OPTICS AND ECOPHYSIOLOGY OF CORAL REEF ORGANISMS

EDITED BY: Daniel Wangpraseurt, Anthony William Larkum, Christine Ferrier-Pagès, Anya Salih, Mark E. Warner, Eric Jeremy Hochberg, Zvy Dubinsky and Michael Kühl

PUBLISHED IN: Frontiers in Marine Science and Frontiers in Microbiology

frontiers Research Topics

frontiers

ISSN 1664-8714
ISBN 978-2-88963-436-1
DOI 10.3389/978-2-88963-436-1

About Frontiers

Frontiers is more than just an open-access publisher of scholarly articles: it is a pioneering approach to the world of academia, radically improving the way scholarly research is managed. The grand vision of Frontiers is a world where all people have an equal opportunity to seek, share and generate knowledge. Frontiers provides immediate and permanent online open access to all its publications, but this alone is not enough to realize our grand goals.

Frontiers Journal Series

The Frontiers Journal Series is a multi-tier and interdisciplinary set of open-access, online journals, promising a paradigm shift from the current review, selection and dissemination processes in academic publishing. All Frontiers journals are driven by researchers for researchers; therefore, they constitute a service to the scholarly community. At the same time, the Frontiers Journal Series operates on a revolutionary invention, the tiered publishing system, initially addressing specific communities of scholars, and gradually climbing up to broader public understanding, thus serving the interests of the lay society, too.

Dedication to Quality

Each Frontiers article is a landmark of the highest quality, thanks to genuinely collaborative interactions between authors and review editors, who include some of the world's best academicians. Research must be certified by peers before entering a stream of knowledge that may eventually reach the public - and shape society; therefore, Frontiers only applies the most rigorous and unbiased reviews.
Frontiers revolutionizes research publishing by freely delivering the most outstanding research, evaluated with no bias from both the academic and social point of view. By applying the most advanced information technologies, Frontiers is catapulting scholarly publishing into a new generation.

What are Frontiers Research Topics?

Frontiers Research Topics are very popular trademarks of the Frontiers Journals Series: they are collections of at least ten articles, all centered on a particular subject. With their unique mix of varied contributions from Original Research to Review Articles, Frontiers Research Topics unify the most influential researchers, the latest key findings and historical advances in a hot research area! Find out more on how to host your own Frontiers Research Topic or contribute to one as an author by contacting the Frontiers Editorial Office: researchtopics@frontiersin.org

OPTICS AND ECOPHYSIOLOGY OF CORAL REEF ORGANISMS

Topic Editors:
Daniel Wangpraseurt, University of Cambridge, United Kingdom
Anthony William Larkum, University of Technology Sydney, Australia
Christine Ferrier-Pagès, Scientific Centre of Monaco, Monaco
Anya Salih, Western Sydney University, Australia
Mark E. Warner, University of Delaware, United States
Eric Jeremy Hochberg, Bermuda Institute of Ocean Sciences, Bermuda
Zvy Dubinsky, Bar-Ilan University, Israel
Michael Kühl, University of Copenhagen, Denmark

Citation: Wangpraseurt, D., Larkum, A. W., Ferrier-Pagès, C., Salih, A., Warner, M. E., Hochberg, E. J., Dubinsky, Z., Kühl, M., eds. (2020). Optics and Ecophysiology of Coral Reef Organisms. Lausanne: Frontiers Media SA. doi: 10.3389/978-2-88963-436-1

Table of Contents

frontiers in Marine Science

EDITORIAL
published: 03 December 2019
doi: 10.3389/fmars.2019.00742

Editorial: Optics and Ecophysiology of Coral Reef Organisms

Daniel Wangpraseurt[1,2], Anthony W. D. Larkum[3], Christine Ferrier-Pagès[4], Anya Salih[5], Mark E. Warner[6], Zvy Dubinsky[7] and Michael Kühl[8]*

[1] Department of Chemistry, University of Cambridge, Cambridge, United Kingdom, [2] Marine Biology Research Division, Scripps Institution of Oceanography, University of California, San Diego, La Jolla, CA, United States, [3] Climate Change Cluster, University of Technology Sydney, Ultimo, NSW, Australia, [4] Ecophysiology Team, Scientific Centre of Monaco, Monaco, Monaco, [5] School of Science and Health, Hawkesbury Institute for the Environment, Western Sydney University, Penrith, NSW, Australia, [6] School of Marine Science and Policy, University of Delaware, Newark, DE, United States, [7] The Mina and Everard Goodman Faculty of Life Sciences, Bar-Ilan University, Ramat Gan, Israel, [8] Department of Biology, Marine Biological Section, University of Copenhagen, Copenhagen, Denmark

Keywords: photosynthesis, coral reefs, photobiology, optics, coral bleaching

Editorial on the Research Topic

Optics and Ecophysiology of Coral Reef Organisms

Light is arguably the most important factor driving the evolutionary success of coral reefs (Falkowski et al., 1990). Solar energy is the prime force underlying the symbiotic interaction between phototrophic dinoflagellates of the family *Symbiodiniaceae* and the heterotrophic coral animal host. Light is also the major energy source for other key coral reef organisms such as crustose coralline algae, sponges, foraminifera, and epi- and endolithic phototrophic biofilms. However, the physical interaction between light and reef organisms is often treated in insufficient detail. For instance, the spectral and directional characteristics of sunlight, as well as the high temporal and spatial variability, can strongly modulate the photosynthetic response of reef organisms, yet are often ignored (Roth, 2014). Likewise, the optical properties of reef organisms, such as the scattering properties of their photosynthetic tissues, the presence of fluorescent pigments and the structural properties of their calcium carbonate skeleton can strongly modulate light absorption and photosynthesis (Salih et al., 2000; Wangpraseurt et al., 2019a). The present Research Topic is a compilation of 14 articles that aim to improve our understanding of how light affects the ecophysiology of coral reef organisms. The topic is divided into (i) articles that discuss the interaction between light and coral reef organisms and (ii) articles that showcase new technologies enabling an improved understanding of the optics of coral reefs.

The articles by Wangpraseurt et al., Swain et al., and Scheufen et al. discuss relationships between optical properties, photophysiology and bleaching susceptibility of shallow water corals. Wangpraseurt et al., used optical microsensors to study the *in vivo* light microhabitat inside coral tissues during bleaching. It is shown how symbiont loss can lead to an exponential acceleration of the internal light field, suggesting an enhanced contribution of coral scattering for the remaining symbionts. Such an optical feedback mechanism was originally proposed by Enriquez et al. (2005), and has now been confirmed by direct measurements of the light microclimate in corals. However, Wangpraseurt et al. found such accelerating light exposure to be species dependent—it was pronounced in thin-tissued *Pocillopora damicornis* corals, while thick-tissued *Favites* sp. showed a more linear increase in irradiance as a function of symbiont loss. Likewise, Swain et al. provide further evidence for the optical feedback loop using low coherence enhanced backscattering spectroscopy and an optical model to understand coral skeletal light propagation. They show that bleaching susceptibility was strongly related to the scattering coefficient of the top 200 μm of the skeletons. A fractal skeletal growth model suggests that corals that grow faster typically have a lower mass-fractal dimension, denser skeletons with lower reduced scattering coefficients and

OPEN ACCESS

Edited and reviewed by:
Raquel Peixoto, Federal University of Rio de Janeiro, Brazil

****Correspondence:***
Daniel Wangpraseurt
dw527@cam.ac.uk

Specialty section:
This article was submitted to Coral Reef Research, a section of the journal Frontiers in Marine Science

Received: *23 September 2019*
Accepted: *14 November 2019*
Published: *03 December 2019*

Citation:
Wangpraseurt D, Larkum AWD, Ferrier-Pagès C, Salih A, Warner ME, Dubinsky Z and Kühl M (2019) Editorial: Optics and Ecophysiology of Coral Reef Organisms. Front. Mar. Sci. 6:742. doi: 10.3389/fmars.2019.00742

higher bleaching susceptibility. Scheufen et al. compared optical traits and structural characteristics of a range of corals, which differ in skeleton morphology, tissue thickness, coral pigmentation, symbiont type and density. The authors show that light absorption capacity was related to the architectural complexity of the coral skeletons, with chalice-type skeletons achieving higher light absorption capacity than meandroid-type skeletons. Together, these three articles highlight the complexity of light-matter interaction in corals, which is modulated by coral tissue properties, skeleton fractal length, and architectural complexity along with the photosynthetic properties of the coral photosymbionts.

Coral optical properties are also strongly affected by spatial and temporal variability. The articles by Einbinder et al., Ezzat et al., and Nitschke et al. focus on photoacclimation and photoadaptation of *Symbiodinum* over time and space. Mesophotic coral reefs have recently been studied with great interest due to their potential to serve as refugia during climate change, but limited knowledge exists on the photosynthetic properties of *Symbiodiniaceae* from such water depths. Einbinder et al. found that mesophotic *Stylophora pistillata* performed below their photosynthetic compensation point and exhibited a distinct light harvesting antenna organization in their photosymbionts, where *Symbiodiniaceae* developed a cooperative system for excitation energy transfer between photosynthetic units that maximizes light utilization. Ezzat et al. also found that shallow water *S. pistillata* associate with *Symbiodinium* clade A, while mesophotic *S. pistillata* preferably associate with *Symbiodinium* clade C that is more efficient at fixing carbon under low light conditions. Thus, both a change in the antenna organization of *Symbiodinium* and differences in symbiont type are successful adaptations to low light environments. Nitschke et al., characterized the PSII photophysiology of corals from shallow reef environments in spring vs. summer. Despite significant seasonal differences in photoacclimation, the thermal tolerance of coral species did overall not shift between seasons.

Green fluorescent protein (GFP)-like host pigment are produced by many corals but the function of GFPs is still disputed with studies showing both a role in photoprotection (Salih et al., 2000), light enhancement, and tissue heating (Lyndby et al., 2016; Smith et al., 2017; Wangpraseurt et al., 2019a). Quick et al. studied the trade-offs associated with photoprotective GFP expression as a driver for coral polymorphism. Excess blue light excitation was less detrimental to highly fluorescent color morphs compared to low fluorescent morphs. Under low irradiance, however, growth rates were lowered in the highly fluorescent morph, highlighting that host pigments synthesis involves energetically costly protein expression. Color polymorphism caused by photoprotective GFPs may thus be a product of balancing selection, in which high pigment content may be beneficial at the upper and detrimental at the lower end of the depth distribution range of symbiotic corals (Quick et al.). This article adds to the apparently multiplex roles that fluorescent host pigments play for coral fitness, which might not always be beneficial.

The light depended physiological activity of corals also implies variations in the local physico-chemical microhabitat, with pronounced diel variations in O_2 and pH. Silveira et al. investigated the role of diel changes in the bacterial community within the momentum boundary layer (MBL) of corals. They found that dominant taxa and functions in the MBL community were stable suggesting that water flow overrules the effects of coral physiology on the MBL bacterial community. Another article in this ebook investigated the role of light scattering in coralline algae. Vasquez-Elizondo and Enríquez studied the role of the skeleton in enhancing thallus light absorption efficiency of red coralline algae. Thicker rhodolith thalli were the most efficient light collectors exhibiting high pigment absorption efficiency and areal photosynthesis rates. This study demonstrates the utility of measuring optical traits to investigate differences in the competitive abilities, abundances, and niche distribution among algal species and/or growth-forms, and further suggests that skeletal scattering is an important light enhancing mechanism in other reef organisms besides corals.

The second part of the ebook deals with new optical techniques related to the characterization of inherent optical properties, chlorophyll *a* and GFP fluorescence. Jacques et al. describe a simple low-cost approach to characterize the bulk absorption and scattering properties of living corals via spatially resolved diffuse reflectance measurements. Mazel describes a new method to quantify the contribution of fluorescence to optical signatures under ambient illumination conditions and argues that fluorescence has an important visual function in the reef environment. Zweifler et al. developed a fluorescence-based technique to acquire daytime photographs enabling identification of coral recruits. The authors envisage that their technique will provide an easy-to-use photographic system that can contribute significantly to the toolkit for coral reef monitoring and management.

Variable chlorophyll *a* fluorescence is a key tool in characterizing coral health and photophysiological characteristics of corals. However, since the spatial origin of PSII chlorophyll fluorescence in coral tissues is uncertain, such signals give limited information on depth-integrated photosynthetic performance of the whole tissue (Wangpraseurt et al., 2019b). Szabó et al. developed a new approach to assess dynamics of photosystem II and I in whole coral tissues based on redox kinetics of the primary electron donor in Photosystem I (P700) and chlorophyll fluorescence kinetics (Fast-Repetition Rate fluorometry, FRRf). The authors show that P700 kinetics measurements can be used as a measure for the integrity of PSII-PSI electron transfer dynamics in corals. Lastly, Hoadley and Warner developed, a low-cost multicolor chlorophyll *a* fluorometer using an open source hardware development platforms (Arduino and Bitscope) to construct a multispectral excitation system. This may inspire further developments of highly customized low-cost instrumentation for coral photophysiology.

In summary, the contributions in this ebook highlight the fundamental role of the interaction between light and reef organisms and its implication for coral ecophysiology, bleaching susceptibility, photosynthetic efficiency, and other

key ecological functions on coral reefs. It also shows that we still need a better mechanistic understanding of fundamental light-matter interactions in reef organisms, which relies on the development and application of novel techniques and experimental approaches for monitoring optical properties, light fields, and photobiological processes in reef organisms in their natural environment.

AUTHOR CONTRIBUTIONS

The editorial was written by DW, MK, CF-P, and AL with contributions from all remaining authors.

FUNDING

DW was supported by grants from the European Union's Horizon 2020 scheme. MK was supported by grants from the Independent Research Fund Denmark (DFF-1323-00065B and DFF-8021-00308B) and the Carlsberg Foundation. MW was supported by the National Science Foundation (award 1635695).

ACKNOWLEDGMENTS

We thank the Frontiers in Marine Science Editorial staff for their invitation and support in producing this Research Topic.

REFERENCES

Enriquez, S., Mendez, E. R., and Iglesias-Prieto, R. (2005). Multiple scattering on coral skeletons enhances light absorption by symbiotic algae. *Limnol. Oceanogr.* 50, 1025–1032. doi: 10.4319/lo.2005.50.4.1025

Falkowski, P. G., Jokiel, P. L., and Kinzie, R. (1990). Irradiance and corals. *Ecosyst. World* 25, 89–107.

Lyndby, N. H., Kühl, M., and Wangpraseurt, D. (2016). Heat generation and light scattering of green fluorescent protein-like pigments in coral tissue. *Sci. Rep.* 6:26599. doi: 10.1038/srep26599

Roth, M. S. (2014). The engine of the reef: photobiology of the coral–algal symbiosis. *Front. Microbiol.* 5:422. doi: 10.3389/fmicb.2014.00422

Salih, A., Larkum, A., Cox, G., Kühl, M., and Hoegh-Guldberg, O. (2000). Fluorescent pigments in corals are photoprotective. *Nature* 408, 850–853. doi: 10.1038/35048564

Smith, E. G., D'angelo, C., Sharon, Y., Tchernov, D., and Wiedenmann, J. (2017). Acclimatization of symbiotic corals to mesophotic light environments through wavelength transformation by fluorescent protein pigments. *Proc. R. Soc. B Biol. Sci.* 284, 1–9. doi: 10.1098/rspb.2017.0320

Wangpraseurt, D., Jacques, S., Lyndby, N., Holm, J. B., Pages, C. F., and Kühl, M. (2019a). Microscale light management and inherent optical properties of intact corals studied with optical coherence tomography. *J. R. Soc. Interface* 16:20180567. doi: 10.1098/rsif.2018.0567

Wangpraseurt, D., Lichtenberg, M., Jacques, S. L., Larkum, A. W., and Kühl, M. (2019b). Optical properties of corals distort variable chlorophyll fluorescence measurements. *Plant Physiol.* 179, 1608–1619. doi: 10.1104/pp.18.01275

Conflict of Interest: The authors declare that the research was conducted in the absence of any commercial or financial relationships that could be construed as a potential conflict of interest.

frontiers in Marine Science

ORIGINAL RESEARCH
published: 17 October 2016
doi: 10.3389/fmars.2016.00195

Novel Adaptive Photosynthetic Characteristics of Mesophotic Symbiotic Microalgae within the Reef-Building Coral, *Stylophora pistillata*

*Shai Einbinder[1,2], David F. Gruber[3], Eitan Salomon[4], Oded Liran[1,5], Nir Keren[4] and Dan Tchernov[1,5]**

[1] The Leon H. Charney School of Marine Sciences, University of Haifa, Mount Carmel, Haifa, Israel, [2] Department of Evolution, Systematics and Ecology, Hebrew University of Jerusalem, Jerusalem, Israel, [3] Department of Natural Sciences, City University of New York, Baruch College and The Graduate Center, New York, NY, USA, [4] Department of Plant and Environmental Sciences, Hebrew University of Jerusalem, Jerusalem, Israel, [5] Interuniversity Institute for Marine Sciences, Eilat, Israel

OPEN ACCESS

Edited by:
Daniel Wangpraseurt, University of Copenhagen, Denmark

Reviewed by:
Susana Enríquez, National Autonomous University of Mexico, Spain
Leïla Ezzat, Scientific Centre of Monaco, Monaco
Gal Eyal, Tel Aviv University and The Interuniversity Institute for Marine Sciences in Eilat, Israel

***Correspondence:**
Dan Tchernov
dtchernov@univ.haifa.ac.il

Specialty section:
This article was submitted to Coral Reef Research, a section of the journal Frontiers in Marine Science

Received: *01 July 2016*
Accepted: *26 September 2016*
Published: *17 October 2016*

Citation:
Einbinder S, Gruber DF, Salomon E, Liran O, Keren N and Tchernov D (2016) Novel Adaptive Photosynthetic Characteristics of Mesophotic Symbiotic Microalgae within the Reef-Building Coral, Stylophora pistillata. Front. Mar. Sci. 3:195. doi: 10.3389/fmars.2016.00195

Photosynthetic coral reef structures extend from the shallow sundrenched waters to the dimly lit, "twilight" mesophotic depths. For their resident endosymbiotic dinoflagellates, primarily from the genus *Symbiodinium* spp., this represents a photic environment that varies ~15-fold in intensity and also differs in spectral composition. We examined photosynthesis in the scleractinian coral *Stylophora pistillata* in shallow (3 m) and mesophotic settings (65 m) in the northern Red Sea. *Symbiodinium* spp. in corals originating from the mesophotic environment consistently performed below their photosynthetic compensation point and also exhibited distinct light harvesting antenna organization. In addition, the non-photochemical quenching activity of *Symbiodinium* spp. from mesophotic corals was shown to be considerably lower than those found in shallow corals, showing they have fewer defenses to high-light settings. Over a period of almost 4 years, we extensively utilized closed circuit Trimix rebreather diving to perform the study. Phylogenetic analysis showed that shallow corals (3 m) transplanted to a deep reef environment (65 m) maintained their initial *Symbiodinium* spp. community (clade A), rather than taking on deep low-light clades (clade C), demonstrating that shallow *S. pistillata* acclimate to low-light mesophotic environments while maintaining their shallow photosynthetic traits. Mesophotic corals exhibited static depth-related chlorophyll content per cell, a decrease in PSI activity and enhanced sigmoidal fluorescence rise kinetics. The sigmoidal fluorescence rise kinetics we observed in mesophotic corals is an indication of energy transfer between photosynthetic units. We postulate that at mesophotic depths, a community of adapted *Symbiodinium* spp. utilize a unique adaptation to lower light conditions by shifting their light harvesting to a PSII based system, where PSII is structured near PSI, with additional PCP soluble

antenna also trapping light that is funneled to the PSI reaction center. In this study, we provide evidence that mesophotic *Symbiodinium* spp. have developed novel adaptive low-light characteristics consisting of a cooperative system for excitation energy transfer between photosynthetic units that maximizes light utilization.

Keywords: *Symbiodinium* spp., mesophotic coral reef, photosynthesis, low-light acclimation, excitation energy transfer

INTRODUCTION

Scleractinian corals build the framework of the world's tropical reefs and their growth relies primarily on photosynthetic dinoflagellate endosymbionts from the genus *Symbiodinium* (Jones et al., 1998). These photosymbionts reside within the corals endoderm and produce photosynthates that are translocated to the host (Muscatine et al., 1975; Falkowski and Dubinsky, 1981). While shallow reefs have been extensively studied, the deeper mesophotic environment (>30 m) has been much less examined due to difficulty to access, such as the need for technical diving or remotely operated vehicles. Light intensity decays exponentially with depth (Gordon, 1989) and therefore, the mesophotic reef environment, known as the "twilight zone," is characterized by light fluxes that vary seasonally between 5 and 100 μmol photons m^{-2} s^{-1}. This dim mesophotic setting, therefore, receives 15–300 times less of a photon flux than shallow reef counterparts ∼1500 μmol photons m^{-2} s^{-1} (Levy et al., 2003). The low light flux in the mesophotic region impacts corals photosynthetic and calcification rates and limits their vertical distribution throughout the photic zone (Wells, 1957; Dubinsky et al., 1984; Franklin et al., 1996; Jones et al., 1998). In addition, deeper reefs receive narrower spectra, primarily blue light spectra centered at 467 nm, than the wider spectral range of shallow waters (Dishon et al., 2013). In mesophotic, low-light conditions, corals have been shown to shift their energetic budget to heterotrophic predation (Muscatine and Kaplan, 1994; Einbinder et al., 2009). *Symbiodinium* has also been shown to acclimate to low-light regimes (Cohen and Dubinsky, 2015). The current understanding is that two mechanisms are involved: (1) an increase in the effective antenna size—antenna pigments per photosynthetic unit (PSU) (Falkowski and Dubinsky, 1981; Franklin et al., 1996) and (2) an increase of photosynthetic units (PSU) per cell (Chang et al., 1983; Prézelin, 1987; Iglesias-Prieto and Trench, 1997; Pratchett et al., 2008; Hennige et al., 2009; Hutchings et al., 2009; Lesser et al., 2010). However, there have also been studies that have reported no significant changes in the *Symbiodinium* chlorophyll content at depths below 25 m (Titlyanov et al., 2002; Mass et al., 2007; Lesser et al., 2010).

In shallow high light conditions thermal dissipation, Non photochemical Quenching (NPQ) provides a mechanism that protects *Symbiodinium* photosynthetic apparatus from excess photosynthetic active radiation (PAR) damage (Hoegh-Guldberg and Jones, 1999). Dinoflagellates contain two types of photosynthetic antenna: A membrane bound intrinsic antenna–acpPC (Chl a-Chl c2-peridinin protein complex) as shown in **Figure 1** (Niedzwiedzki et al., 2014); and a soluble membrane complex PCP (peridinin-Chl a protein). NPQ was shown to be associated with the conversion of diadinoxanthin to diatoxanthin (Brown, 1997). Xanthophyll epoxidation and de-epoxidation decreases photon flux to PSII reaction centers and thus prevents over reduction of the quinone acceptors by reducing the functional absorption cross-section of PSII reaction centers (σPSII). In corals, the quencher in the NPQ processes was suggested to reside in the apcCP antenna (Iglesias-Prieto and Trench, 1997; Kanazawa et al., 2014).

NPQ has a finite capacity and may reach saturation while excess electrons continue to reduce the electron transport chain (Brown et al., 1999; Dustan, 1999; Smith et al., 2005). Alternative sinks for electrons, other than CO_2 assimilation, may provide additional protection mechanisms to help prevent over reduction at high light intensities. PSI can directly reduce O_2 via the Mehler reaction to produce superoxide radicals that are rapidly converted within the chloroplast to hydrogen peroxide by superoxide dismutase (Jones et al., 1998). Hydrogen peroxide is then detoxified to produce water by ascorbate peroxidase, which oxidizes ascorbate to monodehydroascorbate (Asada, 1999).

While there is a wealth of information on short-term processes of light regime change acclimation mechanisms, long-term processes accounting for the diversity of both symbionts and hosts have only recently been explored (Iglesias-Prieto et al., 2004; Bongaerts et al., 2011, 2013; Cooper et al., 2011; van Oppen et al., 2011; Brazeau et al., 2013; Nir et al., 2014). Most indicate distinct deep and shallow symbionts types, with a few generalist types (Lesser et al., 2010).

In this study, we examined *Stylophora pistillata* at 65 and 3 m, as well as those slowly transplanted from shallow to deep, in an attempt to elucidate what long-term acclimation or adaptation processes photosynthetic dinoflagellates possess in high and low light environments. We are also investigated potential mechanisms of efficient energy transfer at mesophotic depths.

MATERIALS AND METHODS

In order to investigate the photosynthetic characteristics of mesophotic and shallow corals we conducted a series of analyses on intact corals and their isolated *Symbiodinium* and determined their net and gross photosynthesis rates as a function of irradiance (PI), PSII quantum yield, non-photochemical quenching (NPQ) parameters, chlorophyll fluorescence emission spectra and PSI activity.

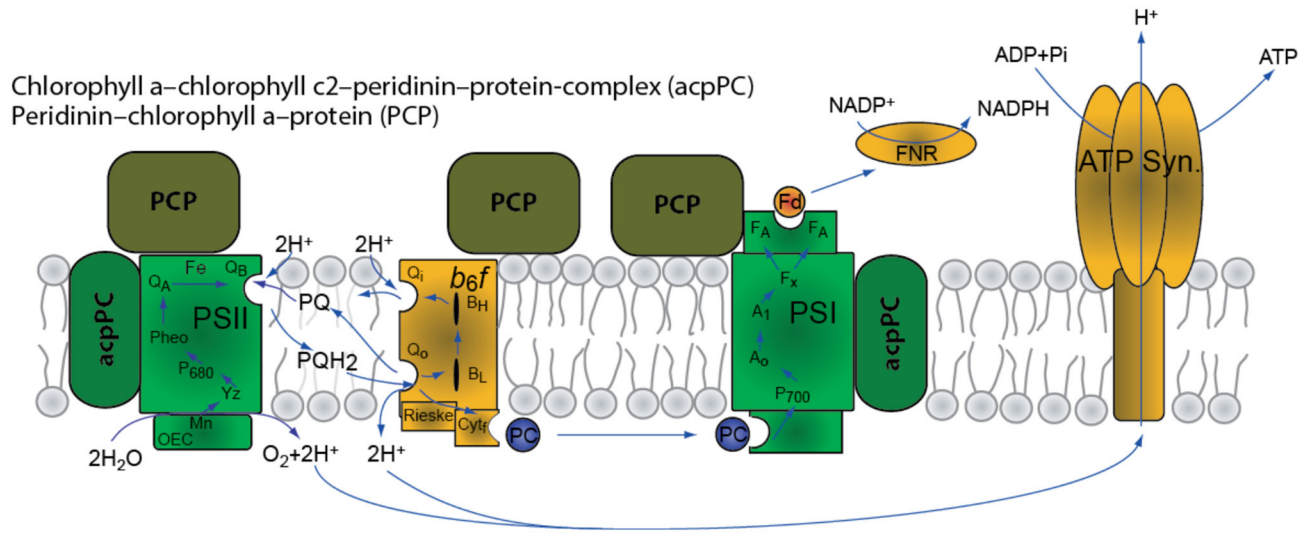

FIGURE 1 | Schematic representation of the photosynthetic apparatus in *Symbiodinium* spp.

Sample Collection and Preparation for Analysis

Coral samples were collected in the Northern Red Sea (29°30′N, 34°56′E) from a gradient of 3 to 65 m along the fore reef slope. Branches of the hermatypic corals *S. pistillata* (wide depth range, 0–70 m) (Fricke and Schuhmacher, 1983) were collected from their natural habitats using closed circuit Trimix rebreather systems (Megalodon™). To distinguish between adaptive or acclimation responses, over almost 4 years (June 2004-April 2008), we gradually transferred (5 m/2 weeks) mesophotic *S. pistillata* from a depth of 65 to 5 m, and shallow *S. pistillata* from 5 m to a final depth of 65 m. The corals then remained at either depth until the conclusion of the experiment when they were removed for analysis. Samples were collected in light-proof black bags and brought to the incubation area where light intensity was controlled to duplicate source depths. The collection was conducted under permit number 31944 from the Israel Nature and Parks Authority. Samples were held for less than 18 h, and then transferred for further analysis.

Fluorescence Parameters (PSII)

Chlorophyll fluorescence parameters were measured using a Fluorescence Induction and Relaxation (FIRe) fluorometer (Satlantic) and a PAM imaging system fluorometer (Walz, GmbH, Effeltrich, Germany). The corals were dark-adapted for 30 min prior to measurements. A single saturating pulse (4000 μmol photons m^{-2} s^{-1}, white-light, 500 ms for the PAM and 10,000 μmol photons m^{-2} s^{-1}, blue-light, 80 μs for the FIRe) was triggered, and PSII maximal fluorescence (F_m) was measured.

NPQ was calculated as described in Schreiber (2004) where $NPQ = (F_m - F'_m)/F'_m$. F'_m was obtained after steady state fluorescence was achieved under an actinic light intensity of (0–1000 μmol photons m^{-2} s^{-1} for the PAM and a 1000 μmol photons m^{-2} s^{-1} (Schott KL2500LCD) for the FIRe measurement.

Oxygen Evolution and Consumption (Net and Gross Photosynthesis)

A quadrupole mass spectrometer (Balzers QMG 421) with a membrane inlet (MIMS) was used to measure dissolved gas in a climate and light controlled chaimber (3.3 ml volume). Simultaneous measurements of argon and mass 14 concentration were used to assess the stability of the system as described in Tchernov et al. (1997, 2001). The action medium consisted of artificial sea water (ASW) pH 8.2 with 2 mM total dissolved inorganic carbon.

PSI Relative Function through Oxygen Consumption

Fresh symbionts were extracted from coral fragments and placed in the action medium that consisted of ASW pH 8.2 with 2 mM total dissolved inorganic carbon. The algae were incubated in the dark in the presence of 10–5 M (3-(3,4-dichlorophenyl)-1,1-dimethylurea) DCMU (D2425 Sigma) for 20 min. When there was no detectable oxygen evolution under illumination at saturating light intensity (400 μmol photons m^{-2} s^{-1}) lights were turned off and 30 μM (sodium 2,6-dichloroindophenol) DCIP, (33125 Sigma), 0.3 mM sodium ascorbate (A7631 Sigma), and 70 μM methyl viologen (856177 Sigma) were added (Kyle et al., 1984). The FIZ were transferred into a temperature controlled (26°C ± 0.5) MIMS chamber. Upon illumination, oxygen was monitored on line using the MIMS as described in Tchernov et al. (1997, 2001). The rate of oxygen consumption was normalized to chlorophyll concentration.

Pigments Analysis

Coral fragments (2 cm) were airbrushed and purified using the same protocol as Stochaj and Grossman (1997) and resuspended in 100% methanol. After ensuring identical samples (chlorophyll concentration), we followed the protocol of Rogers and Marcovich (2007) for pigment HPLC analysis. The samples were incubated in 4°C for 2 h and were vortexed for 2 min every 30 min. The samples were incubated overnight in the presence of ammonium acetate (pH 7.2, −20°C). The mixture was vortexed again and centrifuged (14,000 rpm, 4°C, 20 min). The pellet was discarded and the supernatant was injected into a HPLC equipped with a reverse-phased column (Spherisorb ODS-2 column -silica 5 μm, 3.2 mm × 250 mm (Phenomenex®) analysis.

Photosynthesis/Irradiance Measurements

Coral fragments were airbrushed to release the *Symbiodinium* symbionts, cleaned via triple washing with 0.2 μm filtered seawater and then placed in a temperature-controlled chamber (2.8 ml) at 26°C in artificial seawater (pH 8.2) supplemented with 2 mM dissolved inorganic carbon (S5761 Sigma). For illumination, Schott© KL2500LCD unit with two optic fibers were connected to special optic ports to the chamber. The various chemicals supplied to the cell suspension were introduced via a top injection port. In order to measure respiration during light photosynthesis, isotopic labeling oxygen method incorporated as in Bender et al. (1987). The sample was spiked with $H_2^{18}O$, incubated in light, and measured for labeled oxygen dilution. Detection was performed by a Membrane Inlet Mass Spectrometry (MIMS) apparatus. As all the labeled O_2 is contained in a single well-defined dissolved gas phase and the ambient O_2 pool assumed to be much larger, only a negligible amount of O_2 will be recycled by respiration during the incubation. For normalization, chlorophyll was extracted using 90% acetone, as in Jeffrey and Humphrey (1975). PSI activity values were calculated from the initial slopes.

Phylogenetic Analysis

Phylogenetic analysis of the ITS2 sequences (316 bp) using parsimony (PAUP 4) algorithm carried out with 26 representative sequences of seven clades and three sequences obtained from this study (deep, shallow and transplant, Supplementary Table 1). The ITS2 sequence of *Gymnodinium aureolum* was used as an out-group. Values (%) of 500 bootstrap replicates are given at branching points for parsimony/distance analyses. Corals from shallow water and transplant present zooxanthellae from clade A while the symbiont of the deep-water cluster with clade c.

RESULTS

Dynamics of the Photosynthetic Light Response

For the study of the dynamics of the photosynthetic apparatus we used four groups of corals: shallow and mesophotic coral fragments and two depth transplants groups (3 and 65 m, **Figure 2**). NPQ activity was measured in *S. pistillata* (3 and 65 m), and was up to five times higher in shallow corals than in the mesophotic corals (**Figure 3** and **Table 1**).

The transfer of 65 m mesophotic *Stylophora* colonies to shallow 5 m environments resulted in lethal responses, despite a slow assent rate (5 m every 2 weeks). This is in agreement with (Baker, 2003) that indicates mortality of deeper colonies upon ascending transplant experiments. Yet, the transfer of shallow corals to the mesophotic region was successful. For shallow corals transplanted to 65 m, a marked difference in NPQ from the mesophotic corals was observed, indicating a shallow-type response (**Figure 3**). Phylogenetic sampling showed that transplanted corals retain their original *Symbiodinium* type. This differed from the non-transplanted corals as well as from control corals that were transplanted laterally along the same depth (Supplementary Figure 1). The different symbiont population discovered at mesophotic depths hints that it diverged from shallow population to provide an adaptive advantage. These

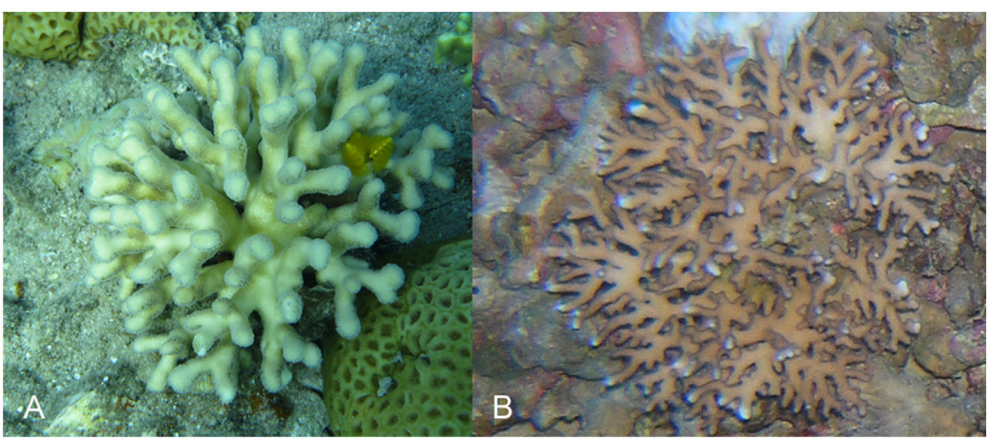

FIGURE 2 | Example of *Stylophora pistillata* from shallow and mesophotic environments. (A) 3 m; **(B)** 65 m.

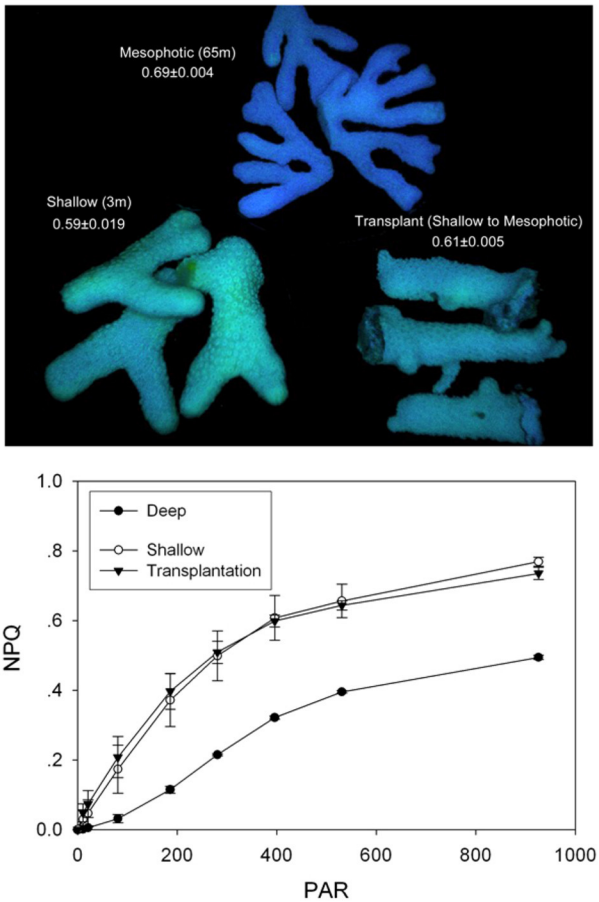

FIGURE 3 | NPQ analysis of mesophotic, shallow and transplanted corals. Measurements were performed using PAM imaging system. The top panel presents a false color image of the coral fragments. The values indicated are Fv/Fm average calculated from three independent fragments. The bottom panel presents NPQ values as a function of incident light intensity for the three coral fragment groups. Mesophotic corals symbionts lose a small fraction of excessive absorbed energy to photoprotective measures.

TABLE 1 | Photosynthetic parameters.

Parameters	Shallow	Deep
α^a	4.9 ± 1.2	2.6 ± 0.9
$P_{max}{}^a$	256 ± 13	160 ± 29
Symbiont density[b]	4E + 05 ± 3E+04	9.47E + 05 ± 9.07E+04
Chl c/Chl a[c]	0.70 ± 0.08	0.46 ± 0.06
Peridinin/Chl a[c]	0.71 ± 0.04	0.58 ± 0.01
Fv/Fm[d]	0.59 ± 0.02	0.68 ± 0.01
$\tau_{Qa}{}^e$	981.34 ± 40	1027.11 ± 20
$\sigma\ \pi_{680}$Å quanta^{-1e}	93 ± 9.4	71.25 ± 8.0
NPQ[d]	2.29 ± 0.15	0.422 ± 0.08
NPQ[e]	0.88 ± 0.21	0.05 ± 0.04
PSI dependent O_2 uptake (μmol O_2 mgChl^{-1}h^{-1})[f]	191 ± 10	71 ± 19

*α—initial slope of the photosynthetic PI curve (**Figure 4**). Pmax—maximal rate of oxygen evolution. τQa—rate of PSII acceptor side reduction measured using a FIRe spectrometer. σ π_{680}Å quanta^{-1}—PSII absorption cross-section measured using a FIRe fluorometer. Fv/Fm—PSII maximal quantum yield measure using a PAM fluorometer. NPQ—non-photochemical quenching of absorbed excitation energy measured using a PAM fluorometer.*

*[a] Based on data presented in **Figure 4**, SE calculated based on three repeats.*

[b] Calculated as described in materials and methods (n = 3).

[c] SE calculated based on four repeats.

[d] SE based on PAM measurements (n = 3).

[e] SE based on FIRe measurements (n = 4).

[f] See methods: PSI Relative Function through Oxygen Consumption); SE (n = 2).

results prompted us to take a closer mechanistic look at the differences in the function of the photosynthetic apparatus.

Organization of the Photosynthetic Apparatus

The rates of oxygen production and uptake reactions were studied in detail using the Membrane Inlet Mass-Spectrometry technique (MIMS). Using MIMS determined that *S. pistillata* from 65 m performed below their photosynthetic compensation point (where oxygen uptake and production rates are equal) at the natural ambient low-light intensities (**Figure 4**). Shallow corals performed close to their photosynthetic P_{max} in their ambient high-light conditions. The P_{max} of mesophotic corals from 65 m was ∼1.6-fold lower than that of their shallow counterparts (**Table 1**), a finding in agreement with (Falkowski and Dubinsky, 1981). Mesophotic corals did not exhibit a decrease in oxygen production when subjected to high-light intensities of nearly two orders of magnitude higher than their natural light environment (**Figure 4**). The relatively low P_{max} is in accordance with the prevalent shade-adapted response in photosynthetic organisms. Mesophotic corals displayed a low initial rate constant (α), comparable to shallow corals (**Table 1**). This differs from the typical response of shade-adapted species that exhibit lower P_{max} at low-light intensities and retain high photosynthetic efficiency (α), due to an increased antenna size (Björkman, 1966).

Using the Fluorescence Induction and Relaxation (FIRe) approach (Kolber et al., 1998), we found that mesophotic PSII traps energy better than shallow PSII; and its variable fluorescence magnitude is higher than the shallow symbionts (**Table 1**). However, mesophotic Q_A-reoxidation time constant (τ) was slightly slower than the shallow PSU constant (**Table 1**,) and the absorption cross-section (σP_{680}) was significantly lower (**Table 1**), implying an overall smaller PSU size.

The photosynthetic pigments concentration ratios were obtained via High Performance Liquid Chromatography (HPLC) (**Table 1**). Mesophotic *Symbiodinium* contain substantially less antenna pigments on a chlorophyll basis. The percent decrease was greater for Chlorophyll C then for Peridinin (34 and 18%, respectively). This data suggests a shift to smaller antenna size in mesophotic corals, with a composition favoring membrane anchored PCP over membrane embedded apcCP. Partial electron transport measurements of freshly isolated *Symbiodinium* (FIZ) were performed using a membrane inlet mass-spectrometer (MIMS). A ratio of 2.7 ± 0.7 in PSI activity was recorded between shallow and mesophotic samples (**Table 1**), suggesting reduced PSI content in mesophotic samples.

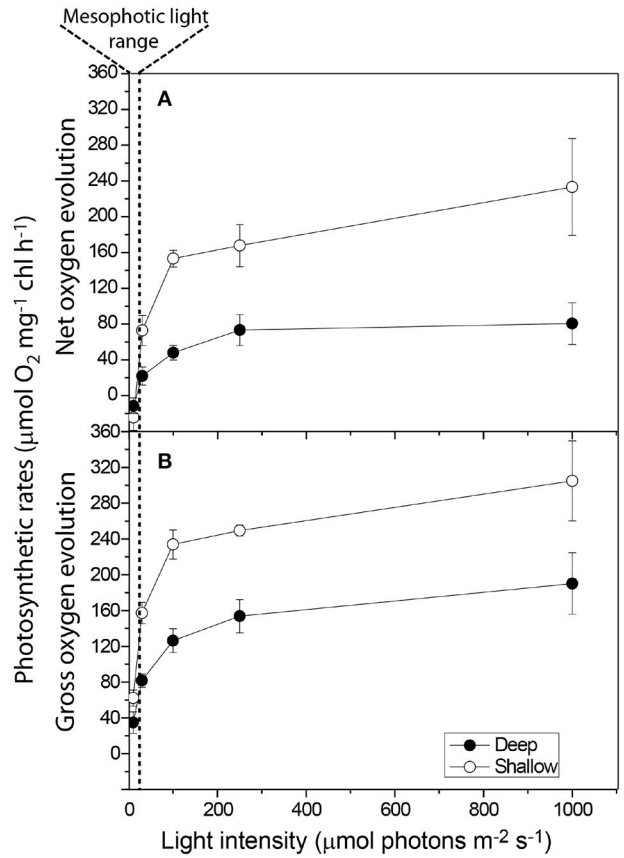

FIGURE 4 | Photosynthesis-Irradiance measurements of the initial mesophotic (65 m) and shallow (3 m) corals *Symbiodinium* sp. depicting (A) Net Photosynthesis and (B) Gross photosynthesis. Mesophotic symbionts do not experience dynamic photoinhibition at shallow light intensities.

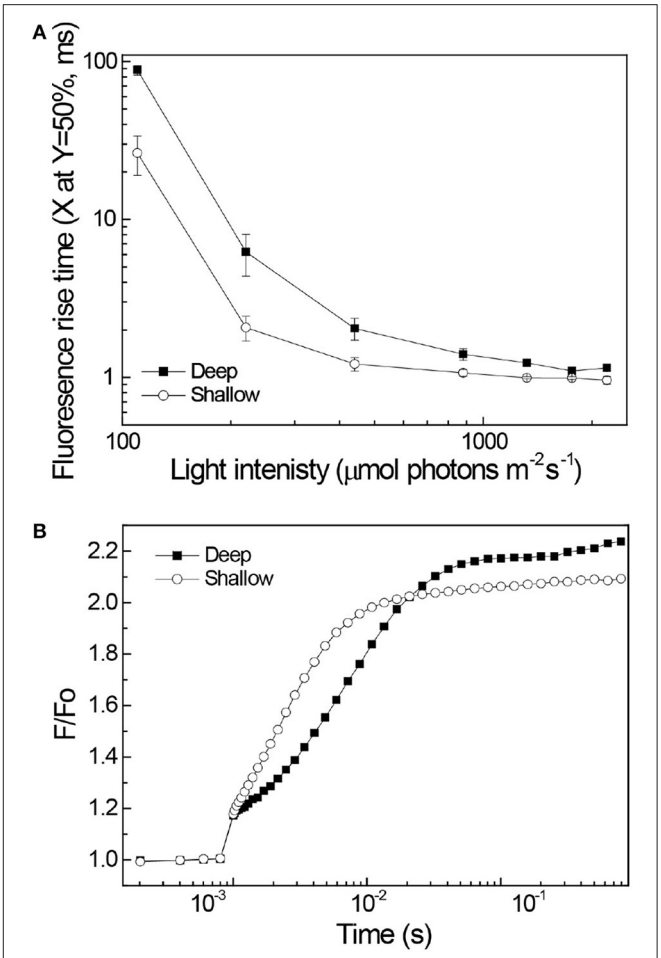

FIGURE 5 | Chlorophyll fluorescence rise kinetics. The actinic light was turned on at 10^{-3} s. **(A)** Shallow corals (3 m) are represented by open symbols, mesophotic corals (65 m) depth are represented by closed symbols. Curves fitted to a sigmoid trandline ($R^2 > 0.97$ for all curves). The fluorescence rise half time, extracted from the sigmoidal fit, for deep and shallow corals is plotted as a function of the actinic light intensity. Standard deviation values calculated from three samples for each depth. Values represent the time for the signal to reach 50% of its maximum excitation. **(B)** An example for the raw data where 220 μmole photons m^{-2} s^{-1} red light excitation (620 nm) was used.

Energy Transfer between Antenna and Reaction Centres

Fluorescence rise kinetics in the presence of DCMU was measured to investigate the dynamics of PSII and antenna energy transfer processes. In the presence of DCMU, blocking electron transport at the Q_B site, fluorescence emission kinetics reflects the interplay of antenna excitation migration and subsequent PSII charge separation. Fluorescence rise kinetics of deep corals was strongly sigmoidal as compared to the shallow corals (**Figure 5**). The sigmoidal nature of the mesophotic corals fluorescence kinetics extended their rise time compared to shallow corals, the difference being most pronounced under low light intensities (**Figure 5**).

DISCUSSION

The combination of static depth-related chlorophyll content per cell (Mass et al., 2007) with a distinct decrease in PSI activity, and enhanced sigmoidal fluorescence rise kinetics suggests a distinct organization of the photosynthetic apparatus of mesophotic corals (**Figure 6**). In the photosynthetic apparatus, PSI supports the linear electron transport process leading to the generation of ATP and NADPH and cyclic electron transport processes affecting ATP/NADPH ratios. Cyclic processes are considered as means for adjusting the redox poise and as a protective mechanism preventing excess excitation induced damages (Munekage et al., 2004; Nawrocki et al., 2015). At low light intensities such protection is not required.

The theoretical limit (Falkowski and Dubinsky, 1981) for enhancing light absorption through an increase in the effective antenna cross section was calculated to be 1650 ± 175 Chl a per P_{700} (Falkowski and Dubinsky, 1981) at a depth equivalent to 30 m (where light intensity is equated to the light intensity at the depth the coral was extracted). This mechanism, therefore, cannot be efficient in the deeper mesophotic reef environment.

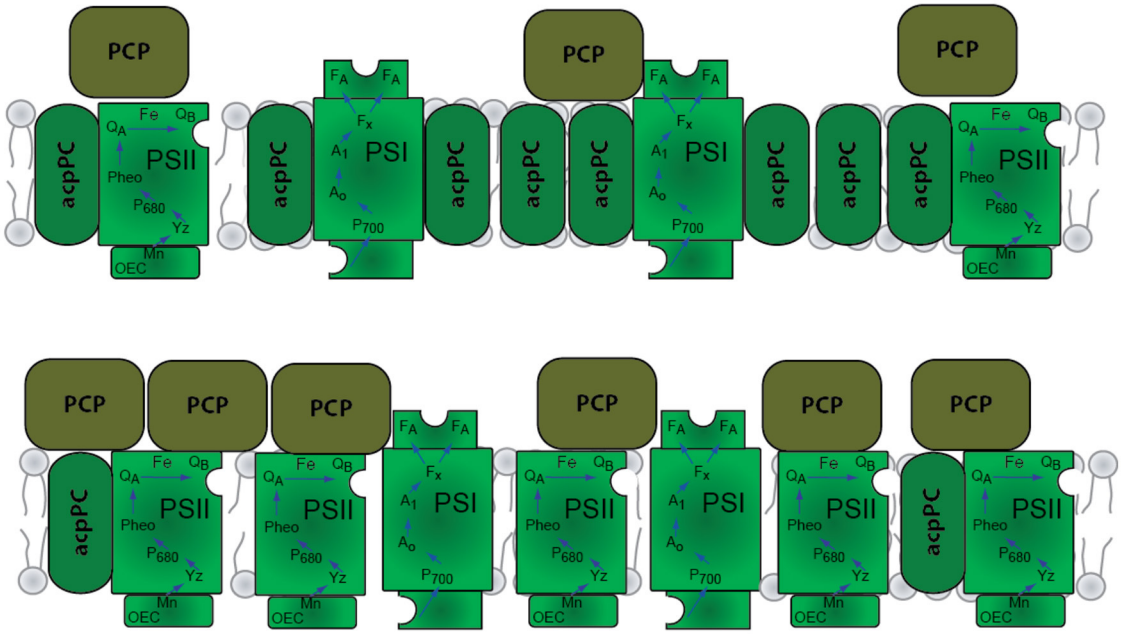

FIGURE 6 | Schematic model of the organization of the photosynthetic apparatus in shallow (top) and mesophotic/deep (bottom) corals.

An increase in PSU per cell may be effective for low-light acclimation, as described by several groups (Chang et al., 1983; Prézelin, 1987; Iglesias-Prieto and Trench, 1997; Hutchings et al., 2009). In this study, as well as in previous work (Mass et al., 2007) evidence of an acclimation pathway mechanism was not found at mesophotic depths.

PSII's shallow energetic trap allows exactions to be distributed between closed and open reaction centers. This creates an efficient low-light energy transfer scheme that is displayed in our data as a sigmoid fluorescence rise kinetics curve, shown only in the deep corals. The sigmoidal fluorescence rise kinetics that we observed in mesophotic corals is an indication of energy transfer between photosynthetic units (Trissl et al., 1993; Lavergne and Trissl, 1995). Under low-light intensities, this energy transfer increases photosynthetic quantum efficiency (Joliot and Joliot, 1964, 2003). The lower PSI content and the shift from a membrane embedded to a membrane-attached light harvesting system can facilitate this type of cooperativity. We postulate that at mesophotic depths, a community of adapted *Symbiodinium* spp. occupies most of the corals and they utilize a unique adaptation to the "twilight" conditions by shifting their light harvesting to a PSII based system, where PSII is structured near PSI, with additional PCP soluble antenna also trapping light that is funneled to the PSI reaction center. Our genetic data suggest that mesophotic *S. pistillata* have one species of symbionts that maintain these traits. Shallow corals and those transplanted from shallow to deep kept their shallow traits, such as high NPQ that serves as a line of defense against photoinhibitory damage (Papageorgiou and Govindjee, 1968; Takahashi et al., 2008). These finding points to an adaptive mechanism in mesophotic corals, rather than the previously noted acclimation strategies. Other species of mesophotic corals and other photosynthetic organisms living in perpetually low-light environments should be examined to determine if they also share this novel, energy efficient low-light photosynthesis strategy.

AUTHOR CONTRIBUTIONS

Planned the study: SE, DG, ES, OL, NK, and DT. Performed Pigments Analysis: SE, ES, OL, NK, and DT. Performed Photosynthesis/Irradiance Measurements: SE, ES, OL, NK, and DT. Wrote the manuscript: SE, DG, ES, OL, NK, and DT.

ACKNOWLEDGMENTS

We thank K. Zendbank for assisting in molecular work and the Interuniversity Institute for Marine Sciences and staff in Eilat, Israel, for contributing to field studies. We greatly thank E. Brokovitch and O. Ben-Sharput for participating in the technical dives. The research was supported by the Israel Science Foundation grant # 981/05 to DT, the Bundesministerium für Bildung und Forschung, Germany, grant # 1923–1300 to DT and the US National Science Foundation grant # 0920572 and 1556213 to DG.

SUPPLEMENTARY MATERIAL

The Supplementary Material for this article can be found online at: http://journal.frontiersin.org/article/10.3389/fmars.2016.00195

REFERENCES

Asada, K. (1999). The water-water cycle in chloroplasts: scavenging of active oxygens and dissipation of excess photons. *Annu. Rev. Plant Physiol. Plant Mol. Biol.* 50, 601–639. doi: 10.1146/annurev.arplant.50.1.601

Baker, A. C. (2003). Flexibility and specificity in coral-algal symbiosis: diversity, ecology, and biogeography of symbiodinium. *Annu. Rev. Ecol. Evol. Syst.* 34, 661–689. doi: 10.1146/annurev.ecolsys.34.011802.132417

Bender, M., Grande, K., Johnson, K., Marra, J., Williams, P., Sieburth, J., et al. (1987). A comparison of four methods for determining planktonic community production. *Limnol. Oceanogr.* 32, 1085–1098. doi: 10.4319/lo.1987.32.5.1085

Björkman, O. (1966). The effect of oxygen concentration on photosynthesis in higher plants. *Physiol. Plant.* 19, 618–633. doi: 10.1111/j.1399-3054.1966.tb07046.x

Bongaerts, P., Frade, P. R., Ogier, J. J., Hay, K. B., van Bleijswijk, J., Englebert, N., et al. (2013). Sharing the slope: depth partitioning of agariciid corals and associated Symbiodinium across shallow and mesophotic habitats (2-60 m) on a Caribbean reef. *BMC Evol. Biol.* 13:205. doi: 10.1186/1471-2148-13-205

Bongaerts, P., Sampayo, E. M., Bridge, T. C. L., Ridgway, T., Vermeulen, F., Englebert, N., et al. (2011). Symbiodinium diversity in mesophotic coral communities on the Great Barrier Reef: a first assessment. *Mar. Ecol. Prog. Ser.* 439, 117–126. doi: 10.3354/meps09315

Brazeau, D. A., Lesser, M. P., and Slattery, M. (2013). Genetic structure in the coral, *Montastraea cavernosa*: assessing genetic differentiation among and within Mesophotic reefs. *PLoS ONE* 8:e65845. doi: 10.1371/journal.pone.0065845

Brown, B. E. (1997). Coral bleaching: causes and consequences. *Coral Reefs* 16, S129–S138. doi: 10.1007/s003380050249

Brown, B. E., Ambarsari, I., Warner, M. E., Fitt, W. K., Dunne, R. P., Gibb, S. W., et al. (1999). Diurnal changes in photochemical efficiency and xanthophyll concentrations in shallow water reef corals : evidence for photoinhibition and photoprotection. *Coral Reefs* 18, 99–105. doi: 10.1007/s003380050163

Chang, S. S., Prézelin, B. B., and Trench, R. K. (1983). Mechanisms of photoadaptation in three strains of the symbiotic dinoflagellate Symbiodinium microadriaticum. *Mar. Biol.* 76, 219–229. doi: 10.1007/BF00393021

Cohen, I., and Dubinsky, Z. (2015). Long term photoacclimation responses of the coral *Stylophora pistillata* to reciprocal deep to shallow transplantation: photosynthesis and calcification. *Front. Mar. Sci.* 2:45. doi: 10.3389/fmars.2015.00045

Cooper, T. F., Ulstrup, K. E., Dandan, S. S., Heyward, A. J., Kühl, M., Muirhead, A., et al. (2011). Niche specialization of reef-building corals in the mesophotic zone: metabolic trade-offs between divergent Symbiodinium types. *Proc. Biol. Sci.* 278, 1840–1850. doi: 10.1098/rspb.2010.2321

Dishon, G., Dubinsky, Z., Fine, M., and Iluz, D. (2013). Underwater light field patterns in subtropical coastal waters: a case study from the Gulf of Eilat (Aqaba). *Isr. J. Plant Sci.* 60, 265–275. doi: 10.1560/IJPS.60.1-2.265

Dubinsky, Z., Falkowski, P. G., Porter, J. W., and Muscatine, L. (1984). Absorption and utilization of radiant energy by light- and shade-adapted colonies of the hermatypic coral *Stylophora pistillata*. *Proc. R. Soc. Lond. Ser. B Biol. Sci.* 222, 203–214. doi: 10.1098/rspb.1984.0059

Dustan, P. (1999). Distribution of zooxanthellae and photosynthetic chloroplast pigments of the reef-building coral montastrea annularis ellis and solander in relation to depth on a West Indian Coral Reef. *Bull. Mar. Sci.* 29, 79–95.

Einbinder, S., Mass, T., Brokovich, E., Dubinsky, Z., Erez, J., and Tchernov, D. (2009). Changes in morphology and diet of the coral *Stylophora pistillata* along a depth gradient. *Mar. Ecol. Prog. Ser.* 381, 167–174. doi: 10.3354/meps07908

Falkowski, P. G., and Dubinsky, Z. (1981). Light-shade adaptation of *Stylophora pistillata*, a hermatypic coral from the Gulf of Eilat. *Nature* 289, 172–174. doi: 10.1038/289172a0

Franklin, L. A., Seaton, G. G. R., Lovelock, C. E., and Larkum, A. W. D. (1996). Photoinhibition of photosynthesis on a coral reef. *Plant Cell Environ.* 19, 825–836. doi: 10.1111/j.1365-3040.1996.tb00419.x

Fricke, H. W., and Schuhmacher, H. (1983). The depth limits of red sea stony corals: an ecophysiological problem (a deep diving survey by submersible). *Mar. Ecol.* 4, 163–194. doi: 10.1111/j.1439-0485.1983.tb00294.x

Gordon, H. R. (1989). Can the Lambert-Beer law be applied to the diffuse attenuation coefficient of ocean water? *Limnol. Oceanogr.* 34, 1389–1409. doi: 10.4319/lo.1989.34.8.1389

Hennige, S., Suggett, D., Warner, M., McDougall, K., and Smith, D. (2009). Photobiology of symbiodinium revisited: bio-physical and bio-optical signatures. *Coral Reefs* 28, 179–195. doi: 10.1007/s00338-008-0444-x

Hoegh-Guldberg, O., and Jones, R. (1999). Photoinhibition and photoprotection in symbiotic dinoflagellates from reef-building corals. *Mar. Ecol. Prog. Ser.* 183, 73–86. doi: 10.3354/meps183073

Hutchings, P., Kingsford, M. J., and Hoegh-Guldberg, O. (eds.). (2009). *The Great Barrier Reef: Biology, Environment and Management*, *1st Edn*. Collingwood, VIC: Springer Netherlands.

Iglesias-Prieto, R., Beltrán, V. H., LaJeunesse, T. C., Reyes-Bonilla, H., and Thomé, P. E. (2004). Different algal symbionts explain the vertical distribution of dominant reef corals in the eastern Pacific. *Proc. Biol. Sci.* 271, 1757–1763. doi: 10.1098/rspb.2004.2757

Iglesias-Prieto, R., and Trench, R. K. (1997). Acclimation and adaptation to irradiance in symbiotic dinoflagellates. II. Response of chlorophyll-protein complexes to different photon-flux densities. *Mar. Biol.* 130, 23–33. doi: 10.1007/s002270050221

Jeffrey, S. W., and Humphrey, G. F. (1975). New spectrophotometric equations for determining chlorophylls a, b, c1 and c2 in higher plants, algae and natural phytoplankton. *Biochem. Physiol. Pflanz.* 167, 191–194.

Joliot, A., and Joliot, P. (1964). Etude cinétique de la réaction photochimique libérant l'oxygène au cours de la photosynthèse. *C.R. Acad. Sci. Paris* 258, 4622–4625.

Joliot, P., and Joliot, A. (2003). Excitation transfer between photosynthetic units: the 1964 experiment. *Photosynth. Res.* 76, 241–245. doi: 10.1023/A:1024908829819

Jones, R. J., Hoegh-Guldberg, O., Larkum, A. W. D., and Schreiber, U. (1998). Temperature-induced bleaching of corals begins with impairment of the CO_2 fixation mechanism in zooxanthellae. *Plant Cell Environ.* 21, 1219–1230. doi: 10.1046/j.1365-3040.1998.00345.x

Kanazawa, A., Blanchard, G. J., Szabó, M., Ralph, P. J., and Kramer, D. M. (2014). The site of regulation of light capture in Symbiodinium: does the peridinin-chlorophyll a-protein detach to regulate light capture? *Biochim. Biophys. Acta* 1837, 1227–1234. doi: 10.1016/j.bbabio.2014.03.019

Kolber, Z. S., Prášil, O., and Falkowski, P. G. (1998). Measurements of variable chlorophyll fluorescence using fast repetition rate techniques: defining methodology and experimental protocols. *Biochim. Biophys. Acta* 1367, 88–106.

Kyle, D. J., Ohad, I., and Arntzen, C. J. (1984). Membrane protein damage and repair: selective loss of a quinone-protein function in chloroplast membranes. *Proc. Natl. Acad. Sci. U.S.A.* 81, 4070–4074.

Lavergne, J., and Trissl, H. W. (1995). Theory of fluorescence induction in photosystem II: derivation of analytical expressions in a model including exciton-radical-pair equilibrium and restricted energy transfer between photosynthetic units. *Biophys. J.* 68, 2474–2492. doi: 10.1016/S0006-3495(95)80429-7

Lesser, M. P., Slattery, M., Stat, M., Ojimi, M., Gates, R. D., and Grottoli, A. (2010). Photoacclimatization by the coral *Montastraea cavernosa* in the mesophotic zone: light, food, and genetics. *Ecology* 91, 990–1003. doi: 10.1890/09-0313.1

Levy, O., Dubinsky, Z., and Achituv, Y. (2003). Photobehavior of stony corals: responses to light spectra and intensity. *J. Exp. Biol.* 206, 4041–4049. doi: 10.1242/jeb.00622

Mass, T., Einbinder, S., Brokovich, E., Shashar, N., Vago, R., Erez, J., et al. (2007). Photoacclimation of *Stylophora pistillata* to light extremes: metabolism and calcification. *Mar. Ecol. Prog. Ser.* 334, 93–102. doi: 10.3354/meps334093

Munekage, Y., Hashimoto, M., Miyake, C., Tomizawa, K., Endo, T., Tasaka, M., et al. (2004). Cyclic electron flow around photosystem I is essential for photosynthesis. *Nature* 429, 579–582. doi: 10.1038/nature02598

Muscatine, L., and Kaplan, I. R. (1994). Resource partitioning by reef corals as determined from stable isotope composition II. 15N of zooxanthellae and animal tissue versus depth. *Pacific Sci.* 48, 304–312.

Muscatine, L., Pool, R. R., and Trench, R. K. (1975). Symbiosis of algae and invertebrates: aspects of the symbiont surface and the host-symbiont interface. *Trans. Am. Microsc. Soc.* 94, 450–469. doi: 10.2307/3225518

Nawrocki, W. J., Tourasse, N. J., Taly, A., Rappaport, F., and Wollman, F.-A. (2015). The plastid terminal oxidase: its elusive function points to multiple contributions to plastid physiology. *Annu. Rev. Plant Biol.* 66, 49–74. doi: 10.1146/annurev-arplant-043014-114744

Niedzwiedzki, D. M., Jiang, J., Lo, C. S., and Blankenship, R. E. (2014). Spectroscopic properties of the Chlorophyll a-Chlorophyll c 2-Peridinin-Protein-Complex (acpPC) from the coral symbiotic dinoflagellate Symbiodinium. *Photosynth. Res.* 120, 125–139. doi: 10.1007/s11120-013-9794-5

Nir, O., Gruber, D. F., Shemesh, E., Glasser, E., and Tchernov, D. (2014). Seasonal mesophotic coral bleaching of *Stylophora pistillata* in the Northern Red Sea. *PLoS ONE* 9:e84968. doi: 10.1371/journal.pone.0084968

Papageorgiou, G., and Govindjee (1968). Light-induced changes in the fluorescence yield of chlorophyll a *in vivo*. II. Chlorella pyrenoidosa. *Biophys. J.* 8, 1316–1328. doi: 10.1016/S0006-3495(68)86558-0

Pratchett, M. S., Munday, P. L., Wilson, S. K., Graham, N. A. J., Cinner, J. E., Bellwood, D. R., et al. (2008). Effects of climate-induced coral bleaching on coral-reef fishes - ecological and economic consequences. *Oceanogr. Mar. Biol. Annu. Rev.* 46, 251–296. doi: 10.1201/9781420065756.ch6

Prézelin, B. (1987). "Photosynthetic physiology of dinoflagellates," in *The Biology of dinoflagellates*, ed F. J. R. Taylor (Oxford: Blackwell Scientific), 174–223.

Rogers, J. E., and Marcovich, D. (2007). A simple method for the extraction and quantification of photopigments from *Symbiodinium* spp. *J. Exp. Mar. Biol. Ecol.* 353, 191–197. doi: 10.1016/j.jembe.2007.08.022

Schreiber, U. (2004). "Pulse-Amplitude-Modulation (PAM) fluorometry and saturation pulse method: an overview," in *Chlorophyll a Fluorescence: A Signature of Photosynthesis*, eds G. Papageorgiou and Govindjee (Dordrecht: Springer), 279–319.

Smith, D. J., Suggett, D. J., and Baker, N. R. (2005). Is photoinhibition of zooxanthellae photosynthesis the primary cause of thermal bleaching in corals? *Glob. Chang. Biol.* 11, 1–11. doi: 10.1111/j.1529-8817.2003.00895.x

Stochaj, W. R., and Grossman, A. R. (1997). Differences in the protein profiles of cultured and endosymbiotic *Symbiodinium* sp. (Pyrrophyta) from the anemone *Aiptasia pallida* (Anthozoa). *J. Phycol.* 33, 44–53. doi: 10.1111/j.0022-3646.1997.00044.x

Takahashi, S., Whitney, S., Itoh, S., Maruyama, T., and Badger, M. (2008). Heat stress causes inhibition of the de novo synthesis of antenna proteins and photobleaching in cultured Symbiodinium. *Proc. Natl. Acad. Sci. U.S.A.* 105, 4203–4208. doi: 10.1073/pnas.0708554105

Tchernov, D., Hassidim, M., Luz, B., Sukenik, A., Reinhold, L., and Kaplan, A. (1997). Sustained net CO_2 evolution during photosynthesis by marine microorganism. *Curr. Biol.* 7, 723–728. doi: 10.1016/S0960-9822(06)00330-7

Tchernov, D., Helman, Y., Keren, N., Luz, B., Ohad, I., Reinhold, L., et al. (2001). Passive entry of CO_2 and its energy-dependent intracellular conversion to HCO_3– in cyanobacteria are driven by a photosystem I-generated $\Delta\mu H+$. *J. Biol. Chem.* 276, 23450–23455. doi: 10.1074/jbc.M101973200

Titlyanov, E., Titlyanova, T., and Yamazato, K. (2002). Acclimation of symbiotic reef-building corals to extremely low light. *Symbiosis* 33, 125–143.

Trissl, H. W., Gao, Y., and Wulf, K. (1993). Theoretical fluorescence induction curves derived from coupled differential equations describing the primary photochemistry of photosystem II by an exciton-radical pair equilibrium. *Biophys. J.* 64, 974–988. doi: 10.1016/S0006-3495(93)81463-2

van Oppen, M. J. H., Bongaerts, P., Underwood, J. N., Peplow, L. M., and Cooper, T. F. (2011). The role of deep reefs in shallow reef recovery: an assessment of vertical connectivity in a brooding coral from west and east Australia. *Mol. Ecol.* 20, 1647–1660. doi: 10.1111/j.1365-294X.2011.05050.x

Wells, J. W. (1957). Corals. *Geol. Soc. Am. Mem.* 67, 1087–1104.

Conflict of Interest Statement: The authors declare that the research was conducted in the absence of any commercial or financial relationships that could be construed as a potential conflict of interest.

The reviewer GE declared a shared affiliation, though no other collaboration, with one of the authors OL to the handling Editor, who ensured that the process nevertheless met the standards of a fair and objective review.

frontiers in Microbiology

ORIGINAL RESEARCH
published: 24 January 2017
doi: 10.3389/fmicb.2017.00059

In vivo Microscale Measurements of Light and Photosynthesis during Coral Bleaching: Evidence for the Optical Feedback Loop?

Daniel Wangpraseurt[1,2†], Jacob B. Holm[1], Anthony W. D. Larkum[2], Mathieu Pernice[2], Peter J. Ralph[2], David J. Suggett[2] and Michael Kühl[1,2*]*

[1] Marine Biological Section, Department of Biology, University of Copenhagen, Helsingør, Denmark, [2] Climate Change Cluster, Department of Environmental Sciences, University of Sydney, Sydney, NSW, Australia

OPEN ACCESS

Edited by:
Virginia Weis,
Oregon State University, USA

Reviewed by:
Melissa Susan Roth,
University of California, Berkeley, USA
Elisha M. Wood-Charlson,
University of Hawaii at Manoa, USA

***Correspondence:**
Daniel Wangpraseurt
wangpraseurt@gmail.com
Michael Kühl
mkuhl@bio.ku.dk

†Present address:
Daniel Wangpraseurt
Department of Chemistry, University of Cambridge, Cambridge, UK

Specialty section:
This article was submitted to Microbial Symbioses, a section of the journal Frontiers in Microbiology

Received: 14 October 2016
Accepted: 09 January 2017
Published: 24 January 2017

Citation:
Wangpraseurt D, Holm JB, Larkum AWD, Pernice M, Ralph PJ, Suggett DJ and Kühl M (2017) In vivo Microscale Measurements of Light and Photosynthesis during Coral Bleaching: Evidence for the Optical Feedback Loop? Front. Microbiol. 8:59. doi: 10.3389/fmicb.2017.00059

Climate change-related coral bleaching, i.e., the visible loss of zooxanthellae from the coral host, is increasing in frequency and extent and presents a major threat to coral reefs globally. Coral bleaching has been proposed to involve accelerating light stress of their microalgal endosymbionts via a positive feedback loop of photodamage, symbiont expulsion and excess *in vivo* light exposure. To test this hypothesis, we used light and O_2 microsensors to characterize *in vivo* light exposure and photosynthesis of *Symbiodinium* during a thermal stress experiment. We created tissue areas with different densities of *Symbiodinium* cells in order to understand the optical properties and light microenvironment of corals during bleaching. Our results showed that in bleached *Pocillopora damicornis* corals, *Symbiodinium* light exposure was up to fivefold enhanced relative to healthy corals, and the relationship between symbiont loss and light enhancement was well-described by a power-law function. Cell-specific rates of *Symbiodinium* gross photosynthesis and light respiration were enhanced in bleached *P. damicornis* compared to healthy corals, while areal rates of net photosynthesis decreased. *Symbiodinium* light exposure in *Favites* sp. revealed the presence of low light microniches in bleached coral tissues, suggesting that light scattering in thick coral tissues can enable photoprotection of cryptic symbionts. Our study provides evidence for the acceleration of *in vivo* light exposure during coral bleaching but this optical feedback mechanism differs between coral hosts. Enhanced photosynthesis in relation to accelerating light exposure shows that coral microscale optics exerts a key role on coral photophysiology and the subsequent degree of radiative stress during coral bleaching.

Keywords: coral bleaching, *Symbiodinium*, photosynthesis, light scattering, coral optics, ecophysiology

Abbreviations: E_d(PAR), incident downwelling photon irradiance (μmol photons m^{-2} s^{-1}); E_0(PAR), photon scalar irradiance (μmol photons m^{-2} s^{-1}); $E_0(\lambda)$, spectral scalar irradiance (μmol photons m^{-2} s^{-1} nm^{-1}); $E_0(PAR)_{bleached}/E_0(PAR)_{healthy}$, photon scalar irradiance enhancement of a bleached coral relative to a healthy coral; $E_0(\lambda)_{bleached}/E_0(\lambda)_{healthy}$, spectral scalar irradiance enhancement of a bleached coral relative to a healthy coral; L_R, light respiration; NIR, near-infrared radiation; PAR, photosynthetically active radiation (400–700 nm); P_N, net photosynthesis; P_G, gross photosynthesis; R_D, dark respiration; $R_H(\lambda)$, spectral holobiont reflectance; $R_H(\lambda)_{bleached}/R_H(\lambda)_{healthy}$, holobiont reflectance enhancement of a bleached coral relative to a healthy coral.

INTRODUCTION

Solar radiation governs coral photophysiology and ultimately drives the productivity and growth of coral reefs (Falkowski et al., 1990). Light stimulates photosynthesis of coral microalgal endosymbionts (*Symbiodinium* spp.), generating O_2 and carbohydrates that are exported to the host fueling coral animal metabolism (Muscatine et al., 1981). However, excess light enhances *Symbiodinium* photodamage (Warner et al., 1999; Takahashi et al., 2004) and, in combination with anomalous seawater temperatures, can induce the breakdown of the coral-algal symbiosis known as coral bleaching (Brown, 1997; Hoegh-Guldberg, 1999). Coral bleaching events are regarded as a major threat to the future of coral reefs (Ainsworth et al., 2016) and hence the physiological mechanisms triggering coral bleaching have been a major research focus for decades (Weis, 2008). Coral bleaching susceptibility is affected by a combination of factors that act on different spatial and temporal scales, including coral thermal history (Brown et al., 2002; Hughes et al., 2003), *Symbiodinium* genotype (Sampayo et al., 2008), as well as biochemical pathways and tissue properties of the coral host species (Baird et al., 2009). At the cellular scale, coral bleaching involves enhanced thermal and radiative exposure of *Symbiodinium* cells, resulting in photodamage and the subsequent generation of reactive oxygen species (ROS) that induce the breakdown of the symbiosis (Lesser, 1996; Hoegh-Guldberg, 1999; Weis, 2008). The *in vivo* light and temperature exposure of *Symbiodinium* within the host tissue ultimately controls whether *Symbiodinium* undergoes photodamage, and it is thus important to resolve the optical and thermal microenvironment of coral hosts (Enriquez et al., 2005; Jimenez et al., 2008; Wangpraseurt et al., 2012; Swain et al., 2016).

Application of light microsensors has shown that the *in vivo* light exposure within coral tissues can be enhanced over the incident downwelling irradiance (Kühl et al., 1995; Wangpraseurt et al., 2012, 2014a,b; Brodersen et al., 2014). Such irradiance enhancement is modulated by the unique optical properties of coral tissue and skeleton (Enriquez et al., 2005; Teran et al., 2010; Kahng et al., 2012; Marcelino et al., 2013; Wangpraseurt et al., 2016a) and can improve photosynthesis under low light conditions (Brodersen et al., 2014; Wangpraseurt et al., 2014a) or lead to light stress under high irradiance (Marcelino et al., 2013; Swain et al., 2016). The loss of *Symbiodinium* spp. cells from corals under environmental stress has been hypothesized to further increase irradiance exposure *in hospite* due to decreased shading by photopigments and increased backscattered light from the coral skeleton (Enriquez et al., 2005; Teran et al., 2010; Swain et al., 2016). According to this so-called optical feedback hypothesis (Enriquez et al., 2005; Swain et al., 2016), skeleton backscattering can further stimulate symbiont loss inducing an accelerating cycle, where symbiont loss promotes light enhancement and vice versa. Several studies have speculated on the relevance of such a feedback loop exacerbating coral bleaching, arguing that the light microenvironment during a stress event could serve as a key factor in determining the severity of a bleaching event (Hoegh-Guldberg, 1999; Franklin et al., 2006; Hoogenboom et al., 2006; Abrego et al., 2008; Weis, 2008; Baird et al., 2009). However, experimental proof of such a mechanism has been lacking.

Here, we provide the first direct measurements of the *in vivo* light environment of *Symbiodinium* during coral bleaching. We performed a thermal stress experiment and monitored changes in the *in vivo* light environment using light microsensors in two coral species with contrasting optical properties in concert with O_2 microsensor-based measurements of gross photosynthesis, net photosynthesis and light respiration. We provide evidence for the acceleration of *in vivo* light exposure upon coral bleaching and show that such light enhancement differs between coral hosts. This highlights the importance of skeleton and tissue optics for coral photophysiology and stress responses.

MATERIALS AND METHODS

Coral Species

Light microenvironments were investigated in two shallow-water corals: the branching coral *Pocillopora damicornis*, and the massive coral *Favites* sp. The coral *P. damicornis* is generally a bleaching-susceptible species (Loya et al., 2001; Swain et al., 2016) with thin tissues (maximum thickness ∼150 and 300 μm for coenosarc and polyp tissues, respectively) and low tissue light attenuation (Szabó et al., 2014). *P. damicornis* from Heron Island is known to harbor different *Symbiodinium* spp. including symbiont type C42ab and C33a (Tonk et al., 2013). *Favites* sp. is a more bleaching-resistant species (Swain et al., 2016) with a polyp tissue thickness of ∼2 mm (Wangpraseurt et al., 2014a) and is known to associate with symbionts of type C1, C21, and C33 (Tonk et al., 2013). Corals were collected at low tide from shallow waters (<2 m depth) on the reef flat off Heron Island, Great Barrier Reef, Australia (152°06′ E, 20°29′ S) in August–September 2014. On a cloudless day during mid-day sun, the incident downwelling photon irradiance integrated over 400–700 nm, i.e., PAR, reached *in situ* values at the level of the sampled colonies of E_d(PAR) > 2000 μmol photons m^{-2} s^{-1} (Wangpraseurt et al., 2014b). Corals were selected from the same small sample area in order to ensure that they were adapted to a comparable light and flow regime. Coral fragments from at least 10 different daughter colonies of *P. damicornis* and *Favites* sp. were collected and sub-fragmented (*P. damicornis* ca. 3–10 cm in length and *Favites* ca. 3 cm in diameter).

Bleaching Experiment

Collected corals were allowed to recover from potential translocation stress for a minimum of 1 week in a shaded outdoor aquarium at Heron Island Research Station before transfer to the experimental incubation set-up consisting of an outdoor aquarium tank (300 L) that was exposed to natural sunlight (13 h of daylight) and continuously supplied with seawater from the reef flat at an exchange rate of about 0.2 L s^{-1}. The set-up mimicked conditions on the Heron Island reef flat for a water depth of 20–30 cm with high solar irradiance exposure. A water heater connected to a thermistor (accuracy: ±1.5°C, Sensor type: KTY81-121, Sentien Electronics, Australia) was

placed in one corner of the tank and two submersible water pumps directed the water flow (3–5 cm s^{-1}) toward the heater, while four additional water pumps recirculated the water in the tank at a comparable flow speed in order to avoid the build-up of temperature gradients within the tank. E_d(PAR) during noon was ∼2000 μmol photons m^{-2} s^{-1} as measured at the water surface with a planar quantum irradiance sensor connected to a light meter (LI-190 and LI-1400, Li-Cor, Lincoln, NE, USA). Temperature was monitored using data loggers (Onset, USA) randomly distributed within the tank and logging at a time interval of 1 min. Coral fragments were randomly distributed within the tank. In order to induce coral bleaching, we followed the protocol of Middlebrook et al. (2010), whereby the water temperature was step-wise increased by about 1°C per day. In total the experiment ran for 13 days during September 2014, and included 3 days of baseline measurements at ambient water temperature (22°C) followed by 10 days ramping of temperature from 22 to 33°C.

Often experimental measurements on coral bleaching use a balanced experimental design where temperature treated corals are assessed on par with healthy corals during the course of the experiment. In the microenvironmental approach used here, the total number of samples was limited by the experimental challenges involving intra-tissue microsensor measurements with a high chance of sensor breakage. As our main aim was to assess the optical mechanisms underlying coral bleaching, we prioritized measuring coral tissues with reduced algal cell densities over a larger number of control measurements on healthy corals. It is important to note that our experimental design does thus not allow for excluding potential experimental treatment effects (e.g., coral disease) on the physiology of the algae. However, all corals were visually expected for tissue necrosis and sloughing, and corals appeared visually free of disease. During the temperature ramping experiment, visual bleaching of *Favites* sp. occurred much slower than in *P. damicornis* and we thus accelerated the bleaching process for *Favites* sp. through a combined temperature and light stress treatment (see Supplementary Methods). Our approach did not allow us to compare differences in photophysiology or the rate of symbiont loss between *P. damicornis* and *Favites* sp.

Optical Measurements

Spectral scalar irradiance $E_0(\lambda)$ and reflectance $R_H(\lambda)$ measurements were performed in a flow chamber that was flushed at a flow rate of 0.5–1 cm s^{-1} with seawater at the same temperature as in the experimental bleaching treatment tank. Fiber-optic scalar irradiance microprobes with a spherical tip diameter of 80 μm (Rickelt et al., 2016) were used to measure the spectral light microenvironment on and within coral coenosarc and polyp tissues as described previously (Wangpraseurt et al., 2012; see Supplementary Methods for details).

Spectral reflectance measurements on intact corals (R_H) were performed with a flat-cut fiber-optic reflectance probe (2 mm diameter, Ocean Optics, USA) positioned at a 45° angle relative to the coral surface at a distance of 1 cm from the sample, using a similar measuring configuration as in Rodriguez-Roman et al. (2006). Vertically incident light [E_d(PAR) = 400 μmol photons m^{-2} s^{-1}] was provided by a fiber-optic tungsten halogen-lamp equipped with a collimating lens (Schott KL-2500, Germany). The coral reflected light measurements were normalized to the reflected light measured under identical optical configuration from a 99% white reflectance standard (Spectralon, Labsphere, USA). Scalar irradiance and reflectance spectra were also measured on bare skeletons (see Supplementary Figure S1).

Photosynthesis and Respiration Measurements

Clark-type O_2 microsensors (tip size of 25 μm, a 90% response time of <0.5 s and a stirring sensitivity of ∼1%; Unisense A/S, Aarhus, Denmark) were used to measure O_2 production and consumption of *P. damicornis* as described previously (Wangpraseurt et al., 2012; Brodersen et al., 2014). Sensor readings were linearly calibrated from measurements in air saturated water and anoxic water (flushed with N_2). Percent air saturation in seawater at experimental temperature and salinity was transformed to O_2 concentration (μmol O_2 L^{-1}) using gas tables (Ramsing and Gundersen, Unisense, Denmark; www.unisense.com). All O_2 microsensor measurements were performed in the same configuration as the scalar irradiance microsensor measurements but with the O_2 microsensors approaching the coral surface at an angle of ∼10° relative to the vertically incident light. Measurements of gross photosynthesis at the coral surface were performed using the light–dark shift technique (see Revsbech and Jorgensen, 1983 for detailed description) followed by measurements of steady-state O_2 concentration profiles from the coral tissue surface through the diffusive boundary layer (DBL) and into the mixed turbulent water phase above (Brodersen et al., 2014) under an incident photon irradiance of E_d(PAR) = 400 μmol photons m^{-2} s^{-1}. Steady-state O_2 conditions were usually achieved within 5–10 min at a constant light level and each microsensor profile took on average about 5 min. We chose E_d = 400 μmol photons m^{-2} s^{-1} as a irradiance level close to the photosynthetic maximum based on previous microsensor measurements under comparable conditions (Ulstrup et al., 2006) and preliminary results from variable chlorophyll fluorimetry-based measurement of relative photosynthetic electron transport rates vs. irradiance (data not shown). The coral was then placed in darkness for >15 min before O_2 profiles measured the dark respiration of the coral holobiont (Schrameyer et al., 2014). Additional measurements of the dark-adapted maximum quantum yield of PSII were done with a commercial variable chlorophyll fluorescence imaging system (Imaging-PAM, Walz GmbH, Germany; see supporting information and Supplementary Figure S2).

Symbiodinium Density and Pigment Dynamics

Symbiodinium cell density was determined for small tissue areas of *Favites* sp. using a microsampling technique (Kemp et al., 2008), where individual polyps were sampled by careful separation of the coral tissue from the underlying skeleton using a syringe and needle (see supporting information and Supplementary Figure S3). This technique was not used for

P. damicornis since the thin tissue of this coral was firmly attached to the skeleton, making it difficult to completely remove the tissue with a syringe. Instead small branch tips (maximum of 0.5–0.8 cm in length) were collected, crushed and centrifuged to separate host tissue, skeleton and *Symbiodinium* (see supporting information). For both coral species, *Symbiodinium* density was then estimated using a haemocytometer. Additional tissue samples were collected (as described above) for HPLC (high performance liquid chromatography) analysis using standard protocols (see supporting information).

Data Analysis

Measured raw spectra were integrated between 400 and 700 nm (PAR) using the mathematical integration function of Origin Pro 9.1 (Origin, USA). The *in vivo* light enhancement relative to the incident downwelling irradiance was calculated as $E_0(PAR)/E_d(PAR)$. Data was averaged for measurements performed on day 1 ('healthy,' water temperature 22°C) and day 10 ('bleached,' water temperature 33°C). We also expressed the enhancement of spectral scalar irradiance, $E_0(\lambda)$, of bleached corals relative to healthy corals as $E_0(\lambda)_{bleached}/E_0(\lambda)_{healthy}$. Areal rates of gross photosynthesis (PG; nmol O_2 cm^{-2} s^{-1}) were calculated by depth integration of the volumetric rates assuming constant rates of photosynthesis over the entire tissue. Tissue thickness of *P. damicornis* was ca. 300 μm for polyp tissues and ca. 150 μm for coenosarc tissues as determined with scalar irradiance microsensors (data not shown, see Wangpraseurt et al., 2014a). Net photosynthesis (PN) and dark respiration (RD) rates were calculated using Fick's first law of diffusion (see Chan et al., 2016 for details). Light respiration of the coral holobiont (LR) was then calculated as the difference between gross and net photosynthesis (Schrameyer et al., 2014). In order to compare *Symbiodinium* dependent gross photosynthetic rates between healthy and bleached corals, we normalized our areal rates to cell density. Values of O_2 production in nmol O_2 cm^{-2} s^{-1} was divided by the average measured cell density (in cells per cm^{-2}) to express gross photosynthesis in fmol O_2 $cell^{-1}$ s^{-1}.

Statistical Analysis

Regression analyses were used to test for the relationship between *Symbiodinium* cell density and *in vivo* coral tissue scalar irradiance. A non-linear curve fitting procedure was applied to test the relationship between the *in vivo* E_0 (expressed in % of E_d) measured in polyp surface, polyp aboral and coenosarc surface tissues of *P. damicornis* and the cell density (cells per cm^{-2}). The fitting used the non-linear Levenberg Marquardt iteration algorithm and applied a power-law function (i.e.,$y = ax^{-b}$) to yield the adjusted R^2 and reduced χ^2 goodness of fit parameters. Physiological and optical parameters measured for *P. damicornis* and *Favites* sp., including F_v/F_m, P_G, P_N, R_D, L_R, $E_0(PAR)/E_d(PAR)$ were compared between healthy (day = 1) and bleached (day = 10) conditions using a two-sample Student's *t*-test (for equal variances) or Welch's *t*-test (for unequal variances). Statistical tests were performed in Origin Pro 9.1 (Origin, USA).

RESULTS

Effect of Bleaching on Cell Density and *Symbiodinium* Pigmentation

Symbiodinium cell density was significantly reduced at the end of the experiment for both *P. damicornis* and *Favites* sp. (**Figure 1**). In *P. damicornis*, the mean cell density was reduced 4.2-fold from 1.43×10^6 (± SE 2.8×10^5) to 3.42×10^5 (± 7.5×10^4 SE) cells cm^{-2} [Student's *t*-test: $t(10) = 3.7$, $p = 0.003$; Supplementary Figure S4]. In *Favites* sp., there was a comparable fourfold reduction in cell density from 2.30×10^6 (3.6×10^5) to 5.6×10^5 (1.4×10^5 SE) cells cm^{-2} tissue surface area [Student's *t*-test: $t(10) = 3.3$, $p = 0.008$]. Chlorophyll *a* density (per g of host tissue biomass) decreased by about 2.1- and 1.7-fold for *P. damicornis* [Student's *t*-test: $t(8) = 1.6$, $p = 0.146$] and *Favites* sp. [Welch's *t*-test: $t(7.5) = 2.4$, $p = 0.047$], respectively although this difference was only statistically significant for *Favites* sp. (**Figure 1**).

Effect of Bleaching on *In vivo* Scalar Irradiance

For all corals and measurement locations, *in vivo* photon scalar irradiance, $E_0(PAR)$, increased in bleached compared to healthy corals (**Figures 2a–e**). In *P. damicornis*, the greatest increase in $E_0(PAR)$ was measured in the aboral polyp tissues, where PAR was about 3.65-fold higher in bleached vs. healthy corals [$E_0(PAR)/E_d(PAR) = 1.97 \pm 0.21$ SE and 0.54 ± 0.09 SE, respectively; Student's *t*-test: $t(10) = -6.1$, $p < 0.001$; **Figure 2d**]. The $E_0(PAR)$ enhancement was less pronounced for oral polyp tissues and coenosarc oral tissues with ratios of $E_0(PAR)/E_d(PAR) = 1.58$ and 1.66, respectively (**Figure 2d**).

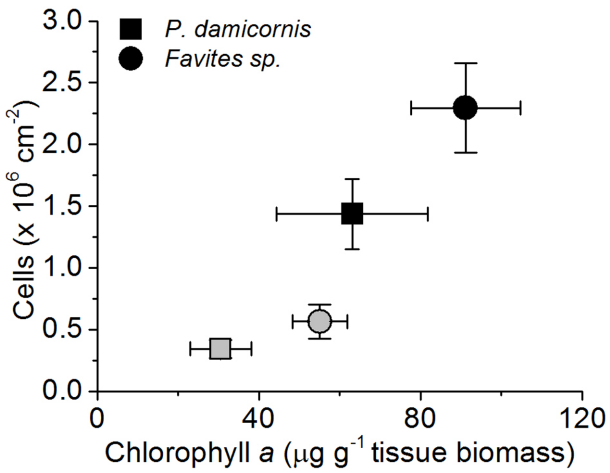

FIGURE 1 | Changes in *Symbiodinium* cell density (cells per cm^{-2} surface area) and chlorophyll *a* density (in μg chlorohyll *a* per g dry host tissue biomass) during the bleaching experiment. Healthy corals (black symbols) and bleached corals (gray symbols) were measured at the beginning (day 1) and the end of the experiment (day 10). Data are mean ± SEM; $n = 4$–8 for cell density estimates and $n = 6$–9 for chlorophyll *a* estimates.

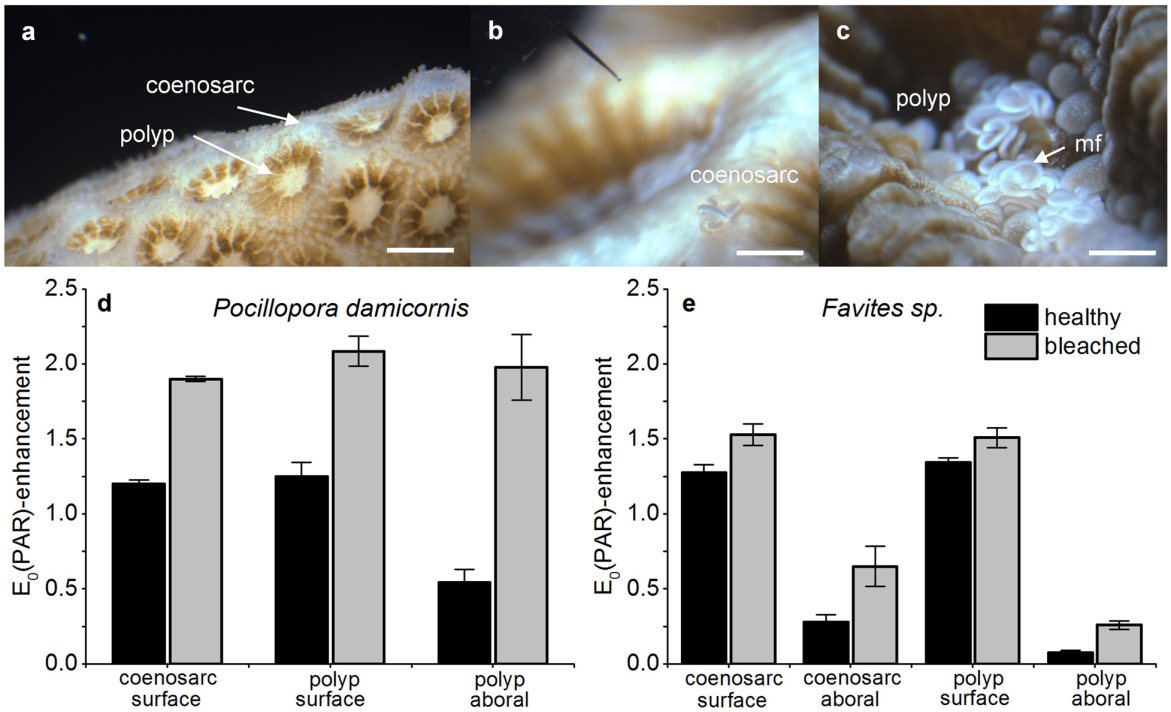

FIGURE 2 | Effect of bleaching on *in vivo* photon scalar irradiance, E_0(PAR)-enhancement. Typical measurement locations over the coenosarc and polyp tissues of *Pocillopora damicornis* **(a)** and *Favites* sp. **(b,c)**. Scale bar = 1 mm **(a)** and 2 mm **(b,c)**. Note the scalar irradiance microprobe **(b)** and extruded mesenterial filaments (mf) in the stressed *Favites* sp. coral **(c)**. E_0(PAR)-enhancement was expressed as E_0(PAR)/E_d(PAR) and was measured in healthy and bleached *P. damicornis* **(d)** and *Favites* sp. **(e)**. Measurements were performed on the surface of coenosarc and polyp tissues as well as in the lowermost aboral tissue layer (vertical depths closest to the skeleton) for healthy (day 1) and bleached corals (day 10). Data are mean ± SE (n = 6 corallite-level replicates).

For *Favites* sp., E_0(PAR) for aboral polyp tissues of bleached corals [E_0(PAR)/E_d(PAR) = 0.26 ± 0.03 SE] was ∼3.5 times higher than in respective healthy tissues [E_0(PAR)/E_d(PAR) = 0.07 ± 0.02 SE] but this difference was not significant [Welch's t-test: $t(3.1) = -2.3$, $p = 0.11$]. E_0(PAR) on the oral polyp tissue increased by 1.13 times upon bleaching [Welch's t-test: $t(3.5) = -5.5$, $p = 0.007$, **Figure 2e**]. For coenosarc tissues, we similarly observed a proportionally greater E_0(PAR) enhancement upon bleaching in aboral tissues E_0(PAR)/E_d(PAR) = 2.3 vs. oral tissues E_0(PAR)/E_d(PAR) = 1.27 (**Figure 2e**). The magnitude of E_0(PAR) enhancement in bleached relative to healthy coral tissues was similar for *Favites* sp. and *P. damicornis*, but the absolute enhancement was different as low light niches remained in *Favites* sp. [E_0(PAR)/E_d(PAR) = 0.25 ± 0.03] (**Figures 2d,e**).

Effect of Bleaching on the *In vivo* Spectral Light Environment

In vivo $E_0(\lambda)$ of bleached corals was increased relative to healthy corals (λ = 400–700 nm) for both species; however, the relative enhancement of $E_0(\lambda)$, i.e., $E_0(\lambda)_{bleached}/E_0(\lambda)_{healthy}$, was dependent on coral species and tissue type (**Figures 3A–D** and **4A,B**). In *P. damicornis*, $E_0(\lambda)_{bleached}/E_0(\lambda)_{healthy}$ in aboral polyp tissues was highest for blue light [$E_0(\lambda)_{bleached}/E_0(\lambda)_{healthy}$ ∼ 5 for λ = 400–500 nm] followed by far red light [$E_0(\lambda)_{bleached}/E_0(\lambda)_{healthy}$ ∼ 4 for λ = 670–690 nm] and least pronounced for green to red light [$E_0(\lambda)_{bleached}/E_0(\lambda)_{healthy}$ ∼ 3 for λ = 550–650 nm] (**Figures 3C** and **4A**). In contrast, tissue surface $E_0(\lambda)$ did not exhibit such pronounced spectral features and scalar irradiance was more evenly enhanced between 400 and 700 nm in both polyp and coenosarc tissues (**Figures 3A,C** and **4A**). A similar trend was observed in *Favites* sp., where maximal $E_0(\lambda)$ enhancement was measured in aboral polyp tissues in the blue ($\lambda \approx 500$ nm) and far-red ($\lambda \approx 650$–695 nm) (**Figures 3B,D** and **4B**). Note that no light enhancement factors were calculated for aboral polyp tissues for wavelengths less than 500 nm, due to a relatively low signal to noise ratio (a result of the almost completely depleted blue light in healthy corals). $E_0(\lambda)$ was fairly evenly enhanced between 400 and 700 nm for surface tissues of *Favites* (**Figure 4B**).

Enhancement of spectral reflectance, $R_H(\lambda)_{bleached}/R_H(\lambda)_{healthy}$ in *P. damicornis* followed a similar wavelength dependency as the $E_0(\lambda)$ enhancement in aboral polyp tissues, i.e., it peaked for λ = 420–550 nm and λ = 650–690 nm (**Figure 4A**; Supplementary Figure S5). However, the $R_H(\lambda)_{bleached}/R_H(\lambda)_{healthy}$ ratio was lower than the $E_0(\lambda)_{bleached}/E_0(\lambda)_{healthy}$ ratio, i.e., the increase in reflectance was lower than the increase in *in vivo* scalar irradiance of bleached tissues relative to healthy tissues (**Figure 4A**). For polyp tissues of *Favites* sp., $R_H(\lambda)_{bleached}/R_H(\lambda)_{healthy}$ was ∼1 and ∼1.5 for λ = 400–500 and 550–690 nm, respectively (**Figure 4B**). For

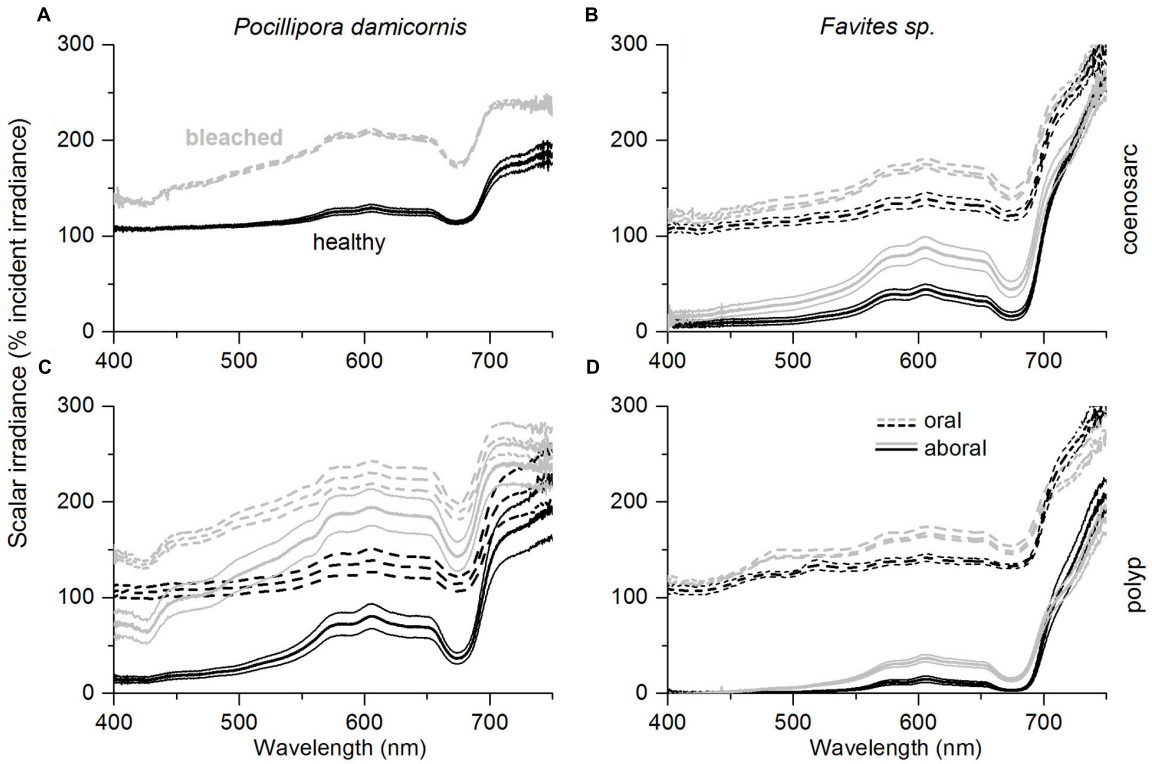

FIGURE 3 | Effect of coral bleaching on *in vivo* spectral scalar irradiance, $E_0(\lambda)$ expressed in % of the incident downwelling irradiance, $E_d(\lambda)$. Measurements were performed on the coenosarc **(A,B)** and polyp tissue **(C,D)** of *P. damicornis* (left panel), and *Favites* sp. (right panel). Solid and dashed lines represent measurements performed in aboral tissues and at the tissue surface, respectively. Measurements were performed on healthy corals (day 1; black) and bleached corals (day 10; gray). Data are mean ± SE ($n = 6$ corallite-level replicates).

coenosarc tissues, $R_H(\lambda)_{bleached}/R_H(\lambda)_{healthy}$ was similar to polyp tissues for wavelengths >550 nm but was <1 at 450–510 nm (**Figure 4B**). Thus reflectance measurements were not able to capture tissue depth- and tissue type-dependent dynamics in scalar irradiance, as can be seen by the more moderate increase in reflectance relative to the *in vivo scalar* irradiance during bleaching (**Figure 4**).

Symbiodinium Cell Density and *In vivo* Scalar Irradiance Dynamics in *Pocillopora damicornis*

In vivo E_0(PAR) enhancement and *Symbiodinium* cell density was described by a power-law function (**Figures 5A–C**) from all data collected throughout the bleaching experiment. The best fit was obtained when *Symbiodinium* cell density was matched against E_0(PAR) enhancement measured in aboral polyp tissues ($R^2 = 0.45$; **Figure 5C**) (compared to R^2 fits of 0.43 and 0.30 for coenosarc surface and polyp surface tissues, respectively; **Figures 5A,B**).

Photosynthesis and Respiration of *Pocillopora damicornis*

Areal rates of gross photosynthesis in bleached coenosarc and polyp tissues were reduced by 70 and 25%, respectively, when compared to the corresponding healthy tissues (**Figure 6A**), but these measurements do not account for symbiont loss after bleaching (**Figure 1**). Instead, cell-specific rates of gross photosynthesis were about 1.3- and 3.2-fold higher in coenosarc and polyp tissues, respectively, for *Symbiodinium* remaining in the bleached corals as compared to the unbleached corals (**Figure 6D**). Measurements of the maximum quantum yield of PSII showed that upon bleaching F_v/F_m was reduced by about 50% as compared to healthy corals (0.38 ± 0.03 vs. 0.8 ± 0.01, respectively; mean ± SEM; Supplementary Figure S2).

Measurements of areal net photosynthesis generally showed net O_2 production except for measurements in bleached coenosarc tissues that exhibited a net O_2 consumption of 0.046 (± 0.015 SE) nmol O_2 cm^{-2} s^{-1} in the light (**Figure 6B**). There was a trend toward increased holobiont light respiration in bleached vs. healthy coenosarc tissues (**Figure 6C**), while a decreased light respiration was found in polyp tissues after bleaching (0.40 ± 0.08 vs. 0.33 ± 0.03 nmol O_2 cm^{-2} s^{-1}; mean ± SEM). In contrast, apparent light respiration rates per *Symbiodinium* cell increased after bleaching by 4.2- and 2.5-fold for coenosarc and polyp tissues, respectively (**Figure 6F**). Areal dark respiration rates did not change significantly after the bleaching experiment for both coensoarc and polyp tissues (Student's *t*-test, $p > 0.05$; **Figure 6E**).

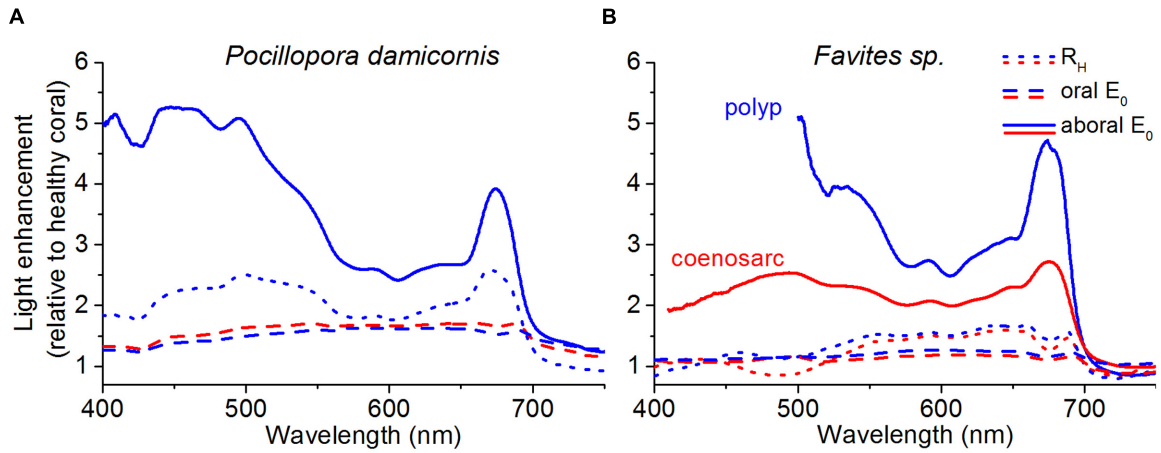

FIGURE 4 | Spectral light enhancement in bleached relative to healthy corals. The enhancement in $E_0(\lambda)$ and $R_H(\lambda)$ due to bleaching was calculated as $E_0(\lambda)_{bleached}/E_0(\lambda)_{healthy}$ and $R_H(\lambda)_{bleached}/R_H(\lambda)_{healthy}$. $R_H(\lambda)$ (dotted lines) was measured at a distance of 1 cm from the tissue surface and $E_0(\lambda)$ was measured at the tissue surface (dashed lines) and in the aboral tissue layers closest to the skeleton (solid lines). Data was collected for both polyp (blue) and coenosarc tissues (red) for *P. damicornis* **(A)**, and *Favites* sp. **(B).** Note that *P. damicornis* $R_H(\lambda)$ measurements include areas covering both polyp and coenosarc tissues, and that $E_0(\lambda)$ measurements were not performed in aboral coenosarc tissues of *P. damicornis* due to lack of sufficient tissue thickness. Original $R_H(\lambda)$ spectra for bleached and healthy corals are shown in Supplementary Figure S5.

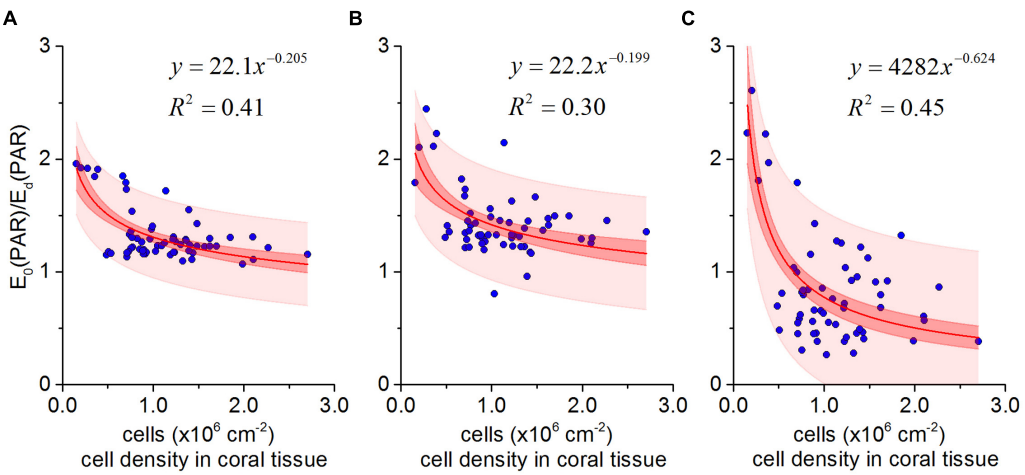

FIGURE 5 | *In vivo* photon scalar irradiance enhancement E_0(PAR)/ E_d(PAR) as a function of *Symbiodinium* cell density in *Pocillopora damicornis* for coenosarc surface tissues (A), polyp surface tissues (B), and polyp aboral tissues (C). The best fit (solid red lines) in all cases was a power-law relationship ($y = ax^{-b}$). Red and light red areas represent 95% confidence and prediction intervals, respectively.

DISCUSSION

Microscale light measurements revealed an average E_0(PAR)-enhancement of ~2 for *P. damicornis*, with maximal values of up to 2.6 within bleached polyp tissues (**Figure 5**). Such measured enhancement in *P. damicornis* can at first approximation be explained by simple light scattering events within the coral skeleton (Enriquez et al., 2005; Wangpraseurt et al., 2014a). As *Symbiodinium* cell density becomes reduced (**Figure 1**), more light penetrates toward the skeleton (**Figure 3A**) and an increased fraction of this light is backscattered (Enriquez et al., 2005). For a flat isotropically scattering skeleton with a reflectance, R, the average path length of upwelling photons is twice that of photons in the incident collimated light beam traversing a thin layer of coral tissue (ignoring tissue scattering) (Kühl and Jørgensen, 1994). Here, the contribution of the coral skeleton reflectance on the scalar irradiance can be calculated as (Kortüm, 2012): $E_o = (1 + 2R)E_d$, where E_d is the incident downwelling irradiance. The flux absorbed by *Symbiodinium* can thus be estimated as $\Phi_{abs} = \Phi_{abs}^{(s)} + \Phi_{abs}^{(i)} = (1 + 2R)\Phi_{abs}^{(i)}$, where $\Phi_{abs}^{(i)}$ is the absorption of the incident beam, i.e., $\Phi_{abs}^{(i)} = A \times E_d$, where A is the absorption cross-section of *Symbiodinium* (Enriquez et al., 2005). Diffuse reflectance of *P. damicornis* skeletons in our study was on average $R = 0.5$ (data not shown), which

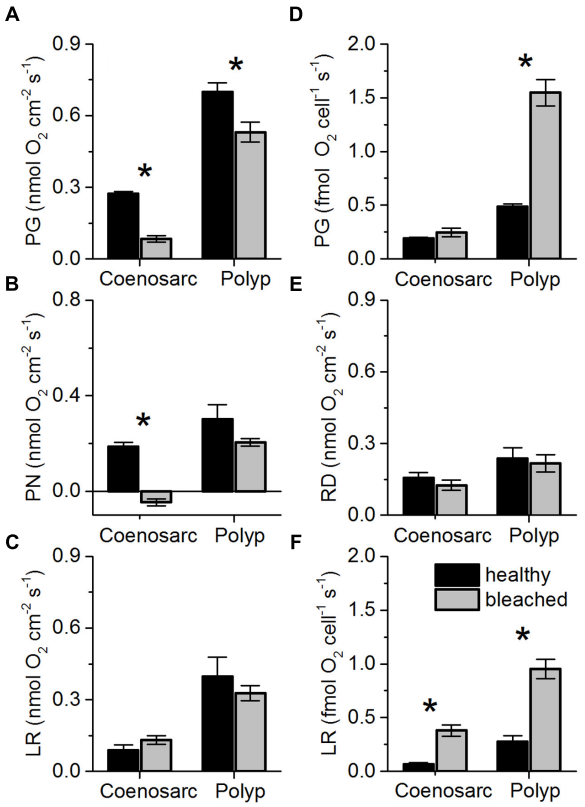

FIGURE 6 | Areal rates (in nmol O_2 cm^{-2} s^{-1}) of gross photosynthesis (A; PG), net photosynthesis (**B**; PN), and apparent light respiration (**C**; LR = PG-PN) and dark respiration (**E**; RD) in coenosarc and polyp tissues of healthy (black bars) and bleached fragments (gray bars) of *Pocillopora damicornis*. **(D,F)** same as left panels but normalized to cell density, i.e., cell specific-rates. Data are mean ± SEM (n = 10–12 corallite-level replicates). Significant differences ($p < 0.05$) between bleached and healthy tissues are marked with an asterisk.

is comparable to previous measurements ($R = 0.36$, Swain et al., 2016). As such, our theoretical calculations would predict an E_0(PAR)-enhancement of 2, a value consistent with our direct measurements for the thin bleached coenosarc tissues of *P. damicornis* (**Figure 5A**).

In contrast to the consistent theoretical and measured E_0(PAR)-enhancement values for *P. damicornis* coenosarc tissues, we observed an E_0(PAR) enhancement of >2 for polyp tissues (**Figures 5B,C**). E_0(PAR) enhancement of >2 suggests an additional scattering contribution from the coral tissue (Wangpraseurt et al., 2014a) and/or from the concave corallite architecture (Ow and Todd, 2010). Indeed, measurements for bare skeletons (Supplementary Figure S1) revealed a higher E_0 within the corallite than over the coenosteum, suggesting that the small concave corallite for *P. damicornis* (width and length ∼1 mm; Nothdurft and Webb, 2007) effectively homogenizes and redirects the incident radiation, through multiple reflections from the skeletal walls toward the center of the corallite, whereas light escapes more easily as diffuse reflectance from the rather flat coenosteum. Given the thin tissue in *P. damicornis*, multiple scattering by such millimeter-sized skeletal structures likely contributes to the observed higher E_0(PAR)-enhancement of *Symbiodinium* in polyp vs. coenosarc tissues in the intact living coral (**Figure 4A**). However, the E_0(PAR)-enhancement observed in intact bleached *P. damicornis* was still higher than for bare skeletons indicating additional light enhancement through tissue scattering. It is possible that diffusely backscattered photons from the skeleton are trapped by the tissue (see detailed discussion in Wangpraseurt et al., 2014a) and/or that the scattering coefficient is higher for coral tissue than for coral skeleton, as is the case for *Favites* sp. (Wangpraseurt et al., 2016a).

The optical feedback hypothesis predicts an inverse power-law relationship between *Symbiodinium* cell density and *in vivo* light exposure, i.e., the rate of light field 'amplification' increases as symbiont cell density decreases (Teran et al., 2010; Swain et al., 2016). For a small cup-shaped polyp, with low tissue absorption and scattering, the greatest effect of corallite architecture on light scattering is expected in close proximity to the skeletal surface at the center of the corallite (Teran et al., 2010; Wangpraseurt et al., 2016a). Our measurements for *P. damicornis* support these predictions since the highest rate of light enhancement was measured within aboral polyp tissues ($R^2 = 0.45$, **Figure 5C**). Scattering by (sub)millimeter-sized skeletal surface elements in such a thin-tissued coral with small polyps thus play a key role in the measured light enhancement dynamics upon bleaching.

Coral bleaching also involves a change in the spectral exposure of the remaining symbionts (**Figure 4**). In a normally pigmented healthy coral, blue light (400–450 nm) is rapidly attenuated vertically within the coral tissue due to peak light absorption by Chl *a*, leaving symbionts in aboral tissue layers exposed to a green to red shifted light spectrum (**Figure 3**; Szabó et al., 2014). As coral bleaching progresses, symbionts in aboral tissues are progressively exposed to greater amounts of blue light (**Figure 4**). It is important to note that such spectral changes could not be captured solely based on surface scalar irradiance or diffuse reflectance measurements (**Figure 4**), highlighting the relevance of depth resolved measurement of *in vivo* scalar irradiance. Minor changes in the spectral composition of light can affect *Symbiodinium* photosynthesis *in vivo* (Wangpraseurt et al., 2014c) and it will be interesting in the future to study the effect of changing spectral exposure on symbiont photosynthesis along a vertical gradient within the tissue (Lichtenberg et al., 2016).

Our data demonstrated the presence of species-specific patterns of light modulation, whereby light gradients were alleviated in polyp tissues of *P. damicornis* but remained present in polyp tissues of *Favites* sp. after bleaching (**Figures 3A–D**). *Favites* sp. are characterized by thick, light scattering tissues (Wangpraseurt et al., 2014a, 2016a) with host pigments such as GFP (Salih et al., 2000; Lyndby et al., 2016) and mycosporine-like amino acids (Dunlap and Shick, 1998; Lesser and Farrell, 2004) that often remain present during bleaching (Smith et al., 2013). Although, *P. damicornis* does also have a GFP-like pigment (Takabayashi and Hoegh-Guldberg, 1995), the GFP-like pigments in *Favites* sp. are arranged in a chromatophore system that strongly enhances light scattering (Lyndby et al., 2016; Wangpraseurt et al., 2016b) facilitating a steep light attenuation along the enhanced optical path within thick scattering coral

tissue (Wangpraseurt et al., 2012; Lyndby et al., 2016). Our finding of low light levels in the aboral polyp tissues therefore suggests that tissue background scattering and absorption effectively attenuate light even in bleached tissues of *Favites* sp. Additionally, differences between *P. damicornis* and *Favites* sp. in skeleton optical properties are likely (Marcelino et al., 2013; Swain et al., 2016; Wangpraseurt et al., 2016a), which would further affect the fraction of light 'amplification' by the skeleton (Marcelino et al., 2013). Thus our results indicate that symbionts in *P. damicornis* will be more severely affected by 'optical feedback' than symbionts in *Favites* sp. during coral bleaching. The moderate light environment in aboral polyp tissues of bleached *Favites* sp. could facilitate photoprotection of remaining cryptic *Symbiodinium* sp. (Silverstein et al., 2012), which could be a key determinant for symbiont repopulation and subsequent coral recovery from bleaching (Rowan et al., 1997).

However, it is likely that a variety of structural design solutions exist that provide photoprotection on different spatial scales (see also Yost et al., 2013). For a branching coral, such as *P. damicornis*, light attenuates along the branch due to shading by neighboring branches (Kaniewska et al., 2011). The magnitude of light attenuation along a single branch is similar to the light attenuation observed within the polyp tissues of *Favites* sp. (compare Kaniewska et al., 2011 and Wangpraseurt et al., 2012). Thus the presence of moderate light microenvironments is expected for *P. damicornis* due to its colony-level architectural complexity, which was however, not assessed in the present study. We visually observed that corals bleached first over the coenosarc tissue area, while symbionts remained within the tentacles of *P. damicornis* despite the enhanced *in vivo* light environment in polyp tissues. It was not possible to measure the light microenvironment within the highly contractile tentacle tissue and it remains unknown, whether a more moderate light microenvironment remained within the tentacles facilitating resistance to bleaching. Additionally, it is possible that bleaching was alleviated for tentacle tissues because of tentacle movement leading to enhanced gas exchange (Shashar et al., 1993) and possibly reducing the build-up of high O_2 levels alleviating oxidative stress.

We observed increased symbiont cell-specific rates of gross O_2 evolution and light respiration in bleached relative to healthy *P. damicornis*, although F_v/F_m values and areal photosynthetic rates (gross and net) decreased (**Figure 6**). Numerous studies have reported lowered F_v/F_m values (Warner et al., 1999; Jones et al., 2000; Supplementary Figure S2) and reduced net photosynthesis of *Symbiodinium* in response to thermal and/or light stress (Iglesias-Prieto and Trench, 1994; Warner et al., 1996, 1999), but few studies have measured gross O_2 evolution independent of light respiration (Kühl et al., 1995; Abrego et al., 2008; Schrameyer et al., 2014). A lowering of F_v/F_m is often interpreted as a sign of photoinhibition of *Symbiodinium* and can result from the formation of non-functional PS II reaction centers, i.e., a downregulation of PSII efficiency that still allows for O_2 evolution to occur (Hill et al., 2004). The high cell-specific gross photosynthetic rate (**Figure 6D**) could be explained as a downregulation of PSII efficiency counteracting the rapidly increasing *in vivo* irradiance (**Figure 4**). It is also possible that the observed dynamics reflect photoacclimation of *Symbiodinium*, as high light acclimation involves an increase in the functional absorption cross section of PSII that leads to a lowering of F_v/F_m (Hennige et al., 2008; Suggett et al., 2009). Additionally, it is possible that bleaching affected the symbiont community, potentially favoring more efficient photosynthesisers under high temperature (Roth, 2014; Sampayo et al., 2016).

The relative increase of cell-specific photosynthesis for bleached relative to healthy corals will depend on the quantity of incident solar radiation. Assuming a scenario where incident radiation saturates photosynthesis in all algal cell layers of a healthy coral, the *in vivo* light enhancement due to bleaching would not allow for a further enhancement of photosynthesis. Likewise, a faster increase in temperature would lead to more severe photoinhibtion and ultimately reduced photosynthetic rates. Additionally, our data showed that cell density (per surface area) declined to a greater extent than chlorophyll content (per g host tissue biomass). The reason for this mismatch remains unknown but could be related to reduced tissue thickness, which would affect chlorophyll but not cell density data, and/or potentially reflect the limited capacity of the HPLC to detect the Chl *a* signals in our microsamples. Normalization of gross photosynthesis data per chlorophyll *a* content of the corals showed that gross photosynthesis was only enhanced for polyp tissues (by about 1.6-fold) of bleached vs. healthy *P. damicornis* corals (data not shown). The enhancement of cell-specific photosynthesis during coral bleaching should thus be interpreted with caution and needs further investigation.

Light respiration significantly increased during the bleaching experiment, accounting for about 35% of gross photosynthesis in healthy tissues up to about 150% of gross photosynthesis in bleached tissues (**Figure 6**). Enhanced, apparently light-driven, O_2 consumption is a sign of increased electron flow through alternative electron pathways, of which the Mehler reaction is especially prevalent in *Symbiodinium* (Roberty et al., 2014). While an upregulation of the Mehler reaction has been interpreted as a photoprotective mechanism to decrease excitation pressure on PSII under high light (Roberty et al., 2014), the Mehler reaction generates ROS that can readily lead to oxidative stress, if antioxidants such as superoxide dismutase and ascorbate peroxidase are not upregulated as well (Krueger et al., 2014; Roberty et al., 2014). Together, the enhanced metabolic activity likely reflects a response of *Symbiodinium* to the strongly accelerated *in vivo* light environment (**Figure 5**) showing that coral microscale optics exert a key role in coral photophysiology.

Climate change-related coral bleaching is arguably the prime cause of global reef decline and better predictions of coral bleaching susceptibility rest on understanding the mechanisms at play (Hoegh-Guldberg, 1999; Hoegh-Guldberg et al., 2007; Weis, 2008). The optical feedback hypothesis (Enriquez et al., 2005), whereby *Symbiodinium* undergoes light exposure 'amplification' during coral bleaching (Enriquez et al., 2005; Swain et al., 2016) has lacked experimental evidence in terms of direct measures of the tissue light field before and during coral bleaching. Here, we give the first experimental proof that the *in vivo* scalar irradiance in corals is enhanced during coral bleaching due to changes in the balance between absorption and

scattering upon loss of *Symbiodinium*. Light amplification differs between coral hosts, as tissue light gradients and optical shelter remained in the massive coral *Favites* sp. but were alleviated in *P. damicornis*. The finding of optical shelter in bleached *Favites* sp. tissues implies a photoprotective microenvironment that could sustain coral resilience by facilitating the repopulation from cryptic *Symbiodinium* after stress. Our study shows that coral bleaching can in fact enhance cell-specific photosynthetic rates of remaining *Symbodinium*, which is interpreted as a response to the accelerated *in vivo* light exposure during bleaching. We conclude that coral microscale optics have a fundamental role in shaping the radiative exposure of *Symbiodinium* and thus photophysiological stress responses during coral bleaching.

AUTHOR CONTRIBUTIONS

All authors designed the experiment. JH and DW analyzed the data. DW, MK, DS, and JH interpreted the data. DW performed microsensor measurements and JH performed symbiont cell density and tissue surface area estimates. DW, JH, AL performed the experimental bleaching treatment. MK and PR provided new reagents, materials and tools: DW, MK, and JH wrote the paper with editorial input and consent from all co-authors.

FUNDING

This study was funded by a Danielle Simmons Award grant from the Australian Coral Reef Society (DW), a Science for Management Award from the Great Barrier Reef Marine Park Authority (DW), a Distinguished Postdoctoral Fellowship from the Carlsberg Foundation (DW), and a Sapere-Aude Advanced grant from the Danish Council for Independent Research | Natural Sciences (MK). The authors declare no competing interests.

ACKNOWLEDGMENTS

We thank Unnikrishnan Kuzhiumparambil for performing the HPLC analysis and Christian Evenhuis for initial discussions. Giovanni Bernal and the staff at Heron Island research station are thanked for help with coral sample collection as well as excellent assistance in the field.

SUPPLEMENTARY MATERIAL

The Supplementary Material for this article can be found online at: http://journal.frontiersin.org/article/10.3389/fmicb.2017.00059/full#supplementary-material

REFERENCES

Abrego, D., Ulstrup, K. E., Willis, B. L., and Van Oppen, M. J. H. (2008). Species-specific interactions between algal endosymbionts and coral hosts define their bleaching response to heat and light stress. *Proc. R. Soc. B* 275, 2273–2282. doi: 10.1098/rspb.2008.0180

Ainsworth, T. D., Heron, S. F., Ortiz, J. C., Mumby, P. J., Grech, A., Ogawa, D., et al. (2016). Climate change disables coral bleaching protection on the Great Barrier Reef. *Science* 352, 338–342. doi: 10.1126/science.aac7125

Baird, A. H., Bhagooli, R., Ralph, P. J., and Takahashi, S. (2009). Coral bleaching: the role of the host. *Trends Ecol. Evol.* 24, 16–20. doi: 10.1016/j.tree.2008.09.005

Brodersen, K. E., Lichtenberg, M., Ralph, P. J., Kühl, M., and Wangpraseurt, D. (2014). Radiative energy budget reveals high photosynthetic efficiency in symbiont-bearing corals. *J. R. Soc. Interface* 11:20130997. doi: 10.1098/rsif.2013.0997

Brown, B., Dunne, R., Goodson, M., and Douglas, A. (2002). Experience shapes the susceptibility of a reef coral to bleaching. *Coral Reefs* 21, 119–126.

Brown, B. E. (1997). Coral bleaching: causes and consequences. *Coral Reefs* 16, S129–S138. doi: 10.1007/s003380050249

Chan, N., Wangpraseurt, D., Kühl, M., and Connolly, S. R. (2016). Flow and coral morphology control coral surface pH: implications for the effects of ocean acidification. *Front. Mar. Sci.* 3:10. doi: 10.3389/fmars.2016.00010

Dunlap, W. C., and Shick, J. M. (1998). Ultraviolet radiation-absorbing mycosporine-like amino acids in coral reef organisms: a biochemical and environmental perspective. *J. Phycol.* 34, 418–430. doi: 10.1046/j.1529-8817.1998.340418.x

Enriquez, S., Mendez, E. R., and Iglesias-Prieto, R. (2005). Multiple scattering on coral skeletons enhances light absorption by symbiotic algae. *Limnol. Oceanogr.* 50, 1025–1032. doi: 10.1364/AO.49.005032

Falkowski, P. G., Jokiel, P. L., and Kinzie, R. (1990). Irradiance and corals. *Ecosyst. World* 25, 89–107.

Franklin, D. J., Cedres, C. M. M., and Hoegh-Guldberg, O. (2006). Increased mortality and photoinhibition in the symbiotic dinoflagellates of the Indo–Pacific coral *Stylophora pistillata* (Esper) after summer bleaching. *Mar. Biol.* 149, 633–642. doi: 10.1007/s00227-005-0230-z

Hennige, S. J., Smith, D. J., Perkins, R., Consalvey, M., Paterson, D. M., and Suggett, D. J. (2008). Photoacclimation, growth and distribution of massive coral species in clear and turbid waters. *Mar. Ecol. Prog. Ser.* 369, 77–88. doi: 10.3354/meps07612

Hill, R., Larkum, A. W., Frankart, C., Kühl, M., and Ralph, P. J. (2004). Loss of functional photosystem II reaction centres in zooxanthellae of corals exposed to bleaching conditions: using fluorescence rise kinetics. *Photosynth. Res.* 82, 59–72. doi: 10.1023/B:PRES.0000040444.41179.09

Hoegh-Guldberg, O. (1999). Climate change, coral bleaching and the future of the world's coral reefs. *Mar. Freshw. Res.* 50, 839–866. doi: 10.1071/MF99078

Hoegh-Guldberg, O., Mumby, P. J., Hooten, A. J., Steneck, R. S., Greenfield, P., Gomez, E., et al. (2007). Coral reefs under rapid climate change and ocean acidification. *Science* 318, 1737–1742. doi: 10.1126/science.1152509

Hoogenboom, M. O., Anthony, K. R. N., and Connolly, S. R. (2006). Energetic cost of photoinhibition in corals. *Mar. Ecol. Prog. Ser.* 313, 1–12. doi: 10.3354/meps313001

Hughes, T. P., Baird, A. H., Bellwood, D. R., Card, M., Connolly, S. R., Folke, C., et al. (2003). Climate change, human impacts, and the resilience of coral reefs. *Science* 301, 929–933. doi: 10.1126/science.1085046

Iglesias-Prieto, R., and Trench, R. K. (1994). Acclimation and adaptation to irradiance in symbiotic dinoflagellates. I. Responses of the photosynthetic unit to changes in photon flux density. *Mar. Ecol. Prog. Ser.* 113, 163–175. doi: 10.3354/meps113163

Jimenez, I. M., Kuhl, M., Larkum, A. W. D., and Ralph, P. J. (2008). Heat budget and thermal microenvironment of shallow-water corals: do massive corals get warmer than branching corals? *Limnol. Oceanogr.* 53, 1548–1561. doi: 10.4319/lo.2008.53.4.1548

Jones, R. J., Ward, S., Amri, A. Y., and Hoegh-Guldberg, O. (2000). Changes in quantum efficiency of photosystem II of symbiotic dinoflagellates of corals after heat stress, and of bleached corals sampled after the 1998 Great Barrier Reef mass bleaching event. *Mar. Freshw. Res.* 51, 63–71. doi: 10.1071/MF99100

Kahng, S. E., Hochberg, E. J., Apprill, A., Wagner, D., Luck, D. G., Perez, D., et al. (2012). Efficient light harvesting in deep-water zooxanthellate corals. *Mar. Ecol. Prog. Ser.* 455, 65–77. doi: 10.3354/meps09657

Kaniewska, P., Magnusson, S. H., Anthony, K. R. N., Reef, R., Kühl, M., and Hoegh-Guldberg, O. (2011). Importance of macro- versus microstructure in modulating light levels inside coral colonies. *J. Phycol.* 47, 846–860. doi: 10.1111/j.1529-8817.2011.01021.x

Kemp, D., Fitt, W., and Schmidt, G. (2008). A microsampling method for genotyping coral symbionts. *Coral Reefs* 27, 289–293. doi: 10.1007/s00338-007-0333-8

Kortüm, G. (2012). *Reflectance Spectroscopy: Principles, Methods, Applications*. New York, NY: Springer Science & Business Media.

Krueger, T., Becker, S., Pontasch, S., Dove, S., Hoegh-Guldberg, O., Leggat, W., et al. (2014). Antioxidant plasticity and thermal sensitivity in four types of *Symbiodinium* sp. *J. Phycol.* 50, 1035–1047. doi: 10.1111/jpy.12232

Kühl, M., Cohen, Y., Dalsgaard, T., Jørgensen, B. B., and Revsbech, N. P. (1995). Microenvironment and photosynthesis of zooxanthellae in scleractinian corals studied with microsensors for O2, pH and light. *Mar. Ecol. Prog. Ser.* 117, 159–172. doi: 10.3354/meps117159

Kühl, M., and Jørgensen, B. B. (1994). The light-field of microbenthic communities – radiance distribution and microscale optics of sandy coastal sediments. *Limnol. Oceanogr.* 39, 1368–1398. doi: 10.4319/lo.1994.39.6.1368

Lesser, M. P. (1996). Elevated temperatures and ultraviolet radiation cause oxidative stress and inhibit photosynthesis in symbiotic dinoflagellates. *Limnol. Oceanogr.* 41, 271–283. doi: 10.4319/lo.1996.41.2.0271

Lesser, M. P., and Farrell, J. H. (2004). Exposure to solar radiation increases damage to both host tissues and algal symbionts of corals during thermal stress. *Coral Reefs* 23, 367–377. doi: 10.1007/s00338-004-0392-z

Lichtenberg, M., Larkum, A. W. D., and Kühl, M. (2016). Photosynthetic acclimation of *Symbiodinium* in hospite depends on vertical position in the tissue of the scleractinian coral *Montastrea curta*. *Front. Microbiol.* 7:230. doi: 10.103389/fmixb.2016.00230

Loya, Y., Sakai, K., Yamazato, K., Nakano, Y., Sambali, H., and Van Woesik, R. (2001). Coral bleaching: the winners and the losers. *Ecol. Lett.* 4, 122–131. doi: 10.1046/j.1461-0248.2001.00203.x

Lyndby, N. H., Kühl, M., and Wangpraseurt, D. (2016). Heat generation and light scattering of green fluorescent protein-like pigments in coral tissue. *Sci. Rep.* 6:26599. doi: 10.1038/srep26599

Marcelino, L. A., Westneat, M. W., Stoyneva, V., Henss, J., Rogers, J. D., Radosevich, A., et al. (2013). Modulation of light-enhancement to symbiotic Algae by light scattering in corals and evolutionary trends in bleaching. *PLoS ONE* 8:e61492. doi: 10.1371/journal.pone.0061492

Middlebrook, R., Anthony, K. R., Hoegh-Guldberg, O., and Dove, S. (2010). Heating rate and symbiont productivity are key factors determining thermal stress in the reef-building coral *Acropora formosa*. *J. Exp. Biol.* 213, 1026–1034. doi: 10.1242/jeb.031633

Muscatine, L., Mccloskey, L. R., and Marian, R. E. (1981). Estimating the daily contribution of carbon from zooxanthellae to coral animal respiration. *Limnol. Oceanogr.* 26, 601–611. doi: 10.4319/lo.1981.26.4.0601

Nothdurft, L. D., and Webb, G. E. (2007). Microstructure of common reef-building coral genera *Acropora*, *Pocillopora*, *Goniastrea* and *Porites*: constraints on spatial resolution in geochemical sampling. *Facies* 53, 1–26. doi: 10.1007/s10347-006-0090-0

Ow, Y., and Todd, P. (2010). Light-induced morphological plasticity in the scleractinian coral *Goniastrea pectinata* and its functional significance. *Coral Reefs* 29, 797–808. doi: 10.1007/s00338-010-0631-4

Revsbech, N. P., and Jorgensen, B. B. (1983). Photosynthesis of benthic microflora measured with high spatial-resolution by the oxygen microprofile method - capabilities and limitations of the method. *Limnol. Oceanogr.* 28, 749–756. doi: 10.4319/lo.1983.28.4.0749

Rickelt, L. F., Lichtenberg, M., Trampe, E. C. L., and Kühl, M. (2016). Fiber-optic probes for small-scale measurements of scalar irradiance. *Photochem. Photobiol.* 92, 331–342. doi: 10.1111/php.12560

Roberty, S., Bailleul, B., Berne, N., Franck, F., and Cardol, P. (2014). PSI Mehler reaction is the main alternative photosynthetic electron pathway in *Symbiodinium* sp., symbiotic dinoflagellates of cnidarians. *New Phytol.* 204, 81–91. doi: 10.1111/nph.12903

Rodriguez-Roman, A., Hernandez-Pech, X., Thome, P. E., Enriquez, S., and Iglesias-Prieto, R. (2006). Photosynthesis and light utilization in the Caribbean coral *Montastraea faveolata* recovering from a bleaching event. *Limnol. Oceanogr.* 51, 2702–2710. doi: 10.4319/lo.2006.51.6.2702

Roth, M. S. (2014). The engine of the reef: photobiology of the coral–algal symbiosis. *Front. Microbiol.* 5:422. doi: 10.3389/fmicb.2014.00422

Rowan, R., Knowlton, N., Baker, A., and Jara, J. (1997). Landscape ecology of algal symbionts creates variation in episodes of coral bleaching. *Nature* 388, 265–269. doi: 10.1038/40843

Salih, A., Larkum, A., Cox, G., Kühl, M., and Hoegh-Guldberg, O. (2000). Fluorescent pigments in corals are photoprotective. *Nature* 408, 850–853. doi: 10.1038/35048564

Sampayo, E. M., Ridgway, T., Bongaerts, P., and Hoegh-Guldberg, O. (2008). Bleaching susceptibility and mortality of corals are determined by fine-scale differences in symbiont type. *Proc. Natl. Acad. Sci. U.S.A.* 105, 10444–10449. doi: 10.1073/pnas.0708049105

Sampayo, E. M., Ridgway, T., Franceschinis, L., Roff, G., Hoegh-Guldberg, O., and Dove, S. (2016). Coral symbioses under prolonged environmental change: living near tolerance range limits. *Sci. Rep.* 6:36271. doi: 10.1038/srep36271

Schrameyer, V., Wangpraseurt, D., Hill, R., Kühl, M., Larkum, A. W., and Ralph, P. J. (2014). Light respiratory processes and gross photosynthesis in two scleractinian corals. *PLoS ONE* 9:e110814. doi: 10.1371/journal.pone.0110814

Shashar, N., Cohen, Y., and Loya, Y. (1993). Extreme diel fluctuations of oxygen in diffusive boundary layers surrounding stony corals. *Biol. Bull.* 185, 455–461. doi: 10.2307/1542485

Silverstein, R. N., Correa, A. M. S., and Baker, A. C. (2012). Specificity is rarely absolute in coral–algal symbiosis: implications for coral response to climate change. *Proc. R. Soc. B* 279, 2609–2618. doi: 10.1098/rspb.2012.0055

Smith, E., D'angelo, C., Salih, A., and Wiedenmann, J. (2013). Screening by coral green fluorescent protein (GFP)-like chromoproteins supports a role in photoprotection of zooxanthellae. *Coral Reefs* 32, 463–474. doi: 10.1007/s00338-012-0994-9

Suggett, D. J., Moore, C. M., Hickman, A. E., and Geider, R. J. (2009). Interpretation of fast repetition rate (FRR) fluorescence: signatures of phytoplankton community structure versus physiological state. *Mar. Ecol. Prog. Ser.* 376, 1–19. doi: 10.3354/meps07830

Swain, T. D., Dubois, E., Gomes, A., Stoyneva, V. P., Radosevich, A. J., Henss, J., et al. (2016). Skeletal light-scattering accelerates bleaching response in reef-building corals. *BMC Ecol.* 16:1. doi: 10.1186/s12898-016-0061-4

Szabó, M., Wangpraseurt, D., Tamburic, B., Larkum, A. W. D., Schreiber, U., Suggett, D. J., et al. (2014). Effective light absorption and absolute electron transport rates in the coral *Pocillopora damicornis*. *Plant Physiol. Bioch.* 83, 159–167. doi: 10.1016/j.plaphy.2014.07.015

Takabayashi, M., and Hoegh-Guldberg, O. (1995). Ecological and physiological differences between two color morphs of the coral *Pocillopora damicornis*. *Mar. Biol.* 123, 705–714. doi: 10.1007/BF00349113

Takahashi, S., Nakamura, T., Sakamizu, M., Van Woesik, R., and Yamasaki, H. (2004). Repair machinery of symbiotic photosynthesis as the primary target of heat stress for reef-building corals. *Plant Cell Physiol.* 45, 251–255. doi: 10.1093/pcp/pch028

Teran, E., Mendez, E. R., Enriquez, S., and Iglesias-Prieto, R. (2010). Multiple light scattering and absorption in reef-building corals. *Appl. Opt.* 49, 5032–5042. doi: 10.1364/AO.49.005032

Tonk, L., Bongaerts, P., Sampayo, E. M., and Hoegh-Guldberg, O. (2013). SymbioGBR: a web-based database of *Symbiodinium* associated with cnidarian hosts on the Great Barrier Reef. *BMC Ecol.* 13:7. doi: 10.1186/1472-6785-13-7

Ulstrup, K. E., Ralph, P. J., Larkum, A. W. D., and Kuhl, M. (2006). Intra-colonial variability in light acclimation of zooxanthellae in coral tissues of *Pocillopora damicornis*. *Mar. Biol.* 149, 1325–1335. doi: 10.1007/s00227-006-0286-4

Wangpraseurt, D., Jacques, S., Petri, T., and Kuhl, M. (2016a). Monte Carlo modeling of photon propagation reveals highly scattering coral tissue. *Front. Plant Sci.* 7:1404. doi: 10.3389/fpls.2016.01404

Wangpraseurt, D., Larkum, A. W., Franklin, J., Szabó, M., Ralph, P. J., and Kühl, M. (2014a). Lateral light transfer ensures efficient resource distribution in symbiont-bearing corals. *J. Exp. Biol.* 217, 489–498. doi: 10.1242/jeb.091116

Wangpraseurt, D., Larkum, A. W., Ralph, P. J., and Kühl, M. (2012). Light gradients and optical microniches in coral tissues. *Front. Microbiol.* 3:316. doi: 10.3389/fmicb.2012.00316

Wangpraseurt, D., Polerecky, L., Larkum, A. W., Ralph, P. J., Nielsen, D. A., Pernice, M., et al. (2014b). The in situ light microenvironment of corals. *Limnol. Oceanogr.* 59, 917–926. doi: 10.4319/lo.2014.59.3.0917

Wangpraseurt, D., Tamburic, B., Szabó, M., Suggett, D., Ralph, P. J., and Kühl, M. (2014c). Spectral effects on *Symbiodinium* photobiology studied with a programmable light engine. *PLoS ONE* 9:e112809. doi: 10.1371/journal.pone.0112809

Wangpraseurt, D., Wentzel, C., Jacques, S. L., Wagner, M., and Kuhl, M. (2016b). In vivo imaging of coral tissue and skeleton with optical coherence tomography. *bioRxiv* doi: 10.1101/088682

Warner, M. E., Fitt, W. K., and Schmidt, G. W. (1996). The effects of elevated temperature on the photosynthetic efficiency of zooxanthellae in hospite from four different species of reef coral: a novel approach. *Plant Cell Environ.* 19, 291–299. doi: 10.1111/j.1365-3040.1996.tb00251.x

Warner, M. E., Fitt, W. K., and Schmidt, G. W. (1999). Damage to photosystem II in symbiotic dinoflagellates: a determinant of coral bleaching. *Proc. Natl. Acad. Sci. U.S.A.* 96, 8007–8012. doi: 10.1073/pnas.96.14.8007

Weis, V. M. (2008). Cellular mechanisms of Cnidarian bleaching: stress causes the collapse of symbiosis. *J. Exp. Biol.* 211, 3059–3066. doi: 10.1242/jeb.009597

Yost, D. M., Wang, L.-H., Fan, T.-Y., Chen, C.-S., Lee, R. W., Sogin, E., et al. (2013). Diversity in skeletal architecture influences biological heterogeneity and *Symbiodinium* habitat in corals. *Zoology* 5, 262–269. doi: 10.1016/j.zool.2013.06.001

Conflict of Interest Statement: The authors declare that the research was conducted in the absence of any commercial or financial relationships that could be construed as a potential conflict of interest.

frontiers in Marine Science

ORIGINAL RESEARCH
published: 13 April 2017
doi: 10.3389/fmars.2017.00102

Carbon and Nitrogen Acquisition in Shallow and Deep Holobionts of the Scleractinian Coral *S. pistillata*

Leïla Ezzat[1]*, *Maoz Fine*[2,3], *Jean-François Maguer*[4], *Renaud Grover*[1] and *Christine Ferrier-Pagès*[1]

[1] Marine Department, Scientific Centre of Monaco, Monaco, Monaco, [2] The Mina and Everard Goodman Faculty of Life Sciences, Bar-Ilan University, Ramat-Gan, Israel, [3] The Interuniversity Institute for Marine Sciences, Eilat, Israel, [4] Laboratoire de l'Environnement Marin, UMR 6539, UBO/Centre Nationnal de la Recherche Scientifique/IRD/IFREMER, Institut Universitaire Européen de la Mer, Plouzané, France

Reef building corals can host different symbiont genotypes (clades), and form distinct holobionts in response to environmental changes. Studies on the functional significance of genetically different *symbionts* have focused on the thermal tolerance rather than on the nutritional significance. Here, we characterized the nitrogen and carbon assimilation rates, the allocation patterns of these nutrients within the symbiosis, and the trophic condition of two distinct holobionts of *Stylophora pistillata*: one associated with *Symbiodinium* clade A in shallow reefs and the other one associated with clade C in mesophotic reefs. The main findings are that: (1) clade C-symbionts have a competitive advantage for the acquisition of carbon at low irradiance compared to clade A-symbionts; (2) light is however the primary factor that determines the positive relationship between the amount of carbon fixed in photosynthesis by the symbionts and the amount of carbon translocated to the host; and (3) by contrast, the dominant *Symbiodinium* type preferentially determines a negative relationship between rates of coral feeding and nitrogen assimilation, although light still plays a relevant role in this relationship. Clade C-holobionts had indeed higher heterotrophic capacities, but lower inorganic nitrogen assimilation rates than clade A-holobionts, at all light levels. Broadly, our results show that the assimilation and translocation rates of inorganic carbon and nitrogen are clade and light-dependent. In addition, the capacity of *S. pistillata* to form mesophotic reefs in the Red Sea relies on its ability to select *Symbiodinium* clade C, as this symbiont type is more efficient to fix carbon at low light.

Keywords: light acclimation, carbon isotopes, nitrogen isotopes, clades, nitrate, ammonium, scleractinian coral, mesophotic coral

OPEN ACCESS

Edited by:
Noga Stambler, Bar-Ilan University, Israel

Reviewed by:
Susana Enríquez, National Autonomous University of Mexico, Mexico
Michael P. Lesser, University of New Hampshire, USA
David Michael Baker, University of Hong Kong, Hong Kong

***Correspondence:**
Leïla Ezzat
leila@centrescientifique.mc

Specialty section:
This article was submitted to Coral Reef Research, a section of the journal Frontiers in Marine Science

Received: *14 December 2016*
Accepted: *27 March 2017*
Published: *13 April 2017*

Citation:
Ezzat L, Fine M, Maguer J-F, Grover R and Ferrier-Pagès C (2017) Carbon and Nitrogen Acquisition in Shallow and Deep Holobionts of the Scleractinian Coral S. pistillata. Front. Mar. Sci. 4:102. doi: 10.3389/fmars.2017.00102

INTRODUCTION

Coral reefs support one of the most diverse and productive biological communities on Earth. Their success owe from the symbiotic relationship that corals build with photosynthetic dinoflagellate algae, commonly named zooxanthellae, that can sustain up to 95% of the daily energetic demand of the symbiotic association (Muscatine et al., 1984; Muscatine, 1990), also called holobiont (Rohwer et al., 2002). While symbionts need light for photosynthesis and constrain their host to mainly develop in the first 30 m depth, corals can however form large structures called mesophotic reefs

in much deeper waters. Mesophotic reefs therefore refer to deep but light-limited coral ecosystems (Hinderstein et al., 2010), ranging between 30 and 80 m in the Gulf of Mexico (Kahng, 2010), to more than 100 m in some locations with exceptionally clear waters, such as the Red Sea (Lesser et al., 2009; Winters et al., 2009). Although, photosynthesis is limited by the low light levels, these reefs host a wide diversity of taxa due to numerous upwelling events and internal waves, that deliver significant amounts of inorganic nutrients and particulate organic matter (Leichter and Genovese, 2006; Lesser et al., 2009).

In response to decreased light intensity, corals can either present host (Brazeau et al., 2013) and/or symbiont genetic diversity (Lesser et al., 2010) as well as adaptations to grow under low irradiance conditions. For example, in order to increase and optimize the light capture and rates of autotrophic carbon production at depth >30 m, corals undergo morphological changes (Mass et al., 2007; Einbinder et al., 2009; Nir et al., 2011) as well as modifications in the photo-physiological traits of their symbionts (Wyman et al., 1987; Lesser et al., 2000, 2009). They also compensate their low photosynthate production by increasing the acquisition of heterotrophic nutrients (Muscatine et al., 1989; Mass et al., 2007; Alamaru et al., 2009; Einbinder et al., 2009; Lesser et al., 2010; Crandall et al., 2016). Corals can finally harbor different *Symbiodinium* clades depending on the depth at which they thrive (Finney et al., 2010; Lesser et al., 2010). In the Caribbean, although some colonies can present a mix of symbiont clades with a zonation pattern (Kemp et al., 2015), Symbiodinium A and B are predominant in tissue exposed to high irradiance (surface waters) while Symbiodinium C is dominant in shaded tissue of deep corals (Rowan and Knowlton, 1995; Rowan et al., 1997). In the northern Red Sea, *Stylophora pistillata* shifts from hosting clade A in shallow waters to clade C below 40 m depth (Mass et al., 2007; Winters et al., 2009). Although, numerous studies have now acknowledged the diversity and flexibility of *Symbiodinium* under different light environments, the functional significance of these associations remains unexplored. It has been suggested that physiological diversification in *Symbiodinium* species can confer growth advantages to their associated coral host, by presenting different thermal and light tolerances as well as capacities in nutrient acquisition (Little et al., 2004; Abrego et al., 2008; Stat et al., 2008; Venn et al., 2008; Jones and Berkelmans, 2010; Lesser et al., 2013). Among studies on the functional significance of the clades, most have focused on their capacity to tolerate thermal stress (Berkelmans and van Oppen, 2006; Howells et al., 2012; Silverstein et al., 2015; Hume et al., 2016) while their nutritional capacities are still poorly known, although it has important physiological consequences for the host (Loram et al., 2007; Baker et al., 2013; Starzak et al., 2014; Leal et al., 2015). Baker et al. (2013) and Pernice et al. (2015) showed that the acquisition of nitrogen and carbon by *Acroporidae* species (*Acropora tenuis* and *Isopora palifera,* respectively) was clade—(Baker et al., 2013; Pernice et al., 2015) and temperature dependent (Baker et al., 2013). Other studies on sea anemones also demonstrated that *Symbiodinium* genotypic diversity affects the quantity and quality of photosynthates translocated to the animal host (Loram et al., 2007; Starzak et al., 2014; Leal et al., 2015), as well as the heterotrophic capacities of the host (Leal et al., 2015). Overall, these studies suggest that symbiont identity directly relates to the trophic plasticity of the holobiont. Because acquisition of both auto-and heterotrophic nutrients is critical for coral growth and reproduction (Muscatine and Porter, 1977; Muscatine et al., 1989; Ferrier-Pages et al., 2000; Houlbreque and Ferrier-Pagès, 2009), a better understanding of the nutritional capacities of different holobionts will help predict their resilience to stress. Until now, no direct simultaneous comparison exists between auto-and heterotrophic performance of shallow and deep corals associated with different *Symbiodinium* genotypes, although deep reefs host a huge biodiversity (Hovland, 2008).

Here we compare the trophic and photosynthetic capacities of two distinct holobionts of the scleractinian coral *S. pistillata* living in shallow and mesophotic reefs of Eilat (Red Sea). *S. pistillata,* harbors clade A1 in shallow waters (<40 m) and clade C in deeper environments (>40 m), forming two different holobionts of the same species (Byler et al., 2013). We measured, under the light conditions of surface and deep waters, the heterotrophic capacities of each holobiont, as well as their rates of photosynthesis and acquisition of inorganic carbon and nitrogen using stable isotopes [$NaH^{13}CO_3$ (^{13}C), $^{15}NH_4Cl$ (NH_4), and $^{15}NaNO_3$ (NO_3)]. Inorganic carbon and nitrogen acquisition by the symbionts, together with host prey capture, provide direct measures to score nutritional plasticity of these symbioses. Getting new insights into the trophic behavior and the metabolic processes associated with mesophotic corals is essential to understand the ecology and biology of these unique habitats as well as the vertical connectivity existing between shallow and deep environments, which may be of great importance for the future health and resilience of their associated ecosystems.

MATERIALS AND METHODS

Biological Material and Experimental Setup

Experiments were performed in November 2014 at the IUI, in the Gulf of Eilat (Israel). While light conditions decreased from 200 to 400 μmol quanta m^{-2} s^{-1} at 5 m depth to 20 to 40 μmol quanta m^{-2} s^{-1} at 50 m depth, the seawater temperature (24 ± 0.5°C) and nutrient concentrations remained stable throughout the investigated depth range (Bednarz et al., 2017). The above environmental data were provided by the Israel National Monitoring Program at the Gulf of Eilat (http://www.iui-eilat.ac.il/Research/NMPMeteoData.aspx) and represented average values collected close to our study site. Ten mother colonies of the Red Sea coral *S. pistillata* were thus sampled directly on the reef, five colonies from 5 m depth and five others from 50 m depth. Field collection of animals complied with a permit issued by the Israel Nature and Parks Authority (2015/40780). Colonies were enclosed in different bags underwater, to keep track of each genotype, and brought back to the laboratory, located few meters from the reef, were they were properly identified. The main *Symbiodinium* genotype hosted by each colony was checked according to the protocol of Santos et al. (2002). As repeatedly observed (Mass et al., 2007; Lampert-Karako et al., 2008; Winters et al., 2009; Nir et al., 2014), the main clade associated to shallow colonies was A1, while C1 and C3 (simplified to clades A and C

throughout the manuscript) populated the deep colonies (Table S5). Fifteen nubbins of about 3 cm long were then cut from each mother colony, tagged, and distributed in 4 open tanks for clade A and four other tanks for clade C. Aquarium system was set up in outdoor water tables, continuously supplied with unfiltered oligotrophic seawater from the reef at a temperature of 24°C ± 0.5. Coral colonies were exposed to photon flux densities (PFD) similar to those found at 50 and 5 m at the month of collection (mean daily PFDs were equivalent to 13.8 mol photons m^{-2} d^{-1} for surface and 0.8 mol photons m^{-2} d^{-1} for deep holobionts). Proper light intensity was calibrated by the use of a light meter (Li-Cor, LI-250A, USA) and UV-filters were disposed above aquaria to protect deep corals against UVR. Coral nubbins were maintained for 2 days prior to the measurements described below, which have been performed (i) at the "natural" light level of each population/holobiont (subsequently called "high-light" for the shallow population and "low light" for the deep population) but also (ii) at the other corresponding light (low light for the shallow population and high light for the deep one). This last measurement was performed to assess the ability of each holobiont to quickly adjust its response to changes in irradiance.

Rates of Net Photosynthesis, Respiration, and Chlorophyll Content Measurements

Changes in oxygen production were monitored for 60 min on 5 nubbins per holobiont (A and C; from 5 mother colonies) at the two mean irradiances corresponding to the surface and deep PFD levels: 350 μmol photons m^{-2} s^{-1} (shallow, High light, HL) and 20 μmol photons m^{-2} s^{-1} (deep, Low light, LL), respectively. Respiration rates (R) were assessed in the dark after the illumination period. Nubbins were individually placed in glass chambers, filled with a known volume of 0.45 μM filtered seawater (FSW) which were stirred using a magnetic stirrer. Glass chambers were maintained at 24°C by the use of a water bath equipped with a PreSense optode (oxygen-sensitive minisensor) connected to the Oxy-4 (4 Channel oxygen meter, PreSense, Regensburg, Germany). Optodes were calibrated against air-saturated and dinitrogen-saturated water for the 100 and 0% oxygen, respectively. Estimations of net photosynthesis (P_n) at LL and HL and respiration (R) were measured by regressing oxygen production against time. Gross photosynthesis (P_g) was assessed by adding R to P_n. At the end of each incubation, coral nubbins were frozen at −20°C prior to the subsequent determination of total chlorophyll content. Briefly, coral tissue was removed from its skeleton in 10 mL filtered seawater (FSW) with an air-brush, homogenized with a potter grinder and transferred into a 15 mL tube before being centrifuged at 8,000 g for 10 min at 4°C. The pellet was re-suspended into 5 mL 100% acetone and stored at 4°C overnight. The next day, samples were centrifuged at 11,000 g for 15 min at 4°C before assessing the chlorophyll content according to the protocol of Jeffrey and Humphrey (1975). Data were normalized to the surface area (cm^2) of each nubbin using the wax-dipping technique (Davies, 1989). Conversions of oxygen fluxes to carbon equivalents, based on molar weights, were calculated according to Anthony and Fabricius (2000) and Gattuso and Jaubert (1990). P:R ratio, which shows the autotrophic capability of an organism to self-maintenance was obtained with the following equation: $P{:}R = (P_C \times 12)/(R_C \times 24)$, where $P_C = Pg \times 12/PQ$ and $R_C = R \times (12 \times RQ)$. P_C represents the amount of carbon acquired during photosynthesis; R_C is the amount of carbon consumed by respiration; 12 is the C molecular mass; PQ and RQ are the photosynthetic and respiratory quotient respectively and vary according to the *in situ* light intensity experienced by the holobionts (Gattuso and Jaubert, 1990; Lesser, 2013). Net photosynthesis was considered to be efficient for 11 h light (length of the day in November in Eilat, http://www.iui-eilat.ac.il/NMP/Default.aspx) and respiration for 24 h. P:R ratio was calculated for a period time of 24 h.

Additional nubbins ($n = 5$ per condition from 5 mother colonies) were used to assess the respiration rates of freshly isolated symbionts. For this, tissues were extracted from live coral samples in 10 mL of FSW and centrifuged at the corresponding temperature. After centrifugation, pellets were re-suspended in 20 mL FSW and disposed for 20 min in aquaria before processing to the respiration rate measurements as previously exposed. Data were normalized to the surface area of each nubbin.

$NaH^{13}CO_3$ and $^{15}NH_4Cl$, $^{15}NaNO_3$ Labeling

The following incubations were performed according to Tremblay et al. (2012) and Grover et al. (2002) (**Figure 1**). For each holobiont (A and C), 40 coral nubbins (8 per colony) were placed in individual beakers filled with 200 mL FSW. Beakers and corals were transferred back to the outdoor water tables; 20 beakers were incubated under ≪ low light ≫ while the other 20 beakers were maintained under ≪ high light ≫ for 5 h (T_0), between 11 a.m. and 4 p.m., to cover the maximal irradiances received at each depth. In addition, for each light level, 10 beakers were enriched with 0.6 mM $NaH^{13}CO_3$ (98 atom $\%^{13}C$, #372382, Sigma-Aldrich, St-Louis, MO, USA) and 3 μM $^{15}NH_4Cl$ (98 atom $\%^{15}N$, #24858029, Sigma-Aldrich, St-Louis, MO, USA) while 10 beakers received 0.6 mM $NaH^{13}CO_3$ and 3 μM $^{15}NaNO_3$ (98 atom $\%^{15}N$, #24862444, Sigma-Aldrich, St-Louis, MO, USA). The concentrations were chosen to provide sufficient enrichment for further analysis. Additional nubbins were incubated in non-enriched water as control samples (natural isotopic abundance). At the end of the 5 h incubation, half nubbins were sampled for T_0 while the other half were transferred into non-enriched seawater for one chase period of 24 h (T_{24}). All nubbins were frozen at −20°C at the end of each time point (T_0 and T_{24}) before tissue extraction (air pick), separation of the symbionts from the animal tissue by centrifugation and freeze-drying of the extracts for conservation.

The subsequent determination of $\%^{13}C$ enrichment, $\%^{15}N$ enrichment, C and N measurements in the algal and animal compartments were performed with a Delta plus Mass spectrometer (Thermofisher Scientific, Bremen, Germany) coupled to a C/N analyser (Flash EA, Thermofisher Scientific). The ^{15}N or ^{13}C enrichments were calculated from ^{15}N-^{13}C values obtained from samples exposed to ^{15}N or ^{13}C enriched seawater and from control samples incubated without isotope addition. From the difference between these two measurements,

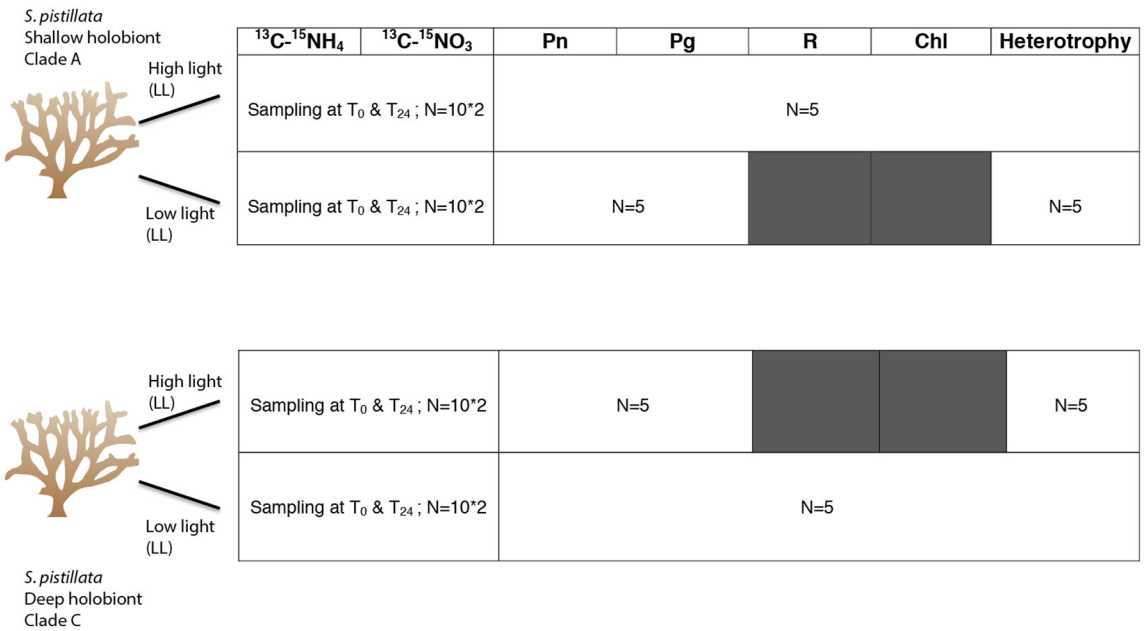

FIGURE 1 | Detailed table summarizing the experimental set up and the different parameters studied according to the number of nubbins used per timesteps [T_0 (5 h incubation) and T_{24} (chase)]. Modified according to: http://ian.umces.edu/imagelibrary/displayimage-77-6640.html.

the enrichment was calculated and considered significant when it was at least three times higher than the standard deviation obtained on control samples. From there, the nitrogen and carbon assimilation rates were calculated according to Montoya et al. (1996) based on the particulate nitrogen or carbon content of the sample, the incubation time, the theoretical ^{15}N and ^{13}C enrichment of the incubation water at the beginning and the skeletal surface area of the corals.

The carbon incorporation rates in the symbionts and animal tissue was thus calculated according to Tremblay et al. (2012):

$$\rho = \frac{(C_{meas} - C_{nat}) * M_s * M_c}{(C_{inc} - C_{meas}) * (t_{pulse} + t_{chase}) * S}$$

Where ρ is the carbon incorporation rate in the algal or animal fraction, C_{meas} and C_{nat} are the percentages of ^{13}C measured in the samples, C_{inc} is the percent ^{13}C enrichment in the incubation medium, M_s is the mass of the freeze-dried sample (mg) and M_c the mass of carbon per milligram of symbiont or animal tissues ($\mu g\ mg^{-1}$); S is the surface area of the nubbin (cm^2) and T_{pulse} and T_{chase} are the incubation time periods (h) in the light in the enriched and non-enriched medium. C_{inc} varies during the pulse-chase period and can be calculated as following:

$$C_{inc} = \frac{(C_{pulse} * t_{pulse}) + (C_{chase} * t_{chase})}{(t_{pusle} + t_{chase})}$$

Where C_{pulse} and C_{chase} are the percent ^{13}C enrichment of the enriched and non-enriched incubation media, respectively ($C_{chase} = 1.1\%$).

Furthermore, the amount of photosynthesized carbon translocated from the symbionts to the host can be calculated using the following equation:

$$Ts = P_c - \rho_s - R_s$$

Where P_c is the total amount of autotrophic carbon produced by the symbionts; ρ_s is the carbon assimilation rate and R_s the respiration rate of the symbionts.

Assimilation rates of ammonium and nitrate ρ were calculated according to Grover et al. (2002, 2003):

$$\rho = \frac{N_{mes} - N_{nat}}{(N_{enr} - N_{mes}) * T_{inc} * S} * M_s * M_N * 10^6$$

Where N_{mes} is the $\%^{15}N$ measured in the sample; N_{nat} is the natural ^{15}N abundance in control nubbin; N_{enr} is the ^{15}N enrichment of the incubation medium; T_{inc} is the incubation time (h) and S is the surface area expressed in cm^2; M_s is the total mass of the sample (mg); M_N is the particulate nitrogen mass (mg).

For more detailed information regarding the calculations, please refer to Tremblay et al. (2012) and Grover et al. (2002). Data were normalized to the coral surface area.

Heterotrophic Feeding

Feeding rates were determined at each light level (LL, HL) on 10 nubbins per holobiont (from 5 colonies) following Houlbrèque et al. (2004), by incubating individual fragments in small 400 mL plexiglas chambers equipped with a motor-driven propeller to insure a proper flow speed of 4 cm s^{-1} as described in Ferrier-Pagès et al. (2010). Chambers were kept in

a water bath to maintain the temperature constant. After the full expansion of the polyps, the experiment started by delivering 1,000 *Artemia salina* nauplii L^{-1} (previously quantified using a Bogorov counting chamber). *Artemia* concentration was then determined in triplicate after 0, 15, 30, 45, and 60 min and nauplii were directly replaced in the chamber after counting. Three additional chambers without coral were used to account for a possible decrease in nauplii concentration due to natural death. Feeding rates were calculated as the decrease in the number of preys during the incubation, and were normalized to the nubbin surface area. The concentration of *A. salina* nauplii used in this study (2,000 cells/L) is high compared to the zooplankton concentration usually measured in the reefs (7 cells/L). However, it is low compared to the concentration of nanoplankton prey (10^6–10^7 cells/L). It has only been used to assess the heterotrophic capacities of each coral population for a same amount of food.

Statistical Analysis

Statistical analyses were performed using Statistica 10 (Statsoft, Chicago, IL). All data were expressed as mean ± standard error. Normality and homoscedasticity of the data residuals were tested using Kolmogorov–Smirnov (using Lilliefors corrections) and Levene tests. A one-way ANOVA was used to test the difference in chlorophyll content and respiration rates of the clade A and C-symbionts. Two-way ANOVAs were performed to test (i) the effects of the holobiont (A/C) and the light level (LL/HL) on the net and gross photosynthesis rates, the grazing rates and the P:R and (ii) to test the effect of holobiont (A/C) and fraction (host/symbiont) on the structural C:N. A factorial analysis of variance (ANOVA) was performed to test the effects of time (T_0 and T_{24}), light level, holobiont and fraction on the rates of carbon and nitrogen (NH_4 and NO_3) assimilation, the rates and percentage of photosynthate translocation, and the structural C and N contents (μmol C or N mg^{-1}). Moreover, there was no significant difference between ^{13}C measurements obtained in presence of $^{15}NH_4$ or $^{15}NO_3$ either for A and C holobionts (ANOVA, $p > 0.05$), therefore data were pooled for analysis. Percentages of photosynthate translocation were log-transformed prior analyses. When there were significant differences, the analyses were followed by *a posteriori* testing (Tukey's test). Finally, Pearson correlations were used to attest the relationships between (i) carbon fixation and translocation and (ii) feeding rates and NH_4 or NO_3 assimilation rates in the algal fraction after 5 h incubation. *P*-values were considered for $p < \alpha, \alpha = 0.05$.

RESULTS

Physiological Measurements

Chlorophyll concentration, which was only dependent on the *in situ* growth conditions of the holobionts (i.e., mainly light) was significantly lower in clade A than clade C-holobionts (**Figure 2A**; Table S1, ANOVA, $p < 0.05$). Net rates of photosynthesis (Pn), significantly increased with light for both holobionts (Figure S1A; Tukey HSD, $p < 0.001$). In addition, while Pn was not different between holobionts under high light,

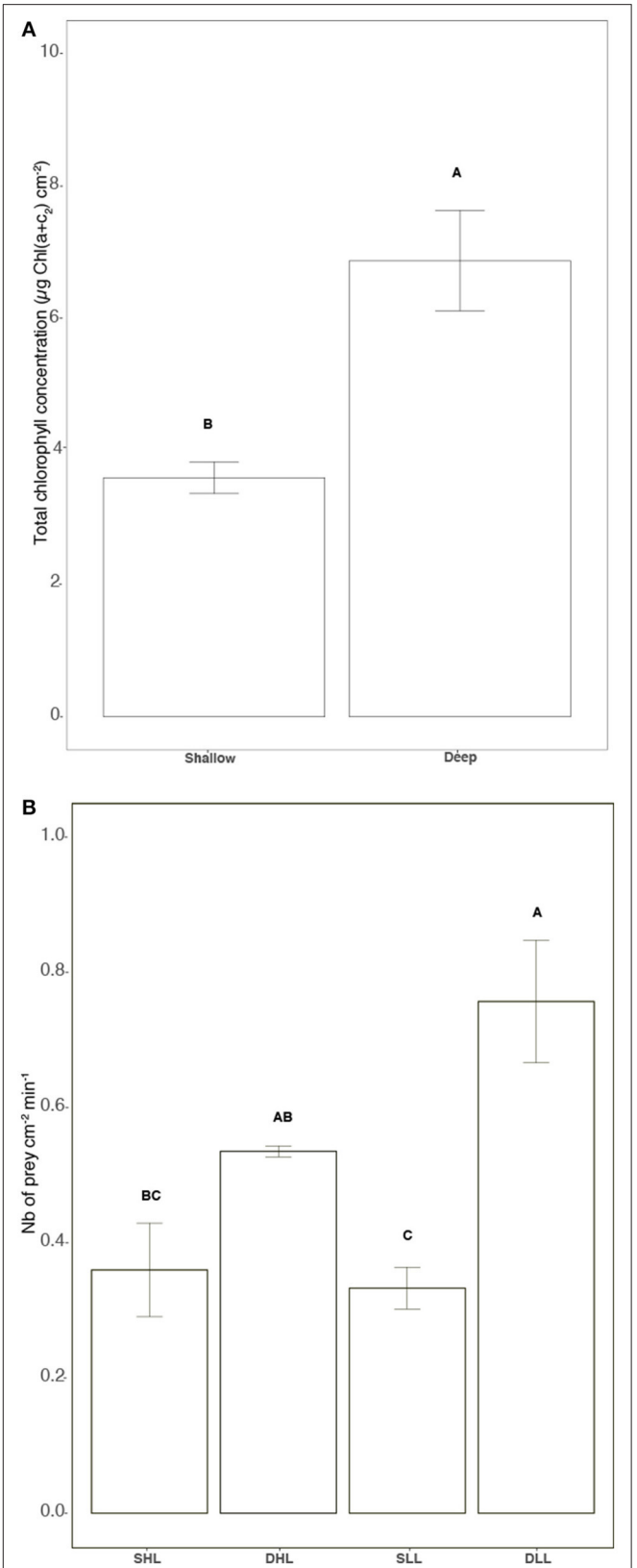

FIGURE 2 | (A) Total chlorophyll concentration [μg Chl ($a+c_2$) cm^{-2}], **(B)** Grazing rates (Number of prey cm^{-2} mn^{-1}). Statistically significances are indicated in bold letters, *p*-values are considered for $p < 0.05$.

clade A-holobionts presented a lower Pn under low light (Figure S1A; Tukey HSD, $p < 0.001$). Respiration rates were significantly lower for clade C-holobionts (Figure S1B; Tukey HSD, $p < 0.01$). Therefore, clade A-holobionts reduced their P:R values with decreasing light intensities from 1.00 ± 0.08 to 0.11 ± 0.1 (Tukey HSD, $p = 0.003$) while the P:R ratio of clade C-holobionts remained unchanged (6.85 ± 1.5–4.3 ± 1.7 at high and low light respectively, Tukey HSD, $p > 0.05$), and was higher than the P:R of clade A-holobionts (Tukey HSD, $p < 0.02$). Feeding rates were significantly lower in clade A than clade C-holobionts, under their natural light level (**Figure 2B**; Table S1, ANOVA, $p < 0.05$ and $p = 0.02$).

$NaH^{13}CO_3$ Labeling—Carbon Assimilation within the Symbiosis

Carbon Acquisition and Allocation within the Symbiosis

The carbon budget of each holobiont was similar in presence of NH_4^+ and NO_3^- for each light level (ANOVA, $p > 0.05$). Therefore, data represent the mean and standard error of the two measurements.

The amounts of carbon fixed by the symbionts and translocated to the host were significantly affected by both the light level and the clade hosted in each holobiont (Table S2; ANOVA, $p < 0.002$). Higher rates were indeed observed under high light for both holobionts (**Figures 3A,B**; Tukey HSD; $p < 0.01$). However, while clade A fixed and translocated 30% more carbon to the host than clade C under high light (**Figures 3A,B**; Table S2;Tukey HSD, $p < 0.001$), the reverse was observed under low light, especially for carbon translocation at T0 (**Figure 3B**; Tukey HSD, $p < 0.05$). The rates of carbon incorporation into the symbionts were generally significantly higher than those measured for the host (**Figures 4A,B**; Tukey HSD, $p < 0.03$). Higher rates were also generally observed under high light both in the animal and algal fractions of both holobionts (**Figures 4A,B**; Tukey HSD, $p < 0.03$).

Ammonium Assimilation

The assimilation of NH_4 within the symbiosis was affected by both the clade present in each holobiont, the fraction (host/symbionts) considered and the length of the incubation (Table S3, ANOVA, $p < 0.0002$). Clade effect was very important as clade A-symbionts assimilated ca. 31 and 95% more NH_4 than clade C-symbionts depending on the light level (Tukey HSD, $p < 0.03$). Clade A symbionts also retained 10–20 times more NH_4 than their host (**Figures 5A,B**; Table S3; Tukey HSD, $p < 0.0001$), while clade C symbionts retained the same amount (Table S3; Tukey HSD, $p > 0.05$). The difference between T_0 and T_{24} in the assimilation rates showed that clade A symbionts translocated to their host 6.2% of the NH_4 assimilated while clade C symbionts translocated 47.5%.

Nitrate Assimilation

The assimilation of NO_3 was affected by both the clade present in each holobiont, and the fraction (host/symbionts) considered (Table S3, ANOVA, $p < 0.001$). Higher assimilation rates were observed in the symbiont fraction compared to the host tissue for both holobionts at any timesteps and light conditions

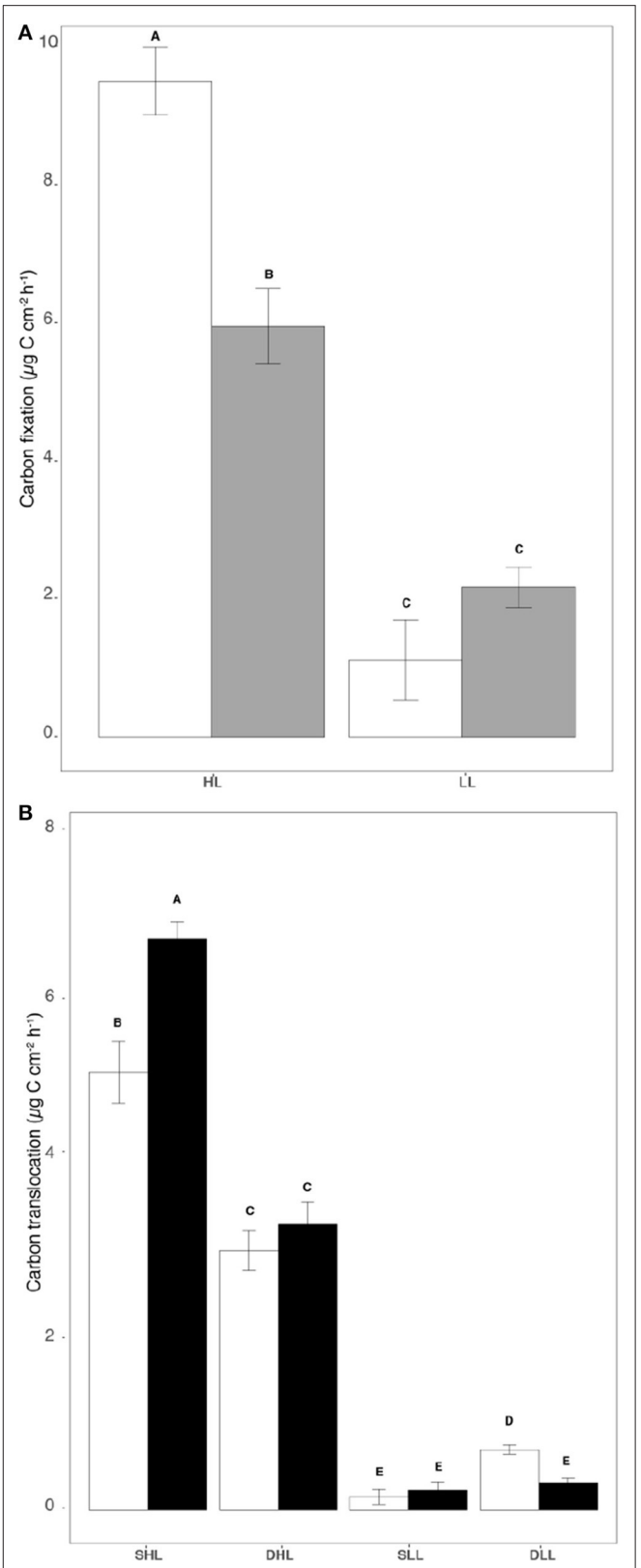

FIGURE 3 | Rates of (A) Carbon fixation (µg C cm^{-2} h^{-1}) and **(B)** Carbon translocation (µg C cm^{-2} h^{-1}) for clade A and C-holobionts according to the light intensity. Statistically significances are indicated in bold letters, *p*-values are considered for $p < 0.05$.

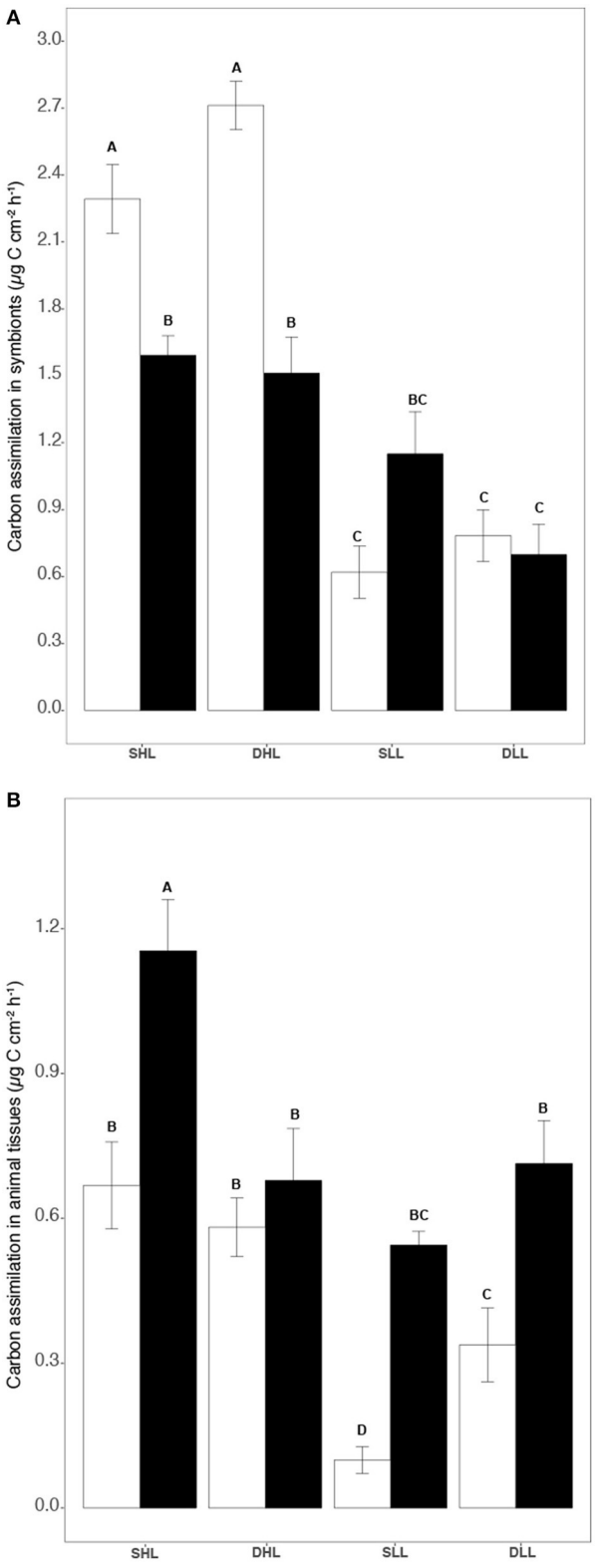

FIGURE 4 | (A) Carbon incorporation rates (μg C cm^{-2} h^{-1}) in symbionts and **(B)** in host for both clade A and C-holobionts according to the different fractions (algal and animal tissue), light intensities (LL/HL), and timesteps (T_0, T_{24}). Statistically significances are indicated in bold letters, *p*-values are considered for $p < 0.05$.

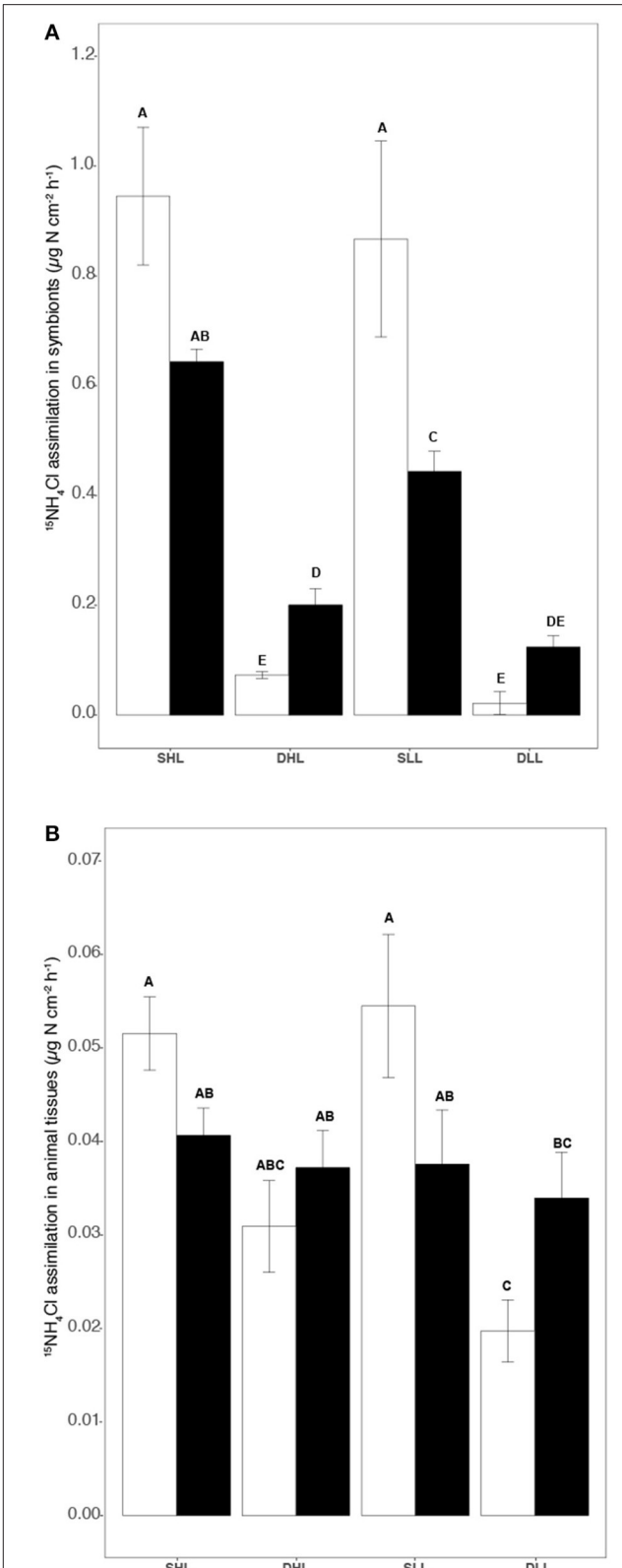

FIGURE 5 | Rates of (A) $^{15}NH_4$ assimilation in symbionts and **(B)** $^{15}NO_3$ host (μg N h^{-1} cm^{-2}) according to the different fractions (algal and animal tissue), light intensities (LL/HL), and timesteps (T_0, T_{24}). Statistically significances are indicated in bold letters, *p*-values are considered for $p < 0.05$.

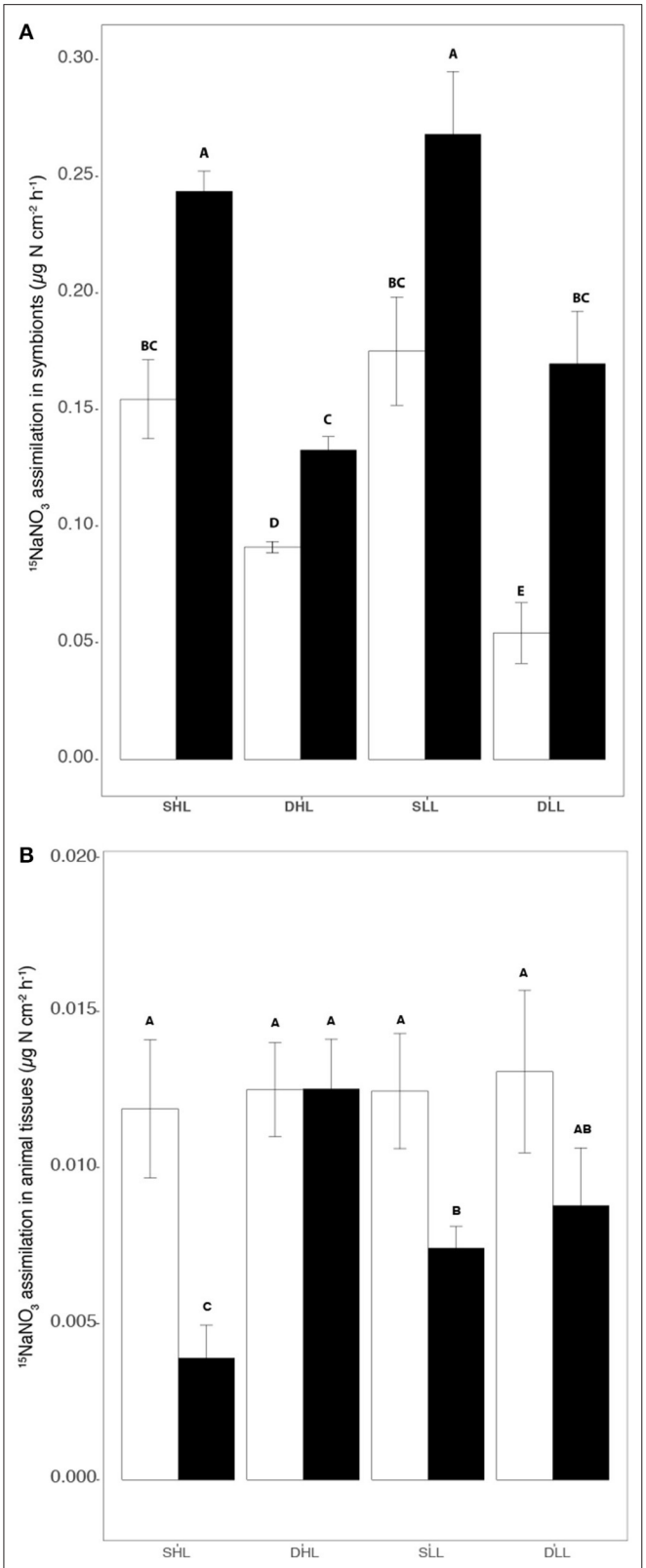

FIGURE 6 | Rates of (A) $^{15}NO_3$ assimilation in symbionts and **(B)** host (μg N h^{-1} cm^{-2}) according to the different fractions (algal and animal tissue), light intensities (LL/HL), and timesteps (T_0, T_{24}). Statistically significances are indicated in bold letters, *p*-values are considered for $p < 0.05$.

(**Figures 6A,B**; Table S3; Tukey HSD, $p < 0.0001$). Clade effect was also very important as clade A-symbionts assimilated ca. 38 and 67% more NO_3 than clade C-symbionts depending on the fraction and time of incubation (Table S3, ANOVA, $p < 0.001$). In addition, the difference between T_0 and T_{24} in the assimilation rates showed that clade A symbionts translocated 14.3% of the NO_3 assimilated while clade C symbionts translocated 19.4%. An increase in the rate of NO_3 assimilation was also observed between T_0 and T_{24} in both clade C and clade A symbionts at any timesteps and light intensities (Table S3; Tukey HSD, $p < 0.05$), except for clade A symbionts exposed to low light (Tukey HSD, $p > 0.05$).

C:N Structural

A significant interaction was observed between the fractions (host/symbionts) and the symbiont clade for the structural C:N ratio (Figure S5, Table S4, ANOVA, $p < 0.001$). The observed difference in C:N between holobionts were due to (1) lower carbon content (μmol C mg^{-1}) of clade C holobionts, mainly in the host (Tukey HSD, $p < 0.05$; Figure S2); and to (2) lower nitrogen content (μmol N mg^{-1}) of clade C- holobionts in both the host and symbionts (Figures S3, S4;Tukey HSD, $p < 0.05$). In addition, clade C symbionts showed higher C:N ratio compared to clade A symbionts (Table S4; Tukey HSD, $p < 0.05$).

Correlation between Studied Parameters

A significant positive correlation was observed between the carbon fixation and translocation rates (**Figure 7A**; $r = 0.918$; d.f. $= 18$; $p < 0.05$). Significant negative correlations were observed between (a) the NH_4 assimilation and feeding rates (**Figure 7B**, $r = -0.737$; d.f $= 18$; $p < 0.05$), (b) the NO_3 assimilation and feeding rates (**Figure 7C**; $r = -0.853$; d.f $= 18$; $p < 0.05$).

DISCUSSION

This study assessed several aspects of the trophic ecology of the Red Sea coral *S. pistillata* associated with *Symbiodinium* clade A in shallow waters and clade C in deep environments (Winters et al., 2003; Mass et al., 2007) forming two different holobionts (Rohwer et al., 2002). The main finding is that clade C-holobionts presented a competitive advantage for the acquisition of carbon at low irradiance compared to clade A-holobionts. This observation is critical to explain the capacity of *S. pistillata* to colonize deep environments in the Red Sea. In addition, light was the primary factor that determined a positive relationship between the amount of carbon fixed in photosynthesis by the symbionts and the amount of carbon translocated to the host. *Symbiodinium* genotype was the primary factor influencing nitrogen assimilation rates, although light still played a relevant role in this relationship. Lastly, we observed a negative relationship between feeding rates and inorganic nitrogen assimilation rates. Overall, our results suggest that hosting different symbiont types allows the scleractinian species *S. pistillata* to colonize both shallow and deep environments in the Red Sea.

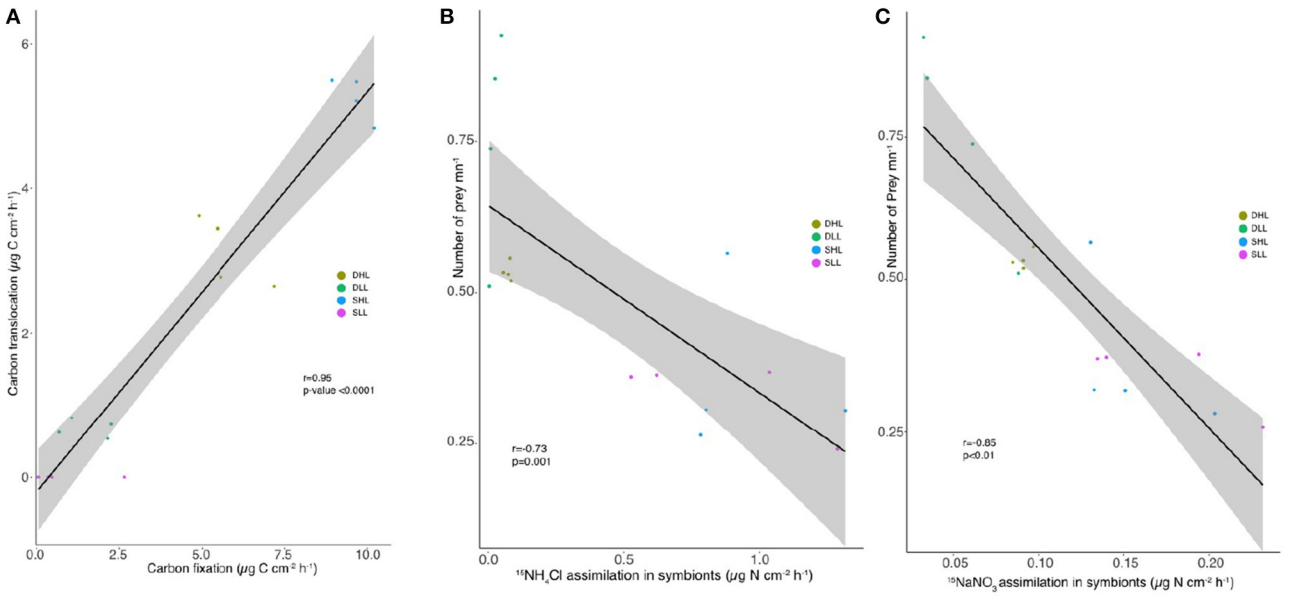

FIGURE 7 | Relationships between (A) rates of carbon fixation (µg C cm^{-2} h^{-1}) and translocation (µg C cm^{-2} h^{-1}), feeding and **(B)** $^{15}NH_4$ or **(C)** $^{15}NO_3$ assimilation rates for clade A and C-holobionts according to the light intensity after 5 h incubation.

Acquisition of Inorganic Nitrogen

The *Symbiodinium* genotype associated with shallow and deep *S. pistillata* was one of the primary factors influencing the rates of nitrogen assimilation and translocation. Clade A-holobionts indeed presented higher NH_4 and NO_3 assimilation rates than clade C-holobionts, independently of the irradiance received during the incubation, and for the same nutrient history (comparable inorganic nutrient levels at 5 and 50 m depth *in situ*, during the sampling month). Consistent with this finding, two recent studies (Baker et al., 2013; Pernice et al., 2015) found that rates of nitrogen acquisition by *Acroporidae* species (*A. tenuis* and *I. palifera,* respectively) were also clade dependent.

Light intensity/history was the second important factor explaining differences in nitrogen assimilation rates between the two holobionts. The importance of light was evidenced by the fact that (i) clade A-holobionts, which came from the highly-lit shallow reef, and which presented a high metabolic activity, showed higher rates of both NO_3 and NH_4 assimilation than clade C-holobionts, sampled in deep environment; (ii) NH_4 assimilation by clade C-holobionts was higher at 350 µmol photons m^{-2} s^{-1} than at 20 µmol photons m^{-2} s^{-1}. According to previous observations made on other photosynthetic organisms (Canvin and Atkins, 1974; Amory et al., 1991) or on coral symbionts in culture (Rodríguez-Román and Iglesias-Prieto, 2005) and *in hospite* (Grover et al., 2002), light can have a direct effect on nitrogen assimilation; this later process is indeed closely dependent on the amount of electrons that can be supplied by the ferredoxin, through the linear electron flow between photosystems I and II. Light can also have an indirect effect on nitrogen assimilation, by changing the metabolic activity of the holobionts. The low C and N contents of clade C-holobionts compared to clade A-holobionts are indicative of a lower metabolic activity, which in turn can lead to lower nitrogen requirements. On the contrary, survival in high light environments for clade A-holobionts can increase both their metabolic activity and their nitrogen demand to repair light-damaged photosystems (Dubinsky and Jokiel, 1994; Dubinsky and Falkowski, 2011).

In addition, the higher assimilation of inorganic nitrogen by clade A-holobiont may compensate for the lack of zooplankton, which is known to be much less abundant in shallow waters compared to deep environments (Schmidt, 1973; Lesser et al., 2009). Conversely, nitrogen can be acquired by clade C-holobionts in deep waters through heterotrophy (Crandall et al., 2016) or through dinitrogen fixation (Lesser et al., 2007). This is confirmed by their higher grazing rates compared to shallow holobionts and by the inverse relationship between heterotrophy and inorganic nitrogen acquisition. This negative correlation suggests that nitrogen assimilation by the holobiont needs to be supported by heterotrophic feeding when the activity of the symbionts is reduced, either due to a reduction in light availability or when the dominant symbiont type presents a reduced ability for nitrogen assimilation.

Additionally, clade A and C-holobionts of *S. pistillata* had unequal translocation rates and allocation patterns of nitrogen within the symbiosis, likely suggesting different needs of the symbionts and animal host in nitrogen. Consistent with previous results on many cnidarian species, clade A-holobionts showed a higher uptake of NH_4 compared to NO_3 (Wilkerson and Trench, 1986; Wilkerson and Kremer, 1993; Grover et al., 2002, 2003; Pernice et al., 2012), and very low translocation rates to the host. Clade A symbionts thus acted as a sink for nitrogen within the symbiosis (Wilkerson and Kremer, 1993; Grover et al., 2002; Pernice et al., 2012; Kopp et al., 2013). In contrast,

clade C-symbionts exhibited similar rates of NH_4 and NO_3 assimilation, and much higher translocation rates to the host. As a consequence, nitrogen was evenly shared between the host and its symbionts.

Carbon Budget

The depths at which *S. pistillata* colonies were sampled (5 and 50 m) account for extreme living conditions because holobionts were exposed either to high irradiance (>350 μmoles photons m^{-2} s^{-1}) or to <30 μmol photons m^{-2} s^{-1} (Cohen and Dubinsky, 2015). By establishing the carbon budget of shallow and deep holobionts of *S. pistillata*, this study first shows that clade C-holobionts have a competitive advantage for the acquisition of autotrophic carbon at low irradiance compared to clade A-holobionts, and that each holobiont has a different environmental optimum along the irradiance gradient. This study thus confirms previous observations, which concluded that *S. pistillata* acclimates to depth through photo-adaptive mechanisms linked to the *Symbiodinium* genotype hosted at each depth distribution (Cohen and Dubinsky, 2015). Overall, many coral species associate with more than one algal taxon, whose relative abundance has been correlated with irradiance gradients (Rowan and Knowlton, 1995; Rowan et al., 1997; Iglesias-Prieto et al., 2004). These changes allow the host to extend its depth range while remaining ecologically dominant. Consistent also with previous observations on deep corals (McCloskey and Muscatine, 1984; Levy et al., 2006; Mass et al., 2007; Cohen and Dubinsky, 2015), low respiration rate was another adaptation of clade C-holobionts to their deep environment. This reduction in respiratory needs maintained the P:R of clade C-holobionts, measured at low light (4.3 ± 1.7), similar to the P:R of clade A-holobionts, measured under high light (1.00 ± 0.08), suggesting that the amount of photosynthates was sufficient to cover the respiratory needs of the deep water colonies. All together, these observations indicate a niche specialization among holobionts of *S. pistillata*, allowing a maximal acquisition and utilization of carbon throughout the depth profile.

The carbon budget also showed that carbon translocation was closely related to carbon fixation in photosynthesis by the symbionts and was therefore more closely related to light availability than to clade identity. This observation is in agreement with a previous study performed on two scleractinian corals (Tremblay et al., 2015), but challenges the hypothesis that carbon translocation is clade dependent (Leal et al., 2015). Further studies should be carried out, by taking into account different light levels and clade genotypes, to better understand this relationship.

CONCLUSION

Collectively, the results presented in this study indicate that the vertical distribution pattern of *S. pistillata* in the Red Sea, and its ability to form mesophotic reefs, can be explained by the presence of specific symbionts adapted to different light regimes. The differential use of light by clade A and C symbionts constitutes an important axis for niche diversification, controlling the abundance and distribution of *S. pistillata* along the depth gradient. Our results also show that the amount of solar energy that the holobionts absorb drives their metabolic activity, nitrogen assimilation rates and needs as well as their structural C:N content.

AUTHOR CONTRIBUTIONS

LE, CF, MF, and RG conceived the experiment. LE, CF, and MF performed the experiments. LE and CF made the extractions. JM performed the mass spectrometry analyses. LE, CF, RG, and JM analyzed the data. LE, CF, RG, MF, and JM wrote the manuscript.

ACKNOWLEDGMENTS

We would like to sincerely thank all the staff at the IUI in Eilat (IL) as well as Dr. JO Irisson from the Observatoire Océanologique de Villefranche-sur-mer (LOV) for his constructive comments and help with the statistical analyses, Vanessa Bednarz and Jérôme Durivault from the CSM. Many thanks to Prof. Denis Allemand, Director of the Centre Scientifique de Monaco for scientific support. Lastly, we would like to thank three reviewers for their constructive comments and time spent on revising our manuscript. This project was supported by the IUI, the Israel Science Foundation for MF, the CSM and the Institut Européen de la mer. Financial support to LE was provided by the Centre Scientifique de Monaco.

SUPPLEMENTARY MATERIAL

The Supplementary Material for this article can be found online at: http://journal.frontiersin.org/article/10.3389/fmars.2017.00102/full#supplementary-material

REFERENCES

Abrego, D., Ulstrup, K. E., Willis, B. L., and van Oppen, M. J. (2008). Species–specific interactions between algal endosymbionts and coral hosts define their bleaching response to heat and light stress. *Proc. R. Soc. Lond. B Biol. Sci.* 275, 2273–2282. doi: 10.1098/rspb.2008.0180

Alamaru, A., Loya, Y., Brokovich, E., Yam, R., and Shemesh, A. (2009). Carbon and nitrogen utilization in two species of Red Sea corals along a depth gradient: insights from stable isotope analysis of total organic material and lipids. *Geochim. Cosmochim. Acta* 73, 5333–5342. doi: 10.1016/j.gca.2009.06.018

Amory, A. M., Vanlerberghe, G. C., and Turpin, D. H. (1991). Demonstration of both a photosynthetic and a nonphotosynthetic CO_2 requirement for NH_4^+ assimilation in the green alga *Selenastrum minutum*. *Plant Physiol.* 95, 192–196. doi: 10.1104/pp.95.1.192

Anthony, K. R. N., and Fabricius, K. E. (2000). Shifting roles of heterotrophy and autotrophy in coral energetics under varying turbidity. *J. Exp. Mar. Bio. Ecol.* 252, 221–253.

Baker, D. M., Andras, J. P., Jordán-Garza, A. G., and Fogel, M. L. (2013). Nitrate competition in a coral symbiosis varies with temperature among *Symbiodinium* clades. *ISME J.* 7, 1248–1251. doi: 10.1038/ismej.2013.12

Bednarz, V. N., Grover, R., Maguer, J.-F., Fine, M., and Ferrier-Pagès, C. (2017). The assimilation of diazotroph-derived nitrogen by scleractinian corals depends on their metabolic status. *Mbio* 8:e02058–16. doi: 10.1128/mBio.02058-16

Berkelmans, R., and van Oppen, M. J. (2006). The role of zooxanthellae in the thermal tolerance of corals: a 'nugget of hope' for coral reefs in an era of climate change. *Proc. R. Soc. Lond. B Biol. Sci.* 273, 2305–2312. doi: 10.1098/rspb.2006.3567

Brazeau, D. A., Lesser, M. P., and Slattery, M. (2013). Genetic structure in the coral, *Montastraea cavernosa*: assessing genetic differentiation among and within mesophotic reefs. *PLoS ONE* 8:e65845. doi: 10.1371/journal.pone.0065845

Byler, K. A., Carmi-Veal, M., Fine, M., and Goulet, T. L. (2013). Multiple symbiont acquisition strategies as an adaptive mechanism in the coral *Stylophora pistillata*. *PLoS ONE* 8:e59596. doi: 10.1371/journal.pone.0059596

Canvin, D. T., and Atkins, C. A. (1974). Nitrate, nitrite and ammonia assimilation by leaves: effect of light, carbon dioxide and oxygen. *Planta* 116, 207–224. doi: 10.1007/BF00390228

Cohen, I., and Dubinsky, Z. (2015). Long term photoacclimation responses of the coral *Stylophora pistillata* to reciprocal deep to shallow transplantation: photosynthesis and calcification. *Front. Mar. Sci.* 2:45. doi: 10.3389/fmars.2015.00045

Crandall, J., Teece, M., Estes, B., Manfrino, C., and Ciesla, J. (2016). Nutrient acquisition strategies in mesophotic hard corals using compound specific stable isotope analysis of sterols. *J. Exp. Mar. Biol. Ecol.* 474, 133–141. doi: 10.1016/j.jembe.2015.10.010

Davies, P. S. (1989). Short-term growth measurements of corals using an accurate buoyant weighing technique. *Mar. Biol.* 101, 389–395. doi: 10.1007/BF00428135

Dubinsky, Z., and Falkowski, P. (2011). "Light as a source of information and energy in zooxanthellate corals," in *Coral Reefs: An Ecosystem in Transition,* eds Z. Dubinsky and N. Stambler (Springer), 107–118.

Dubinsky, Z., and Jokiel, P. L. (1994). Ratio of energy and nutrient fluxes regulates symbiosis between zooxanthellae and corals. *Pac. Sci.* 48, 313–324.

Einbinder, S., Mass, T., Brokovich, E., Dubinsky, Z., Erez, J., and Tchernov, D. (2009). Changes in morphology and diet of the coral *Stylophora pistillata* along a depth gradient. *Mar. Ecol. Prog. Ser.* 381, 167–174. doi: 10.3354/meps07908

Ferrier-Pages, C., Gattuso, J.-P., Dallot, S., and Jaubert, J. (2000). Effect of nutrient enrichment on growth and photosynthesis of the zooxanthellate coral *Stylophora pistillata*. *Coral Reefs* 19, 103–113. doi: 10.1007/s003380000078

Ferrier-Pagès, C., Rottier, C., Beraud, E., and Levy, O. (2010). Experimental assessment of the feeding effort of three scleractinian coral species during a thermal stress: effect on the rates of photosynthesis. *J. Exp. Mar. Biol. Ecol.* 390, 118–124. doi: 10.1016/j.jembe.2010.05.007

Finney, J. C., Pettay, D. T., Sampayo, E. M., Warner, M. E., Oxenford, H. A., and LaJeunesse, T. C. (2010). The relative significance of host–habitat, depth, and geography on the ecology, endemism, and speciation of coral endosymbionts in the genus *Symbiodinium*. *Microb. Ecol.* 60, 250–263. doi: 10.1007/s00248-010-9681-y

Gattuso, J. P., and Jaubert, J. (1990). Effect of light on oxygen and carbon dioxide fluxes and on metabolic quotients measured *in situ* in a zooxanthellate coral. *Limnol. Oceanogr.* 35, 1796–1804. doi: 10.4319/lo.1990.35.8.1796

Grover, R., Maguer, J.-F., Allemand, D., and Ferrier-Pages, C. (2003). Nitrate uptake in the scleractinian coral *Stylophora pistillata*. *Limnol. Oceanogr.* 48, 2266–2274. doi: 10.4319/lo.2003.48.6.2266

Grover, R., Maguer, J.-F., Reynaud-Vaganay, S., and Ferrier-Pages, C. (2002). Uptake of ammonium by the scleractinian coral *Stylophora pistillata*: effect of feeding, light, and ammonium concentrations. *Limnol. Oceanogr.* 47, 782–790. doi: 10.4319/lo.2002.47.3.0782

Hinderstein, L. M., Marr, J. C. A., Martinez, F. A., Dowgiallo, M. J., Puglise, K. A., Pyle, R. L., et al. (2010). Theme section on "Mesophotic coral ecosystems: characterization, ecology, and management". *Coral Reefs* 29, 247–251. doi: 10.1007/s00338-010-0614-5

Houlbreque, F., and Ferrier-Pagès, C. (2009). Heterotrophy in tropical scleractinian corals. *Biol. Rev.* 84, 1–17. doi: 10.1111/j.1469-185X.2008.00058.x

Houlbrèque, F., Tambutté, E., Allemand, D., and Ferrier-Pagès, C. (2004). Interactions between zooplankton feeding, photosynthesis and skeletal growth in the scleractinian coral *Stylophora pistillata*. *J. Exp. Biol.* 207, 1461–1469. doi: 10.1242/jeb.00911

Hovland, M. (2008). *Deep-Water Coral Reefs: Unique Biodiversity Hot-Spots*. Springer Science & Business Media.

Howells, E., Beltran, V., Larsen, N., Bay, L., Willis, B., and van Oppen, M. (2012). Coral thermal tolerance shaped by local adaptation of photosymbionts. *Nat. Clim. Chang.* 2, 116–120. doi: 10.1038/nclimate1330

Hume, B. C. C., Voolstra, C. R., Arif, C., D'Angelo, C., Burt, J. A., Eyal, G., et al. (2016). Ancestral genetic diversity associated with the rapid spread of stress-tolerant coral symbionts in response to Holocene climate change. *Proc. Natl. Acad. Sci. U.S.A.* 113, 4416–4421. doi: 10.1073/pnas.1601910113

Iglesias-Prieto, R., Beltran, V., LaJeunesse, T., Reyes-Bonilla, H., and Thome, P. (2004). Different algal symbionts explain the vertical distribution of dominant reef corals in the eastern Pacific. *Proc. R. Soc. Lond. B Biol. Sci.* 271, 1757–1763. doi: 10.1098/rspb.2004.2757

Jeffrey, S., and Humphrey, G. (1975). New spectrophotometric equations for determining chlorophylls *a, b, c1* and *c2* in higher plants, algae and natural phytoplankton. *Biochem. Physiol. Pflanz BPP* 167, 191–194. doi: 10.1016/S0015-3796(17)30778-3

Jones, A., and Berkelmans, R. (2010). Potential costs of acclimatization to a warmer climate: growth of a reef coral with heat tolerant vs. sensitive symbiont types. *PLoS ONE* 5:e10437. doi: 10.1371/journal.pone.0010437

Kahng, S., Garcia-Sais, J. R., Spalding, H. L., Brokovich, E., Wagner, D., Weil, E., et al. (2010). Community ecology of mesophotic coral reef ecosystems. *Coral Reefs* 29, 255–275. doi: 10.1007/s00338-010-0593-6

Kemp, D. W., Thornhill, D. J., Rotjan, R. D., Iglesias-Prieto, R., Fitt, W. K., and Schmidt, G. W. (2015). Spatially distinct and regionally endemic *Symbiodinium* assemblages in the threatened Caribbean reef-building coral *Orbicella faveolata*. *Coral Reefs* 34, 535–547. doi: 10.1007/s00338-015-1277-z

Kopp, C., Pernice, M., Domart-Coulon, I., Djediat, C., Spangenberg, J. E., Alexander, D. T. L., et al. (2013). Highly dynamic cellular-level response of symbiotic coral to a sudden increase in environmental nitrogen. *MBio* 4:e00052–13. doi: 10.1128/mBio.00052-13

Lampert-Karako, S., Stambler, N., Katcoff, D. J., Achituv, Y., Dubinsky, Z., and Simon-Blecher, N. (2008). Effects of depth and eutrophication on the zooxanthella clades of *Stylophora pistillata* from the Gulf of Eilat (Red Sea). *Aquat. Conserv.* 18, 1039. doi: 10.1002/aqc.927

Leal, M. C., Hoadley, K., Pettay, D. T., Grajales, A., Calado, R., and Warner, M. E. (2015). Symbiont type influences trophic plasticity of a model cnidarian–dinoflagellate symbiosis. *J. Exp. Biol.* 218, 858–863. doi: 10.1242/jeb.115519

Leichter, J. J., and Genovese, S. J. (2006). Intermittent upwelling and subsidized growth of the scleractinian coral *Madracis mirabilis* on the deep fore-reef slope of Discovery Bay, Jamaica. *Mar. Ecol. Prog. Ser.* 316, 95–103. doi: 10.3354/meps316095

Lesser, M. (2013). Using energetic budgets to assess the effects of environmental stress on corals: are we measuring the right things? *Coral Reefs* 32, 25–33. doi: 10.1007/s00338-012-0993-x

Lesser, M., Stat, M., and Gates, R. (2013). The endosymbiotic dinoflagellates (*Symbiodinium* sp.) of corals are parasites and mutualists. *Coral Reefs* 32, 603–611. doi: 10.1007/s00338-013-1051-z

Lesser, M. P., Falcón, L. I., Rodríguez-Román, A., Enríquez, S., Hoegh-Guldberg, O., and Iglesias-Prieto, R. (2007). Nitrogen fixation by symbiotic cyanobacteria provides a source of nitrogen for the scleractinian coral *Montastraea cavernosa*. *Mar. Ecol. Prog. Ser.* 346, 143–152. doi: 10.3354/meps07008

Lesser, M. P., Mazel, C., Phinney, D., and Yentsch, C. S. (2000). Light absorption and utilization by colonies of the congeneric hermatypic corals *Montastraea faveolata* and *Montastraea cavernosa*. *Limnol. Oceanogr.* 45, 76–86. doi: 10.4319/lo.2000.45.1.0076

Lesser, M. P., Slattery, M., and Leichter, J. J. (2009). Ecology of mesophotic coral reefs. *J. Exp. Mar. Biol. Ecol.* 375, 1–8. doi: 10.1016/j.jembe.2009.05.009

Lesser, M. P., Slattery, M., Stat, M., Ojimi, M., Gates, R. D., and Grottoli, A. (2010). Photoacclimatization by the coral *Montastraea cavernosa* in the mesophotic zone: light, food, and genetics. *Ecology* 91, 990–1003. doi: 10.1890/09-0313.1

Levy, O., Achituv, Y., Yacobi, Y., Dubinsky, Z., and Stambler, N. (2006). Diel 'tuning' of coral metabolism, physiological responses to light cues. *J. Exp. Biol.* 209, 273–283. doi: 10.1242/jeb.01983

Little, A. F., Van Oppen, M. J., and Willis, B. L. (2004). Flexibility in algal endosymbioses shapes growth in reef corals. *Science* 304, 1492–1494. doi: 10.1126/science.1095733

Loram, J., Trapido-Rosenthal, H., and Douglas, A. (2007). Functional significance of genetically different symbiotic algae *Symbiodinium* in a coral reef symbiosis. *Mol. Ecol.* 16, 4849–4857. doi: 10.1111/j.1365-294X.2007.03491.x

Mass, T., Einbinder, S., Brokovich, E., Shashar, N., Vago, R., Erez, J., et al. (2007). Photoacclimation of *Stylophora pistillata* to light extremes: metabolism and calcification. *Mar. Ecol. Prog. Ser.* 334, 93–102. doi: 10.3354/meps334093

McCloskey, L., and Muscatine, L. (1984). Production and respiration in the Red Sea coral *Stylophora pistillata* as a function of depth. *Proc. R. Soc. Lond. B Biol. Sci.* 222, 215–230. doi: 10.1098/rspb.1984.0060

Montoya, J. P., Voss, M., Kahler, P., and Capone, D. G. (1996). A simple, high-precision, high-sensitivity tracer assay for N (inf2) fixation. *Appl. Environ. Microbiol.* 62, 986–993.

Muscatine, L. (1990). The role of symbiotic algae in carbon and energy flux in reef corals. *Ecosyst. World* 25, 75–87.

Muscatine, L., Falkowski, P., Dubinsky, Z., Cook, P., and McCloskey, L. (1989). The effect of external nutrient resources on the population dynamics of zooxanthellae in a reef coral. *Proc. R. Soc. Lond. B Biol. Sci.* 236, 311–324. doi: 10.1098/rspb.1989.0025

Muscatine, L., Falkowski, P., Porter, J., and Dubinsky, Z. (1984). Fate of photosynthetic fixed carbon in light-and shade-adapted colonies of the symbiotic coral *Stylophora pistillata*. *Proc. R. Soc. Lond. B Biol. Sci.* 222, 181–202. doi: 10.1098/rspb.1984.0058

Muscatine, L., and Porter, J. W. (1977). Reef corals: mutualistic symbioses adapted to nutrient-poor environments. *Bioscience* 27, 454–460. doi: 10.2307/1297526

Nir, O., Gruber, D., Einbinder, S., Kark, S., and Tchernov, D. (2011). Changes in scleractinian coral *Seriatopora hystrix* morphology and its endocellular *Symbiodinium* characteristics along a bathymetric gradient from shallow to mesophotic reef. *Coral Reefs* 30, 1089–1100. doi: 10.1007/s00338-011-0801-z

Nir, O., Gruber, D. F., Shemesh, E., Glasser, E., and Tchernov, D. (2014). Seasonal mesophotic coral bleaching of *Stylophora pistillata* in the Northern Red Sea. *PLoS ONE* 9:e84968. doi: 10.1371/journal.pone.0084968

Pernice, M., Meibom, A., Van Den Heuvel, A., Kopp, C., Domart-Coulon, I., Hoegh-Guldberg, O., et al. (2012). A single-cell view of ammonium assimilation in coral–dinoflagellate symbiosis. *ISME J.* 6, 1314–1324. doi: 10.1038/ismej.2011.196

Pernice, M., Dunn, S. R., Tonk, L., Dove, S., Domart-Coulon, I., Hoppe, P., et al. (2015). A nanoscale secondary ion mass spectrometry study of dinoflagellate functional diversity in reef?building corals. *Environ. Microbiol.* 17, 3570–3580. doi: 10.1111/1462-2920.12518

Rodríguez-Román, A., and Iglesias-Prieto, R. (2005). Regulation of photochemical activity in cultured symbiotic dinoflagellates under nitrate limitation and deprivation. *Mar. Biol.* 146, 1063–1073. doi: 10.1007/s00227-004-1529-x

Rohwer, F., Seguritan, V., Azam, F., and Knowlton, N. (2002). Diversity and distribution of coral-associated bacteria. *Mar. Ecol. Prog. Ser.* 243, 1–10. doi: 10.3354/meps243001

Rowan, R., and Knowlton, N. (1995). Intraspecific diversity and ecological zonation in coral-algal symbiosis. *Proc. Natl. Acad. Sci. U.S.A.* 92, 2850–2853. doi: 10.1073/pnas.92.7.2850

Rowan, R., Knowlton, N., Baker, A., and Jara, J. (1997). Landscape ecology of algal symbionts creates variation in episodes of coral bleaching. *Nature* 388, 265–269. doi: 10.1038/40843

Santos, S. R., Taylor, D. J., Kinzie, R. A. III, Hidaka, M., Sakai, K., and Coffroth, M. A. (2002). Molecular phylogeny of symbiotic dinoflagellates inferred from partial chloroplast large subunit (23S)-rDNA sequences. *Mol. Phylogenet. Evol.* 23, 97–111. doi: 10.1016/S1055-7903(02)00010-6

Schmidt, H.-E. (1973). The vertical distribution and diurnal migration of some zooplankton in the Bay of Eilat (Red Sea). *Helgoländer Wiss. Meeresunters.* 24, 333–340. doi: 10.1007/BF01609523

Silverstein, R. N., Cunning, R., and Baker, A. C. (2015). Change in algal symbiont communities after bleaching, not prior heat exposure, increases heat tolerance of reef corals. *Glob. Chang. Biol.* 21, 236–249. doi: 10.1111/gcb.12706

Starzak, D. E., Quinnell, R. G., Nitschke, M. R., and Davy, S. K. (2014). The influence of symbiont type on photosynthetic carbon flux in a model cnidarian–dinoflagellate symbiosis. *Mar. Biol.* 161, 711–724. doi: 10.1007/s00227-013-2372-8

Stat, M., Morris, E., and Gates, R. D. (2008). Functional diversity in coral–dinoflagellate symbiosis. *Proc. Natl. Acad. Sci. U.S.A.* 105, 9256–9261. doi: 10.1073/pnas.0801328105

Tremblay, P., Grover, R., Maguer, J. F., Legendre, L., and Ferrier-Pagès, C. (2012). Autotrophic carbon budget in coral tissue: a new ^{13}C-based model of photosynthate translocation. *J. Exp. Biol.* 215, 1384–1393. doi: 10.1242/jeb.065201

Tremblay, P., Maguer, J. F., Grover, R., and Ferrier-Pagès, C. (2015). Trophic dynamics of scleractinian corals: stable isotope evidence. *J. Exp. Biol.* 218, 1223–1234. doi: 10.1242/jeb.115303

Venn, A., Loram, J., Trapido-Rosenthal, H., Joyce, D., and Douglas, A. (2008). Importance of time and place: patterns in abundance of *Symbiodinium* clades A and B in the tropical sea anemone *Condylactis gigantea*. *Biol. Bull.* 215, 243–252. doi: 10.2307/25470708

Wilkerson, F. P., and Kremer, P. (1993). DIN, DON and PO_4 flux by a medusa with algal symbionts. *Mar. Ecol. Prog. Ser.* 90, 237–237. doi: 10.3354/meps090237

Wilkerson, F., and Trench, R. (1986). Uptake of dissolved inorganic nitrogen by the symbiotic clam *Tridacna gigas* and the coral *Acropora* sp. *Mar. Biol.* 93, 237–246. doi: 10.1007/BF00508261

Winters, G., Beer, S., Zvi, B. B., Brickner, I., and Loya, Y. (2009). Spatial and temporal photoacclimation of *Stylophora pistillata*: zooxanthella size, pigmentation, location and clade. *Mar. Ecol. Prog. Ser.* 384, 107–119. doi: 10.3354/meps08036

Winters, G., Loya, Y., Rottgers, R., and Beer, S. (2003). Photoinhibition in shallow-water colonies of the coral *Stylophora pistillata* as measured *in situ*. *Limnol. Oceanogr.* 48, 1388–1393. doi: 10.4319/lo.2003.48.4.1388

Wyman, K., Dubinsky, Z., Porter, J., and Falkowski, P. (1987). Light absorption and utilization among hermatypic corals: a study in Jamaica, West Indies. *Mar. Biol.* 96, 283–292. doi: 10.1007/BF00427028

Conflict of Interest Statement: The authors declare that the research was conducted in the absence of any commercial or financial relationships that could be construed as a potential conflict of interest.

The handling Editor declared a shared affiliation, though no other collaboration, with one of the authors MF and states that the process nevertheless met the standards of a fair and objective review.

frontiers in Microbiology

ORIGINAL RESEARCH
published: 22 May 2017
doi: 10.3389/fmicb.2017.00784

Bacterial Community Associated with the Reef Coral *Mussismilia braziliensis's* Momentum Boundary Layer over a Diel Cycle

Cynthia B. Silveira[1,2], Gustavo B. Gregoracci[3], Felipe H. Coutinho[1,4], Genivaldo G. Z. Silva[5], John M. Haggerty[2], Louisi S. de Oliveira[1], Anderson S. Cabral[1], Carlos E. Rezende[6], Cristiane C. Thompson[1], Ronaldo B. Francini-Filho[7], Robert A. Edwards[5], Elizabeth A. Dinsdale[1] and Fabiano L. Thompson[1,8]**

[1] Instituto de Biologia, Universidade Federal do Rio de Janeiro, Rio de Janeiro, Brazil, [2] Department of Biology, San Diego State University, San Diego, CA, USA, [3] Universidade Federal de São Paulo - Baixada Santista, Santos, Brazil, [4] Centre for Molecular and Biomolecular Informatics, Radboud Institute for Molecular Life Sciences, Radboud University Medical Centre, Nijmegen, Netherlands, [5] Department of Computational Science, San Diego State University, San Diego, CA, USA, [6] Laboratório de Ciências Ambientais, Universidade Estadual do Norte Fluminense, Campos dos Goytacazes, Brazil, [7] Departamento de Engenharia e Meio Ambiente, Universidade Federal da Paraíba, Rio Tinto, Brazil, [8] Laboratório de Sistemas Avançados de Gestão da Produção, COPPE, Universidade Federal do Rio de Janeiro, Rio de Janeiro, Brazil

Corals display circadian physiological cycles, changing from autotrophy during the day to heterotrophy during the night. Such physiological transition offers distinct environments to the microbial community associated with corals: an oxygen-rich environment during daylight hours and an oxygen-depleted environment during the night. Most studies of coral reef microbes have been performed on samples taken during the day, representing a bias in the understanding of the composition and function of these communities. We hypothesized that coral circadian physiology alters the composition and function of microbial communities in reef boundary layers. Here, we analyzed microbial communities associated with the momentum boundary layer (MBL) of the Brazilian endemic reef coral *Mussismilia braziliensis* during a diurnal cycle, and compared them to the water column. We determined microbial abundance and nutrient concentration in samples taken within a few centimeters of the coral's surface every 6 h for 48 h, and sequenced microbial metagenomes from a subset of the samples. We found that dominant taxa and functions in the coral MBL community were stable over the time scale of our sampling, with no significant shifts between night and day samples. Interestingly, the two water column metagenomes sampled 1 m above the corals were also very similar to the MBL metagenomes. When all samples were analyzed together, nutrient concentration significantly explained 40% of the taxonomic dissimilarity among dominant genera in the community. Functional profiles were highly homogenous and not significantly predicted by any environmental variables measured. Our data indicated that water flow may overrule the effects of coral physiology in the MBL bacterial community, at the scale of centimeters, and suggested that sampling resolution at the scale of millimeters may be necessary to address diurnal variation in community composition.

Keywords: coral reef microbiome, diurnal cycle, Abrolhos, coral momentum boundary layer, coral physiology, coral mucus

OPEN ACCESS

Edited by:
Michael Kühl,
University of Copenhagen, Denmark

Reviewed by:
Haiwei Luo,
The Chinese University of Hong Kong, Hong Kong
Paulina Kaniewska,
The University of Queensland, Australia
Michael Sweet,
University of Derby, UK
Pedro Rodrigues Frade,
University of the Algarve, Portugal

****Correspondence:***
Cynthia B. Silveira
cynthiabsilveira@gmail.com
Fabiano Thompson
fabianothompson1@gmail.com

Specialty section:
This article was submitted to Aquatic Microbiology, a section of the journal Frontiers in Microbiology

Received: *01 August 2016*
Accepted: *18 April 2017*
Published: *22 May 2017*

Citation:
Silveira CB, Gregoracci GB, Coutinho FH, Silva GGZ, Haggerty JM, de Oliveira LS, Cabral AS, Rezende CE, Thompson CC, Francini-Filho RB, Edwards RA, Dinsdale EA and Thompson FL (2017) Bacterial Community Associated with the Reef Coral Mussismilia braziliensis's Momentum Boundary Layer over a Diel Cycle. Front. Microbiol. 8:784. doi: 10.3389/fmicb.2017.00784

INTRODUCTION

The rules governing associations between bacteria and corals represent a current theme of debate (Thompson et al., 2015; Douglas and Werren, 2016; Theis et al., 2016). Temporal dynamics of bacterial community composition and functional roles in coral holobionts add important information to this debate (Garren and Azam, 2012; Bourne et al., 2016). The majority of studies on the changes in coral bacterial community composition over time have been focused on stress and disease conditions (Ritchie, 2006; Garren et al., 2009; Sweet et al., 2014; Zaneveld et al., 2016). However, coral-associated bacteria can change over coral animal developmental stages and natural mucus aging (Apprill et al., 2009; Sweet et al., 2011b; Sharp et al., 2012; Glasl et al., 2016). When colony size is utilized as a proxy for age, bacterial community diversity in the coral *Coelastrea aspera* increases in a step-wise pattern from juveniles to medium colonies, decreasing again in older, larger colonies (Williams et al., 2015). Short time scale changes in response to tides have also been reported in *C. aspera*, and are dependent of colony age (Sweet et al., 2017). Understanding the dynamics of coral-microbe associations over time is necessary in order to predict coral's response to disturbance and design manipulation strategies to improve coral resilience (Ainsworth and Gates, 2016; Sweet and Brown, 2016).

Corals experience fundamental physiological changes in response to light availability over day–night cycles. They switch from autotrophic holobionts during the day, when intracellular zooxanthellae produce carbon surpluses through photosynthesis, to heterotrophs during the night, when polyps prey on zooplankton (Shashar et al., 1993; Anthony and Fabricius, 2000). Animal tissue respiration is higher at night and early morning compared to the afternoon due to digestion of prey captured at night (Schneider et al., 2009). This physiologic switch results in hyperoxic conditions in the holobiont during the day, and hypoxia during the night, with the polyp oral cavity becoming almost anoxic (Shashar et al., 1993; Haas et al., 2013). Coral respiration and calcification also reduces the pH of the surrounding environment during the night (Smith et al., 2013). Coral's molecular responses to light, pH, and redox potential changes over the day includes overexpression of cryptochromes, antioxidant enzymes such as catalase and carbonic anhydrase, which may explain light-enhanced coral calcification (Chalker and Taylor, 1975; Levy et al., 2011). Increased expression of protective enzymes against reactive oxygen species, such as superoxide dismutase and catalase is reflected in enhanced activity of these enzymes during the day, a protective mechanism for the cnidarian-zooxanthellae association (Levy et al., 2006). Enzymes involved in glycolysis and several biosynthetic pathways are among the ones overexpressed during the night (Levy et al., 2011). Diel transcriptomic patterns of photoreceptors, putative circadian regulation genes, stress response genes, and metabolic genes were also observed in the coral *Acropora cervicornis* (Hemond and Vollmer, 2015). The production of microsporine-like aminoacids follows sunlight cycles, and it is speculated to protect corals from ultraviolet radiation damage (Yakovleva and Hidaka, 2004). Microbes recycle up to 45% of the carbon fixed by *Symbiodinium* and exuded as coral mucus, highlighting bacterial dependence on coral physiology for growth (Brown and Bythell, 2005). Changes in oxygen availability and pH in coral tissues are expected to reflect changes in microbial community composition and metabolism. Nevertheless, virtually all studies on coral-associated and reef microbiomes are based on samples taken during the day due to logistical restrictions. This sampling bias could heavily distort the understanding of microbial community composition and function in the coral holobiont.

Biological rhythms often account for periodicity in host–parasite interactions in many animal models (Martinez-Bakker and Helm, 2015). In corals, diel physiological changes are important in black band disease development by interfering with the metabolism of coral-associated Cyanobacteria (Carlton and Richardson, 1995). Although anoxic conditions are consistently maintained at the coral–mat interface, sulfide production at night accelerates band progression by creating a toxic environment for coral tissues (Carlton and Richardson, 1995). In an analogous case, compounds produced during the day by symbiotic zooxanthellae, such as dimethylsulfoniopropionate (DMSP) and dimethylsulfide (DMS), intermediate coral-microbe associations (Raina et al., 2010). In the coral *Pocillopora damicornis*, DMSP functions as a chemotaxis and chemokinesis cue for the potential pathogen *Vibrio coralliliyticus* (Garren et al., 2014). Diurnal changes in pH are also predicted to alter the coral-associated microbiota. Sustained reduced pH, simulating ocean acidification scenarios, lead to distinct bacterial community composition with implications for coral physiological adaptation (Meron et al., 2011; Webster et al., 2013; O'Brien et al., 2016). These studies indicate that under stress conditions, normal diurnal physiological cycles may interfere with the progression of disease and coral survival, particularly in cases of polymicrobial diseases (Bourne et al., 2009; Sweet and Bulling, 2017).

Corals influence the reef overlying water and surrounding sediments through the release of organic carbon-rich mucus (Wild et al., 2004, 2005; Bythell and Wild, 2011). The level of influence corals have on the water is dependent of the mucus composition and solubility, ranging from particulate material that serve as particle traps to dissolved labile molecules readily utilized for bacterial growth (Wild et al., 2004; Haas et al., 2011). Mucus constantly released by corals and benthic physiologic processes create three boundary layers over the reef benthos: the first, called diffusive boundary layer, is millimeters thick and is formed by the diffusion of benthic metabolism, such as photosynthesis and respiration; the second, called momentum boundary layer (MBL), is a viscous sublayer centimeters thick, and is formed by a combination of products released by the benthos and the friction of water movement over corals; the third, called benthic boundary layer, is about 1 m thick, is formed by water turbulence and controls interactions of the reef with the open sea waters (Shashar et al., 1993, 1996; Barott and Rohwer, 2012). Coral mucus release rate and mucus composition varies in response to light. In *Acropora acuminata*, the lipid content varies between night and day in response to photosynthesis rates by zooxanthellae, as the endosymbiotic algae are the primary sites of mucus lipid production (Crossland, 1987). Therefore, coral influence on benthic boundary layers

is predicted to differ between day and night. Water column reef communities experience diurnal physiological changes in response to photosynthesis/respiration rates (Kayanne et al., 1995). Yet, these changes are thought to be a result of benthic respiration and calcification, as most reef production is of benthic origin (Kayanne et al., 1995; Silveira et al., 2015). The water column microbial communities in Heron Island, Great Barrier Reef, was significantly different between day and night (Sweet et al., 2010). However, the lack of differences between tides was interpreted as a weak connection between the benthos and the water column, with planktonic processes governing the differences observed or, alternatively, rapid turnover and mixing offsetting the benthic–pelagic coupling (Sweet et al., 2010).

Here, we hypothesized that the microbial community within coral MBL responds to changes in coral physiology. We investigated the microbial community associated with the MBL over the Brazilian endemic reef coral *Mussismilia braziliensis* in response to light availability. This genus forms ∼70% of the reef structure in the Abrolhos and is highly adapted to high turbidity stress periodically observed in the region due to continental runoff and sediment resuspension (Leão and Kikuchi, 2005; Segal et al., 2012; Loiola et al., 2013). *Proteobacteria, Bacteroidetes, Firmicutes, Cyanobacteria*, and *Actinomycetes* are the main groups associated to *M. braziliensis* (Reis et al., 2009; Castro et al., 2010; Garcia et al., 2013). In the present study, microbial community composition and functional profiles were compared between *M. braziliensis*'s MBL and water column over one diel cycle. Microbial metagenomes were also compared with changes in nutrient concentrations and microbial, viral and picoeukaryotic abundances. We found that the coral MBL did not display a diurnal pattern in the time scale analyzed. The similarity between MBL and water column, and the correlation with nutrient concentrations suggested that water flow over corals outweighs the effect of coral physiology on the MBL microbial community.

MATERIALS AND METHODS

Sampling

Samples were collected from Santa Bárbara island (17.9647778S, 38.7027778W), inside the Abrolhos Marine National Park (SISBIO permit 27147-2) in August 14th to 16th, 2011, during the austral winter. The main organisms contributing to benthic cover in Santa Bárbara are: coral 7.7%, crustose coralline algae (CCA) 6.6%, fleshy algae 22.4%, and turf algae 66.4%. Our sampling strategy targeted the MBL above visually healthy *M. braziliensis* corals. MBL samples were taken within 5 cm from the coral surface by scuba divers using a manual bilge pump (Haas et al., 2014). To minimize the amount of overlying water into the MBL sample, material was pumped from the surface of eight adjacent colonies at each time point, for a total of 80 l. Due to the sampling method, this sample was mainly composed of coral MBL over the corals, but include some benthic boundary layer (further above the corals) and coral mucus that detaches from the colony (Barott and Rohwer, 2012). Water column samples were taken from 1 m above the corals. Coral's MBL and water column were sampled at 5 and 4 m depth, respectively. Corals were sampled every 6 h for 48 h starting at 12:00 h on August 14th, for a total of nine samples through time. Water column was sampled every 6 h for 24 h starting at the same time, for a total of five samples through time. The reef area where the sampled coral heads were located was marked so we could return to the same location each time. Samples for nutrient and metagenomic analysis were collected and preserved according to Haas et al. (2014). From each sample, three 50 ml aliquots were flash frozen in liquid nitrogen for nutrient concentration analysis. For Chlorophyll *a* analysis, triplicate 2 l subsamples were immediately filtered through 0.45 μm pore-size ester-cellulose filters (Millipore) and the filters were frozen. Three 2 l subsamples were filtered through 0.7 μm pore GF/F glass fiber filter and aliquots of 50 ml of the filtrate were conserved in amber bottles with 1 ml of phosphoric acid for Dissolved Organic Carbon (DOC) determination (Rezende et al., 2010). Triplicate 1 ml subsamples were fixed with paraformaldehyde, glutaraldehyde and a mix of paraformaldehyde and glutaraldehyde (1, 0.5, and 1 + 0.05% final concentrations) for the fixation of eukaryotic autotrophs, viruses and bacteria, respectively. Sixty liters of each sample were concentrated through 100 kDa tangential flow filtration and subsequently filtered through a 0.22 μm Sterivex to concentrate microbes. Sterivex were frozen in liquid nitrogen until laboratory processing for metagenomics sequencing.

Nutrients and Microbial Abundance Measurements

Inorganic nutrients concentrations were determined using standard oceanographic methods (Grasshoff et al., 2009). Briefly: (1) ammonia was determined by indophenol, (2) nitrite was determined by diazotization, (3) nitrate was determined by reduction in Cd–Cu column followed by diazotization, (4) total nitrogen was determined by digestion with potassium persulfate following nitrate determination, (5) orthophosphate was determined by reaction with ascorbic acid, (6) total phosphorous by acid digestion to phosphate, and (7) silicate by reaction with molybdate. DOC concentration in the filtrates was determined by high catalytic oxidation using a TOC/TDN analyser (Shimadzu) (Rezende et al., 2010). Chlorophyll filters were extracted overnight in 90% acetone at 4°C and analyzed by fluorometry for chlorophyll concentration using a Turner Designs TD-700 fluorometer (Sunnyvale, CA, USA). Prokaryotic and viral abundances were determined by flow cytometry after incubating the samples with SYBR Green nucleic acid staining (Life Technologies, Carlsbad, CA) as previously described (Andrade et al., 2003). Autotrophic eukaryotes abundance (pico and nanoeukaryotes) was determined by flow cytometry through chlorophyll autofluorescence.

Metagenomic Sequencing and Anotation

To investigate the composition of microbial assemblages associated to *M. braziliensis* MBL we sequenced three metagenomes at "dark" time points: 00:00 on August 15th, 00:00 on August 16th, and 06:00 on August 16th (at the end of the second night). Three "day" time points were sequenced: 18:00 on August 14th (the first sampling day), 18:00 on August 15th, and 12:00 on August 16th, the last sampling day. We also

sequenced one "night" water column sample from 00:00 on August 15th and one "day" water column sample from 12:00 on August 15th. Samples from 18:00 were taken before sunset, at the end of 12 h of daylight exposure, and therefore were grouped as "day." The same criteria was applied to 06:00 samples grouped as "night."

DNA was extracted from Sterivex after proteinase K/SDS treatment by phenol/chloroform/isoamyl alcohol technique, and sequenced on an Ion Torrent sequencer (Life Sciences, USA). Reads shorter than 100 bp and with mean quality scores lower than 25 were removed using PrinSeq (Schmieder and Edwards, 2011b). High quality sequences were then de-replicated with TagCleaner (Schmieder et al., 2010) and potential contaminants matching lambda or human DNA sequences removed with DeconSeq (Schmieder and Edwards, 2011a). A summary of metagenomic sequencing, quality control, and sample grouping used in multivariate analyses is presented in **Table 1**. Taxonomic annotation was performed using FOCUS and functional annotation using SUPERFOCUS (Silva et al., 2014, 2016). Metagenomes are publically available on FigShare (https://doi.org/10.6084/m9.figshare.4614745.v1) and MG-RAST under the project *Diel Mussismilia* (http://metagenomics.anl.gov/linkin.cgi?project=mgp14437; Meyer et al., 2008). Taxonomic and functional annotation tables utilized in multivariate analysis are provided as online Supplementary Materials.

Statistical Analysis

Statistical analyses were performed using Vegan package in R (Dixon, 2003) or using Primer 6 (PRIMER-E, Plymouth). Relative abundances (%) of taxonomic and functional groups were analyzed through non-metric multidimentional scaling (NMDS) in Vegan (Dixon, 2003). The presence of significant clusters (time or sample source) was determined using Permutational ANOVA (PERMANOVA) using Bray-Curtis dissimilarities (Anderson, 2001). To test for correlation between environmental variables and taxonomic and functional profiles we reduced the dataset to taxa or functions representing >1% of the annotated sequences (mean across all eight samples). The use of abundant groups is expected to reduce stochastic effects associated with rare members or functions (Shade and Gilbert, 2015). Distance-based linear models (DistLM) analysis using Bray Curtis dissimilarity and scaled environmental variables was used to determine the contribution of each environmental variable to the total dissimilarity on taxonomic and functional profiles (McArdle and Anderson, 2001). DistLM was ran stepwise with a second order Akaike Information Criteria (AICc) in Primer. We selected variables that contributed to 10% or more to the dissimilarity and performed a Canonical Correspondence Analysis (CCA) using Vegan in R to visualize the relationship between environmental variables and taxa/function. We performed a Pearson correlation test followed by Holm's *p*-values post-correction to determine significant correlations between environmental variables and taxa/functions (Holm, 1979). Microbial communities can be modulated by the available nutrients, but the opposite scenario, where nutrient availability is a product of microbial metabolism, is also possible. Therefore, we also tested taxonomic and functional profiles as predictor of environmental variables in a separate DistLM-test.

RESULTS

Chlorophyll, Organic, and Inorganic Nutrients

Variation in organic and inorganic forms of nitrogen and phosphorous over time are shown in **Table 2**. Concentration of total phosphorus and nitrogen, ammonium, and nitrite did not co-vary over time (Pearson correlation, $p > 0.05$), while orthophosphate and nitrate were positively correlated (Pearson correlation $r = 0.72$, $p = 0.003$). Nitrate contributed to most of the inorganic nitrogen pool both in the coral MBL and the water column (1.70 ± 0.04 μM, mean $\pm$ *SE* for coral and 1.79 ± 0.26 for water column, compared to 0.15 ± 0.05 and 0.05 ± 0.05 for nitrite and 0.17 ± 0.07 and 0.29 ± 0.14 for ammonium in coral and water column, respectively). Concentration of DOC and Chlorophyll *a* are shown in **Table 2**. DOC correlated with total nitrogen, including the organic nitrogen pool (Pearson correlation $r = 0.79$, $p < 0.001$). Chlorophyll *a*, DOC, and nutrient concentrations were not significantly different between day and night samples (Welch Two Sample *t*-test $p > 0.05$ for all tests on the coral MBL only, water column only, and MBL and water combined). Therefore, we were not able to identify diurnal patterns in nutrient concentration in the MBL above *M. braziliensis* or the water column at this time scale.

TABLE 1 | Metagenomes summary.

Sample	Time group	Sequences generated	Sequences after QC	Passed QC (%)	MG-RAST ID
Coral MBL_08.15.11_18:00	Day	799,095	601,398	75.26	4644203.3
Coral MBL_08.15.11_00:00	Night	4,820,694	4,096,018	84.97	4644204.3
Coral MBL_08.15.11_18:00	Day	2,007,447	1,466,499	73.05	4644206.3
Coral MBL_08.16.11_00:00	Night	1,946,874	1,495,057	76.79	4644206.3
Coral MBL_08.16.11_06:00	Night	47,502	37,850	79.68	4644208.3
Coral MBL_08.16.11_12:00	Day	71,627	42,363	59.14	4644207.3
Water column_08.15.11_00:00	Night	1,397,498	1,114,569	79.75	4644209.3
Water column_08.15.11_12:00	Day	5,74,364	4,47,371	77.89	4644210.3

Number of sequences generated and percentage of sequences that passed quality control using Prinseq. Sample source and time group indicate sample clustering for PERMANOVA-tests.

TABLE 2 | Inorganic nutrients, Chlorophyll a and DOC concentrations in *M. braziliensis* boundary layer and water column over a diel cycle.

Sample	Date	Time	Ortophosphate	Total Phosphorus	NH_3	Nitrite	Nitrate	Total Nitrogen	Chlorophyll *a*	DOC
Coral MBL	08/14	12:00	0.12 (0.00)	0.29 (0.01)	0.05 (0.01)	0.05 (0.00)	1.69 (0.02)	5.61 (0.25)	0.06 (0.02)	115.8 (00.0)
Coral MBL	08/14	18:00	0.18 (0.01)	0.39 (0.01)	0.15 (0.03)	0.06 (0.01)	1.80 (0.01)	7.56 (0.83)	0.26 (0.03)	113.3 (15.8)
Coral MBL	08/15	00:00	0.10 (0.01)	0.22 (0.01)	0.42 (0.04)	0.05 (0.00)	1.63 (0.03)	6.77 (0.39)	0.46 (0.06)	129.1 (25.0)
Coral MBL	08/15	06:00	0.18 (0.01)	0.36 (0.01)	0.61 (0.09)	0.07 (0.00)	1.58 (0.02)	9.00 (1.75)	0.26 (0.06)	140.8 (37.5)
Coral MBL	08/15	12:00	0.14 (0.01)	0.37 (0.01)	0.05 (0.00)	0.08 (0.01)	1.75 (0.08)	11.24 (1.74)	1.62 (0.39)	155.8 (1.66)
Coral MBL	08/15	18:00	0.14 (0.01)	0.27 (0.01)	0.05 (0.00)	0.07 (0.01)	1.49 (0.11)	7.38 (0.48)	0.35 (0.03)	125.0 (39.1)
Coral MBL	08/16	00:00	0.73 (0.03)	na	na	0.47 (0.01)	1.69 (0.05)	7.7 (0.86)	0.62 (0.11)	129.1 (25.0)
Coral MBL	08/16	06:00	0.14 (0.00)	0.25 (0.01)	0.06 (0.01)	0.08 (0.02)	1.88 (0.07)	6.65 (0.57)	0.35 (0.17)	104.1 (3.33)
Coral MBL	08/16	12:00	4.07 (0.05)	na	0.08 (0.01)	0.41 (0.01)	na	7.7 (0.86)	0.45 (0.21)	105.8 (9.16)
Water Column	08/14	12:00	0.08 (0.00)	0.24 (0.01)	<0.05 (0.00)	0.04 (0.01)	1.72 (0.09)	5.09 (0.54)	0.31 (0.02)	169.1 (49.1)
Water Column	08/14	18:00	0.08 (0.00)	0.21 (0.01)	0.08 (0.01)	0.05 (0.01)	1.67 (0.02)	5.50 (0.69)	0.31 (0.24)	135.8 (45.0)
Water Column	08/15	00:00	0.11 (0.01)	0.23 (0.00)	1.00 (0.09)	0.05 (0.01)	1.82 (0.04)	5.17 (0.50)	0.30 (0.22)	103.3 (7.5)
Water Column	08/15	06:00	0.11 (0.02)	0.21 (0.01)	0.33 (0.04)	0.05 (0.00)	1.93 (0.08)	5.15 (0.01)	0.15 (0.04)	136.6 (67.5)
Water Column	08/15	12:00	0.09 (0.01)	0.21 (0.03)	0.05 (0.00)	0.06 (0.01)	1.81 (0.01)	5.08 (0.40)	0.30 (0.08)	114.1 (12.5)

Values represent means of triplicate measurements, in $\mu mol.l^{-1}$, and standard deviation in parenthesis.

Microbial Abundance

Prokaryotic abundances ranged from 3.2×10^5 to 7.0×10^5 ml^{-1} in the coral MBL, and from 4.4×10^5 to 6.6×10^5 ml^{-1} in the water column. Viral abundances ranged from 4.8×10^6 to 10.6×10^6 ml^{-1} on the coral and 5.1×10^6 to 7.3×10^6 ml^{-1} in the water column. When analyzing MBL and water column samples together, viruses and prokaryotes showed a significant negative correlation to each other (Pearson $r = -0.57$, $p = 0.03$). Prokaryotic abundance also correlated negatively to total phosphorous concentration (Pearson $r = -0.72$, $p = 0.003$), while viral abundance correlated positively to total phosphorous (Pearson $r = 0.56$, $p = 0.03$). The abundance of autotrophic pico- and nanoeukayotes ranged from 4.2×10^3 to 10×10^3 ml^{-1} and from 3.6×10^2 to 10.8×10^2 ml^{-1}, respectively. Pico and nanoeukaryote abundances were positively correlated to each other (Pearson $r = 0.66$, $p = 0.008$) and were both negatively correlated to viral abundance (Pearson $r = -0.61$, $p = 0.01$ and $r = -0.65$, $p = 0.01$ for pico- and nanoeukaryotes, respectively). Prokaryotic and picoeukaryote abundances correlated positively (Pearson $r = 0.76$, $p = 0.001$). No diurnal patterns were observed in the microbial and viral abundances on the coral MBL or in the water column (Welch Two Sample *t*-test $p > 0.05$ for all tests on the coral MBL only, water column only, and MBL and water combined). However, over the course of the diurnal monitoring we detected a viral burst event that occurred at 18:00 of the first night. At this time, prokaryotic abundances in the MBL dropped to the lowest values recorded during the cycles, while viral abundances peaked (**Figure 1**).

Microbial Taxonomic and Functional Profiles

The microbial community associated with *M. braziliensis* MBL at night was dominated by *Proteobacteria* (mean of 32.2% of annotated reads), *Firmicutes* (21.5%), *Thaumarchaeota* (9.6%), *Euryarchaeota* (8.4%), *Cyanobacteria* (5.9%), and *Bacteroidetes* (4.4%). During the day, the same phyla were dominant, except for *Euryarchaeota*: *Proteobacteria* (41.6%), *Bacteroidetes* (13.79%), *Cyanobacteria* (8.3%), *Firmicutes* (8.2%), *Thaumarchaeota* (4.3%), and *Tenericutes* (4.2%). The main phyla in the water column at night were *Proteobacteria* (39.4%), Cyanobacteria (17.2%), *Firmicutes* (9.4%), *Thaumarchaeota* (7.4%), and *Euryarchaota* (5.7%). Overall, the same phyla dominated all three groups of samples.

At the genus level, the microbial community associated with *M. braziliensis* MBL at night was dominated by members of the genera *Anaplasma* (9.2%, mean of annotated sequences), *Coprococcus* (6.05%), *Staphylococcus* (5.6%), unclassified *Alphaproteobacteria* (5.0%), *Coprothermobacter* (5.0%), and the archaeal genus *Nitrosopumilus* (5.0%) (**Figure 2A** and Supplementary Material 1). During the day, the dominant members were unclassified *Alphaproteobacteria* (6.9%), *Fluviicola* (4.8%), *Vibrio* (4.6%), *Synechococcus* (4.6%), *Glaciecola* (3.8%), and *Alteromonas* (3.5%). The most abundant genera in the water column were *Synechococcus* (12.5%), unclassified *Alphaproteobacteria* (8.3%), *Hirschia* (5.3%), *Anaplasma* (4.9%), *Prochorococcus* (4.4%), and *Nitrosopumilus* (3.0%). NMDS analysis based on relative abundances of genera showed no significant clusters among the three tested groups (water column, MBL daytime and MBL nighttime, PERMANOVA $p > 0.05$, **Figure 3A**). Bacterial richness, diversity, and evenness at the species level did not significantly differ between day and night in the MBL (**Table 3**, *t*-test $p = 0.29$, 0.347, and 0.0516 for Chao richness, Shannon diversity (H'), and Pielou's evenness, respectively).

Abundant functional subsystems were remarkably similar across MBL and water samples at night and day (**Figure 2B** and Supplementary Material 2). The most abundant functions at the level 1 Subsystems according to SEED database were carbohydrates ($13.1 \pm 0.5\%$, mean $\pm$ *SD*); amino acids and derivatives ($11.9 \pm 1.4\%$); protein metabolism ($9.6 \pm 1.2\%$); cofactors, vitamins, prosthetic groups, pigments ($8.7 \pm 0.5\%$), and RNA metabolism ($6.3 \pm 1.1\%$). At the level 2, most

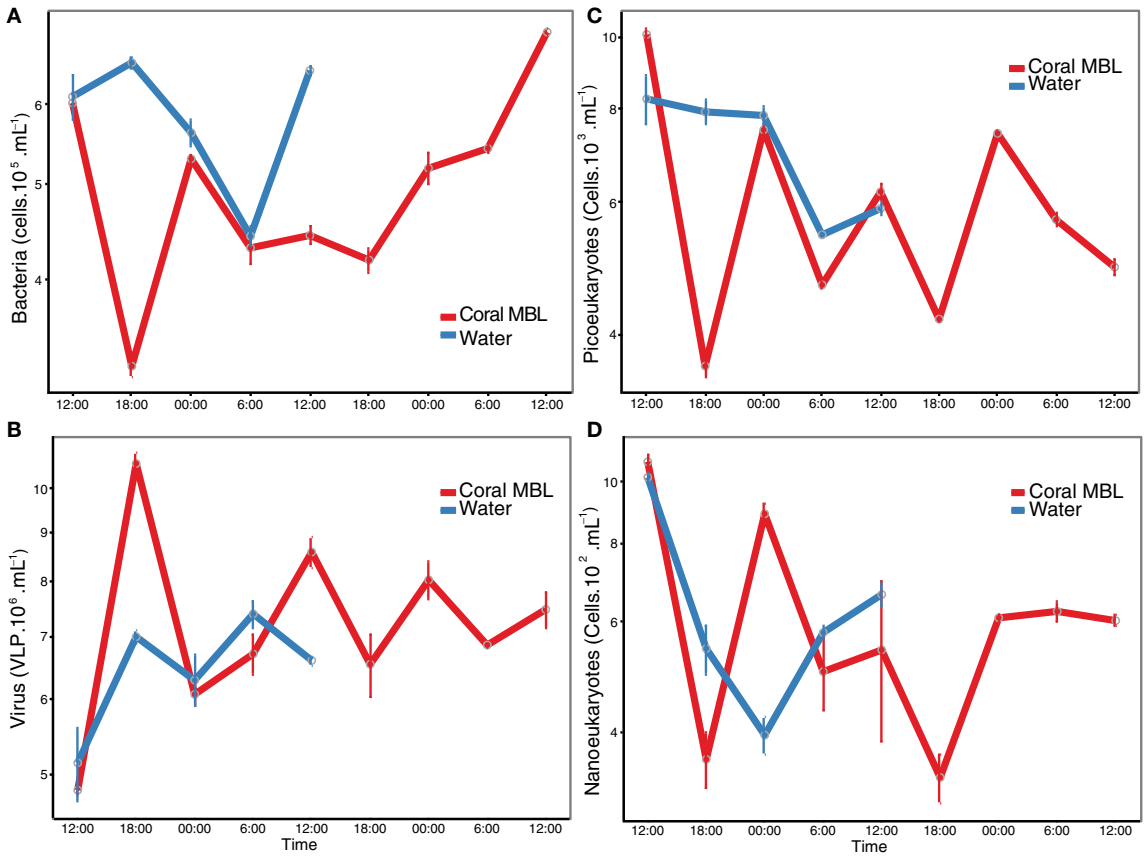

FIGURE 1 | Microbial abundance over time. Abundance of **(A)** prokaryotic cells, **(B)** viral-like particles, autotrophic **(C)** pico- and **(D)** nanoeukaryotes was determined by flow cytometry. Red line indicates the coral momentum boundary layer and blue indicates the water column one meter above the corals.

of the predicted proteins were unclassified (20.9 ± 1.5%, mean ± *SD*), followed by protein biosynthesis (6.3 ± 0.5%), central carbohydrate metabolism (6.3 ± 0.3%), lysine, threonine, methionine, and cysteine (3.7 ± 1.4%), RNA processing and modification (3.4 ± 0.7%), and transcription (2.9 ± 0.6%). NMDS analysis was performed based on the abundance of functions classified at the level 2 subsystems (as opposed to level 1 described above). PERMANOVA-tests showed no significant difference in functional profiles between MBL and water column or between daytime and nighttime MBL (PERMANOVA $p > 0.05$, **Figure 3B**).

Environmental Predictors of Dominant Taxa and Functions

We investigated if taxonomic profiles in both MBL and water column samples were determined by nutrient concentrations. We performed these analyses with 26 dominant genera, defined as those with at least 1% relative abundance, which contributed to a total of 70.6% of the community composition. The relationship between environmental variables and dominant taxa can be visualized in the Canonical Correspondence Analysis (CCA) plot (**Figure 4A**). DistLM analysis tested the contribution of each environmental variable to the dissimilarity among dominant community members. DistLM showed that nitrate was the best predictor of taxonomic dissimilarity (40% of community dissimilarity, $p = 0.019$). Following, DOC contributed to 27%, prokaryotic abundance and source (MBL or water column) each contributed with 17.8%, time of collection with 14%, and total phosphorus with 13.9%. All the other variables contributed to 10% or less the community dissimilarity. We tested significant correlations between nitrate, which had the highest explanatory proportion, and each taxon. *Coprothermobacter* was negatively correlated with nitrate ($r = -0.91$, Holm's post-test correction $p = 0.04$). We then performed a reverse DistLM-test where taxonomic dissimilarity was tested as predictor for environmental variable dissimilarity. *Synechococcus* was the genus explaining the highest proportion of environmental variable dissimilarity (25%, $p = 0.04$).

Analyses of relationships between environmental variables and dominant functional profiles were performed on 25 SEED level 2 subsystems, each one with abundances of at least 1%, contributing to a total of 51.9% of all functionally annotated reads. Correlations between dominant functions and environmental variables can be visualized in the CCA (**Figure 4B**). DistLM analysis showed that dissimilarity among functional profiles was poorly explained by environmental

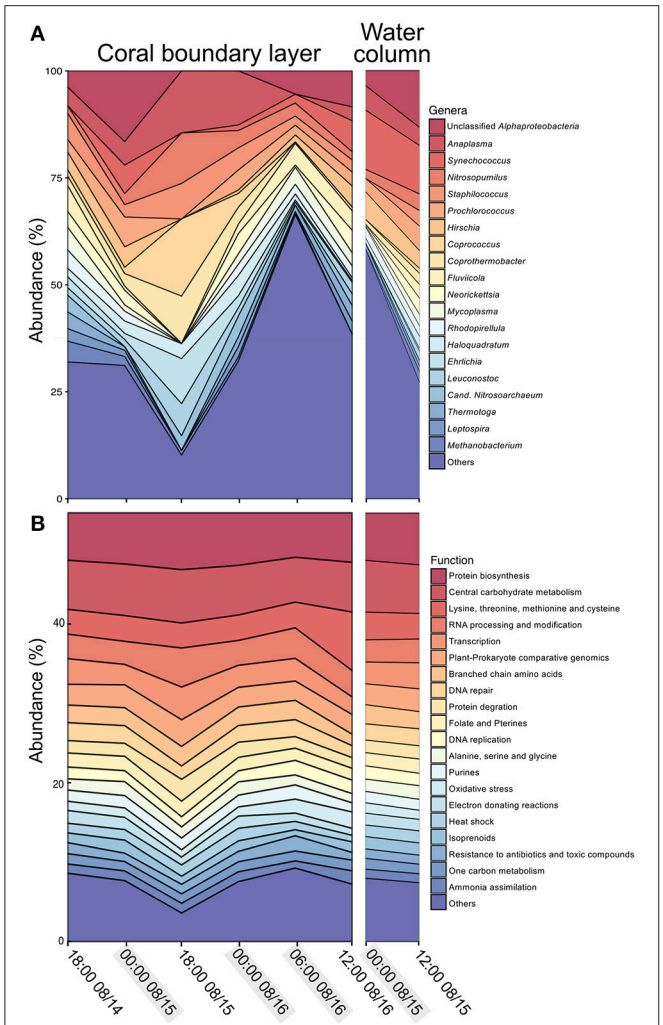

FIGURE 2 | Taxonomic and functional profiles. Abundance of **(A)** dominant genera as assigned by FOCUS in the coral boundary layer (left panel) and water column (right panel), and **(B)** dominant level 2 Subsystem functions in SEED database as assigned by SUPERFOCUS the coral boundary layer (left panel) and water column (right panel). Shadowed time points indicate samples grouped as "night."

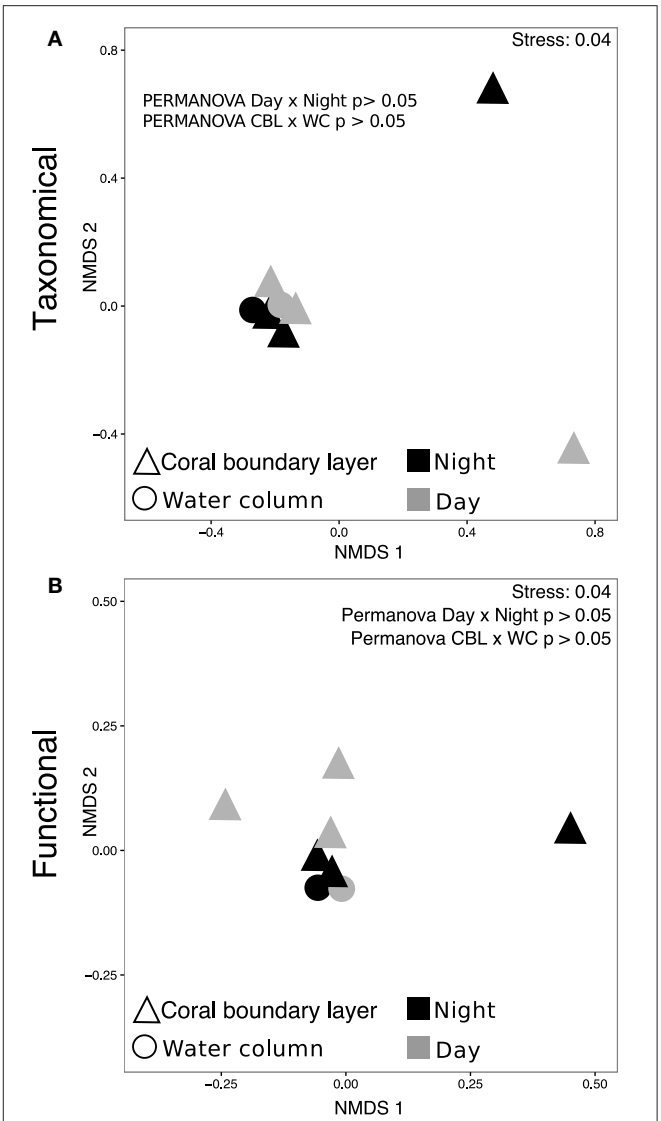

FIGURE 3 | Taxonomic and functional clustering. NMDS plots and PERMANOVA tests based on the abundance of **(A)** genera and **(B)** level 2 Subsystems functions SEED database.

variables. Orthophosphate, nitrate, and cell abundance were the variables contributing to the highest proportion of explanation (45, 29, and 24%, respectively), however *p*-values were not significant (0.08, 0.1, and 0.1, respectively). Accordingly, the reverse test where functional profiles were tested as predictors of environmental variables showed no significant functions.

DISCUSSION

Current coral microbiome studies are mostly focused on finding species-specific associations across geographical patterns and disturbance response (Hester et al., 2015; Bourne et al., 2016; Hernandez-agreda et al., 2016). Most studies investigating temporal variability in coral microbiomes are focused on relatively long time scales, weeks to months, with little information available on temporal variability at the diel scale (Glasl et al., 2016; Zaneveld et al., 2016). This contrasts with the strong diurnal variation imposed by coral physiology (Sorek et al., 2014). Here, we aimed to fill this gap by analyzing microbial dynamics on the MBL above the coral *M. braziliensis* at the diel scale. We found no evidence for a diel pattern in bacterial taxonomic and functional profiles at the time scale sampled, and observed that the variability of taxonomic profiles correlated with nutrient concentrations, suggesting that the coral MBL was more influenced by water column dynamics than by coral physiology. This result is consistent with previous findings in water column bacterial communities in the Great Barrier Reef, and supports the hypothesis that diurnal patterns in community composition are related to planktonic processes rather than to benthic–pelagic coupling (Sweet et al., 2010).

TABLE 3 | Bacterial richness and diversity indexes at the species level.

Sample	Species count	Chao	Shannon (*H'*)	Evenness
Coral MBL_08.15.11_18:00	1,363	1,402	5.527721	0.7658835
Coral MBL_08.15.11_00:00	1,446	1,456	4.906071	0.6742298
Coral MBL_08.15.11_18:00	1,088	1,245	5.510376	0.7880864
Coral MBL_08.16.11_00:00	1,403	1,424	5.238537	0.722919
Coral MBL_08.16.11_06:00	1,049	1,254	5.203073	0.7480417
Coral MBL_08.16.11_12:00	604	935	4.977831	0.7773519
Water column_08.15.11_00:00	1,408	1,424	5.145579	0.7097424
Water column_08.15.11_12:00	1,391	1,435	4.963443	0.6857689

The dominant taxa observed in *M. braziliensis* MBL belong to *Proteobacteria*, *Firmicutes, Thaumarchaeota,* and *Cyanobacteria* phyla, which were previously reported as abundant in *M. braziliensis* mucus, along with *Planctomycetes* and *Bacteroidetes* (Reis et al., 2009; Garcia et al., 2013). Other coral species within the *Mussismilia* genus, however, were previously shown to harbor distinct bacterial community profile even at the phylum level, with higher abundance of *Actinobacteria, Acidobacteria, Lentisphaera,* and *Nitrospira* (Castro et al., 2010). This result shows that both the MBL sample and the water above are under influence of coral mucus and support the hypothesis of stable interactions between microbes and the *Mussismilia* genus (Carlos et al., 2013; Fernando et al., 2014). Growing evidence suggest that different coral species select for specific bacterial assemblages, even at large geographic scales (Hernandez-agreda et al., 2016; Neave et al., 2016). Stable members of the bacterial community were found in low abundance in Porites corals across the Pacific, while abundant members were often sporadic (Ainsworth et al., 2015; Hester et al., 2015). Likewise, rare or low-abundance prokaryotic families drive the differences in microbial community composition between depths within the depth generalist coral *Stephanocoenia intersepta* (Glasl et al., 2017). Microbial community associated with the coral *Seriatopora hystrix* correlated more with habitat than with coral host genotype (Pantos et al., 2015). The lack of diurnal differences observed here may be a result of abundant, sporadic members that do not respond to quick changes in coral physiology compared to stable, low abundance members. We predict that stable members of the holobiont that co-evolve with their hosts would respond to changes in host physiology by synchronizing growth and metabolism. This type of relationship is not expected in transient members that are highly subject to stochastic processes.

Microbial association with corals can be shaped by host genotype and environmental features (Rohwer et al., 2002; Zilber-Rosenberg and Rosenberg, 2008). Although our sampling procedure targets microbes from the MBL, predicted to have a relatively weak relationship with the coral compared to tissue-associated microbes, we observed high abundance of typical symbiotic genera such as *Anaplasma, Hirchia, Neoricketsia, Mycoplasma,* and *Ehrlichia*. These groups comprise obligate endosymbionts of some arthropods and have reduced genomes that retain only essential functions, often including genes that serve the hosts (López-Madrigal et al., 2011; McCutcheon and Moran, 2011). It is possible that the sequences observed here came from obligate coral symbiont species belonging to these genera, but not yet described. These microbes could be both naturally expelled from the coral surface during mucus exudation or we could have accidentally sampled fragments of coral tissue during the MBL pumping. Although bacterial assemblages differ between compartments within the coral holobiont, endosymbiotic microorganisms are found in coral mucus samples collected by the milking method, showing that differentiating between these compartments requires fine-scale sampling procedures (Sweet et al., 2011a).

Association between specific microbial community functional profiles and environmental conditions are consistently observed over time and space, regardless of species composition (Huttenhower et al., 2012). The highly similar functional profiles found here in both diurnal and nocturnal MBL, and lack of correlation with short-term fluctuation in nutrient concentration corroborates the idea of a functional profile characteristic of the studied reefs. Functions related to carbohydrate metabolism, amino acids, and protein metabolism were the most abundant, as observed before in water column microbial metagenomes of the Abrolhos region (Bruce et al., 2012). This profile differs from those of pristine coral reefs in the Pacific, where respiration and virulence were the most abundant functions (Dinsdale et al., 2008a,b). These differences may, however, be a result of method variability, from DNA extraction to sequencing (Wood-Charlson et al., 2015).

Despite the lack of a diel pattern in nutrients and microbial abundance during the sampled period, we identified a synchronized change in total prokaryotic and viral abundance that indicated a lytic event. Studies of short time scale variation in viral abundances in marine environments have conflicting results, and most of them did not display diel cycles (Jiang and Paul, 1994; Winter et al., 2004; Winget and Wommack, 2009). Likewise, little empirical evidence exists for Kill-the-Winner dynamics in complex mixed communities (Thingstad, 2000; Knowles et al., 2016). Interestingly, pico- and nanoeukaryotes abundance were negatively correlated with total viral abundance ($r = -0.61$ and -0.65, respectively). This suggests that a significant fraction of the active community might be comprised of eukaryotic viruses, despite the fact that these viruses comprise only about 10% of total the viral community (Brussaard et al., 2010; Silveira et al., 2015). It was not possible to differentiate groups V1, V2, and V3 in our samples, which correspond to bacteriophages or eukaryotic viruses, preventing to conclusively determine if the largest variance was indeed in the eukaryotic virus group (Brussaard, 2004; Brussaard et al., 2010).

The lack of diel patterns and the correlations between taxonomic dissimilarities and nutrients suggest that water flow over corals determines microbial community composition in the MBL, rather than diel switches in coral physiology. Community assembly patterns observed here in the MBL, and before in the coral holobiont, indicate that stochastic processes such as migration or nutrient fluctuations due to hydrodynamics are important forces shaping the short-term fluctuations in the microbiome, as opposed to deterministic processes (Sloan et al., 2006; Hester et al., 2015). This pattern has been observed

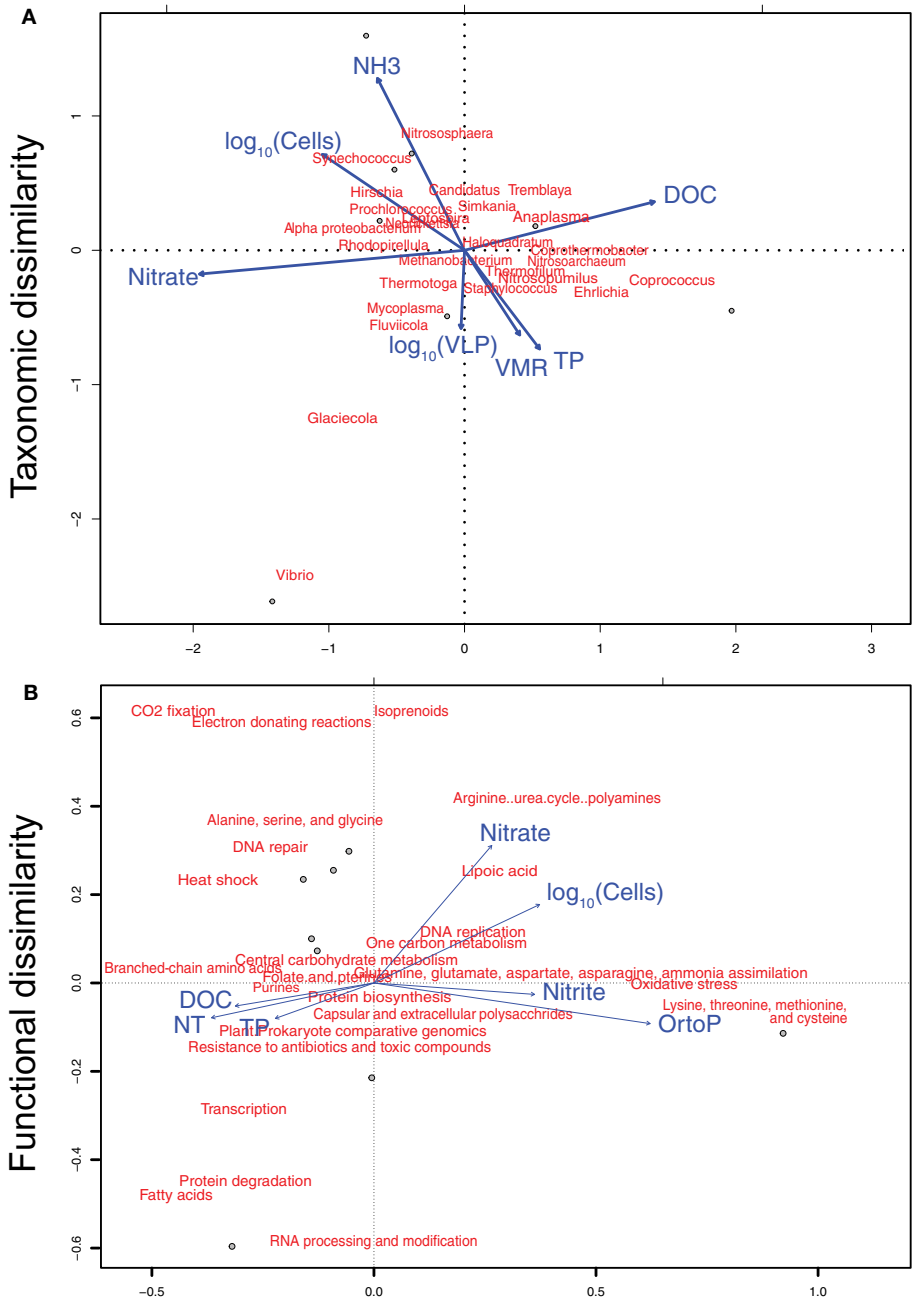

FIGURE 4 | Canonical correspondence analysis of environmental variables and (A) dominant genera, and **(B)** dominant functions. Environmental variables used in the analysis are shown in **Figure 1** and **Table 2**. Dominant genera and functions were defining as those with at least 1% abundance. Twenty-five genera and twenty-six functions were utilized in the analysis, summing up to a total of 70.6 and 51.9% of taxonomically and functionally annotated reads, respectively.

in several microbial communities and can be explained by a stochastic neutral community model (Sloan et al., 2006). It is also possible that significant diurnal changes in the community happen in the coral holobiont and in the diffusive boundary layer at the millimeter scale. The diffusive boundary layer of *S. pistillata* is significantly thinner when a 5 cm/s current is applied (Shashar et al., 1993). To address whether diurnal patterns in community composition occur on coral diffuse boundary layer, tank, and field approaches that target spatially-defined sampling at the scale of millimeters, reduce water flow, or amplify the effect of coral physiology are necessary.

In conclusion, we show that the microbial community in the MBL of the coral *M. braziliensis* do not display significant diurnal patterns. Instead, this community is similar to the water column 1 m above the corals and responds to environmental fluctuations in nutrient concentrations. Our results suggest that despite coral

mucus contribution to the MBL community composition, the overlying water currents contribute more to short term variability in community assembly than diurnal changes in coral physiology. These results expand the view of short-term temporal dynamics of coral microbiome, often bypassed in studies on coral health and reef ecology.

AUTHOR CONTRIBUTIONS

CS, GG, and FT designed the study; CS, GG, FC, GS, JH, LO, AC, CR, CT, RF, RE, and ED generated and analyzed the data; CS and FT wrote the manuscript and all authors contributed to revisions.

ACKNOWLEDGMENTS

The work was funded by CNPq, CAPES, and FAPERJ. ED was supported by NSF (Grants 1323809 and 1330800). Computational resources for bioinformatic analyses were funded by NSF grant CNS-1305112 to RE.

SUPPLEMENTARY MATERIAL

The Supplementary Material for this article can be found online at: http://journal.frontiersin.org/article/10.3389/fmicb.2017.00784/full#supplementary-material

REFERENCES

Ainsworth, T. D., and Gates, R. D. (2016). Corals' microbial sentinels. *Science* 352, 1518–1520. doi: 10.1126/science.aad9957

Ainsworth, T. D., Krause, L., Bridge, T., Torda, G., Raina, J., Zakrzewski, M., et al. (2015). The coral core microbiome identifies rare bacterial taxa as ubiquitous endosymbionts. *ISME J.* 9, 2261–2274. doi: 10.1038/ismej.2015.39

Anderson, M. J. (2001). A new method for non-parametric multivariate analysis of variance. *Austral Ecol.* 26, 32–46. doi: 10.1111/j.1442-9993.2001.01070.pp.x

Andrade, L., Gonzalez, A., Araujo, F., and Paranhos, R. (2003). Flow cytometry assessment of bacterioplankton in tropical marine environments. *J. Microbiol. Methods* 55, 841–850. doi: 10.1016/j.mimet.2003.08.002

Anthony, K. R. N., and Fabricius, K. E. (2000). Shifting roles of heterotrophy and autotrophy in coral energetic under varying turbidity. *J. Exp. Mar. Bio. Ecol.* 221–253. doi: 10.1016/S0022-0981(00)00237-9

Apprill, A., Marlow, H. Q., Martindale, M. Q., and Rappé, M. S. (2009). The onset of microbial associations in the coral *Pocillopora meandrina*. *ISME J.* 3, 685–699. doi: 10.1038/ismej.2009.3

Barott, K. L., and Rohwer, F. L. (2012). Unseen players shape benthic competition on coral reefs. *Trends Microbiol.* 20, 621–628. doi: 10.1016/j.tim.2012.08.004

Bourne, D. G., Garren, M., Work, T. M., Rosenberg, E., Smith, G. W., and Harvell, C. D. (2009). Microbial disease and the coral holobiont. *Trends Microbiol.* 17, 554–562. doi: 10.1016/j.tim.2009.09.004

Bourne, D. G., Morrow, K. M., and Webster, N. S. (2016). Insights into the coral microbiome: underpinning the health and resilience of reef ecosystems. *Annu. Rev. Microbiol.* 70, 102215–195440. doi: 10.1146/annurev-micro-102215-095440

Brown, B. E., and Bythell, J. C. (2005). Perspectives on mucus secretion in reef corals. *Mar. Ecol. Prog. Ser.* 296, 291–309. doi: 10.3354/meps296291

Bruce, T., Meirelles, P. M., Garcia, G., Paranhos, R., Rezende, C. E., de Moura, R. L., et al. (2012). Abrolhos bank reef health evaluated by means of water quality, microbial diversity, benthic cover, and fish biomass data. *PLoS ONE* 7:e36687. doi: 10.1371/journal.pone.0036687

Brussaard, C. (2004). Optimization of procedures for counting viruses by flow cytometry. *Appl. Environ. Microbiol.* 70, 1506–1513. doi: 10.1128/AEM.70.3.1506-1513.2004

Brussaard, C. P. D., Payet, J. P., Winter, C., and Weinbauer, M. G. (2010). Quantification of aquatic viruses by flow cytometry. *Man. Aquat. Viral Ecol.* 102–109. doi: 10.4319/mave.2010.978-0-9845591-0-7.102

Bythell, J. C., and Wild, C. (2011). Biology and ecology of coral mucus release. *J. Exp. Mar. Bio. Ecol.* 408, 88–93. doi: 10.1016/j.jembe.2011.07.028

Carlos, C., Torres, T. T., and Ottoboni, L. M. M. (2013). Bacterial communities and species-specific associations with the mucus of Brazilian coral species. *Sci. Rep.* 3:1624. doi: 10.1038/srep01624

Carlton, R. G., and Richardson, L. L. (1995). Oxygen and sulfide dynamics in a horizontally migrating cyanobacterial mat: black band disease of corals. *FEMS Microbiol. Ecol.* 18, 155–162. doi: 10.1111/j.1574-6941.1995.tb00173.x

Castro, A. P., Araújo, S. D., Reis, A. M. M., Moura, R. L., Francini-Filho, R. B., Pappas, G., et al. (2010). Bacterial community associated with healthy and diseased reef coral *Mussismilia hispida* from Eastern Brazil. *Microb. Ecol.* 59, 658–667. doi: 10.1007/s00248-010-9646-1

Chalker, B. E., and Taylor, D. L. (1975). Light-enhanced calcification, and the role of oxidative phosphorylation in calcification of the coral *Acropora cervicornis*. *Proc. R. Soc. London B Biol. Sci.* 190, 323–331. doi: 10.1098/rspb.1975.0096

Crossland, C. J. (1987). *In situ* release of mucus and DOC-lipid from the corals *Acropora variabilis* and *Stylophora pistillata* in different light regimes. *Coral Reefs* 6, 35–42. doi: 10.1007/BF00302210

Dinsdale, E. A., Edwards, R. A., Hall, D., Angly, F., Breitbart, M., Brulc, J. M., et al. (2008a). Functional metagenomic profiling of nine biomes. *Nature* 452, 629–632. doi: 10.1038/nature06810

Dinsdale, E. A., Pantos, O., Smriga, S., Edwards, R. A., Angly, F., Wegley, L., et al. (2008b). Microbial ecology of four coral atolls in the Northern Line Islands. *PLoS ONE* 3:e1584. doi: 10.1371/journal.pone.0001584

Dixon, P. (2003). VEGAN, a package of R functions for community ecology. *J. Veg. Sci.* 14, 927–930. doi: 10.1111/j.1654-1103.2003.tb02228.x

Douglas, A. E., and Werren, J. H. (2016). Holes in the hologenome: why host-microbe symbioses are not holobionts. *MBio* 7:e02099. doi: 10.1128/mBio.02099-15

Fernando, S. C., Wang, J., Sparling, K., Garcia, G. D., Francini-Filho, R. B., de Moura, R. L., et al. (2014). Microbiota of the Major South Atlantic reef building coral Mussismilia. *Microb. Ecol.* 69, 267–280. doi: 10.1007/s00248-014-0474-6

Garcia, G. D., Gregoracci, G. B., Santos, E. O., Meirelles, P. M., Silva, G. G. Z., Edwards, R., et al. (2013). Metagenomic analysis of healthy and white plague-affected *Mussismilia braziliensis* corals. *Microb. Ecol.* 65, 1076–1086. doi: 10.1007/s00248-012-0161-4

Garren, M., and Azam, F. (2012). Corals shed bacteria as a potential mechanism of resilience to organic matter enrichment. *ISME J.* 6, 1159–1165. doi: 10.1038/ismej.2011.180

Garren, M., Raymundo, L., Guest, J., Harvell, C. D., and Azam, F. (2009). Resilience of coral-associated bacterial communities exposed to fish farm effluent. *PLoS ONE* 4:e7319. doi: 10.1371/journal.pone.0007319

Garren, M., Son, K., Raina, J.-B., Rusconi, R., Menolascina, F., Shapiro, O. H., et al. (2014). A bacterial pathogen uses dimethylsulfoniopropionate as a cue to target heat-stressed corals. *ISME J.* 8, 999–1007. doi: 10.1038/ismej.2013.210

Glasl, B., Bongaerts, P., Elisabeth, N. H., Hoegh-Guldberg, O., Herndl, G. J., and Frade, P. R. (2017). Microbiome variation in corals with distinct depth distribution ranges across a shallow–mesophotic gradient (15–85 m). *Coral Reefs* 1–6. doi: 10.1007/s00338-016-1517-x

Glasl, B., Herndl, G. J., and Frade, P. R. (2016). The microbiome of coral surface mucus has a key role in mediating holobiont health and survival upon disturbance. *ISME J.* 10, 2280–2292. doi: 10.1038/ismej.2016.9

Grasshoff, K., Kremling, K., and Ehrhardt, M. (eds.). (2009). *Methods of Seawater Analysis*. John Wiley & Sons.

Haas, A. F., Gregg, A. K., Smith, J. E., Abieri, M. L., Hatay, M., and Rohwer, F. (2013). Visualization of oxygen distribution patterns caused by coral and algae. *PeerJ* 1:e106. doi: 10.7717/peerj.106

Haas, A. F., Knowles, B., Lim, Y. W., McDole Somera, T., Kelly, L. W., Hatay, M., et al. (2014). Unraveling the unseen players in the ocean - a field guide to

water chemistry and marine microbiology. *J. Vis. Exp.* 21, 1–16. doi: 10.3791/52131

Haas, A. F., Nelson, C. E., Wegley Kelly, L., Carlson, C. A., Rohwer, F., Leichter, J. J., et al. (2011). Effects of coral reef benthic primary producers on dissolved organic carbon and microbial activity. *PLoS ONE* 6:e27973. doi: 10.1371/journal.pone.0027973

Hemond, E. M., and Vollmer, S. V. (2015). Diurnal and nocturnal transcriptomic variation in the Caribbean *Staghorn coral*, *Acropora cervicornis*. *Mol. Ecol.* 24, 4460–4473. doi: 10.1111/mec.13320

Hernandez-agreda, A., Leggat, W., Bongaerts, P., and Ainsworth, D. (2016). The microbial signature provides insight into the mechanistic basis of coral success across reef habitats. *MBio* 7, 1–10. doi: 10.1128/mBio.00560-16

Hester, E. R., Barott, K. L., Nulton, J., Vermeij, M. J., and Rohwer, F. L. (2015). Stable and sporadic symbiotic communities of coral and algal holobionts. *ISME J.* 10, 1157–1169. doi: 10.1038/ismej.2015.190

Holm, S. (1979). A simple sequentially rejective multiple test. *Scand. J. Stat.* 6, 65–70.

Huttenhower, C., Gevers, D., Knight, R., Abubucker, S., Badger, J. H., Chinwalla, A. T., et al. (2012). Structure, function and diversity of the healthy human microbiome. *Nature* 486, 207–214. doi: 10.1038/nature11234

Jiang, S. C., and Paul, J. H. (1994). Seasonal and diel abundance of viruses and occurrence of lysogeny/bacteriocinogeny in the marine environment. *Mar. Ecol. Prog. Ser.* 104, 163–172. doi: 10.3354/meps104163

Kayanne, H., Suzuki, H., and Saito, H. (1995). Diurnal changes in the partial pressure of carbon dioxide in coral reef water. *Science* 269, 214–216. doi: 10.1126/science.269.5221.214

Knowles, B., Silveira, C., Bailey, B. A., Barrot, K., Cantu, V. A., Cobián-Güemes, A., et al. (2016). Lytic to temperate switching of viral communities. *Nature* 531, 466–470. doi: 10.1038/nature17193

Leão, Z. M. A. N., and Kikuchi, R. K. P. (2005). A relic coral fauna threatened by global changes and human activities, Eastern Brazil. *Mar. Pollut. Bull.* 51, 599–611. doi: 10.1016/j.marpolbul.2005.04.024

Levy, O., Achituv, Y., Yacobi, Y. Z., Dubinsky, Z., and Stambler, N. (2006). Diel "tuning" of coral metabolism: physiological responses to light cues. *J. Exp. Biol.* 209, 273–283. doi: 10.1242/jeb.01983

Levy, O., Kaniewska, P., Alon, S., Eisenberg, E., Karako-Lampert, S., Bay, L. K., et al. (2011). Complex diel cycles of gene expression in coral-algal symbiosis. *Science* 331, 175. doi: 10.1126/science.1196419

Loiola, M., Oliveira, M. D. M., and Kikuchi, R. K. P. (2013). Tolerance of Brazilian brain coral *Mussismilia braziliensis* to sediment and organic matter inputs. *Mar. Pollut. Bull.* 77, 55–62. doi: 10.1016/j.marpolbul.2013.10.033

López-Madrigal, S., Latorre, A., Porcar, M., Moya, A., and Gil, R. (2011). Complete genome sequence of "*Candidatus Tremblaya princeps*" strain PCVAL, an intriguing translational machine below the living-cell status. *J. Bacteriol.* 193, 5587–5588. doi: 10.1128/JB.05749-11

Martinez-Bakker, M., and Helm, B. (2015). The influence of biological rhythms on host–parasite interactions. *Trends Ecol. Evol.* 30, 314–326. doi: 10.1016/j.tree.2015.03.012

McArdle, B. H., and Anderson, M. J. (2001). Fitting multivariate models to community data: a comment on distance-based redundancy analysis. *Ecology* 82, 290–297. doi: 10.1890/0012-9658(2001)082[0290:FMMTCD]2.0.CO;2

McCutcheon, J. P., and Moran, N. A. (2011). Extreme genome reduction in symbiotic bacteria. *Nat. Rev. Microbiol.* 10, 13–26. doi: 10.1038/nrmicro2670

Meron, D., Atias, E., Kruh, L. I., Elifantz, H., Minz, D., Fine, M., et al. (2011). The impact of reduced pH on the microbial community of the coral *Acropora eurystoma*. *ISME J.* 5, 51–60. doi: 10.1038/ismej.2010.102

Meyer, F., Paarmann, D., D'Souza, M., Olson, R., Glass, E. M., Kubal, M., et al. (2008). The metagenomics RAST server - a public resource for the automatic phylogenetic and functional analysis of metagenomes. *BMC Bioinformatics* 9:386. doi: 10.1186/1471-2105-9-386

Neave, M. J., Apprill, A., Ferrier-Pagès, C., and Voolstra, C. R. (2016). Diversity and function of prevalent symbiotic marine bacteria in the genus Endozoicomonas. *Appl. Microbiol. Biotechnol.* 100, 8315–8324. doi: 10.1007/s00253-016-7777-0

O'Brien, P. A., Morrow, K. M., Willis, B., and Bourne, D. (2016). Implications of ocean acidification for marine microorganisms from the free-living to the host-associated. *Front. Mar. Sci.* 3:47. doi: 10.3389/fmars.2016.00047

Pantos, O., Bongaerts, P., Dennis, P. G., Tyson, G. W., and Hoegh-Guldberg, O. (2015). Habitat-specific environmental conditions primarily control the microbiomes of the coral *Seriatopora hystrix*. *ISME J.* 9, 1916–1927. doi: 10.1038/ismej.2015.3

Raina, J. B., Dinsdale, E. A., Willis, B. L., and Bourne, D. G. (2010). Do the organic sulfur compounds DMSP and DMS drive coral microbial associations? *Trends Microbiol.* 18, 101–108. doi: 10.1016/j.tim.2009.12.002

Reis, A. M. M., Araújo S. D. Jr., Moura, R. L., Francini-Filho, R. B., Pappas, G. Jr., Coelho, A. M. A., et al. (2009). Bacterial diversity associated with the Brazilian endemic reef coral *Mussismilia braziliensis*. *J. Appl. Microbiol.* 106, 1378–1387. doi: 10.1111/j.1365-2672.2008.04106.x

Rezende, C. E., Pfeiffer, W. C., Martinelli, L. A., Tsamakis, E., Hedges, J. I., and Keil, R. G. (2010). Lignin phenols used to infer organic matter sources to Sepetiba Bay - RJ, Brasil. *Estuar. Coast. Shelf Sci.* 87. 479–486. doi: 10.1016/j.ecss.2010.02.008

Ritchie, K. B. (2006). Regulation of microbial populations by coral surface mucus and mucus-associated bacteria. *Mar. Ecol. Prog. Ser.* 322, 1–14. doi: 10.3354/meps322001

Rohwer, F., Seguritan, V., Azam, F., and Knowlton, N. (2002). Diversity and distribution of coral-associated bacteria. *Mar. Ecol. Prog. Ser.* 243, 1–10. doi: 10.3354/meps243001

Schmieder, R., and Edwards, R. (2011a). Fast identification and removal of sequence contamination from genomic and metagenomic datasets. *PLoS ONE* 6:e17288. doi: 10.1371/journal.pone.0017288.

Schmieder, R., and Edwards, R. (2011b). Quality control and preprocessing of metagenomic datasets. *Bioinformatics* 27, 863–864. doi: 10.1093/bioinformatics/btr026

Schmieder, R., Lim, Y., Rohwer, F., and Edwards, R. (2010). TagCleaner: identification and removal of tag sequences from genomic and metagenomic datasets. *BMC Bioinformatics* 11:341. doi: 10.1186/1471-2105-11-341

Schneider, K., Levy, O., Dubinsky, Z., and Erez, J. (2009). *In situ* diel cycles of photosynthesis and calcification in hermatypic corals. *Limnol. Oceanogr.* 54, 1995–2002. doi: 10.4319/lo.2009.54.6.1995

Segal, B., Negrão, F., and Calderon, E. N. (2012). Four-year monthly sediment deposition on turbid southwestern Atlantic coral reefs, with a comparison of benthic assemblages. *Brazil. J. Oceanogr.* 60, 49–63. doi: 10.1590/S1679-87592012000100006

Shade, A., and Gilbert, J. A. (2015). Temporal patterns of rarity provide a more complete view of microbial diversity. *Trends Microbiol.* 23, 335–340. doi: 10.1016/j.tim.2015.01.007

Sharp, K. H., Distel, D., and Paul, V. J. (2012). Diversity and dynamics of bacterial communities in early life stages of the Caribbean coral *Porites astreoides*. *ISME J.* 6, 790–801. doi: 10.1038/ismej.2011.144

Shashar, N., Cohen, Y., and Loya, Y. (1993). Extreme diel fluctuations of oxygen in diffusive boundary layers surrounding stony corals. *Biol. Bull.* 185, 455–461. doi: 10.2307/1542485

Shashar, N., Kinaneb, S., Jokiel, P. L., and Pattersond, M. R. (1996). Hydromechanical boundary layers over a coral reef. *J. Exp. Mar. Biol. Ecol.* 199, 17–28. doi: 10.1016/0022-0981(95)00156-5

Silva, G. G. Z., Cuevas, D. A., Dutilh, B. E., and Edwards, R. A. (2014). FOCUS: an alignment-free model to identify organisms in metagenomes using non-negative least squares. *PeerJ* 2:e425. doi: 10.7717/peerj.425

Silva, G. G. Z., Green, K. T., Dutilh, B. E., and Edwards, R. A. (2016). Sequence analysis SUPER-FOCUS: a tool for agile functional analysis of shotgun metagenomic data. *Bioinformatics* 32, 354–361. doi: 10.1093/bioinformatics/btv584

Silveira, C. B., Silva-Lima, A. W., Francini-Filho, R. B., Marques, J. S. M., Almeida, M. G., Thompson, C. C., et al. (2015). Microbial and sponge loops modify fish production in phase-shifting coral reefs. *Environ. Microbiol.* 17, 3832–3846. doi: 10.1111/1462-2920.12851

Sloan, W. T., Lunn, M., Woodcock, S., Head, I. M., Nee, S., and Curtis, T. P. (2006). Quantifying the roles of immigration and chance in shaping prokaryote community structure. *Environ. Microbiol.* 8, 732–740. doi: 10.1111/j.1462-2920.2005.00956.x

Smith, J. E., Price, N. N., Nelson, C. E., and Haas, A. F. (2013). Coupled changes in oxygen concentration and pH caused by metabolism of benthic coral reef organisms. *Mar. Biol.* 160, 2437–2447. doi: 10.1007/s00227-013-2239-z

Sorek, M., Díaz-Almeyda, E. M., Medina, M., and Levy, O. (2014). Circadian clocks in symbiotic corals: the duet between *Symbiodinium* algae and their coral host. *Mar. Genomics* 14, 47–57. doi: 10.1016/j.margen.2014.01.003

Sweet, M. J., and Brown, B. E. (2016). Coral responses to anthropogenic stress in the twenty-first century: an ecophysiological perspective. *Oceanogr. Mar. Biol. Annu. Rev.* 54, 271–314. doi: 10.1201/9781315368597-6

Sweet, M. J., Brown, B. E., Dunne, R. P., Singleton, I., and Bulling, M. (2017). Evidence for rapid, tide-related shifts in the microbiome of the coral *Coelastrea aspera*. *Coral Reefs* 1–14. doi: 10.1007/s00338-017-1572-y

Sweet, M. J., and Bulling, M. T. (2017). On the importance of the microbiome and pathobiome in coral health and disease. *Front. Mar. Sci.* 4:9. doi: 10.3389/fmars.2017.00009

Sweet, M. J., Croquer, A., and Bythell, J. C. (2010). Temporal and spatial patterns in waterborne bacterial communities of an island reef system. *Aquat. Microb. Ecol.* 61, 1–11. doi: 10.3354/ame01433

Sweet, M. J., Croquer, A., and Bythell, J. C. (2011a). Bacterial assemblages differ between compartments within the coral holobiont. *Coral Reefs* 30, 39–52. doi: 10.1007/s00338-010-0695-1

Sweet, M. J., Croquer, A., and Bythell, J. C. (2011b). Development of bacterial biofilms on artificial corals in comparison to surface-associated microbes of hard corals. *PLoS ONE* 6:e21195. doi: 10.1371/journal.pone.0021195

Sweet, M. J., Croquer, A., and Bythell, J. C. (2014). Experimental antibiotic treatment identifies potential pathogens of white band disease in the endangered Caribbean coral *Acropora cervicornis*. *Proc. R. Soc. B* 281:20140094. doi: 10.1098/rspb.2014.0094

Theis, K. R., Dheilly, N. M., Klassen, J. L., Brucker, R. M., Baines, J. F., Bosch, T. C. G., et al. (2016). Getting the hologenome concept right: an eco-evolutionary framework for hosts and their microbiomes. *Msystems* 1:e00028-16. doi: 10.1128/mSystems.00028-16

Thingstad, T. F. (2000). Elements of a theory for the mechanisms controlling abundance, diversity, and biogeochemical role of lytic bacterial viruses in aquatic systems. *Limnol. Oceanogr.* 45, 1320–1328. doi: 10.4319/lo.2000.45.6.1320

Thompson, J. R., Rivera, H. E., Closek, C. J., and Medina, M. (2015). Microbes in the coral holobiont: partners through evolution, development, and ecological interactions. *Front. Cell. Infect. Microbiol.* 4:176. doi: 10.3389/fcimb.2014.00176

Webster, N. S., Uthicke, S., Botté, E. S., Flores, F., and Negri, A. P. (2013). Ocean acidification reduces induction of coral settlement by crustose coralline algae. *Glob. Change Biol.* 19, 303–315. doi: 10.1111/gcb.12008

Wild, C., Huettel, M., Klueter, A., Kremb, S. G., Rasheed, M. Y. M., and Jørgensen, B. B. (2004). Coral mucus functions as an energy carrier and particle trap in the reef ecosystem. *Nature* 428, 63–66. doi: 10.1038/nature02344

Wild, C., Woyt, H., and Huettel, M. (2005). Influence of coral mucus on nutrient fluxes in carbonate sands. *Mar. Ecol. Prog. Ser.* 287, 87–98. doi: 10.3354/meps287087

Williams, A. D., Brown, B. E., Putchim, L., and Sweet, M. J. (2015). Age-related shifts in bacterial diversity in a reef coral. *PLoS ONE* 10:e0144902. doi: 10.1371/journal.pone.0144902

Winget, D. M., and Wommack, K. E. (2009). Diel and daily fluctuations in virioplankton production in coastal ecosystems. *Environ. Microbiol.* 11, 2904–2914. doi: 10.1111/j.1462-2920.2009.02038.x

Winter, C., Herndl, G. J., and Weinbauer, M. G. (2004). Diel cycles in viral infection of bacterioplankton in the North Sea. *Aquat. Microb. Ecol.* 35, 207–216. doi: 10.3354/ame035207

Wood-Charlson, E. M., Weynberg, K. D., Suttle, C. A., Roux, S., and van Oppen, M. J. H. (2015). Metagenomic characterization of viral communities in corals: mining biological signal from methodological noise. *Environ. Microbiol.* 17, 3440–3449. doi: 10.1111/1462-2920.12803

Yakovleva, I., and Hidaka, M. (2004). Diel fluctuations of mycosporine-like amino acids in shallow-water scleractinian corals. *Mar. Biol.* 145, 863–873. doi: 10.1007/s00227-004-1384-9

Zaneveld, J. R., Burkepile, D. E., Shantz, A. A., Pritchard, C. E., McMinds, R., Welsh, R., et al. (2016). Overfishing and nutrient pollution interact with temperature to disrupt coral reefs down to microbial scales. *Nat. Commun.* 7:11833. doi: 10.1038/ncomms11833

Zilber-Rosenberg, I., and Rosenberg, E. (2008). Role of microorganisms in the evolution of animals and plants: the hologenome theory of evolution. *FEMS Microbiol. Rev.* 32, 723–735. doi: 10.1111/j.1574-6976.2008.00123.x

Conflict of Interest Statement: The authors declare that the research was conducted in the absence of any commercial or financial relationships that could be construed as a potential conflict of interest.

frontiers in Marine Science

ORIGINAL RESEARCH
published: 17 August 2017
doi: 10.3389/fmars.2017.00269

Non-intrusive Assessment of Photosystem II and Photosystem I in Whole Coral Tissues

Milán Szabó[1,2], Anthony W. D. Larkum[1], David J. Suggett[1], Imre Vass[3], László Sass[3], Barry Osmond[2,4], Alonso Zavafer[2], Peter J. Ralph[1] and Wah S. Chow[2]*

[1] Climate Change Cluster (C3), University of Technology Sydney, Ultimo, NSW, Australia, [2] Division of Plant Sciences, Research School of Biology, Australian National University, Acton, ACT, Australia, [3] Biological Research Centre, Institute of Plant Biology, Hungarian Academy of Sciences, Szeged, Hungary, [4] Centre for Sustainable Ecosystem Solutions, School of Biological Sciences, University of Wollongong, Wollongong, NSW, Australia

OPEN ACCESS

Edited by:
Zvy Dubinsky,
Bar-Ilan University, Israel

Reviewed by:
Itay Cohen,
Hebrew University of Jerusalem, Israel
Susana Enríquez,
National Autonomous University of Mexico, Mexico

***Correspondence:**
Milán Szabó
milan.szabo@uts.edu.au

Specialty section:
This article was submitted to Coral Reef Research, a section of the journal Frontiers in Marine Science

Received: *02 March 2017*
Accepted: *03 August 2017*
Published: *17 August 2017*

Citation:
Szabó M, Larkum AWD, Suggett DJ, Vass I, Sass L, Osmond B, Zavafer A, Ralph PJ and Chow WS (2017) Non-intrusive Assessment of Photosystem II and Photosystem I in Whole Coral Tissues. Front. Mar. Sci. 4:269. doi: 10.3389/fmars.2017.00269

Reef building corals (phylum Cnidaria) harbor endosymbiotic dinoflagellate algae (genus *Symbiodinium*) that generate photosynthetic products to fuel their host's metabolism. Non-invasive techniques such as chlorophyll (Chl) fluorescence analyses of Photosystem II (PSII) have been widely used to estimate the photosynthetic performance of *Symbiodinium in hospite*. However, since the spatial origin of PSII chlorophyll fluorescence in coral tissues is uncertain, such signals give limited information on depth-integrated photosynthetic performance of the whole tissue. In contrast, detection of absorbance changes in the near infrared (NIR) region integrates signals from deeper tissue layers due to weak absorption and multiple scattering of NIR light. While extensively utilized in higher plants, NIR bio-optical techniques are seldom applied to corals. We have developed a non-intrusive measurement method to examine photochemistry of intact corals, based on redox kinetics of the primary electron donor in Photosystem I (P700) and chlorophyll fluorescence kinetics (Fast-Repetition Rate fluorometry, FRRf). Since the redox state of P700 depends on the operation of both PSI and PSII, important information can be obtained on the PSII-PSI intersystem electron transfer kinetics. Under moderate, sub-lethal heat stress treatments (33°C for ~20 min), the coral *Pavona decussata* exhibited down-regulation of PSII electron transfer kinetics, indicated by slower rates of electron transport from Q_A to plastoquinone (PQ) pool, and smaller relative size of oxidized PQ with concomitant decrease of a specifically-defined P700 kinetics area, which represents the active pool of PSII. The maximum quantum efficiency of PSII (F_v/F_m) and functional absorption cross-section of PSII (σ_{PSII}) remained unchanged. Based on the coordinated response of P700 parameters and PSII-PSI electron transport properties, we propose that simple P700 kinetics parameters as employed here serve as indicators of the integrity of PSII-PSI electron transfer dynamics in corals.

Keywords: corals, photosynthesis, P700, chlorophyll fluorescence, heat stress

INTRODUCTION

Coral reefs are one of the world's most productive and diverse ecosystems, sustained through a symbiosis between reef-building corals and their endosymbiont eukaryotic microalgal partner (*Symbiodinium* sp.) and a complex bacterial consortia (Ainsworth et al., 2010). Nutrient exchange between partners is fuelled primarily by *Symbiodinium*'s photosynthetic productivity and hence light utilization is a key factor driving coral metabolism from the organismal (Roth, 2014) to the entire ecological (Muir et al., 2015) reef scale. As the highly orchestrated symbiotic metabolic exchange can be threatened by several environmental stress factors that may impact coral metabolism, it is crucial to understand stress impacts at the holobiont level through integrated bio-optical/bio-physical, metabolomics and molecular approaches (Pernice and Levy, 2014). The importance of understanding the photosynthetic processes is particularly critical to revealing the light utilization efficiency and thus niche specialization of corals across a range of biogeographical habitats. Such knowledge also characterizes a range of regulatory mechanisms that respond to environmental stress that define the resilience of the coral holobiont (Roth, 2014; Warner and Suggett, 2016). Photosynthetic productivity of *Symbiodinium* sp. is highly regulated via the coupled inter-system electron transfer processes between photosystem II (P680) and photosystem I (P700), but the regulation mechanisms of this process in *Symbiodinium* are still poorly understood.

Under steady state environmental conditions, PSII and PSI work in series to ensure the linear flow of electrons from the donor side of PSII to the acceptor side of PSI, and in turn drive CO_2 fixation via the Calvin-Benson Cycle. This linear electron flow is coupled with translocation of protons from the stroma to the lumen to build up a proton motive force that drives ATP synthase activity, producing a defined ratio of ATP and NADPH (e.g., Kramer and Evans, 2011). Over-reduction of the plastoquinone pool that could naturally occur under midday high irradiance levels e.g., in shallow reefs (Gorbunov et al., 2001) or as a result of impaired CO_2 fixation may initiate alternative pathways of electron flow to dissipate excessive excitation energy to avoid photo-oxidative stress while maintaining coordinated level of ATP production and NADPH synthesis (Cardol et al., 2011). For *Symbiodinium*, these processes are much less characterized than in higher plants or green algae (Warner and Suggett, 2016), but evidence suggests that alternative electron transport can manifest itself in the form of cyclic electron flow (CEF) operating between PSI and the cytochrome b_6/f complex possibly via the ferredoxin-dependent pathway (Aihara et al., 2016), or pseudo-cyclic electron flow of Mehler reaction, that plays a significant role in excess energy dissipation (Roberty et al., 2014). Expression of these pathways, however, may differ significantly between different *Symbiodinium* genotypes (Aihara et al., 2016; Warner and Suggett, 2016).

To characterize photosynthetic efficiency on multiple levels of organization of the symbiont algae, e.g., from free living state to single nubbins and *in situ* colonies, one of the most frequently applied methods is the detection of variable fluorescence of chlorophyll *a* (Chl *a*) (Warner et al., 2010). Such methods have been broadly applied to investigate light use efficiency (Gorbunov et al., 2001; Ralph et al., 2005; Szabó et al., 2014), photoacclimation (Hill and Ralph, 2005; Hennige et al., 2008; Lichtenberg et al., 2016), and photodamage (Ragni et al., 2010; Hill et al., 2011; Hill and Takahashi, 2014; Schrameyer et al., 2016) of intact corals under various environmental stress conditions. However, chlorophyll *a* fluorescence measurements of whole coral tissues are not always straightforward due to a strong light gradient and other complex optical properties specific to coral tissues (Enríquez et al., 2005; Wangpraseurt et al., 2012, 2014; Schrameyer et al., 2014; Lichtenberg et al., 2016). Light attenuation within coral tissue is strongly wavelength dependent (Wangpraseurt et al., 2012; Szabó et al., 2014), which particularly influences both the penetration depth of the excitation light beam projected onto the coral surface and the re-absorption of the fluorescence. Attempts to overcome this fundamental problem, based on attenuation of the functional absorption-cross section of PSII (σ) as a measure of effective irradiance within the tissue, are limited by the fact that these measurements are still performed at the coral surface thereby giving rise to potential artifacts of light attenuation of the probing and actinic light from the surface (Szabó et al., 2014). More recently, combined microfiber PAM and dissolved oxygen measurements were performed throughout the entire depth of the tissue, revealing stratification of chlorophyll *a* fluorescence signals from different symbiont layers with potentially different photoacclimation states (Lichtenberg et al., 2016). In addition, such measurements are still fundamentally invasive and less convenient for rapid monitoring of photosynthetic performance of whole corals, and do not provide information about PSI operation and/or electron transfer, an important regulatory process of alternative electron flow processes.

Whilst past studies have applied a combination of biophysical/photobiological methods (e.g., oxygen evolution and uptake measurements, variable chlorophyll *a* fluorescence and PSI reaction center (P700) redox kinetics) to evaluate the mechanisms underpinning photobiological operation (e.g., Suggett et al., 2008; Roberty et al., 2014; Aihara et al., 2016), most of these measurements require invasive treatment that is impractical on intact corals. Simultaneous measurements of Photosystems I and II electron transport rates [ETR(I) and ETR(II), respectively] in intact corals have been reported (Hoogenboom et al., 2012). However, their approach did not enable meaningful information to be derived about the kinetics

Abbreviations: DCMU, 3-(3,4-dichlorophenyl)-1,1-dimethyl-urea; FR, far red light; F_o, intrinsic fluorescence signal with fully oxidized Q_A in the dark; F_m, maximal fluorescence signal with fully reduced Q_A; F_v, Variable fluorescence in the dark (proportional to reducible Q_A); GA, glycolaldehyde; F_v/F_m, Maximum quantum efficiency of open PSII centers in the dark based on full Q_A reduction; MT, multiple turnover; LIFT-FRRF, laser-induced fluorescence transient fast repetition rate fluorometry; PAR, photosynthetically active radiation (400-700 nm); PSII, photosystem II; PSI, photosystem I; P700, special chlorophyll dimer acting as the primary electron donor in PSI; $P700^+$, oxidized state of P700; P_m, maximum $P700^+$ signal in weak FR light; PQ, plastoquinone pool σ_{PSII}—functional absorption cross section of PSII in the dark; Q_A, primary quinone electron acceptor in PSII; Q_B, secondary quinone electron acceptor in PS II; NIR, near infrared light; ST, single turnover.

of the intersystem electron transfer and the plastoquinone (PQ) pool size, which are the most significant descriptors of "active" PSII. Moreover, no assessment of the active pool of PSII based on P700 redox kinetics signal has been undertaken. P700 kinetics based on near-infrared (NIR) reflectance detection is a known whole-tissue measure for whole chain PSII and PSI electron transport e.g., in plant leaves (Jia et al., 2014), but its applicability for concerted PSII-PSI activity has not yet been evaluated in corals.

Our objective here was therefore to determine the applicability of simple P700 redox kinetic measurements to (i) assay both PSII and PSI activity, (ii) evaluate the applicability of PSI redox kinetics measurements in comparison with PSII chlorophyll *a* fluorescence kinetics measurements and (iii) reveal the behavior of coupled PSII-PSI electron transport under acute heat stress in the common Great Barrier Reef coral *Pavona decussata*, which is considered a relatively heat tolerant species in terms of photosynthetic activity. Due to such high thermal tolerance, this model species allows the investigation of fine changes of photosynthetic activity under short, acute stress conditions without initiating major alterations in photosynthetic pigment content, permanent physiological damage or symbiont expulsion e.g., during coral bleaching (McClanahan, 2004; Hill et al., 2012; Krämer et al., 2013; Schrameyer et al., 2014, 2016).

We show that (i) P700 redox kinetics as applied here provide accurate estimate of both the active PSII electron pool and the steady-state and maximal levels of $P700^+$ and (ii) sub-lethal heat stress impacts the redox state of $P700^+$ and PSII electron transfer processes, maintaining an enhanced electron turnover via PSI, even when linear electron flow from PSII is transiently impaired.

MATERIALS AND METHODS

Coral Material

Colonies of the coral species *P. decussata* (Dana) were collected from Heron Island lagoon, located on the southern Great Barrier Reef of Australia (151°55′E, 23°270′S) during July 2015. Prior to experimentation, coral colonies were maintained for 4–6 months in a recirculating 500-L aquarium at the University of Technology Sydney under constant temperature of 25°C, salinity of 32 ppt, and irradiance of 150 μmol photons m^{-2} s^{-1} (provided by Hydra FiftyTwo HD LED array, Aquaillumination®, C2 Development, Inc., USA) on a 12 h:12 h light:dark cycle. Before all measurements, *P. decussata* fragments (2–4 cm) were cut from the parent colonies and maintained for at least 12 h in 10-L aquaria aerated by bubbling of ambient air at 25°C and irradiance of 150 μmol photons m^{-2} s^{-1}.

For experimental treatments, coral nubbins were transiently moved to an optical glass cuvette (4 × 4 × 4 cm, Hellma Inc.) filled with seawater and constantly aerated with an air pump at a temperature of 25°C (control conditions) or set to a desired temperature using a heater/chiller (Julabo Ltd.) as described in the heat treatment section.

Simultaneous Measurements of PSII and PSI Photosynthetic Electron Transport

In order to measure the operation of PSII and PSI reaction center simultaneously, PSII chlorophyll fluorescence parameters (described in details in *"Active chlorophyll a fluorometry"*) and P700 kinetics (described in details in "*Measurement of redox kinetics of P700"* section) were recorded on the same spot of the same specimen, and under identical conditions (the configuration of the setup is shown in Figure S1). This was achieved using a multi-furcated fiber optics light-guide (Heinz Walz GmbH, Effeltrich, Germany) that integrated various probing light sources into a single light-guide aligned to the coral nubbin within the cuvette (described in "*Coral material"* section). The same multi-furcated fiber optic system also served for guiding P700/fluorescence signals to the chlorophyll fluorescence detectors and P700 emitter-detector unit. With this setup (Figure S1), potential artifacts resulting from differences in optical geometry and measuring conditions were minimized.

Measurement of Redox Kinetics of P700

Measurement of P700 redox changes in the current study is based on the principle that absorbance changes at ∼820 nm are related to changes in redox levels of the photosystem I reaction center P700, varying between 100% reduced (P700) and 100% oxidized ($P700^+$) states (Klughammer and Schreiber, 1994). The lowest signal level is related to 100% reduced P700, which upon application of far-red background light, is oxidized to the steady-state $P700^+$ level. Upon application of a saturation pulse (usually of white light that saturates both PSII and PSI), P700 becomes fully oxidized, representing 100% $P700^+$. After cessation of the saturation pulse, electron flow from PSII reduces $P700^+$, lowering the signal levels usually below the initial steady-state P700 level (because of the strong reducing pressure of electrons from PSII electrons, if active). With the far-red light continuously turned on, P700 is re-oxidized to the given steady state level. The corresponding changes in absorbance were monitored using a dual wavelength (820/870 nm) unit (ED-P700DW) attached to a pulse amplitude modulation (PAM) fluorometer (Heinz Walz GmbH, Effeltrich, Germany) in reflectance mode, in a custom made setup that synchronizes illumination and data acquisition using a multi-channel programmable pulse/delay generator, as described in details previously (Kou et al., 2013).

The amount of photo-oxidisable P700 was initially obtained by illuminating each coral nubbin with continuous far-red light illumination (∼200 μmol photons m^{-2} s^{-1}, peak wavelength 740 nm, from an LED735-66-60 diode array, Roithner LaserTechnik, Vienna, Austria) for ∼10 s to reach steady-state P700 oxidation. A measuring sequence was then initiated, which consisted of (i) a 50 ms delay phase to record the steady-state $P700^+$, (ii) a single-turnover saturating xenon flash (ST, irradiance $>10^6$ μmol photons m^{-2} s^{-1}, Heinz Walz GmbH, Effeltrich, Germany) to fully photo-oxidize P700 to form 100% $P700^+$ and (iii) a subsequent 900 ms phase to record P700 redox kinetics changes after cessation of the saturation pulse, but with background far-red light continuously present during the entire cycle. The peak level of the signal immediately after the saturation flash was denoted as P_m, representing the maximum photo-oxidisable P700. P700 kinetics signals following the saturation pulse were analyzed using a mathematical integration of the area that is bounded by the horizontal line representing the initial and final steady-state $P700^+$ levels in continuous far-red light, and the dipping curve representing the transient reduction of $P700^+$ by

electrons donated by PSII after a saturating flash—termed the "P700 kinetics area" for short (Kou et al., 2012; Hu et al., 2013; Fan et al., 2016b). One measuring cycle lasted for 950 ms, and 8 sequences, at 0.2 Hz, were averaged into a single trace to improve signal-to-noise.

Active Chlorophyll *a* Fluorometry

Variable chlorophyll fluorescence parameters were determined by Fast-Repetition Rate fluorometry (LIFT-FRRf, Soliense Inc.) using the "Q_A flash excitation" protocol, based on single turnover (ST) flashes. The instrument and the principle of the Q_A flash excitation protocol are described in detail Osmond et al. (2017). Briefly, excitation light provided by a blue LED (∼470 nm peak wavelength) is focused by the custom-built, 12 cm aperture telescope onto a ∼2 cm diameter spot that was aligned with one of the entry arms of the fiber-optics used for P700 and PAM measurements, providing a combined exit point of the fiber-optics facing the coral sample side (described above). The Q_A flash excitation protocol from the LIFT-FRRf marine instrument applied ∼1 μs flashlets of blue excitation light in a saturation sequence of 180 flashlets at 50% duty cycle (average excitation power of about 6300 μmol photons m^{-2} s^{-1}), spaced at 2 μs intervals, and a relaxation sequence with 90 flashlets with exponentially increasing intervals starting at 20 μs, resulting in a 362 μs long saturation sequence and a 28788 μs long relaxation sequence (29150 μs in total). The same telescope collected the red chlorophyll fluorescence signal, separated from the 470 nm excitation light using a 45° dichroic mirror (Edmund Optics NT47-948) and conveyed by a 12.5 mm diameter flexible 1 m optical fiber to the detector unit of the instrument. A 685 nm interference filter (25 nm bandwidth, 75% transmission; custom-made by Intor Inc.) further separated the chlorophyll fluorescence emission from the reflected excitation light.

The Q_A flash-induced fluorescence changes were analyzed using the automated fitting algorithm of the Soliense software (http://soliense.com/LIFT_Method.php) according to the biophysical FRR model of Kolber et al. (1998). The variable fluorescence yield, F_v is calculated as $F_v = F_m - F_o$, where F_o is minimal fluorescence and F_m is maximal fluorescence with fully reduced Q_A. The maximum photochemical efficiency of PSII is thus expressed as F_v/F_m. In addition, the functional absorption cross-section of PSII (σ_{PSII}), the kinetics of electron transport between PSII and PSI and the oxidized portion of PQ pool were estimated by fitting the LIFT-FRR fluorescence transients to the FRR model [http://soliense.com/LIFT_Method.php, "Size of the oxidized portion of PQ pool (PQ_{ox})"]. The decline in fluorescence yield during the relaxation of Q_A flash acquisition is fitted by two exponentials (τ_1 and τ_2) corresponding to the half times for electron transfer from faster component (in plants commonly referred as Q_A to the PQ) and slower component (in plants commonly referred as PQ pool to PSI, respectively, Osmond et al., 2017; and http://soliense.com/LIFT_Method.php).

Another method to monitor chlorophyll fluorescence is the so called OJIP protocol or the Kautsky induction curve or the polyphasic rise of chlorophyll fluorescence. This method consists of monitoring the kinetics of the chlorophyll induction curve in the transition between dark to light adapted state (Kalaji et al., 2017). This protocol primary measures the transition between the point where all PSII reaction center are open (refer as O step or F_o at 20 μs) to the point where all reaction centers are closed and the fluorescence intensity reaches its maximum, nominally called Peak (refer as P step or F_m) (Strasser, 1992). Additionally, two inflections can be observed at 2 ms (J step) and at 20 ms (I step). These four steps delimit three phases: OJ, JI and IP and conventionally it is believed that they are associated with events in the electron transport chain (ETC) (Strasser, 1992; Kalaji et al., 2017). The OJ, photochemical phase, relates to the reduction of the acceptor side of PSII (Strasser, 1992). The JI phase relates to the transport beyond Q_A and IP phase relates to several processes, in particular the electrons reaching PSI (Schansker et al., 2005; Kalaji et al., 2017). The induction curve of the chlorophyll *a* fluorescence (OJIP transient) was measured at 25°C using a Multichannel-Plant Efficiency Analyzer 2 (M-PEA, Hansatech Instruments, UK) (for a full description of the instrument refer to Strasser et al., 2010). The excitation, saturating and actinic light was 660 nm with an intensity of 5000 photons m^{-2} s^{-1} for 10 s. Fragments of corals were placed in an optical glass cuvette (described in "Coral material") filled with seawater. The cuvette was placed in front of the sensor head without the use of a leaf clip. To increase the light homogeneity within the sample holder, the cuvette was covered in aluminum foil. The sample was kept in darkness for 10 min with constant air bubbling.

Heat Stress and Recovery Experiment

Coral nubbins ($n = 3$) in the optical glass cuvette were dark-acclimated at 25°C for 10 min under continuous aeration to measure P_m, the P700 kinetics area, steady-state $P700^+$ and F_v/F_m in the dark-acclimated state (denoted as "control"). After recording photophysiological parameters in the "control" phase, the temperature was elevated to 33°C within ∼15 min. Following 20 min of elevated temperature treatment, the effects of the heat stress were recorded (denoted as "heat"). Samples were then returned to 25°C within ∼15 min, and after a further 20 min, the measurement sequence was repeated (denoted as "recovery"). In order to avoid any potential changes in the electron transport chain due to long dark acclimation periods (Hill and Ralph, 2008), samples were kept at growth irradiance ∼100 μmol photons m^{-2} s^{-1} of white light under constant aeration in the same optical glass cuvette throughout. This background light was kept on for the entire experiment, during the control, heat and recovery measurements, except the 10 min dark adaptation periods where the maximum quantum yield and the dark adapted P700 parameters were recorded. Measurements were performed through the fiber optic system on the same spot for the control, heat treatment and recovery phases, on three separate nubbins (independent biological replicates).

Inhibitor Treatments

Pavona decussata nubbins were first measured without the application of any inhibitor to determine baseline responses. Various chemical inhibitors were then added directly to the seawater surrounding the nubbins during the

control measurements. DCMU (3-(3,4-dichlorophenyl)-1,1-dimethylurea) was applied at a final concentration of 40 μM in complete darkness for ∼20 min, after which P700 measurements were performed. In the case of DCMU treatment, a combined heat treatment was also performed as described above ("Heat stress and recovery"). In a second experiment, the Calvin-Benson cycle inhibitor glycolaldehyde (GA) was applied at a final concentration of 5 mM in the same manner as for DCMU.

Statistical Analyses

Paired Sample *t*-test was applied for paired comparisons of parameter means (specified in Results) of heat-treated and control samples (with equal variances) using Origin Pro 9.1 (Origin, USA).

RESULTS

P700 Redox Kinetics under Heat Stress and Recovery

Steady-state $P700^+$ reflects the actual oxidized level of the $P700^+$ pool under weak far-red illumination, which attained the maximal level of $P700^+$ (P_m) upon receiving a strong saturation pulse (SP). As a result of the high intensity of the saturation pulse, electron flow from PSII led to the re-reduction of $P700^+$, with a decline in $P700^+$ below the initial steady-state $P700^+$. As the background FR light was continuously on, $P700^+$ increased again (due to the reoxidation of P700) and within ∼1000 ms attained a steady-state level. In the same specimen, under heat stress, the $P700^+$ trace exhibited similar pattern; however, the initial $P700^+$ level decreased and the P700 kinetics area became smaller, indicating slowing of electron flow from PSII under heat stress. These changes partially recovered to the original level upon cooling back to 25°C (**Figure 1**, representative traces).

As the absolute values of P_m, steady-state $P700^+$ and P700 kinetics area varies from specimen to specimen due to potential differences in symbiont density and optical properties etc., heat induced changes in P700 parameters are represented as relative changes (**Figure 2**). P_m significantly declined by ∼25% under heat stress and did not fully recover after the stress removal, compared to the untreated control (**Figure 2A**). Steady-state $P700^+$ significantly declined by ∼50% and recovered to ∼80% of the untreated control values (**Figure 2B**). P700 kinetics area significantly declined by ∼50% and exhibited only a partial recovery to ∼70% of the untreated control (**Figure 2C**). These trends suggest overall that the reduced form of PSI (i.e., less $P700^+$) is more prevalent under acute heat stress.

P700 Redox Kinetics under Heat Stress Conditions, When Linear Electron Flow was Chemically Inhibited by DCMU

Under acute heat stress $P700^+$ decreased; however, under these conditions it was not possible to judge to what extent linear electron flow from PSII might have contributed to redox changes of $P700^+$. Therefore, in order to investigate the behavior of P700 kinetics independently from PSII processes, the heat treatment experiment was performed on coral fragments when the linear electron flow was chemically blocked with DCMU (Jones et al., 2003). Treatment of *P. decussata* nubbins with DCMU completely eliminated the P700 kinetics area below the steady level (at 25°C) (**Figure 3**).

The parameter P_m did not change significantly with DCMU and heat treatment (**Figure 4A**). Steady-state $P700^+$ significantly increased by ∼45% upon DCMU treatment (at 25°C, **Figure 4B**), indicating elevated $P700^+$. In the presence of DCMU, heat treatment caused a reversible decline in steady-state $P700^+$ by ∼15%; however these changes were not statistically significant as compared to non-heat treated but DCMU treated samples.

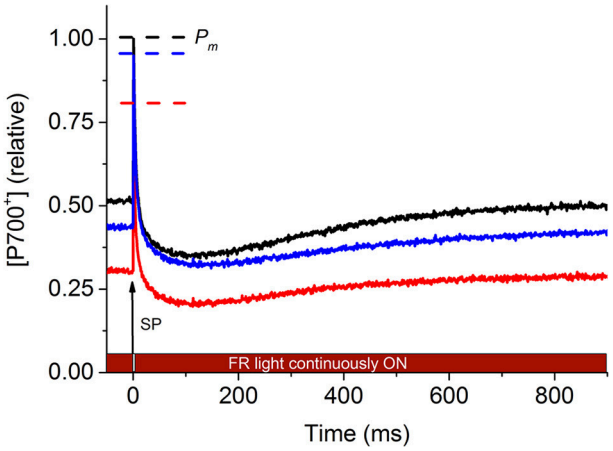

FIGURE 1 | Representative $P700^+$ kinetics signals of *P. decussata* estimated based on the absorbance changes at 820 nm (in reflectance mode). Measurements were done at 25°C (control, black line), at 33°C (heat, red line), and 25°C after the heat treatment (recovery, blue line). $P700^+$ signal intensity is shown in relative units as [$P700^+$] (relative). The initial 50 ms of the signal represents the steady state P700 level in the presence of weak far-red light. At time point $t = 0$ ms, a saturating pulse (SP) was applied to fully oxidize P700 (thus all P700 reaction centers are in the form of $P700^+$, denoted as P_m, representing the highest absorbance at 820 nm, dashed line with the respective colors of the different treatments). Electrons from PSII reduce $P700^+$, causing a decline in 820 nm absorbance to a level below the initial (first 50 ms) P700 redox level (because the reducing electron flow originating presumably from PSII exceeds the rate of forward electron flow out of PSI). As the weak FR light is continuously on (as indicated over the X axis), P700 gets reoxidized, causing the 820 nm signal to return to the steady-state level within ∼900 ms. For detailed description of P700 kinetics measurements, refer to Materials and methods. For heat-induced changes in P700 kinetics signal, refer to main text.

P700 Kinetics after Chemically Blocking Calvin-Benson Cycle

We further investigated whether the changes in $P700^+$ redox state could be related to the operation of Calvin-Benson cycle. This was performed by incubating coral fragments with the Calvin-Benson cycle inhibitor glycolaldehyde (GA). GA induced a decrease in the steady-state $P700^+$ levels and P700 kinetics area at the initial time points; upon prolonged incubation the P700 kinetics area completely disappeared (**Figure 5**), indicating that GA inhibition of Calvin-Benson cycle perturbs the photosynthetic pathways in a similar manner as heat stress, i.e.,

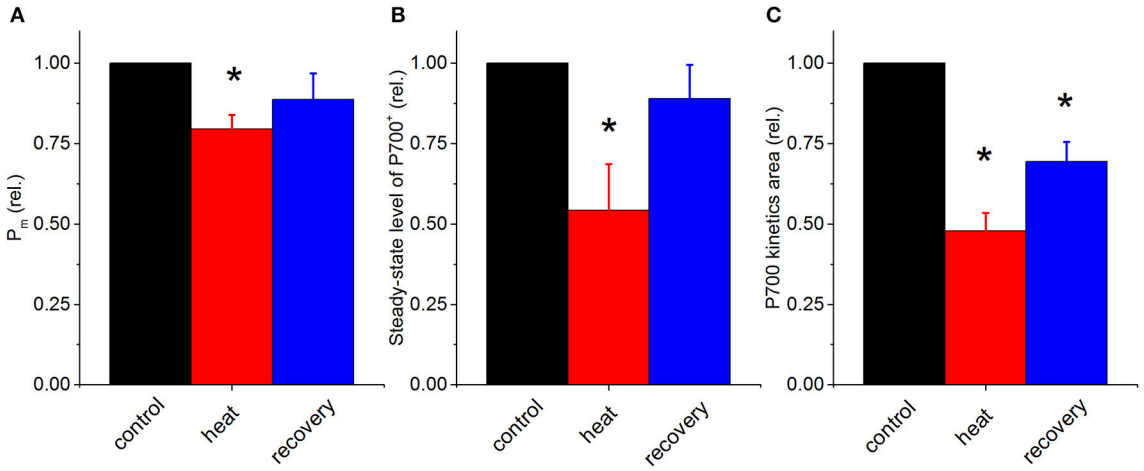

FIGURE 2 | Relative changes in P700 parameters in the coral *P. decussata* over the course of heat treatment and recovery period. P_m **(A)**, initial steady-state level of $P700^+$ **(B)**, and the values of P700 kinetics area ("PSII area") **(C)**; control, black column; heat treatment, red column and recovery, blue column. Signals were recorded on the same samples under the same temperature treatment as described in **Figure 1**. Statistically significant differences of parameters between control and treatment ($p < 0.05$) are denoted with asterisks. Error bars are standard errors of mean (SEM), $n = 3$.

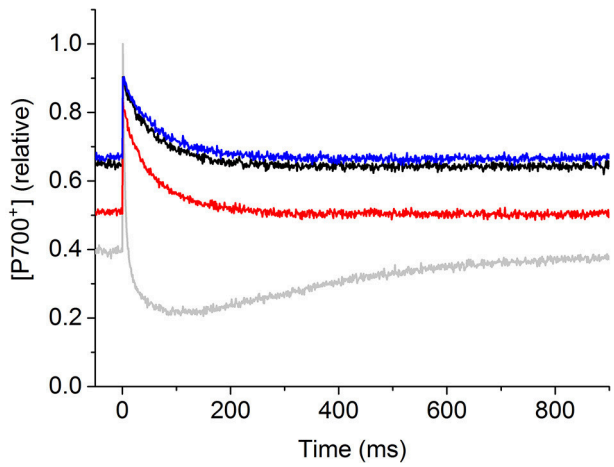

FIGURE 3 | Representative $P700^+$ kinetics signals of *P. decussata* when linear electron flow was chemically blocked by DCMU. Measurements were done at 25°C (control, black line), at 33°C (heat, red line), and 25°C after the heat treatment (recovery, blue line) all in the presence of 40 μM DCMU. Grey lines show the control signal in the absence of DCMU (recorded at 25°C). The same illumination protocol was applied as shown and described in **Figure 1**. $P700^+$ signal intensity is shown in relative units as [$P700^+$] (relative).

more reduced state of PSI and decreased electron flow from PSII to PSI; however the effect of chemical inhibition by GA was more pronounced than that of the acute heat stress (see Discussion).

Fast-Repetition Rate Fluorescence (FRRf) and Fast Induction Curve (OJIP) Parameters under Heat Stress

In order to investigate the PSII electron transfer kinetics under heat stress alongside PSI, under the same conditions as for the P700 measurements, fast fluorescence induction-relaxation chlorophyll fluorescence measurements were performed. Small changes could be observed in fluorescence kinetics during the saturation phase of the FRRf signal in heat stressed relative to control fragments (**Figure 6**); the calculated parameters, maximum quantum efficiency of PSII (F_v/F_m) (**Figure 7A**) and functional absorption cross-section (σ_{PSII}) (**Figure 7B**), did not change significantly, indicative of unaltered inherent properties of PSII reaction centers. In contrast, more substantial changes were observed during the relaxation phase of the fluorescence kinetics (**Figure 6**), as the relative oxidation state of the PQ pool significantly declined (i.e., the PQ pool became more reduced) (**Figure 7C**). Consistent with this, although the forward electron transfer time constant component τ_1 increased upon heating, this change was not significant (**Figure 7D**), whereas the longer relaxation time constant component, τ_2 increased significantly upon heat stress and partially recovered (**Figure 7E**), indicative of slowing electron transport rates between the PQ pool and PSI. This effect was largely reversed after recovery at 25°C.

Additional multi-phasic fast induction chlorophyll fluorescence measurements were performed to reveal the relative changes in the various phases of fluorescence rise during a multiple turnover saturating flash (**Figure 8**). In the double normalized curves, F_o (the "O" phase) is set to 0, whereas F_m (the "P" phase) is set to 1 to display relative changes. "Control" curve shows a typical OJIP rise of corals, with a distinguishable OJ phase (10^{-5} to 2×10^{-3} s) representing the photochemical phase of Q_A reduction to Q_A^- and the JI (2×10^{-3} to 10^{-1} s) and IP (10^{-1} to 2×10^{0} s) phases representing the thermal phase of fluorescence induction (e.g., Hill et al., 2004a). In heat treated samples, the fluorescence rise is almost complete already at the J phase, whereas the JIP phase largely disappeared. Under recovery conditions, the OJIP fluorescence induction curve regained its original characteristics of control samples, but the recovery was only partial.

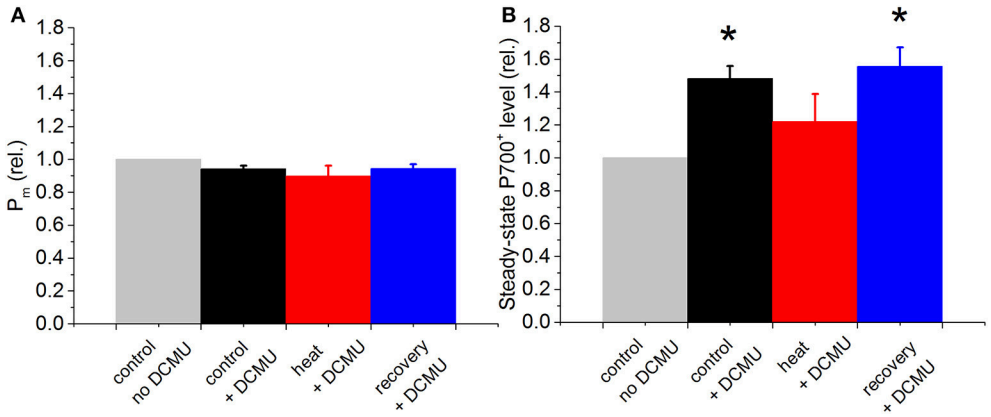

FIGURE 4 | Relative changes in P700 kinetics signals in the coral *P. decussata* over the course of heat treatment and recovery period, in the presence of DCMU. P_m **(A)**, and initial steady-state level of P700$^+$ **(B)** were recorded on the same dark-adapted samples, at the same time point. Control, black column; heat treatment, red column and recovery, blue column. Gray bars show the signal in the absence of DCMU, normalized to 1, to show relative changes caused by the treatments. Signals were recorded on the same samples under the same temperature treatment as described for Figure. Statistically significant differences between −DCMU and +DCMU control samples ($p < 0.05$) are shown with asterisk. Error bars are standard errors of mean (SEM), $n = 3$.

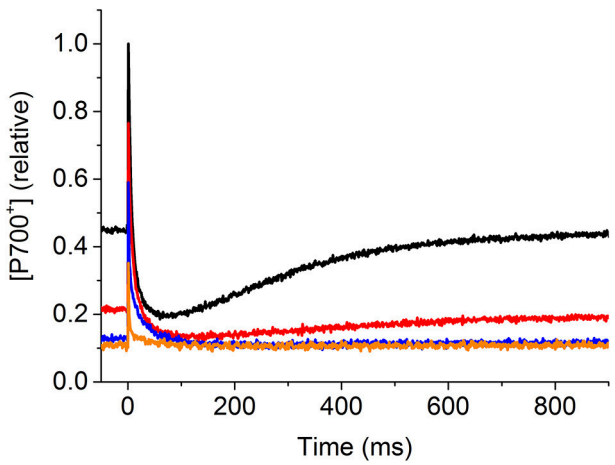

FIGURE 5 | Effect of the Calvin-Benson cycle inhibitor glycolaldehyde (GA) on P700 kinetics. Control nubbins were measured in the absence of the inhibitor (−GA, black line), then the same nubbins were incubated with 5 mM GA (+GA) and P700 measurements were performed at different time points: 50 min, red line; 2 h, blue line; 4.5 h, orange line. The same illumination protocol was applied as shown and described in **Figure 1**. P700$^+$ signal intensity is shown in relative units as [P700$^+$] (relative).

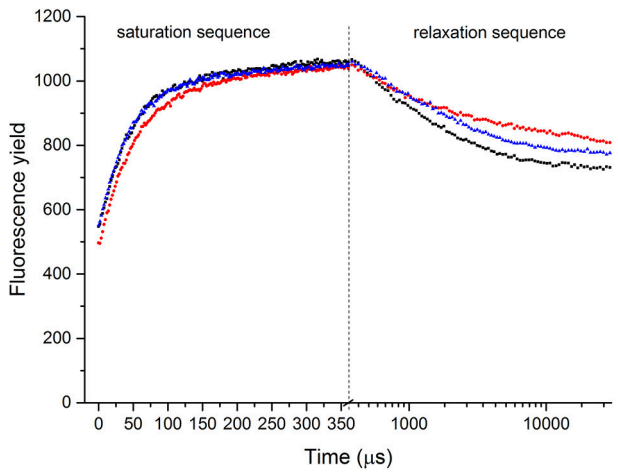

FIGURE 6 | Representative FRRf saturation-relaxation fluorescence traces of *P. decussata*. Measurements were done at 25°C (control, black line), at 33°C (heat, red line), and 25°C after the heat treatment (recovery, blue line). Saturation sequence is displayed on a linear timescale, whereas relaxation sequence is on a $\log_{10}$ timescale (the two sequences are visually separated with a dashed line). Y axis represents fluorescence yield.

DISCUSSION

Photosynthetic performance of reef-building corals plays a key role in determining their ecological success under normal growth conditions as well as in response to transient stressors (Warner et al., 2002; Anthony et al., 2007). Photobiological performance and photosynthetic energy budgets of *Symbiodinium* in hospite have been characterized and reviewed in several studies (Brodersen et al., 2014; Roth, 2014; Warner and Suggett, 2016). However, surprisingly, the available data regarding the fundamental intersystem PSII-PSI electron transport properties in corals is scarce. While changes in PSII activity represent one of the best known indicators of heat stress sensitivity (Warner et al., 1999; Hill et al., 2004b), the loss of PSII quantum efficiency, deduced from variable Chl fluorescence measurements, usually manifests itself under severe prolonged heat impacts which lead to extensive loss of photosynthetic performance (e.g., Hill et al., 2012). Intuitively, severe inhibition of PSII activity should be preceded by more subtle temperature perturbations of the electron transport flow through the whole photosynthetic machinery, lowering photosynthetic performance. Such

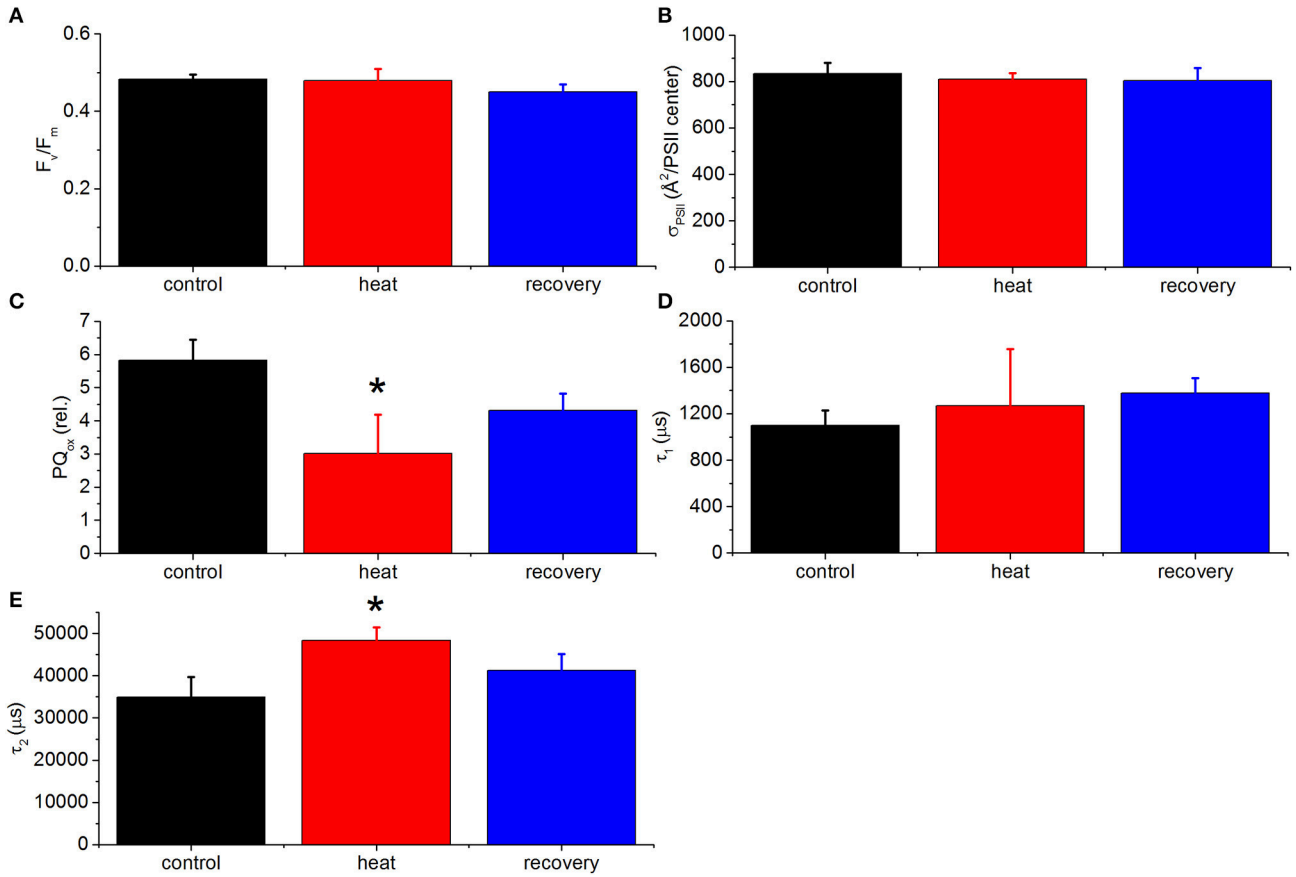

FIGURE 7 | Calculated FRRf parameters of *P. decussata*. F_V/F_M **(A)**, functional absorption cross-section of PSII **(B)**, relative oxidation state of the plastoquinone pool (PQ_{ox}) **(C)**, τ_1 **(D)**, and τ_2 **(E)**. Measurements were done at 25°C (control, black line), at 33°C (heat, red line) and 25°C after the heat treatment (recovery, blue line). Representative FRRf traces are shown in **Figure 6**. Statistically significant differences are shown with asterisks ($p < 0.05$). Error bars are standard errors of mean (SEM), $n = 3$.

decline in photosynthetic activity, if persistent, may lead to a *gradual deterioration of the photosynthetic performance of the endosymbiont algae without impacting the most characteristic indicator of the stress, the decline in PSII quantum efficiency*. Unfortunately, the PSII quantum efficiency is generally used as the most universal (and in most cases the only) indicator of the stress presence in corals. Earlier studies (Hoogenboom et al., 2012) indicated that PSII is a more vulnerable component to heat stress than PSI, which is in agreement with our finding that forward electron transfer kinetics slow down (**Figure 7**). However, the main aim of our approach was to ascertain whether using a single measurement of P700 redox kinetics yields information about both active PSII and PSI, possibly complementing the performance indicators obtained by more commonly applied chlorophyll fluorescence measurements.

The fact that acute heat stress caused remarkable changes in P700 kinetics, the steady-state level of $P700^+$ and the P700 kinetics area suggests that electron flow from PSII has a strong impact on the redox state of $P700^+$, similarly to the situation in higher plants (Oguchi et al., 2011; Jia et al., 2014). This is corroborated with the observations that the P700 kinetics area completely disappeared in the presence of DCMU (**Figure 3**) and the steady state $P700^+$ increased, as the linear electron flow from PSII reducing $P700^+$ has completely stopped. When heat stress was applied in the presence of DCMU, the steady-state $P700^+$ decreased, although to a much lesser extent as compared to the heat treatment in the absence of inhibitor (cf. **Figures 2**, **4**). The fact that the steady-state $P700^+$ level drops even in the presence of DCMU (when linear electron flow is blocked) indicates that alternative electron transport pathways might have been initiated under heat stress, the existence of which has been shown in *Symbiodinium* (Reynolds et al., 2008; Roberty et al., 2014; Aihara et al., 2016). The diminished response of steady-state $P700^+$ under heat stress, when DCMU was applied might be due to the disturbance of the redox poise of P700 by DCMU (Fan et al., 2016a). Our chlorophyll fluorescence measurements indicated that under moderate heat stress conditions, maximum PSII quantum efficiency and the functional cross-section of PSII were marginally affected by the heat stress. Instead, kinetic parameters of the photosynthetic electron transport responded to a higher degree. In plants, τ_1 reflects electron transport from Q_A to PQ, whereas τ_2 reflects a slower electron transfer component from

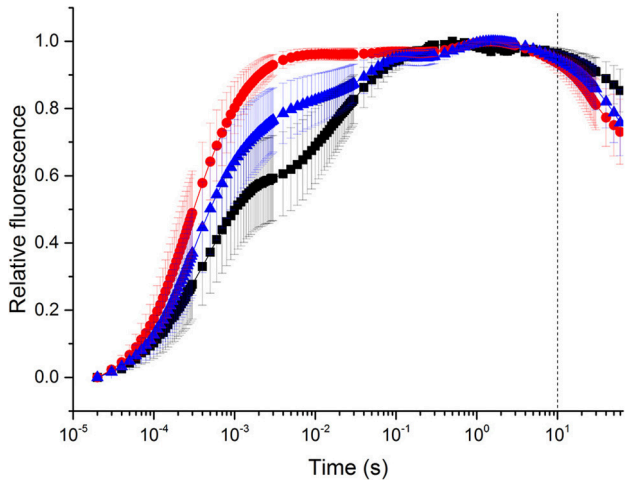

FIGURE 8 | Fast fluorescence induction (OJIP) curves. Measurements were done at 25°C (control, black line), at 33°C (heat, red line), and 25°C after the heat treatment (recovery, blue line). Illumination was applied from the beginning of data recording; the dashed line represents the timepoint when the illumination was turned off. Fluorescence traces are double-normalized (F_O set to 0 and F_m to 1) in order to represent relative changes. Error bars are standard errors of mean (SEM), $n = 3$.

PQ to PSI (Osmond et al., 2017). However, these electron transfer steps are uncharacterised in detail for corals; as such, here we refer to τ_1 as the fast component of electron transfer, an inherent property of PSII, which is largely unchanged under acute heat stress. In contrast, τ_2 is most likely closely related to the reduction level of the PQ pool (and possibly the electron transfer steps beyond PQ pool, indicated by the large time constant values), which is related to the phenomenon that the Q_B site is occupied by an electron that is unable to proceed to the PQ pool, because an oxidized PQ molecule from the PQ pool is unavailable. This is corroborated by the calculated oxidized portion of the PQ pool, which strongly declined upon heating. The concentration of oxidized PQ decreases when the PQ pool is more reduced due to limitation of electron transport at the acceptor side of PSI. This is in agreement with earlier findings that persistent reduction of the PQ pool was more prevalent under heat stress or bleaching conditions (Jones and Hoegh-Guldberg, 2001; Hill et al., 2004a).

This interpretation is further corroborated by the finding that when active electron flow from PSII to PSI is impaired under heat stress, maximal fluorescence of the fast induction (OJIP) curves occurs already at the J level, ~2 ms, with only a small thermal phase (JIP) present. Together these measurements indicate that the maximal photochemical capacity of PSII reaction centers is not affected (unchanged F_v/F_m and presence of photochemical OJ phase) under moderate heat stress, whereas the subsequent electron transfer steps became significantly impaired probably due to the heat-induced reduction of the PQ pool, as has been shown for higher plants (Tóth et al., 2007). Taken together, our observations suggest that when referring to the "active PSII electron transfer" involved in reducing $P700^+$, the critical steps appear to be the efficiency of electron transfer after the primary acceptor, Q_A^-, rather than the actual photochemical activity of PSII reaction centers (represented by the presence of OJ phase). While F_v/F_m measurements indicated little stress, the simultaneous measurements of PSII to PSI electron transfer rates clearly indicated severe impacts on the PSII-PSI intersystem electron flow, i.e. the forward electron transfer from Q_A to Q_B and the PQ pool. Steady-state $P700^+$ levels recorded at 820 nm, in the presence of weak FR light (740 nm) were very sensitive to heat-induced changes, indicating that under acute heat stress there is less $P700^+$ under continuous weak FR light, possibly due to enhanced electron pressure, which may originate from non-linear electron flow pathways.

The P700 kinetics signal underwent similar changes to heat stress when chemical inhibition of the Calvin-Benson cycle was applied. Glycolaldehyde (GA) is a known inhibitor of Calvin-Benson cycle in corals (Bhagooli, 2013; Hill et al., 2014) and earlier applications have demonstrated that under conditions when CO_2 fixation is impaired by chemical inhibition (Hill et al., 2014) or by decreased concentrations of dissolved inorganic carbon (Oakley et al., 2014), linear electron flow of photosynthesis is downregulated even at ambient temperatures in the absence of heat stress (Hill et al., 2014; Oakley et al., 2014). Such a response is in agreement with the current study, where P700 kinetics area (bounded by the horizontal line corresponding to steady-state illumination with far-red light and the dipping curve of $P700^+$ signal upon application of a saturating flash, representing the delivery of PSII electrons to PSI), completely disappears in the presence of GA, but in the absence of heat stress (**Figure 5**), in agreement with earlier findings on decreased oxygen evolution in corals as a result of GA treatment (Hill et al., 2014). In parallel with the loss of P700 kinetics area, the initial steady-state P700 level decreases, possibly because inhibition of Calvin-Benson cycle leads to elevated NADPH and ferredoxin levels that cause over-reduction of PQ pool through cyclic electron transport pathway(s) and blockage of the PSI acceptor side. This in fact leads to more reduced P700 (lower steady-state $P700^+$) and slower electron transfer rates (smaller P700 kinetics area). Therefore, GA treatment alone mimics the heat-induced changes in photosynthetic electron flow, but the acute heat stress applied in the current study may cause only partial inactivation of Calvin cycle (P700 kinetics area not completely lost), which can be recovered during the applied recovery period at 26°C. As for all dinoflagellates, *Symbiodinium* sp. carry a type II Rubisco (Whitney et al., 1995) that is considered generally more heat sensitive than type I Rubisco (Leggat et al., 2004). The same heat stress assay employed here was applied in earlier studies to cause partial inactivation of Rubisco in *Symbiodinium* (Lilley et al., 2010), which may lead to a decrease in relative oxidation level of PQ and thus electron flow back-pressure on PSII (Hill et al., 2014).

In summary, we suggest that under conditions when the chlorophyll fluorescence signals may be complex to interpret i.e., due to the vertical light heterogeneity in coral tissues (Wangpraseurt et al., 2012), P700 kinetics measurements performed in the NIR region may serve as a whole tissue marker for operation of both PSII and PSI and a non-invasive stress indicator of photosynthetic efficiency of coral endosymbionts (the combination of P700 and chlorophyll fluorescence methods

to understand intersystem PSII-PSI electron transfer properties are shown in Figure S2). How these current findings under transient and rapid (acute) heat stress ultimately apply to more prolonged heat stress events that drive coral bleaching in nature will be an important next question to investigate, as is, for example, whether the transient perturbation of intersystem electron flow, represented by the P700 kinetics signal, provides a sensitive marker of photosynthetic activity under other sub-lethal stress conditions as well. It has to be noted that during prolonged stress exposure, the P700 signal might also be influenced by bio-optical/physiological alterations of coral tissues (e.g., symbiont expulsion, changes in pigment concentrations across the tissue) that need to be investigated further. Physiological phenomena of the coral holobiont such as tentacle movement and/or contraction could have occurred in the experimental timeframe applied in the current study, and it may have influenced the cross-section and thus light availability within the coral tissues. However, we suggest that such impacts are minimal, because the functional absorption cross-section of PSII was found unchanged (**Figure 7B**). It also remains to be investigated whether P700 redox signal can be assigned as a functional trait, as it has been shown that chlorophyll fluorescence parameters can be associated with the different *Symbiodinium* genetic types as photobiological traits (Suggett et al., 2015; Goyen et al., 2017).

Finally, our results are in agreement with earlier observations (Jones et al., 1998; Lilley et al., 2010; Bhagooli, 2013; Hill et al., 2014) that a general weakness in corals (potentially leading to coral bleaching) could be the heat sensitivity of the Type II Rubisco, which causes partial inhibition of the Calvin-Benson cycle and CO_2 fixation, although the direct effect of acute heat stress on the Rubisco and on the whole photosynthetic productivity remains to be investigated. Under these circumstances, as indicated here, there may be side effects on cyclic electron transport and the Mehler-Ascorbate-Peroxidase (MAP) pathway. Recent works (Reynolds et al., 2008; Roberty et al., 2014; Aihara et al., 2016) have indicated the possibility that singlet oxygen production is generated when PQ pool is reduced, i.e., the relative size of oxidized PQ pool is smaller (and thus charge recombination in PSII reaction centers is promoted), which may be a primary factor in coral bleaching (Vass, 2012; Rehman et al., 2016). Nevertheless, these effects have to be documented individually in corals, where it is known that there are varied responses to similar acute thermal stress scenarios (Downs et al., 2013; Gardner et al., 2017). It is entirely possible that despite the "Achilles Heel" of a heat sensitive Rubisco, different *Symbiodinium* types have evolved different strategies to cope with this problem, and that the diversity of these strategies account for the different heat sensitivities of corals to coral bleaching.

AUTHOR CONTRIBUTIONS

MS, AL, IV, and WC planned the study. MS and AZ collected the data. MS, AL, AZ, IV, LS, DS, BO, and WC interpreted and analyzed the data. PR and WC provided consumables, reagents and tools. All authors contributed to drafting, critical commenting the manuscript and approved it for publication.

FUNDING

This work was supported by the award of Australian Research Council Discovery Project (ARC DP120101360) to WC and Future Fellowship (FT130100202) to DS. IV and LS were partly supported by a grant from the Hungarian National Research, Development and Innovation Office (NN110960). Construction of the prototype LIFT-FRRf instrument was supported by a development grant to BO from the University of Wollongong.

ACKNOWLEDGMENTS

The authors thank Dr. Zbigniew Kolber for his advice on LIFT-FRRf data analysis, Paul Brooks, Graeme Poleweski and David Hughes for maintenance of UTS coral tanks, Drs. Ross Lilley, Mathieu Pernice, Dimitri Tolleter and Duncan Fitzpatrick for fruitful discussions.

SUPPLEMENTARY MATERIAL

The Supplementary Material for this article can be found online at: http://journal.frontiersin.org/article/10.3389/fmars.2017.00269/full#supplementary-material

REFERENCES

Aihara, Y., Takahashi, S., and Minagawa, J. (2016). Heat induction of cyclic electron flow around photosystem I in the symbiotic dinoflagellate Symbiodinium. *Plant physiol.* 171, 522–529. doi: 10.1104/pp.15.01886

Ainsworth, T. D., Thurber, R. V., and Gates, R. D. (2010). The future of coral reefs: a microbial perspective. *Trends Ecol. Evol.* 25, 233–240. doi: 10.1016/j.tree.2009.11.001

Anthony, K., Connolly, S. R., and Hoegh-Guldberg, O. (2007). Bleaching, energetics, and coral mortality risk: effects of temperature, light, and sediment regime. *Limnol. Oceanogr.* 52, 716–726. doi: 10.4319/lo.2007.52.2.0716

Bhagooli, R. (2013). Inhibition of Calvin–Benson cycle suppresses the repair of photosystem II in Symbiodinium: implications for coral bleaching. *Hydrobiologia* 714, 183–190. doi: 10.1007/s10750-013-1535-4

Brodersen, K. E., Lichtenberg, M., Ralph, P. J., Kühl, M., and Wangpraseurt, D. (2014). Radiative energy budget reveals high photosynthetic efficiency in symbiont-bearing corals. *J. R. Soc. Int.* 11:20130997. doi: 10.1098/rsif.2013.0997

Cardol, P., Forti, G., and Finazzi, G. (2011). Regulation of electron transport in microalgae. *Biochim. Biophys. Acta* 1807, 912–918. doi: 10.1016/j.bbabio.2010.12.004

Downs, C., McDougall, K. E., Woodley, C. M., Fauth, J. E., Richmond, R. H., Kushmaro, A., et al. (2013). Heat-stress and light-stress induce different cellular pathologies in the symbiotic dinoflagellate during coral bleaching. *PLoS ONE* 8:e77173. doi: 10.1371/journal.pone.0077173

Enríquez, S., Méndez, E. R., and Iglesias-Prieto, R. (2005). Multiple scattering on coral skeletons enhances light absorption by symbiotic algae. *Limnol. Oceanogr.* 50, 1025–1032. doi: 10.4319/lo.2005.50.4.1025

Fan, D.-Y., Fitzpatrick, D., Oguchi, R., Ma, W., Kou, J., and Chow, W. S. (2016a). Obstacles in the quantification of the cyclic electron flux

around Photosystem I in leaves of C3 plants. *Photosyn. Res.* 129, 239–251. doi: 10.1007/s11120-016-0223-4

Fan, D.-Y., Ye, Z.-P., Wang, S.-C., and Chow, W. S. (2016b). Multiple roles of oxygen in the photoinactivation and dynamic repair of Photosystem II in spinach leaves. *Photosyn. Res.* 127, 307–319. doi: 10.1007/s11120-015-0185-y

Gardner, S. G., Raina, J.-B., Ralph, P. J., and Petrou, K. (2017). Reactive oxygen species (ROS) and dimethylated sulphur compounds in coral explants under acute thermal stress. *J. Exp. Biol.* 220, 1787–1791. doi: 10.1242/jeb.153049

Gorbunov, M. Y., Kolber, Z. S., Lesser, M. P., and Falkowski, P. G. (2001). Photosynthesis and photoprotection in symbiotic corals. *Limnol. Oceanogr.* 46, 75–85. doi: 10.4319/lo.2001.46.1.0075

Goyen, S., Pernice, M., Szabó, M., Warner, M. E., Ralph, P. J., and Suggett, D. J. (2017). A molecular physiology basis for functional diversity of hydrogen peroxide production amongst *Symbiodinium* spp. (Dinophyceae). *Mar. Biol.* 164:46. doi: 10.1007/s00227-017-3073-5

Hennige, S. J., Smith, D. J., Perkins, R., Consalvey, M., Paterson, D. M., and Suggett, D. J. (2008). Photoacclimation, growth and distribution of massive coral species in clear and turbid waters. *Mar. Ecol. Prog. Ser.* 369, 77–88. doi: 10.3354/meps07612

Hill, R., Brown, C. M., DeZeeuw, K., Campbell, D. A., and Ralph, P. J. (2011). Increased rate of D1 repair in coral symbionts during bleaching is insufficient to counter accelerated photo-inactivation. *Limnol. Oceanogr.* 56, 139–146. doi: 10.4319/lo.2011.56.1.0139

Hill, R., Larkum, A. W. D., Prasil, O., Kramer, D. M., Szabó, M., Kumar, V., et al. (2012). Light-induced dissociation of antenna complexes in the symbionts of scleractinian corals correlates with sensitivity to coral bleaching. *Coral Reefs* 31, 963–975. doi: 10.1007/s00338-012-0914-z

Hill, R., Larkum, A. W., Frankart, C., Kühl, M., and Ralph, P. J. (2004a). Loss of functional Photosystem II reaction centres in Zooxanthellae of corals exposed to bleaching conditions: using fluorescence rise kinetics. *Photosyn. Res.* 82, 59–72. doi: 10.1023/B:PRES.0000040444.41179.09

Hill, R., and Ralph, P. J. (2005). Diel and seasonal changes in fluorescence rise kinetics of three scleractinian corals. *Funct. Plant Biol.* 32, 549–559. doi: 10.1071/FP05017

Hill, R., and Ralph, P. J. (2008). Dark-induced reduction of the plastoquinone pool in zooxanthellae of scleractinian corals and implications for measurements of chlorophyll a fluorescence. *Symbiosis* 46, 45–56.

Hill, R., Schreiber, U., Gademann, R., Larkum, A. W. D., Kühl, M., and Ralph, P. J. (2004b). Spatial heterogeneity of photosynthesis and the effect of temperature-induced bleaching conditions in three species of corals. *Mar. Biol.* 144, 633–640. doi: 10.1007/s00227-003-1226-1

Hill, R., Szabó, M., ur Rehman, A., Vass, I., Ralph, P. J., and Larkum, A. W. (2014). Inhibition of photosynthetic CO_2 fixation in the coral Pocillopora damicornis and its relationship to thermal bleaching. *J. Exp. Biol.* 217, 2150–2162. doi: 10.1242/jeb.100578

Hill, R., and Takahashi, S. (2014). Photosystem II recovery in the presence and absence of chloroplast protein repair in the symbionts of corals exposed to bleaching conditions. *Coral Reefs* 33, 1101–1111. doi: 10.1007/s00338-014-1188-4

Hoogenboom, M. O., Campbell, D. A., Beraud, E., Dezeeuw, K., and Ferrier-Pages, C. (2012). Effects of light, food availability and temperature stress on the function of photosystem II and photosystem I of coral symbionts. *PLoS ONE* 7:e30167. doi: 10.1371/journal.pone.0030167

Hu, Y.-Y., Fan, D.-Y., Losciale, P., Chow, W. S., and Zhang, W.-F. (2013). Whole-tissue determination of the rate coefficients of photoinactivation and repair of photosystem II in cotton leaf discs based on flash-induced P700 redox kinetics. *Photosyn. Res.* 117, 517–528. doi: 10.1007/s11120-013-9822-5

Jia, H., Dwyer, S. A., Fan, D.-Y., Han, Y., Badger, M. R., von Caemmerer, S., et al. (2014). A novel P700 redox kinetics probe for rapid, non-intrusive and whole-tissue determination of photosystem II functionality, and the stoichiometry of the two photosystems *in vivo*. *Physiol. Plant* 152, 403–413. doi: 10.1111/ppl.12235

Jones, R., and Hoegh-Guldberg, O. (2001). Diurnal changes in the photochemical efficiency of the symbiotic dinoflagellates (Dinophyceae) of corals: photoprotection, photoinactivation and the relationship to coral bleaching. *Plant Cell Environ.* 24, 89–99. doi: 10.1046/j.1365-3040.2001.00648.x

Jones, R. J., Hoegh-Guldberg, O., Larkum, A. W. D., and Schreiber, U. (1998). Temperature-induced bleaching of corals begins with impairment of the CO_2 fixation mechanism in zooxanthellae. *Plant Cell Environ.* 21, 1219–1230. doi: 10.1046/j.1365-3040.1998.00345.x

Jones, R. J., Muller, J., Haynes, D., and Schreiber, U. (2003). Effects of herbicides diuron and atrazine on corals of the Great Barrier Reef, Australia. *Mar. Ecol. Prog. Ser.* 251, 153–167. doi: 10.3354/meps251153

Kalaji, H. M., Schansker, G., Brestic, M., Bussotti, F., Calatayud, A., Ferroni, L., et al. (2017). Frequently asked questions about chlorophyll fluorescence, the sequel. *Photosyn. Res.* 132, 13–66. doi: 10.1007/s11120-016-0318-y

Klughammer, C., and Schreiber, U. (1994). An improved method, using saturating light-pulses, for the determination of photosystem-I quantum yield via $P700^+$-absorbance changes at 830 nm. *Planta* 192, 261–268. doi: 10.1007/BF01089043

Kolber, Z. S., Prasil, O., and Falkowski, P. G. (1998). Measurements of variable chlorophyll fluorescence using fast repetition rate techniques: defining methodology and experimental protocols. *Biochim. Biophys. Acta Bioenerg.* 1367, 88–106. doi: 10.1016/S0005-2728(98)00135-2

Kou, J., Oguchi, R., Fan, D.-Y., and Chow, W. S. (2012). The time course of photoinactivation of photosystem II in leaves revisited. *Photosyn. Res.* 113, 157–164. doi: 10.1007/s11120-012-9743-8

Kou, J., Takahashi, S., Oguchi, R., Fan, D.-Y., Badger, M. R., and Chow, W. S. (2013). Estimation of the steady-state cyclic electron flux around PSI in spinach leaf discs in white light, CO2-enriched air and other varied conditions. *Funct. Plant Biol.* 40, 1018–1028. doi: 10.1071/FP13010

Kramer, D. M., and Evans, J. R. (2011). The Importance of energy balance in improving photosynthetic productivity. *Plant Physiol.* 155, 70–78. doi: 10.1104/pp.110.166652

Krämer, W. E., Schrameyer, V., Hill, R., Ralph, P. J., and Bischof, K. (2013). PSII activity and pigment dynamics of Symbiodinium in two Indo-Pacific corals exposed to short-term high-light stress. *Mar. Biol.* 160, 563–577. doi: 10.1007/s00227-012-2113-4

Leggat, W., Whitney, S., and Yellowlees, D. (2004). Is coral bleaching due to the instability of the zooxanthellae dark reactions? *Symbiosis* 37, 137–153.

Lichtenberg, M., Larkum, A. W., and Kühl, M. (2016). Photosynthetic acclimation of Symbiodinium in hospite depends on vertical position in the tissue of the scleractinian coral Montastrea curta. *Front. Microbiol.* 7:230. doi: 10.3389/fmicb.2016.00230

Lilley, R. M., Ralph, P. J., and Larkum, A. W. (2010). The determination of activity of the enzyme Rubisco in cell extracts of the dinoflagellate alga *Symbiodinium* sp. by manganese chemiluminescence and its response to short-term thermal stress of the alga. *Plant Cell Environ.* 33, 995–1004. doi: 10.1111/j.1365-3040.2010.02121.x

McClanahan, T. (2004). The relationship between bleaching and mortality of common corals. *Mar. Biol.* 144, 1239–1245. doi: 10.1007/s00227-003-1271-9

Muir, P. R., Wallace, C. C., Done, T., and Aguirre, J. D. (2015). Limited scope for latitudinal extension of reef corals. *Science* 348, 1135–1138. doi: 10.1126/science.1259911

Oakley, C. A., Schmidt, G. W., and Hopkinson, B. M. (2014). Thermal responses of Symbiodinium photosynthetic carbon assimilation. *Coral Reefs* 33, 501–512. doi: 10.1007/s00338-014-1130-9

Oguchi, R., Douwstra, P., Fujita, T., Chow, W. S., and Terashima, I. (2011). Intra-leaf gradients of photoinhibition induced by different color lights: implications for the dual mechanisms of photoinhibition and for the application of conventional chlorophyll fluorometers. *New Phytol.* 191, 146–159. doi: 10.1111/j.1469-8137.2011.03669.x

Osmond, C. B., Chow, W. S., Wyber, R., Zavafer, A., Keller, B., Muller, O., et al. (2017). Relative functional and optical absorption cross sections of PSII and other photosynthetic parameters monitored *in situ*, at a distance with a time resolution of a few seconds, using a prototype Light Induced Fluorescence Transient (LIFT) device. *Funct. Plant Biol.* doi: 10.1071/FP17024. [Epub ahead of print].

Pernice, M., and Levy, O. (2014). Novel tools integrating metabolic and gene function to study the impact of the environment on coral symbiosis. *Front. Microbiol.* 5:448. doi: 10.3389/fmicb.2014.00448

Ragni, M., Airs, R. L., Hennige, S. J., Suggett, D. J., Warner, M. E., and Geider, R. J. (2010). PSII photoinhibition and photorepair in Symbiodinium (Pyrrhophyta) differs between thermally tolerant and sensitive phylotypes. *Mar. Ecol. Prog. Ser.* 406, 57–70. doi: 10.3354/meps08571

Ralph, P. J., Schreiber, U., Gademann, R., Kühl, M., and Larkum, A. W. D. (2005). Coral photobiology studied with a new imaging pulse amplitude modulated fluorometer. *J. Phycol.* 41, 335–342. doi: 10.1111/j.1529-8817.2005.04034.x

Rehman, A. U., Szabó, M., Deák, Z., Sass, L., Larkum, A., Ralph, P., et al. (2016). *Symbiodinium* sp. cells produce light-induced intra-and extracellular singlet oxygen, which mediates photodamage of the photosynthetic apparatus and has the potential to interact with the animal host in coral symbiosis. *New Phytol.* 212, 472–484. doi: 10.1111/nph.14056

Reynolds, J. M., Bruns, B. U., Fitt, W. K., and Schmidt, G. W. (2008). Enhanced photoprotection pathways in symbiotic dinoflagellates of shallow-water corals and other cnidarians. *Proc. Natl. Acad. Sci. U.S.A.* 105, 13674–13678. doi: 10.1073/pnas.0805187105

Roberty, S., Bailleul, B., Berne, N., Franck, F., and Cardol, P. (2014). PSI Mehler reaction is the main alternative photosynthetic electron pathway in *Symbiodinium* sp., symbiotic dinoflagellates of cnidarians. *New Phytol.* 204, 81–91. doi: 10.1111/nph.12903

Roth, M. S. (2014). The engine of the reef: photobiology of the coral–algal symbiosis. *Front. Microbiol.* 5:422. doi: 10.3389/fmicb.2014.00422

Schansker, G., Toth, S. Z., and Strasser, R. J. (2005). Methylviologen and dibromothymoquinone treatments of pea leaves reveal the role of photosystem I in the Chl a fluorescence rise OJIP. *Biochim. Biophys. Acta Bioenerg.* 1706, 250–261. doi: 10.1016/j.bbabio.2004.11.006

Schrameyer, V., Krämer, W., Hill, R., Jeans, J., Larkum, A. W., Bischof, K., et al. (2016). Under high light stress two Indo-Pacific coral species display differential photodamage and photorepair dynamics. *Mar. Biol.* 163, 1–13. doi: 10.1007/s00227-016-2940-9

Schrameyer, V., Wangpraseurt, D., Hill, R., Kühl, M., Larkum, A. W., and Ralph, P. J. (2014). Light respiratory processes and gross photosynthesis in two scleractinian corals. *PLoS ONE* 9:e110814. doi: 10.1371/journal.pone.0110814

Strasser, R. J. (1992). The Fo and the OJIP fluorescence rise in higher plants and algae. *Regul. Chloroplast Biogenesis*. 226, 423–426.

Strasser, R. J., Tsimilli-Michael, M., Qiang, S., and Goltsev, V. (2010). Simultaneous *in vivo* recording of prompt and delayed fluorescence and 820 nm reflection changes during drying and after rehydration of the resurrection plant *Haberlea rhodopensis*. *Biochim. Biophys. Acta Bioenerg.* 1797, 122–122. doi: 10.1016/j.bbabio.2010.04.365

Suggett, D. J., Goyen, S., Evenhuis, C., Szabó, M., Pettay, D. T., Warner, M. E., et al. (2015). Functional diversity of photobiological traits within the genus Symbiodinium appears to be governed by the interaction of cell size with cladal designation. *New Phytol.* 208, 370–381. doi: 10.1111/nph.13483

Suggett, D. J., Warner, M. E., Smith, D. J., Davey, P., Hennige, S., and Baker, N. R. (2008). Photosynthesis and production of hydrogen peroxide by Symbiodinium (Pyrrhophyta) phylotypes with different thermal tolerances. *J. Phycol.* 44, 948–956. doi: 10.1111/j.1529-8817.2008.00537.x

Szabó, M., Wangpraseurt, D., Tamburic, B., Larkum, A. W., Schreiber, U., Suggett, D. J., et al. (2014). Effective light absorption and absolute electron transport rates in the coral *Pocillopora damicornis*. *Plant Physiol. Biochem.* 83, 159–67. doi: 10.1016/j.plaphy.2014.07.015

Tóth, S. Z., Schansker, G., and Strasser, R. J. (2007). A non-invasive assay of the plastoquinone pool redox state based on the OJIP-transient. *Photosyn. Res.* 93, 193–203. doi: 10.1007/s11120-007-9179-8

Vass, I. (2012). Molecular mechanisms of photodamage in the Photosystem II complex. *Biochim. Biophys. Acta Bioenerg.* 1817, 209–217. doi: 10.1016/j.bbabio.2011.04.014

Wangpraseurt, D., Larkum, A. W., Franklin, J., Szabó, M., Ralph, P. J., and Kühl, M. (2014). Lateral light transfer ensures efficient resource distribution in symbiont-bearing corals. *J. Exp. Biol.* 217, 489–498. doi: 10.1242/jeb.091116

Wangpraseurt, D., Larkum, A. W., Ralph, P. J., and Kühl, M. (2012). Light gradients and optical microniches in coral tissues. *Front. Microbiol.* 3:316. doi: 10.3389/fmicb.2012.00316

Warner, M., Chilcoat, G., McFarland, F., and Fitt, W. (2002). Seasonal fluctuations in the photosynthetic capacity of photosystem II in symbiotic dinoflagellates in the Caribbean reef-building coral Montastraea. *Mar. Biol.* 141, 31–38. doi: 10.1007/s00227-002-0807-8

Warner, M. E., Fitt, W. K., and Schmidt, G. W. (1999). Damage to photosystem II in symbiotic dinoflagellates: a determinant of coral bleaching. *Proc. Natl. Acad. Sci. U.S.A.* 96, 8007–8012. doi: 10.1073/pnas.96.14.8007

Warner, M. E., Lesser, M. P., and Ralph, P. J. (2010). "Chlorophyll fluorescence in reef building corals," in *Chlorophyll a Fluorescence in Aquatic Sciences: Methods and Applications Developments in Applied Phycology*, Vol. 4, eds D. J. Suggett, O. Prášil, and M. A. Borowitzka (Dordrecht: Springer), 209–222.

Warner, M. E., and Suggett, D. J. (2016). "The Photobiology of *Symbiodinium* spp.: linking physiological diversity to the implications of stress and resilience," in *The Cnidaria, Past, Present and Future*, eds S. Goffredo and Z. Dubinsky (Cham: Springer), 489–509.

Whitney, S. M., Shaw, D. C., and Yellowlees, D. (1995). Evidence that some dinoflagellates contain a Ribulose-1, 5-bisphosphate carboxylase/oxygenase related to that of the $ alpha $-proteobacteria. *Proc. Biol. Sci.* 259, 271–275. doi: 10.1098/rspb.1995.0040

Conflict of Interest Statement: The authors declare that the research was conducted in the absence of any commercial or financial relationships that could be construed as a potential conflict of interest.

frontiers in Marine Science

METHODS
published: 21 August 2017
doi: 10.3389/fmars.2017.00266

Method for Determining the Contribution of Fluorescence to an Optical Signature, with Implications for Postulating a Visual Function

Charles Mazel *

NIGHTSEA, Lexington, MA, United States

The fluorescence of many marine organisms is a visually compelling phenomenon. Descriptions of the phenomenon have at times been accompanied by suggestions of a visual function, but with minimal supporting evidence. It is possible to make quantitative estimates of the contribution of fluorescence emission to a visual signal under arbitrary illumination conditions. This analysis can help in deciding whether further research into a visual function is warranted, or whether the fluorescence is an interesting epiphenomenon associated with biomaterials that are present for other purposes. This paper describes the concepts associated with visual signals consisting of both reflected and fluoresced light, and methods for determining the underlying optical properties and using that information to model visual signal under environmentally relevant illumination conditions.

Keywords: fluorescence, vision, optical signature, visual signature modeling, fluorescence and marine life

OPEN ACCESS

Edited by:
Daniel Wangpraseurt, University of Cambridge, United Kingdom

Reviewed by:
Jörg Wiedenmann, University of Southampton, United Kingdom
Daniel Osorio, University of Sussex, United Kingdom

***Correspondence:**
Charles Mazel
mazelcharles@gmail.com

Specialty section:
This article was submitted to Coral Reef Research, a section of the journal Frontiers in Marine Science

Received: *01 May 2017*
Accepted: *02 August 2017*
Published: *21 August 2017*

Citation:
Mazel C (2017) Method for Determining the Contribution of Fluorescence to an Optical Signature, with Implications for Postulating a Visual Function. Front. Mar. Sci. 4:266. doi: 10.3389/fmars.2017.00266

INTRODUCTION

The fluorescence of many marine organisms is a visually compelling phenomenon. It is typically discovered and documented by illuminating the subject with an intense light source of appropriate wavelength and viewing it through a complementary barrier filter that blocks the reflected excitation light and transmits the fluorescence. The emitted colors are highly saturated and create a strikingly beautiful effect. There tends to be strong contrast against the background, especially since the exploration is generally done in darkness. It is natural to ask "Why does that happen?" This question can be interpreted either mechanistically (What is the physical source of the fluorescence?) or functionally (What, if any, is the purpose of the fluorescence?).

The equipment for locating and documenting fluorescence *in situ* or *in vivo* has become readily available in recent years, leading to an explosion of observations that in turn have led to an increase in scientific research. Much of this has focused on origin and possible ecophysiological roles of the fluorescing proteins in reef corals (Salih et al., 2000; Kelmanson and Matz, 2003; Ugalde et al., 2004; Bou-Abdallah et al., 2006; Palmer et al., 2009; Gittins et al., 2015; Smith et al., 2017), but some studies have touched on possible visual functions in fish and other marine organisms (Mazel et al., 2004; Haddock et al., 2005; Matz et al., 2006; Michiels et al., 2008; Gerlach et al., 2014; Sparks et al., 2014; Haddock and Dunn, 2015; Gruber et al., 2016). A few of these latter have had a strong foundation in measurement and analysis, while others have been more speculative and suggestive, based purely on observation and correlation.

When we view and photograph fluorescence *in situ* or in the laboratory we are almost always doing so under highly artificial conditions-in the dark, armed with an intense narrow-band excitation light source and an efficient barrier filter that rejects reflected light and isolates the fluorescence. Observations made in this way do not in themselves tell you anything about how the fluorescence might contribute to the appearance of the organism under natural environmental lighting conditions. And while it is always valid to ask "Why?" in the functional sense, there is no reason to presuppose a visual function. The existence of any characteristic in an organism is not a priori evidence of a functional role for that characteristic. It may simply be an epiphenomenon present in materials evolved for other purposes. For example, human teeth fluoresce quite strongly when excited and viewed under identical conditions to those used with marine organisms (**Figure 1**), but this emission is not noticeable under natural conditions and no one has yet suggested that this might be functional.

This paper describes a method for collecting and analyzing the data needed to investigate one of the criteria that must be satisfied to demonstrate a visual function for fluorescence—that the fluorescence is sufficiently intense to make a meaningful contribution to the optical signature under realistic illumination conditions. After describing the basis we go through the method with a test case for a fluorescent shark.

BACKGROUND

The criteria to demonstrate a visual function for fluorescence are listed below. Note that there can be alternative ways of formulating these, but they will all include the same basic elements.

1. Fluorescence exists when the subject is illuminated at wavelengths that are naturally present in its habitat.
2. The organism for which a viewing function is postulated is physiologically capable of perceiving the wavelengths of the fluorescence emission.
3. There is enough energy transferred into the fluorescence band to make a meaningful contribution to the visual signal under relevant illumination conditions.
4. The viewing organism's behavior is influenced by the presence vs. absence of fluorescence in the subject.

Demonstrating #1 is straightforward. As noted above, the technology to explore for and document fluorescence is robust and readily available commercially. The excitation wavelengths most commonly used for exploration are typically in the mid-blue portion of the spectrum (~440–460 nm), a range that is transmitted well in seawater, is generally available in the environment, and has proved to be effective in exciting fluorescence in a wide range of organisms. There is, however, no "ideal" wavelength range for exciting all instances of fluorescence, and there is a potential for other naturally available wavelengths to be involved.

Demonstrating #2 takes more specialized equipment, but the requirements and techniques are known. You need to show that the fluorescence can reach the light-sensing cells and be absorbed by the visual pigments. The latter is typically determined by microspectrophotometry on receptor cells (e.g., Hanaoka and Fujimoto, 1957; Chung and Marshall, 2016). Incident light can also be affected by intraocular filters before it reaches the retina (Heinermann, 1983; Douglas and Marshall, 1999). The absorption properties of such filters can be measured with a spectrometer. Lens filters can potentially act as barrier filters to enhance the fluorescence relative to reflected light but could also block fluorescence wavelengths.

Demonstrating #3 requires specialized equipment and data analysis, and one methodological approach to this is the focus of this paper.

Demonstrating #4 is perhaps hardest of all. It can be extremely difficult to set up experimental conditions that eliminate the fluorescence while not affecting other visual factors at the same time but this has been done for several cases (Arnold et al., 2002; Gerlach et al., 2014; Haddock and Dunn, 2015).

There have been peer-reviewed publications that have strongly suggested, or even claimed, demonstration of a visual function based simply on criteria 1, or 1 and 2, combined with a hypothesis (untested) about the role the fluorescence might play in the organism's life (Sparks et al., 2014; Gruber et al., 2016). This is not sufficient. Considering the fluorescence of human teeth, the fluorescence certainly exists (#1), and humans certainly have the *ability* to see the emitted wavelengths (#2), but that does not mean that there is enough energy in the fluorescence to make a noticeable difference in appearance under natural lighting conditions (#3) nor is there any evidence to suggest that it influences our behavior (#4).

Before delving into the measurements needed to evaluate #3 it is worth thinking about what is involved in fluorescence constituting a meaningful visual signal. To be meaningful the fluorescence would have to make a material contribution to the organism's appearance in a way that is involved in behavior. This generally means that it either increases contrast against the viewing background such that the organism can be seen *more* easily (mating attraction, warning or threat displays, lures to attract prey, etc.) or reduces that contrast so that it can be seen *less*

FIGURE 1 | Fluorescence photograph of human teeth. Photograph made using the same methods as generally used for fluorescence images of marine organisms.

easily (camouflage to reduce the chance of being preyed upon, or to increase the chance of prey capture).

It has been noted (Lythgoe, 1979; Johnsen, 2011) that fluorescence has a greater potential to play a role in visual function in the marine than in the terrestrial environment. This is because the world above water is generally awash in broadband illumination (white light) and it is more of a challenge for fluorescence, which tends to be a relatively weak effect, to enhance coloration relative to simple reflectance. Water, by contrast, is an optical filter, selectively removing wavelengths of visible light exponentially as a function of depth. First to be absorbed are the long wavelength reds, then the oranges, then the yellows. Next are either the greens or the blues, depending on the water type. In clear tropical waters blue light penetrates the furthest, while in temperate coastal waters that contain high loads of blue-absorbing colored dissolved organic matter (CDOM) the water color tends more toward the green (Mobley, 1994).

Because fluorescence is a transformation of energy from one wavelength to another it is potentially a means of producing colors that would not otherwise be present in this spectrally limited environment. Moving energy from wavelengths that are naturally present to wavelengths that are not has the greatest potential to create visual contrast. Oranges and reds are a great "choice" for fluorescence contrast in the sea since those wavelengths are effectively not present in downwelling light once one reaches a depth of ∼20 m, even in clear tropical waters. The coral that appears distinctly orange in the photograph on the left in **Figure 2** attracted a diver's attention since it was encountered at a depth at which there is effectively no orange light and it stood out in strong contrast with the washed-out blue of its surroundings. This image was made with ambient light alone. When photographed again with an electronic flash (right) the coral is not particularly distinctive. Note that the coral must still be fluorescing in that image, and even more so than in the image on the left, since it is being illuminated by the same ambient light *plus* the light from the electronic flash. The orange fluorescence is completely overwhelmed by the reflected light from the flash.

The most commonly encountered fluorescence color, both in corals and fish, is green. Transferring energy from the blue to the green has less potential to create contrast since green light generally travels quite well in water, so it is "available" to be reflected, and the fluorescence must be intense if it is to have an enhancement effect. There are many corals that appear quite intensely green under blue light excitation in the dark but that give no hint of that color under daylight illumination. There are others, however, in which the fluorescence energy transfer is great enough that the green fluorescence is evident (at least to a human) even in relatively shallow water. We can call the first type "covert fluorescence" in the sense that the fluorescence is present but not obviously visible, while in the latter case we can call it "overt fluorescence." Examples of both types often coexist in the same habitat, so they are exposed to exactly the same downwelling light. The difference is in the efficiency of the fluorescence.

Diver observation like this (overt vs. covert) might give a hint of fluorescence contribution, but in the end the issue of factor #3–whether the process of fluorescence is contributing enough photons to feasibly make a contribution to appearance–must be considered from the point of view of whatever organism is hypothesized to view the fluorescence. What is covert to a human might be overt to another organism, possibly only at certain times of day or depth. It is possible to make quantitative measurements that enable modeling of the light leaving the surface of a fluorescing organism, including both the reflected and fluoresced components.

OPTICAL SIGNATURE

The light leaving a fluorescing organism under any illumination condition will be a combination of two components—ambient light that has been reflected from the surface of the organism, without a change of wavelength, and light that has been absorbed and then re-emitted in a different wavelength band by the fluorescence. The totality of light leaving the surface is termed

FIGURE 2 | Coral (*Scolymia* sp.) at a depth of ∼20 m photographed with ambient light **(left)** shows distinct natural fluorescence compared to image made with electronic flash **(right)**, Saba, Lesser Antilles. Images © Conrad Blickenstorfer.

the *exitance*. It is possible, and indeed desirable, to make direct measurements of the exitance either *in situ* or *in vivo* under realistic lighting conditions. However, it is generally not practical to make those measurements under what is likely to be the very wide range of possible ambient lighting conditions that the subject might be exposed to through the course of the day and year, and as a function of depth, cloud cover, and other variables.

In this paper we outline the information needed to compute the exitance under arbitrary illumination conditions, and methods to collect the necessary data. In addition to providing the overall spectral signature, the results can also be used to calculate the extent to which fluorescence enhances the signal relative to the same system without fluorescence. The principles and methods are then illustrated with a case study of fluorescence in a shark. The methods to be described were originally developed to model the contribution of fluorescence to the perceived color of corals (Mazel and Fuchs, 2003), but can be applied to any subject.

METHODS

We describe here a method for calculating the light that leaves a fluorescing surface under any illumination conditions. This is not the only possible way to do this, but it has been successfully applied to the analysis of fluorescing marine organisms (Mazel and Fuchs, 2003; Mazel et al., 2004). Alternative approaches are described, for example, in the analyses of the contribution of fluorescence to the appearance of flowers (Iriel and Lagorio, 2010), a frog (Taboada et al., 2017), and a red-fluorescent fish (Bitton et al., 2017).

The light leaving the surface is the *exitance*, which we will designate as *E*. This and other quantities to be discussed here, unless otherwise noted, vary with wavelength and are designated in the form $E(\lambda)$. Exitance can be in energy or photon flux units, and for this discussion we will assume the latter.

The total exitance at any wavelength consists of photons produced by reflection without a change of wavelength, *R*, and photons resulting from fluorescence, *F*.

$$E(\lambda) = R(\lambda) + F(\lambda) \tag{1}$$

The reflected component is the product of the incident light, I_0, and the true reflectance, R_T, again on a wavelength by wavelength basis (Equation 2). Reflectance is a non-dimensional quantity designating the fraction of photons reflected at each wavelength. Measurement of reflectance from a fluorescing surface is complicated by the presence of both reflected and fluoresced photons, the exact question that we are addressing here. The "true reflectance" refers only to the reflected component.

$$R(\lambda) = I_0(\lambda) * R_T(\lambda) \tag{2}$$

The fluoresced photons will have a spectral distribution that corresponds to the shape of the emission spectrum, which we will designate by $M(\lambda)$. When fluorescence arises from a single entity, such as a particular fluorescent protein in a coral, the spectral distribution of the emitted light is independent of the excitation wavelength. The processes of absorption and fluorescence are decoupled at the level of atomic transitions, with the result that at the time that the emission occurs the molecule does not "know" what wavelength produced the excited state. This is not the case when the fluorescence arises from a complex mixture of substances, such as CDOM (colored dissolved organic matter), but measurements of excitation/emission spectra for corals and fish so far indicate that this condition applies.

The emission spectrum is typically normalized to some value such as 1 or 100. The actual fluoresced component, $F(\lambda)$, will have the same spectral distribution (shape) as the normalized emission spectrum, but we need to determine the magnitude of this spectrum. There will be some constant scaling factor *S* (not spectral) that we can apply to the prototype emission spectrum to convert it into photon flux units (Equation 3).

$$F(\lambda) = S * M(\lambda) \tag{3}$$

This factor *S* will be determined by how much useful light is available to excite the fluorescence, combined with the efficiency of conversion of incident energy to fluorescence. "Useful light" must be distinguished from the total incident light since not all wavelengths have the same potential to result in fluorescence. The relative ability of different wavelengths of light to excite fluorescence is described by the excitation spectrum, designated here by $X(\lambda)$. Like the emission spectrum *M* this is typically normalized to some value. We can scale the incident light spectrum I_0 by the excitation spectrum *X* to find the spectrum of "useful" incident light, *U*.

$$U(\lambda) = I_0(\lambda) * X(\lambda) \tag{4}$$

The greater the fraction of this useful incident light is re-emitted as fluorescence, the stronger the fluoresced component of exitance will be. The conventional quantity for describing fluorescence efficiency is the "quantum yield," defined as the number of photons fluoresced divided by the number of photons *absorbed*. The measurement is typically done with isolated, extracted pigment. The process of extraction has the potential to alter the fluorescence properties, however, and in the real world in which the fluorescing organism exists the incident light will be striking a complex surface that may have multiple layers and closely situated molecules, not all of which are fluorescing. In the case of corals, for example, there are factors such as mucus layers, bacteria, symbiotic algae, and more involved. There is no way of knowing what portion of the incident light is being absorbed by the fluorescent substance and how much by other molecular entities. Fortunately, knowing this is not necessary. We are concerned with what is happening under real-world conditions, and for our prior work with corals (Mazel and Fuchs, 2003) we developed the concept of "practical fluorescence efficiency." This is defined as the number of photons fluoresced divided by the number of photons *available* to be absorbed. This treats the organism as a "black box" and provides a useful means to make measurements and predictions based on intact organisms with all their associated complexity. We will designate the practical fluorescence efficiency here by Φ_P. The method to determine it

will be described below. With this methodology the total photons fluoresced will be the total photons available to be fluoresced times Φ_P. The "total photons available to be fluoresced" is the integral of the potentially useful photons U.

$$\Phi_P = {\int F(\lambda)d\lambda} \Big/ {\int U(\lambda)d\lambda} \quad (5)$$

Substituting from Equation (3) and rearranging, we have,

$$\Phi_P * \int U(\lambda)\, d\lambda = S * \int M(\lambda)d\lambda \quad (6)$$

And we can find S as

$$S = {\Phi_P * \int U(\lambda)d\lambda} \Big/ {\int M(\lambda)d\lambda} \quad (7)$$

So finally we have

$$E(\lambda) = I_0(\lambda) * R_T(\lambda) + S * M(\lambda), \quad (8)$$

where S is calculated for each case from Equation (7).

With the exitance spectrum and its components the change in the available optical signature due to fluorescence can be visualized, and the fractional contribution of fluorescence to the signal in any wavelength band can be computed.

To perform the modeling using the methodology described above we need five pieces of information:

- I_0 - Incident (ambient) light spectrum
- R_T - True reflectance spectrum
- X - Fluorescence excitation spectrum
- M - Fluorescence emission spectrum
- Φ_P - Practical fluorescence efficiency

Note that other than I_0, all of these quantities are inherent optical properties of the organism that only need to be determined once. All of the other quantities needed can be calculated from these for each case.

We will now describe how each of these pieces of information can be obtained. After that we will illustrate the procedure by going step by step through a recent exercise to determine the potential for fluorescence to contribute to the appearance of the chain catshark (*Scyliorhinus retifer*).

I_0 – Incident Light Spectrum

The incident light used for modeling should be relevant to the organism's natural illumination conditions. If the fluorescence is postulated to have a visual function under particular constraints, such as depth or time of day, the spectrum should be appropriate to those conditions. Data may be measured *in situ* with an underwater spectrometer, or may be modeled with a radiance modeling program such as Hydrolight (Sequoia Scientific, Seattle, WA).

R_T – True Reflectance Spectrum

Reflectance is a non-dimensional quantity specifying the fraction of incident light that is reflected at an interface. There is no change of wavelength in this process. If a surface is not fluorescent then the observable optical signal consists entirely of reflected light. The reflectance of a surface can also be a function of the angle of incidence of the light reaching the surface. For purposes of this discussion we assume that light is diffusely reflected, neglecting angular dependencies. While this may not be true of any given surface, it is not likely to affect the results significantly and there is no need to over-complicate the problem when primarily trying to sort out the potential contribution of fluorescence to the signal.

Reflectance is typically measured by providing broadband illumination (full visible spectrum) and making successive measurements of the light reflected from the subject of interest and from a diffusely reflecting reference surface with known reflectance properties, such as Spectralon™ (Labsphere, Sutton, NH). The reflectance is computed as the light reflected by the sample divided by the light reflected by the reference surface as a function of wavelength, after correcting for the reflectance of the reference surface itself. For a fluorescing surface this procedure is complicated by the fact that the broadband illumination source will itself excite fluorescence and the "reflected" light will include a fluorescence component. There is a measurement procedure for separating the reflected and fluoresced components of the light (Fuchs, 2001), but it is also possible to make the correction using the efficiency data, since the determination of efficiency (described below) does not require knowledge of the "true" reflectance.

X – Fluorescence Excitation Spectrum

As described above, the excitation spectrum is a measurement of the relative ability of different incident wavelengths to produce fluorescence. Measurement of the excitation spectrum requires specialized instrumentation, typically a laboratory spectrofluorometer. This instrument incorporates a means to illuminate the subject with a very narrow range of wavelengths (typically a few nanometers bandwidth) at a time, and scan that illumination through a defined wavelength range. At each excitation wavelength the intensity of the emission at a fixed wavelength is recorded, with corrections applied to account for variations in the excitation light source intensity as a function of wavelength. The result is a graph of the intensity of emitted light as a function of incident wavelength. As with the emission spectrum it is typically presented normalized to a maximum of 1 (or 100, as preferred).

M – Fluorescence Emission Spectrum

The emission spectrum is a measure of the distribution of emitted light as a function of wavelength. This can be measured with the same spectrofluorometer used to measure the excitation, this time fixing the excitation wavelength and recording the emission either with a scanning monochromator or by collecting the full spectrum at once with an array detector. The data must be corrected for the spectral sensitivity of the detector system as a function of wavelength. Such correction factors are often included with the instrument but can also be determined by measuring the output of a light source with known spectrum.

The emission spectrum can also be measured with a much simpler spectrometer. There are many small diode array spectrometers available on the market (e.g., Ocean Optics,

Dunedin, FL). Excite the subject with a light source that emits in a wavelength range that produces reasonably strong fluorescence but does not overlap with the emission spectrum. A barrier filter can be used to prevent the excitation light from reaching the spectrometer, but it is usually possible to see the two separate wavelength bands simultaneously in the spectrometer readout.

Φ_P – Practical Fluorescence Efficiency

To find the practical fluorescence efficiency Φ_P we need three pieces of information, all of which can be measured:

- Incident light spectrum, I_0 – controlled as described below
- Light leaving the surface
- Fluorescence excitation spectrum, X

Note that for this Φ_P determination the incident light spectrum is *not* an arbitrary illumination I_0. In this case it must be a light source *that excites the fluorescence but does not overlap with the fluorescence emission*. This is important, as otherwise it would be difficult to sort out what portion of the light in the emission band results from fluorescence and what portion from reflectance. Isolating the excitation and the emission for this measurement removes that difficulty.

We define the practical fluorescence efficiency Φ_P as the number of photons fluoresced, N_F, divided by the number of photons available to be absorbed, N_A.

$$\Phi_P = {}^{N_F}\!/_{N_A} \tag{9}$$

The number of photons available to be absorbed is the integral of the "useful" spectrum, the incident light spectrum scaled by the excitation spectrum,

$$N_A = \int I_0\,(\lambda)\,X\,(\lambda)\,d\lambda \tag{10}$$

while the number of photons fluoresced is found from a direct measurement of fluorescence emitted from the surface,

$$N_F = \int F(\lambda) d\lambda \tag{11}$$

The procedure is as follows:

- Measurements
  - Measure the incident spectral intensity (I_O) produced by the excitation source. Direct the source at a non-fluorescent reference surface with known reflectance characteristics and direct the spectrometer fiber at that surface. This surface must either have uniform reflectance across the spectrum, or the actual reflectance spectrum must be accounted for. Position the light source and detector to avoid specular reflection.
  - Measure the fluorescence (F) leaving the surface of the specimen. The surface should be positioned in the same relationship (distance and angle) to the light source and detector as the reference surface. There will be two peaks in the measured spectrum—one from reflected excitation light and the other from the fluorescence. For this efficiency measurement we are only concerned with the fluorescence portion. If the light leaving the surface is much weaker than that reflected from the reference surface it may be necessary to set the spectrometer to a longer integration time to acquire a useful signal, allowing the reflected portion of the signal to saturate. If so, this difference in integration time will have to be accounted for in the calculations that follow.
- Calculations
  - Apply any spectrometer spectral correction factors to both of the measured spectra (reference surface and sample) and normalize them to the same integration time if different times were used.
  - Account for the fact that not all of the incident wavelengths are as effective as others at exciting the fluorescence, as described by the excitation spectrum. Multiply the incident light spectrum by the normalized excitation spectrum at each wavelength, as in Equation (4). If the instruments used to collect the spectra do not provide data at the same wavelength intervals it will be necessary to interpolate data so that they match (typically to 1 nm intervals).
  - If the spectrometers are calibrated in energy flux (intensity) units, as is often the case, convert both spectra to relative photon units by multiplying by wavelength.
  - Integrate over the entire wavelength range in which there is measurable excitation or emitted light energy to compute the total number of photons contained in the incident light and the fluorescence spectra (Equations 10 and 11). The result for the incident light spectrum is the total number of photons available to be absorbed, N_A, and for the emitted light spectrum the total of numbers fluoresced, N_F.
  - Take the ratio of the above numbers, N_F/N_A to find Φ_P.

SAMPLE CASE

Example data dealing with all of the above can be found in the paper on the contribution of fluorescence to the perceived color of corals (Mazel and Fuchs, 2003) and example results of this kind of analysis can be found in the paper on the potential visual function of fluorescence in a stomatopod (mantis shrimp) (Mazel et al., 2004). Presented here is a data set recently collected to explore the potential significance of fluorescence in the chain catshark, *Scyliorhinus rotifer*. This was one of the two species that was discussed in a recent publication (Gruber et al., 2016) that argued strongly for a visual function. The data in that paper only demonstrated criteria 1 and 2 as outlined above—that fluorescence exists and that the shark visual system has the potential to respond to the fluorescence wavelengths. Here we address criterion #3, whether there is a significant amount of energy transferred into the fluorescence band.

Access to live specimens and a room that could be darkened was provided by the Seacoast Science Center (Rye, NH). For

the measurements the sharks were kept in small plastic tubs of seawater lined with a black cloth to minimize stray light effects.

At a qualitative level these specimens appeared the same as those shown in Figure 5 of Gruber et al. (2016). The lower image of **Figure 3** was made with broadband white light illumination while the top image was made with blue light excitation (Sola NIGHTSEA, Light and Motion, Marina, CA) and a Yellow #12 filter (Tiffen, Hauppauge, NY) to block the reflectance and reveal the fluorescence.

It can be seen in **Figure 3** that areas of different shades of brown/beige in the white light image correspond to areas of different fluorescence intensity in the fluorescence image. The measurements described here were made from the lighter (higher reflectance) areas, which also exhibited the brighter fluorescence.

Fluorescence excitation and emission spectra were measured from two specimens with a Fluoromax 2 spectrofluorometer (SPEX Industries, Edison, NJ) fitted with a bifurcated fiber optic probe. The common end of the fiber was held with a laboratory clamp to maintain a fixed position relative to the shark. **Figure 4** shows the fiber positioned next to the shark, with the excitation light illuminating the skin.

Figure 5 shows the excitation and emission spectra for the brightly fluorescent area of the skin. The results were identical for both specimens, showing an excitation maximum at ∼450 nm and an emission maximum at ∼520 nm.

Incident light, reflected light, and total exitance were measured with a Model USB2000 fiber optic spectrometer (Ocean Optics, Dunedin, FL). For reflectance measurements illumination was provided by a halogen lamp. Reference measurements were made from a Spectralon^{TM} disk with either nominal 50 or 99% reflectance across the visible spectrum. The nominal 50% reference surface was itself calibrated by measuring its reflectance relative to the 99% reference surface. The linearity of the spectrometer with respect to integration time was checked by measuring the same signal using different integration times and verifying that they matched after scaling.

Reflectance was computed as the ratio of the signal measured from the shark surface to that from the reference surface after the appropriate scaling factors (reference surface reflectance, integration time) were applied. **Figure 6** shows a typical reflectance spectrum for a patch of skin with brighter fluorescence.

There may be a small hint of a "bump" in the reflectance spectrum, indicated by the arrow in **Figure 6**. This corresponds to the location of the fluorescence emission peak and illustrates the point made above that when making reflectance measurements under broadband illumination the fluorescence component will be included. As more photons are absorbed at shorter wavelengths and transferred into longer wavelengths by fluorescence one expects to see a reflectance dip corresponding to the excitation spectrum and a reflectance peak corresponding to the emission spectrum. The stronger the fluorescence, the more accentuated these features would be. The reflectance measurement shown in **Figure 6** indicates that the fluorescence does not contribute much to the apparent reflectance under this illumination. Note that this does not indicate that a fluorescence contribution will be inconsequential under all lighting conditions. Under narrow band blue illumination, for

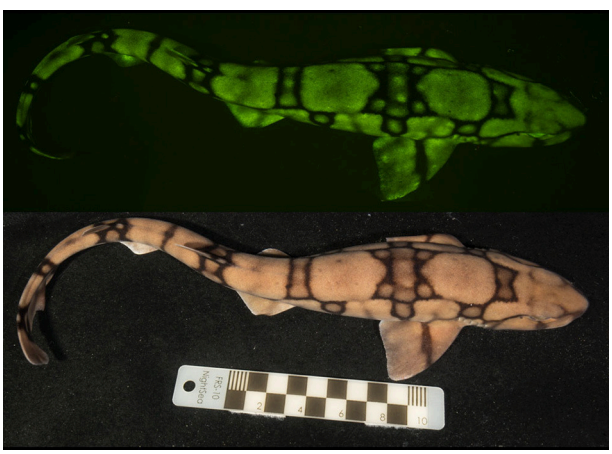

FIGURE 3 | Photographs of a chain catshark under white light illumination **(bottom)** and fluorescing **(top)** under blue light illumination imaged through a yellow longpass filter. Scale in cm.

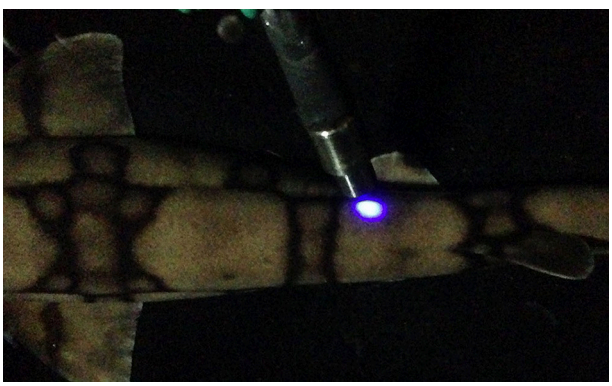

FIGURE 4 | Bifurcated fiber optic probe of the Fluoromax-2 spectrofluorometer directed at a shark's skin, showing the excitation spot on the surface.

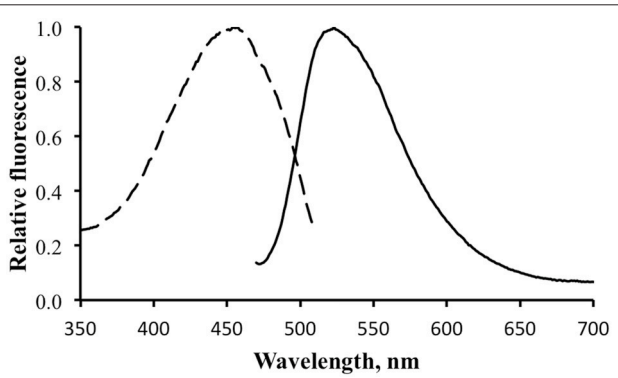

FIGURE 5 | Fluorescence excitation (dotted line) and emission (solid line) for the shark fluorescence. Excitation measured with emission monochromator set at 530 nm. Emission measure with excitation monochromator set at 450 nm.

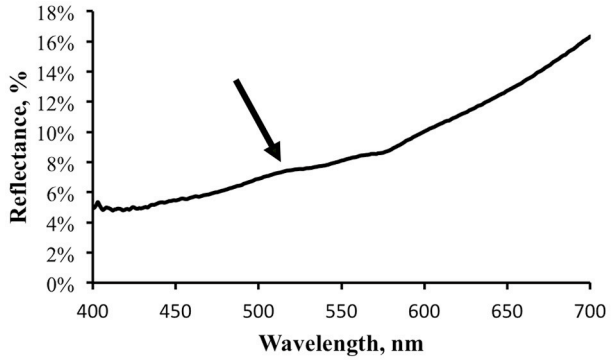

FIGURE 6 | Reflectance spectrum, in percent, for the same light area of the shark skin for which the fluorescence was measured. Arrow indicates possible small increase in apparent reflectance due to fluorescence contribution.

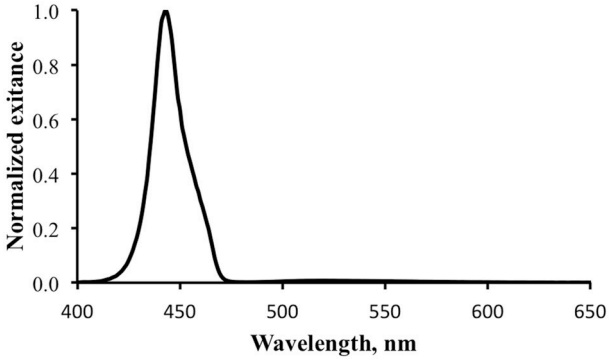

FIGURE 7 | Normalized total exitance from the surface of the shark. The large peak at ∼450 nm is reflected excitation light. The fluorescence is barely evident between 500 and 550 nm.

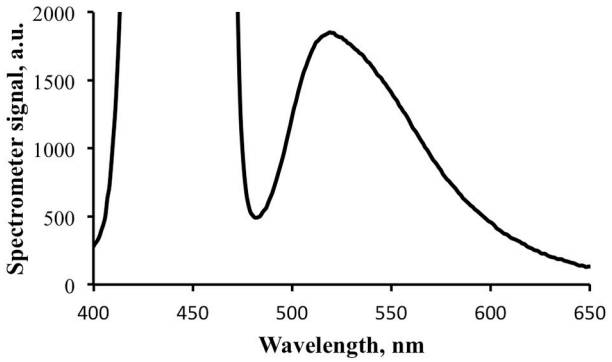

FIGURE 8 | Fluorescence portion of the exitance signal shown in **Figure 7**. The signal for the reflected blue light is saturated at the integration time for this data collection.

example, the fluorescence will comprise 100% of the exitance signal at the emission wavelengths. The significance of the fluorescence must always be analyzed relative to the total light field.

For the practical fluorescence efficiency determination the narrow band blue light source (Sola NIGHTSEA) was used for excitation. **Figure 7** shows the measurement of the light leaving the surface of the shark. The measurement was made with an integration time selected to prevent the reflected blue light from saturating the detector. At this scale the fluorescence peak is barely visible. The data for the blue light reflected from the reference surface is not shown, but is essentially the same spectral distribution as the blue portion of the peak in **Figure 7**.

An additional measurement was made at a longer integration time to provide greater signal strength for the fluorescence portion of the exitance, elevating it above the noise floor (**Figure 8**). This caused the blue light signal to be saturated, but provided cleaner data for the fluorescence calculations. Note that the shape of the emission spectrum measured with the spectrometer is essentially identical to that measured with the spectrofluorometer (**Figure 5**).

The incident and emitted light spectral data were interpolated to 1 nm increments over the range of 400–700 nm. A spectral correction factor was then applied, determined separately by measuring the output of a light source with known spectral intensity distribution. The data were then converted to relative photon units by multiplying each data point by its corresponding wavelength. Note that it is not necessary for the data to be calibrated in *absolute* energy or photon units as long as the same processing procedure is used for all spectra. The incident blue light spectrum was further processed by multiplying by the excitation spectrum at corresponding wavelengths to find the "useful" incident light spectrum.

The processed data sets were then summed across the appropriate wavelength ranges to determine the total photons in the useful incident light and emitted fluorescence bands to find N_A and N_F, respectively. For the former this range was 420–470 nm, and for the latter it was 480–650 nm. While not perfect, these captured the bulk of the distribution under each curve. The practical fluorescence efficiency, Φ_P. was then computed as N_F/N_A.

This procedure was followed for multiple measurements from three sharks and yielded Φ_P values ranging from 0.1 to 0.4%, with one reading closer to 1%.

This information can be used to model the spectrum of light leaving the surface of the shark under arbitrary illumination conditions. We do this with downwelling light spectra previously computed (Mazel, 2005) using Hydrolight for two cases—relatively clear tropical waters (Bahamas) and temperate coastal water (New England). The Hydrolight spectra were computed with water optical property data measured *in situ* in these environments. The following is not intended as a comprehensive investigation, but rather to illustrate the modeling process and what can be learned from it.

The contribution of fluorescence to an optical signal will be maximized when (1) the downwelling light spectrum overlaps significantly with the excitation spectrum and (2) the fluorescence emission occurs at wavelengths that are not strongly present in the downwelling light. Satisfying these two conditions

means maximizing "pumping" of fluorescence and minimizing competition from reflected photons. **Figure 9** shows normalized downwelling light spectra at a depth of 21 m at 0800 local time, 50% cloud cover, and a flat sea surface for both the tropical (thick solid line) and temperate (thin solid line) cases. The normalized excitation (dashed line) and emission (dotted line) spectra are overlaid to show their relationship to the available light. The tropical case indicates a predominantly blue light field while the temperate case is strongly peaked in the green. The minimal energy at wavelengths longer than 600 nm in both cases results from absorption by water itself, while the strong attenuation of blue light in the temperate case results from dissolved organic matter. Note that these spectra are normalized, and the overall light level at this depth in temperate waters would be much lower than that in tropical. We can see from the plot that there is reasonable overlap between the available light and the excitation spectrum for the tropical water case, but not for the temperate. There is downwelling light that overlaps with the emission spectrum in both cases, indicating that any fluorescence will have to "compete" with reflected light.

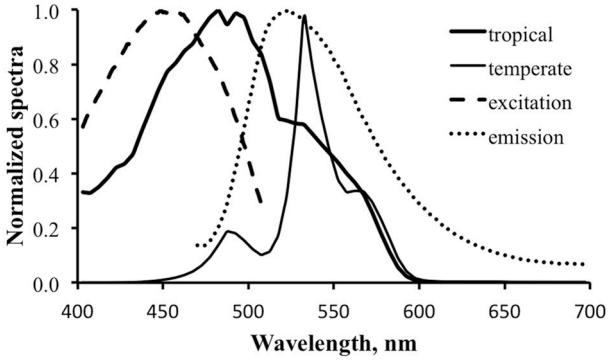

FIGURE 9 | Normalized downwelling light spectra at a depth of 21 m at 0800 local time, 50% cloud cover, and a flat sea surface for tropical (thick solid line) and New England temperate (thin solid line) cases. Normalized excitation (dashed line) and emission (dotted line) spectra show their relationship to the available light.

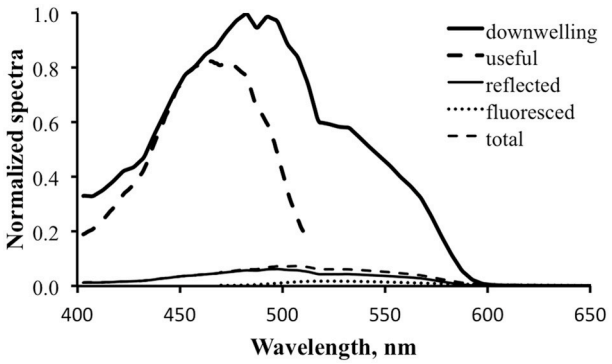

FIGURE 10 | Fluorescence enhancement modeling for the tropical water case. Downwelling light—thick solid line; computed "useful" downwelling light—thick dashed line; computed reflectance—thin solid line; fluoresced light computed with 3% practical fluorescence efficiency—dotted line; modeled total exitance—thin dashed line.

Figure 10 shows the computed results for fluorescence enhancement for the tropical water case. The thick dark line is the downwelling light spectrum, identical to that in **Figure 9**. The thick dashed line is the "useful" spectrum, calculated by multiplying the downwelling spectrum by the excitation spectrum (Equation 4). This is the data that will be converted to relative photons and integrated to calculate total available photons (N_A). This is in turn multiplied by the practical fluorescence efficiency (Φ_P) to find the total fluoresced photons (N_F). That number is used to calculate the scale factor, *S,* to be applied to the prototype fluorescence emission spectrum, *M* (Equation 7). For the purposes of generating **Figure 10** an arbitrary value of 3% was used for Φ_P. Note that this is about an order of magnitude greater than the actual Φ_P determined for the shark fluorescence, but it was necessary to use a larger value for the spectrum to be evident in the figure.

Figure 11 is a detail of the lower portion of **Figure 10**. The calculated reflected light spectrum (Equation 2) is represented by the thin dark line, the scaled prototype fluorescence emission spectrum by the dotted line, and the total exitance, the sum of the reflected light spectrum and the scaled fluorescence emission spectrum, by the thin dashed line. If this were an actual efficiency value the fluorescence would indeed be boosting the available optical signal.

We can use the data to explore the potential for a fluorescence contribution under any given illumination condition by holding everything else constant and varying Φ_P. To generate the data for **Figure 12** we used the tropical data and Φ_P values of 0.5, 1, and 5%. The 0.5% value is closest to the actual measured values. The results indicate that it would require a fluorescence efficiency much larger than this to have a significant effect on the total exitance.

Figure 13 shows the results for fluorescence enhancement for the temperate water case. As with **Figure 10**, the thick dark line is the downwelling light spectrum and the thick dashed line is the computed "useful" spectrum. Note how wavelength-limited and weak this is relative to that for the tropical case. This is because of the poor overlap between the available downwelling light and the fluorescence excitation spectrum. The thin dark line is the computed reflected light. A value of 5% was used for Φ_P to generate the data for this graph, but even at this enhanced level the fluorescence is essentially "invisible."

Figure 14 is similar to **Figure 12**, exploring the effect of varying fluorescence efficiency on the potential for fluorescence to contribute to the optical signature for the temperate water case. The combination of the inefficient "pumping" of fluorescence and the significant competition from reflected light in these green-shifted temperate waters renders the fluorescence contribution insignificant for the visual signal.

DISCUSSION

Observations of fluorescence in nature are intriguing and each one potentially opens a new direction for research into visual

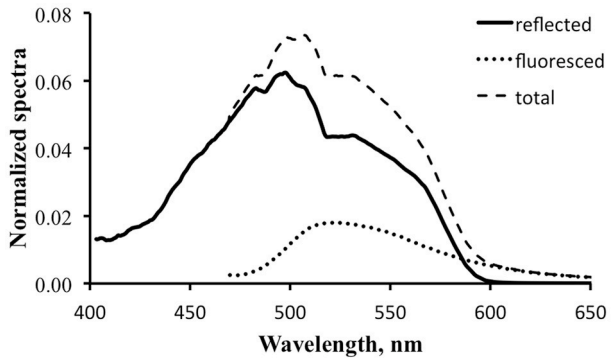

FIGURE 11 | Detail of reflected light (solid line), fluorescence (dotted line), and computed total exitance (dashed line) for the tropical water case using a value of 3% for practical fluorescence efficiency.

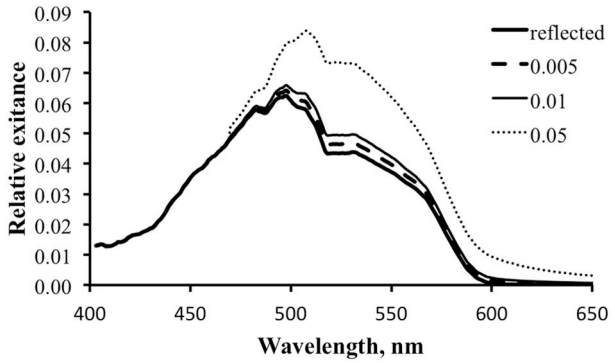

FIGURE 12 | Modeled spectral exitance for the tropical water case with Φ_P values of 0.5 (dashed line), 1 (thin solid line), and 5% (dotted line).

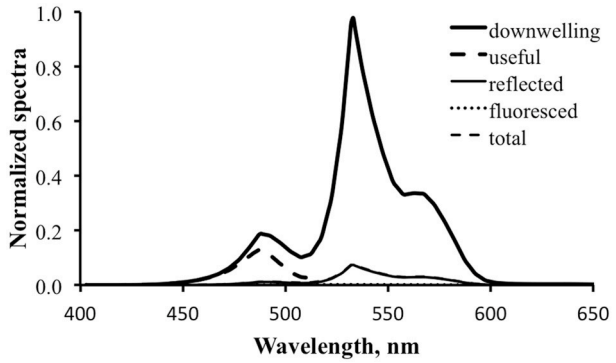

FIGURE 13 | Fluorescence enhancement modeling for the tropical water case. Downwelling light—thick solid line; computed "useful" downwelling light—thick dashed line; computed reflectance—thin solid line; fluoresced light computed with 5% practical fluorescence efficiency—dotted line; modeled total exitance—thin dashed line. At this scale the fluorescence contribution is not visible.

ecology. The existence of fluorescence, however, is not in itself evidence that the fluorescence is visually functional. Fluorescence can only play a role in vision if it makes a material contribution to the exitance, the total light leaving the surface. The exitance from a fluorescent surface will include contributions from both light that has been reflected without a change in wavelength and light that has been absorbed and re-emitted at longer wavelengths by fluorescence. For the contribution of the latter to be "material" it must change the spectral signature relative to that which is produced only by the former. This will generally occur when either or both of the following are true: (1) the fluorescence intensity is intense due to a combination of good overlap of the available light with the fluorescence excitation spectrum and a high practical fluorescence efficiency; (2) the fluorescence wavelength is in a region of the spectrum that is either weak or not present under the relevant illumination conditions.

The methods described in this manuscript provide a framework and means for measuring optical properties quantitatively and using that data to compute the spectral distribution of light leaving the surface under arbitrary illumination conditions. The results can also be used to compute the signal enhancement resulting from the fluorescence, either as a function of wavelength or as a total photon contribution within a defined spectral band. Modeling over a range of conditions such as depth, time of day, and water optical properties can help in identifying scenarios in which the fluorescence has the potential to be a useful visual signal.

There are alternative ways to approach the measurement and modeling of fluorescence contribution (e.g., Bitton et al., 2017; Taboada et al., 2017). While these differ in detail from the approach described here they lead to the same end: an estimate of the contribution of fluorescence to the optical signal.

The results of quantitative measurement and modeling are not the complete story in regard to a visual function. As outlined in the introduction there are four conditions that must be satisfied for fluorescence to be demonstrated to play a role in vision:

1. Fluorescence exists when the subject is illuminated at wavelengths that are naturally present in its habitat.
2. The organism for which a viewing function is postulated is physiologically capable of perceiving the wavelengths of the fluorescence emission.
3. There is enough energy transferred into the fluorescence band to make a meaningful contribution to the visual signal under relevant illumination conditions.
4. The viewing organism's behavior is influenced by the presence vs. absence of fluorescence in the subject.

The work described here addresses condition #3. If fluorescence measurement and modeling indicate the *potential* for fluorescence to make a significant contribution it will still be necessary to determine if the exitance spectrum is further modulated by transmission through the medium between the subject and the putative viewer, and the nature of ocular filters (Heinermann, 1983; Douglas and Marshall, 1999) or preferential retinal spectral sensitivities in that viewer, as determined by microspectrophotometry (Hanaoka and Fujimoto, 1957; Chung and Marshall, 2016). This analysis also does not account for the background, whether open water or some variety of benthic

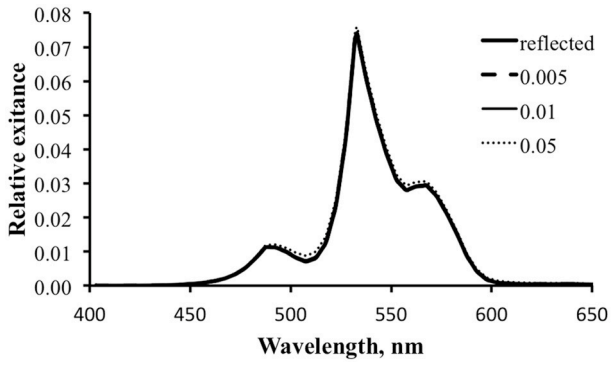

FIGURE 14 | Modeled spectral exitance for the temperate water case with Φ_P values of 0.5 (dashed line), 1 (thin solid line), and 5% (dotted line).

habitat, against which the subject is situated. The background is important as the fluorescence can only be functional if it creates contrast (in the cases of intraspecific communication, mate attraction, display, warning coloration, and the like) or reduces contrast (in the case of camouflage) relative to the spectral signature in the absence of fluorescence. And finally, a behavioral response must be demonstrated.

It is also possible that measurement and modeling indicate that while a subject appears brightly fluorescent when viewed under intense excitation in the dark, the practical fluorescence efficiency is so low, or there is so much competition from reflected ambient light at the wavelengths of fluorescence, that the fluorescence contribution would be trivial under natural illumination conditions. This information would then be a factor in deciding whether further investigation of a visual function is warranted.

Differences in the way that the question of visual function of fluorescence is addressed can be seen in the literature. Arnold et al. (2002) demonstrated all criteria for a fluorescence function in a bird (budgerigar, *Melopsittacus undulatus*), including a behavioral response. The quantitative approaches of Mazel et al. (2004), Taboada et al. (2017), and Bitton et al. (2017) indicated the potential for fluorescence to play a visual role in a stomatopod (*Lysiosquillina glabriuscula*), frog (*Hypsiboas punctatus*) and fish (*Trypterygion delaisi*), respectively. Another quantitative treatment (Iriel and Lagorio, 2010) indicated that the fluorescence of the flowers investigated was too weak relative to reflected light to have a functional role.

In contrast, several recent papers either imply or ascribe a visual function based on conditions 1 and 2 alone, without a quantitative evaluation of fluorescence contribution (Sparks et al., 2014; Gruber et al., 2016; Wails et al., 2017). The lack of quantitative support does not mean there is *not* a visual function in these cases, just that it is premature to suggest that there is without also considering the possibility that the fluorescence may be a non-functional epiphenomenon. The conditions for demonstrating a fluorescence function are known, as are the tools and methods for performing the quantitative analyses. These should be brought to bear in any investigation of visual function of fluorescence.

ETHICS STATEMENT

Measurements on live sharks were made in cooperation with the Seacoast Science Center, Rye NH. These were non-contact optical measurements with no invasive procedures. The handling of the specimens in order to enable the research was carried out by Science Center staff and did not differ from their normal handling of the specimens.

AUTHOR CONTRIBUTIONS

The author confirms being the sole contributor of this work and approved it for publication.

FUNDING

The original work in developing methods for analyzing the contribution of fluorescence to an optical signal was carried out with support from the Environmental Optics Program of the Office of Naval Research, award N0001402C0089. The more recent measurements of shark fluorescence were self-funded.

REFERENCES

Arnold, K. E., Owens, I. P. F., and Marshall, N. J. (2002). Fluorescent signaling in parrots. *Science* 295:92. doi: 10.1126/science.295.5552.92

Bitton, P. P., Harant, U. K., Fritsch, R., Champ, C. M., Temple, S. E., and Michiels, N. K. (2017). Red fluorescence of the triplefin *Tripterygion delaisi* is increasingly visible against background light with increasing depth. *R. Soc. Open Sci.* 4:161009. doi: 10.1098/rsos.161009

Bou-Abdallah, F., Chasteen, N. D., and Lesser, M. P. (2006). Quenching of superoxide radicals by green fluorescent protein. *Biochimica Et Biophysica Acta General Subjects* 1760, 1690–1695. doi: 10.1016/j.bbagen.2006.08.014

Chung, W. S., and Marshall, N. J. (2016). Comparative visual ecology of cephalopods from different habitats. *Proc. R. Soc. B* 283:20161346. doi: 10.1098/rspb.2016.1346

Douglas, R. H., and Marshall, N. J. (1999). "A review of vertebrate and invertebrate ocular filters," in *Adaptive Mechanisms in the Ecology of Vision,* eds S. N. Archer, M. B. A. Djamgoz, E. R. Loew, J. C. Partridge and S. Vallerga (Dordrecht: Springer), 95–162. doi: 10.1007/978-94-017-0619-3_5

Fuchs, E. (2001). Separating the fluorescence and reflectance components of coral spectra. *Appl. Opt.* 40, 3614–3621. doi: 10.1364/AO.40.003614

Gerlach, T., Sprenger, D., and Michiels, N. K. (2014). Fairy wrasses perceive and respond to their deep red fluorescent coloration. *Proc. R. Soc. B* 281:20140787. doi: 10.1098/rspb.2014.0787

Gittins, J. R., D'Angelo, C., Oswald, F., Edwards, R. J., and Wiedenmann, J. (2015). Fluorescent protein-mediated colour polymorphism in reef corals: multicopy genes extend the adaptation/acclimatization potential to variable light environments. *Mol. Ecol.* 24, 453–465. doi: 10.1111/mec.13041

Gruber, D. F., Loew, E. R., Deheyn, D. D., Akkaynak, D., Gaffney, J. P., Smith, W. L., et al. (2016). Biofluorescence in catsharks (Scyliorhinidae): fundamental description and relevance for elasmobranch visual ecology. *Sci. Rep.* 6:24751. doi: 10.1038/srep24751

Haddock, S. H., and Dunn, C. W. (2015). Fluorescent proteins function as a prey attractant: experimental evidence from the hydromedusa *Olindias formosus* and other marine organisms. *Biol. Open.* 4, 1094–1104. doi: 10.1242/bio.012138

Haddock, S. H., Dunn, C. W., Pugh, P. R., and Schnitzler, C. E. (2005). Bioluminescent and red-fluorescent lures in a deep-sea siphonophore. *Science* 309, 263–263. doi: 10.1126/science.1110441

Hanaoka, T., and Fujimoto, K. (1957). Absorption spectrum of a single cone in carp retina. *Jpn. J. Physiol.* 7, 276–285. doi: 10.2170/jjphysiol.7.276

Heinermann, P. H. (1983). Yellow intraocular filters in fishes. *Exp. Biol.* 43, 127–147.

Iriel, A., and Lagorio, M. G. (2010). Is the flower fluorescence relevant in biocommunication? *Naturwissenschaften* 97, 915–924. doi: 10.1007/s00114-010-0709-4

Johnsen, S. (2011). *The Optics of Life: A Biologist's Guide to Light in Nature*. Princeton, NJ: Princeton University Press.

Kelmanson, I. V., and Matz, M. V. (2003). Molecular basis and evolutionary origins of color diversity in great star coral *Montastraea cavernosa* (Scleractinia: Faviida). *Mol. Biol. Evol.* 20, 1125–1133. doi: 10.1093/molbev/msg130

Lythgoe, J. N. (1979). *Ecology of Vision*. Oxford: Clarendon Press.

Matz, M. V., Marshall, N. J., and Vorobyev, M. (2006). Are corals colorful? *Photochem. Photobiol.* 82, 345–350. doi: 10.1562/2005-08-18-RA-653

Mazel, C. H. (2005). Underwater fluorescence photography in the presence of ambient light. *Limnol. Oceanogr. Methods* 3, 499–510. doi: 10.4319/lom.2005.3.499

Mazel, C. H., Cronin, T. W., Caldwell, R. L., and Marshall, N. J. (2004). Fluorescent enhancement of signaling in a mantis shrimp. *Science* 303:51. doi: 10.1126/science.1089803

Mazel, C. H., and Fuchs, E. (2003). Contribution of fluorescence to the spectral signature and perceived color of corals. *Limnol. Oceanogr.* 48, 390–401. doi: 10.4319/lo.2003.48.1_part_2.0390

Michiels, N., Anthes, N., Hart, N., Herler, J., Meixner, A., Schleifenbaum, F., et al. (2008). Red fluorescence in reef fish: a novel signalling mechanism? *BMC Ecol.* 8:16. doi: 10.1186/1472-6785-8-16

Mobley, C. D. (1994). *Light and Water: Radiative Transfer in Natural Waters*. San Diego, CA: Academic Press.

Palmer, C. V., Modi, C. K., and Mydlarz, L. D. (2009). Coral fluorescent proteins as antioxidants. *PLoS ONE* 4:e7298. doi: 10.1371/journal.pone.0007298

Salih, A., Larkum, A., Cox, G., Kuhl, M., and Hoegh-Guldberg, O. (2000). Fluorescent pigments in corals are photoprotective. *Nature* 408, 850–853. doi: 10.1038/35048564

Smith, E. G., D'Angelo, C., Sharon, Y., Tchernov, D., and Wiedenmann, J. (2017). Acclimatization of symbiotic corals to mesophotic light environments through wavelength transformation by fluorescent protein pigments. *Proc. R. Soc. B Biol. Sci.* 284:20170320. doi: 10.1098/rspb.2017.0320

Sparks, J. S., Schelly, R. C., Smith, W. L., Davis, M. P., Tchernov, D., Pieribone, V. A., et al. (2014). The covert world of fish biofluorescence: a phylogenetically widespread and phenotypically variable phenomenon. *PLoS ONE* 9:e83259. doi: 10.1371/journal.pone.0083259

Taboada, C., Brunetti, A. E., Pedron, F. N., Neto, F. C., Estrin, D. A., Bari, S. E., et al. (2017). Naturally occurring fluorescence in frogs. *Proc. Natl. Acad. Sci. U.S.A.* 114, 3672–3677. doi: 10.1073/pnas.1701053114

Ugalde, J. A., Chang, B. S. W., and Matz, M. V. (2004). Evolution of coral pigments recreated. *Science* 305:1433. doi: 10.1126/science.1099597

Wails, C. N., Gruber, E. D., Slattery, E., Smith, L., and Major, H. L. (2017). Glowing in the light: fluorescence of bill plates in the Crested Auklet (*Aethia cristatella*). *Wilson J. Ornithol.* 129, 155–158. doi: 10.1676/1559-4491-129.1.155

Conflict of Interest Statement: CM is the proprietor of NIGHTSEA, a company that designs and makes equipment for viewing fluorescence. Individuals pursuing marine or terrestrial fluorescence research utilizing the methods described here could potentially be purchasers of some of the equipment, but there are alternatives on the market.

frontiers in Marine Science

ORIGINAL RESEARCH
published: 05 September 2017
doi: 10.3389/fmars.2017.00273

In situ Analysis of Coral Recruits Using Fluorescence Imaging

Adi Zweifler[1,2], *Derya Akkaynak*[1,3], *Tali Mass*[2]* and *Tali Treibitz*[1]*

[1] Marine Technologies Department, Leon H. Charney School of Marine Sciences, University of Haifa, Haifa, Israel, [2] Marine Biology Department, Leon H. Charney School of Marine Sciences, University of Haifa, Haifa, Israel, [3] Interuniversity Institute of Marine Sciences, Eilat, Israel

Recruitment is a fundamental process that influences coral population dynamics as well as reef community structure. To date, coral recruitment success rates are poorly quantified because survey methods are labor-intensive and require manual interpretation. Thus, they are prone to human errors and have low repeatability—a gap we aim to bridge in this research. Since both corals and their symbiotic algae contain fluorescent pigments (chlorophyll and fluorescent proteins), we used the non-invasive Fluorescence Imaging System (FluorIS) and developed a methodology to acquire daytime fluorescent photographs and identify coral recruits in them. We tested our method by monitoring 20 random quadrats at two sites in the Gulf of Aqaba, Israel. The quadrats were surveyed once a month for 8 months in order to track the settlement, mortality and survival rates of new coral recruits. We demonstrate daytime imaging using our method and identification of coral recruits as small as 1 mm in diameter, in a 20 × 20 cm quadrat. Our results show that this photographic method reduces surveyor errors and improves precision. The surveys revealed that on average, there are ∼2 new coral recruit settlements (<2 cm) for a quadrat (40 cm^2) per month and that 83% of them survive the first month. Our study suggests a relative stability in the Gulf of Aqaba coral population during the survey period. The ability to survey recruits during the day using low-cost, easy-to-use photographic equipment has the potential to contribute significantly to the standardization of coral reef monitoring and management tools, at a time when the world's coral reefs are declining due to local and global stressors.

Keywords: underwater imaging, ecological monitoring, recruitment, survival, survey

OPEN ACCESS

Edited by:
Zvy Dubinsky,
Bar-Ilan University, Israel

Reviewed by:
Ulisse Cardini,
Stazione Zoologica Anton Dohrn, Italy
Jörg Wiedenmann,
University of Southampton,
United Kingdom

***Correspondence:**
Tali Mass
tmass@univ.haifa.ac.il
Tali Treibitz
ttreibitz@univ.haifa.ac.il

Specialty section:
This article was submitted to Coral Reef Research, a section of the journal Frontiers in Marine Science

Received: *25 January 2017*
Accepted: *08 August 2017*
Published: *05 September 2017*

Citation:
Zweifler A, Akkaynak D, Mass T and Treibitz T (2017) In situ Analysis of Coral Recruits Using Fluorescence Imaging. Front. Mar. Sci. 4:273. doi: 10.3389/fmars.2017.00273

INTRODUCTION

Recruitment and formation of new juvenile coral colonies indicate good conditions for development and growth of coral reefs and is essential to their recovery (Glassom et al., 2004; Baird et al., 2006). Coral recruitment success is most commonly quantified by examination of artificial settlement plates. The plates are easy to use, as the recruits are inspected in the lab using a microscope under UV light. However, this method does not allow continuous monitoring because the plates are taken out for inspection (Mundy, 2000; Soong et al., 2003; Field et al., 2007). In addition, they were shown to be biased (Yerushalmi, 2016). Alternatively, *in situ* visual surveys are also conducted (Edmunds et al., 1998; Miller et al., 2000; Martinez and Abelson, 2013). Both of these methods are labor-intensive and time-consuming (Piniak et al., 2005; Shlesinger and Loya, 2016). Settlement plates require manual and microscopic examination of the surface, while many visual surveys rely on fluorescence and are therefore conducted at night using specialized

equipment (Piniak et al., 2005; Roth and Knowlton, 2009; Salinas-de-Leon et al., 2011; Martinez and Abelson, 2013). Small-scale macro photography has also been used for imaging coral recruits (Edmunds et al., 1998). In the larger scale, using photographic surveys of the seabed is becoming a common method for mapping reef communities (Shihavuddin et al., 2013; Cardini et al., 2015). Advances in computer vision have enabled the processing and automated annotation of these large-scale coral reef surveys (Stokes and Deane, 2009; Beijbom et al., 2012, 2016), offering a powerful alternative to manually annotated visual surveys (Singh et al., 2004; Beijbom et al., 2015). However, such large-scale photographic surveys are impractical and are rarely used for coral recruits, which are very small and often cryptic under natural light, making them difficult to detect with traditional photographic techniques (Baird et al., 2006).

Most scleractinian coral and their symbiotic algae (*Symbiodinium* spp.) contain fluorescent pigments including GFP-like fluorescent proteins (FPs) and chlorophyll, respectively, that fluoresce under UV or blue light (Alieva et al., 2008). The FluorIS system was shown to acquire high resolution, wide field-of-view (FOV) *in situ* images of coral fluorescence during daytime (Treibitz et al., 2015). This system uses a modified consumer camera, which images both the green (520–630 nm), and red (630–800 nm) broadband components of the fluorescence spectra that correspond to the emission spectra of green, GFP-like fluorescence proteins and chlorophyll-a, respectively. The use of fluorescence has recently been shown to improve accuracy in automated image annotation of coral colonies (Beijbom et al., 2016). Fluorescence imaging is conducted through the use of filtered excitation strobes that emit short wavelengths, usually UV or blue light with emission maxima at 420–620 nm, and a barrier filter that is mounted on the camera lens to block reflected light (Mazel, 1997). At night, only fluorescence excited by the strobes is recorded. During the day, an additional additive signal from the ambient light is recorded (Treibitz et al., 2015). The reflected ambient component, which is not filtered by the barrier filter, appears in the image in green or yellow and is mixed with the fluorescence signal, as seen in **Figure 1D**. Consequently, most studies detecting fluorescence *in situ* take place at night to avoid ambient light illumination (Piniak et al., 2005; Baird et al., 2006). Treibitz et al. (2015) showed that fluorescence could be imaged during daytime by subtracting the ambient light image (captured with the strobes off).

In this study we optimized the FluorIS with specific components for surveying coral recruits under 2 cm in diameter (**Figure 1**), automated ambient light subtraction, and developed a custom software, "RecruitTracker" (Akkaynak, 2017), that improves the efficiency and accuracy of image analysis. We implemented the method in long-term field surveys for recording coral recruit settlement and survival. Our results show that this method reduces errors in identification caused by other fluorescent organisms and/or surveyor errors. In addition, during our surveys we were able to record the settlement, growth, and mortality of coral recruits from 1 mm in diameter and up. Our results indicate relative stability in coral recruit population in the Gulf of Aqaba, with high survival rates of 75% during the first month after settlement.

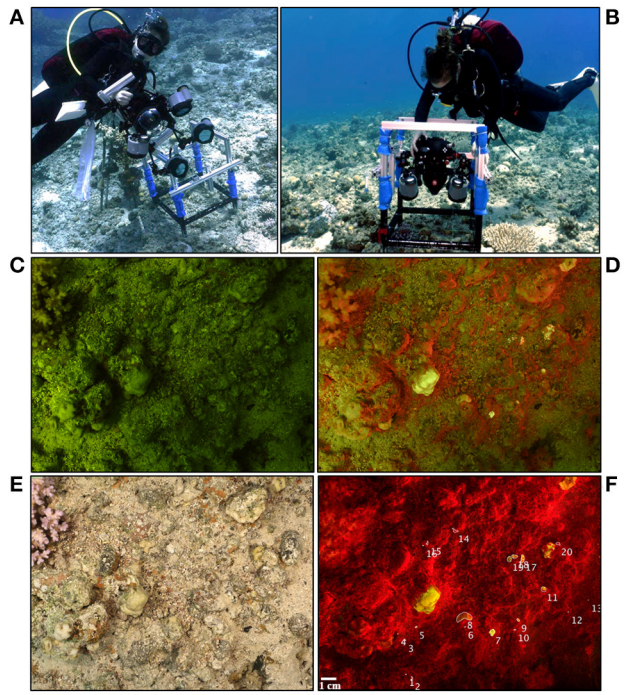

FIGURE 1 | (A) A diver attaching the FluorIS to a custom-made frame in order to **(B)** image co-located image pairs (ambient and fluorescence) after positioning the frame. **(C)** Ambient image (blue strobes off) and **(D)** Fluorescence image (blue strobes on) taken using the FluorIS. **(E)** Reflectance image taken under white illumination with a standard camera. All images were taken during daytime at the Inter University Institute (IUI), Gulf of Eilat, Israel at 8 m depth. Quadrat size is 20 × 20 cm. **(F)** Fluorescence image after subtracting image **(C)** from image **(D)**. Numbers represent coral recruits marked using the MATLAB code developed for this study.

MATERIALS AND METHODS

Imaging System

We used a fluorescence imaging system constructed of two cameras: the FluorIS (Treibitz et al., 2015) for fluorescence imaging, and a standard camera for reflectance (white light) imaging (Table S1). Both systems consist of a Nikon D810 camera and a Nikkor 35 mm f1.8 lens, and were enclosed in a Hugyfot (Erembodegem, Belgium) housing with a fisheye dome port for diving. In the FluorIS system, the camera was modified by replacing the IR filter over its sensor with a clear filter that transmits the entire light spectrum the sensor is sensitive to (roughly 300–1200 nm). The IR internal filter strongly attenuates long wavelengths above 650 nm in order to imitate the human visual system, which is not sensitive to these wavelengths. The presence of this filter limits chlorophyll-a fluorescence imaging by standard off-the-shelf cameras. Four INON Z240 strobes with blue EX-INON filters (NightSea) were used as excitation sources for fluorescence. Since the modified FluorIS camera has an expanded spectral range in the long wavelengths (>650 nm), an additional Schott BG39 filter was mounted on the strobes to block IR wavelengths that pass through the primary excitation filter. A yellow Tiffen #12 barrier filter was mounted on the camera's lens in order to block the blue light reflected from the

strobes. The reflectance images were taken with two INON Z240 strobes with no additional filters on the strobe or on the camera.

Development of the Imaging System

In order to determine the lens and field-of-view of the camera system and estimate the size of detectable coral recruits, we tracked 10 *Stylophora pistillata* recruits for a month, from settlement or until they reached 2cm in diameter, using both fluorescence and reflectance imaging in a controlled environment aquarium. We collected planula from adult *S. pistillata* colonies located in front of the Interuniversity Institute for Marine Sciences (IUI), Eilat, Israel (Red Sea, 29°30′.07 N, 34°55′.02 E) during April-May 2015, following peak release (Shlesinger et al., 1998). Planula were transferred to the lab and held in a 70 × 70 × 70 cm controlled environment aquarium. The temperature in the aquarium was maintained at ∼25°C, which is close to seawater values for April-May in the Gulf of Aqaba (Shaked and Genin, 2012). Light was set to ∼150–200μm q m^2 s^{-1} on a 12:12 h light:dark cycle. The coral recruits were fed every 2 days with freshly hatched Artemia. We placed a custom made frame on top of the aquarium, which fixed the camera in a permanent position, mid-aquarium above the surface (Figure S1). Once a week a set of images was taken using the FluorIS and the standard camera with a Nikkor 24–70 mm lens in several zoom settings (24, 35, 50, and 70 mm). Following this experiment, we chose to use a 35 mm lens with a 20 × 20 cm FOV, where the camera is 30 cm above the ground.

In situ Deployment of the Imaging System

A custom-made frame was built from aluminum profiles to enable rapid and easy attachment and release of the imaging modules holding the cameras and strobes. The frame was attached to a 50 × 50 cm quadrat, with four, 70 cm long legs. The height of the frame could be adjusted in order to increase resolution by reducing the quadrat size. In order to image a 20 × 20 cm quadrat, the camera holder was located 30 cm above the ground and the 20 × 20 cm quadrat was demarcated within the original quadrat by string. The quadrat itself was elevated 10 cm above the ground to minimize disturbance to the reef while acquiring the pictures (**Figures 1A,B**).

Image Subtraction for Daytime Fluorescence

In order to eliminate the reflectance and fluorescence from ambient light in daytime imaging, we used the *ambient light subtraction method* (Treibitz et al., 2015). This method uses two images taken with the FlourIS; one with the blue strobes on (I_{day}), and one with the blue strobes off ($I_{ambient}$). The fluorescent image is obtained by subtracting the strobes-off image from the strobes-on image ($F_{strobes} = I_{day} - I_{ambient}$). The subtraction will only succeed if these images are perfectly aligned with each other. Even though the camera was placed on a frame positioned on the seabed, there were still small movements that caused slight differences between the images. In Treibitz et al. (2015) the images were aligned manually. In the present case, to overcome these movements and register the image pairs automatically, we developed an image registration algorithm written in MATLAB (Mathworks, Inc.; Akkaynak, 2017). In this algorithm, the fluorescence image is warped into the ambient light image, i.e., it is stretched and resized such that prominent image features are aligned in both images, using a projective transformation. The transformation is computed using matches of SURF (Speeded Up Robust Feature) keypoints (Bay et al., 2008) filtered with RANSAC (RANdom SAmple Consensus, (Zuliani, 2008). The SURF local feature detector function finds corresponding points between two images, allowing them to be rotated and scaled with respect to each other. RANSAC finds the transformation on which the most pairs agree on, and discards the pairs that did not (**Figures 2A,B**). This is the transformation that is used for warping. As opposed to standard image registration applications, the challenge in this case is that the images are from different sources (i.e., fluorescent and ambient). Hence, in our code, RecruitTracker (Akkaynak, 2017), we modified some of the parameter values used in standard registration to match these differences. In addition, although the images were taken subsequently, we sometimes experienced small intensity changes in the ambient light between the image pair. We compensated for that by automatically calculating the ambient light gain by limiting the number of allowed negative values in the subtraction result. After registration, the strobes-off image was subtracted from the strobes-on image. The result of the subtraction is a fluorescence image excited solely by the blue strobes (**Figures 1F**, **2D**). We conducted the same image registration process with the reflectance image as well.

In situ Imaging

In order to find the optimal imaging depth and time most suitable for daytime imaging in local conditions, 400 co-located reflectance and fluorescence image pairs were captured randomly during daytime. A set of images was taken every 2 m between 4 and 15 m at 8:00 a.m., 12:00 and 16:00 p.m. These times of day represent the three significant directions and intensities of sunrays at the Gulf of Aqaba. The purpose of this test was to assess the effect of different light intensities on the quality of ambient light subtraction for daytime images.

To examine whether the fluorescence signal excited by the blue strobes is strong in relation to the ambient light, we calculated the ratio of pixel intensities between the fluorescence image to the ambient one in the red and green channels. The fluorescent pixels were determined by thresholding the fluorescence image after subtraction using a dynamic threshold (using the MATLAB function *multithresh*, based on Otsu, 1979). After thresholding, we conducted a pixel-wise division of the fluorescent image by the ambient light image. This yielded a ratio image for each image pair (fluorescence and ambient). **Figure 3** depicts the histogram of the resulting ratio for all pixels identified as fluorescent in all image pairs acquired during the long-term field study ($N = 275$).

Sensitivity Test

To test the sensitivity of our method in comparison to visual surveys, we asked three experienced coral biologists to participate in a survey in which they draw a sketch of the coral recruits in a given quadrat under ambient light and fluorescent light during

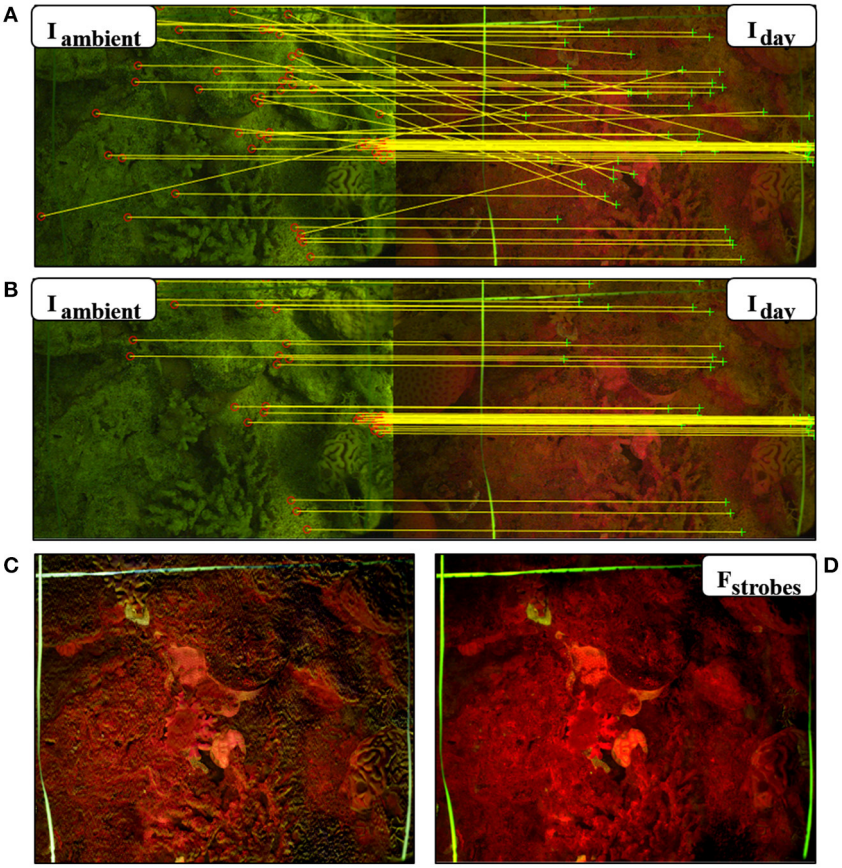

FIGURE 2 | Automatic ambient light subtraction. **(A,B)** Fluorescence image pairs taken during the day using the FluorIS, with the blue strobes off ($I_{ambient}$) and blue strobes on (I_{day}). **(A)** Matching interest points found using SURF descriptors in the algorithm before RANSAC. **(B)** Matching points after RANSAC. Ambient signal in $I_{ambient}$ helps find the matching interest points. **(C)** Result of image subtraction without registration. The image is not sharp and is missing the fine details. **(D)** $F_{strobes} = I_{day} - I_{ambient}$ is the result of the automatic subtraction algorithm with registration. It exhibits high contrast and detail.

daytime, while diving. Forty-eight random quadrats were imaged both in fluorescence and reflectance mode and in addition, the divers draw detailed sketches of the coral recruits they identified in the same imaged quadrat *in situ*, during the dive in which the images were acquired. Each diver scanned the quadrat twice: first in ambient light and then using a blue strobe and a yellow filter mask over his diving mask. Corals found in the second scan were added to the same drawing with a special mark. The reflectance images, the fluorescence images and the drawings were compared.

Long-Term Survey

Following the finalization of the experiment parameters, field surveys were conducted once a month between September 2015 and May 2016 with an additional survey in September 2016. The survey period covers the peak spawning season of most of the coral species at the Gulf of Aqaba (Shlesinger et al., 1998). Forty quadrats were chosen randomly at 8–10 m depth in the coral reef in front of the IUI and in a Marine Protected Area (MPA), in the Gulf of Aqaba, Israel. Twenty 20 × 20 cm quadrats were photographed at each site. Each quadrat was imaged with the FluorIS and with the reflectance camera. In order to return to the same quadrats month after month, we used a transect line in the MPA whereas at the IUI we marked the quadrats' locations with white epoxy glue marking the frame's corners.

Image Annotation

We designed a graphical user interface in MATLAB to allow the user to manually draw a contour around each coral recruit on the fluorescence image (subtraction result) of a given quadrat (Akkaynak, 2017). The program automatically calculates a pixel-to-cm ratio for each image using the 1 cm markings on a rope that was photographed in each image as a scale bar. All images had a resolution of 4,928 × 7,380 pixels, in which 1 cm corresponded to 250 pixels on average. Small variations were observed due to the vertical placement of the frame and the rope. Once the user marks all recruits, the program saves the following outputs: an image with the contours marked, a binary mask (i.e., a map) containing the coordinates of the contours of each coral, and a spreadsheet with the recruit's number and area in cm^2. The areas of the coral recruits in cm^2 were calculated from their areas in pixels, using the pixel-to-cm ratio extracted from each image. To detect the

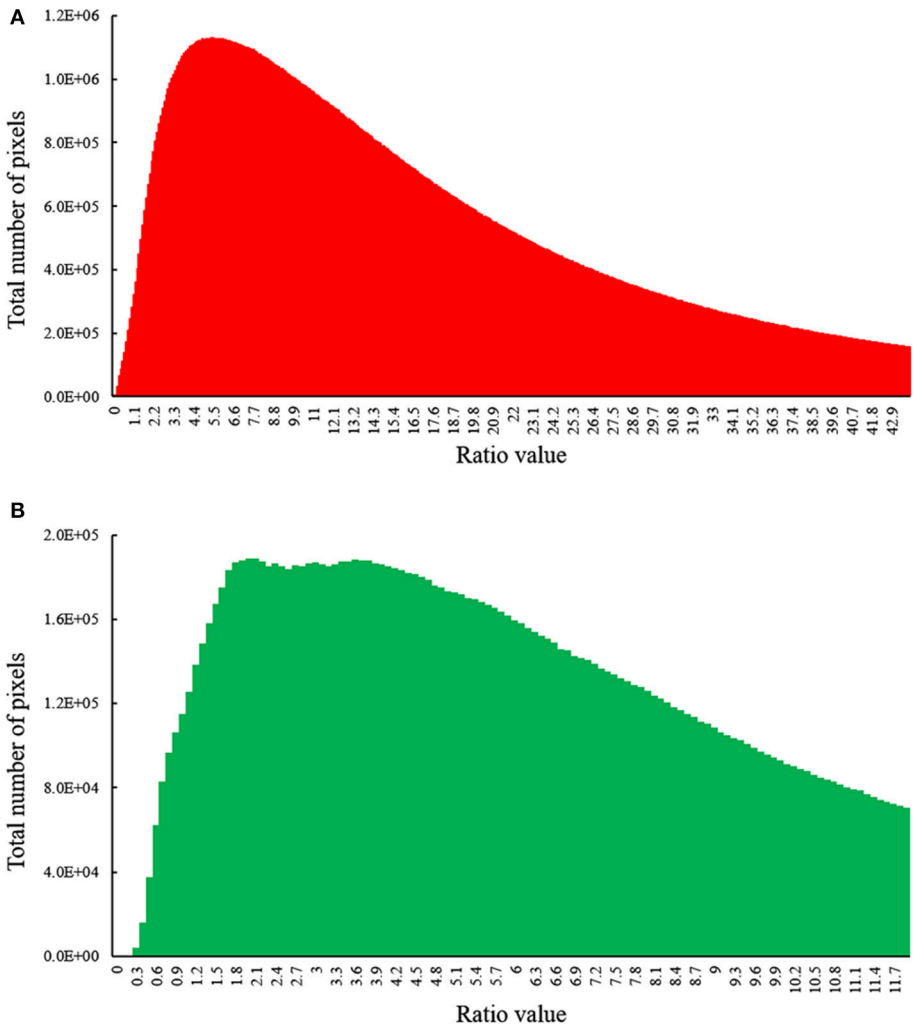

FIGURE 3 | Histogram of ratio values between the fluorescence image ($F_{strobes}$) to the ambient image ($I_{ambient}$) in **(A)** red channel (chlorophyll) and **(B)** green channel (GFP) for all image pairs photographed during our survey ($n = 275$). The fluorescence is mostly in the order of the ambient light or higher, resulting in high signal-to-noise-ratio in the subtracted images. Histograms depict fluorescent pixels only.

recruits that did not express GFP, we used the reflectance image of the annotated quadrat as a source of verification. The coordinates of the contours were saved in the binary masks in order to return to the same corals for future analysis. We eliminated corals with major axis diameters greater than 2 cm, which roughly limited the area of the largest recruits to be $\pi * (1\,cm)^2 = 3.14\,cm^2$, assuming they were circular.

Statistical Analysis

Since our results did not meet the ANOVA normality assumption, a Kruskal-Wallis test was performed to obtain the method sensitivity results and a Friedman's test for non-parametric repeated measures was performed to obtain coral recruits settlement and survival results. No transformations were made to the data. All statistical analyses were done with IBM SPSS 23, with α set to 0.05.

RESULTS

Fluorescence Imaging of Recruits During the Day

Using the FluorIS, we successfully recorded wide field-of-view fluorescence images of coral recruits from 0.001 cm^2 (~1 mm in diameter) during daytime in a quadrat of 20 × 20 cm. The automatic registration algorithm for image subtraction (**Figure 2**) was successful on 92% of the image pairs, and on the rest, we could perform the subtraction with manual registration; thus, all acquired images were used for the subsequent analysis. We were able to image during daytime in a wide range of ambient light intensities. The quadrats were located at depths from 5 to 12 m where the spectral irradiance of GFP measured at noon at 520 nm can typically be between 85 and 155 $\mu W\,cm^{-2}\,nm^{-1}$ and for chlorophyll at 680 nm, the spectral irradiance is typically between 0 and 95 $\mu W\,cm^{-2}\,nm^{-1}$ (Eyal et al., 2015). We

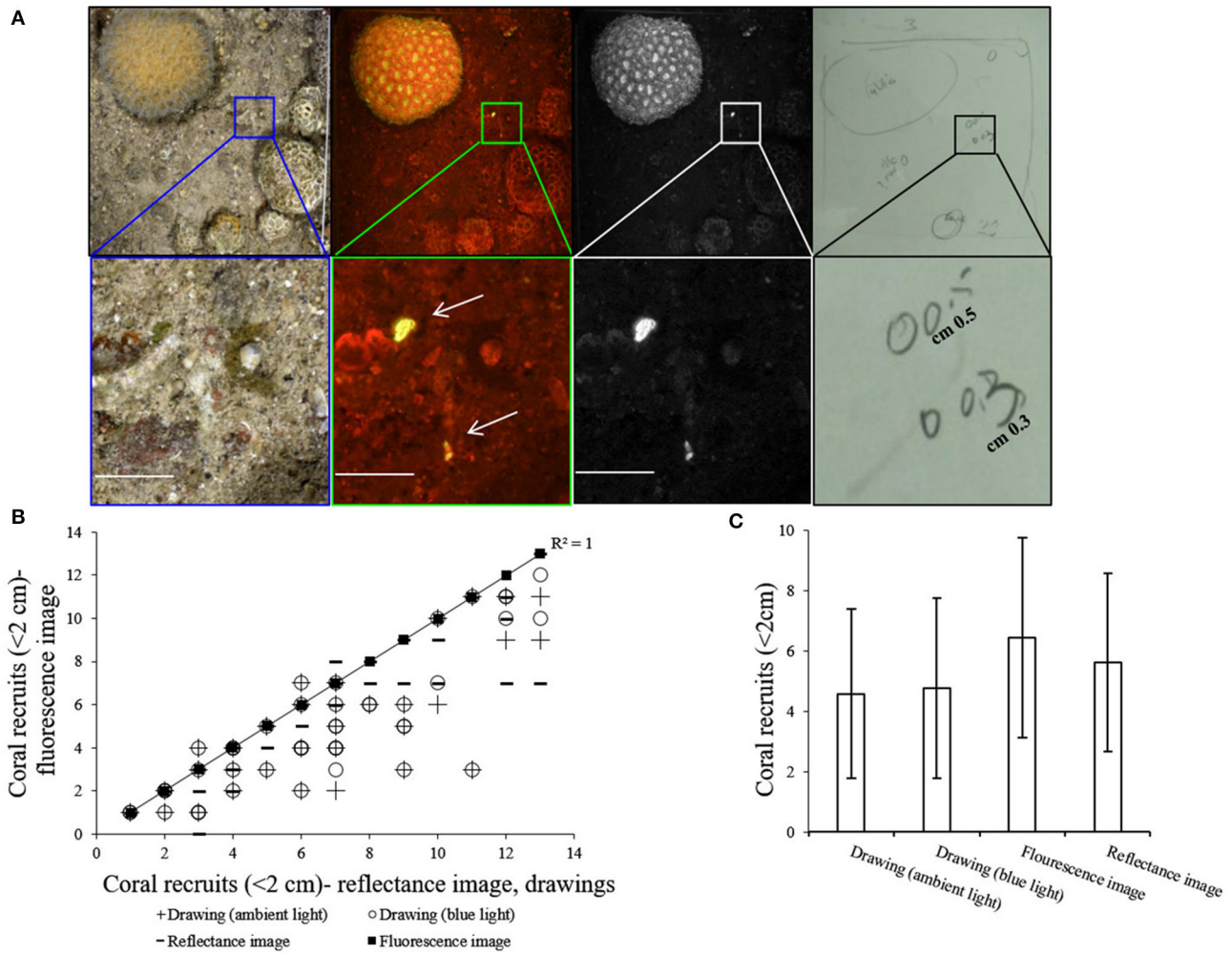

FIGURE 4 | (A) Top row (left to right)–reflectance image, fluorescence image, green channel of fluorescence image, and drawing of the same quadrat. Bottom row-magnification of the inset at the top row shows two coral recruits that were identified and drawn by the diver and are clearly seen in the fluorescence image compared to the reflectance image in which it is difficult to locate them (all scale bars are 1 cm). **(B)** Correlation between number of coral recruits counted in each of the fluorescence images to the number of coral recruits counted with the other methods on the same quadrat. Y axis = fluorescence image, X axis = drawing (ambient light), drawing (blue light), and reflectance image. Trendline ($R^2 = 1$) represents least-squares linear regression of fluorescence imaging vs. other methods ($n = 48$). **(C)** Mean number ($\pm SD$) of coral recruits counted with each of the methods ($n = 48$).

identified that for daytime conditions our camera's ISO should range between 200 and 400, the aperture at a max of f/8 and the shutter speed at 1/200th. Since we imaged 30 cm above the ground, which is rather close, the signal from the strobes is strong in relation to the ambient light. The images are a combination of fluorescent and ambient light, thus the fluorescence level in the original image cannot be adjusted by, for example, changing the exposure time. For the image subtraction to be meaningful, the fluorescence signal should be above camera sensitivity. Therefore, we compared the fluorescence intensity to the ambient light intensity. Histograms of this ratio (**Figure 3**) show that not only the fluorescence signal is above camera sensitivity but it is also usually stronger than the ambient signal (i.e., ratio above 1). As red attenuates much faster than green in the water column, the fluorescence compared to reflectance from the sun is stronger in the red channel. Nevertheless, green fluorescence also had a strong signal compared to the ambient one.

Method Sensitivity

In each quadrat, coral recruits were identified in the fluorescence image, reflectance image and in the drawing with and without the blue flashlight, as demonstrated in **Figure 4A**. A strong correlation was found between the fluorescence imaging method and the other methods (Spearman's test, $n = 48$, $P < 0.001$, $r_s > 0.5$) (**Figure 4B**). The number of recruits counted in the fluorescence images is 24% higher than the number counted in the drawings executed with and without the blue flashlight (Kruskal-Wallis test, $p < 0.01$, df = 3, chi-square = 11.75) (**Figure 4C**). A comparison of the drawings executed with and without the blue flashlight, reveals no significant difference in

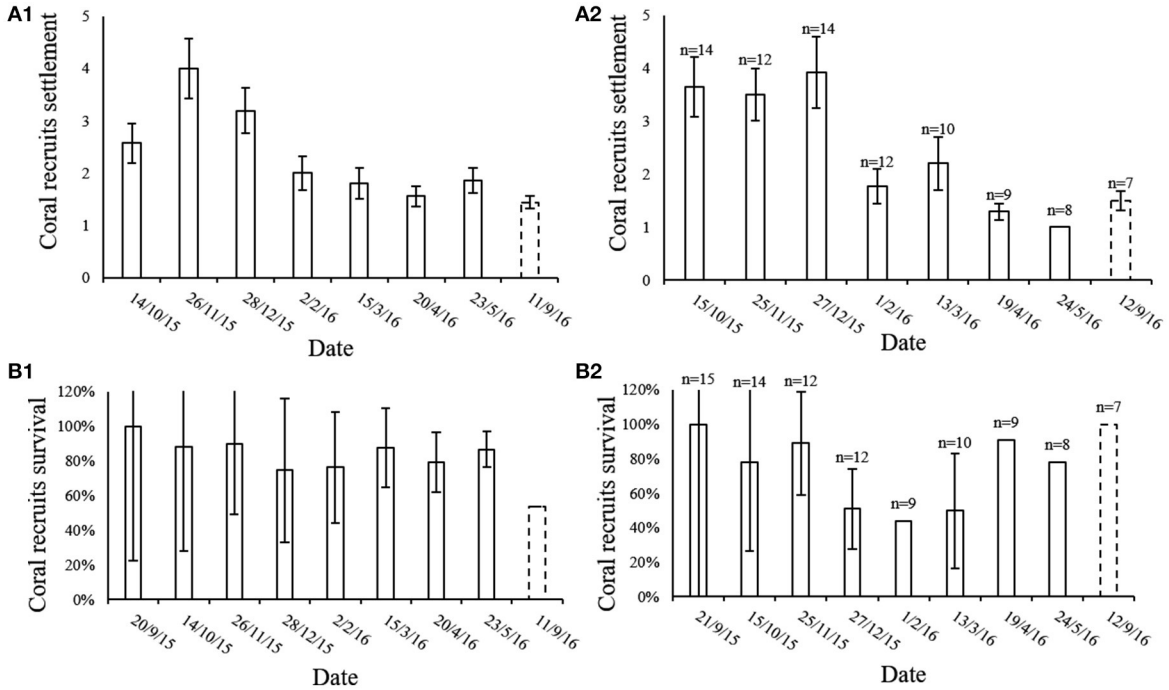

FIGURE 5 | (A) Mean number (±SE) of coral recruits settled in the 20 × 20 cm quadrat during each month of our survey both in the **(A1)** MPA ($n = 18$) and in the **(A2)** IUI sites. September 2015 is t = 0 and therefore not shown. **(B)** Percentage (mean ± SE) of coral recruits that survived their first month during the 8 month of survey at the reserve ($n = 18$) **(B1)** and at the IUI **(B2)**. Since September 2015 is $t = 0$ we assume the survival for that month is 100%. Dashed line representing September 2016 emphasizes the 4 month gap from last survey and the return to the survey sites after 1 year.

the coral recruit count (Kruskal-Wallis test, $p = 0.8$, df = 1, chi-square = 0.07). In 93% of the fluorescence images we found the same or more coral recruits in comparison to the other methods. From the recruits identified in the reflectance images, 11% did not exhibit a fluorescence signal.

Settlement and Survival

The average number of new recruit settlements every month in the MPA and at the IUI is presented in **Figure 5A**. The MPA showed the greatest amount of new settlements in November 2015, significantly differing from the period between March to September 2016 (Friedman's test, $p < 0.01$, chi-square = 26.7, df = 7, $n = 18$). At the IUI, the largest amount of new settlements was recorded in December 2015 and differed significantly from the period between February and September 2016 (Friedman's test, $p < 0.01$, chi-square = 36.46, df = 7, $n = 7$) (**Figure 5A2**). An average of 83 and 67% of the new recruits survived their first month in the MPA and at the IUI respectively (**Figure 5B**). An average of 43 and 47% of the coral recruits survived the entire year in the MPA and at the IUI respectively (**Figure 5B**). During our 8-months survey, we recorded an average of 2.35 and 2.43 new recruit settlement per 40 cm^2 $month^{-1}$ at the IUI and in the MPA respectively (**Figure 6**).

Fusion, Growth and Competition

Throughout our surveys we recorded several distinct phenomena: (1) Within 3 months, two *Montipora verrucosa* recruits had fused to form one colony (**Figure 7A**). Due to the algae bloom observed during March-May, it was difficult to detect the fusion in the reflectance images taken during those months; however, in the fluorescence images the fused colony is clearly detected. (2) Using RecruitTracker (see image annotation in methods), we were able to calculate the area of the coral recruits that were marked in cm^2; therefore, growth rate can be calculated (**Figure 7B**). This example displays a *Porites* sp. recruit that grew by ∼0.036 cm^2 within 1 year. (3) survival and death of two adjacent recruits, *Porites* sp. and *Echinopora tiranesis* (**Figure 7C**). From September 2015 to March 2016 both recruits look healthy and grew naturally however, in April the *E. tiranesis* started shrinking and by September 2016 both recruits had died.

DISCUSSION

Compared to previous surveys of coral recruits, the fluorescence imaging method developed in this study enables *in situ*, high resolution, wide field-of-view daytime fluorescence imaging of coral recruits. We demonstrated that using the FlourIS imaging system with RecruitTracker improved surveys of coral recruits in a spatial and temporal scale. Our method can be used for various research applications and enables further ecological and physiological studies of coral recruits by simplifying large-scale daytime fluorescence surveys.

Until recently, fluorescence imaging systems were limited either by resolution (Winters et al., 2009), spatial coverage of the

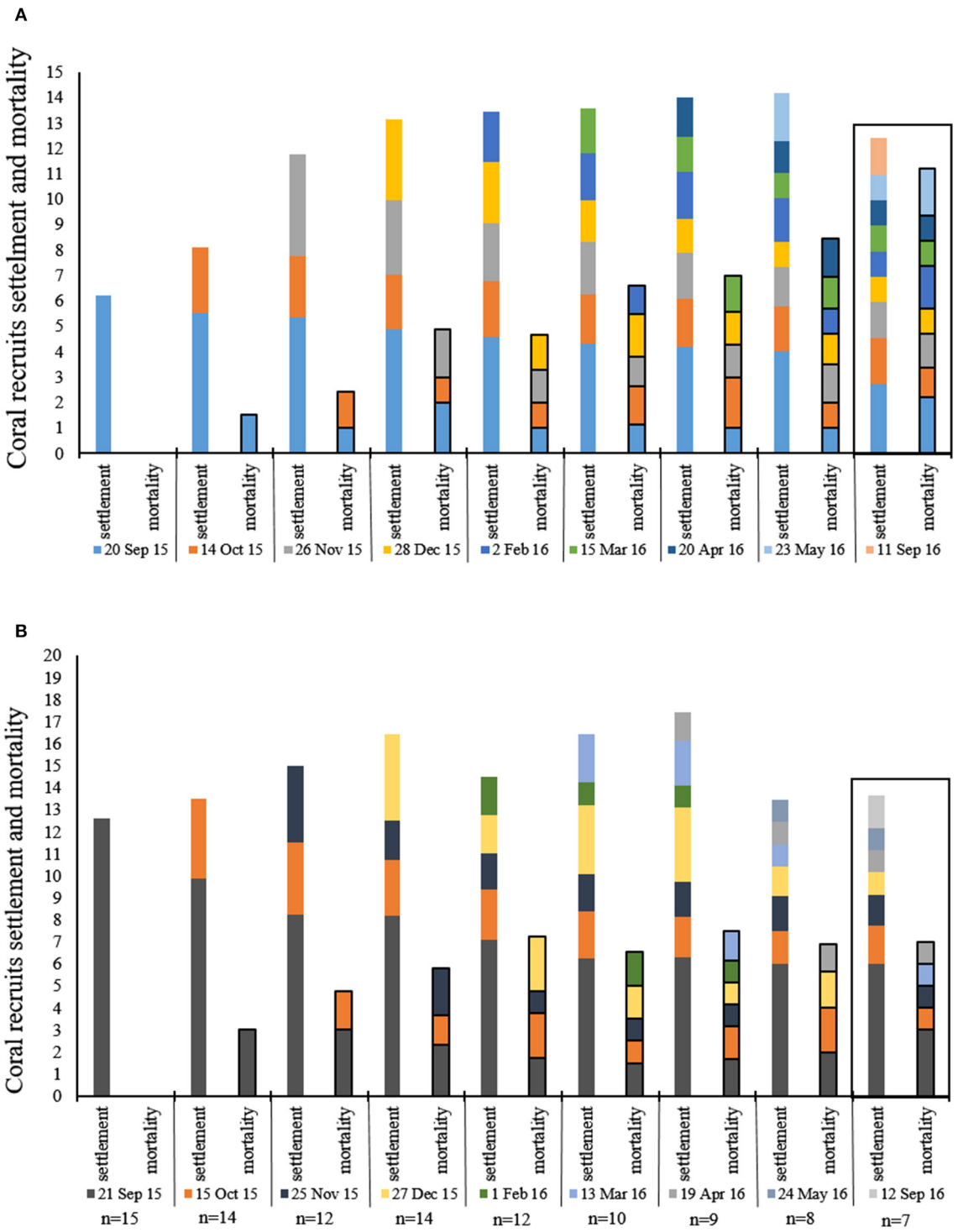

FIGURE 6 | Mean number (20 × 20 cm quadrat) of coral recruits settlement and mortality during each month of the survey. Each color represents 1 month in which new recruites were recorded, the same color follows the same recruits signifies their survival and mortlity from month to month. **(A)** reserve ($n = 18$), **(B)** IUI. Box around September 2016 emphasizes the 4 month gap from last survey and the return to the survey sites after 1 year.

measurements and/or ease of operation (Mazel, 1997; Mazel et al., 2003). Using a high-resolution camera with a wide-angle lens enabled us to identify small recruits (from ∼1 mm in diameter) in a relatively large field-of-view (20 × 20 cm). The system is built with off-the-shelf components and is easy to use and replicate, allowing standardization and widespread use.

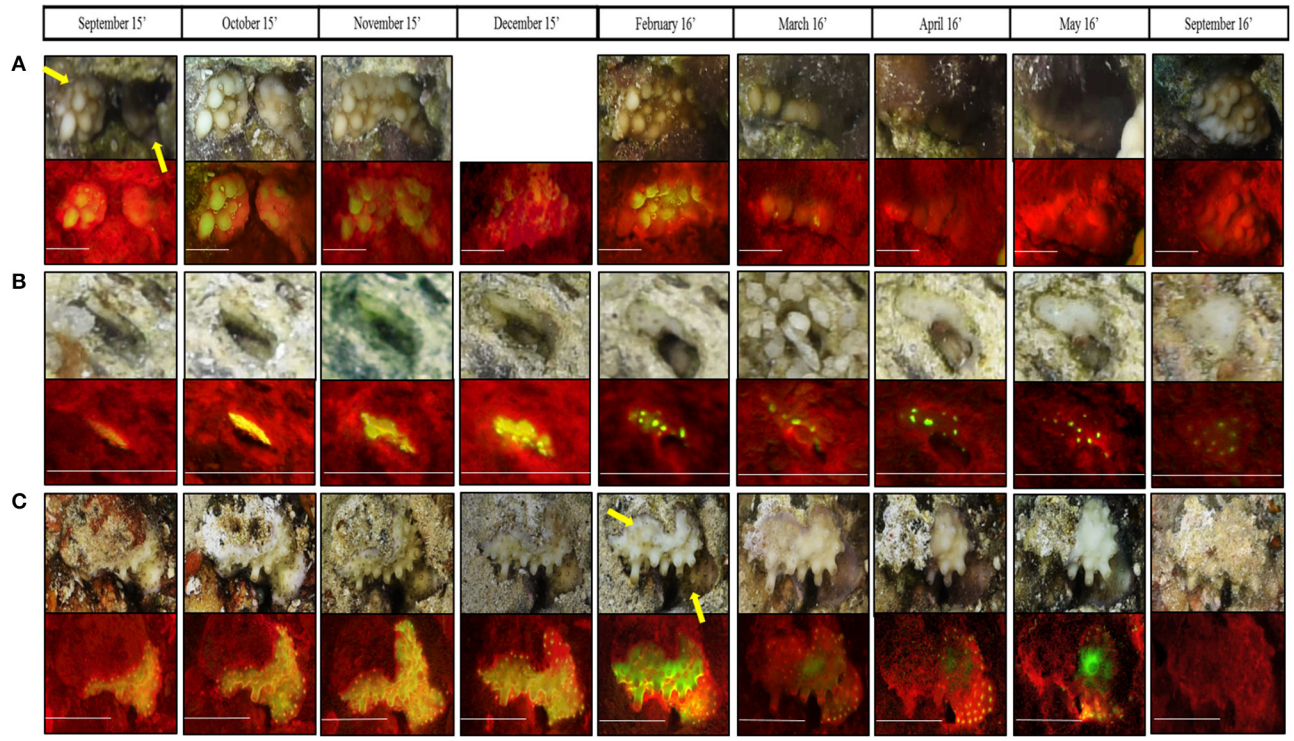

FIGURE 7 | Magnification of three phenomena recorded both in fluorescence and reflectance imaging during the present surveys; **(A)** Two *Montipora verrucosa* recruits fused to one colony from November 2015, **(B)** the growth of *Porites* sp. in 0.036 cm^2 during the survey period, and **(C)** competition between *Porites* sp. (botom coral) to *Echinopora tiranesis* (top coral). All scale bars are 0.5 cm. In **(A)** December 2015 reflectance image is missing since the camera moved while imaging so the coral was cutout of the image.

The ability to conduct daytime surveys has several advantages for the diver, including safety, ease of navigation, coverage of larger areas, spotting subjects from a distance and reducing fatigue (Zawada and Mazel, 2014). Thus, one of our main goals was to achieve daytime fluorescence imaging. This required overcoming two challenges. First, we implemented automatic registration of the fluorescent and ambient light images, which has not been previously demonstrated. This was not an easy task as the images are from different sources. Nevertheless, our algorithm (RecruitTracker) achieved high success rate of 92%. As opposed to nighttime fluorescence images, the fact that ambient light signal exists in the original fluorescence image works in our benefit and aids in the automatic registration (**Figure 2**). Second, when imaging during daytime, if the fluorescence signal is significantly lower than the ambient sunlight, the subtraction results in a noisy, less useful, image. To overcome this, we used a wide-angle lens (rather than a macro lens), which allowed us to place the camera very close to the seabed (30 cm). This resulted in high irradiance from the strobes on the coral and hence a strong fluorescence signal in comparison to the subtracted ambient signal (**Figure 3**). In this case, it was important to use a camera that had high sensitivity and bit-depth. These two system characteristics yield a high signal-to-noise-ratio in the fluorescence image (Treibitz et al., 2015).

Another challenge we faced while developing the system was the fact that fluorescence is not species-specific and there are other organisms besides corals that contain fluorescent pigments, e.g., algae, sponges, and worms. This, combined with user error, could lead to high error rates (Piniak et al., 2005). Many taxa have diverse fluorescent pigments, which helps to distinguish them from scleractinian recruits. In addition, there are corals that express a very weak GFP signal if any, (e.g., *Porites* sp.) (Roth et al., 2010) whose identification was only possible by their texture and shape in the fluorescence images. Light intensity is known to modulate pigmentation in corals of the species Acroporidae, Merulinidae, and Pocilloporidae (D'Angelo et al., 2008). However, here we do not aim to follow quantitative changes, but use the fluorescence to find the recruits. If high taxonomic resolution is required, utilizing the FluorIS along with a standard reflectance camera is essential (Baird et al., 2006). We followed this recommendation and compared each recruit identified in the fluorescence image to a high-resolution reflectance image. One inherent limitation of *in situ* imaging surveys is the fact that we can only photograph the surface of the reef, and cannot see recruits that settle on the side or beneath rocks.

We demonstrated the higher precision of this system in comparison to regular images and visual surveys. The advantages of using an imaging method over a visual survey are that field-time is reduced, images can be taken by a diver with no taxonomic expertise (or an autonomouse vehicle) and re-examined by multiple observers for accurate analysis, and

potentially be analyzed by automated annotation programs (Edmunds et al., 1998; Piniak et al., 2005; Burgess et al., 2010). We have shown here that by using our fluorescence images we found more coral recruits compared to the amount we would have found using only reflectance images and diver observations. In addition, due to the camera's high resolution and modification carried out on the FluorIS, expanding spectral range in the long wavelengths, errors in identification caused by other fluorescent organisms and/or surveyor errors were significantly reduced (**Figure 4**). Moreover, the number of non-fluorescent recruits was ∼11%. This suggests that to speed identification, it can be done only on the fluorescence images, with a cross-check to the reflectance images to verify that the fluorescent organism is indeed a coral recruit.

In this study, we covered most of the known reproduction periods of the dominant corals in the northern part of the Gulf of Aqaba. The spawning is known to be a year round process, in which the different coral species have different spawning dates (Shlesinger et al., 1985, 1998). We found relative stability in recruitment/mortality rates with high survival rates at the two surveyed sites (**Figure 6**). The coral reefs in the Gulf of Aqaba have been reported in decline and at risk of collapse, due to both local and global stressors (Glassom et al., 2004, 2006; Loya, 2004; Abelson et al., 2005). Nevertheless, our results are in line with a recent study (Shlesinger and Loya, 2016) which suggested that the reefs in Eilat (Gulf of Aqaba) are recovering. It is likely that our findings are an underestimation of the actual rates since we only surveyed a one-year reproduction period. Therefore, consistent *in situ* monitoring studies should be performed to reveal the full picture of the settlement and survival of coral recruits in order to estimate the true status of the reef.

We recorded 16% less survival during the first month at the IUI site in comparison to the MPA. The two sites are only a few 100 m away from each other. Nevertheless, they differ in the following parameters: the MPA was declared by the Israeli Nature and Parks Authority 20 years ago and has been closed to the public since, whereas the IUI area is subject to frequent diving activity. In addition, the topography of the reef at the MPA is more complex and three-dimetional whereas at the IUI the reef is mostly flat. These facts can explain the lower survival rates during the first month after settlement at the IUI in comparision to the MPA. Extensive human activity, structural complexity and availability of substrate for settlement was reported to have an important impact on the recruitment process at different locations (Hughes and Connell, 1999; Alvarez-Filip et al., 2011). Based on our data, we estimate ∼72 recruits settled per m^2 $year^{-1}$. This result significantly differs from other studies conducted on natural substrate such as Shlesinger and Loya (2016), who conducted their surveys at the same sites and found ∼15 recruits per m^2 $year^{-1}$. Other studies found ∼7 recruits per m^2 $year^{-1}$ at the Great Barrier Reef (Connell et al., 1997; Hughes et al., 2007) and ∼4 recruits per m^2 $year^{-1}$ in the western Atlantic (Smith, 1992; Miller et al., 2000).

Significant differences between similar studies using different methods were demonstrated by Abelson et al. (2005) and Yerushalmi (2016), as well as inconsistent findings in recruitment studies using different experimental protocols. Yerushalmi (2016) showed significant differences in number and in species distribution between artificial and natural substrate of coral recruit settlement, the author reported more recruits on artificial substrate as opposed to more species diversity on natural substrate. Moreover, several studies that examined coral recruitment processes in the Gulf of Aqaba using *in situ* settlement plates followed by microscopic analysis (Glassom et al., 2004, 2006; Abelson et al., 2005; Martinez and Abelson, 2013), presented significantly different recruit numbers at the same study site. In this study, we demonstrated these biases by showing different recruit counts when using different methods. We counted more recruits with our method due to its higher precision. Hence, there is a crucial need for a standardized method of recruitment assessment in coral reefs worldwide (Abelson and Gaines, 2005), which could be fulfilled by our method.

In this study, we also showed that various phenomena and morphological changes in recruits could be tracked using our imaging system (**Figure 7**). For example, we were able to record fusion, also known as a chimerism, of two recruits. This could open the way for a larger genomic study on chimerism in coral reefs. Chimerism is known to exist in several marine colonial animals from different phyla including sponges, cnidarians, bryozoans and tunicates, as well as in protists and plants. To date, the amount of chimerism in reef corals *in situ* is unknown (Heyward and Stoddart, 1985; Rinkevich and Weissman, 1987; Puill-Stephan et al., 2009). In addition, the ability to calculate growth rate with a non-distractive method *in situ* is crucial for large scale monitoring. The growth rate of *Porites* sp. recruit presented here (∼0.036 cm^2 $year^{-1}$) corresponds with the growth rates of *Porites* sp. known from the Great Barrier Reef and the Gulf of Aqaba (Lough and Barnes, 1997; Al-Rousan and Felis, 2013). We have to note, that since corals are three dimensional whereas the images taken by this method are two dimensional, natural changes in the environment such as seasonal algal blooms, which cover large areas of the substrate, changes in the quadrat positioning and camera angle can affect the calculation.

Coral recruitment, particularly settlement patterns and survival rates, has been long identified as a vital process in the ability of reefs to recover from anthropogenic and natural disturbances (Hughes et al., 2007, 2010; Urvoix et al., 2012). Therefore, understanding the recruitment process is essential for developing suitable reef conservation and management strategies. We believe that our low-cost, non-destructive, and easy-to-use method will help standardize surveys and long-term monitoring of coral recruits. In addition, it can be applied via underwater vehicles for rapid and automated surveys. In the future, we plan to develop automatic annotation methods to speed up image analysis. The recorded data can be easily uploaded to create universal databases contributing to improved understanding of this vital and delicate life stage in the coral's life cycle. This will help predict the destiny of coral reefs that are at risk of decline due to numerous environmental stressors.

AUTHOR CONTRIBUTIONS

TT conceived the project, built the system, and advised algorithm development. AZ led lab and *in situ* experiments, performed data analysis, and provided consent for the publication of the

identifiable images. TM helped and advised throughout the experiments and contributed to experiment design and data collection and analysis. DA wrote the image annotation code and helped in field experiments. AZ. TT, TM, and DA wrote the manuscript.

FUNDING

The study was supported by the Leona M. and Harry B. Helmsley Charitable Trust, the Maurice Hatter Foundation and Paul Amir Foundation. DA was also funded by the IUI post-doctoral fellowship.

ACKNOWLEDGMENTS

We thank the Leona M. and Harry B. Helmsley Charitable Trust, the Maurice Hatter Foundation and Paul Amir Foundation. AZ was an Awardee of the Hollis Gear Award—American Academy of Underwater Sciences (AAUS). A special thanks to Aviel Nahum for writing the image subtraction code. We thank the Interuniversity Institute for Marine Sciences in Eilat, Israel, for their hospitality and the use of their facilities, as well as Deborah Levi, Dotan Shreiber, Maayan Neder, Sivan Haviv, Tom Shlesinger, and Tal Cohen for their generous assistance during dives in Eilat. We also thank Avigdor Abelson and Stephane Martinez for their guidance regarding the data analysis and to Ido Itzhaki for assisting with the statistical analysis. The study was performed in accordance with regulations and guidelines set by the Israeli Nature and Parks Authority.

SUPPLEMENTARY MATERIAL

The Supplementary Material for this article can be found online at: http://journal.frontiersin.org/article/10.3389/fmars.2017.00273/full#supplementary-material

REFERENCES

Abelson, A., and Gaines, S. (2005). A call for a standardized protocol of coral recruitment research and outlines for its conception. *Mar. Pollut. Bull.* 50, 1745–1748. doi: 10.1016/j.marpolbul.2005.09.046

Abelson, A., Olinky, R., and Gaines, S. (2005). Coral recruitment to the reefs of Eilat, Red Sea: temporal and spatial variation, and possible effects of anthropogenic disturbances. *Mar. Pollut. Bull.* 50, 576–582. doi: 10.1016/j.marpolbul.2005.02.021

Akkaynak, D. (2017). *dakkaynak/recruitTracker: Original Version of recruit Tracker [Data Set]*. doi: 10.5281/zenodo.583534

Alieva, N. O., Konzen, K. A., Field, S. F., Meleshkevitch, E. A., Hunt, M. E., Beltran-Ramirez, V., et al. (2008). Diversity and evolution of coral fluorescent proteins. *PLoS ONE* 3:e2680. doi: 10.1371/journal.pone.0002680

Al-Rousan, S., and Felis, T. (2013). Long-term variability in the stable carbon isotopic composition of *Porites* corals at the northern Gulf of Aqaba, Red Sea. *Palaeogeogr. Palaeoclimatol. Palaeoecol.* 381–382, 1–14. doi: 10.1016/j.palaeo.2013.03.025

Alvarez-Filip, L., Cote, I. M., Gill, J. A., Watkinson, A. R., and Dulvy, N. K. (2011). Region-wide temporal and spatial variation in Caribbean reef architecture: is coral cover the whole story? *Glob. Chang. Biol.* 17, 2470–2477. doi: 10.1111/j.1365-2486.2010.02385.x

Baird, A. H., Salih, A., and Trevor-jones, A. (2006). Fluorescence census techniques for the early detection of coral recruits. *Coral Reefs* 25, 73–76. doi: 10.1007/s00338-005-0072-7

Bay, H., Ess, A., Tuytelaars, T., and Van Gool, L. (2008). Speeded-Up Robust Features (SURF). *Comput. Vis. Image Underst.* 110, 346–359. doi: 10.1016/j.cviu.2007.09.014

Beijbom, O., Edmunds, P. J., Kline, D. I., Mitchell, B. G., and Kriegman, D. (2012). "Automated annotation of coral reef survey images," in *Proceedings of the IEEE Computer Society Conference on Computer Vision and Pattern Recognition* (Washington, DC).

Beijbom, O., Edmunds, P. J., Roelfsema, C., Smith, J., Kline, D. I., Neal, B. P., et al. (2015). Towards automated annotation of benthic survey images: variability of human experts and operational modes of automation. *PLoS ONE* 10:e0130312. doi: 10.1371/journal.pone.0130312

Beijbom, O., Treibitz, T., Kline, D. I., Eyal, G., Khen, A., Neal, B., et al. (2016). Improving automated annotation of benthic survey images using wide-band fluorescence. *Sci. Rep.* 6:23166. doi: 10.1038/srep23166

Burgess, S. C., Osborne, K., Sfiligoj, B., and Sweatman, H. (2010). Can juvenile corals be surveyed effectively using digital photography?: implications for rapid assessment techniques. *Environ. Monit. Assess.* 171, 345–351. doi: 10.1007/s10661-009-1282-1

Cardini, U., Van Hoytema, N., Schuhmacher, H., Wild, C., and Naumann, M. S. (2015). 37 Years later: revisiting a Red Sea long-term monitoring site Biodiversity. *Coral Reefs* 34:1111. doi: 10.1007/s00338-015-1321-z

Connell, J. H., Hughes, T. P., and Wallace, C. C. (1997). A 30-year study of coral abundance, recruitment, and disturbance at several scales in space and time. *Ecol. Monogr.* 67, 461–488. doi: 10.1890/0012-9615(1997)067[0461:AYSOCA]2.0.CO;2

D'Angelo, C., Denzel, A., Vogt, A., Matz, M. V., Oswald, F., Salih, A., et al. (2008). Blue light regulation of host pigment in reef-building corals. *Mar. Ecol. Prog. Ser.* 364, 97–106. doi: 10.3354/meps07588

Edmunds, P. J., Aronson, R. B., Swanson, D. W., Levitan, D. R., and Precht, W. F. (1998). Photographic versus visual census techniques for the quantification of juvenile corals. *Bull. Mar. Sci.* 62, 937–946.

Eyal, G., Wiedenmann, J., Grinblat, M., D'Angelo, C., Kramarsky-Winter, E., Treibitz, T., et al. (2015). Spectral diversity and regulation of coral fluorescence in a mesophotic reef habitat in the Red Sea. *PLoS ONE* 10:e0128697. doi: 10.1371/journal.pone.0128697

Field, S. N., Glassom, D., and Bythell, J. (2007). Effects of artificial settlement plate materials and methods of deployment on the sessile epibenthic community development in a tropical environment. *Coral Reefs* 26, 279–289. doi: 10.1007/s00338-006-0191-9

Glassom, D., and Chadwick, N. E. (2006). Recruitment, growth and mortality of juveniles corals at Eilat, northern Red Sea. *Mar. Ecol. Prog. Ser.* 318, 111–122. doi: 10.3354/meps318111

Glassom, D., Zakai, D., and Chadwick-Furman, N. E. (2004). Coral recruitment: a spatio-temporal analysis along the coastline of Eilat, northern Red Sea. *Mar. Biol.* 144, 641–651. doi: 10.1007/s00227-003-1243-0

Heyward, A. J., and Stoddart, J. A. (1985). Genetic structure of two species of *Montipora* on a patch reef: conflicting results from electrophoresis and histocompatibility. *Mar. Biol.* 85, 117–121. doi: 10.1007/BF00397429

Hughes, T. P., Graham, N. A. J., Jackson, J. B. C., Mumby, P. J., and Steneck, R. S. (2010). Rising to the challenge of sustaining coral reef resilience. *Trends Ecol. Evol.* 25, 633–642. doi: 10.1016/j.tree.2010.07.011

Hughes, T. P., Rodrigues, M. J., Bellwood, D. R., Ceccarelli, D., Hoegh-Guldberg, O., McCook, L., et al. (2007). Phase shifts, herbivory, and the resilience of coral reefs to climate change. *Curr. Biol.* 17, 360–365. doi: 10.1016/j.cub.2006.12.049

Hughes, T. P., and Connell, J. H. (1999). Multiple stressors on coral reefs: a long-term perspective. *Limnol. Oceanogr.* 44, 864–877. doi: 10.4319/lo.1999.44.3_part_2.0932

Lough, J. M., and Barnes, D. J. (1997). Several centuries of variation in skeletal extension, density and calcification in massive *Porites* colonies from the Great Barrier Reef: a proxy for seawater temperature and a background of variability against which to identify unnatural change. *J. Exp. Mar. Biol. Ecol.* 211, 29–67. doi: 10.1016/S0022-0981(96)02710-4

Loya, Y. (2004). "The coral reefs of Eilat-past, present and future: three decades of coral community structure studies," in *Coral Health and Disease*, eds E. Rosenberg and Y. Loya (Berlin; Heidelberg: Springer), 1–34.

Martinez, S., and Abelson, A. (2013). Coral recruitment: the critical role of early post-settlement survival. *ICES J. Mar. Sci.* 70, 1294–1298. doi: 10.1093/icesjms/fst035

Mazel, C. (1997). Coral fluorescence characteristics: excitation/emission spectra, fluorescence efficiencies, and contribution to apparent reflectance. *Ocean Opt.* XIII, 2963. doi: 10.1117/12.266450

Mazel, C. H., Strand, M. P., Lesser, M. P., Crosby, M. P., Coles, B., and Nevis, A. J. (2003). High resolution determination of coral reef bottom cover from multispectral fluorescence laser line scan imagery. *Limnol. Oceanogr.* 48, 522–534. doi: 10.4319/lo.2003.48.1_part_2.0522

Miller, M. W., Weil, E., and Szmant, A. M. (2000). Coral recruitment and juvenile mortality as structuring factors for reef benthic communities in Biscayne National Park, *Coral Reefs* 19, 115–123. doi: 10.1007/s003380000079

Mundy, C. N. (2000). An appraisal of methods used in coral recruitment studies. *Coral Reefs* 19, 124–131. doi: 10.1007/s003380000081

Otsu, N. (1979). A threshold selection method from gray-level histograms. *IEEE Trans. Syst. Man Cybern.* 9, 62–66. doi: 10.1109/TSMC.1979.4310076

Piniak, G. A., Fogarty, N. D., Addison, C. M., and Kenworthy, W. J. (2005). Fluorescence census techniques for coral recruits. *Coral Reefs* 24, 496–500. doi: 10.1007/s00338-005-0495-1

Rinkevich, B., and Weissman, I. L. (1987). Chimeras in colonial invertebrates - a synergistic symbiosis or somatic-cell and germ-cell parasitism. *Symbiosis* 4, 117–134.

Roth, M. S., and Knowlton, N. (2009). Distribution, abundance, and microhabitat characterization of small juvenile corals at Palmyra Atoll. *Mar. Ecol. Prog. Ser.* 376, 133–142. doi: 10.3354/meps07787

Roth, M. S., Latz, M. I., Goericke, R., and Deheyn, D. D. (2010). Green fluorescent protein regulation in the coral *Acropora yongei* during photoacclimation. *J. Exp. Biol.* 213, 3644–3655. doi: 10.1242/jeb.040881

Salinas-de-Leon, P., Costales-Carrera, A., Zeljkovic, S., Smith, D. J., and Bell, J. J. (2011). Scleractinian settlement patterns to natural cleared reef substrata and artificial settlement panels on an Indonesian coral reef. *Estuar. Coast. Shelf Sci.* 93, 80–85. doi: 10.1016/j.ecss.2011.02.016

Shaked, Y., and Genin, A. (2012). *Israel National Monitoring Program at the Gulf of Eilat.* Eilat: The Interuniversity Institute for Marine Sciences.

Shihavuddin, A. S. M., Gracias, S. M. N., Garcia, R., Gleason, A., and Gintert, B. (2013). Image-based Coral Reef classification and thematic mapping. *Remote Sens.* 5, 1809–1841. doi: 10.3390/rs5041809

Shlesinger, T., and Loya, Y. (2016). Recruitment, mortality, and resilience potential of scleractinian corals at Eilat, Red Sea. *Coral Reefs* 35, 1357–1368. doi: 10.1007/s00338-016-1468-2

Shlesinger, Y., Goulet, T. L., and Loya, Y. (1998). Reproductive patterns of scleractinian corals in the northern Red Sea. *Mar. Biol.* 132, 691–701. doi: 10.1007/s002270050433

Shlesinger, Y., Loya, Y., Masters, W. M., and Simmons, A. (1985). Coral Community reproductive patterns: Red Sea versus the Great Barrier Reef. *Science* 14, 1333–1335. doi: 10.1126/science.228.4705.1333

Singh, H., Armstrong, R., Gilbes, F., Eustice, R., Roman, C., Pizarro, O., et al. (2004). Imaging coral I: imaging coral habitats with the SeaBED AUV. *Subsurface Sens. Technol. Appl.* 5, 25–42. doi: 10.1023/B:SSTA.0000018445.25977.f3

Smith, S. R. (1992). Patterns of coral recruitment and post-settlement mortality on bermuda's reefs: comparisons to Caribbean and pacific reefs. *Integr. Comp. Biol.* 32, 663–673. doi: 10.1093/icb/32.6.663

Soong, K., Chen, M., Chen, C., Dai, C., Fan, T., Li, J., et al. (2003). Spatial and temporal variation of coral recruitment in Taiwan. *Coral Reefs* 22, 224–228. doi: 10.1007/s00338-003-0311-8

Puill-Stephan, E., Willis, B. L., van Herwerden, L., and van Oppen, M. J. H. (2009). Chimerism in wild adult populations of the broadcast spawning coral *Acropora millepora* on the Great Barrier Reef. *PLoS ONE* 4:e7751. doi: 10.1371/journal.pone.0007751

Stokes, M. D., and Deane, G. B. (2009). Automated processing of coral reef benthic images. *Limnol. Oceanogr. Methods* 7, 157–168. doi: 10.4319/lom.2009.7.157

Treibitz, T., Neal, B. P., Kline, D. I., Beijbom, O., and Roberts, P. L. D. (2015). Wide field-of-view fluorescence imaging of Coral Reefs. *Sci. Rep.* 5, 1–5. doi: 10.1038/srep07694

Urvoix, L., Fauvelot, C., and Bouchon, C. (2012). "Monitoring of coral larval recruitment on artificial settlement plates at three different depths using genetic identification of recruits (Guadeloupe Island)," in *Proceedings of* the *65th Gulf and Caribbean Fisheries Institute* (Santa Marta), 114–120.

Winters, G., Holzman, R., Blekhman, A., Beer, S., and Loya, Y. (2009). Photographic assessment of coral chlorophyll contents: Implications for ecophysiological studies and coral monitoring. *J. Exp. Mar. Biol. Ecol.* 380, 25–35. doi: 10.1016/j.jembe.2009.09.004

Yerushalmi, M. (2016). *Assessing Coral Recruitment Properties in Eilat's Reef using DNA Barcoding Tools*. Master's thesis, University of Haifa, Haifa

Zawada, D. G., and Mazel, C. H. (2014). Fluorescence-based classification of Caribbean coral reef organisms and substrates. *PLoS ONE* 9:e84570. doi: 10.1371/journal.pone.0084570

Zuliani, M. (2008). *RANSAC for Dummies with Examples using the RANSAC Toolbox for Matlab and More*.

Conflict of Interest Statement: The authors declare that the research was conducted in the absence of any commercial or financial relationships that could be construed as a potential conflict of interest.

frontiers in Marine Science

ORIGINAL RESEARCH
published: 14 September 2017
doi: 10.3389/fmars.2017.00297

Light Absorption in Coralline Algae (Rhodophyta): A Morphological and Functional Approach to Understanding Species Distribution in a Coral Reef Lagoon

*Román M. Vásquez-Elizondo and Susana Enríquez **

Laboratorio de Fotobiología, Unidad de Sistemas Arrecifales Puerto Morelos, Instituto de Ciencias del Mar y Limnología, Universidad Nacional Autónoma de Mexico, Cancún, Mexico

Red coralline algae are a cosmopolitan group with the ability to precipitate $CaCO_3$ within the walls of their vegetative cells. The resultant carbonate structure is key for explaining their ecological success, as it provides protection against herbivores and resistance to water motion. However, its potential contribution to enhance thallus light absorption efficiency through multiple light scattering on algal skeleton, similar to the effect documented for scleractinian corals, has not been yet investigated. Here, we initiate this analysis, characterizing thallus optical properties of three coralline species, which differed in pigment content and thallus mass area (TMA, gDW m^{-2}). The three species, the rhodolith *Neogoniolithon* sp., the crustose coralline alga (CCA), *Lithothamnion* sp., and the articulated alga *Amphiroa tribulus,* represent the more distinctive coralline growth-forms and are able to colonize contrasting light environments in Caribbean coral reefs. The thicker thalli of the rhodoliths were the most efficient light collectors, as evidenced by their higher pigment absorption efficiency (a^*_{Chla}; m^2 $mgChla^{-1}$) and photosynthetic rates per unit area. This could explain rhodolith success in oligotrophic, highly illuminated reef environments. In contrast, the thinner thalli of the CCA, a low-light specialist, showed the highest metabolic rates normalized to mass and the highest light absorption efficiencies per unit mass (a^*_M; m^2 gdw^{-1}). Therefore, the ecological success of the CCA in cryptic habitats within the reef cannot be explained only by its low-light physiology, but also by its capacity to reduce the structural costs of their thalli, and thus of its new growth. Lastly, the ecological success of *Amphiroa tribulus,* which displayed intermediate values for the efficiency of light absorption, metabolic rates and TMA, was explained by its ability to construct the largest light collectors (algal canopies) thanks to the presence of flexible, non-calcified segments (genicula). This ability enables enhanced photosynthetic and carbonate production at the organism/canopy level. The resulting fragile canopy survives best within the protection provided by colonies of the lettuce coral *Agaricia agaricites.* In conclusion, our study demonstrates the utility of optical traits as powerful tools to investigate differences in the competitive abilities, abundances and niche distribution among algal species and/or growth-forms.

Keywords: optical traits, photosynthesis, niche differentiation, rhodoliths, CCA, articulated alga, coral reefs, *Amphiroa tribulus*

OPEN ACCESS

Edited by:
Daniel Wangpraseurt, University of Cambridge, United Kingdom

Reviewed by:
Charles Alan Jacoby, St. Johns River Water Management District, United States
Hollie Putnam, Hawai'i Institute of Marine Biology, United States

****Correspondence:***
Susana Enríquez
enriquez@cmarl.unam.mx;
susana.enriquezdominguez@gmail.com

Specialty section:
This article was submitted to Coral Reef Research, a section of the journal Frontiers in Marine Science

Received: *31 March 2017*
Accepted: *30 August 2017*
Published: *14 September 2017*

Citation:
Vásquez-Elizondo RM and Enríquez S (2017) Light Absorption in Coralline Algae (Rhodophyta): A Morphological and Functional Approach to Understanding Species Distribution in a Coral Reef Lagoon. Front. Mar. Sci. 4:297. doi: 10.3389/fmars.2017.00297

INTRODUCTION

Coralline algae are a diverse group of red macroalgae with the ability to calcify within the walls of their vegetative cells (Johansen, 1981). This broad taxonomic group is present in virtually every coastal ecosystem, from highly illuminated, intertidal regions to extremely light-limited habitats like rock crevices or depths of 250 m (Johansen, 1981; Littler et al., 1985; Payri et al., 2001; Burdett et al., 2014). The ecological significance of coralline algae varies from playing a fundamental role as ecosystem engineers of highly diverse communities (Foster, 2001; Steller et al., 2003) to being the preferred substrate for settlement of invertebrate larvae (Heyward and Negri, 1999; Williams et al., 2008). In certain ecosystems, corallines are the main contributors to carbon budgets (Chisholm, 2003; Martin et al., 2006; Bensoussan and Gattuso, 2007). On coral reefs, corallines are fundamental for cementing the primary reef framework and maintain habitat diversity (Littler, 1972; Littler and Doty, 1975; Adey, 1998; Perry and Hepburn, 2008; Perry et al., 2008). Carbonate skeletons are considered responsible for the distribution and abundance of many species (Steneck, 1986; Vadas and Steneck, 1988; Steneck et al., 1991; Steneck and Dethier, 1994; Steller and Foster, 1995; Foster, 2001), and ultimately for the ecological success of coralline algae in marine habitats, as they play fundamental roles providing protection against herbivores and resistance to water motion.

The ability of coralline algae to colonize contrasting marine environments (Algarra and Niell, 1987; Häder et al., 1997; Payri et al., 2001; Schubert and García-Mendoza, 2008; Enríquez et al., 2009; Vásquez-Elizondo and Enríquez, 2016) relies on multiple physiological and structural adaptations. Among them, the optical properties of thalli may play a central role, as they are fundamental regulators of algal photosynthetic responses by controlling the entrance of solar energy. Changes in the efficiency of light absorption could help to elucidate the differential ability of organisms to acclimate or adapt to differing light regimes and the consequences of these responses on coralline photosynthetic performance. Unfortunately, little is known about the optical properties of coralline algae. The technical difficulties of performing optical measurements on highly dispersive structures, have strongly limited this area of research (Vásquez-Elizondo et al., 2017). Several studies have characterized the optical properties of multicellular photosynthetic tissues in aquatic organisms, such as marine macroalgae (Ramus, 1978; Frost-Christensen and Sand-Jensen, 1992; Enríquez et al., 1994, 2009; Mercado et al., 1996; Schubert et al., 2011); seagrasses and freshwater angiosperms (e.g., Enríquez et al., 1992; Frost-Christensen and Sand-Jensen, 1992; Olesen et al., 2002; Enríquez and Sand-Jensen, 2003; Enríquez, 2005; Cayabyab and Enríquez, 2007; Durako, 2007), and scleractinian corals (Shibata, 1969; Enríquez et al., 2005; Rodríguez-Román et al., 2006; Wangpraseurt et al., 2017). All these studies have documented large within and among species variation in optical properties of multicellular photosynthetic structures. Some of them documented common trends among species related to basic structural traits, such as pigment content, tissue thickness and specific mass area (Ramus et al., 1976a,b; Ramus, 1978, 1990; Enríquez et al., 1992, 1994, 2005; Olesen et al., 2002; Enríquez and Sand-Jensen, 2003; Enríquez, 2005). Small structural modifications in key photosynthetic structures may lead to significant changes in optical properties of tissues, with subsequent implications for photosynthetic performance. Many aquatic organisms reduce the optical absorption cross-sections of their multicellular photosynthetic structures (i.e., thalli/leaves) at increasing light levels and become thinner when light limits their growth (Lüning and Dring, 1985; Markager and Sand-Jensen, 1992; Enríquez and Sand-Jensen, 2003). These photoacclimatory responses are similar to the widely documented response of unicells (e.g., Raven and Geider, 2003), but they contrast with descriptions for terrestrial leaves, which generally exhibit little variation in light absorption and no clear pattern of change in pigment content with irradiance (i.e., Björkman, 1981). Scattering of light within terrestrial leaves produces significant enhancements in their internal light field, even above external incident irradiance levels (Vogelmann and Björn, 1984; Vogelmann et al., 1996). This phenomenon, which strongly depends on the anatomical characteristics of the leaf and the presence/absence of light-reflecting structures (Vogelmann et al., 1988, 1996), is known as multiple light scattering. Multiple scattering of light has important consequences for leaf photosynthetic performance (Vogelmann et al., 1989, 1996) and strongly reduces the role of pigment content as a fundamental control of tissue light absorption. Multiple scattering of light on carbonate skeletons of corals has been demonstrated to enhance the ability of symbiotic algae to collect light *in hospite,* despite the fact that pigment contents of symbiotic corals are lower than leaves of land plants (Enríquez et al., 2005). Furthermore, the ecological and evolutionary success of symbiotic *Scleractinia* in oligotrophic, tropical environments has been attributed to the extraordinary light absorption properties of the host-symbiont-skeleton unit (Enríquez et al., 2005, 2017).

In coralline algae, however, the capacity of carbonate skeleton to enhance light absorption and photosynthetic performance remains unknown (see Payri et al., 2001; Burdett et al., 2014). Recently, Vásquez-Elizondo and Enríquez (2016) documented significant differences in the light absorption properties of three coralline species, before and after exposing the experimental organisms to heat-stress. These authors attributed the differences in coralline sensibility to heat-stress to differing abilities to withstand light-stress induced by elevated temperature. Similar exacerbations of light-stress have been documented for symbiotic scleractinian corals exposed to heat-stress (Warner et al., 1996; Iglesias-Prieto and Trench, 1997). Interestingly, corals share with coralline algae similar sensitivity to ocean warming and acidification, two major global threats that affect marine habitats (Hoegh-Guldberg et al., 2007; McCoy and Kamenos, 2015; Vásquez-Elizondo and Enríquez, 2016).

In the present study we analyzed the optical properties of the same three coralline species examined by Vásquez-Elizondo and Enríquez (2016), as model organisms to investigate the association between optical traits and structural descriptors, such as pigment content and thallus mass area: the rhodolith forming species *Neogoniolithon* sp.; the articulated algae *Amphiroa tribulus;* and the low-light incrusting alga-CCA *Lithothamnion*

sp. The optical traits characterize were: (i) absorptance (A), defined as the fraction of incident light absorbed by thallus photosynthetic pigments, which describes the capacity of light absorption by algal thalli to sustain photosynthetic activity; and (ii) two descriptors for light absorption efficiency, pigment-specific absorption coefficient (a^*_{pigm}, m^2 mg $pigm^{-1}$) and mass-specific absorption coefficient (a^*_M, m^2 g DW^{-1}). The first, a^*_{pigm}, describes pigment efficiency of the light collector (algal thalli), and the second, a^*_M, describes light absorption efficiency of thallus structural mass. Both descriptors have been previously determined for the leaves of an amphibious plant, *Mentha aquatica* (Enríquez and Sand-Jensen, 2003) and for the leaves of the seagrass *Thalassia testudinum* (Enríquez, 2005). The analysis of a^*_M follows previous suggestions by Falkowski et al. (1985), Ramus (1990), and Enríquez et al. (1994).

MATERIALS AND METHODS

Sample Collection and Experimental Manipulation of Organisms

Samples of three species (**Figure 1**) were collected from the reef lagoon of Puerto Morelos (Mexican Caribbean, 20°51′N, 86°55′W) between 2011 and 2013. Specimens of the rhodolith forming species *Neogoniolithon* sp. were collected at 3 m depth by snorkeling within the seagrass bed. Samples of the articulated alga *Amphiroa tribulus* and the crustose coralline (CCA) *Lithothamnion* sp. were collected by SCUBA diving at a depth of 5–6 m within the back-reef coral community. The three species inhabit contrasting light environments, and show contrasting photobiology and growth-forms (Vásquez-Elizondo and Enríquez, 2016). *Neogoniolithon* sp. colonizes mobile substrates (sand) inside open seagrass beds in the highly illuminated, shallow reef lagoon, and exhibits a high-light acclimatory response (Vásquez-Elizondo and Enríquez, 2016). The articulated and CCA algae colonize less illuminated habitats within the reef community and show contrasting photobiology. The CCA *Lithothamnion* sp. is a low light specialist, which grows underneath or adjacent to colonies of *Orbicella faveolata* and *O. annularis*, in cryptic environments within the reef that do not receive direct solar radiation (Vásquez-Elizondo and Enríquez, 2016). The articulated alga, *Amphiroa tribulus,* grows within colonies of the lettuce-leaf coral *Agaricia agaricites* (Figure S1 in Supporting Information, SI) and exhibits contrasting pigmentation between both sides of its thalli. The irradiance reaching each of the sites was estimated about 37% of surface irradiance (Es) for the back-reef at 5–6 m depth, and 47% of Es for the open seagrass bed (calculated from *in situ* measurements of water column attenuation coefficients, K_d = 0.198 m^{-1}, similar to values reported by Enríquez and Pantoja-Reyes, 2005). After collection, samples were transported in black plastic bags to the outdoor tank facilities of the Universidad Nacional Autónoma de México (UNAM) at the Unidad Académica de Sistemas Arrecifales (UASA) in Puerto Morelos (Quintana Roo, Mexico). This approach avoids degradation of pigments and damage to thalli due to exposure to full solar radiation. The outdoor facilities consist of 48 experimental tanks of 30-L, connected to eight 1,000-L header tanks. Each header tank was supplied with constant seawater from the reef lagoon, which then supplied the experimental tanks. Water temperature in the tanks was controlled using commercial aquarium heaters (Process, Technology, USA). Light conditions were simulated to match the particular habitat of each of the species using neutral screens: attenuation of 53% Es for the rhodoliths; 75% Es for the articulated alga; and about ≈98% Es for the CCA, as this species inhabits an extremely low-light environment (cf., Vásquez-Elizondo and Enríquez, 2016). Most experimental determinations were made 2–3 days after collection, and all were completed within a week. Prior to experimental determinations, branches of the rhodolith and articulated algae, and 2–3 cm^2

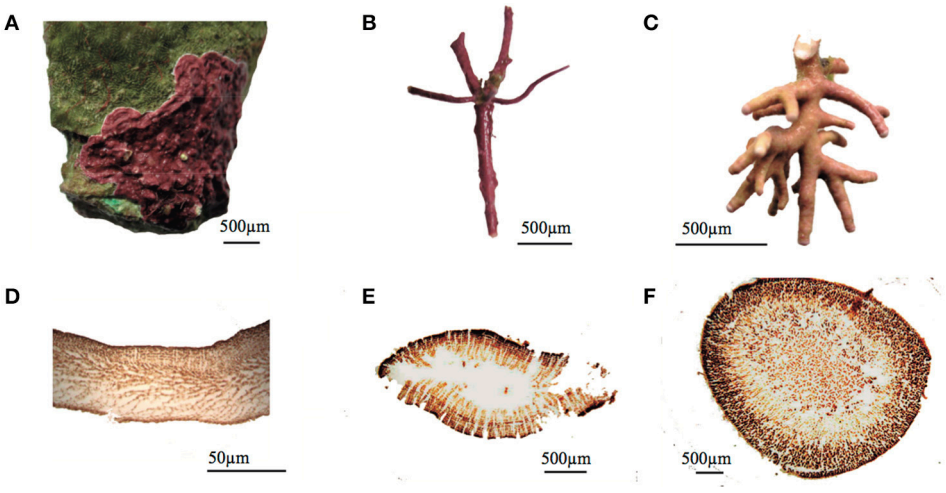

FIGURE 1 | Images of the three coralline algae (Rhodophyta) characterized in this study. (**A**) The crustose coralline alga (CCA), *Lithothamnion* sp. growing on some dead coral skeleton of the genus *Orbicella*. (**B**) The articulated alga *Amphiroa tribulus*. (**C**) The rhodolith forming species belonging to the genus *Neogoniolithon* sp. **(D–F)** show a microscopic cross section of their respective thalli.

segments of the CCA were cleaned gently to remove epiphytes (mainly fleshy algae) and minimize potential interferences during optical characterizations. Two optical determinations were performed for each thallus of the articulated alga, as this species presented a heterogeneous anatomy with two distinct pigmentations on the opposite sides of their branches. The optical properties of each side were characterized, referred as to the highly-pigmented (HP) upper side, and lesser-pigmented (LP) lower side. CCA segments were detached from the substratum before optical characterization.

Thallus Structural Descriptions

Pigment content was measured spectrophotometrically on the same samples used for light absorption determinations. Fragments of coralline thalli were manually homogenized before pigment extraction. Phycobiliprotein extraction (phycoerythrin PE, phycocyanin PC, and allophycocyanin APC) was performed adding a phosphate potassium buffer (0.1 M, pH 6.8) to the homogenized sample. Pigment extractions were analyzed in a conventional spectrophotometer (Elyptica, Ensenada, Mexico) after centrifuging samples maintained in darkness at 4°C for 2 h. The residual carbonate pellet was re-suspended in 80% acetone for chlorophyll *a* extraction. Samples were maintained overnight in darkness, at 4°C. Phycobiliprotein and chlorophyll *a* contents were calculated according to the equations of, respectively, Kursar et al. (1983) and Lichtenthaler and Wellburn (1983).

Thallus mass area (TMA, g cm^{-2}) was calculated as the ratio between thallus dry mass and its projected area. This parameter is the inverse of the specific leaf area (SLA, cm^2 gDW^{-1}), a common descriptor in plant ecology (e.g., Garnier et al., 1997; Poorter and De Jong, 1999; Evans and Poorter, 2001), and equivalent to leaf mass area (1/SLA=LMA; i.e., Witkowski and Lamont, 1991; de la Riva et al., 2016). Dry weight was determined by drying the samples for 48 h at 60°C. These measurements allowed description of an association for each species between thallus fresh (blotting dry) and dry weight ($R^2 > 0.95$, $P < 0.05$, $n = 7$). Subsequent dry weight estimations were derived from direct fresh weight measurements. We also determined thallus thickness (mm) from indirect estimations, using its linear association with TMA previously described [thallus thickness (mm) = 5.96*TMA + 0.033; $R^2 = 0.90$; $P < 0.001$; $n = 32$; $SE = 0.158$]. Ash-free dry weight (organic content) was estimated by decalcification of dried thalli of known weight with HCl (10% v:v). Calcium carbonate content per total dry mass (% $CaCO_3$) was further determined by subtracting the organic dry weight, according to Steller et al. (2007). The surface area of rhodoliths and the articulated alga was measured using digital images and IMAGE J™ software. For CCA segments, the projected area or cross-section area was obtained by covering the alga with aluminum foil, weighing the aluminum piece and comparing it to a reference of known area and weight (aluminum foil technique, Marsh, 1970). Special care was taken to minimize overlap. Pigment content values were normalized to surface area and dry mass for estimations of two descriptors: thallus pigment density (mg m^{-2}), and thallus pigment content (mg g DW^{-1}).

Finally, for the description of the three-dimensional (3D-) coralline morphology (algal canopy), we calculated the total-one sided surface area referenced by its vertical projection (no units or m^2 m^{-2}). This calculation is equivalent to the leaf area index (LAI; Watson, 1947), which is a common descriptor for terrestrial plant canopies. Complete individuals of each species were photographed from a vertical perspective using a white bottom plate, and the projected area was obtained using IMAGE J™ software. Subsequently, branches were manually separated to estimate the total one-sided area of the thalli, following the protocol described previously. Coralline LAI was calculated as the ratio between total surface area of the organisms against its projected ground area.

Optical Determinations

Reflectance spectra (R) were performed according to Vásquez-Elizondo et al. (2017), using a miniature Ocean Optics USB2000 spectroradiometer (Ocean Optics, Inc., Dunedin, Fl, USA). Reflected light was collected with a 2 mm fiber optic placed over the thallus surface at an angle of 45° and a distance of 3–5 mm. Algal segments were placed in a black container filled with seawater, and we prevented the fiber optic from shading the sample. The spectral variability collected between 400 and 750 nm, was registered by the spectroradiometer using the software SpectraSuite® (Ocean Optics, Inc., Fl, USA). Reflectance was expressed as the ratio between radiance measurements from the surface of pigmented thalli relative to radiance reflected by a white reference (Teflon). Homogeneous diffuse illumination was provided from a semi-sphere coated with barium oxide (BaO), which was illuminated from below using different commercial light sources in order to fulfill the PAR range illumination (400–700 nm). This semi-sphere was placed above the black container at approximately 25 cm from the algal fragments. Reflectance spectra of pigmented fragments were corrected by normalizing them to the reflectance of nearly identical but bleached fragments. All determinations showed reflectance values above 0.94 ($R_{725-750nm} = 94\%$ light reflected) in the range between 725 and 750 nm, which implies that the magnitude of residual light scattering was sufficiently low, around 6%.

Determinations of light transmission (Absorbance, D) were performed using a spectrophotometer AMINCO DW2 (USA) controlled by an OLIS data collection system, equipped with an opal-glass in front of the detector (Shibata, 1959). Thallus fragments were mounted in a 3 ml cuvette, filled with filtered seawater. Algal thalli were held against the wall of the cuvette using a holder specifically developed to avoid misplacement during determinations (Enríquez, 2005). Measurements were performed between 400 and 750 nm at intervals of 1 nm. Attenuance (apparent absorbance) was corrected for residual scattering by subtracting absorbance at 750 nm. All spectra produced absorbance (D) values below 0.1 for the range 725–750 nm ($D_{725-750}$). Naturally bleached samples of coralline algae were used as blanks for subtraction of non-photosynthetic absorption (Enríquez, 2005; Vásquez-Elizondo et al., 2017).

We calculated the optical descriptors as follows:

(1) thallus absorptance (A) was calculated as:

$$A(\lambda) = 1 - 10^{-D(\lambda)} - R(\lambda) \quad (1)$$

where $10^{-D(\lambda)}$, $D(\lambda)$ and $R(\lambda)$ denote, respectively, transmittance (T), absorbance (D), and reflectance (R) at a particular

wavelength (λ). Absorptance was estimated for the average PAR range (A_{PAR}) and for the chlorophyll *a* (Chl*a*) peak at 680 nm (A_{Chla}). Pigmented branches of the rhodolith *Neogoniolithon* sp. that are about 1.4 ± 0.21 mm thick transmit on average 1.2% ± 0.21 ($n = 6$) of the incident light (Vásquez-Elizondo et al., 2017). Therefore, we considered transmission through rhodolith branches to be 0 for samples thicker than 1.4 mm, and that absorptance could be derived directly from reflectance data as proposed by Enríquez et al. (2005) and confirmed by Vásquez-Elizondo et al. (2017). Absorptance for these samples was calculated as:

$$A(\lambda) = 1 - R(\lambda) \quad (2)$$

(2) the efficiency of light collection was quantified using two parameters, pigment specific absorption coefficient (a^*_{pigm} in m^2 mg $pigm^{-1}$) calculated as:

$$a^*_{pigm} = (D/\rho)\ln 10 \quad (3)$$

and mass specific absorption coefficient (a^*_M, in m^2 gDW^{-1}) calculated as:

$$a^*_M = (D/TMA)\ln 10 \quad (4)$$

where *D* is absorbance, ρ is pigment cross section in mg m^{-2}, and TMA is thallus mass area. a^*_{pigm} was calculated for the PAR range (a^*_{Pigm}) and for the Chl*a* peak at 680 nm (a^*_{Chla}), using, respectively, total pigment and Chl*a* density values. Similarly, a^*_M was estimated for the PAR region (a^*_{MPAR}) and for the Chl*a* peak at 680 nm (a^*_{M680}).

Absorbance for thalli of rhodoliths was estimated from reflectance measurements using the transformation D(λ)=log[1/R(λ)] proposed by Shibata (1969) and Enríquez et al. (2005). Optical determinations on rhodoliths only required one measurement (reflectance), whereas the other two species needed two optical measurements (transmittance and reflectance) to estimate absorptance. This explains why the number of determinations for rhodoliths was higher than for the other two species.

Photosynthetic Determinations

The physiological data used in this comparison were derived from Vásquez-Elizondo and Enríquez (2016), who characterized photosynthetic rates of samples exposed to control conditions (summer conditions of 30°C and ambient pH) and three experimental treatments: heat-stress (32°C); reduced pH (7.9) and combined heat-stress and reduced pH (32°C and pH = 7.9), at the UNAM mesocosms facilities. Experimental organisms were collected in August 2013 from the same sites described previously of the reef lagoon of Puerto Morelos, and expressed, thus, the summer *"phenotype"* for the three coralline populations. Photosynthetic rates were estimated polarographically using oxygen Clark type electrodes, in closed chambers (Hansatech, Nortfolk, UK) connected to a circulating bath with temperature control (RTE-100/RTE 101LP; Neslab Instruments Inc., Portsmouth, NH, USA). Samples were incubated for 45 min under saturating irradiances (>Ek) according to the particular photobiology of each species, which was previously characterized by Vásquez-Elizondo and Enríquez (2016), through the description of the photosynthetic response to irradiance (P vs. E) curve. Post-illumination respiration (R_L) was determined in darkness, right after P_{max} incubations. R_L allowed estimation of gross photosynthesis rates from knowledge of oxygen consumption at P_{max}. Maximum gross photosynthesis, P_{max}, was normalized either per projected area (μmol O_2 cm^{-2} h^{-1}) or dry weight (μmol O_2 gDW^{-1} h^{-1}). Photosynthesis data from Vásquez-Elizondo and Enríquez (2016) are available at https://search.datacite.org/works/10.1594/PANGAEA.860802 (doi: 10.1594/PANGAEA.860802).

Photosynthetic Production Estimations

Total photosynthetic production per individual was calculated by multiplying thallus photosynthetic rates per area by the estimated Leaf Area Index of each morphology. For comparison among coralline growth-forms, we assumed the simplest scenario using estimates of net photosynthetic production for 1 h at saturation irradiance (P_{max}).

Comparison of Optical Properties among Different Photosynthetic Structures

Using data from the literature for pigment specific absorption normalized to chlorophyll *a* (a^*_{Chla}, m^2 mg $Chla^{-1}$), we compared these published values against the variability estimated for the three coralline species in our study. The aquatic photosynthetic structures considered in this comparison were >30 species from Atlantic and Mediterranean coastal habitats, mostly non-calcifying red algae, characterized by Enríquez et al. (1994); the amphibious aquatic angiorperm *Mentha aquatica* described by Enríquez and Sand-Jensen (2003); the seagrass *Thalassia testudinum* characterized by Enríquez (2005); and the scleractinian coral, *Porites branerii* documented by Enríquez et al. (2005). Data from Enríquez et al. (1994) were re-calculated from original D_{680} and Chl*a* values, which allowed estimation of a^*_{Chla} according to Enríquez and Sand-Jensen (2003) and Enríquez (2005).

Data Analyses

One-way analysis of variance, ANOVA-test, was used to find differences among species in their structural and optical descriptors, after testing for normality and homoscedasticity assumptions. Pearson correlation coefficients (r) were used to determine association of variation between log-log transformed, structural and optical descriptors. Least-squares (LS) regression analyses of log-log transformed data were used to describe the associations of variation according to the equation: [$\log Y = a + b \log X$], which allows description of the allometric function [$Y = aX^b$].

Analyses of covariance, ANCOVA tests, were also used to test for significant differences in the intercept or the slope of the linear LS-regression associations. For testing differences among species in the covariation between the capacity of light absorption (absorptance) and pigment density, we used an exponential model [$y = A_{max}*(1\text{-}e^{-b*x})$], where A_{max} denotes

maximum absorptance and b is the initial exponential rise of this association. All statistics were performed using the IBM-SPSS™ Statistics (Statistical Package for the Social Sciences).

RESULTS

The three coralline algae displayed significant differences in thallus structure and optical properties (**Figures 1**, **2**, Table S1 in the supporting information, SI). The rhodolith, *Neogoniolithon* sp., had the thickest thalli, largest TMA and highest carbonate content, together with the lowest thallus pigmentation per unit area and dry weight (**Figure 2**, Table S1 in SI). In contrast, the CCA, *Lithothamnion* sp., had the thinnest thalli, lowest TMA and highest pigment content normalized to dry weight (**Figures 2C,D**). The highest pigment content per area (pigment density), however, was found in the articulated alga, *Amphiroa tribulus* (**Figure 2A**). Thallus thickness was positively correlated with TMA and negatively with thallus pigmentation (Table S2 in SI). Other relationships varied among species, with TMA being positively correlated with Chl*a* per unit area for all three coralline species, and positively correlated with total pigmentation per area only for the rhodolith and CCA. No correlation was observed between TMA and thallus pigmentation per unit mass (Tables S2–4, SI).

Transmission absorption spectra showed the typical features of *Rhodophyta*, with an absorption band at 620–625 nm for PC; peaks at 490, 545, and 576 nm for PE; and at 650 nm for APC. The presence of Chl*a* was evidenced at 430–434 nm and at its red peak at 680 nm (**Figures 3A–C**). This Chl*a* red absorption peak masked PC and APC peaks, which were only seen for low-pigmented samples. Reflectance spectra showed opposite features: lower values in the absorption bands of the photosynthetic pigments (**Figures 3D–F**) and higher in the non-absorbing PAR regions. When transforming reflectance spectra of the rhodolith branches into absorbance values following the equation $D(\lambda)=\log[1/R(\lambda)]$, we observed in the newly calculated spectra similar absorption bands and peaks to those obtained directly through transmission measurements (**Figure 3C**).

The optical descriptors estimated from transmission and reflectance measurements showed significant differences among species (**Figures 2G–L**, Table S1, SI). A higher absorptance was found for the rhodolith *Neogoniolithon* sp., whereas the lowest was shown by the CCA *Lithothamnion* sp. (**Figures 2G,H**). *A. tribulus* thalli exhibit a more complex optical behavior with higher absorptance at the upper higher-pigmented side relative to the lower side (**Figures 2G,H**). Larger differences were observed for pigment- and mass-specific absorption coefficients (**Figures 2I,L**). Pigment specific coefficients, a^*_{Pigm} and $a^*_{\mathrm{Chl}a}$, were three-fold higher for the rhodoliths relative to the values shown by the articulated alga and the CCA (**Figures 2I,J**, Table S1, SI). In contrast, light absorption efficiency per mass, a^*_{MPAR} and a^*_{M680}, were three-fold higher for the CCA than for the rhodoliths. Contrasting differences between both sides of *A. tribulus* thalli were also observed for these coefficients: the upper side showed similar values to the rhodoliths, whereas the lower side to the CCA (**Figures 2K,L**, Table S1 in SI).

All these optical parameters showed species-specific non-linear associations with coralline structural descriptors (**Figures 4**, **5**; **Tables 2**, **3**). Absorptance (A_{PAR} and $A_{\mathrm{Chl}a}$) increased non-linearly as total pigmentation or Chl*a* per area increased to a maximum value, A_{max} (**Figures 4A,B**, **Table 1**). The CCA *Lithothamnion* sp. showed the lowest A_{max} despite its high pigment content, while rhodoliths achieved A_{max} at the lowest thallus pigmentation (**Figures 4A,B**, **Table 1**).

To better understand these differences, we analyzed the covariation between pigment absorption efficiency, a^*_{Pigm} or $a^*_{\mathrm{Chl}a}$, and pigment density. This analysis showed two strong, non-linear and negative associations, which highlighted significant differences among species for this common trend (**Figures 4C,D**; **Tables 2, 3**). The thick and low-pigmented thalli of the rhodolith *Neogoniolithon* sp. exhibited higher pigment absorption efficiency at low pigmentation than the thinner thalli of the other two species (**Figures 4C,D**; Table S1 in SI). Furthermore, small changes in pigmentation resulted in larger variations in a^*_{Pigm} and $a^*_{\mathrm{Chl}a}$ for the rhodolith.

On the other hand, thallus pigmentation normalized to mass showed negative associations with a^*_{Pigm} and $a^*_{\mathrm{Chl}a}$, but positive with mass specific absorption (a^*_{MPAR}, a^*_{M680}; **Figures 4E,F**; Tables S2–S4 in SI). These positive associations resulted in part from a negative colinearity between TMA and thallus pigmentation (Tables S2–S4 in SI). Specifically, we observed for TMA: (i) a positive effect on coralline absorptance (A_{PAR} and $A_{\mathrm{Chl}a}$) and on pigment specific absorption (a^*_{Pigm} and $a^*_{\mathrm{Chl}a}$) (**Figures 5A–D**; **Table 2**); and (ii) a negative effect on the variation of mass specific absorption (a^*_{MPAR} and a^*_{M680}; **Figures 5E,F**; **Tables 2, 3**). Interestingly, variation in TMA was able to explain 45–50% variability analyzed in coralline absorptance (**Figures 5A,B**; **Table 2**). However, such positive effect of TMA on enhancing light absorption capacity of coralline thalli was not observed for the intra-specific comparison. On the contrary, negative associations were found between TMA and a^*_{Pigm}, which were significant for rhodoliths and CCA thalli but not for the articulated alga (**Tables 2, 3**; **Figures 5A–D**).

In contrast to the large species-specific component observed for the associations of variation of pigment specific absorption (a^*_{Pigm} and $a^*_{\mathrm{Chl}a}$), mass specific absorption (a^*_{MPAR}, a^*_{M680}) showed a common trend for the three coralline species investigated (**Figures 4**, **5**). We observed a single non-linear and negative association with TMA (**Figures 5E,F**, **Tables 2**, **3**), which supports the interpretation that the simplest CCA coralline morphology can achieve the highest a^*_M values thanks to its thin and highly pigmented thalli, whereas the thick and low pigmented thalli of the rhodolith constrain this morphotype to low a^*_M (**Figures 5E,F**). In addition, small changes in TMA result in large variation in a^*_{MPAR} and a^*_{M680} for both, CCA and articulated alga, whereas the rhodolith exhibited the lowest a^*_M and the lowest variation for this optical descriptor.

To better understand the different contributions of TMA and thallus pigmentation to the variation of pigment and mass specific absorption, a multiple regression analysis was conducted. Two quantitative models enable description of this differential contribution:

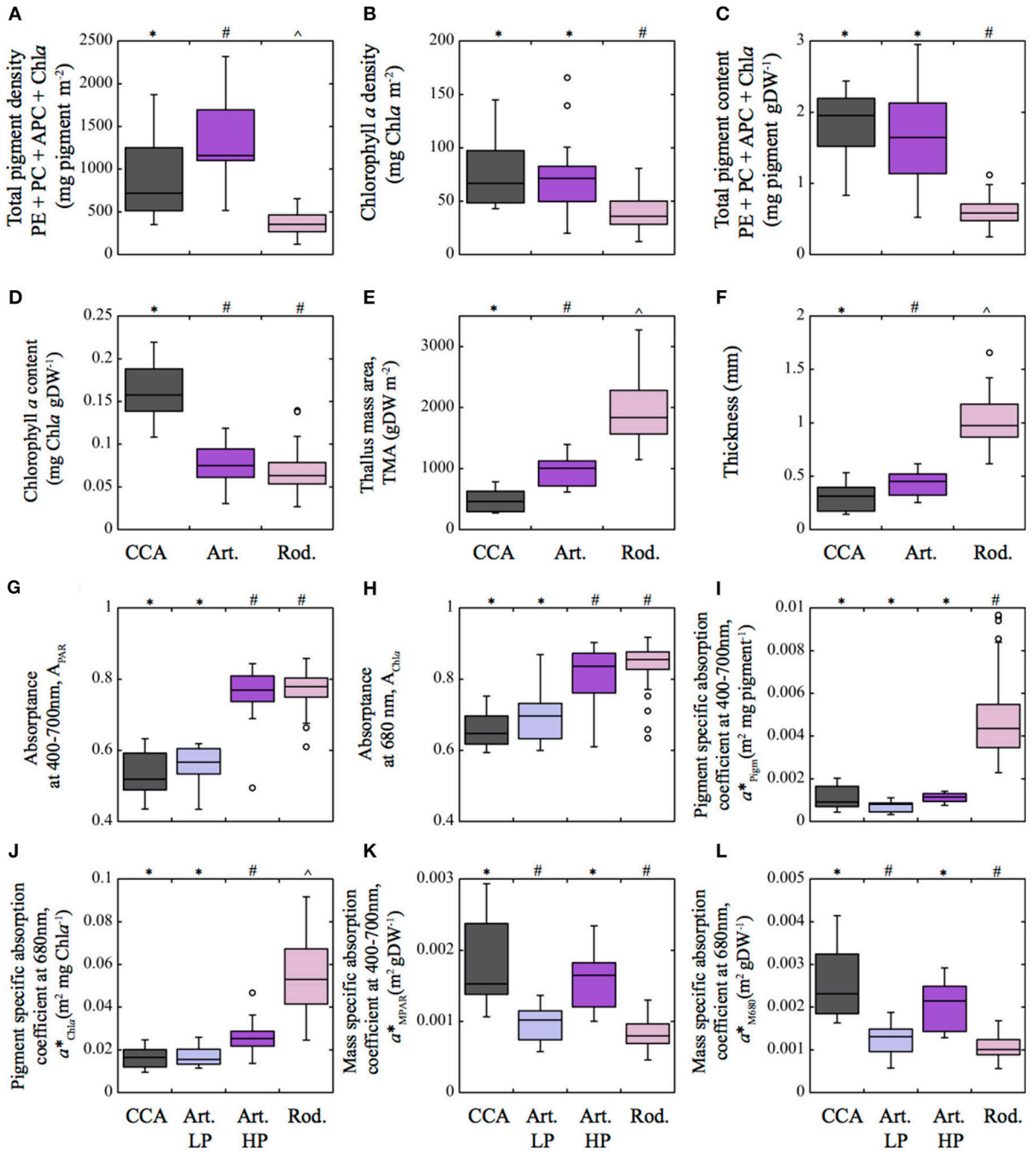

FIGURE 2 | Box plot showing the distribution of the different structural and optical thallus descriptors of the three coralline algae characterized in this study. **(A)** Total pigment density (mg pigm m^{-2}) and **(B)** Chlorophyll *a* density (mg Chl*a* m^{-2}); **(C)** Total pigment content (mg pigm gDW^{-1}) and **(D)** Chlorophyll *a* content (mg Chl*a* gDW^{-1}); **(E)** Thallus mass area (TMA, gDW m^{-2}); **(F)** thallus thickness (mm); **(G)** Absorptance for the PAR average (A_{PAR}) and **(H)** for the Chl*a* red peak at 680 nm (A_{Chla}); **(I)** pigment specific absorption coefficient for the PAR average (a^*_{Pigm}; m^2 mg $pigm^{-1}$) and **(J)** for the Chl*a* red peak at 680 nm (a^*_{Chla}; m^2 mg $Chla^{-1}$); **(K)** mass specific absorption coefficient (a^*_{MPAR}; m^2 gDW^{-1}) for the PAR average and **(L)** for the Chl*a* red peak at 680 nm (a^*_{M680}; m^2 gDW^{-1}). Total pigment refers to the sum of phycoerythrin (PE), phycocyanin (PC), allophycocyanin (APC) as well as chlorophyll *a* (Chl*a*). *Boxes* encompass the 25 and 75% quartiles of all the data for each growth-form, the *central horizontal line* represents the median, *bars* extend to the 95% confidence limits, and *open circles* represent observations extending beyond the 95% confidence limits. Different symbols above the occurence of boxes indicate significant differences between species (one way ANOVA $P < 0.05$, Tukey *post-hoc* $P < 0.05$). Color of the boxes: pink for the rhodolith *Neogoniolithon* sp; purple for the articulated alga; and gray for the crustose coralline *Lithothamnion* sp. (CCA). In **(G–L)** the purple and blue color corresponds, respectively, to the highly pigmented (HP) and lesser pigmented (LP) sides of the thalli of the articulated alga. Sample size for the descriptors: rhodoliths $n = 54$–63, articulated $n = 15$–19, CCA $n = 12$.

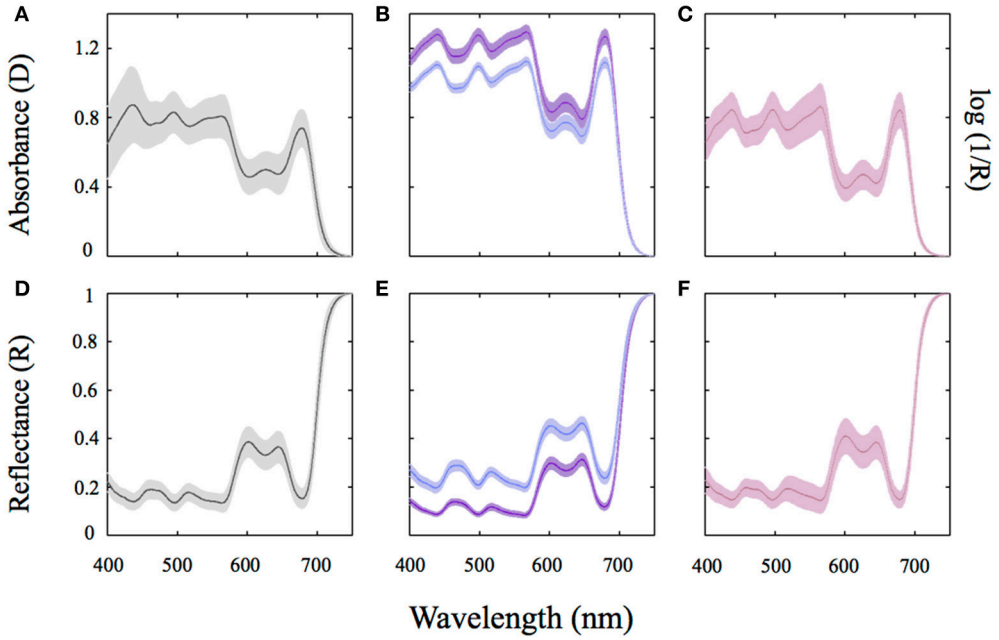

FIGURE 3 | Absorption and reflectance spectra of the three coralline algae characterized in this study. Average absorbance (D) for thallus spectra of the CCA *Lithothamnion* sp **(A)** and the articulated alga *Amphiroa tribulus* **(B)**; Average absorption spectra of thalli of the rhodolith forming species *Neogoniolithon* sp. using reflectance (R) determinations and the transformation log(1/*R*) **(C)**. **(D–F)** Show the respective average reflectance (R) spectra of the coralline species studied. The solid line represents an average spectrum of ≥8 independent spectra whereas the shaded area represents the SD of the mean. Color of the lines: pink for the rhodolith *Neogoniolithon* sp.; Purple and blue for highly pigmented (HP) and lesser pigmented (LP) sides of the articulated alga *Amphiroa tribulus;* And gray for the crustose coralline (CCA) *Lithothamnion* sp.

Model I

$$\log\ a^*_{\mathrm{Chl}a} = -3.13 \pm 0.22 + \mathbf{0.25} \pm 0.08^* \log\ \mathrm{TMA} \\ \mathbf{-0.78} \pm 0.10^* \log\ \mathrm{Chl}a\mathrm{W(mg\ gDW^{-1})} \\ (R^2 = 0.54, \mathrm{SE} = 0.177, n = 106, P < 0.05)$$

Model II

$$\log\ \mathrm{a}^*_{\mathrm{M680}} = -0.95 \pm 0.10 - \mathbf{0.53} \pm 0.04^* \log\ \mathrm{TMA} \\ \mathbf{+0.24} \pm 0.05^* \log\ \mathrm{Chl}a\mathrm{W(mg\ gDW^{-1})} \\ (R^2 = 0.78, \mathrm{SE} = 0.08, n = 88, P < 0.001)$$

The first model (Model I) indicates that increases in TMA can offset (positive effect) the strong reduction in pigment absorption efficiency, $a^*_{\mathrm{Chl}a}$, that results from increases in thallus pigmentation. In contrast, the second model (Model II) supports the opposite trend on mass specific absorption (a^*_{M680}), as the decline in a^*_{M680} caused by increases in TMA, can be compensated by increases in thallus pigmentation. Therefore, this quantitative description supports the existence of a morpho-functional trade-off in the regulation of the optical properties of coralline algae.

Association of Variation between Optical Traits and Thallus Photosynthesis

As optical traits are not direct descriptors of thallus photosynthesis, we examined the association of variation between optical and physiological descriptors. Significant linear and positive associations between coralline a^*_{Pigm} and a^*_{M} and thallus photosynthetic rates normalized to projected area ($R^2 = 0.90$, $P < 0.05$; $n = 5$; Figure S2 in SI), and to dry mass ($R^2 = 0.92$, $P < 0.05$; $n = 5$), were observed for the same organisms measured by Vásquez-Elizondo and Enríquez (2016). To support the generalization of these associations, however, more species and coralline morphologies need to be added to this comparison.

Estimates of coralline photosynthetic production require information about the variation in canopy size, in addition to knowledge of differences in thallus photosynthetic rates, as the size of algal canopy significantly contributes to total photosynthetic production of the whole individual. Algal canopy size was described in this study by means of the Leaf Area Index (LAI). Average LAI values for the rhodolith, articulated alga, and CCA were, respectively, 1.27 ± 0.1, 1.95 ± 0.17 and 1.15 ± 0.01 (Table S1 in SI). According to these values, the three dimensional-(3D) ramification pattern of the rhodolith and the articulated alga allow both morphologies to achieve LAI values above 1, whereas the 2D-structure of the CCA constrains this growth-form to values close to 1 (**Figure 6A**). LAI variability for each species population within the reef lagoon of Puerto Morelos, however, showed significant differences (**Figure 6B**). The articulated alga was the species that constructed the largest canopies (LAI ∼2.5; **Figure 6B**; Figure S1 in SI), while variability in LAI was minimal for the CCA associated with small protuberances on its surface, which explain the

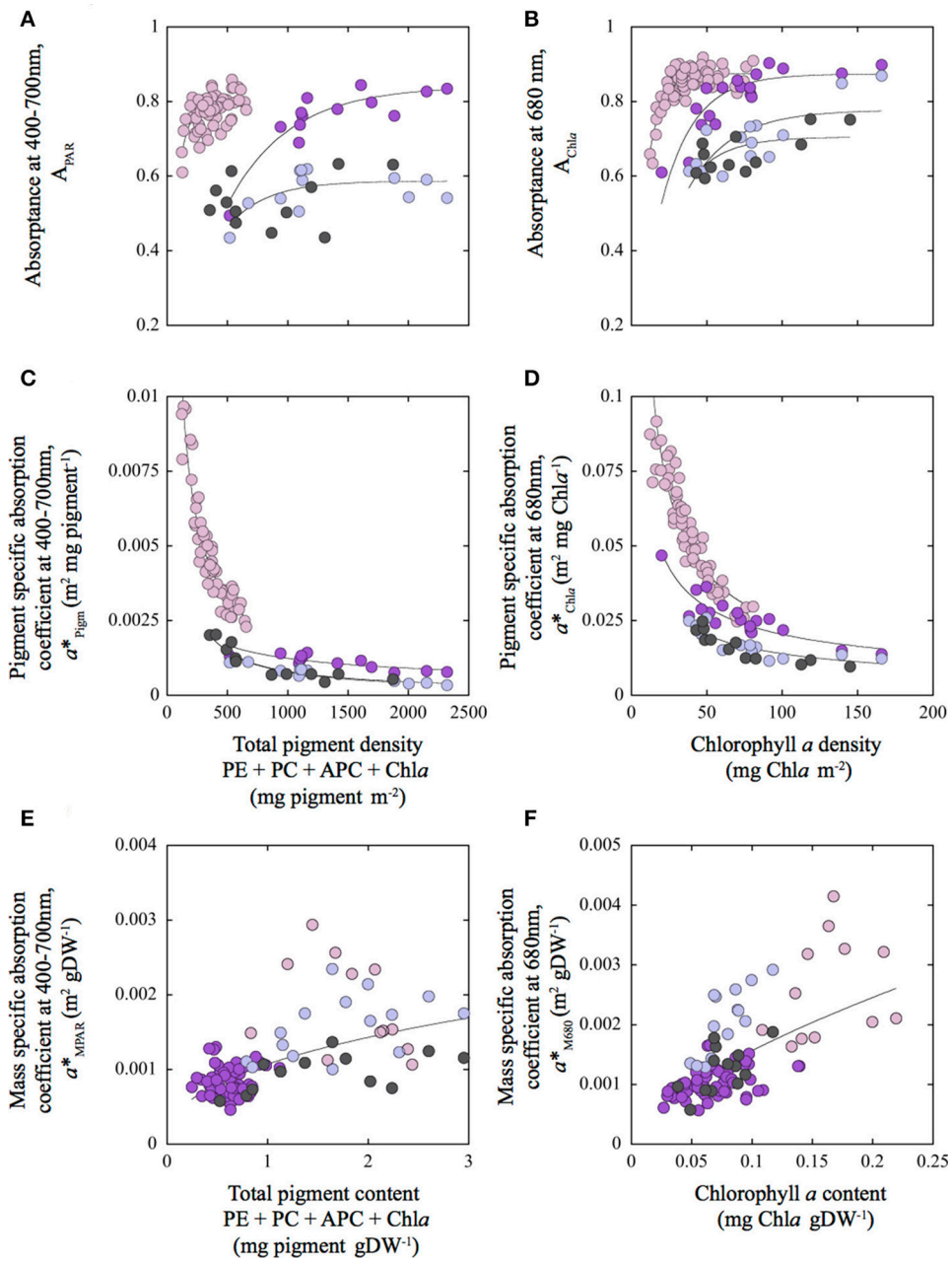

FIGURE 4 | Variation of the optical descriptors as a function of changes in thallus pigmentation for the three coralline algae characterized in this study. Variation of Absorptance for the PAR average (A_{PAR}) **(A)**; for the Chl*a* red peak at 680 nm (A_{Chla}) **(B)**; for pigment specific absorption coefficients for the PAR average (a^*_{Pigm}; m^2 mg $pigm^{-1}$) **(C)**; and for the Chl*a* red peak at 680 nm (a^*_{Chla}; m^2 mg $Chla^{-1}$) **(D)**; for as a function of changes in total pigment (mg pigm m^{-2}) and chlorophyll *a* (mg Chla m^{-2}) density respectively. Variation of mass specific absorption coefficients for the PAR average (a^*_{MPAR}; m^2 g DW^{-1}) **(E)**; and for the Chl*a* red peak at 680 nm (a^*_{M680}; m^2 g DW^{-1}) **(F)** as a function of changes in, respectively, total pigment content (PigmW; mg pigm gDW^{-1}) and chlorophyll *a* content (ChlaW; mg Chl*a* gDW^{-1}). Total pigment refers to the sum of phycoerythrin (PE), phycocyanin (PC), allophycocyanin (APC) as well as, chlorophyll *a* (Chl*a*). Colors of the symbols: pink for the rhodolith *Neogoniolithon* sp.; purple and blue, for the highly pigmented (HP) and lesser pigmented (LP) sides of the thalli of the articulated alga *Amphiroa tribulus*; and gray for the crustose coralline (CCA) *Lithothamnion* sp. Solid lines correspond to a power function fit [$y = a^*x^b$] representing species-specific trends **(A–D)** and the common trend found for the three species **(E,F)**.

slightly higher values above 1 estimated for this simple 2D-morphology. Estimations of photosynthetic production per individual per hour exhibited large differences among the three coralline growth-forms (**Figure 6C**). The articulated alga *Amphiroa tribulus* and *Neogoniolithon* sp. showed the highest production, while the CCA the lowest.

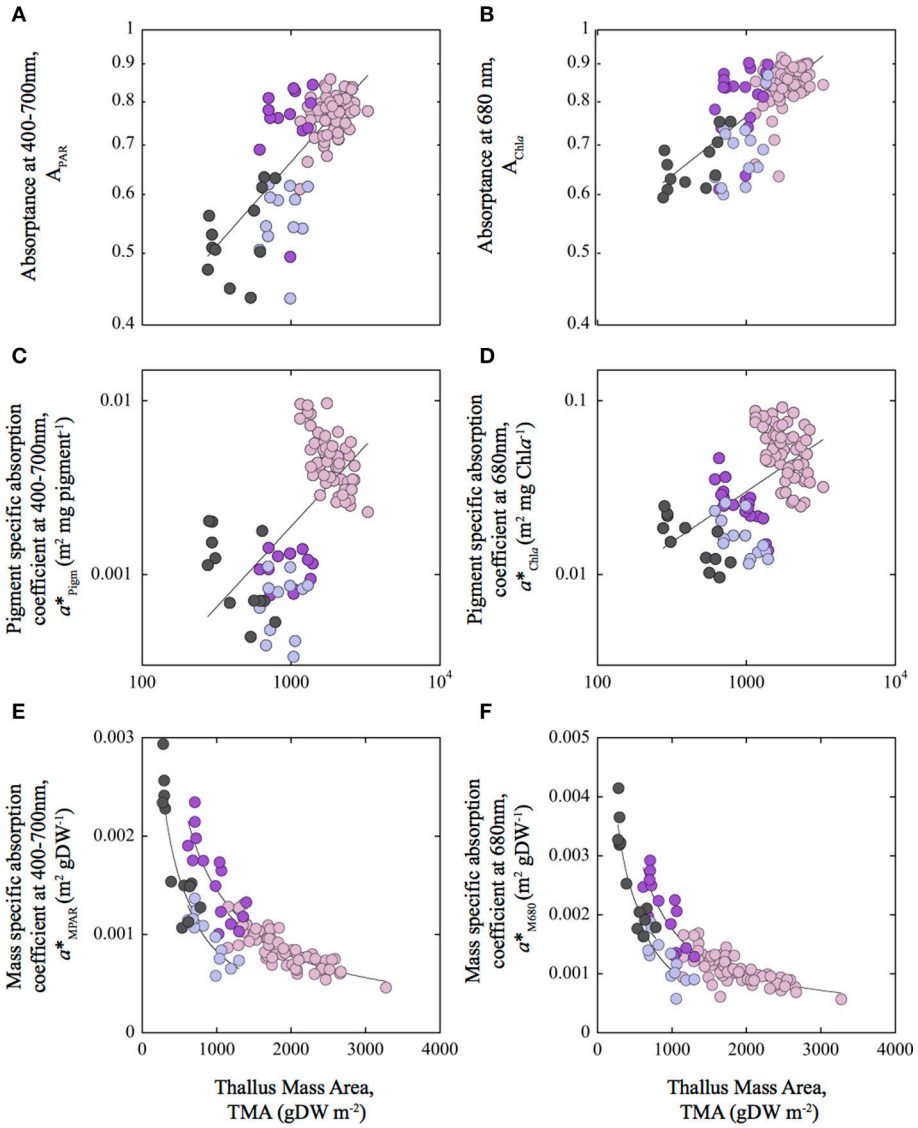

FIGURE 5 | Associations of variation between optical descriptors and Thallus Mass Area: Variation of absorptance for the PAR average (A_{PAR}) **(A)** and for the Chl*a* red peak at 680 nm (A_{Chla}) **(B)**; for pigment specific absorption coefficients for the PAR average (a^*_{Pigm}; m^2 mg pigm^{-1}) **(C)** and for the Chl*a* red peak at 680 nm (a^*_{Chla}) **(D)**; and for mass specific absorption coefficients for the PAR average (a^*_{MPAR}; m^2 g DW^{-1}) **(E)** and for the Chl*a* red peak at 680 nm (a^*_{M680}) **(F)**, as a function of changes in thallus mass area (TMA). Colors of the symbols: pink, for the rhodolith *Neogoniolithon* sp.; purple and blue for the highly pigmented (HP) and lesser pigmented (LP) sides of the thalli of the articulated alga *Amphiroa tribulus;* and gray for the crustose coralline (CCA) *Lithothamnion* sp. Solid lines correspond to a power function fit [$y = a^*x^b$] representing the general trend observed among species **(A–D)**, and the species-specific trends **(E,F)**. Note the axis in log scale in **(A–D)**.

DISCUSSION

This first optical characterization of coralline algae revealed that, on average, the three species examined reflected between 10 and 30% of the incident light, which represent values up to three times higher than those previously described for non-calcifying tissues (Lüning and Dring, 1985; Bauerle et al., 2004; Enríquez, 2005; Durako, 2007), but below reflectance of pubescent (Ehleringer et al., 1976) or stressed (Carter and Knapp, 2001) terrestrial leaves. Such high back-scattering supports the technical challenge that this important group of marine primary producers has represented for the development of optical studies. Our characterization indicates that the optical properties of coralline thalli follow similar trends to those previously described for non-calcified photosynthetic tissues of aquatic macrophytes (e.g., Enríquez et al., 1992, 1994; Enríquez and Sand-Jensen, 2003; Enríquez, 2005). Increases in thallus pigmentation result in non-linear declines in pigment absorption efficiency, as predicted by the "pigment packaging effect" (Morel and Bricaud, 1981; Kirk, 1994; Enríquez and Sand-Jensen, 2003). However, we also documented significant differences among coralline species for this common trend, with the thickest and less pigmented

TABLE 1 | Parameters describing non-linear association between absorptance, estimated for the PAR average (A_{PAR}) and for the chlorophyll *a* –Chl*a*- red peak at 680 nm (A_{Chla}), and total pigment (mg pigment m^{-2}) and chlorophyll *a* (mg Chl*a* m^{-2}) densities, respectively.

	Growth-form—species	R^2	A_{max}	*b*	A_{max} : *b*
A_{PAR}	Rhodoliths—*Neogoniolithon* sp.	0.33	0.78 ± 0.006	0.014 ± 0.001	55.7
	Articulated—*Amphiroa tribulus* (HP)	0.85	0.84 ± 0.02	0.019 ± 0.0002	442.1
	(LP)	0.5	0.58 ± 0.01	0.003 ± 0.0006	193.3
	CCA - *Lithothamnion* sp.	< 0.05ns			
A_{Chla}	Rhodoliths—*Neogoniolithon* sp.	0.72	0.87 ± 0.004	0.11 ± 0.005	7.9
	Articulated—*Amphiroa tribulus* (HP)	0.74	0.87 ± 0.017	0.04 ± 0.004	21.7
	(LP)	0.43	0.77 ± 0.03	0.03 ± 0.006	25.6
	CCA—*Lithothamnion* sp.	0.34	0.70 ± 0.02	0.04 ± 0.008	17.5

A_{max} is the maximum absorptance and b is the exponential increase of A with pigment density increases, for the model [$y = A_{max}*(1-e^{-b*x})$]. The ratio between the A_{max} and b [A_{max}: b] allows estimation of the amount of pigment density required to reach A_{max}.. HP and LP denote the highly pigmented (upper) and the lesser-pigmented (lower) sides of the thalli of the articulated algae Amphiroa tribulus.

TABLE 2 | Equations derived from Least Squares (LS) regression analysis of log-log transformed data, describing the variation of the optical descriptors as a function of changes in the structural traits of the three coralline algae characterized in this study: the rhodolith *Neogoniolithon* sp., the articulated alga *Amphiroa tribulus,* and the crustose coralline algae (CCA) *Lithothamnion* sp.

Equation (log-log)	Statistics
$\log a^*_{Pigm} = 0.49(\pm0.12) - 1.22(\pm0.04)^*$ log Pigm	($R^2 = 0.87$, $n = 94$, S.E. = 0.13, $P \leq 0.001$)
$\log a^*_{Chla} = 0.17(\pm0.08) - 1.11(\pm0.05)^*$ log Chl*a*	($R^2 = 0.77$, $n = 106$, S.E. = 0.12, $P \leq 0.001$)
$\log a^*_{MPAR} = -2.97(\pm0.01) + 0.64(\pm0.05)^*$ log PigmW	($R^2 = 0.41$, $n = 96$, S.E. = 0.13, $P \leq 0.001$)
$\log a^*_{M680} = -2.15(\pm0.08) + 0.96(\pm0.06)^*$ log Chl*a*W	($R^2 = 0.45$, $n = 102$, S.E. = 0.13, $P \leq 0.001$)
$\log A_{PAR} = -0.85(\pm0.06) + 0.30(\pm0.02)^*$ log TMA	($R^2 = 0.55$, $n = 94$, S.E. = 0.05, $P \leq 0.001$)
$\log A_{Chla} = -0.59(\pm0.04) + 0.22(\pm0.01)^*$ log TMA	($R^2 = 0.51$, $n = 107$, S.E. = 0.03, $P \leq 0.001$)
$\log a^*_{Pigm} = -5.51(\pm0.37) + 1.37(\pm0.12)^*$ log TMA	($R^2 = 0.37$, $n = 94$, S.E. = 0.30, $P \leq 0.001$)
$\log a^*_{Chla} = -3.26(\pm0.27) + 1.03(\pm0.09)^*$ log TMA	($R^2 = 0.29$, $n = 107$, S.E. = 0.21, $P \leq 0.001$)
$\log a^*_{MPAR} = -1.19(\pm0.11) - 0.68(\pm0.03)^*$ log TMA	($R^2 = 0.71$, $n = 96$, S.E. = 0.09, $P \leq 0.001$)
$\log a^*_{M680} = -0.89(\pm0.11) - 0.74(\pm0.03)^*$ log TMA	($R^2 = 0.74$, $n = 102$, S.E. = 0.09, $P \leq 0.001$)

Abbreviations and units: total pigment (pigm) density (mg pigm m^{-2}); chlorophyll a (Chla) density (mg Chla m^{-2}); Total pigment (PigmW) content (mg pigm gDW^{-1}) and chlorophyll a (ChlaW) content (mg Chla gDW^{-1}); absorptance for the PAR average (A_{PAR}) and for the Chla red peak at 680 nm (A_{Chla}); pigment specific absorption coefficient for the PAR average (a^*_{Pigm}; m^2 mg $pigm^{-1}$) and for the Chla red peak at 680 nm (a^*_{Chla}; m^2 mg $Chla^{-1}$);mass specific absorption coefficient for the PAR average (a^*_{MPAR}; m^2 g DW^{-1}) and for the Chla red peak at 680 nm (a^*_{M680}; m^2 g DW^{-1}); Thallus Mass Area (TMA; g DW m^{-2}).

thalli of the rhodolith *Neogoniolithon* sp. showing significantly higher pigment absorption efficiency than the thalli of both the articulated and CCA species. These differences were explained through the positive effects of thallus pigmentation and mass area (TMA) on the capacity (A) and pigment efficiency (a^*_{pigm}) of light absorption, which overcome the negative correlation between TMA or thallus thickness and thallus pigmentation (Table S2 in SI), revealing similar trends documented previously for marine macrophytes (Enríquez et al., 1994) and terrestrial leaves (Vile et al., 2005). The optical theory developed for unicells does not yield with this conclusion (Duysens, 1956; Kirk, 1975, 1976, 1994; Morel and Bricaud, 1981), as this theory predicts that a^*_{pigm} declines with increases in both cell size and cellular pigment content. Furthermore, the first study that applied this optical descriptor, a^*_{pigm}, to multicellular tissues, the leaves of an amphibious plant *Mentha aquatica,* yielded results similar to unicells, as both parameters, leaf pigment content and leaf mass area, LMA, were negatively associated with a^*_{pigm} (Enríquez and Sand-Jensen, 2003). The trend documented in our comparison for three coralline species agrees with the findings of Enríquez et al. (1994), who compared 90 spp. of macroalgae and 12 of seagrasses. In that study, the authors concluded that increases in tissue thickness are more effective for enhancing absorbance (*D*) than increases in tissue pigmentation (Enríquez et al., 1994), attributing the capacity for thick tissues to reduce "pigment packaging," to enhanced light scattering within thicker photosynthetic structures. For coralline algae, increases in thallus size result from increases in carbonate skeleton thickness. This implies that coralline skeletons may play and important role in the regulation of the optical properties of coralline thalli, as they do in symbiotic corals (Enríquez et al., 2005). This conclusion, however, is only valid when comparing different coralline morphologies, as within each species we observed the same trend documented for unicells and the leaves of *Mentha aquatica* (Duysens, 1956; Kirk, 1975, 1976, 1994; Morel and Bricaud, 1981; Enríquez and Sand-Jensen, 2003). According to all these findings, increases in skeleton thickness or TMA of coralline thalli may yield a morphotype with reduced pigment packaging, but it does not completely offset this phenomenon, as within any given morphology, increases in pigmentation still induce non-linear declines in pigment absorption efficiency.

Incorporating data from previous studies into the coralline interspecific a^*_{Chla} analysis, we observed that the rhodolith *Neogoniolithon* sp. had an average value similar to the *Rhodophyta* a^*_{Chla} mean recalculated from Enríquez et al. (1994)

TABLE 3 | Slopes and intercepts of the linear associations (log-log transformed data) between the structural and optical descriptors of the three coralline species characterized in this study: the rhodolith *Neogoniolithon* sp., the articulated alga *Amphiroa tribulus* (both sides) and the crustose coralline (CCA) *Lithothamnion* sp.

y, x trait	Growth-form	Slope	Intercept	R^2	*n*	SE	*P*
a^*_{Pigm} vs. Pigm	Rhodoliths	−0.88 ± 0.03	−0.22 ± 0.09	0.89	57	0.05	<0.001
	Articulated HP	−0.55 ± 0.31	−1.56 ± 0.10	0.64	13	0.06	0.001
	Articulated LP	−0.86 ± 0.10	−0.59 ± 0.28	0.89	12	0.06	<0.001
	CCA	−0.97 ± 0.29	−0.34 ± 0.31	0.87	12	0.08	<0.001
a^*_{Chla} vs. Chl*a*	Rhodoliths	−0.78 ± 0.03	−0.14 ± 0.05	0.86	62	0.05	<0.001
	Articulated HP	−0.59 ± 0.06	−0.62 ± 0.11	0.81	18	0.05	<0.001
	Articulated LP	−0.63 ± 0.09	−0.77 ± 0.17	0.73	14	0.06	<0.001
	CCA	−0.78 ± 0.08	−0.44 ± 0.15	0.89	12	0.04	<0.001
a^*_{MPAR} vs. PigmW	Rhodoliths						0.50ns
	Articulated HP	0.68 ± 0.15	−2.8 ± 0.04	0.32	15	0.10	0.026
	Articulated LP	0.51 ± 0.12	−3.07 ± 0.33	0.41	12	0.09	0.023
	CCA						0.33ns
a^*_{M680} vs. Chl*a*W	Rhodoliths	0.65 ± 0.07	−2.65 ± 0.09	0.18	63	0.09	0.001
	Articulated HP	1.17 ± 0.20	−1.63 ± 0.22	0.65	14	0.07	0.001
	Articulated LP	1.14 ± 0.27	−2.12 ± 0.31	0.36	13	0.11	0.001
	CCA						0.28ns
a^*_{Pigm} vs. TMA	Rhodoliths	−1.53 ± 0.15	0.87 ± 0.51	0.41	57	0.12	<0.001
	Articulated HP						0.93ns
	Articulated LP						0.80ns
	CCA	−1.34 ± 0.32	0.70 ± 0.86	0.41	12	0.18	0.023
a^*_{Chla} vs. TMA	Rhodoliths	−1.43 ± 0.15	1.004 ± 0.51	0.24	63	0.12	0.001
	Articulated HP	−1.18 ± 0.14	1.06 ± 0.43	0.70	18	0.07	0.001
	Articulated LP	−0.95 ± 0.21	0.046 ± 0.63	0.41	13	0.09	0.013
	CCA	−0.81 ± 0.15	−0.97 ± 0.39	64	12	0.08	0.002
a^*_{MPAR} vs. TMA	Rhodoliths	−0.97 ± 0.07	−0.44 ± 0.23	0.69	57	0.05	<0.001
	Articulated HP	−1.002 ± 0.16	−0.41 ± 0.48	0.65	15	0.07	0.001
	Articulated LP	−1.1 ± 0.19	−0.31 ± 0.58	0.68	12	0.07	0.001
	CCA	−0.86 ± 0.13	−0.75 ± 0.34	0.76	12	0.07	<0.001
a^*_{M680} vs. TMA	Rhodoliths	−0.99 ± 0.08	−0.58 ± 0.27	0.54	63	0.07	<0.001
	Articulated HP	−1.18 ± 0.2	−0.10 ± 0.59	0.64	14	0.07	0.001
	Articulated LP	−1.37 ± 0.26	−0.18 ± 0.78	0.59	13	0.09	0.002
	CCA	−0.81 ± 0.09	−0.59 ± 0.24	0.87	12	0.05	<0.001

Abbreviations and units as described in ***Table 2****.*

data (**Figure 7**). Both average a^*_{Chla} values for the rhodolith (this study) and *Rhodophyta* (data from Enríquez et al., 1994) were significantly above the averages estimated for *Amphiroa tribulus* and the CCA (**Figure 7**). Interestingly, the scleractinian coral *P. branneri* was, as predicted by Enríquez et al. (2005), the photosynthetic structure with the highest a^*_{Chla}, whereas the leaves of the two aquatic higher plants showed similar a^*_{Chla} averages to, respectively, *A. tribulus* (*T. testudinum*) and the CCA (*M. aquatica*). To better understand these interspecific differences, we analyzed the associations of variation between a^*_{Chla} and chlorophyll *a* density (**Figure 7B**). This inter-specific comparison revealed that the diverse group of red algae (34 spp.) characterized by Enríquez et al. (1994) displayed the largest variability within this association. Most of the species examined in that study were non-calcifying thalli, although 5 spp. were also corallines belonging to the genus *Peysonnelia* and *Jania*. It is remarkable that the three species characterized here were among the *Rhodophyta* with the highest a^*_{Chla} (**Figure 7B**), as supported by an ANCOVA test (intercept *t*-test $p < 0.01$; *Rhodophyta* intercept $= -0.69 \pm 0.10$; corallines intercept $= 0.17 \pm 0.08$ in **Table 2**). No differences were found, however, for the slopes of these associations (slope *t*-test $p > 0.05$). Values for the coral *Porites branneri* from Enríquez et al. (2005) showed a trend similar to that of rhodoliths (ANCOVA, *t*-test $P > 0.05$). The low chlorophyll *a* density of the symbiotic coral explains its high a^*_{Chla} average (**Figure 7**). Rhodoliths and CCA showed significant differences for this trend (ANCOVA, intercept *t*-test, $p < 0.01$, **Table 3**), supporting the notion that coralline algae with thicker thalli and higher TMA can reduce "pigment packaging" more efficiently, developing structures with higher a^*_{Pigm} for similar thallus pigmentation. Yet, this comparative analysis supports the conclusion that the presence of highly reflective structures (i.e., coralline carbonate skeletons) plays a key role in thallus optics of multicellular photosynthetic tissues,

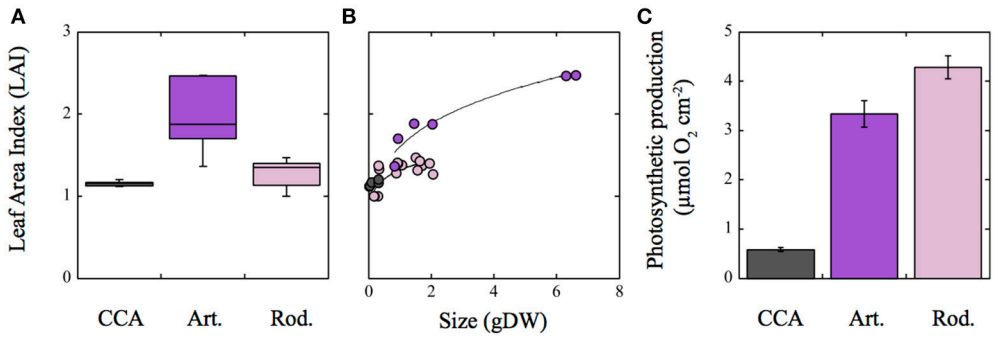

FIGURE 6 | Variation of the Leaf Area Index (LAI) in the three growth-forms of coralline algae characterized in this study. **(A)** Box plot describing LAI variability for each coralline growth-form; **(B)** variation of LAI as a function of coralline algal size in g DW; **(C)** estimated photosynthetic production for each coralline growth-form for 1 h assuming a constant P_{max} (µmol 0_2 cm^{-2}). Photosynthetic data were derived from Vásquez-Elizondo and Enríquez (2016). For **(A)**: *Boxes* encompass the 25 and 75% quartiles of all data, the *central horizontal line* represents the median, *bars* extend to the 95% confidence limits, and *open circles* represent observations extending beyond the 95% confidence limits. Solid lines in **(B)** correspond to a power function fit [$y = a^*x^b$]. Colors denote: pink for the rhodolith *Neogoniolithon* sp.; purple for the articulated alga *Amphiroa tribulus;* and gray for the crustose coralline (CCA) *Lithothamnion* sp. Error bars in **(C)** correspond to SE ($n = 6$).

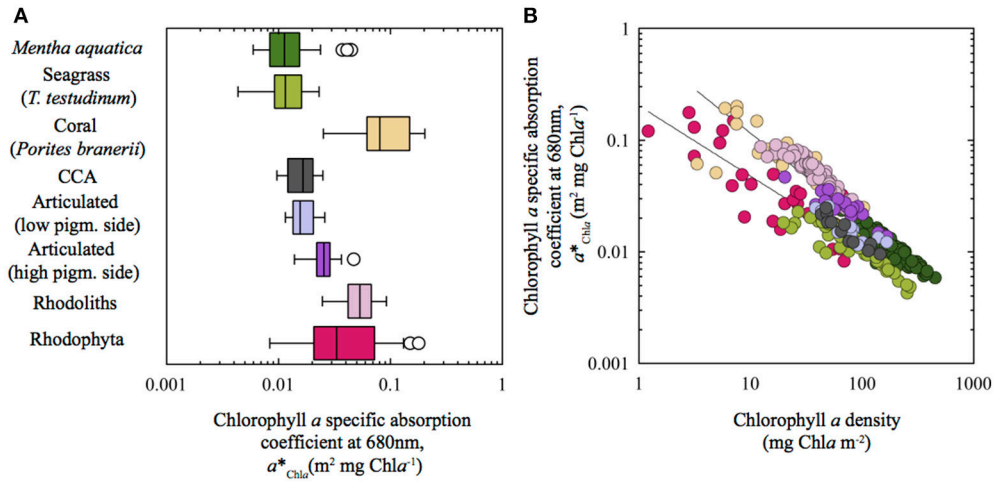

FIGURE 7 | Inter-specific variation of pigment specific absorption for the Chl*a* red peak (a^*_{Chla}) across different aquatic photosynthetic structures: **(A)** Box plot showing a^*_{Chla} variation for the different species characterized; and **(B)** log/log variation of a^*_{Chla} as a function of changes in chlorophyll *a* density (mg Chl*a* m^{-2}). Data from: Corallines (this study); *Rhodophyta* (Enríquez et al., 1994); *Mentha aquatica* (Enríquez and Sand-Jensen, 2003); coral *Porites branerii* (Enríquez et al., 2005); *Thalassia testudinum* (Enríquez, 2005). Trend lines in **(B)** correspond to power function fits [$y=a^*x^b$] for: (1) *Rhodophyta* and *T. testudinum* (bottom trend line) and, (2) corallines (rhodoliths, articulated and CCA), *Porites branerii* and *Mentha aquatica*. LS regression analysis of the log-log transformed data: For fit (1), log $a^*_{Pigm} = -0.69\ (\pm\ 0.10) - 0.63\ (\pm 0.08)^*$ log Chl*a* ($R^2 = 0.76$, $n = 26$, $SE = 0.21$, $P < 0.001$; for fit (2), log $a^*_{Pigm} = -0.15\ (\pm\ 0.07) - 0.91\ (\pm 0.04)^*$ log Chl*a* ($R^2 = 0.68$, $n = 123$, $SE = 0.15$, $P < 0.001$).

through enhancing the efficiency with which photosynthetic pigments collect solar energy. Accordingly, we may explain why the leaves of the seagrass *Thalassia testudinum* showed a similar positive effect of LMA on a^*_{Chla} (Enríquez, 2005) in contrast to the opposite trend reported for the thinner leaves of *Mentha aquatica* (Enríquez and Sand-Jensen, 2003), as the seagrass leaves produce oxalate crystals within the pigmented epidermal cells (Dobbs et al., 2004), and also present the ability to precipitate aragonites crystals within their cell walls (Enríquez and Schubert, 2014).

With respect to the variation of light absorption efficiency per mass (a^*_M), we observed in the present comparison a strong and negative association between this optical descriptor and coralline TMA, in accordance with previous analyses (Enríquez et al., 1994; Enríquez and Sand-Jensen, 2003). Significant differences for the effect of TMA on a^*_M variation were also found among the three coralline species. Both, CCA and the articulated alga showed the highest a^*_M values and the largest reductions in a^*_M as TMA increases. Rhodoliths, in contrast, had the lowest a^*_M and a reduced sensitivity to change a^*_M with TMA variation. Therefore, our comparison also supports the utility of a^*_M to quantify functional differences among species, although we agree with Falkowski et al. (1985) and Ramus (1990), that this parameter is a mathematical construction as only photosynthetic

pigments have a real absorption cross-section. Mass or carbon specific absorption has been proposed as a functional descriptor for the efficiency of the photosynthetic light collector to return the energy collected to structural mass or carbon (Ramus, 1990; Enríquez et al., 1994; Enríquez and Sand-Jensen, 2003). Our study supports this interpretation but also the existence of a potential trade-off between both optical traits (a^* and a^*_M). According to this trade-off, species with thick structures, low pigmentation and high TMA can reduce pigment content and thus the amount of nitrogen required to build the light collector (high a^*_{Pigm}) at the expense of increasing its structural costs (carbon) and diminishing the return of the solar energy collected into new structural carbon (lower a^*_M). In contrast, thin and cheap photosynthetic structures can minimize the structural costs of their thalli and maximize carbon return (higher a^*_M), at the expense of increasing "pigment packaging" (lower a^*_{Chla}) and the construction costs of the photosynthetic apparatus in terms of pigment and nitrogen investments. The first strategy, represented by the rhodolith *Neogoniolithon* sp., would be an optimal solution for colonizing oligotrophic and highly illuminated environments, while the second option, represented by the CCA *Lithothamnion* sp., would maintain positive carbon balances under extremely low light conditions within the reef framework. The ecological and/or evolutionary success of the articulated alga *Amphiroa tribulus,* which combines both strategies in a specialized bifacial thallus, may not depend on its complex thallus optics, but on its ability to construct large 3D-canopies. We estimated for *A. tribulus* intermediate values in thallus light absorption efficiency, metabolic rates and TMA, but photosynthetic production per individual was as high as that of the rhodolith, thanks to its ability to form one the largest light collectors at the organism/canopy level. For the quantification of the size of the light collector of the whole organism, we used a parameter, LAI, common in terrestrial plant ecology, but not so common in marine ecology, although it has been successfully applied for the characterization of seagrass habitats (Olesen et al., 2002; Enríquez and Pantoja-Reyes, 2005; Collier et al., 2007). Seagrass LAI can explain changes in the magnitude of leaf self-shading within seagrass beds (Enríquez and Pantoja-Reyes, 2005) and leaf photoprotection (Schubert et al., 2015). In addition, LAI has been successfully applied to understand the response to depth of *Jania adherens* in association with a sponge (Enríquez et al., 2009). Our comparison provides new support for the functional relevance of LAI to characterize benthic communities in marine habitats.

In summary, by enhancing a^*_{Chla} the rhodolith *Neogoniolithon* sp. not only produces a more efficient light collector under nutrient limitation, but a more productive thallus with high photosynthetic rates per area. In contrast, the structurally cheap and simple crustose 2D-morphology of *Lithothamnion* sp. allows maximizing thallus efficiency for energy collection per structural mass. Thereby, this growth-form allows maintaining positive carbon balances under the extremely limited light conditions that occur within the coral reef framework, insuring species survival. The third growth-form represented by the articulated alga *Amphiroa tribulus*, is able to compensate for its intermediate optical and photosynthetic thallus capabilities, by constructing large light collectors (canopies). In our simulation, this species achieved values of photosynthetic production per organism similar to the rhodoliths despite its lower thallus photosynthetic rates. Yet, the capacity to construct complex 3D-canopies explains the higher productivity of the rhodolith *Neogoniolithon* sp. and *Amphiroa tribulus*, while algal production of the simplest crustose 2D-morphology of *Lithothamnion* sp. depends entirely on thallus photosynthesis. *Neogoniolithon* sp. colonizes open areas within the reef seagrass bed, whereas *A. tribulus* and *Lithothamnion* sp. require a fixed substrate within the coral reef community. The low light specialist *Lithothamnion* sp. grows on cryptic habitats within the coral reef framework, while the weak canopy of *A. tribulus* finds the appropriate niche within the protection provided by colonies of the lettuce coral *Agaricia agaricites* (Figure S1 in SI). Our analysis, therefore, supports the utility of optical traits in marine ecology, as powerful tools to investigate differences in competitive abilities, morpho-functional constraints, abundances and niche distribution among algal species and growth-forms.

AUTHOR CONTRIBUTIONS

SE designed research, RV performed research, RV and SE analyzed data and wrote the paper.

ACKNOWLEDGMENTS

Two Mexican research projects granted to SE, DGAPA (IN206710) and CONACYT (Conv-CB-2009: 129880), provided financial support to this research, which was part of the PhD thesis of RV in the postgraduate program of the Universidad Nacional Autónoma de México (UNAM- *Posgrado en Ciencias del Mar y Limnología -PCMyL*). The Mexican Consejo Nacional de Ciencia y Tecnología (CONACyT) is acknowledged for providing 4 years Ph.D fellowship to support RV. We thank Darren Brown for useful comments on the manuscript and Roberto Iglesias-Prieto for his valuable input, optimism, technical support and "good energy" during the development of this project. The experiments performed in this work comply with the current laws of Mexico. An ethics approval was not required as per national regulations. The study was supported by the Mexican permit: "Permiso de Pesca de Fomento" No PPF/DGOPA-031/13, to SE; issued by the Secretaría de Agricultura, Ganadería, Desarrollo rural, Pesca y Alimentación of the United States of Mexico, to support the development of the project: "*Evaluación del efecto de la limitación de carbono sobre diferentes productores primarios de la laguna arrecifal de Puerto Morelos: Importancia de la calcificación.*"

SUPPLEMENTARY MATERIAL

The Supplementary Material for this article can be found online at: http://journal.frontiersin.org/article/10.3389/fmars.2017.00297/full#supplementary-material

REFERENCES

Adey, W. H. (1998). Coral reefs: algal structured and mediated ecosystems in shallow, turbulent, alkaline waters. *J. Phycol.* 34, 393–406. doi: 10.1046/j.1529-8817.1998.340393.x

Algarra, P., and Niell, F. X. (1987). Structural adaptations to light reception in two morphotypes of *Corallina elongata* ELLIS and SOLAND. *Mar. Ecol.* 8, 253–261. doi: 10.1111/j.1439-0485.1987.tb00187.x

Bauerle, W. L., Weston, D. J., Bowden, J. D., Dudley, J. B., and Toler, J. E. (2004). Leaf absorptance of photosynthetically active radiation in relation to chlorophyll meter estimates among woody plant species. *Sci. Horticult.* 101, 169–178. doi: 10.1016/j.scienta.2003.09.010

Bensoussan, N., and Gattuso, J.-P. (2007). Community primary production and calcification in a NW Mediterranean ecosystem dominated by calcareous macroalgae. *Mar. Ecol. Prog. Ser.* 334, 37–45. doi: 10.3354/meps334037

Björkman, O. (1981). "Responses to different quantum flux densities," in *Physiological Plant Ecology I: Responses to the Physical Environment*, eds O. L. Lange, P. S. Nobel, C. B. Osmond, and H. Ziegler (Berlin; Heidelberg: Springer Berlin Heidelberg), 57–107.

Burdett, H. L., Keddie, V., MacArthur, N., McDowall, L., McLeish, J., Spielvogel, E., et al. (2014). Dynamic photoinhibition exhibited by red coralline algae in the red sea. *BMC Plant Biol.* 14:139. doi: 10.1186/1471-2229-14-139

Carter, G. A., and Knapp, A. K. (2001). Leaf optical properties in higher plants: linking spectral characteristics to stress and chlorophyll concentration. *Am. J. Bot.* 88, 677–684. doi: 10.2307/2657068

Cayabyab, N. M., and Enríquez, S. (2007). Leaf photoacclimatory responses of the tropical seagrass *Thalassia testudinum* under mesocosm conditions: a mechanistic scaling-up study. *New Phytol.* 176, 108–123. doi: 10.1111/j.1469-8137.2007.02147.x

Chisholm, J. R. M. (2003). Primary productivity of reef-building crustose coralline algae. *Limnol. Oceanogr.* 48, 1376–1387. doi: 10.4319/lo.2003.48.4.1376

Collier, C. J., Lavery, P. S., Masini, R. J., and Ralph, P. J (2007). Morphological, growth and meadow characteristics of the seagrass *Posidonia sinuosa* along a depth-related gradient of light availability. *Mar. Ecol. Prog. Ser.* 337, 103–115. doi: 10.3354/meps337103

de la Riva, E. G., Olmo, M., Poorter, H., Ubera, J. L., and Villar, R. (2016). Leaf Mass per Area (LMA) and its relationship with leaf structure and anatomy in 34 mediterranean woody species along a water availability gradient. *PLoS ONE* 11:e0148788. doi: 10.1371/journal.pone.0148788

Dobbs, F. C., Zimmerman, R. C., and Drake, L. A. (2004). Occurrence of intracellular crystals in leaves of *Thalassia testudinum*. *Aquat. Bot.* 80, 23–28. doi: 10.1016/j.aquabot.2004.03.003

Durako, M. J. (2007). Leaf optical properties and photosynthetic leaf absorptance in several Australian seagrasses. *Aquat. Bot.* 87, 83–89. doi: 10.1016/j.aquabot.2007.03.005

Duysens, L. N. (1956). The flattening of the absorption spectrum of suspensions, as compared to that of solutions. *Biochim. Biophys. Acta* 19, 1–12. doi: 10.1016/0006-3002(56)90380-8

Ehleringer, J., Björkman, O., and Mooney, H. A. (1976). Leaf pubescence: effects on absorptance and photosynthesis in a desert shrub. *Science* 192, 376–377. doi: 10.1126/science.192.4237.376

Enríquez, S. (2005). Light absorption efficiency and the package effect in the leaves of the seagrass *Thalassia testudinum*. *Mar. Ecol. Prog. Ser.* 289, 141–150. doi: 10.3354/meps289141

Enríquez, S., Agustí, S., and Duarte, C. (1992). Light absorption by seagrass *Posidonia oceanica* leaves. *Mar. Ecol. Prog. Ser.* 86, 201–201. doi: 10.3354/meps086201

Enríquez, S., Agustí, S., and Duarte, C. M. (1994). Light absorption by marine macrophytes. *Oecologia* 98, 121–129. doi: 10.1007/BF00341462

Enríquez, S., Ávila, E., and Carballo, J. L. (2009). Phenotypic plasticity induced in transplant experiments in a mutualistic association between the red alga *Jania adhaerens* (Rhodophyta, Corallinales) and the sponge *haliclona caerulea* (Porifera: Haplosclerida): morphological responses of the alga. *J. Phycol.* 45, 81–90. doi: 10.1111/j.1529-8817.2008.00640.x

Enríquez, S., Méndez, E. R., Hoegh-Guldberg, O., and Iglesias-Prieto, R. (2017). Key functional role of the optical properties of coral skeletons in coral ecology and evolution. *Proc. R. Soc. B Biol. Sci.* 284:20161667. doi: 10.1098/rspb.2016.1667

Enríquez, S., Méndez, E. R., and Iglesias-Prieto, R. (2005). Multiple scattering on coral skeletons enhances light absorption by symbiotic algae. *Limnol. Oceanogr.* 50, 1025–1032. doi: 10.4319/lo.2005.50.4.1025

Enríquez, S., and Pantoja-Reyes, N. (2005). Form-function analysis of the effect of canopy morphology on leaf self-shading in the seagrass *Thalassia testudinum*. *Oecologia* 145, 235–243. doi: 10.1007/s00442-005-0111-7

Enríquez, S., and Sand-Jensen, K. (2003). Variation in light absorption properties of *Mentha aquatica* L. as a function of leaf form: implications for plant growth. *Int. J. Plant Sci.* 164, 125–136. doi: 10.1086/344759

Enríquez, S., and Schubert, N. (2014). Direct contribution of the seagrass *Thalassia testudinum* to lime mud production. *Nat. Commun.* 5:3835. doi: 10.1038/ncomms4835

Evans, J. R., and Poorter, H. (2001). Photosynthetic acclimation of plants to growth irradiance: the relative importance of specific leaf area and nitrogen partitioning in maximizing carbon gain. *Plant Cell Environ.* 24, 755–767. doi: 10.1046/j.1365-3040.2001.00724.x

Falkowski, P. G., Dubinsky, Z., and Wyman, K. (1985). Growth-Irradiance relationships in phytoplankton. *Limnol. Oceanogr.* 30, 311–321. doi: 10.4319/lo.1985.30.2.0311

Foster, M. S. (2001). Rhodoliths: between rocks and soft places. *J. Phycol.* 37, 659–667. doi: 10.1046/j.1529-8817.2001.00195.x

Frost-Christensen, H., and Sand-Jensen, K. (1992). The quantum efficiency of photosynthesis in macroalgae and submerged angiosperms. *Oecologia* 91, 377–384. doi: 10.1007/BF00317627

Garnier, E., Cordonnier, P., Guillerm, J.-L., and Sonié, L. (1997). Specific leaf area and leaf nitrogen concentration in annual and perennial grass species growing in Mediterranean old-fields. *Oecologia* 111, 490–498. doi: 10.1007/s004420050262

Häder, D.-P., Lebert, M., Flores-Moya, A., Jiménez, C., Mercado, J., Salles, S., et al. (1997). Effects of solar radiation on the photosynthetic activity of the red alga *Corallina elongata* Ellis et Soland. *J. Photochemi. Photobiol. B Biol.* 37, 196–202. doi: 10.1016/S1011-1344(96)07402-7

Heyward, A. J., and Negri, A. P. (1999). Natural inducers for coral larval metamorphosis. *Coral Reefs* 18, 273–279. doi: 10.1007/s003380050193

Hoegh-Guldberg, O., Mumby, P. J., Hooten, A. J., Steneck, R. S., Greenfield, P., Gomez, E., et al. (2007). Coral reefs under rapid climate change and ocean acidification. *Science* 318, 1737–1742. doi: 10.1126/science.1152509

Iglesias-Prieto, R., and Trench, R. K. (1997). "Photoadaptation, photoacclimation and niche diversification in invertebrate-dinoflagellate symbioses," in *Proceedings of the 8th International Coral Reef Symposium* (Panama), 1319–1324.

Johansen, H. W. (1981). *Coralline Algae, A First Synthesis*. Boca Raton, FL: CRC Press.

Kirk, J. T. O. (1975). A theoretical analysis of the contribution of algal cells to the attenuation of light within natural waters I. General treatment of suspensions of pigmented cells. *New Phytol.* 75, 11–20. doi: 10.1111/j.1469-8137.1975.tb01366.x

Kirk, J. T. O. (1976). A theoretical analysis of the contribution of algal cells to the attenuation of light natural waters. *New Phytol.* 77, 341–358. doi: 10.1111/j.1469-8137.1976.tb01524.x

Kirk, J. T. O. (1994). *Light and Photosynthesis in Aquatic Ecosystems, 2nd Edn*. Cambridge: Cambridge Uniersity Press.

Kursar, T., van der Meer, J., and Alberte, R. (1983). Light-harvesting system of the red alga *Gracilaria tikvahiae*: I. Biochemical analyses of pigment mutations. *Plant Physiol.* 73, 353–360. doi: 10.1104/pp.73.2.353

Lichtenthaler, H. K., and Wellburn, A. R. (1983). Determination of total carotenoids and chlorophylls a and b of leaf extracts in different solvents. *Biochem. Soc. Trans.* 11, 591–592. doi: 10.1042/bst0110591

Littler, M. M. (1972). The crustose corallinaceae. *Oceanogr. Mar. Biol.* 10, 103–120.

Littler, M. M., and Doty, M. S. (1975). Ecological components structuring the seaward edges of tropical pacific reefs: the distribution, communities and productivity of porolithon. *J. Ecol.* 63, 117–129. doi: 10.2307/2258846

Littler, M. M., Littler, D. S., Blair, S. M., and Norris, J. N. (1985). Deepest known plant life discovered on an uncharted seamount. *Science* 227, 57–59. doi: 10.1126/science.227.4682.57

Lüning, K., and Dring, M. J. (1985). Action spectra and spectral quantum yield in marine macroalgae with thin and thick thalli. *Mar. Biol.* 87, 119–129. doi: 10.1007/BF00539419

Markager, S., and Sand-Jensen, K. (1992). Light requirements and depth zonation of marine macroalgae. *Mar. Ecol. Prog. Ser.* 88, 83–83. doi: 10.3354/meps088083

Marsh, J. A. (1970). Primary productivity on reef-building calcareous red algae. *Ecology* 51, 255–263. doi: 10.2307/1933661

Martin, S., Castets, M.-D., and Clavier, J. (2006). Primary production, respiration and calcification of the temperate free-living coralline alga *Lithothamnion corallioides*. *Aquat. Bot.* 85, 121–128. doi: 10.1016/j.aquabot.2006.02.005

McCoy, S., and Kamenos, N. A. (2015). Coralline algae (Rhodophyta) in a changing world: integrating ecological, physiological, and geochemical responses to global change. *J. Phycol.* 51, 6–24. doi: 10.1111/jpy.12262

Mercado, J. M., Jiménez, C., Niell, F. X., and Figueroa, F. L. (1996). Comparison of methods for measuring light absorption by algae and their application to the estimation of the package effect. *Sci. Mar.* 60, 39–45.

Morel, A., and Bricaud, A. (1981). Theoretical results concerning light-absorption in a discrete medium, and application to specific absorption of phytoplankton. *Deep Sea Res. A. Oceanogr. Res. Pap.* 28, 1375–1393. doi: 10.1016/0198-0149(81)90039-X

Olesen, B., Enríquez, S., Duarte, C. M., and Sand-Jensen, K. (2002). Depth-acclimation of photosynthesis, morphology and demography of *Posidonia oceanica* and *Cymodocea nodosa* in the Spanish Mediterranean Sea. *Mar. Ecol. Prog. Ser.* 236, 89–97. doi: 10.3354/meps236089

Payri, C. E., Maritorena, S., Bizeau, C., and Rodière, M. (2001). Photoacclimation in the tropical coralline alga *Hydrolithon onkodes* (Rhodophyta, Corallinaceae) from a French Polynesian reef. *J. Phycol.* 37, 223–234. doi: 10.1046/j.1529-8817.2001.037002223.x

Perry, C. T., and Hepburn, L. J. (2008). Syn-depositional alteration of coral reef framework through bioerosion, encrustation and cementation: taphonomic signatures of reef accretion and reef depositional events. *Earth Sci. Rev.* 86, 106–144. doi: 10.1016/j.earscirev.2007.08.006

Perry, C. T., Spencer, T., and Kench, P. S. (2008). Carbonate budgets and reef production states: a geomorphic perspective on the ecological phase-shift concept. *Coral Reefs* 27, 853–866. doi: 10.1007/s00338-008-0418-z

Poorter, H., and De Jong, R. O. B. (1999). A comparison of specific leaf area, chemical composition and leaf construction costs of field plants from 15 habitats differing in productivity. *New Phytol.* 143, 163–176. doi: 10.1046/j.1469-8137.1999.00428.x

Ramus, J. (1978). Seaweed anatomy and photosynthetic performance: the ecological significance of light guides, heterogeneous absorption and multiple scatter. *J. Phycol.* 14, 352–362. doi: 10.1111/j.1529-8817.1978.tb00312.x

Ramus, J. (1990). A form-function analysis of photon capture for seaweeds. *Hydrobiologia* 204, 65–71. doi: 10.1007/BF00040216

Ramus, J., Beale, S., and Mauzerall, D. (1976a). Correlation of changes in pigment content with photosynthetic capacity of seaweeds as a function of water depth. *Mar. Biol.* 37, 231–238. doi: 10.1007/BF00387608

Ramus, J., Beale, S., Mauzerall, D., and Howard, K. (1976b). Changes in photosynthetic pigment concentration in seaweeds as a function of water depth. *Mar. Biol.* 37, 223–229. doi: 10.1007/BF00387607

Raven, J. A., and Geider, R. J. (2003). "Adaptation, acclimation and regulation in algal photosynthesis," in *Photosynthesis in Algae,* eds A. W. D. Larkum, S. E. Douglas, and J. A. Raven (Dordrecht: Springer Netherlands), 385–412.

Rodríguez-Román, A., Hernández-Pech, X., Thomé, P. E., Enríquez, S., and Iglesias-Prieto, R. (2006). Photosynthesis and light utilization in the Caribbean coral *Montastraea faveolata* recovering from a bleaching event. *Limnol. Oceanogr.* 51, 2702–2710. doi: 10.4319/lo.2006.51.6.2702

Schubert, N., Colombo-Pallota, M. F., and Enríquez, S. (2015). Leaf and canopy scale characterization of the photoprotective response to high-light stress of the seagrass *Thalassia testudinum*. *Limnol. Oceanogr.* 60, 286–302. doi: 10.1002/lno.10024

Schubert, N., and García-Mendoza, E. (2008). Photoinhibition in red algal species with different carotenoid profiles. *J. Phycol.* 44, 1437–1446. doi: 10.1111/j.1529-8817.2008.00590.x

Schubert, N., García-Mendoza, E., and Enríquez, S. (2011). Is the photoacclimatory response of Rhodophyta conditioned by the species carotenoid profile? *Limnol. Oceanogr.* 56, 2347–2361. doi: 10.4319/lo.2011.56.6.2347

Shibata, K. (1959). Spectrophotometry of translucent biological materials: opal glass transmission method. *Methods Biochem. Anal.* 7, 77–109. doi: 10.1002/9780470110232.ch3

Shibata, K. (1969). Pigments and a UV-absorbing substance in corals and a blue-green alga living in the Great Barrier Reef. *Plant Cell Physiol.* 10, 325–335.

Steller, D., Hernández-Ayón, J., Riosmena-Rodríguez, R., and Cabello-Pasini, A. (2007). Effect of temperature on photosynthesis, growth and calcification rates of the free-living coralline alga *Lithophyllum margaritae*. *Ciencias Mar.* 33, 441–456. doi: 10.7773/cm.v33i4.1255

Steller, D. L., and Foster, M. S. (1995). Environmental factors influencing distribution and morphology of rhodoliths in Bahía Concepción, B.C.S., México. *J. Exp. Mar. Biol. Ecol.* 194, 201–212. doi: 10.1016/0022-0981(95)00086-0

Steller, D. L., Riosmena-Rodríguez, R., Foster, M. S., and Roberts, C. A. (2003). Rhodolith bed diversity in the Gulf of California: the importance of rhodolith structure and consequences of disturbance. *Aquat. Conserv. Mar. Freshw. Ecosyst.* 13, S5–S20. doi: 10.1002/aqc.564

Steneck, R., and Dethier, M. (1994). A functional group approach to the structure of algal-dominated communities. *Oikos* 69, 476–498. doi: 10.2307/3545860

Steneck, R. S. (1986). The ecology of coralline algal crusts: convergent patterns and adaptative strategies. *Annu. Rev. Ecol. Syst.* 17, 273–303. doi: 10.1146/annurev.es.17.110186.001421

Steneck, R. S., Hacker, S. D., and Dethier, M. N. (1991). Mechanisms of competitive dominance between crustose coralline algae: an herbivore-mediated competitive reversal. *Ecology* 72, 938–950. doi: 10.2307/1940595

Vadas, R. L., and Steneck, R. S. (1988). Zonation of deep water benthic algae in the Gulf of Maine. *J. Phycol.* 24, 338–346. doi: 10.1111/j.1529-8817.1988.tb04476.x

Vásquez-Elizondo, R. M., and Enríquez, S. (2016). Coralline algal physiology is more adversely affected by elevated temperature than reduced pH. *Sci. Rep.* 6:19030. doi: 10.1038/srep19030

Vásquez-Elizondo, R. M., Legaria-Moreno, L., Pérez-Castro, M. Á., Krämer, W. E., Scheufen, T., Iglesias-Prieto, R., et al. (2017). Absorptance determinations on multicellular tissues. *Photosyn. Res.* 132, 311–324. doi: 10.1007/s11120-017-0395-6

Vile, D., Garnier, É., Shipley, B., Laurent, G., Navas, M.-L., Roumet, C., et al. (2005). Specific leaf area and dry matter content estimate thickness in laminar leaves. *Ann. Bot.* 96, 1129–1136. doi: 10.1093/aob/mci264

Vogelmann, T. C., and Björn, L. O. (1984). Measurement of light gradients and spectral regime in plant tissue with a fiber optic probe. *Physiol. Plant.* 60, 361–368. doi: 10.1111/j.1399-3054.1984.tb06076.x

Vogelmann, T. C., Bornman, J. F., and Josserand, S. (1989). Photosynthetic light gradients and spectral regime within leaves of *Medicago sativa*. *Phil. Trans. R. Soc. Lond. B* 323, 411–421. doi: 10.1098/rstb.1989.0020

Vogelmann, T. C., Knapp, A. K., McClean, T. M., and Smith, W. K. (1988). Measurements of light within thin plant tissues with fiber optic microprobes. *Physiol. Plant.* 72, 623–630. doi: 10.1111/j.1399-3054.1988.tb09173.x

Vogelmann, T. C., Nishio, J. N., and Smith, W. K. (1996). Leaves as light capture: light propagation and gradients of carbon fixation within leaves. *Trends Plant Sci.* 1, 65–70. doi: 10.1016/S1360-1385(96)80031-8

Wangpraseurt, D., Wentzel, C., Jacques, S. L., Wagner, M., and Kühl, M. (2017). *In vivo* imaging of coral tissue and skeleton with optical coherence tomography. *J. R. Soc. Interface* 14:20161003. doi: 10.1098/rsif.2016.1003

Warner, M. E., Fitt, W. K., and Schmidt, G. W. (1996). The effects of elevated temperature on the photosynthetic efficiency of zooxanthellae in hospite from four different species of reef coral: a novel approach. *Plant Cell Environ.* 19, 291–299. doi: 10.1111/j.1365-3040.1996.tb00251.x

Watson, D. J. (1947). Comparative physiological studies in the growth of field crops. I. Variation in net assimilation rate and leaf area between species and varieties, and within and between years. *Ann. Bot.* 11, 41–76. doi: 10.1093/oxfordjournals.aob.a083148

Williams, E. A., Craigie, A., Yeates, A., and Degnan, S. M. (2008). Articulated coralline algae of the genus *Amphiroa* are highly effective natural inducers of settlement in the tropical abalone *Haliotis asinina*. *Biol. Bull.* 215, 98–107. doi: 10.2307/25470687

Witkowski, E. T. F., and Lamont, B. B. (1991). Leaf specific mass confounds leaf density and thickness. *Oecologia* 88, 486–493. doi: 10.1007/BF00317710

Conflict of Interest Statement: The authors declare that the research was conducted in the absence of any commercial or financial relationships that could be construed as a potential conflict of interest.

frontiers in Marine Science

ORIGINAL RESEARCH
published: 26 September 2017
doi: 10.3389/fmars.2017.00309

Changes in the Number of Symbionts and *Symbiodinium* Cell Pigmentation Modulate Differentially Coral Light Absorption and Photosynthetic Performance

Tim Scheufen[1,2], *Roberto Iglesias-Prieto*[1,3] *and Susana Enríquez*[1]*

[1] *Unidad Académica de Sistemas Arrecifales Puerto Morelos, Universidad Nacional Autónoma de México, Cancun, Mexico,*
[2] *Posgrado de Ciencias del Mar y Limnología of the Universidad Nacional Autónoma de México, Mexico City, Mexico,*
[3] *Department of Biology, The Pennsylvania State University, University Park, PA, United States*

OPEN ACCESS

Edited by:
Daniel Wangpraseurt, University of Cambridge, United Kingdom

Reviewed by:
Ross Cunning, Hawaii University, United States
Noga Stambler, Bar-Ilan University, Israel

***Correspondence:**
Susana Enríquez
enriquez@cmarl.unam.mx; susana.enriquezdominguez@gmail.com

Specialty section:
This article was submitted to Coral Reef Research, a section of the journal Frontiers in Marine Science

Received: *03 May 2017*
Accepted: *08 September 2017*
Published: *26 September 2017*

Citation:
Scheufen T, Iglesias-Prieto R and Enríquez S (2017) Changes in the Number of Symbionts and Symbiodinium Cell Pigmentation Modulate Differentially Coral Light Absorption and Photosynthetic Performance. Front. Mar. Sci. 4:309. doi: 10.3389/fmars.2017.00309

In order to understand the contribution of pigmented coral tissues to the extraordinary optical properties of the coral-symbiont-skeleton unit, we analyzed the associations between structural and optical traits for four coral species, which broadly differ in skeleton morphology, tissue thickness and in the variation of coral pigmentation, symbiont content, *Symbiodinium* dominant type and *Symbiodinium* cell pigmentation (Ci). Significant differences among species were found for the maximum capacity of light absorption (A_{max}) and for the minimum pigmentation required to reach that maximum. The meandroid morphotype represented by *Pseudodiploria strigosa* showed a slightly lower A_{max} than the other three chalice-type species, while the thickest species, *Montastraea cavernosa*, required 2–3.5 times higher pigmentation to reach A_{max}. In contrast, *Orbicella faveolata* and *Orbicella annularis*, which were able to harbor high number of symbionts and achieve the highest photosynthetic rates per area, showed the largest abilities for light collection at decreasing symbiont densities, leading to a more fragile photophysiological condition under light and heat-stress. Holobiont photosynthesis was more dependent on *Symbiodinium* performance in the less populated organisms. At reduced pigmentation, we observed a similar non-linear increase in holobiont light absorption efficiency (a^*_{Chla}), which was differentially modulated by reductions in the number of symbionts and *Symbiodinium* Ci. For similar pigmentation, larger symbiont losses relative to Ci declines resulted in smaller increases in a^*_{Chla}. Two additional optical traits were used to characterize light absorption efficiency of *Symbiodinium* (a^*_{sym}) and coral host (a^*_M). Optimization of a^*_{sym} was well represented by *P. strigosa*, whereas a^*_M was better optimized by *O. annularis*. The species with the largest symbiont content, *O. faveolata*, and with the thickest tissues, *M. cavernosa,* represented, respectively, less efficient solutions for both coral traits. Our comparison demonstrates the utility of optical traits to characterize inter-specific differences in coral acclimatization and performance. Furthermore, holobiont light absorption efficiency (a^*_{Chla}) appeared as a better proxy for the "bleached phenotype"

than simple reductions in coral color. The analysis of a putative coordinated variation in the number of symbionts and in *Symbiodinium* cell pigmentation deserves special attention to understand holobiont optimization of energy collection (a^*_{Chla}) and photosynthetic performance.

Keywords: light absorption, scleractinian coral, symbiont population, symbiont cell pigmentation, optical traits

INTRODUCTION

The maintenance of a healthy mutualistic endosymbiosis between a simple animal and an unicellular photoautotroph in the genus *Symbiodinium* is one of the cornerstones for the construction and maintenance of coral reefs. The solar energy that drives coral photosynthesis is collected by the photosynthetic apparatus of the symbionts and transformed efficiently into organic carbon. Photosynthates translocated to the host have been recognized as a major source of the energy that supports coral metabolism (Muscatine et al., 1981) and calcification rates (Pearse and Muscatine, 1971; Colombo-Pallotta et al., 2010). Therefore, any reduction in the production and translocation of photosynthates to the coral host will affect coral performance and growth. This places the photosynthetic activity of the symbionts at the center of the cellular processes that regulate coral performance. Furthermore, coral photosynthesis is directly affected by symbiosis instability under elevated temperatures (heat stress), but specially when this ancient and successful symbiosis collapses (coral bleaching). Therefore, coral bleaching not only results in severe losses in coral pigmentation and symbionts, but also in the generation of a dysfunctional holobiont. Such dysfunctional condition is expressed in a massive loss of symbionts and pigmentation (Weis, 2008), but also in the full suppression of coral photosynthesis (Scheufen et al., 2017). Anomalous seawater temperatures associated with global warming have been identified as the primary cause of mass coral bleaching events (Hoegh-Guldberg, 1999; Lesser and Farrell, 2004; Smith et al., 2005). Other environmental stressors like anomalous light increases, anomalous low temperatures, diseases, changes in salinity, etc., can also cause coral bleaching (i.e., Glynn, 1996; Lesser, 1996; Hoegh-Guldberg, 1999; Brown et al., 2000; Hoegh-Guldberg et al., 2005; Kemp et al., 2011).

Changes in coral pigmentation, however, are also related to seasonal variation in the number of symbionts (Fagoonee et al., 1999; Fitt et al., 2000) and/or in symbiont cell pigmentation (Brown et al., 1999; Fitt et al., 2000). Reductions in symbiont number are preferentially associated with increases in seawater temperature (e.g., Brown et al., 1999; Fagoonee et al., 1999; Fitt et al., 2000; Scheufen et al., 2017) while higher nutrient availability may better explain increases in symbiont density (Dubinsky et al., 1990; Stimson and Kinzie, 1991; Brown et al., 1999; Ferrier-Pagès et al., 2001). Reductions in coral pigmentation often occur during acclimation to high-light conditions (Falkowski and Dubinsky, 1981; Iglesias-Prieto and Trench, 1994; Hennige et al., 2009). Therefore, changes in coral pigmentation not only reflect symbiosis instability, but holobiont acclimatization to seasonal changes or variable environmental conditions.

The variability displayed by a single colony in the number of symbionts, in *Symbiodinium* cell pigmentation, and in the dominant symbiont type (Brown et al., 2000; Kemp et al., 2014) can be as large as inter-specific variation (Brown et al., 1999). However, although species that present low variation in the dominant *Symbiodinium* type, do display large changes in coral pigmentation and symbiont content, little attention has received the analysis of this variation and its functional meaning for coral performance. By contrast, a significant effort has been invested in the analysis of changes in the dominant symbiont type and coral susceptibility to bleach (e.g., Savage et al., 2002; Baker, 2004; Tchernov et al., 2004; Berkelmans and van Oppen, 2006; Kemp et al., 2006; Robison and Warner, 2006; Warner et al., 2006; Suggett et al., 2008; Fitt et al., 2009; Pettay et al., 2015). Interestingly, species that have shown low mortality rates during massive bleaching events, also had higher symbiont content per area (Stimson et al., 2002).

Changes in coral pigmentation directly affect the amount of solar energy absorbed by the symbiotic algae and potentially used in photosynthesis. Scleractinian corals have been recognized as one of the most efficient solar energy collectors (Enríquez et al., 2005) and users of this energy through photosynthesis (Rodríguez-Román et al., 2006), thanks to multiple scattering of light on coral carbonate skeletons. The extraordinary optical properties of scleractinian corals vary among skeleton morphologies (Terán et al., 2010; Marcelino et al., 2013; Enríquez et al., 2017), colony growth-forms (Anthony et al., 2005; Enríquez et al., 2017), coral pigmentation (Enríquez et al., 2005; Wangpraseurt et al., 2012), and differences among symbionts in their chlorophyll-specific absorption coefficient, a^* (Wyman et al., 1987; Dubinsky et al., 1990; Lesser et al., 2000; Stambler and Dubinsky, 2005; Hennige et al., 2009). However, our understanding of the association between changes in coral pigmentation and absorptance (i.e., fraction of incident light absorbed by the photosynthetic apparatus of *Symbiodinium*) is still insufficient. Only one study has documented so far this association for the species *Porites branneri* (Enríquez et al., 2005). In that study, the authors reported that the maximum capacity of light absorption of *P. branneri* ($A_{max} = \sim 93\%$) is already achieved at 20 mg Chl*a* m^{-2}, a value far below estimations for terrestrial leaves (e.g., Carter and Knapp, 2001; Davis et al., 2011) and submerged macrophytes (Frost-Christensen and Sand-Jensen, 1992; Enríquez et al., 1994). How variable is the maximum capacity of light absorption (i.e., absorptance) among coral species, and how variable is the minimum amount of coral pigmentation required to reach that maximum, remains still uncertain.

The aim of this study was to contribute to fill this gap of knowledge through the characterization of the optical properties

of four coral species, *Orbicella annularis*, *Orbicella faveolata*, *Montastraea cavernosa*, and *Pseudodiploria strigosa,* which widely differ in their skeleton morphology, tissue thickness and in the species plasticity for changing coral pigmentation, symbiont content, *Symbiodinium* dominant type and *Symbiodinium* cell pigmentation (Ci) and size (cell diameter). A second objective of this analysis was to elucidate potential differences between the number of symbionts (# symbionts cm^{-2}) and *Symbiodinium* pigmentation (Ci, pg Chl*a* sym^{-1}), in their direct effects on holobiont optical properties. The data set analyzed corresponds to data from a recent study by Scheufen et al. (2017), who performed two experiments, one in March 2011 and the other in October 2011, and we also included unpublished data from a third experiment performed in June 2012 on the same four species and coral populations from the reef lagoon of Puerto Morelos (Mexican Caribbean). Scheufen et al. (2017) investigated differences in the thermal sensitivity of two seasonal coral phenotypes, winter and summer, of these four Caribbean species. Experimental corals were exposed to three temperature treatments (control, +2 and +4°C). The interest of the present comparison was also to test if changes in holobiont optical properties can contribute to explain the functional significance of the seasonal coral phenotypes documented by Scheufen et al. (2017). These authors reported for the winter coral condition, holobionts with reduced photosynthetic rates per area, per symbiont and per mass. In summer, however, corals generally increase their photosynthetic productivity and calcification rates (Barnes and Lough, 1989; Scheufen et al., 2017), producing holobionts with reduced number of symbionts per area but more pigmented cells (Brown et al., 1999; Fitt et al., 2000; Scheufen et al., 2017). Thus, this comparison analyses variation among four coral species and two seasonal phenotypes in optical and structural traits, but also in gross photosynthesis, as well as changes associated with experimental exposures to heat-stress.

MATERIALS AND METHODS

Skeleton Characteristics

Coral skeleton macrostructure differs significantly among the four species (**Figure 1**), except for *O. annularis* and *O. faveolata*, which showed small but significant differences at micro-scale level, as *O. faveolta* has thinner septa (cf. Budd and Klaus, 2001). The three chalice-type species, *M. cavernosa, O. faveolata,* and *O. annularis*, present middle-sized corallites (<4 and <15 mm diameter), significantly smaller for both *Orbicella* spp. (**Figure 1**), and a slightly plocoid morphology with irregular presence of coenosteum. *P. strigosa* is the only species with a meandroid morphology, characterized by a distribution of septa as parallel lines running over the walls (**Figure 1**).

Sample Collection

The data-set analyzed was generated as part of a series of heat-stress experiments conducted during 2011 and 2012, to investigate the differential sensitivity of Caribbean coral reef

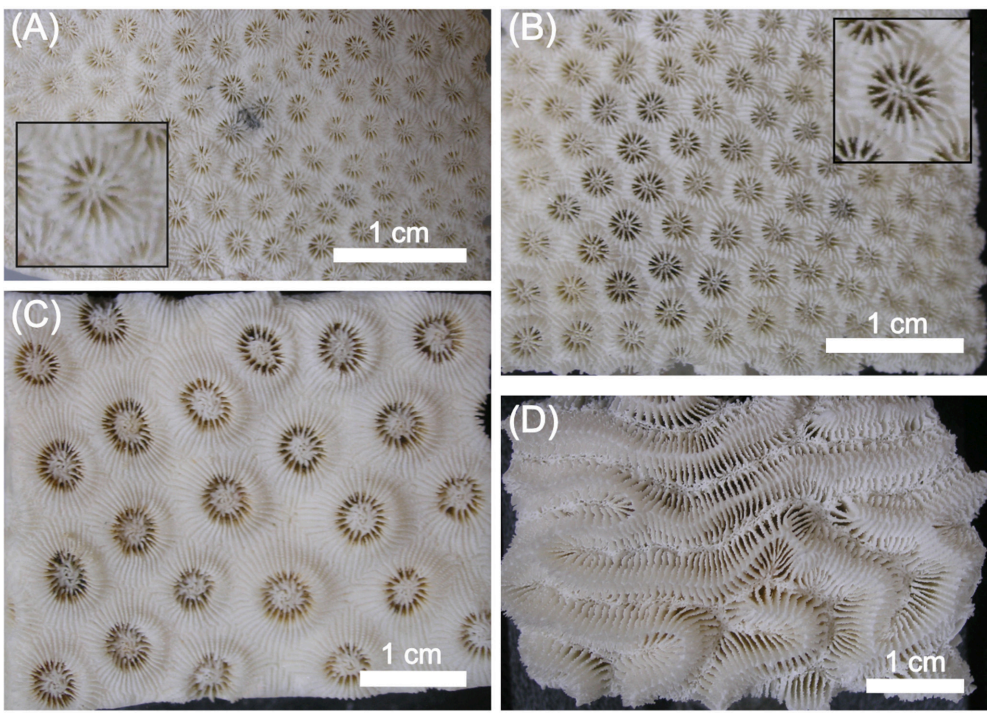

FIGURE 1 | Images of coral skeletons for **(A)** *Orbicella annularis*, **(B)** *Orbicella faveolata*, **(C)** *Montastraea cavernosa*, and **(D)** *Pseudodiploria strigosa*. The inserts in **(A,B)** show a close-up of the calyx structure of *O. annularis* and *O. faveolata*, respectively. The scale bar in each panel is 1 cm.

builders to global warming. The methodology employed for the determinations of the different parameters analyzed in this comparison, as well as for the experimental treatments that induced the variability investigated, is extensively described in Scheufen et al. (2017). See Supplementary Table 1 for number of samples of each parameter and species. Experimental organisms were obtained from three different colonies of *O. annularis*, *O. faveolata*, *M. cavernosa*, and *P. strigosa* collected by Scuba diving at a depth of 5 m in the same sites of the lagoon of Puerto Morelos (Mexico), on February 23rd and September 8th 2011, as well as on May 14th 2012. Coral pieces were cut into equally sized explants of ca. 10 cm^2, and fixed to PVC plates using non-toxic underwater epoxy (Z-Spar Splash Zone, A–788). These experimental nubbins were returned back to the reef lagoon for full recovery, where they were placed on tables at 5 m depth, located near the back-reef. After 15 days, the organisms were transported back to the UNAM mesocoms tank system, where they were distributed over three outdoor 152 L tanks equipped with running seawater. The temperature of the water was maintained at 28°C using commercial aquaria heaters (Process Technology, USA) located in the header tanks and connected to thermocouple sensors (J type, TEI Ingeniería, Mexico).

Definition of the Different Coral Phenotypes Used in This Comparison

Corals exposed to control conditions (28°C) represent the "unstressed" phenotypes developed by the experimental organisms in the mesocosms facilities of the UNAM. These corals were collected at 5 m depth and at three different seasons (February, May, and September) in the reef lagoon of Puerto Morelos. Heat-stress was induced exposing corals to 30°C (+2°C) and 32°C (+4°C). The maximum photochemical efficiency of photosystem II, F_v/F_m, was monitored daily at dusk using a diving PAM fluorometer (Heinz-Walz GmbH, Germany; see Scheufen et al., 2017 for details). As local MMM = 30°C, control corals exposed to 30°C in September did not experience any negative effect of the heat-stress treatment on F_v/F_m (cf., Scheufen et al., 2017). Therefore, only when significant changes in F_v/F_m were observed between control and heat-stressed samples, we considered that corals had expressed the "heat-stressed" phenotypes. As concluded by Scheufen et al. (2017), only when the heat-stressed corals showed gross photosynthesis values not significantly different from 0, we considered that corals had achieved the "bleached" phenotype.

Chlorophyll *a* and Symbiont Determinations

Chlorophyll *a* and symbiont extractions were performed by airbrushing coral samples with filtered seawater (0.45 μm) and subsequent homogenization of coral tissue slurries with a tissue homogeniser (T 10 basic Ultra-Turrax, IKA). Symbiont samples were preserved adding 200 μl of iodine (Lugol), until symbiont cells were counted in a hemocytometer. Pigment extraction was performed in acetone/dimethyl sulfoxide (95:5, vol/vol). For the calculation of the final chlorophyll *a* density, we used the equations for dinoflagellates provided by Jeffrey and Humphrey (1975). Protein content was also estimated spectrophotometrically (Ocean Optics USB 4000 spectroradiometer, Ocean Optics Ltd, FL), using the equation of Whitaker and Granum (1980). Coral surface area was determined by covering the cleaned coral skeletons with aluminum foil following the method of Marsh (1970).

Reflectance and Absorptance Determinations

Coral reflectance (R) was measured according to Enríquez et al. (2005) and Vásquez-Elizondo et al. (2017). Samples were placed in a black container filled with filtered seawater and illuminated with homogeneous diffuse light. This illumination was provided from reflected light from a semi-sphere coated with barium oxide (BaO) and placed above the sample and the black container. The semi-sphere was illuminated from below using a submersible LED ring placed around the coral sample inside the container, and enriched with halogen lamps and violet-blue LEDs illumination. Both illumination enrichments allowed enhancing the light reflected by the semi-sphere in, respectively, red-infrared and violet-blue light. Reflected light was collected by placing a 2 mm diameter fiber-optics over the surface of the sample at an angle of 45° and a distance of 1 cm from the coral surface. Measurements were performed between 400 and 750 nm using an Ocean Optics USB 4000 spectroradiometer (Ocean Optics Ltd, FL), averaging 10 scans per measurement with a boxcar width of 1.4 nm and a resolution of 0.2 nm. For calibration, we used bleached coral skeletons of the respective species. **Figures 2A–D** shows reflectance spectra for each coral species together with the variability characterized for the unstressed, and for the stressed and bleached samples. Estimated absorbance spectra (**Figures 2E–H**) according to Shibata (1969) and Enríquez et al. (2005), were also calculated from reflectance data as [log (1/R)]. From these optical determinations, we estimated absorptance (A) for the chlorophyll *a* peak at 675 nm, as $A_{675} = 1 - R_{675}$, assuming that the amount of light transmitted (T) through the coral skeleton was negligible (Vásquez-Elizondo et al., 2017).

Determinations of the Specific Absorption Coefficients

The chlorophyll *a* specific absorption coefficient for the chlorophyll *a* peak at 675 nm (a^*_{Chla}; m^2 Chla^{-1}) was calculated according to Enríquez et al. (2005), using the following equation:

$$a^*_{Chla} = (De/\rho) \cdot \ln(10) \quad (1)$$

Where De is the estimated absorbance value at 675 nm, calculated as [$De_{675} = \log(1/R_{675})$], and ρ is the chlorophyll *a* cross-section in mg Chl*a* m^{-2}. This parameter, a^*_{Chla}, is considered a descriptor of the pigment light absorption efficiency of the holobiont, as it combines changes in the photoacclimatory condition of *Symbiodinium* (cell pigmentation) *in hospite*, in the size of the symbiotic population, and in the dominant *Symbiodinium* type. In addition to this holobiont optical

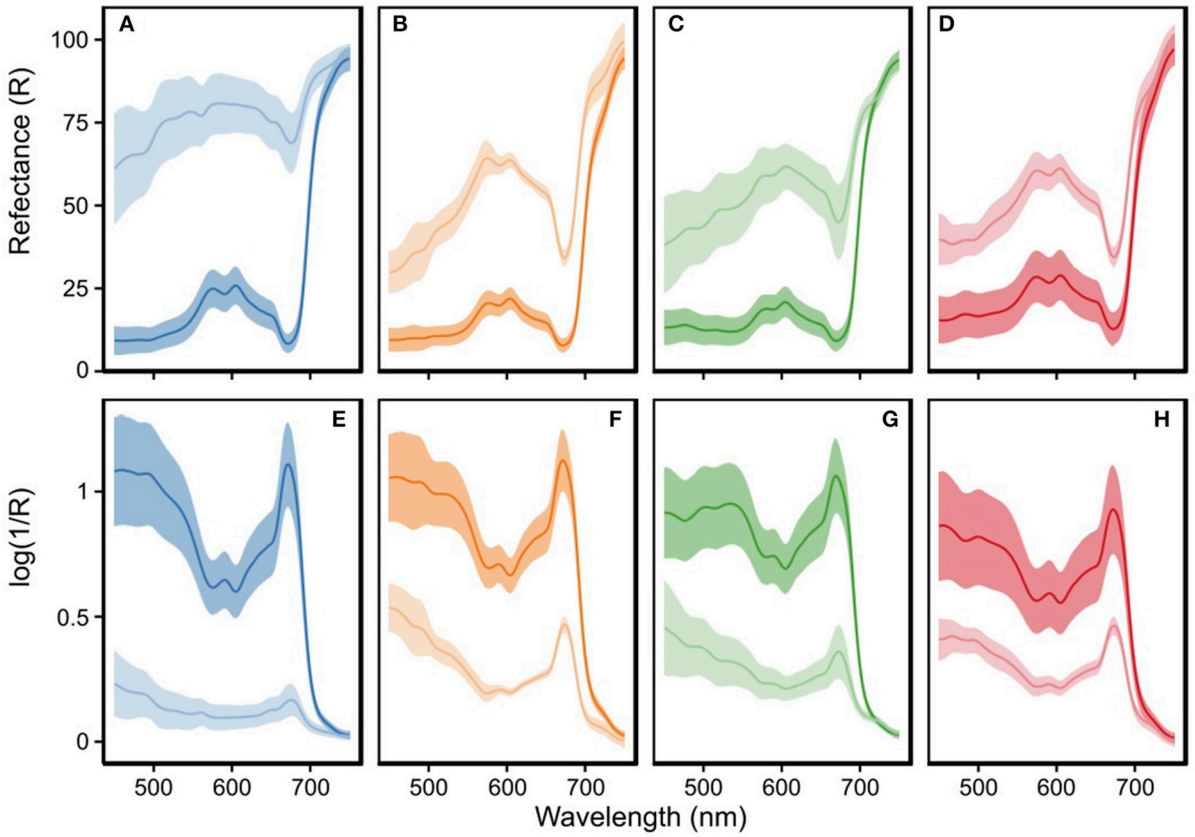

FIGURE 2 | Spectroscopic determinations for *Orbicella annularis* (blue), *Orbicella faveolata* (orange), *Montastraea cavernosa* (green), and *Pseudodiploria strigosa* (red) for unstressed (dark color) and stressed/bleached (light color) coral samples: **(A–D)** reflectance spectra and **(E-H)** calculated absorbance **(D)** spectra from reflectance (R) measurements as log(1/R), according to Shibata (1969). Shading colored area represents the standard deviation (STD) variability for >90 determinations for unstressed samples of *O. annularis* ($n = 123$), *O. faveolata* ($n = 96$), *M. cavernosa* ($n = 110$), and *P. strigosa* ($n = 194$); and $n > 10$ for stressed/bleached samples of *O. annularis* ($n = 122$), *O. faveolata* ($n = 13$), *M. cavernosa* ($n = 28$), and *P. strigosa* ($n = 54$). Unstressed samples represent a subset of the 28°C treatment of all experiments, while for the stressed/bleached group data describe all samples characterized.

descriptor, two more specific absorption coefficients were estimated: the first named mass-specific absorption (a^*_M, m^2 mg protein^{-1}), allowed the quantification of the potential benefits returned to the host of the capacity of this symbiosis to collect solar energy; the second, symbiont-specific absorption (a^*_{sym}, m^2 sym^{-1}), allowed estimation of changes in the light absorption efficiency of *Symbiodinium in hospite*. For the calculation of the first descriptor we substituted ρ by host protein content (mg protein cm^{-2}), whereas for the calculation of a^*_{sym} we used symbiont density (# sym cm^{-2}). Briefly, a^*_{Chla} was defined as a descriptor of holobiont light absorption efficiency; a^*_M describes host light absorption efficiency; and a^*_{sym} the light absorption efficiency of *Symbiodinium* (see **Table 1**).

Oxygen Evolution Determinations

Oxygen fluxes were measured polarographically, using Clark-type O_2 electrodes (Hansatech Instruments Ltd, Norfolk, UK) connected to a custom acrylic water-jacketed chambers (200 ml) filled with filtered seawater (0.45 μm). Coral samples were placed inside the chambers, and $NaHCO_3$ (5 mM) was added to prevent CO_2 limitation during incubations in small volume chambers (cf., Iglesias-Prieto et al., 1992; Enríquez et al., 2002; Cayabyab and Enríquez, 2007). The temperature within the water-jacketed chambers was maintained constant with an external water re-circulating bath equipped with a temperature control system (Model AD07R–20, PolyScience, Niles, IL). Five coral samples per species belonging to three different colonies, were used for each physiological determination. Maximum net photosynthesis (net P_{max}) was determined exposing the samples to a known saturation irradiance of 500 μmol photons m^{-2} s^{-1} during 15 min. The saturation irradiance was previously determined characterizing the photosynthesis response curve (P vs. E) of each species. Oxygen evolution rates were measured again in darkness for five additional minutes to determine post-illumination respiration (R_{PI}). Gross-photosynthesis (P_{max}) was estimated by adding O_2 consumption through respiration, to the previously

TABLE 1 | Table of terms, definitions, and units for the structural, optical, and photosynthetic traits used in this comparison.

Parameter	Definition	Units
STRUCTURAL TRAITS		
Chlorophyll *a* density	Chlorophyll *a* per area	mg Chl*a* m^{-2}
Symbiont density	Number of symbionts per area	$\times 10^6$ #sym cm^{-2}
Ci	Chlorophyll *a* per symbiont cell	pg Chl*a* sym^{-1}
Soluble host protein	Soluble host protein per area	mg protein cm^{-2}
OPTICAL TRAITS (at 675 nm)		
Absorptance (A)	Fraction of incident light absorbed	Dimensionless
a^*_{Chla}	Chlorophyll *a* specific absorption coefficient	m^2 mg $Chla^{-1}$
a^*_{sym}	Symbiont specific absorption coefficient	m^2 sym^{-1}
a^*_M	Protein specific absorption coefficient	m^2 mg $protein^{-1}$
PHOTOSYNTHETIC TRAITS		
P_{max}	Gross-photosynthesis per area	μmol O_2 cm^{-2} h^{-1}
P_{sym}	Gross-photosynthesis per symbiont	pmol O_2 sym^{-1} h^{-1}
P_M	Gross-photosynthesis per host protein	μmol O_2 $protein^{-1}$ h^{-1}

determined net photosynthetic rates under saturation irradiance (net P_{max}).

Data Analysis

As mentioned above, the dataset analyzed represents pooled data from three heat-stress experiments. Supplementary Table 1 shows the number of samples per species and stress-level used in this comparative analysis. One-way ANOVA and *Post-Hoc* Tukey HSD tests allowed determination of significant differences among the unstressed samples, as well as the three different coral phenotypes investigated within each species (unstressed, stressed, and bleached). To analyse the association between absorptance and chlorophyll *a* density, we used an asymptotic exponential function:

$$y = A_{max}(1 - e^{(-b^* Chla\ density)})$$

where A_{max} is the maximum absorptance reached and **b** is the exponential rise of the function.

Least-square regression analyses of log/log transformed data ($\log y = \log a + b \log x$) were used to derive the allometric function: $[y = a^* x^b]$ between changes in the specific absorption coefficients (a^*_{Chla}, a^*_M, a^*_{sym}) and structural coral traits. Pearson correlation coefficients (r) were used to describe the associations of variation between log-transformed parameters. Finally, principal component analysis (PCA) allowed exploring patterns at a multidimensional scale.

All analyses were conducted using R (Version 3.3.2; R Core Team, 2017) with the "car" (Fox and Weisberg, 2011), and "agricolae" (de Mendiburu, 2016) packages loaded.

RESULTS

Structural and Functional Variability of the Un-stressed Samples

For the unstressed corals, chlorophyll *a* density showed significant differences between the more pigmented (*O. faveolata* and *M. cavernosa*) and less pigmented (*O. annularis*) species (one-way ANOVA, Tukey HSD, $p < 0.05$; **Figure 3A**). The coefficients of variation (CV) were slightly higher for *P. strigosa* (CV = 43%) relative to the values found for *O. annularis* (CV = 29%), *O. faveolata* (CV = 28%), and *M. cavernosa* (CV = 28%). The highest symbiont densities (**Figure 3B**), and the lowest chlorophyll *a* content per symbiont (Ci, **Figure 3C**) were found for the two *Orbicellas* spp., while *M. cavernosa* and *P. strigosa* presented significantly lower symbiont density and higher Ci (one-way ANOVA, Tukey HSD, $p < 0.05$). The species that showed the highest soluble host protein content was *M. cavernosa* (6 ± 0.7 mg protein cm^{-2}), whereas *O. annularis* showed the lowest average value (2.4 ± 0.2 mg protein cm^{-2}; **Figure 3D**). However, no significant differences were observed among *O. annularis*, *O. faveolata,* and *P. strigosa* for host protein content in the unstressed samples (one-way ANOVA, Tukey HSD, $p > 0.05$).

Maximum photosynthetic rates per area (P_{max}) were significantly higher in both *Orbicella* spp. (one-way ANOVA, Tukey HSD, $p < 0.05$; **Figure 3F**), but symbiont contribution to holobiont photosynthetic production (P_{sym}) was the lowest (**Figure 3G**). P_{sym} showed a similar pattern of variation to Ci: the highest P_{sym} was observed in the unstressed samples of *P. strigosa* and *M. cavernosa*. These P_{sym} differences among species were however only significant for *P. strigosa* (one-way ANOVA, Tukey HSD, $p < 0.05$; **Figure 3G**). Photosynthetic rates normalized to soluble protein content (P_M) were highest for *O. annularis* and lowest for *M. cavernosa* (one-way ANOVA, Tukey HSD, $p < 0.05$; **Figure 3H**).

With respect to the optical traits, unstressed samples of *O. annularis, O. faveolata,* and *M. cavernosa* showed equal maximum capacity for light absorption ($A_{max} > 90\%$). The lowest A_{max} for the unstressed specimens was determined for *P. strigosa* ($A_{max} = 88\%$; one-way ANOVA, Tukey HSD, $p < 0.05$, **Figure 3I**). All unstressed samples showed low values for chlorophyll *a* specific absorption (a^*_{Chla}; **Figure 3J**). The highest values were estimated for *O. annularis* (one-way ANOVA, Tukey HSD, $p < 0.05$); which also showed the highest mass specific absorption (a^*_M; one-way ANOVA, Tukey HSD, $p < 0.05$; **Figure 3L**). On the other hand, the highest symbiont specific absorption (a^*_{sym}) was estimated for *M. cavernosa* and *P. strigosa* (one-way ANOVA, Tukey HSD, $p < 0.05$; **Figure 3K**).

Principal Component Analysis (PCA) for Non-stressed Holobionts

Un-stressed samples of the four species investigated were clearly discriminated by PCA analysis (**Table 2**, **Figure 4**). The principal component 1 (PC1) was determined by four functional (P_M, P_{sym}, a^*_M, a^*_{sym}) and three structural (symbiont density, Ci, and protein content) traits, and explained 39% of the variability (**Table 2**). This component was able to distinguish between the

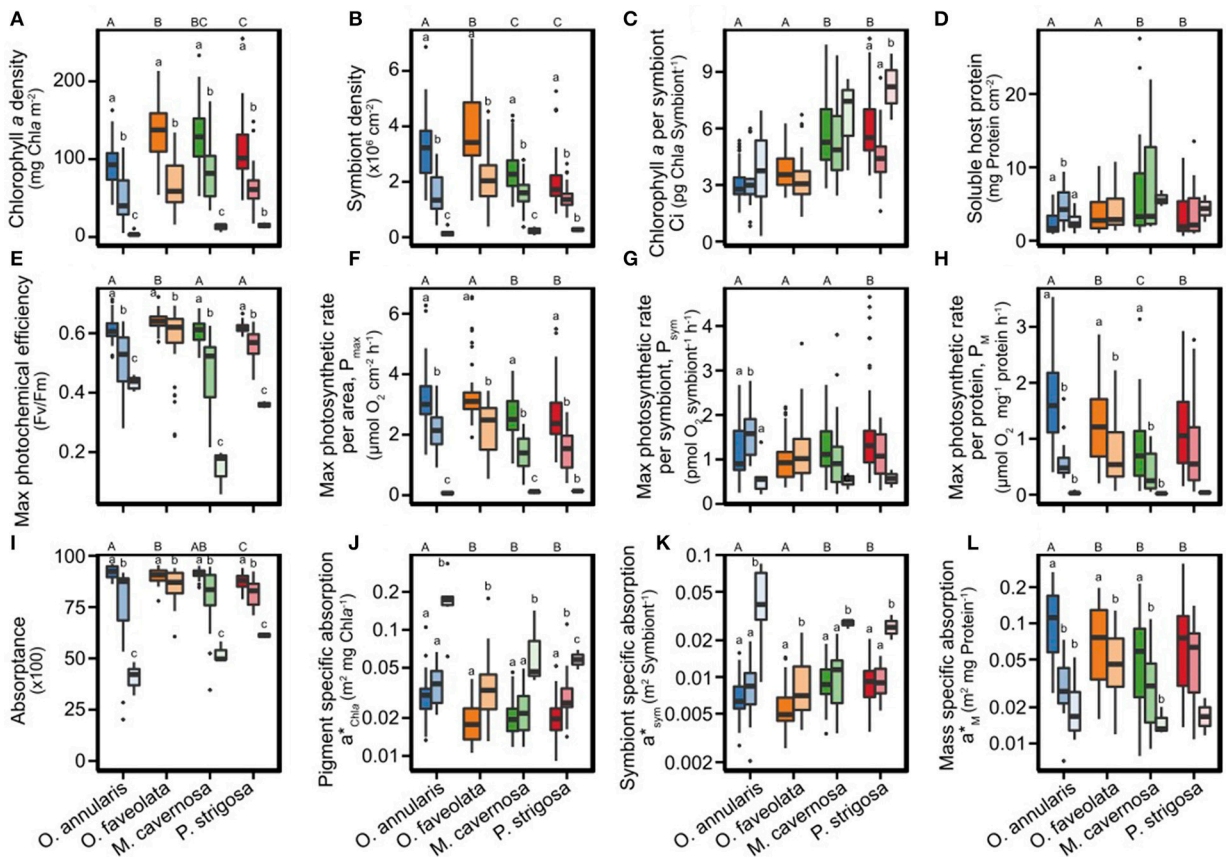

FIGURE 3 | Box plots of the variation of structural **(A–D)**, photosynthetic **(E–H)**, and optical **(I–L)** descriptors of the holobiont phenotype of *Orbicella annularis* (blue), *Orbicella faveolata* (orange), *Montastraea cavernosa* (green), and *Pseudodiploria strigosa* (red). Different shading describes the unstressed (dark), heat-stressed (light), and bleached phenotypes (lighter). Boxes encompass the 25 and 75% quartiles. The central line corresponds to the median, and bars extend to the 95 and 5% of the confidence limits. Uppercase letters indicate significant differences among species, while lowercase letters denote differences among coral phenotypes (ANOVA tests were performed across species using two-way ANOVA). The lack of lowercase letters indicate that changes were not significant.

two species that harbored higher number of symbionts, both *Orbicellas* spp., and the species with higher host protein content and *Symbiodinium* Ci, *P. strigosa* and *M. cavernosa.* The second component (PC2) diferentiated between the more pigmented (*O. faveolata* and *M. cavernosa*) and the less pigmented species (*O. annularis* and *P. strigosa*). This component increased the variability explained to 66%, thanks to the contribution of changes in holobiont pigmentation (Chl*a* density) and holobiont light absorption efficiency (a^*_{Chla}), with smaller contributions of coral descriptors normalized to symbiont and mass (**Table 2**). No correlation was found between this component and holobiont photosynthetic production. Finally, a third component (PC3) increased the variability explained to 80%, thanks to the contribution of P_{max}, *Symbiodinium* Ci and two optical descriptors, a^*_M and a^*_{sym} (**Table 2**).

Structural and Functional Variability of the Stressed Corals

Exposure to heat-stress induced in the two *Orbicellas* and *M. cavernosa* significant chlorophyll *a* (>90%) and symbiont (>89%) losses (one-way ANOVA, Tukey HSD, $p < 0.001$; **Figures 3A,B**). *P. strigosa* showed smaller changes but this species also reduced significantly its chlorophyll *a* and symbiont number when compared with the unstressed samples (one-way ANOVA, Tukey HSD, $p < 0.001$). No significant change was observed for *Symbiodinium* Ci in samples of *O. annularis*, *O. faveolata*, and *M. cavernosa* exposed to heat-stress. Unexpectly, in *P. strigosa* we found a reduction in *Symbiodinium* Ci in the heat-stressed samples, but not in the bleached ones, which showed the highest values (one-way ANOVA, Tukey HSD, $p < 0.001$; **Figure 3C**). Host soluble protein content did not present significant changes in the stressed samples of *O. faveolata*, *M. cavernosa*, and *P. strigosa*, while it increased significantly in *O. annularis* (**Figure 3D**).

F_v/F_m and holobiont gross photosynthesis declined in all samples that suffered heat-stress (**Figures 3E–H**). F_v/F_m reductions were largest for *M. cavernosa* (77%), intermediate for *P. strigosa* and *O. annularis* (30–40%) and lowest for *O. faveolata* (**Figure 3E**). Only three species, *O. annularis*, *M. cavernosa*, and *P. strigosa,* showed P_{max} and P_M values no significantly different to 0 for some of the samples exposed to heat-stress

TABLE 2 | PCA analysis for the structural, optical, and photo-physiological coral descriptors of the un-stressed samples of *Orbicella annularis, O. faveolata*, *Montastraea cavernosa,* and *Pseudodiploria strigosa*.

	PC1	PC2	PC3
Chlorophyll *a* (mg Chl*a* m^{-2})	0.14	**−0.52**	0.05
Symbionts (x10^6 # sym cm^{-2})	**0.43**	−0.19	−0.25
Ci (pg Chl*a* sym^{-1})	**−0.33**	−0.23	**0.40**
Soluble host protein (mg cm^{-2})	**−0.35**	−0.26	−0.14
a^*_{Chla} (m^2 mg $Chla^{-1}$)	−0.07	**0.52**	−0.03
a^*_{sym} (m^2 sym^{-1})	**−0.41**	0.21	0.29
a^*_M (m^2 mg $protein^{-1}$)	**0.36**	0.28	**0.34**
P_{max} (µmol O_2 cm^{-2} h^{-1})	−0.09	0.11	**−0.70**
P_{sym} (pmol O_2 sym^{-1} h^{-1})	**−0.39**	0.23	−0.23
P_M (µmol O_2 $protein^{-1}$ h^{-1})	**0.33**	**0.34**	0.10
Standard deviation	1.96	1.63	1.21
Proportion of variance	0.39	0.27	0.15
Cumulative proportion	0.39	0.65	0.80

Bold values highlight strong correlations [loading > 0.3] between original variables and PCs. The table shows the correlation values of each coral trait for the first three principal components. The table also shows the cumulative variation accounted for each component.

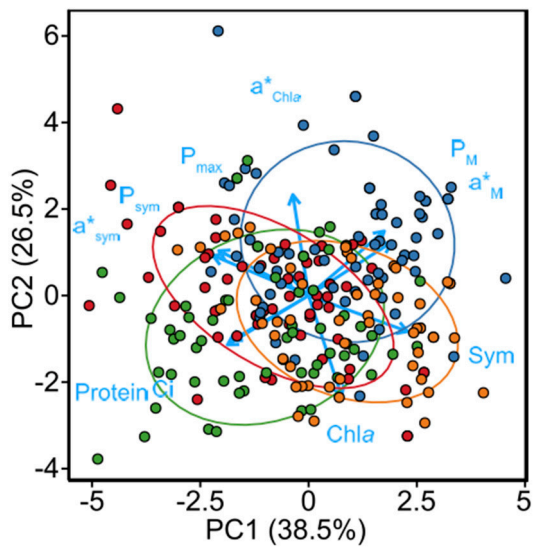

FIGURE 4 | Principal component analysis (PCA) plot showing the grouping of the unstressed specimens of *Orbicella annularis* (blue), *Orbicella faveolata* (orange), *Montastraea cavernosa (*green), and *Pseudodiploria strigosa* (red), based on the structural (chlorophyll *a*, symbiont, Ci, protein content), optical (a^*_{Chla}, a^*_{sym}, a^*_M) and photosynthetic (P_{max}, P_{sym}, P_M) descriptors. Blue arrows indicate the correlation of the different parameters with PC1 and PC2.

(**Figures 3F,H**). We considered that these samples had reached the bleached phenotype, according to Scheufen et al. (2017), as these holobiont were fully dysfunctional with respect to photosynthesis. The only species that did not develop the bleached phenotype was *O. faveolata*, although some stressed specimens showed highly reduced F_v/F_m values (**Figure 3E**), but still mantained significant photosynthetic activity. *Symbiodinium* photosynthetic rates (P_{sym}) were also significantly reduced in the bleached phenotypes (**Figure 3G**).

Association of Variation between Coral Pigmentation and Optical Traits

The declines observed in chlorophyll *a* and symbiont density in the stressed organisms, induced significant reductions in coral absorptance (**Figure 3I**) together with large increases in the specific absorption coefficients (a^*_{Chla} and a^*_{sym}, **Figures 3J,K**). The greatest reductions in absorptance (55%) were estimated for *O. annularis*, while *M. cavernosa* and *P. strigosa* experienced losses of, respectively, 43 and 30% (one-way ANOVA, Tukey HSD, $p < 0.001$). *O. faveolata* was the species that showed the smallest declines in absorptance (7%; one-way ANOVA, Tukey HSD, $p < 0.001$). Only a few stressed samples experienced large reductions in absorptance (∼50%), but these holobionts still maintained significant photosynthetic activity ($P_{max} = 0.7 \pm 0.15$). In addition to absorptance, the most prominent changes in the specific absorption coefficients were observed in *O. annularis*, followed by *P. strigosa*, and *M. cavernosa*, whereas *O. faveolata* showed the smallest variation in a^*_{Chla} and a^*_{sym} (**Figures 3J,K**). Bleached organisms for all species showed the highest values for a^*_{Chla} and a^*_{sym} and the lowest for a^*_M (**Figures 3J–H**).

Principal Component Analysis (PCA) of the Heat-Stressed Corals

The three main coral phenotypes, unstressed, stressed and bleached, were clearly grouped in a second PCA analysis, performed using exclusively coral functional descriptors (**Table 3**, **Figure 5**). The previous structural and functional differences became smaller in comparison with the variability generated by heat-stress. The principal component 1 (PC1) explained 39% of this variability thanks to P_M, a^*_M, and P_{max}, which were negatively associated with a^*_{Chla} a^*_{sym}. The second component 2 (PC2), which increased the variability explained to 66%, was mainly determined by P_{sym} and P_{max} (**Table 3**). Accordingly, the dramatic reduction in coral photosynthesis induced by heat-stress, which was reflected in the holobiont rates (P_{max}), in *Symbiodinium* photosynthesis (P_{sym}), and in the relative contribution of coral photosynthesis to the host (P_M), was paired with large increases in the efficiency of solar energy collection of the holobiont (a^*_{Chla}) and *Symbiodinium* (a^*_{sym}). However, light absorption efficiency of the host (a^*_M) was positively associated with holobiont photosynthesis (**Figure 5**, **Table 3**).

Variation of Holobiont Optical Properties

Optical traits (a^*_{Chla}, a^*_{sym}, a^*_M) showed: (i) a positive association between a^*_{Chla} and a^*_{sym}; (ii) a negative association between a^*_{sym} and a^*_M; and (iii) no association between a^*_{Chla} and a^*_M (**Table 4**). Strong correlations were also found between optical and structural coral traits (**Table 4**), as absorptance and the specific absorption coefficients were positively associated with increases in chlorophyll *a*, symbiont density, and Ci (**Table 4**). A negative colinearity was detected between symbiont density and Ci (Pearson $r = -0.29$, $p < 0.001$; **Table 4**). This general pattern

TABLE 3 | PCA analysis for the optical and photo-physiological coral descriptors of the un- stressed, stressed and bleached samples of *Orbicella annularis, O. faveolata, Montastraea cavernosa,* and *Pseudodiploria strigosa*.

	PC1	PC2	PC3
a^*_{Chla} (m^2 mg $Chla^{-1}$)	**−0.37**	−0.18	**0.56**
a^*_{sym} (m^2 sym^{-1})	**−0.46**	−0.05	**0.49**
a^*_M (m^2 mg $protein^{-1}$)	**0.49**	**−0.36**	**0.37**
P_{max} (μmol O_2 cm^{-2} h^{-1})	**0.33**	**0.60**	0.13
P_{sym} (pmol O_2 sym^{-1} h^{-1})	−0.07	**0.68**	**0.34**
P_M (μmol O_2 $protein^{-1}$ h^{-1})	**0.55**	−0.11	**0.42**
Standard deviation	1.54	1.25	1.14
Proportion of variance	0.39	0.26	0.22
Cumulative proportion	0.39	0.66	0.87

Bold values highlight strong correlations [loading > 0.3] between original variables and PCs. The table shows the correlation values of each coral trait for the first three principal components of this PCA analysis. The table also shows the cumulative variation accounted for each component.

presented some deviations when analyzing the variation within coral species (Supplementary Table 2), as symbiont density and Ci were not significantly correlated in *O. annularis*, *O. faveolata*, and *M. cavernosa*.

The associations of variation between absoptance and, both, chlorophyll *a* and symbiont density (**Figure 6**) were described using the asymptotic function:

$$A = A_{max}(1 - e^{(-b^*Chla\ density)}) \quad (1)$$

where A_{max} is the maximum absorptance value achieved at increasing pigmentation or symbiont density, and b describes the exponential rise of this association. This model allowed estimation for each coral species of the amount of chlorophyll *a* and/or symbiont density required to reach A_{max} *O. faveolata* required the lowest pigmentation (27 mg Chl*a* m^{-2}), followed by *O. annularis* (41 mg Chl*a* m^{-2}), *P. strigosa* (41 mg Chl*a* m^{-2}), and *M. cavernosa* (80 mg Chl*a* m^{-2}). Similarly, the minimum symbiont density required to reach that maximum was lowest for *O. faveolata* (0.76×10^6 # cells cm^{-2}) and *P. strigosa* (0.92×10^6 # cells cm^{-2}); and highest for *O. annularis* (1.37×10^6 # cells cm^{-2}) and *M. cavernosa* (1.58×10^6 symbionts cm^{-2}; **Figure 6**).

A power function was used to describe the non-linear associations between the specific absorption coefficients and holobiont structural traits (**Figures 6C,D**; Supplementary Tables 3, 4). Least-square regression analyses of log/log transformed data according to the equation:

$$\log(y) = \log(a) + b^*\log(x) \quad (2)$$

allowed estimation of the allometric morpho-functional associations, as: $y = a\ X^b$, where log(a) describes the intercept and b the "scaling factor" of the allometric association or the linear slope of the log/log transformed data.

Two common models described the variation of a^*_{Chla} as a function of changes in chlorophyll *a* or symbiont density for all coral species investigated. The first model explained 75% of the variation examined in a^*_{Chla}:

$$\log a^*_{Chla}(m^2\ mg^{-1}\ Chla) = -0.39 \pm 0.04 - 0.63 \pm 0.02^*\log Chla\ density\ (mg\ Chla\ m^{-2})$$
$$(r^2 = 0.75, n = 360, F = -1063.1, p < 0.001) \quad Model(1)$$

The second was able to describe 35% of a^*_{Chla} variation based on only changes in symbiont density:

$$\log a^*_{Chla}(m^2 mg^{-1} Chla) = -1.47 \pm 0.04 - 0.45 \pm 0.03^*\log symbiont\ density\ (\times 10^6 \#\ sym\ cm^{-2})$$
$$(r^2 = 0.35, n = 360, F = 195.03, p < 0.001) \quad Model(2)$$

Multiple Regression Analyses

To better understand the dependence of coral optical traits (A and a^*_{chla}) on the variation of holobiont pigmentation, we performed multiple regression analyses in order to distinguish between direct and combined effects of changes in the number of symbionts (symbiont density) and in *Symbiodinium* pigmentation (Ci) on this variation. The models found allow quantification of the effect of changes in the distribution of coral pigmentation on coral optics. According to these models:

(i) increases in symbiont density result in larger enhancements in coral absorptance than increases in *Symbiodinium* Ci:

$$\log A = 1.77 \pm 0.01 + \mathbf{0.26} \pm 0.02^*\log symbiont\ density\ (\times 10^6 cm^{-2}) + \mathbf{0.16} \pm 0.02^*\log Ci\ (mg\ Chla\ cell^{-1}) - 0.1 \pm 0.04^*\log symbiont\ density^*\log Ci$$
$$(R^2 = 0.57, n = 360, F = 157.58, p < 0.001) \quad Model(3)$$

and,

(ii) increases in *Symbiodinium* Ci result in larger reductions in pigment light absorption efficiency than increases in symbiont density:

$$\log a^*_{Chla}(m^2\ mg\ Chla^{-1}) = -0.97 \pm 0.02 - \mathbf{0.48} \pm 0.05^*\log sym\ density(\times 10^6\ \#symcm^{-2}) - \mathbf{0.74} \pm 0.03^*\log Ci(mg\ Chla\ cell^{-1}) - 0.19 \pm 0.08^*\log sym\ density^*\log Ci$$
$$(R^2 = 0.77, n = 360, F = 393.86, p < 0.001) \quad Model(4)$$

Thus, holobionts that distribute their pigmentation over more symbionts at expenses of reducing *Symbiodinium* cell pigmentation will be able to collect more light (A) and more efficiently (a^*_{Chla}) reducing holobiont pigment packaging. However, the significant interaction found for symbiont density and Ci in both models indicates that at increasing coral pigmentation the contribution of both parameters to enhance A or reduce a^*_{Chla} is smaller.

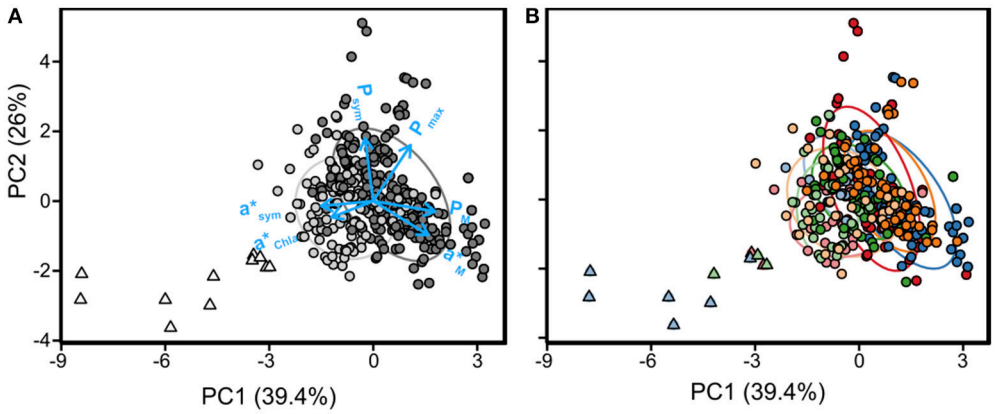

FIGURE 5 | Principal component analysis (PCA) plot showing **(A)** the grouping of samples in un-stressed (dark gray), stressed (gray), and bleached (light gray) coral phenotypes, based on the optical (a^*_{Chla}, a^*_{sym}, a^*_M) and photo-physiological (P_{max}, P_{sym}, P_M) descriptors. Blue arrows indicate the correlation of the different descriptors with PC1 and PC2. Plot **(B)** described the same grouping identifying coral species with different color: *Orbiella annularis* in blue, *Orbicella faveolata* in orange, *Montastraea cavernosa* in green, and *Pseudodiploria strigosa* in red. Different shading describes coral phenotypes from unstressed (dark) to bleached (lighter).

TABLE 4 | Pearson correlation between optical, structural, and photo-physiological descriptors.

	Optical				Structural			Photo-physiological	
	log A	**log a^*_{chla}**	**log a^*_{sym}**	**log a^*_M**	**log Chl*a***	**log sym**	**log Ci**	**log P_{max}**	**log P_{sym}**
log A									
log a^*_{Chla}	−0.34***								
log a^*_{sym}	−0.24***	0.57***							
log a^*_M	0.38***	−0.08	−0.36***						
log Chl*a*	0.74***	−0.87***	−0.54***	0.28***					
log sym	0.66***	−0.59***	−0.85***	0.48***	0.79***				
log Ci	0.14**	−0.44***	0.44***	−0.30***	0.35***	−0.29***			
log P_{max}	0.67***	−0.44***	−0.46***	0.26***	0.67***	0.70***	−0.03		
log P_{sym}	0.1	0.14**	0.43***	−0.24***	−0.06	−0.28***	0.32***	0.49***	
log P_M	0.49***	−0.28***	−0.54***	0.83***	0.48***	0.66***	−0.28***	0.70***	0.14**

*Significants levels: ***0.001; **0.01; *0.05.*

Significant differences among species were also detected for these trends (Supplementary Tables 5, 6). For example, *O. faveolata* showed the largest scaling factor between a^*_{Chla} and chlorophyll *a* density (−0.89 ± 0.04, Supplementary Table 3), significantly larger than the smallest value estimated for *O. annularis* (−0.5 ± 0.03). These findings indicate that "pigment packaging" within coral tissues presents a relevant species-specific component that still needs to be characterized (Supplementary Tables 3, 4).

Effects of Optical Traits on Holobiont Photosynthetic Rates

PCA analyses and Pearson correlations highlighted significant colinearities between coral photosynthetic rates and optical descriptors (**Tables 2–4**, **Figures 3–4**). The optical trait better related to holobiont photosynthetic rates was a^*_M, whereas a^*_{Chla} and a^*_{sym} showed significant but negative associations with P_{max} and P_M (**Table 4**, **Figure 4**). Interestingly, increases in *Symbiodinium* light absorption efficiency (a^*_{sym}) were significantly and positively associated with symbiont contribution to holobiont photosynthetic production (P_{sym}). The three photosynthetic descriptors (P_{max}, P_{sym}, and P_M) were also positively related: a strong Pearson correlation was found between P_{max} and P_M, and a significant association was also observed between P_{max} and P_{sym} (**Table 4**).

DISCUSSION

This comparative characterization of the optical properties of scleractinian corals revealed that the three species with the chalice-type skeleton, *O. annularis*, *O. faveolata*, and *M. cavernosa,* were able to achieve higher maximum light absorption capacities (A_{max} > 90%) than the species with the meandroid skeleton morphology, *P. strigosa* (A_{max} = 88%). This finding agrees with the results of a recent description of the variation of the optical properties of coral skeletons, where the meandroid morphotype was categorized as a skeleton with lower abilities to enhance multiple light scattering (Enríquez

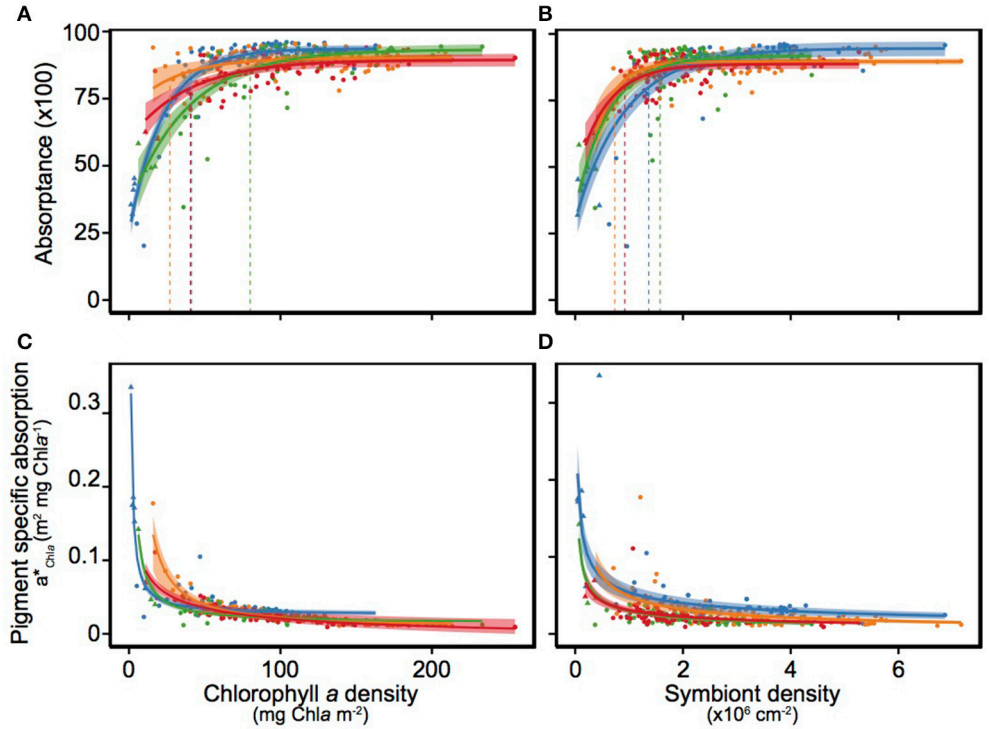

FIGURE 6 | Description of the variation of absorptance **(A)** and pigment specific absorption (a^*_{Chla}) as a function of changes in chlorophyll *a* **(A,C)** and symbiont density **(B,D)**, for *Orbicella annularis* (blue), *Orbicella faveolata* (orange), *Montastraea cavernosa* (green), and *Pseudodiploria strigosa* (red). Solid lines mark the asymptotic fits for each coral species and the shade area represents the extension of the 95 and 5% confident intervals. Discontinuous vertical color lines mark the values of chorophyll *a* or symbiont density where A_{max} was achieved for each species.

et al., 2017). The small although significant differences found for the maximum light absorption capacity of the holobiont were also reflected in large variation among species in the amount of pigmentation and/or symbionts required to achieve that maximum, A_{max}. *O. faveolata* was the species that showed the highest ability to maximize light absorption at the lowest pigmentation and symbiont densities. In contrast, *M. cavernosa* required the largest pigmentation to maximize light absorption but similar number of symbionts to *O. annularis*. Interestingly, despite the lower A_{max} estimated for *P. strigosa,* this species was able to maximize absorptance with one of the lowest number of symbionts and holobiont pigmentation. According to these findings, this first comparison highlighted significant differences among coral species in holobiont capacity and efficiency to collect solar energy, either per unit of pigment or symbiont content. The inter-specific variability documented, however, still supports the extraordinary efficiency of scleractinian corals as solar energy collectors previously documented (Enríquez et al., 2005; Terán et al., 2010), as the amount of chlorophyll *a* required to reach maximum absorptance was remarkably lower for three species (<50 mg Chl*a* m^{-2}) if comparing with terrestrial leaves (>200 mg Chl*a* m^{-2}; see Carter and Knapp, 2001; Davis et al., 2011) or marine macrophyte tissues (>100 mg Chl*a* m^{-2}; see Frost-Christensen and Sand-Jensen, 1992; Enríquez et al., 1994). Previous characterizations for *Stylophora pistillata,* which did not consider the contribution of coral skeleton to the emergent optical properties of the coral-symbionts-skeleton unit, were also largely above (120 mg Chl*a* m^{-2}; see Dubinsky et al., 1984, 1990).

Our comparison also supports that "pigment packaging" (Duysens, 1956) still affects coral tissues. Non-linear reductions in light absorption efficiency, a^*_{Chla}, at increasing coral pigmentation per projected area (cross-section) were found for all species characterized, similarly to previous descriptions for multicellular structures (Enríquez and Sand-Jensen, 2003; Enríquez, 2005; Enríquez et al., 2005) and phytoplankton (e.g., Morel and Bricaud, 1981; Kirk, 2011). However, according to models 3 and 4, increases in symbiont density are more effective to counterbalance "pigment packaging" and enhance coral absorptance than increases in *Symbiodinium* cell pigmentation (Ci) in agreement with the results of Terán et al. (2010). These authors documented using Monte Carlo simulations of 2D skeleton models, that changes in the number of symbionts are more effective to collect light than changes in the absorptivity of *Symbiodinium* cells. Hence, the distribution of photosynthetic pigments over a higher number of symbionts results in larger enhancements in coral capacity (absorptance) and efficiency (a^*_{Chla}) of light absorption. On the other side, for similar coral pigmentation increases in *Symbiodinium* pigment content (Ci) at the same time that the number of symbionts is reduced, leads to higher "pigment packaging" (lower a^*_{Chla}) within the

coral-symbiont-skeleton unit. This coral structural adjustment produces a more inefficient holobiont to collect solar energy, but with perhaps functional advantages under increasing levels of light stress. Our comparative study also highlighted a species-specific component in that "pigment packaging," which needs still to be characterized. This component has to be related to the optical properties of coral skeletons, optical properties of *Symbiodinium* cells (i.e., cell diameter and pigment content, Ci), coral tissue thickness, *Symbiodinium* distribution within coral tissue, and also species plasticity for changing symbiont content and *Symbiodinium* cell pigmentation (Ci). Among them, variation in the optical properties of coral skeleton, tissue thickness, and species plasticity for changing symbiont content and *Symbiodinium* cell pigmentation (Ci), are more likely the most important coral traits involved in the regulation of holobiont optical properties.

Seasonal changes in the number of symbionts and in *Symbiodinium* Ci (e.g., Brown et al., 1999; Fagoonee et al., 1999; Fitt et al., 2000) may express the optimization of holobiont optical properties to: (i) minimize pigment packaging under optimal conditions or decreasing light levels; or (ii) enhance photoprotection under increasing light stress. Therefore, we propose that the summer coral phenotype recently documented by Scheufen et al. (2017) characterized by increasing *Symbiodinium* Ci at the same time that the number of symbionts is reduced, may be the optimal holobiont adjustment to the seasonal increase in seawater temperature, in order to enhance the high-light photoprotective response of *Symbiodinium in hospite*. However, too large increases in *Symbiodinium* Ci at reduced number of symbionts may produce a more sensitive holobiont under high light and/or heat stress conditions, as small loses in the number of cells will lead to larger changes in coral pigmentation and thus, larger enhancements in a^*_{Chla} (**Figure 7**). The extremely high a* values found for the bleached phenotype supports the relevance of this optical descriptor to determine a functional "tipping point" for this symbiosis, set when a* rises to levels unacceptable for maintaining symbiont photosynthesis due to extremely high local light fields for *Symbiodinium*. In contrast, winter increases in the number of symbionts may require reductions in *Symbiodinium* Ci to counterbalance pigment packaging and enhance the penetration of light into coral tissues to illuminate sufficiently the different symbiont layers. This adjustment would be particularly important for coral species with skeletons with reduced efficiency to enhance multiple light scattering (Enríquez et al., 2017). In the holobiont acclimatization to summer, however, the decrease in the number of symbionts would result in very efficient holobionts to collect solar energy (high a^*_{Chla}) but with higher risk of reaching the bleached phenotype under light and/or heat stress, if such declines are not associated with increases in *Symbiodinium* Ci (**Figure 7**). According to this interpretation, the functional link between structural and optical coral traits could explain the effect of changes in the number of symbionts and/or *Symbiodinium* Ci on holobiont performance, irrespective of the occurrence or not of additional changes in the dominant *Symbiodinium* type, and thus, in the physiological response of the symbionts. In this study, we did not characterize these changes, but previous

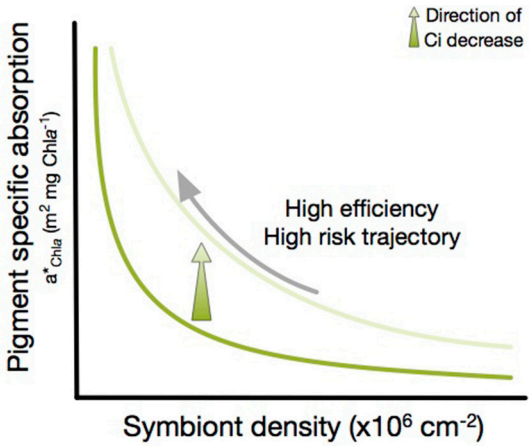

FIGURE 7 | Theoretical scheme of the modulating effect of *Symbiodinium* Ci on the association of a^*_{Chla} with changes in symbiont density. The lower (dark green) line shows the variation of a^*_{Chla} with a constant Ci calculated form the standard deviation above the mean Ci (high Ci condition). The upper (light green) line shows the variation with a constant Ci value calculated from the standard deviation below the mean Ci. The green arrow indicates the direction of a^*_{Chla} increases when a stable symbiont density decreases its Ci. The upper trajectory leads to faster increase in a^*_{Chla}, but also a higher risk of collection too much light under heat stress and suffering higher photo-damage. The real trajectories for each species can be found in Supplementary Figure 1.

descriptions of the variability of *Symbiodinium* dominant type for the four species investigated from the reef lagoon of Puerto Morelos (Mexico) have reported the presence of C3d (C3e) in *M. cavernosa*; B1 and C1 types in *P. strigosa*; and C7 and D1a/*Symbiodinium trenchii* in *O. faveolata* (LaJeunesse, 2002). A more detailed study by Kemp et al. (2015) on *O. faveolata* growing at the "Bocana" in the reef lagoon of Puerto Morelos, reported the presence of A3, B1, B17, C17, and D1a/*S. trenchii.* With respect to *O. annularis* LaJeunesse (2002) documented the presence of B1, C3, and D1a/*S. trenchii* in corals collected from reefs at Lee Stocking islands, in Bahamas. From our own previous analyses, we found A3 and B1 in *O. annularis* and A3, B17, C7, and D1a/*S. trenchii* in *O. faveolata*, in colonies growing at similar sites and depths to those analyzed in this study from the reef lagoon of Puerto Morelos (unpublished data). Such variability in the dominant *Symbiodinium* type could also help to explain part of the variation not accounted in this study for a* and P_{max}.

Structural and Functional Variability among Coral Species

PCA was able to describe 80% of the inter-specific variability displayed by non-stressed holobionts (**Figure 4**), highlighting relevant association of variation between structural and functional traits. The first component (PC1) discriminated between the species with the ability to harbor high number of symbionts, the two *Orbicellas*, and *P. strigosa* and *M. cavernosa,* two species characterized by thick tissues (high host soluble protein content) and highly pigmented symbionts. The second component (PC2) distinguished between highly pigmented

(*O. faveolata* and *M. cavernosa*) and less pigmented species (*O. annularis* and *P. strigosa*). Thus, the reduced host mass and high number of symbionts of the two *Orbicellas* allowed these species to achieve higher light absorption efficiency and photosynthetic production per mass (a^*_M and P_M). Accordingly, the "evolutionary solution" represented by the two *Orbicellas,* but in particular by *O. annularis* characterized by low pigmented thin tissues, has produced holobionts with high efficiency for solar energy collection (a^*_{Chla}) and high photosynthetic returns to the host (P_M). The third component (PC3) of the PCA analysis accounted for the effect on holobiont photosynthetic production (P_{max}) of the interspecific structural and optical variability analyzed in this study. This component showed that the most productive holobionts (P_{max}) tend to present lower light absorption efficiencies for both symbiotic partners, host (a^*_M) and *Symbiodinium* (a^*_{sym}), and harbor symbionts with lower Ci values (**Table 2**, **Figure 4**). All these associations of variation between structural and functional coral traits support the potential of this approach to understand differences among coral species in the advantages or constraints that these symbioses may provide to the holobiont and to each member of the mutualistic association, the animal and the alga. Furthermore, a trade-off between increases in the number of symbionts and reductions in *Symbiodinium* Ci may be inferred from this analysis. The first strategy requires higher light scattering abilities of coral skeleton (Enríquez et al., 2017) to offset the packaging effect, enhance the local light field of *Symbiodinium* and ensure higher benefits for the host (P_M and a^*_M). In contrast, the ecological and/or evolutionary success of the second option would primarily depend on the capacity of *Symbiodinium* to maximize light collection efficiency (a^*_{sym}) and its contribution to holobiont photosynthetic production (P_{sym}).

Structural and Functional Variability among Coral Phenotypes

In addition to these inter-specific differences, our comparison also revealed common changes among species for the heat-stressed and bleached coral phenotypes. Indeed, PCA analysis allowed distinction between the bleached and the heat-stressed samples (**Figure 5**). Changes in holobiont photosynthesis (P_{max}), positively associated with a^*_M and negatively with a^*_{sym} and a^*_{Chla}, were able to describe 40% of the variability contained in the whole data set (PC1). This finding supports previous conclusions by Scheufen et al. (2017), who documented that the bleached coral phenotype is determined by the full suppression of coral photosynthesis and large increases in the light absorption efficiency of *Symbiodinium* (a^*_{sym}) and the holobiont (a^*_{Chla}). We also found here that the un-stressed holobiont condition was better described by a^*_M, which may quantify the efficiency of the symbiosis to return to the host the solar energy collected (**Table 3**). The second (PC2) and third (PC3) components, which increased the variability explained to 66 and 87%, respectively, discriminated between two un-stressed holobionts: one that favors enhancing the photosynthetic contribution of *Symbiodinium* to holobiont production (P_{sym}); and a second strategy that favors enhancing the benefits for the host (P_M and a^*_M). According to this, PC1 described the evolution of the stressed phenotype of all species toward a common bleached condition; whereas PC2 and PC3 allowed distinction among un-stressed species and/or seasonal phenotypes.

Another conclusion of this analysis in agreement with Scheufen et al. (2017), is that reductions in coral pigmentation are insufficient to define the bleached coral phenotype. Yet, other holobiont descriptors in addition to coral color are needed to determine the dysfunctional condition of these ancient symbioses. Coral photosynthetic rates appeared as the strongest descriptors, but our study supports the capacity of optical traits to recognize a bleached coral (**Figure 3**). Severe reductions in coral absorptance (A), but also dramatic increases in light absorption efficiency of chlorophyll *a* (a^*_{chla}) and light absorption efficiency of *Symbiodinium* (a^*_{sym}) can be used to differentiate an stressed coral from a dysfunctional symbiosis. More work is, however, needed to fully understand the natural variability displayed by coral optical traits and its relation to holobiont performance and colonial growth.

Micro-scale approaches are useful tools for the characterization of the internal light fields of the symbionts (Kühl et al., 1995; Wangpraseurt et al., 2012, 2014, 2016; Brodersen et al., 2014). This approach has documented the presence of light gradients (Wangpraseurt et al., 2012) and lateral light transfer within coral tissues (Wangpraseurt et al., 2014), which apparently are more pronounced in corals with thicker tissues. Optical characterizations of coral skeletons (e.g., Enríquez et al., 2005, 2017; Terán et al., 2010; Marcelino et al., 2013) are also fundamental to understand the direct contribution of the skeleton to modify the internal light field of *Symbiodinium*. In addition to these approaches, the understanding of the optical properties of the whole coral-alga-skeleton unit cannot be overlooked, as it is central to recognize differences among species and phenotypes in coral performance and competitive abilities. Our analysis is a first attempt to investigate this potential, analyzing the optical properties for four coral species. Further research is still needed to characterize the diversity of structural and functional solutions achieved by these ancient symbioses along their evolutionary history, and the utility of optical coral traits for the development of the coral *Trait-based approach* proposed by Madin et al. (2016).

AUTHOR CONTRIBUTIONS

SE and RI designed research, TS performed research, TS and SE analyzed data and wrote the paper. All authors contributed to the final edited version of the manuscript.

ACKNOWLEDGMENTS

Two Mexican research projects granted to SE, DGAPA (IN206710), and CONACYT (Conv-CB-2009: 129880), and an European project (PFP7-FORCE-244161) provided financial support to this research. This research was part of the PhD thesis of TS in the program *Posgrado en Ciencias del Mar y Limnología (PCMyL)* of the Universidad Nacional Autónoma de

México (UNAM). The Consejo Nacional de Ciencia y Tecnología (CONACyT) is acknowledged for providing 3 years fellowship to support TS during his PhD program and the FORCE project is also acknowledged for providing 1 year fellowship to TS. The experiments performed in this work comply with the current laws of Mexico. An ethics approval was not required as per national regulations. The study was supported by two Mexican permits: "Permiso de Pesca de Fomento" No DGOPA.07342.010810.4121, to SE; and No DGOPA.08606.251011.3021, to RI; issued by the Secretaría de Agricultura, Ganadería, Desarrollo rural, Pesca y Alimentación of the United States of Mexico, to support, respectively, the development of the projects: "*Evaluación del efecto de la limitación de carbono sobre diferentes productores primarios de la laguna arrecifal de Puerto Morelos: Importancia de la calcificación*"; and "*Efectos del calentamiento y acidificación del Océano en las tasas de calcificación de los corales.*"

SUPPLEMENTARY MATERIAL

The Supplementary Material for this article can be found online at: http://journal.frontiersin.org/article/10.3389/fmars.2017.00309/full#supplementary-material

REFERENCES

Anthony, K. R. N., Hoogenboom, M. O., and Connolly, S. R. (2005). Adaptive variation in coral geometry and the optimization of internal colony light climates. *Funct. Ecol.* 19, 17–26. doi: 10.1111/j.0269-8463.2005.00925.x

Baker, A. C. (2004). "Symbiont diversity on coral reefs and its relationship to bleaching resistance and resilience," in *Coral Health and Disease*, eds E. Rosenberg and Y. Loya (Berlin: Springer Verlag), 177–194.

Barnes, D. J., and Lough, J. M. (1989). The Nature of skeletal density banding in scleractinian corals: fine banding and seasonal patterns. *J. Exp. Mar. Biol. Ecol.* 126, 119–134. doi: 10.1016/0022-0981(89)90084-1

Berkelmans, R., and van Oppen, M. J. H. (2006). The role of zooxanthellae in the thermal tolerance of corals: a "nugget of hope" for coral reefs in an era of climate change. *Proc. R. Soc. Lond. B* 272, 2305–2312. doi: 10.1098/rspb.2006.3567

Brodersen, K. E., Lichtenberg, M., Ralph, P. J., Kühl, M., and Wangpraseurt, D. (2014). Radiative energy budget reveals high photosynthetic efficiency in symbiont-bearing corals. *J. R. Soc. Interface* 11:20130997. doi: 10.1098/rsif.2013.0997

Brown, B. E., Dunne, R. P., Ambarsari, I., Le Tissier, M. D. A., and Satapoomin, U. (1999). Seasonal fluctuations in environmental factors and variations in symbiotic algae and chlorophyll pigments in four Indo-Pacific coral species. *Mar. Ecol. Prog. Ser.* 191, 53–69. doi: 10.3354/meps191053

Brown, B. E., Dunne, R. P., Goodson, M. S., and Douglas, A. E. (2000). Marine ecology: bleaching patterns in reef corals. *Nature* 404, 142–143. doi: 10.1038/35004657

Budd, A. F., and Klaus, J. S. (2001). The origin and early evolution of the Montastraea "annularis" species complex (Anthozoa: Scleractinia)'. *J. Paleontol.* 75, 527–545. doi: 10.1017/S0022336000039640

Carter, G. A., and Knapp, A. K. (2001). Leaf optical properties in higher plants: linking spectral characteristics to stress and chlorophyll concentration. *Am. J. Bot.* 88, 677–684. doi: 10.2307/2657068

Cayabyab, N. M., and Enríquez, S. (2007). Leaf photoacclimatory responses of the tropical seagrass Thalassia testudinum under mesocosm conditions: a mechanistic scaling-up study. *New Phytol.* 176, 108–123. doi: 10.1111/j.1469-8137.2007.02147.x

Colombo-Pallotta, M. F., Rodríguez-Román, A., and Iglesias-Prieto, R. (2010). Calcification in bleached and unbleached *Montastraea faveolata*: evaluating the role of oxygen and glycerol. *Coral Reefs* 29, 899–907. doi: 10.1007/s00338-010-0638-x

Davis, P. A., Caylor, S., Whippo, C. W., and Hangarter, R. P. (2011). Changes in leaf optical properties associated with light-dependent chloroplast movement. *Plant Cell Environ.* 34, 2047–2059. doi: 10.1111/j.1365-3040.2011.02402.x

de Mendiburu, F. (2016). *Agricolae: Statistical Procedures for Agricultural Research*. R package version 1.2-4. Available online at: https://CRAN.R-project.org/package=agricolae

Dubinsky, Z., Falkowski, P. G., Porter, J. W., and Muscatine, L. (1984). Absorption and utilization of radiant energy by light- and shade-adapted colonies of the hermatypic coral *Stylophora pistillata*. *Proc. R. Soc. Lond. B* 222:203–214. doi: 10.1098/rspb.1984.0059

Dubinsky, Z., Stambler, N., Ben-Zion, M., McCloskey, L., Muscatine, L., and Falkowski, P. G. (1990). The effect of external nutrient resources on the optical properties and photosynthetic efficiency of *Stylophora pistillata*. *Proc. R. Soc. Lond. B* 239, 231–246. doi: 10.1098/rspb.1990.0015

Duysens, L. N. (1956). The flattering of the absorption spectrum of suspensions, as compared to that of solutions'. *Biochim. Biophys. Acta* 19, 1–12. doi: 10.1016/0006-3002(56)90380-8

Enríquez, S. (2005). Light absorption efficiency and the package effect in the leaves of the seagrass Thalassia testudinum. *Mar. Ecol. Prog. Ser.* 289, 141–150. doi: 10.3354/meps289141

Enríquez, S., Agustí, S., and Duarte, C. M. (1994). Light absorption by marine macrophytes. *Oecologia* 98, 121–129. doi: 10.1007/BF00341462

Enríquez, S., and Sand-Jensen, K. (2003). Variation in light absorption properties of *Mentha aquatica* L. as a function of leaf form: implications for plant growth. *Int. J. Plant Sci.* 164, 125–136. doi: 10.1086/344759

Enríquez, S., Méndez, E. R., Hoegh-Guldberg, O., and Iglesias-Prieto, R. (2017). Key functional role of the optical properties of coral skeletons in coral ecology and evolution. *Proc. R. Soc. Lond. B* 284:20161667. doi: 10.1098/rspb.2016.1667

Enríquez, S., Méndez, E. R., and Iglesias-Prieto, R. (2005). Multiple scattering on coral skeletons enhances light absorption by symbiotic algae. *Limnol. Oceanogr.* 50, 1025–1032. doi: 10.4319/lo.2005.50.4.1025

Enríquez, S., Merino, M., and Iglesias-Prieto, R. (2002). Variation in the photosynthetic performance along the leaves of the tropical seagrass Thalassia testudinum. *Mar. Biol.* 140, 891–900. doi: 10.1007/s00227-001-0760-y

Fagoonee, I., Wilson, H. B., Hassell, M. P., and Turner, J. R. (1999). The dynamics of zooxanthellae populations: a long-term study in the field. *Science* 283, 843–845. doi: 10.1126/science.283.5403.843

Falkowski, P. G., and Dubinsky, Z. (1981). Light-shade adaptation of *Stylophora pistillata*, a hermatypic coral from the Gulf of Eilat. *Nature* 289, 172–174. doi: 10.1038/289172a0

Ferrier-Pagès, C., Schoelzke, V., Jaubert, J., Muscatine, L., and Hoegh-Guldberg, O. (2001). Response of a scleractinian coral, *Stylophora pistillata*, to iron and nitrate enrichment. *J. Exp. Mar. Biol. Ecol.* 259, 249–261. doi: 10.1016/S0022-0981(01)00241-6

Fitt, W. K., McFarland, F. K., Warner, M. E., and Chilcoat, G. C. (2000). Seasonal patterns of tissue biomass and densities of symbiotic dinoflagellates in reef corals and relation to coral bleaching. *Limnol. Oceanogr.* 45, 677–685. doi: 10.4319/lo.2000.45.3.0677

Fitt, W. K., Gates, R. D., Hoegh-Guldberg, O., Bythell, J. C., Jatkar, A., Grottoli, A. G., et al. (2009). Response of two species of Indo-Pacific corals, Porites cylindrical and *Stylophora pistillata*, to short-term thermal stress: the host does matter in determining the tolerance of corals to bleaching. *J. Exp. Mar. Biol. Ecol.* 373, 102–110. doi: 10.1016/j.jembe.2009.03.011

Fox, J., and Weisberg, S. (2011). *An R Companion to Applied Regression, 2nd Edn*. Thousand Oaks CA: Sage.

Frost-Christensen, H., and Sand-Jensen, K. (1992). The quantum efficiency of photosynthesis in macroalgae and submerged angiosperms. *Oecologia* 91, 377–384. doi: 10.1007/BF00317627

Glynn, P. W. (1996). Coral reef bleaching: facts, hypotheses and implications. *Glob. Change Biol.* 2, 495–509. doi: 10.1111/j.1365-2486.1996.tb00063.x

Hennige, S. J., Suggett, D. J., Warner, M. E., McDougall, K. E., and Smith, D. J. (2009). Photobiology of Symbiodinium revisited: bio-physical and bio-optical signatures. *Coral Reefs* 28, 179–195. doi: 10.1007/s00338-008-0444-x

Hoegh-Guldberg, O. (1999). Climate change, coral bleaching and the future of the world's coral reefs. *Mar. Freshw. Res.* 50, 839–866. doi: 10.1071/MF99078

Hoegh-Guldberg, O., Fine, M., Skirving, W., Johnstone, R., Dove, S., and Strong, A. (2005). Coral bleaching following wintry weather. *Limnol. Oceanogr.* 50, 265–271. doi: 10.4319/lo.2005.50.1.0265

Iglesias-Prieto, R., and Trench, R. K. (1994). Acclimation and adaptation to irradiance in symbiotic dinoflagellates. I. Responses of the photosynthetic unit to changes in photon flux density. *Mar. Ecol. Prog. Ser.* 113, 163–175. doi: 10.3354/meps113163

Iglesias-Prieto, R., Matta, J. L., Robins, W. A., and Trench, R. K. (1992). Photosynthetic response to elevated temperature in the symbiotic dinoflagellate Symbiodinium microadriaticum in culture. *Proc. Natl. Acad. Sci. U.S.A.* 89, 10302–10305. doi: 10.1073/pnas.89.21.10302

Jeffrey, S. W., and Humphrey, G. F. (1975). New spectrophotometric equations for determining chlorophylls a, b, c1, and c2 in higher plants, algae, and natural phytoplankton. *Biochem. Physiol. Pflanz.* 167, 191–194. doi: 10.1016/S0015-3796(17)30778-3

Kemp, D. W., Cook, C. B., LaJeunesse, T. C., and Brooks, W. R. (2006). A comparison of the thermal bleaching responses of the zoanthid Palythoa caribaeorum from three geographically different regions in south Florida. *J. Exp. Mar. Biol. Ecol.* 335, 266–276. doi: 10.1016/j.jembe.2006.03.017

Kemp, D. W., Hernandez-Pech, X., Iglesias-Prieto, R., Fitt, W. K., and Schmidt, G. W. (2014). Community dynamics and physiology of *Symbiodinium* spp. before, during, and after a coral bleaching event. *Limnol. Oceanogr.* 59, 788–797. doi: 10.4319/lo.2014.59.3.0788

Kemp, D. W., Oakley, C. A., Thornhill, D. J., Newcomb, L. A., Schmidt, G. W., and Fitt, W. K. (2011). Catastrophic mortality on inshore coral reefs of the Florida Keys due to severe low-temperature stress. *Glob. Change Biol.* 17, 3468–3477. doi: 10.1111/j.1365-2486.2011.02487.x

Kemp, D. W., Thornhill, D. J., Rotjan, R. D., Iglesias-Prieto, R., Fitt, W. K., and Schmidt, G. W. (2015). Spatially distinct and regionally endemic Symbiodinium assemblages in the threatened Caribbean reef-building coral *Orbicella faveolata*. *Coral Reefs* 34, 535–547. doi: 10.1007/s00338-015-1277-z

Kirk, J. T. O. (2011). *Light and Photosynthesis in Aquatic Ecosystems, 3rd Edn*. New York, NY: Cambridge University Press.

Kühl, M., Cohen, Y., Dalsgraad, T., Jørgensen, B. B., and Revsbech, N. P. (1995). Mircoenvironment and photosynthesis of zooxanthellae in scleratinian corals studied with microsensors for O2, pH and light. *Mar. Ecol. Prog. Ser.* 117, 159–172. doi: 10.3354/meps117159

LaJeunesse, T. C. (2002). Diversity and community structure of symbiotic dinoflagellates from Caribbean coral reefs. *Mar. Biol.* 141, 387–400. doi: 10.1007/s00227-002-0829-2

Lesser, M. P., Mazel, C., Phinney, D., and Yentsch, C. S. (2000). Light absorption and utilization by colonies of the congeneric hermatypic corals *Montastraea faveolata* and *Montastraea cavernosa*. *Limnol. Oceanogr.* 45, 76–86. doi: 10.4319/lo.2000.45.1.0076

Lesser, M. P. (1996). Exposure of symbiotic dinoflagellates to elevated temperatures and ultraviolet radiation causes oxidative stress and photosynthesis. *Limnol. Oceanogr.* 41, 271–283. doi: 10.4319/lo.1996.41.2.0271

Lesser, M. P., and Farrell, J. (2004). Solar radiation increases the damage to both host tissues and algal symbionts of corals exposed to thermal stress. *Coral Reefs* 23, 367–377. doi: 10.1007/s00338-004-0392-z

Madin, J. S., Hoogenboom, M. O., Connolly, S. R., Darling, E. S., Falster, D. S., Huang, D., et al. (2016). A trait-based approach to advance coral reef science. *Trends Ecol. Evol.* 31, 419–428. doi: 10.1016/j.tree.2016.02.012

Marcelino, L. A., Westneat, M. W., Stoyneva, V., Henss, J., Rogers, J. D., Radosevich, A., et al. (2013). Modulation of light-enhancement to symbiotic algae by light-scattering in corals and evolutionary trends in bleaching. *PLoS ONE* 8:e61492. doi: 10.1371/journal.pone.0061492

Marsh, J. A. (1970). Primary productivity of reef-building calcareous red algae. *Ecology* 51, 255–263. doi: 10.2307/1933661

Morel, A., and Bricaud, A. (1981). Theoretical results concerning light absorption in a discrete medium, and application to specific absorption of phytoplankton. *Deep Sea Res.* 28, 1375–1393. doi: 10.1016/0198-0149(81)90039-X

Muscatine, L., McCloskey, L. R., and Marian, R. E. (1981). Estimating the daily contribution of carbon from zooxanthellae to coral animal respiration. *Limnol. Oceanogr.* 26, 601–611. doi: 10.4319/lo.1981.26.4.0601

Pearse, V. B., and Muscatine, L. (1971). Role of symbiotic algae (zooxanthellae) in coral calcification. *Bio. Bull.* 141, 350–363. doi: 10.2307/1540123

Pettay, D. T., Wham, D. C., Smith, R. T., Iglesias-Prieto, R., and LaJeunesse, T. C. (2015). Microbial invasion of the Caribbean by an Indo-Pacific coral zooxanthella. *Proc. Natl. Acad. Sci. U.S.A.* 112, 7513–7518. doi: 10.1073/pnas.1502283112

R Core Team (2017). *R: A Language and Environment for Statistical Computing*. Vienna: R Foundation for Statistical Computing. Available online at: https://www.R-project.org/

Robison, J. D., and Warner, M. E. (2006). Differential impacts of photoacclimation and thermal stress on the photobiology of four different phylotypes of Symbiodinium (Pyrrhophyta). *J. Phycol.* 42, 568–569. doi: 10.1111/j.1529-8817.2006.00232.x

Rodríguez-Román, A., Hernández-Pech, X., Tome, P. E., Enríquez, S., and Iglesias-Prieto, R. (2006). Photosynthesis and light utilization in the Caribbean coral *Montastraea faveolata* recovering form a bleaching event. *Limnol. Oceanogr.* 51, 2702–2710. doi: 10.4319/lo.2006.51.6.2702

Savage, A. M., Trapido-Rosenthal, H., and Douglas, A. E. (2002). On the functional significance of molecular variation in Symbiodinium, the symbiotic algae of cnidarian: photosynthetic response to irradiance. *Mar. Ecol. Prog. Ser.* 244, 27–37. doi: 10.3354/meps244027

Scheufen, T., Krämer, W. E., Iglesias-Prieto, R., and Enríquez, S. (2017). Seasonal variation modulates coral sensibility to thermal-stress and explains annual changes in coral productivity. *Sci. Rep.* 7:4937. doi: 10.1038/s41598-017-04927-8

Shibata, K. (1969). Pigments and a UV-absorbing substance in corals and blue-green alga living in the Great Barrier Reef. *Plant Cell Physiol.* 10, 325–335.

Smith, D. J., Suggett, D. J., and Baker, N. R. (2005). Is photoinhibition of zooxanthellae photosynthesis the primary cause of thermal bleaching in corals. *Glob. Change Biol.* 11, 1–11. doi: 10.1111/j.1529-8817.2003.00895.x

Stambler, N., and Dubinsky, Z. (2005). Corals as light collectors: an integrating sphere approach. *Coral Reefs* 24, 1–9. doi: 10.1007/s00338-004-0452-4

Stimson, J., and Kinzie, I. I. I., R. A. (1991). The temporal pattern and rate of release of zooxanthellae from the reef coral Pocillopora damicornis (Linnaeus) under nitrogen-enrichment and control conditions. *J. Exp. Mar. Biol. Ecol.* 153, 63–74. doi: 10.1016/S0022-0981(05)80006-1

Stimson, J., Sakai, K., and Sembali, H. (2002). Interspecific comparison of the symbiotic relationship in corals with high and low rates of bleaching-induced mortality. *Coral Reefs* 21, 409–421. doi: 10.1007/s00338-002-0264-3

Suggett, D. J., Warner, M. E., Smith, D. J., Davey, P., Hennige, S., and Baker, N. R. (2008). Photosynthesis and production of hydrogen peroxide by Symbiodinium (pyrrhophyta) phylotypes with different thermal tolerances. *J. Phycol.* 44, 948–956. doi: 10.1111/j.1529-8817.2008.00537.x

Tchernov, D., Gorbunov, M. Y., de Vargas, C., Narayan Yadav, S., Milligan, A. J., Haggblom, M., et al. (2004). Membrane lipids of symbiotic algae are diagnostic of sensitivity to thermal bleaching in corals. *Proc. Natl. Acad. Sci. U.S.A.* 101, 13531–13535. doi: 10.1073/pnas.0402907101

Terán, E., Méndez, E. R., Enríquez, S., and Iglesias-Prieto, R. (2010). Multiple light scattering and absorption in reef-building corals. *Appl. Opt.* 49, 5032–5042. doi: 10.1364/AO.49.005032

Vásquez-Elizondo, R. M., Legaria-Moreno, L., Pérez-Castro, M. A., Krämer, W. E., Scheufen, T., Iglesias-Prieto, R., et al. (2017). Absorptance determinations in multicellular tissues. *Photosynth. Res.* 3, 311–324. doi: 10.1007/s11120-017-0395-6

Wangpraseurt, D., Jacques, S. L., Petrie, T., and Kühl, M. (2016). Monte carlo modeling of photon propagation reveals highly scattering coral tissue. *Front. Plant Sci.* 7:1404. doi: 10.3389/fpls.2016.01404

Wangpraseurt, D., Larkum, A. W., Franklin, J., Szabó, M., Ralph, P. J., and Kühl, M. (2014). Lateral light transfer ensures efficient resource distribution in symbiont-bearing corals. *J. Exp. Biol.* 217, 489–498. doi: 10.1242/jeb.091116

Wangpraseurt, D., Larkum, A. W., Ralph, P. J., and Kühl, M. (2012). Light gradients and optical microniches in coral tissues. *Front. Microbiol.* 3:316. doi: 10.3389/fmicb.2012.00316

Warner, M. E., LaJeunesse, T. C., Robison, J. D., and Thur, R. M. (2006). The ecological distribution and comparative photobiology of symbiotic dinoflagellates from reef corals in Belize: potential implications for

coral bleaching. *Limnol. Oceanogr.* 51, 1887–1897. doi: 10.4319/lo.2006.51.4.1887

Weis, V. M. (2008). Cellular mechanisms of Cnidarian bleaching: stress causes the collapse of symbiosis. *J. Exp. Biol.* 211, 3059–3066. doi: 10.1242/jeb.009597

Whitaker, J. R., and Granum, P. E. (1980). An absolute method for protein determination based on difference in absorbance at 235 and 280 nm. *Anal. Biochem.* 109, 156–159. doi: 10.1016/0003-2697(80)90024-X

Wyman, K. D., Dubinsky, Z., Porter, J. W., and Falkowski, P. G. (1987). Light absorption and utilization among hermatypic corals: a study in Jamaica, West Indies. *Mar. Biol.* 96, 283–292. doi: 10.1007/BF00427028

Conflict of Interest Statement: The authors declare that the research was conducted in the absence of any commercial or financial relationships that could be construed as a potential conflict of interest.

frontiers in Marine Science

ORIGINAL RESEARCH
published: 17 November 2017
doi: 10.3389/fmars.2017.00365

Use of Open Source Hardware and Software Platforms to Quantify Spectrally Dependent Differences in Photochemical Efficiency and Functional Absorption Cross Section within the Dinoflagellate *Symbiodinium* spp.

Kenneth D. Hoadley[*†] *and Mark E. Warner*

School of Marine Science and Policy, University of Delaware, Lewes, DE, United States

OPEN ACCESS

Edited by:
Thomas K. Frazer, University of Florida, United States

Reviewed by:
Bojan Tamburic, University of Technology Sydney, Australia
Oscar Schofield, Rutgers University, The State University of New Jersey, United States

***Correspondence:**
Kenneth D. Hoadley
khoadley@mbari.org

†Present Address:
Kenneth D. Hoadley, Monterey Bay Aquarium Research Institute. Moss Landing, CA, United States

Specialty section:
This article was submitted to Coral Reef Research, a section of the journal Frontiers in Marine Science

Received: *18 May 2017*
Accepted: *30 October 2017*
Published: *17 November 2017*

Citation:
Hoadley KD and Warner ME (2017) Use of Open Source Hardware and Software Platforms to Quantify Spectrally Dependent Differences in Photochemical Efficiency and Functional Absorption Cross Section within the Dinoflagellate Symbiodinium spp. Front. Mar. Sci. 4:365. doi: 10.3389/fmars.2017.00365

Active chlorophyll *a* fluorescence is an essential tool for understanding photosynthetic activity within cnidarian/dinoflagellate symbioses. Fluorescence measurement is typically achieved by utilizing a blue or red monochromatic excitation light source. However, algal photosynthetic pigments can differ in their absorption spectra, potentially leading to excitation wavelength dependent measurements of maximal and light acclimated PSII photosynthetic quantum yield (Fv/Fm or Fq′/Fm′) and functional absorption cross section (σ_{PSII} or $\sigma_{PSII'}$). Here we utilized an open source hardware development platform to construct a multispectral excitation fluorometer to assess spectrally dependent differences in photochemistry within four different *Symbiodinium* species (two of each ITS2-type A4 and B1). Multivariate analysis of light acclimated photochemical signatures showed separation between most alga types. These spectrally dependent differences in light acclimated PSII efficiency and PSII functional absorption cross section likely reflect changes in light harvesting compounds, their connectivity to the PSII reaction centers and the balance between photochemical and non-photochemical fluorescence quenching. Additionally, acclimation to low (20 μmol photons m^{-2} s^{-1}) and high (200 μmol photons m^{-2} s^{-1}) light conditions was examined in two of these symbionts types (ITS-2 type A4 and B1) As expected, chlorophyll a $cell^{-1}$ decreased under high light acclimation in both symbionts. However, only A4 saw a subsequent reduction in absorbance whereas cellular volume decreased in the B1 (*S. minutum*) symbiont. In response to high light acclimation, Fv/Fm was significantly lower at all excitation wavelengths for the B1 symbiont where as efficiencies remained the same for A4. However, high-light acclimated Fq′/Fm′ levels decreased in both symbionts, but only when measured using the 615 or 625 nm excitation wavelengths. Non-photochemical quenching within the antennae bed was downregulated under high light acclimation in the A4 symbiont, but only when measured using the 505 and 530 nm excitation wavelengths. Such changes in Fq′/Fm′ and antennae bed quenching highlight the

benefits of spectrally resolved photochemical measurements. Additionally, the utilization of Arduino and Bitscope hardware exemplifies the potential of open source development platforms for construction of highly customizable instrumentation for photosynthetic research.

Keywords: multispectral fluorometer, absorbance, light acclimation, open source, coral photobiology

INTRODUCTION

Dinoflagellates within the genus *Symbiodinium* can form unique symbioses with various marine invertebrate species, including jellyfish, sea anemones, giant clams, soft corals, and hard corals or scleractinians. These symbioses are pivotal for the ecological success of many of these organisms as they provide a major carbon source to their hosts via translocation of energy rich photosynthate (Muscatine et al., 1984; Muscatine, 1990). This genus contains a high degree of genetic diversity which is currently organized into nine broad clades (designated by the letters A–I), some of which contain hundreds of distinct species (LaJeunesse, 2001). Importantly, different *Symbiodinium*s can have significant influence on the host's response to changes in the environment (Baker, 2003). For example, in corals, thermal tolerance is often associated with the specific symbiont type (Kemp et al., 2006; LaJeunesse et al., 2009; Silverstein et al., 2011; Ortiz et al., 2012). However, matching physiological characteristics with specific symbiont types can be difficult and time consuming. There is a real need within the coral reef community to match physiological variability with genetic variance across symbiont types to better understand what/how these symbioses will respond under future climate conditions.

Such phenotypic assessment (Phenomics) is gaining momentum within other photobiological fields where comprehension of genetic variability has far outpaced phenotypic descriptions (Furbank and Tester, 2011). Phenotypic structure across different symbiont types grown in culture has been documented using photophysiological metrics as measured using active chlorophyll fluorometric measurements (Suggett et al., 2015). However, environmental variables such as light intensity and the spectral characteristics inherent to the coral host in which the symbiont resides can also influence photobiological behavior (Iglesias-Prieto and Trench, 1997b; Iglesias-Prieto et al., 2004; Wangpraseurt et al., 2012, 2014). The potential for phenotypic variance within a single species also increases the difficulty of matching physiology with genotype in symbiodinium (Iglesias-Prieto and Trench, 1997b; Iglesias-Prieto et al., 2004).

The genus *Symbiodinium* contains a number of different photopigments, some involved with light harvesting, while others act as accessory pigments where they can either channel additional energy toward the photosynthetic reaction centers, or dissipate excess light energy (Iglesias-Prieto and Trench, 1994, 1997b). The light harvesting compounds; peridinin-chlorophyll-a-protein (PCP) and chl a-chl c(2)-peridinin-protein (acpPC) have been particularly well-studied and comprise the primary light harvesting units within *Symbiodinium* (Iglesias-Prieto et al., 1991, 1993; Niedzwiedzki et al., 2013, 2014). The relative abundance of these different photopigments can differ across symbiont types (Hennige et al., 2009) and potentially offer another biological parameter that can be utilized to study species specific phenotypes within the genus *Symbiodinium.* As was demonstrated with symbionts housed within *Porites* and *Montipora,* host coral specimens found in Kaneohe Bay, absorbance based measurements can under certain circumstances provide some information on the abundance of photopigment concentrations (Hochberg et al., 2006). However, additional instrumentation is needed to understand the active role of these pigments within the photosynthetic apparatus.

Single turnover (ST) active chlorophyll-*a* fluorometers utilize a short (<300 μs) saturation light pulse to induce charge separation and reduction of the primary electron acceptor Q_a within the PSII reaction center (Kolber and Falkowski, 1998). A major advantage of ST fluorometery is the additional measurement of the functional absorption cross section of PSII (σ_{PSII}) (Suggett et al., 2003), which measures the proportion of light captured by light harvesting proteins attached to a reaction center and utilized by PSII. In these instruments, saturation/excitation lamps are typically centered at a 450–500 nm wavelength to target peak absorbance of chlorophyll-*a*. However, by adjusting the excitation wavelength, it is possible to preferentially target other light harvesting photopigments. For example, by utilizing LEDs with peak emission centered at 447, 505 or 530 nm, we are able to preferentially excite at the peak absorption "soret" bands for the pigments Chl a/c_2, diadinoxanthin, and peridinin, respectively (Niedzwiedzki et al., 2013, 2014). Longer wavelengths such as 625 nm may transfer energy directly to the Chl *a* molecule (Niedzwiedzki et al., 2014). Preferential excitation may provide further insight into how pigment orientation and connectivity to the PSII reaction center may differ across environmental conditions or across symbiont types. However, such systems come at a high cost and alternative systems could be highly beneficial toward improving our understanding of *Symbiodinium* photobiology.

Hardware and software platforms designed to help teach coding and programming languages to the next generation of engineers are becoming increasingly popular within the scientific community. These platforms offer sophisticated microcontrollers as a base with which to design customized instrumentation at a low cost. The high cost of commercially available research instrumentation can be heavily restrictive to many laboratories. Research questions/initiatives often must cater to the available instrumentation, thereby limiting the scope of possible questions or experimental options. Open-sourced hardware and software platforms have the potential to revolutionize how scientists conduct research by allowing for cheap purpose built instrumentation. Sophisticated

instrumentation can be cheaply designed and built around a specific research question/topic. For example, the MultispeQ is an instrument developed to compare photophysiological parameters in plants across the world in an effort to tie in physiological differences with known genetic variance (Kuhlgert et al., 2016). The OpenROV project (www.openrov.com) represents another open-source platform which utilizes both the Arduino and Beaglebone hardware to construct a low cost remotely operated underwater vehicle which can be adapted with different instrumentation for both recreational and/or research purposes. These low-cost, yet highly sophisticated instruments represent an emerging trend in research that have great potential moving forward.

In this study, we utilize open source platforms to construct a low-cost multispectral ST fluorometer to characterize potential photo-physiological differences across four symbiont types from two clades (A and B) living within the anemone *Exaptasia pallida*. We further characterized the light acclimation process within two of these symbionts and describe a spectrally dependent response which differed across the *Symbiodinium* types. This study serves as an example of the potential for furthering scientific inquiry through customized, purpose built instruments via the open source concept and designed for specific research questions.

MATERIALS AND METHODS

Development of Host and Symbiont Combinations

Symbiont strain identification was determined through partial amplification of the ITS2 nuclear ribosomal DNA region and a region of the chloroplast 23S rDNA as described in LaJeunesse and Trench (2000) and Zhang et al. (2000). The two strains of ITS-2 type A4 utilized within this study were collected from *E. pallida* anemones in a mangrove habitat in Key Largo, FL (Hawkins et al., 2016). The A4-a strain represents a natural host and symbiont combination whereas the A4-b strain represents the genotype KLAp2 isolated from the anemone population and then utilized to re-infect aposymbiotic anemones originating from the same Key Largo mangrove habitat (as described in Hawkins et al., 2016). Both the B1-a and B1-b strains represent separate *S. minutum* genotypes and are housed within *E. pallida* (clone CC7, donated by J. Pringle, Stanford University) (Sunagawa et al., 2009). The B1-a strain represents a *S. minutum* variant that is naturally found within *E. pallida* and the B1-b strain was originally isolated from a Caribbean gorgonian (*Plexaura kuna*) (the BURR culture collection, donated by M.A. Coffroth, University of Buffalo). All host symbiont combinations were maintained in stable symbioses for at least 6 months prior to experimentation.

Each host/symbiont combination was maintained in small glass bowls (9 cm diameter, 130-mL volume) filled with artificial seawater (Instant Ocean) at a temperature of 26°C and salinity of 34 ppt. Lighting was maintained at 40 μmol photons m^{-2} s^{-1} with a 14:10 h light dark cycle using cool white fluorescent bulbs. Anemones were fed *Artemia nauplii* twice per week and seawater in each bowl was changed every 3 days.

Experimental Conditions

For comparisons of spectrally dependent quantum yield and functional absorption cross section measurements across symbiont types, four different host/symbiont combinations (A4-a, A4-b, B1-a, and B1-b) were maintained in separate glass bowls with 3–4 anemones per bowl. Anemones were maintained at 20 μmol photons m^{-2} s^{-1} on a 14:10 h light:dark cycle. For spectrally dependent characterization across low and high light acclimated cells, additional bowls for A4-a and B1-a were kept at 200 μmol photons m^{-2} s^{-1} on a 14:10 h light:dark cycle. All bowls were cleaned and filled with fresh artificial seawater every 3 days and anemones were fed twice per week. Temperature was maintained at 26°C. Anemones were acclimated to their respective light conditions over a 2-week period prior to taking chlorophyll a fluorescence measurements and sampling anemones for chlorophyll a concentration, cell count, and cell volume measurements.

Chlorophyll a Fluorescence Measurements

Construction of Open-Sourced Fluorometer

The fluorometer prototype consists of combining several commercially available pieces of electronics. The Bitscope comes with a fully functional software program whereas the Arduino comes with its own code compiler. A schematic of the constructed fluorometer is provided in **Figure 1** and the components are listed in **Table 1**. In brief, excitation was achieved using CREE XLamp XP-E2 LED. Three LEDs wired in series on a metal core printed circuit board (MCPCB) were utilized per excitation color (Channel). Specific LED colors (447, 505, 530, 597, 615, and 625 nm) were chosen due to their commercial availability and for their overlap with peak photopigment absorption values (Niedzwiedzki et al., 2013, 2014). Excitation of each Channel was controlled using logic MOSFET transistors connected to separate IO pins on an Arduino UNO microcontroller board. Power to the LEDs was supplied by a 12-volt AC-DC power converter (Mean-Well). A voltage regulator controlled power to each LED. However, due to performance differences across the LED colors, irradiance differed across wavelengths (447 nm = 34,172; 505 nm = 16,209; 530 nm = 18,401; 597 nm = 24,089; 615 nm = 35,983; 625 nm = 43,662 μmol photons m^{-2} s^{-1}). Although similar irradiance across all excitation wavelengths is ideal, such differences should not affect the calculation of absorption cross section so long as light levels are not so low as to allow for reoxidation of the Q_A^- site within the PSII reaction center (Kolber and Falkowski, 1998). Excitation irradiance values were monitored throughout using an incident quantum sensor (LI-192, LiCor) to ensure stability throughout measurements. Fluorescence rise kinetics were detected with a PIN photodiode (Hammamatsu) connected to a LT122 operational amplifier (Linear Technology) along with a longband pass filter (Schott-RG695). The operational amplifier circuit came prefabricated as part of a Demonstration Circuit Board (1416; Linear Technology) and powered using a ± 15 volt DC-DC (CUI) power supply. The resulting analog output from the PIN photodiode was recorded using a 10AU pocket analyzer (Bitscope). Control of each excitation channel, and the trigger to record data with the

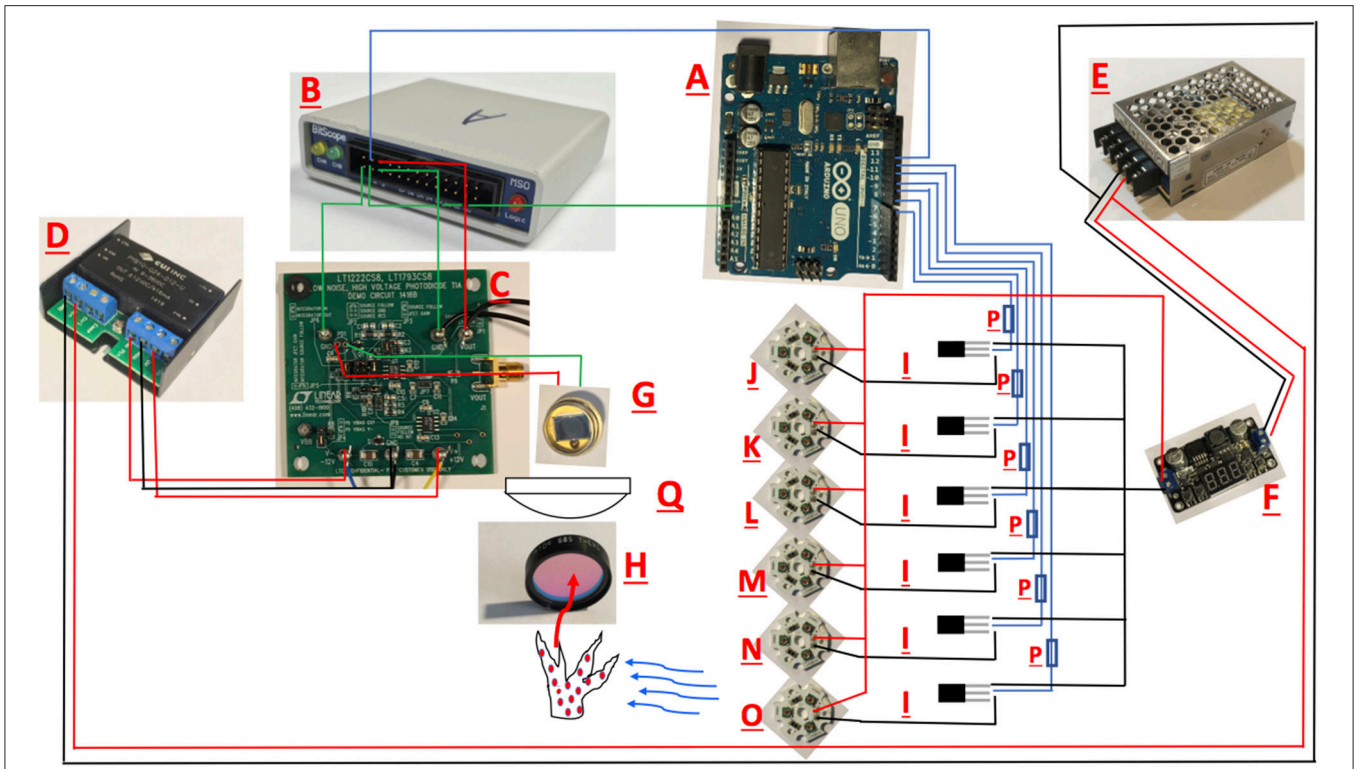

FIGURE 1 | Schematic for the open source multispectral fluorometer. Names of Individual parts are listed in **Table 1**. Black and red lines illustrate wire connections between hardware.

10 AU pocket analyzer was achieved using the Arduino IDE. The Arduino control script is available on github (https://github.com/khoadley/Fluorometer). Light emission and fluorescence detection were directed by glass fiber optic light guides (19.05-mm diameter) oriented at a 90-degree angle to each other.

Measurements were made 1 h after lights were turned off and consisted of six iterations of a 150 μs flash for each of the six excitation wavelengths. Light acclimated fluorescence measurements were then recorded following a 5-min exposure to a cool white actinic LED light source (CREE R5) at an intensity of 200 μmol photons m^{-2} s^{-1}. Reference curves for each channel and light stage were recorded using a solid fluorescence standard (Walz). Fluorescence induction curves were processed in R with the non-linear curve (nlc) fitting package using equations adapted from Kolber and Falkowski (1998) by Dr. Matt Oliver (University of Delaware). Briefly, the data is fit to the equation:

$$F = F_{0EST} + F_{vEST}{}^{*}(1 - \exp(-(C^{*}x)/1))$$

Where F_{0EST}, $F_{vEST,}$ and C are derived through iterative curve fitting. F_0 and F_m are equal to F at the initial and final time point within the curve, respectively. The functional absorption cross section is determined by dividing C by the light irradiance measured from the corresponding excitation LED (R script is also available via Github: https://github.com/khoadley/Fluorometer). The proportion of non-photochemical quenching which is occurring within the light harvesting pigments (non-photochemical quenching in the antennae bed) was calculated as 1-(σ_{PSII}'/σ_{PSII}) where σ'_{PSII} and σ_{PSII} reflect the light and dark acclimated functional absorption cross section of PSII (Gorbunov et al., 2001; Hennige et al., 2009).

Commercially Available Instrument

On the final sampling interval, the maximum quantum yield of photosystem II (PSII, Fv/Fm) and the functional absorption cross section of PSII (σ_{PSII}) were also measured using a fluorescence induction and relaxation (FIRe) fluorometer (Satlantic Inc., Halifax) (**Figure 6**). Measurements were taken 1 h after the start of the dark period and consisted of five iterations of a 120 μs single turnover flash and analyzed by fitting each fluorescence transient curve using the *FIREPRO* software (Kolber and Falkowski, 1998; Hennige et al., 2009).

Algal Cell Number, Volume, and Chlorophyll a Concentration

Each anemone was ground in 1 mL of seawater using a 1.5 mL glass tenbroeck tissue grinder. A 200-μL sample of the resulting homogenate was removed and fixed with 10 μL 1% glutaraldehyde and used for algal cell counts and volume as described below. The remaining homogenate was centrifuged (5,000 × g) for 5 min to separate the host and symbiont portions. The supernatant was removed

TABLE 1 | Equipment list for fluorometer build.

Letter	Hardware	Company	Description	Approximate Price (USD)
A	Arduino UNO	Arduino	Microcontroller	$24.95
B	BitScope BS10	BitScope	Oscilloscope	$245.00
C	1416A	Linear Tech	Photodiode amplifier	$70
D	± 15 vdc power source	CUI	DC-DC power converter	$30
E	24 vdc power source	Mean-Well	AC-DC Converter	$35
F	Voltage Regulator	Drok	Voltage Regulator	$16.89
G	PDB-C109-ND	Digi-Key	PIN photodiode	$71.60
H	RG695	Schott	Long Bandpass filter	$40
I	IRL-520	Vishay	MOSFET	<$2.00 each
J	XP-E (Royal Blue)	Cree LED	447 nm Excitation	$15
K	Luxeon Rebel (Blue)	Luxeon LED	505 nm Excitation	$15
L	XP-E (Green)	Cree LED	530 nm Excitation	$15
M	XP-E (Amber)	Cree LED	597 nm Excitation	$15
N	XP-E (Red Orange)	Cree LED	615 nm Excitation	$15
O	XP-E (Red)	Cree LED	625 nm Excitation	$15
P		Digikey	Resistor	<$1 each
Q	Aspheric Lens	Newport	Aspheric condenser	71
				Total: $712.44

Figure letters correspond to ***Figure 1****.*

for calculating host protein concentration. The remaining algal cell pellet was utilized for calculating chlorophyll a concentration. Algal cell density and volume was assessed by replicate hemocytometer counts ($n = 6$) under 100x magnification. Samples were photographed using a Nikon microphot-FXA epifluorescent microscope and then analyzed by computer using Image J software (NIH) using methods similar to Suggett et al. (2015). For photopigment quantification, pelleted cells were lysed in 90% methanol with a bead beater (BioSpec) for 60 s, incubated at −20°C for 2 h and then centrifuged for 5 min at 5,000 rpm to remove remaining debris. Chlorophyll *a* concentration was then calculated using established protocols (Porra et al., 1989). Host protein concentrations were measured by the BCA method (Thermo Scientific), with bovine serum albumin used for standards. All absorbance measurements (chlorophyll and protein) were performed with a plate reader (FLUOstar Omega BMG labtech).

Spectral Absorbance

For high and low light acclimated symbiont types, spectral absorbance measurements were performed as described in Enríquez et al. (2005) with reflectance (R) measured using a spectrometer (USB2000 Ocean Optics) and absorbance (A) calculated as $A = \log[1/R]$. Three traces were recorded per sample and a spectralon reflectance standard was utilized as a blank. Irradiance was provided by a full spectrum halogen light source (KL2500 LCD Schott). A running average was applied to each replicate trace prior to averaging. Significant differences among high and low light treatments were tested at absorbance wavelengths corresponding to those utilized by the chlorophyll *a* fluorometer (447, 505, 530, 597, 615, 625 nm).

Statistical Analysis

Data-sets were tested for homogeneity of variance and normality of distribution using the Levene and Shapiro-Wilks tests, respectively. Data violating assumptions of normality and homoscedasticity ($p < 0.05$) were log transformed and retested. Significant differences in Fq′/Fm′ and σ_{PSII}' values across all four symbiont types were tested by a one-way ANOVA (**Figures 2A,B**), followed by pairwise comparison across all four symbiont types with Tukey *post-hoc* analyses. Significant separation across symbiont types was assessed using an ANalyses Of SIMilarities test (ANOSIM) with 9,999 permutations. A *post-hoc* analysis of separation was not performed due to low replicate numbers ($n = 3$). Photo-physiological differences across all four symbiont types were visualized using non-metric multidimensional scaling (nMDS) on Euclidean distances after log (x+1) transformation (Ziegler et al., 2014). For high and low light acclimation comparisons, data were compared with a T-test with Bonferonni correction (**Figures 3–5**). Data comparison between the FIRe and Open-Sourced fluorometer was performed by a two-way analysis of variance (ANOVA) between light and symbiont type (**Figure 6**). As the primarily focus was to assess the similarity of responses detected between fluorimeters, significant effects were not followed up with *post-hoc* analyses. All statistical analyses were performed using R software with the "vegan," "car," "edgeR," "gplots," and "pgirmess" packages installed.

RESULTS

Effective Quantum Yield and Functional Absorption Cross Section in Different Symbionts

Effective quantum yield of PSII (Fq′/Fm′) varied across symbiont types and excitation wavelengths (**Figure 2A**). Symbiont type B1-b had between 15 and 23% higher yields than all others ($P = 0.0005$) at 505 nm. In addition, Fq′/Fm′ in anemones harboring B1-b was 30% greater than strain B1-a at 447 nm ($P = 0.02456$) and 24% higher than strains B1-a and A4-a at 530 nm ($P = 0.01324$) (**Figure 2A**). Symbiont strain A4-b had significantly greater (at least 42% higher) light acclimated absorption cross section values than the A4-a strain under all excitation wavelengths ($P < 0.034$) (**Figure 2B**). The A4-b symbiont strain had at least 28% greater light acclimated absorption cross section values than the two B1 strains when measured using 505, 597, and 615 nm excitation wavelengths ($P < 0.009$) (**Figure 2B**). Analysis of similarity (ANOSIM)

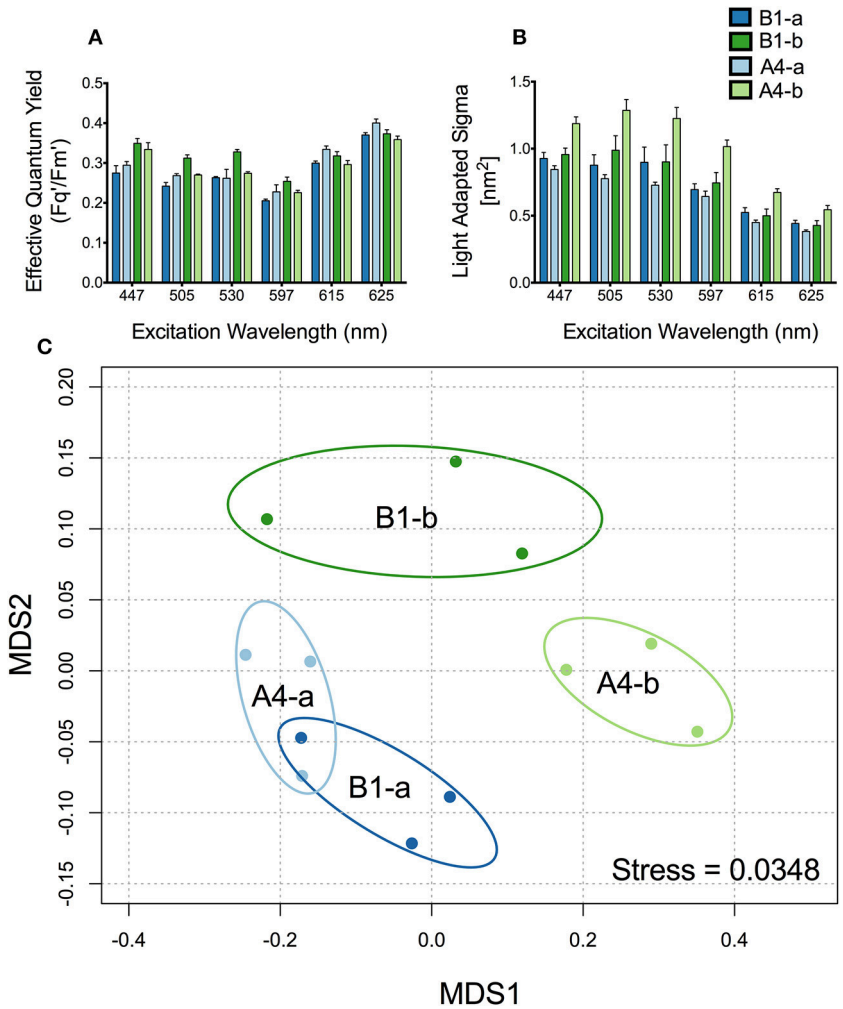

FIGURE 2 | Differences in fluorescence signature across symbiont types. **(A)** Effective quantum efficiency of PSII and **(B)** Light adapted absorption cross section (σ_{PSII}) for (dark blue) B1-a, (light blue) A4-a, (dark green) B1-b, and (light green) A4-b. Bars represent the mean and ±SE for low light adapted samples. **(C)** Principle components analysis using light adapted σ_{PSII} and Fv'/Fm' for all four species. Ellipses represent a 95% confidence around the mean for each symbiont type.

confirmed a strong separation across symbiont types (R = 0.7068, P = 0.0014). Additionally, the MDS analysis shows that the direction of separation between the two Clade A symbionts differs from that of the two Clade B symbionts (**Figure 2C**). This is likely due to differences in Fq′/Fm′ driving the majority of separation between the two clade B symbionts (**Figure 2A**) whereas differences in the absorption cross section account for separation between clade A symbionts (**Figure 2B**).

Spectrally Dependent Maximum Quantum Yield of PSII and Antennae Bed Quenching

The maximum quantum yield of PSII was statistically indistinguishable between low and high light acclimated animals harboring the A4-a symbiont strain at all excitation wavelengths (**Figure 3A**). However, Fv/Fm declined by 12–23% under high light acclimation across all six excitation wavelengths in anemones harboring the B1-a strain (P = 0.02875, 0.0054, 0.0071, 0.0093, 0.0053, 0.0015 for 447, 505, 530, 597, 615, and 625 nm, respectively) (**Figure 3B**). There was a significant drop in the effective quantum yield in both sets of anemones, but only under the longer excitation wavelengths, with reductions for 615 nm (P = 0.0121, 31% reduction) and 625 nm (P = 0.0055, 27% reduction) for A4-a anemones and 597 nm (P = 0.0088, 19% reduction), 615 nm (P = 0.0140, 26% reduction) and 625 nm (P = 0.0381, 25% reduction) for B1-a anemones (**Figures 3C,D**). High light acclimation in the A4-a anemones resulted in a significant decrease in non-photochemical quenching within the antennae bed at excitation wavelengths of 505 nm (P = 0.0372, 40% reduction) and 530 nm (P = 0.0385, 29% reduction) (**Figure 4A**). Non-significant reduction in antennae bed quenching was also observed using a 447 nm excitation wavelength, with a P-value of 0.05032 (**Figure 4A**), There were no significant changes in

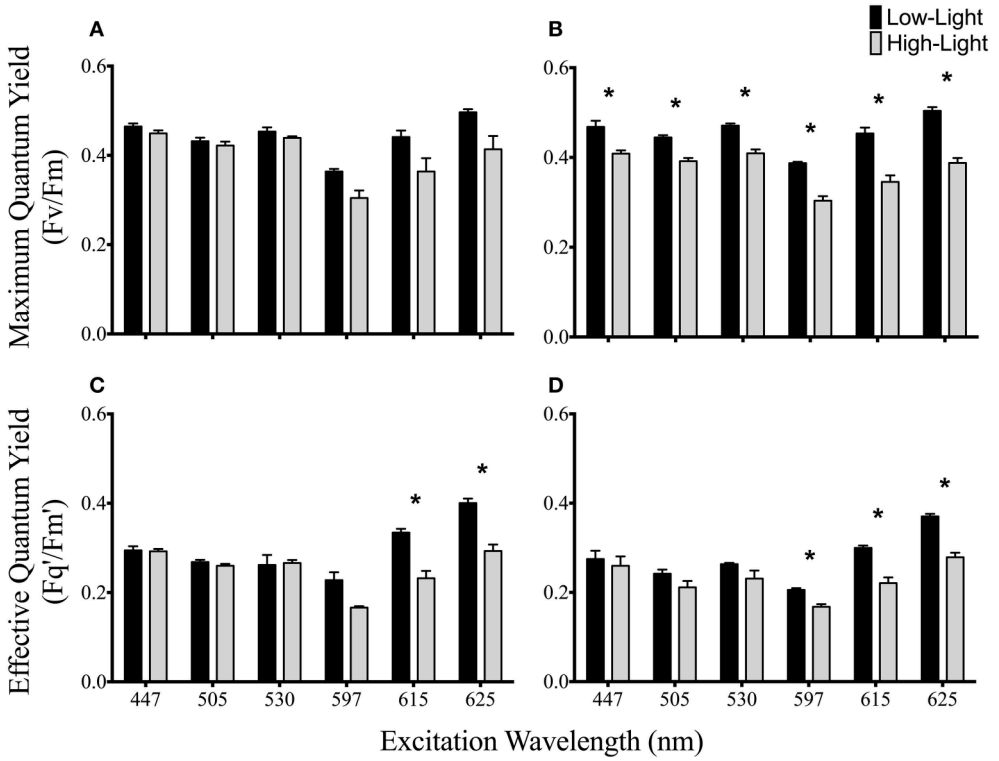

FIGURE 3 | Spectrally dependent maximum and effective quantum yields of PSII photochemistry in anemones photoacclimated to two light levels. Maximum quantum yields for high and low light acclimated **(A)** A4-a and **(B)** B1-a symbiont strains. High and low light acclimated effective quantum yields for **(C)** A4-a and **(D)** B1-a symbiont types. Dark bars represent low-light and gray bars represent high-light acclimated anemones. Error bars represent ±SE. Asterisks represent significant differences between low and high light conditions.

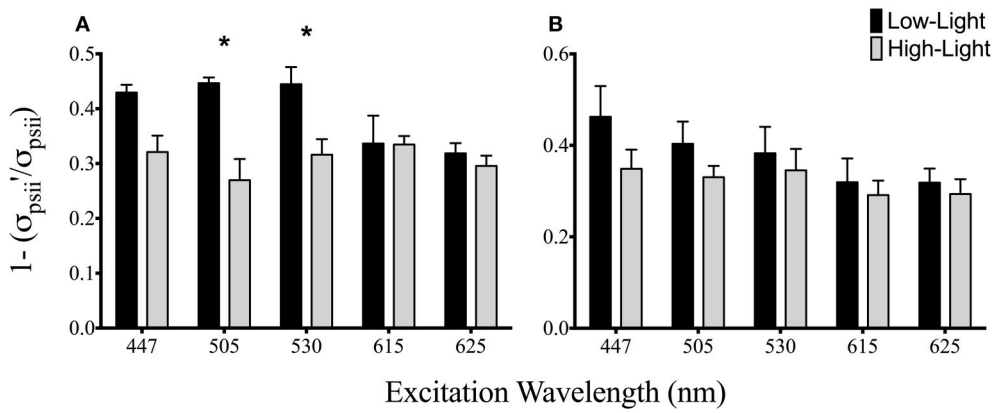

FIGURE 4 | Spectrally dependent antennae bed non-photochemical quenching for A4-a **(A)** and B1-a *Symbiodinium* **(B)**. Bars represent the mean and ±SE for (black) low and (gray) high light acclimated samples. Asterisks represent significant differences between low and high light conditions.

non-photochemical quenching in the antennae bed for the B1-a symbiont (**Figure 4B**). Excitation wavelength 597 nm was excluded from **Figure 4** as antennae bed quenching was very low as the wavelength has limited overlap with any major photopigments (Iglesias-Prieto et al., 1991; Iglesias-Prieto and Trench, 1997a).

Absorption Spectra and Instrument Comparison

There were no differences between absorption spectra of high and low light acclimated anemones harboring the B1-a strain (**Figure 5B**). However, differences were observed for the A4-a strain, where absorption was significantly lower (57%)

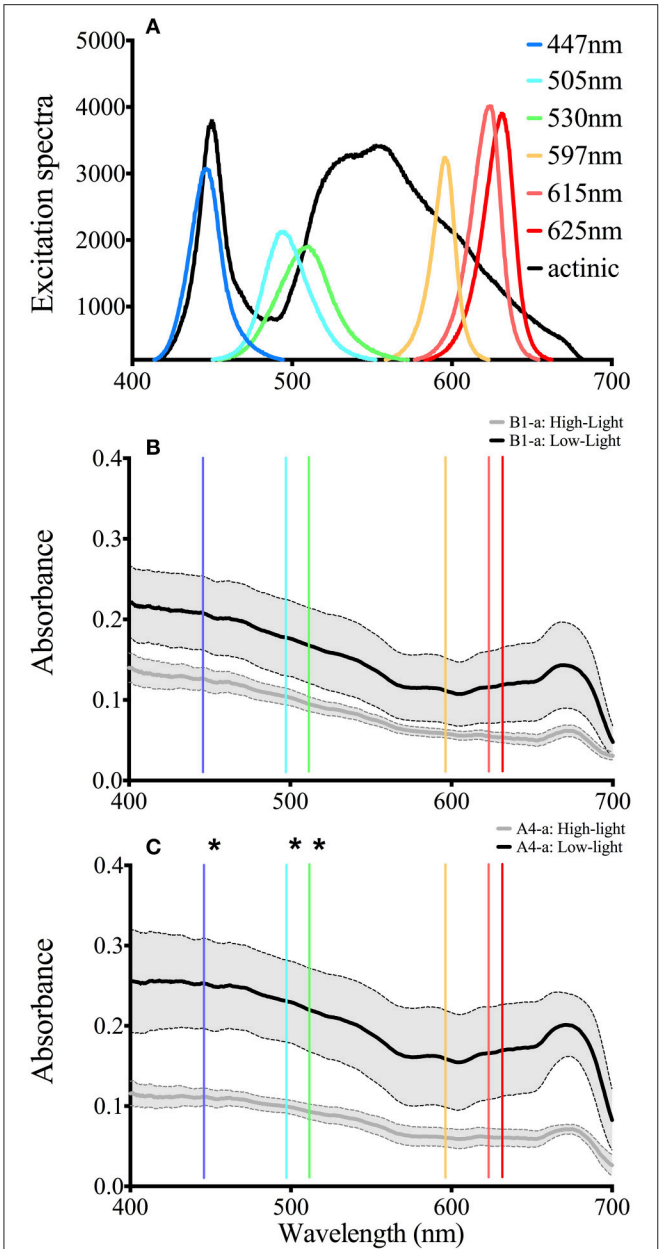

FIGURE 5 | LED output and whole anemone absorption Spectra. **(A)** Spectral characteristics for all six LED as well as the actinic light source. **(B)** Absorption spectra for the B1 symbiont under low (black) and high (gray) light conditions. **(C)** Absorption spectra for the B1 symbiont under low (black) and high (gray) light conditions. The solid line represents the average value and the gray area bounded by the dotted lines represent the standard deviation. Asterisks represent significant differences between low and high light conditions at the specific wavelengths.

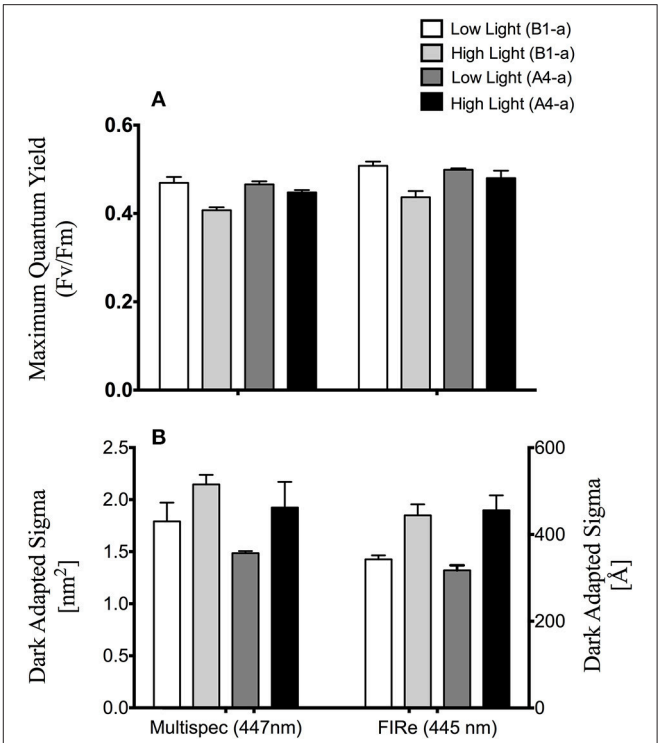

FIGURE 6 | Comparison of open source and FIRe fluorometers. **(A)** Average maximum quantum yield of PSII (Fv/Fm) and **(B)** functional absorption cross section of PSII (σ_{PSII}). Left and right axes reflect σ_{PSII} units for the open-sourced and FIRe fluorometers respectively. Error bars represent ±SE.

at 447, 498, and 513 nm in high light acclimated animals (**Figure 5C**). When comparing the open-source instrument to the commercially produced FIRe fluorometer, similar absolute values, along with a significant reduction in Fv/Fm in response to high light was noted with both devices ($P = 0.0033$ and $P = 0.0057$, respectively; **Figure 6A**). However, using the open-sourced fluorometer, an interactive effect between symbiont type and light was also found ($P = 0.041$) as high-light reductions in Fv/Fm were only significant for the B1-a strain (**Figure 6A**). Although PSII functional absorption cross section is calculated in different units, both instruments detected similar total responses to high light acclimation where σ_{PSII} was significantly higher under high light acclimation ($P = 0.0007$ for FIRe and $P = 0.0289$ for open-sourced (**Figure 6B**).

Symbiont Cell Density, Volume, and Chlorophyll Content

Under low light conditions, cell density was 49–57% higher in B1-b as compared to the other symbiont strains ($P = 0.0099$). No significant differences in chlorophyll cell^{-1} were observed across symbiont strains. However, symbiont strain B1-a had 49–76% higher cell volume ($P = 0.0066$) (**Table 2**) than the other three symbiont types. With respect to high-light acclimation, a two-way ANOVA revealed an interactive effect between light and symbiont type as B1-a cell volume significantly decreased by 28% under high light conditions, were as the A4-a symbiont did not change ($P = 0.0216$). Only chlorophyll content significantly declined by 73 and 59% under high light ($P = 0.0132$) within B1-a and A4-a symbiont strains, respectively (**Table 2**).

TABLE 2 | Symbiont physiology.

Symbiont type	Light level	Cell density (μg host protein^{-1})	Cell volume (μm^{-3})	Chlorophyll (pg cell^{-1})
B1-b	Low	3453 ± 397	394 ± 34	5.18 ± 0.7
A4-b	Low	2226 ± 104	466 ± 39	4.44 ± 0.6
B1-a	Low	2196 ± 129	694 ± 63	4.17 ± 0.8
A4-a	Low	2317 ± 237	452 ± 51	4.10 ± 1.4
B1-a	High	2019 ± 125	502 ± 58	1.14 ± 0.5
A4-a	High	2070 ± 353	470 ± 21	1.69 ± 0.2

DISCUSSION

Our results demonstrate wavelength dependent responses in both effective quantum yield and the functional absorption cross section of PSII across different symbionts. *Symbiodinium* have two major light harvesting complexes, the membrane bound Chla a-Chla C_2-peridinin-protein-complex (acpPC) and the soluble Peridinin-Chlorophyll Protein (PCP) complex, both of which absorb light predominantly between 400 and 550 nm (Iglesias-Prieto et al., 1991, 1993; Niedzwiedzki et al., 2013, 2014). Importantly, Iglesias-Prieto and Trench (1997b) demonstrated how the relative abundance of these different light harvesting compounds could vary across symbiont types growing in culture and/or with respect to high vs. low light acclimation. This was further refined by Hennige et al. (2009) whom used high performance liquid chromatography (HPLC) to compare the relative photopigment concentrations across eight different symbiont types. Such differences may give rise to the spectrally dependent differences across algal species observed here (**Figure 2**). Data from this study largely agree with previous work that used a commercially available multi-spectral pulse amplitude modulation (PAM) fluorometer with a symbiotic coral, that also documented clear wavelength dependencies in *Symbiodinium* photochemical activity (Szabó et al., 2014). In particular, the A4-b (strain: KLAp2) symbiont displayed a higher absolute PSII functional absorption cross section in the light activated state ($\sigma_{PSII'}$) relative to the other symbiotic algae, and similar to the results of Szabó et al. (2014) (albeit in their dark acclimated samples), higher ($\sigma_{PSII'}$) in lower excitation wavelengths (447–530 nm) which then decreased toward red excitation (**Figure 2A**). In contrast, the light acclimated PSII absorption cross section of the A4-a symbiont steadily decreased as excitation light moved from the blue to the red spectrum. Because the photopigments diadinoxanthin and peridinin have peak absorbance values near 505 and 530 nm, respectively, such divisions in $\sigma_{PSII'}$ could be driven by different levels of Chl *a*:diadinoxanthin or Chl *a*:peridinin ratios as well as light harvesting protein content. The decline in functional absorption cross section toward the red excitation spectrum is also naturally due to lower light harvesting complex absorption in the higher wavelength range. In corals, this also correlates to a higher scalar irradiance at higher wavelengths (Wangpraseurt et al., 2012), however, it is not known if a similar irradiance pattern exists in a symbiotic sea anemone that lacks a calcium carbonate skeleton.

The significant drop in chlorophyll *a* concentration in the high light acclimated A4-a and B1-a symbionts is a common photoacclimation response which significantly decrease the amount of light captured by the cell, thereby reducing the potential for excess excitation energy under high irradiance levels. Photoacclimation in *Symbiodinium* has been documented among a number of different species and the overall response is well-understood (Iglesias-Prieto and Trench, 1994, 1997b; Hennige et al., 2009; Finney et al., 2010). Similar to that observed during stress conditions, total organism absorbance may also decline, as symbionts reduce the amount of light that is absorbed and channeled toward photosynthesis (Rodriguez-Román et al., 2006; Hoadley et al., 2016). Although absorbance decreased in the high light acclimated anemones harboring the A4-a alga, there was no significant change in absorbance between the two acclimation light levels for the anemones harboring the B1-a symbiont. Despite the decline in Chl *a* cell^{-1} in the high light acclimated B1-a, this lower absorption difference may have been due, in part, to the alga cell size which also declined during high light acclimation, thus chlorophyll cellular volume^{-1} and pigment packaging may have remained similar across the two light levels.

Interestingly, acclimation to high light conditions reduced Fq′/Fm′ in both symbiont types, but only when excited with red spectrum (597–625 nm) wavelengths. Because photoprotective pigments such as xanthophylls do not absorb at these wavelengths, it is possible that the observed reductions in Fq′/Fm′ are indicative of decoupling between PSII reaction centers and light harvesting proteins. Apart from this reduction in Fq′/Fm′, the two holobionts showed marked photochemical differences in their patterns of photoacclimation, as the B1-a alga displayed a consistent down-regulation of functional PSII reaction centers (i.e., significant decline in Fv/Fm) (**Figure 3B**), while the A4-a symbiont reduced overall absorbance more and displayed a reduction in antennae-based non-photochemical quenching (**Figure 4A**) while Fv/Fm remained stable (**Figure 3A**). Under high light acclimation, microalgae tend to increase photo-protective mechanisms such as antennae-based non-photochemical quenching (Suggett et al., 2007). The reductions in non-photochemical quenching within the antennae bed observed for A4-a may possibly reflect a difference in optics associated with living inside the host anemone as opposed to free-living as is the case for most microalgal light acclimation studies. Coral tissues contain numerous fluorescent proteins which can substantially change the perceived light field for *in situ* symbionts (Dove, 2004). These host derived proteins may also differ across light and temperature gradients thus potentially also influencing symbiont response to elevated light conditions (Salih et al., 2000). Current efforts in understanding the miroenvironments in which *Symbiodinium* live (Wangpraseurt et al., 2012; Lichtenberg et al., 2016) are critical for improving our knowledge of coral/algal photoprotective mechanisms.

To ground-truth our fluorometer, we compared measurements of the same samples against a single excitation (peak 447 nm) Fluorescence Induction and Relaxation (FIRe) fluorometer (Satlantic Inc.). Both systems reported similar Fv/Fm values and overall trends in response to low and high light

acclimation (**Figure 6**). Likewise, a similar response in functional absorption cross section was noted for both instruments, as high light acclimation led to elevated σ_{PSII} values. The slight reduction in Fv/Fm in the B1-a alga under high light acclimation noted with both systems is consistent with previously published work with most cultured *Symbiodinium* and reef corals (Lesser and Gorbunov, 2001; Hennige et al., 2009), however, the rise in σ_{PSII} under high light is not as common, and σ_{PSII} in cultured *Symbiodinium* tend to decrease slightly under high light (see Hennige et al., 2009 for one exception to this in a cultured F2 alga).

It is interesting to note that while the symbiont-anemone combinations used in this study contained a similar symbiont density and Chl. *a* algal cell^{-1} (**Table 2**), multispectral active chlorophyll fluorescence revealed clear differences in symbiont photochemical efficiency that would be missed by a conventional fluorometer using a single wavelength band excitation light source. Importantly, symbiont density was normalized to the quantity of total soluble animal protein, and this does not account for possible structural differences between these two anemone populations, symbiont distributions across anemone location (e.g., tentacles vs. oral disc), or light absorbing animal pigments, all of which could significantly alter the photosynthetically usable radiation (PUR) in these animals further.

Different algal populations were separated by their light acclimated photochemical patterns (**Figure 2C**), but were not resolvable from dark acclimated samples alone (not shown). Spectrally dependent differences in algal photochemistry can not only provide more detail of photochemical differences within a single symbiosis, and also may potentially be a powerful tool for resolving genetically (and functionally) different *Symbiodinium* populations across diverse cnidarian hosts, including reef building corals. These results, while limited in scope, are similar to those of a more extensive study by Suggett et al. (2015) that examined 18 genetically distinct cultured *Symbiodinium* isolates with a single waveband excitation (peak excitation, 450 nm) fast repetition rate fluorometer. Specifically, that work noted that different phylotypes of *Symbiodinium* could be grouped into particular clusters based on the balance of how symbionts used the fraction of open PSII reaction centers (i.e., photochemical quenching or [1-*C*] vs. non-photochemical quenching [1-*Q*]).

There is a growing interest in the field of plant biology to better characterize genomic expression by characterizing specific phenotypic traits in a given environment, also known as phenomics (Furbank and Tester, 2011). Similar to the desire to link genomics to plant function and favorable agricultural traits, there is a growing need to characterize specific physiological traits of symbiotic reef building corals to their environment (Madin et al., 2016; Warner and Suggett, 2016). Active chlorophyll fluorescence is one such tool that has the potential to allow for rapid high throughput screening of photochemical response to different environmental conditions.

This work suggests that low-cost multispectral chlorophyll *a* fluorescence may prove useful in delineating functional traits as well as groups of different symbionts. Open source hardware and software platforms are becoming increasingly popular within the research community as their ease of use and low cost promotes high levels of customization for specific applications and a broad user base that reaches beyond traditional academic research. For example, the MultspeQ is a recently developed fluorometer designed to promote greater utilization across both scientific and community users interested in assessing terrestrial plant physiological responses via a phenomics-based approach (Kuhlgert et al., 2016). By utilizing chlorophyll fluorescence and absorbance based parameters, it is designed to provide a common platform to compare the photochemical traits of plant species worldwide. This device is relatively low cost, in part, due to the utilization and promotion of open access hardware and software platforms. The advantage of a greater user base also allows for higher level interpretation and analysis of the collected data. Although this current study does not offer a fully developed product for other users, it serves as an example of the type of research that can be achieved through the integration of open source platforms with specific research questions in mind and relatively inexpensive hardware. As more advanced hardware platforms adopt the open source concept, it is possible that even more sophisticated and low-cost instrumentation will become more accessible to a larger community of scientific and public community users interested in monitoring the physiological stability of algal-invertebrate symbioses as well.

In conclusion, spectrally dependent characteristics of symbiont photochemistry were effectively quantified using a multispectral chlorophyll-*a* fluorometer. It is likely that the spectrally dependent characteristics observed here correlate with differences in photopigment abundance across symbiont types as has been previously shown using immunoblot and HPLC analyses (Iglesias-Prieto et al., 1991; Iglesias-Prieto and Trench, 1997b; Hennige et al., 2009). With respect to symbiont types A4-a and B1-a, spectrally resolved Fv/Fm and σ_{PSII} values revealed additional changes in response to high-light acclimation that would not be possible if using more conventional active chlorophyll-*a* fluorometers with a single excitation wavelength centered at 450 nm. Importantly, these spectrally resolved fluorescence measurements were made using a custom built fluorometer using open source hardware and software platforms. Our work serves as an example of the potential for open source platforms to be utilized to construct purpose built and relatively low-cost instruments.

AUTHOR CONTRIBUTIONS

All authors listed have made a substantial, direct and intellectual contribution to the work, and approved it for publication.

ACKNOWLEDGMENTS

This project was supported by funding from the National Science Foundation (awards 1316055 and 1258065 to MW).

REFERENCES

Baker, A. C. (2003). Flexibility and specificity in coral-algal symbiosis: diversity, ecology, and biogeography of *Symbiodinium*. *Annu. Rev. Ecol. Evol. Syst.* 34, 661–689. doi: 10.1146/annurev.ecolsys.34.011802.132417

Dove, S. (2004). Scleractinian corals with photoprotective host pigments are hypersensitive to thermal bleaching. *Mar. Ecol. Prog. Ser.* 272, 99–116. doi: 10.3354/meps272099

Enríquez, S., Méndez, E. R., and Iglesias-Prieto, R. (2005). Multiple scattering on coral skeletons enhances light absorption by symbiotic algae. *Limnol. Oceanogr.* 50, 1025–1032. doi: 10.4319/lo.2005.50.4.1025

Finney, J. C., Pettay, D. T., Sampayo, E. M., Warner, M. E., Oxenford, H. A., and LaJeunesse, T. C. (2010). The relative significance of host-habitat, depth, and geography on the ecology, endemism, and speciation of coral endosymbionts in the genus *Symbiodinium*. *Microb. Ecol.* 60, 250–263. doi: 10.1007/s00248-010-9681-y

Furbank, R. T., and Tester, M. (2011). Phenomics–technologies to relieve the phenotyping bottleneck. *Trends Plant Sci.* 16, 635–644. doi: 10.1016/j.tplants.2011.09.005

Gorbunov, M. Y., Kolber, Z. S., Lesser, M., and Falkowski, P. G. (2001). Photosynthesis and photoprotection in symbiotic corals. *Limnol. Oceanogr.* 46, 75–85. doi: 10.4319/lo.2001.46.1.0075

Hawkins, T. D., Hagemeyer, J., and Warner, M. E. (2016). Temperature moderates the infectiousness of two conspecific Symbiodinium strains isolated from the same host population. *Environ. Microbiol.* 18, 5204–5217. doi: 10.1111/1462-2920.13535

Hennige, S. J., Suggett, D. J., Warner, M. E., McDougall, K. E., and Smith, D. J. (2009). Photobiology of *Symbiodinium* revisited: bio-physical and bio-optical signatures. *Coral Reefs* 28, 179–195. doi: 10.1007/s00338-008-0444-x

Hoadley, K. D., Pettay, D. T., Dodge, D., and Warner, M. E. (2016). Contrasting physiological plasticity in response to environmental stress within different cnidarians and their respective symbionts. *Coral Reefs* 35, 529–542. doi: 10.1007/s00338-016-1404-5

Hochberg, E. J., Apprill, A. M., Atkinson, M. J., and Bidigare, R. R. (2006). Bio-optical modeling of photosynthetic pigments in corals. *Coral Reefs* 25, 99–109. doi: 10.1007/s00338-005-0071-8

Iglesias-Prieto, R., Beltran, V. H., LaJeunesse, T. C., Reyes-Bonilla, H., and Thome, P. E. (2004). Different algal symbionts explain the vertical distribution of dominant reef corals in the eastern Pacific. *Proc. R. Soc. Lond. B.* 271, 1757–1763. doi: 10.1098/rspb.2004.2757

Iglesias-Prieto, R., Govind, N., and Trench, R. (1991). Apoprotein composition and spectroscopic characterization of the water- soluble peridinin-chlorophyll a-proteins from three symbiotic dinoflagellates. *Philos. Trans. R. Soc. Lond. B.* 246, 275–283. doi: 10.1098/rspb.1991.0155

Iglesias-Prieto, R., Govind, N., and Trench, R. (1993). Isolation and characterization of three membrane-bound chlorophyll-protein complexes from four dinoflagellate species. *Philos. Trans. R. Soc. Lond. B*. 340, 381–392. doi: 10.1098/rstb.1993.0080

Iglesias-Prieto, R., and Trench, R. (1994). Acclimation and adaptation to irradiance in symbiotic dinoflagellates. I. Responses of the photosynthetic unit to changes in photon flux density. *Mar. Ecol. Prog. Ser*. 113, 163–175. doi: 10.3354/meps113163

Iglesias-Prieto, R., and Trench, R. (1997a). "Photoadaptation, photoacclimation and niche diversification in invertebrate- dinoflagellate symbioses," in *Proceedings of the 8th International Coral Reef Symposium*, eds H. Lessios and I. Macintyre (Balboa: Smithsonian Tropical Research Institute), 1319–1324.

Iglesias-Prieto, R., and Trench, R. K. (1997b). Acclimation and adaptation to irradiance in symbiotic dinoflagellates. II. Response of chlorophyll-protein complexes to different photon-flux densities. *Mar. Biol.* 130, 23–33. doi: 10.1007/s002270050221

Kemp, D. W., Cook, C. B., LaJeunesse, T. C., and Brooks, W. R. (2006). A comparison of the thermal bleaching responses of the zoanthid *Palythoa caribaeorum* from three geographically different regions in south Florida. *J. Exp. Mar. Biol. Ecol.* 335, 266–276. doi: 10.1016/j.jembe.2006.03.017

Kolber, Z., and Falkowski, P. (1998). Measurements of variable chlorophyll fluorescence using fast repetition rate techniques: defining methodology and experimental protocols. *Biochim. Biophys.* 1367, 88–107. doi: 10.1016/S0005-2728(98)00135-2

Kuhlgert, S., Austic, G., and Zegarac, R. (2016). MultispeQ Beta: a tool for large-scale plant phenotyping connected to the open PhotosynQ network. *R. Soc. Open Sci.* 3:160592. doi: 10.1098/rsos.160592

LaJeunesse, T. C. (2001). Investigating the biodiversity, ecology, and phylogeny of endosymbiotic dinoflagellates in the genus *Symbiodinium* using the ITS region: in search of a "species" level marker. *J. Phycol.* 37, 866–880. doi: 10.1046/j.1529-8817.2001.01031.x

LaJeunesse, T. C., Smith, R. T., Finney, J., and Oxenford, H. (2009). Outbreak and persistence of opportunistic symbiotic dinoflagellates during the 2005 Caribbean mass coral 'bleaching' event. *Proc. R. Soc. B.* 276, 4139–4148. doi: 10.1098/rspb.2009.1405

LaJeunesse, T., and Trench, R. (2000). Biogeography of two species of Symbiodinium (Freudenthal) inhabiting the intertidal sea anemone *Anthopleura elegantissima* (Brandt). *Biol. Bull.* 199, 126–134. doi: 10.2307/1542872

Lesser, M. P., and Gorbunov, M. Y. (2001). Diurnal and bathymetric changes in chlorophyll fluorescence yields of reef corals measured *in situ* with a fast repetition rate fluorometer. *Mar. Ecol. Prog. Ser.* 212, 69–77. doi: 10.3354/meps212069

Lichtenberg, M., Larkum, A. W. D., and Kühl, M. (2016). Photosynthetic acclimation of Symbiodinium in hospite depends on vertical position in the tissue of the scleractinian coral *Montastrea curta*. *Front. Microbiol.* 7:230. doi: 10.3389/fmicb.2016.00230

Madin, J. S., Hoogenboom, M. O., and Connolly, S. R. (2016). A trait-based approach to advance coral reef science. *Trends Ecol. Evol.* 31, 419–428. doi: 10.1016/j.tree.2016.02.012

Muscatine, L. (1990). "The role of symbiotic algae in carbon and energy flux in reef corals," in *Ecosystems of the World: Coral Reefs,* ed Z. Dubinsky (Amsterdam: Elsevier), 75–87.

Muscatine, L., Falkowski, P., Porter, J., and Dubinsky, Z. (1984). Fate of photosynthetic fixed carbon in light and shade-adapted colonies of the symbiotic coral *Stylophora pistillata*. *Proc R. Soc. Lond. B*. 222, 181–202. doi: 10.1098/rspb.1984.0058

Niedzwiedzki, D. M., Jiang, J., and Lo, C. S. (2014). Spectroscopic properties of the Chlorophyll a–Chlorophyll c2–Peridinin-Protein-Complex (acpPC) from the coral symbiotic dinoflagellate Symbiodinium. *Photosyn. Res.* 120, 125–139. doi: 10.1007/s11120-013-9794-5

Niedzwiedzki, D. M., Jiang, J., Lo, C. S., and Blankenship, R. E. (2013). Low-temperature spectroscopic properties of the peridinin–chlorophyll a–protein (PCP) complex from the coral symbiotic dinoflagellate Symbiodinium. *J. Phys. Chem. B*. 117, 11091–11099. doi: 10.1021/jp401022u

Ortiz, J. C., González-Rivero, M., and Mumby, P. J. (2012). Can a thermally tolerant symbiont improve the future of Caribbean coral reefs? *Global Change Biol*. 19, 273–281. doi: 10.1111/gcb.12027

Porra, R. J., Thompson, W. A., and Kriedemann, P. E. (1989). Determination of accurate extinction coefficients and simultaneous equations for assaying chlorophylls *a* and *b* extracted with four different solvents: verification of the concentration of chlorophyll standards by atomic absorption spectroscopy. *Biochim. Biophys. Acta* 975, 384–394. doi: 10.1016/S0005-2728(89)80347-0

Rodriguez-Román, A., Hernández-Pech, X., Thome, P. E., Enriquez, S., and Iglesias-Prieto, R. (2006). Photosynthesis and light utilization in the Caribbean coral *Montastraea faveolata* recovering from a bleaching event. *Limnol. Oceanogr.* 51, 2702–2710. doi: 10.4319/lo.2006.51.6.2702

Salih, A., Larkum, A., Cox, G., Kühl, M., and Hoegh-Guldberg, O. (2000). Fluorescent pigments in corals are photoprotective. *Nature* 408, 850–853. doi: 10.1038/35048564

Silverstein, R. N., Correa, A. M. S., LaJeunesse, T. C., and Baker, A. C. (2011). Novel algal symbiont (*Symbiodinium* spp.) diversity in reef corals of Western Australia. *Mar. Ecol. Prog Ser*. 422, 63–75. doi: 10.3354/meps08934

Suggett, D. J., Goyen, S., Evenhuis, C., Szabó, M., Pettay, D. T., Warner, M. E., et al. (2015). Functional diversity of photobiological traits within the genus Symbiodinium appears to be governed by the interaction of cell size with cladal designation. *New Phytol.* 208, 370–381. doi: 10.1111/nph.13483

Suggett, D. J., Le Floc'H, E., Harris, G. N., Leonardos, N., and Geider, R. J. (2007). Different strategies of photoacclimation by two strains of *Emiliania huxleyi* (Haptophyta). *J. Phycol.* 43, 1209–1222. doi: 10.1111/j.1529-8817.2007.00406.x

Suggett, D. J., Oxborough, K., Baker, N. R., MacIntyre, H. L., Kana, T. M., and Geider, R. J. (2003). Fast repetition rate and pulse amplitude modulation

chlorophyll a fluorescence measurements for assessment of photosynthetic electron transport in marine phytoplankton. *Eur. J. Phycol.* 38, 371–384. doi: 10.1080/09670260310001612655

Sunagawa, S., Wilson, E. C., Thaler, M., Smith, M. L., Caruso, C., Pringle, J. R., et al. (2009). Generation and analysis of transcriptomic resources for a model system on the rise: the sea anemone *Aiptasia pallida* and its dinoflagellate endosymbiont. *BMC Genomics* 10:258. doi: 10.1186/1471-2164-10-258

Szabó, M., Wangpraseurt, D., and Tamburic, B. (2014). Effective light absorption and absolute electron transport rates in the coral *Pocillopora damicornis*. *Plant Physiol. Biochem.* 83, 159–167. doi: 10.1016/j.plaphy.2014.07.015

Wangpraseurt, D., Larkum, A. W. D., Ralph, P. J., and Kuhl, M. (2012). Light gradients and optical microniches in coral tissues. *Front. Microbiol.* 3:316. doi: 10.3389/fmicb.2012.00316

Wangpraseurt, D., Tamburic, B., Szabó, M., and Suggett, D. (2014). Spectral effects on Symbiodinium photobiology studied with a programmable light engine. *PLoS ONE* 9:e112809. doi: 10.1371/journal.pone.0112809

Warner, M. E., and Suggett, D. J. (2016). "The photobiology of *Symbiodinium* spp.: linking physiological diversity to the implications of stress and resilience," in *The Cnidaria, Past, Present and Future*, eds S. Goffredo and Z. Dubinsky (Cham: Springer), 489–509.

Zhang, Z., Green, B. R., and Cavalier-Smith, T. (2000). Phylogeny of ultra-rapidly evolving dinoflagellate chloroplast genes: a possible common origin for sporozoan and dinoflagellate plastids. *J. Mol. Evol.* 51, 26–40. doi: 10.1007/s002390010064

Ziegler, M., Roder, C. M., Büchel, C., and Voolstra, C. R. (2014). Limits to physiological plasticity of the coral Pocillopora verrucosa from the central Red Sea. *Coral Reefs* 33, 1115–1129. doi: 10.1007/s00338-014-1192-8

Conflict of Interest Statement: The authors declare that the research was conducted in the absence of any commercial or financial relationships that could be construed as a potential conflict of interest.

frontiers in Marine Science

ORIGINAL RESEARCH
published: 06 February 2018
doi: 10.3389/fmars.2018.00011

Trade-Offs Associated with Photoprotective Green Fluorescent Protein Expression as Potential Drivers of Balancing Selection for Color Polymorphism in Reef Corals

Cathryn Quick[1], *Cecilia D'Angelo*[1,2] *and Jörg Wiedenmann*[1,2]*

[1] *Coral Reef Laboratory, Ocean and Earth Science, University of Southampton, Southampton, United Kingdom,* [2] *Institute for Life Sciences, University of Southampton, Southampton, United Kingdom*

OPEN ACCESS

Edited by:
Daniel Wangpraseurt, University of Cambridge, United Kingdom

Reviewed by:
Anya Salih, Western Sydney University, Australia
Anthony William Larkum, University of Technology Sydney, Australia
Aldo Cróquer, Simón Bolívar University, Venezuela

***Correspondence:**
Jörg Wiedenmann
joerg.wiedenmann@noc.soton.ac.uk

Specialty section:
This article was submitted to Coral Reef Research, a section of the journal Frontiers in Marine Science

Received: *12 April 2017*
Accepted: *16 January 2018*
Published: *06 February 2018*

Citation:
Quick C, D'Angelo C and Wiedenmann J (2018) Trade-Offs Associated with Photoprotective Green Fluorescent Protein Expression as Potential Drivers of Balancing Selection for Color Polymorphism in Reef Corals. Front. Mar. Sci. 5:11. doi: 10.3389/fmars.2018.00011

Photodamage of symbiotic algae exposed to thermal stress is involved in mass coral bleaching, a major cause of reef decline. Photoprotection is therefore a vital part of coral stress physiology. Corals produce a variety of green fluorescent protein (GFP)-like proteins, some of which screen the symbiotic algae from excess sun light. Different tissue concentrations of these GFP-like proteins distinguish color morphs that are characteristic for many coral species. The question arises whether these pigmentation differences may diversify the niches that can be occupied by corals along the steep light gradient that structures coral reef communities. We assessed the implications of GFP-like protein expression in two color morphs of the symbiotic coral *Hydnophora grandis,* both associated with the same *Symbiodinium* sp. (subclade C40). The color morphs of this species (high fluorescent, HF; and low fluorescent, LF), characterized by markedly different contents of a cyan fluorescent protein, were exposed to different quantities of blue light (470 nm) that matched the major absorption band of the host pigment (473 nm). High intensities of blue light caused less photodamage to the symbiotic algae of the HF morph and resulted in higher growth rates of these corals compared to representatives of the LF morph. In contrast, under low intensities of blue light, the HF morph showed lower growth rates than the LF morph, indicating that trade-offs are associated with high levels of fluorescent protein expression under this condition. Both morphs showed highest growth rates at medium light intensities with no obvious influence of the tissue pigmentation. Reef coral color polymorphism caused by photoprotective GFP-like proteins may therefore be a product of balancing selection in which high pigment contents may be beneficial at the upper and detrimental at the lower end of the depth distribution range of symbiotic corals. Conversely, color morphs with GFP-like proteins that function to optimize symbiont photosynthesis in low light environments could gain an advantage from the benefits offered by high pigment levels in deeper waters.

Keywords: coral color, green fluorescent protein, photoprotection, color polymorphism, balancing selection, light stress, coral bleaching

INTRODUCTION

Elevated sea water temperatures are a major cause of mass bleaching events and associated coral mortality (Hoegh-Guldberg, 1999; Hughes et al., 2017). Heat stress inhibits the repair of photosystem II (Takahashi et al., 2009) and lowers the photoinhibitory threshold of the symbiotic algae (Jones et al., 1998; Warner et al., 1999; Bhagooli and Hidaka, 2003; Takahashi et al., 2009), thereby facilitating light-induced damage to Photosystem II reaction centers, particularly the D1 protein (Aro et al., 1993). The resulting faults in energy transfer and electron transport can lead to oxidative stress (reviewed by Pospíšil, 2016) that can cause the breakdown of the symbiotic association and loss of algal cells from the coral tissue (Lesser, 1997; Rehman et al., 2016). The susceptibility of corals to heat and light stress-induced bleaching is increased by unfavorable levels of nutrients in the water, in particular by phosphate deficiency (D'Angelo and Wiedenmann, 2014; Rosset et al., 2017). Bleached corals die unless the symbiont population recovers (Glynn et al., 2001; Baker et al., 2008). Corals and zooxanthellae have therefore evolved protective mechanisms to reduce the impact of light stress. In zooxanthellae, these mechanisms include: xanthophyll cycling (Ambarsari et al., 1997), the use of alternative electron pathways (Reynolds et al., 2008); and the downregulation of photosystem II reaction centers (Gorbunov et al., 2001). Both corals and zooxanthellae produce antioxidant enzymes (Lesser, 2006; Levy et al., 2006) and mycosporine-like amino acids (Banaszak et al., 2000; Shick, 2004; Starcevic et al., 2010) that help to protect the organisms from the negative impact of high light intensities.

A photoprotective function has been also assigned to fluorescent pigments that are often produced by corals and other cnidarians (Wiedenmann et al., 1999; Salih et al., 2000). These pigments belong to the family of GFP-like proteins (Matz et al., 1999; Dove et al., 2001; Alieva et al., 2008). Based on their optical properties they can be divided into fluorescent proteins (FPs) and non-fluorescent chromo-proteins (CPs), noting that CPs are the product of multiple parallel evolution (Gittins et al., 2015). GFP-like proteins can contribute up to ∼7–14% to the soluble cellular proteins in coral tissues (Leutenegger et al., 2007; Oswald et al., 2007) suggesting that they fulfill a significant function within the host. Experimental studies have confirmed that CPs (Smith et al., 2013) as well as green and red FPs (Salih et al., 2000; Gittins et al., 2015) in shallow water corals can exert a photoprotective function by screening the algal symbionts from excess light. However, this function may not always be evident (Dove et al., 1995; Mazel et al., 2003). High levels of fluorescent proteins also occur in mesophotic corals (Eyal et al., 2015; Roth et al., 2015) and other deep-water cnidarians (Vogt et al., 2008), suggesting that these pigments can have functions other than photoprotection. In low light conditions, for example, coral GFP-like proteins have been suggested to enhance light availability for photosynthesis of the algal symbionts (Salih et al., 2000; Eyal et al., 2015; Lyndby et al., 2016). Indeed, recent studies have demonstrated that Förster Resonance Energy Transfer (FRET)-mediated wavelength conversion by orange-red fluorescent proteins promotes the light penetration in symbiont-containing tissue in corals from blue-light dominated deep water habitats (Bollati et al., 2017; Smith et al., 2017).

Among FPs, four color groups have been identified: cyan, green, yellow, and red (Alieva et al., 2008; Nienhaus and Wiedenmann, 2009). In contrast to yellow FPs that are rarely encountered in reef organisms (Alieva et al., 2008), red fluorescent proteins are fairly common. Based on the biochemistry of the chromophore and distinct spectral features, red FPs can be divided into a group in which the red chromophore is formed in an autocatalytic reaction (Matz et al., 1999; Wiedenmann et al., 2002) and a group in which the chromophore is formed by photoconversion of a green precursor (Ando et al., 2002; Wiedenmann et al., 2004; Oswald et al., 2007). The latter optimize the internal light environment for the symbionts in corals from less light exposed habitats (Smith et al., 2017) whereas members of the first group can be found in shallow water corals where they exert a photoprotective function similar to CPs (Smith et al., 2013; Gittins et al., 2015). Cyan and green fluorescent proteins (GFPs) can be frequently encountered in most reef environments (Salih et al., 2000; Eyal et al., 2015; Roth et al., 2015) and representatives of this color group have also been shown to be photoprotective in shallow water corals (Salih et al., 2000). Cyan fluorescent proteins (CFPs) contain the same chromophore as GFPs (Henderson and Remington, 2005) but have characteristically broad absorption/excitation spectra with peaks at 440–460 nm (Alieva et al., 2008) that overlap with the absorption / excitation spectrum of photosynthetic pigments of the symbiotic algae (Smith et al., 2013). CFPs with emission maxima around 485–495 nm have evolved as a product of positive natural selection (Field et al., 2006) and are therefore recognized as a separate color class (Alieva et al., 2008). Their production in corals is often regulated by the intensities of blue light (D'Angelo et al., 2008).

Many coral species exhibit color polymorphisms caused by stable differences in CP and FP expression (Kelmanson and Matz, 2003; Klueter et al., 2006; Oswald et al., 2007; Gittins et al., 2015). In *Acropora millepora*, the pigment concentration in the tissue of different morphs is strongly correlated with the number of gene copies with a particular promoter type, indicating that color polymorphism in reef corals is caused by the differential expression of multicopy genes (Gittins et al., 2015). We have proposed that the balancing selection driving the evolution of color morphs could be due to the benefits from photoprotection offered by the pigments in niches with high levels of light stress and the trade-offs associated with the productions of large quantities of pigments in the absence of light stress (Gittins et al., 2015). Such a balancing selection may allow different color morphs to persist within a population and increase the range of niches that can be occupied by a species across the steep light gradient that structures coral reef communities. However, at present it is unknown whether measurable trade-offs are associated with the expression of photoprotective FPs. On the one hand, no other enzymes and co-factors are required for the pigment production and the proteins have a slow turnover with a half-life of ∼20 days, suggesting the energetic costs for their production could be relatively low (Leutenegger et al., 2007). On the other hand, a high-level expression of at least eight FP gene

copies is required to accumulate pigment concentrations in the tissue that are sufficiently high to fulfill a light screening function (Gittins et al., 2015). Therefore, we have assessed whether the expression of a photoprotective FP in *Hydnophora grandis* is associated with trade-offs that manifest in changes of growth rates in different light environments. The two color morphs of choice were associated with the same *Symbiodinium* sp. (C40), but differed markedly in their expression of CFPs (D'Angelo et al., 2008). The capacity of the CFPs to exert a photoprotective function by selective screening of symbionts in the blue spectral range was assessed by exposing the corals to either blue or orange-red light. Orange-red light was chosen for the control treatment as it is not absorbed by the CFPs and should therefore negatively affect both the high and low fluorescent morphs due to the detrimental effect of this waveband on algal photosynthesis (Smith et al., 2013; Wijgerde et al., 2014).

We predicted that the CFP plays a photoprotective role in *H. grandis* and that therefore the high fluorescent (HF) color morph would show a higher growth rate than the low fluorescent (LF) color morph under high intensities of blue light. We also predicted that removal of essential photons by CFP under low intensities of blue light together with the energetic cost of their high level production would cause the HF morph grow at a slower rate than the LF morph.

MATERIALS AND METHODS

Origin and Maintenance of Corals

The experimental corals, produced in aquaculture at Fiji, were obtained via Tropical Marine Centre London. Corals were cultured in the experimental mesocosm of the Coral Reef Laboratory at the University of Southampton (D'Angelo and Wiedenmann, 2012) and propagated by fragmentation for >5 years before the start of the experiments. Hence, the corals were fully acclimated to the conditions in the experimental aquarium. While the being genetically homogeneous, replicate colonies within each color morph represent independent units with individual life histories.

Identification of Algal Symbionts

The *Symbiodinium* present in each color morph of *H. grandis* were identified to the subclade level by analyzing the ITS2 region of genomic DNA samples from each color morph. A modified CTAB type extraction was carried out (D'Angelo et al., 2015). The region spanning the 18S, ITS1, 5.8S, ITS2, 28S region of the *Symbiodinium* spp. ribosomal DNA was amplified by performing a PCR using the primers SYM-VAR-FWD, and SYM-VAR-REV (Hume et al., 2013).

Amplification was accomplished in the presence of 2 μl of 50 × dNTP mix, 1 μl of each primer, 1 μl of template DNA, 0.5 μl of Advantage 2 polymerase mix (Clontech), 5 μl of 10 x Advantage 2 PCR buffer, and 40 μl PCR grade water. The PCR encompassed an initial denaturation step of 1 min at 95°C, followed by 30 cycles of denaturation (95°C for 30 s), annealing (62°C for 30 s), and elongation (68°C for 30 s). A final elongation step of 5 min at 70°C performed. The PCR products were then cloned as describes in the StrataClone PCR Cloning Kit protocol. Plasmid DNA was prepared from 10 *Escherichia coli* colonies using a ThermoScientific GeneJET Plasmid Miniprep Kit. Sequencing services were provided by Eurofins MWG.

The ITS2 region of the PCR fragment was isolated using reference sequences available in Genbank using the BLAST tool (www.ncbi.nlm.nih.gov/blast). The software package Geneious was used to visualize the vector sequences. The ITS2 regions of the 10 samples were then compared to reference sequences available in Genbank.

Light Exposure Experiments

Coral growth and changes in CFP concentration were assessed in three experiments set up in different flow-through compartments of our experimental mesocosm system (D'Angelo and Wiedenmann, 2012). Five replicate colonies of each color morph were used per condition. All experimental tanks were connected to the same recirculating water system (D'Angelo and Wiedenmann, 2012). Replete levels of dissolved inorganic nutrients were used since imbalanced nutrient levels or low phosphate concentrations can significantly increase the susceptibility of symbiotic corals to light stress (D'Angelo and Wiedenmann, 2014; Rosset et al., 2015, 2017). The water temperature was kept constant at ∼25°C. Prior to the start of the light exposure experiments, the corals were cultured under white metal halide light (Aqualine 10000) at a photon flux of 250 μmol photons $m^{-2}s^{-1}$ on a 10:14 h light:dark cycle. LED stripes (Reef Blue, Aquaray, Tropical Marine Centre London) with controllable output were used to expose the corals to narrow-banded blue light (∼470 nm) that matches the excitation spectrum of the coral CFPs (**Figure 1C**). Colonies were acclimated for 3 weeks to the experimental light condition by changing the light intensities of blue LEDs gradually from ∼150 μmol photons $m^{-2}s^{-1}$ to reach final photon fluxes of 1,100 μmol $m^{-2}s^{-1}$ (high light treatment), 300 μmol $m^{-2}s^{-1}$ medium light treatment), and 10 μmol $m^{-2}s^{-1}$ (low light treatment). Light intensity was measured using a LI-COR LI-250A Light Meter directly at the water surface level, situated ∼3 cm above the coral colonies. The height of the LEDs above the water surface was adjusted until the desired light intensity was reached. The weight of the replicate colonies was determined after a 30 s drip-off step on absorbing tissue to remove excess water. Quantitative fluorescence data of the colonies were measured every 2–3 weeks (D'Angelo et al., 2008) using a Varian Cary Eclipse fluorescence spectrophotometer for recording of spectra in the range of 250–510 nm with the emission wavelength set to 540 nm (slit-width 5; scan speed medium). For imaging purposes, coral fluorescence was excited by ∼470 nm light provided by the Aquaray Reef Blue LEDS, which closely matches to the absorption maximum of CFPs. Photographs were taken with a Olympus Tough camera (Olympus Corporation, Tokyo, Japan) equipped with a yellow long-pass filter (Nightsea, Andover, USA) to block reflected excitation light. Due to the optical properties of the filter, only the green portion of light emitted by the CFPs is detected by the camera and, accordingly, the corals in the photographs appear green. Since the corals under study contain only CFPs, these images nevertheless give a truthful representation of intensity of cyan tissue fluorescence.

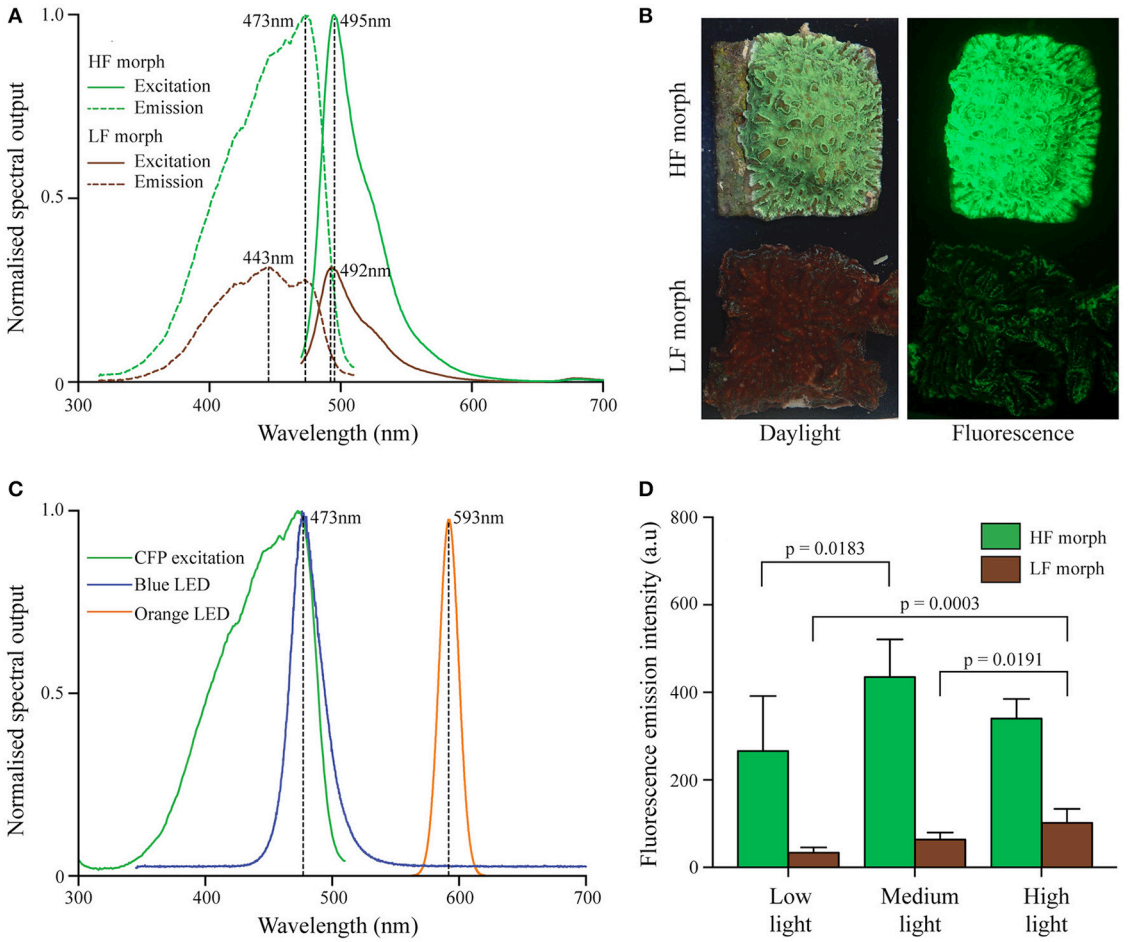

FIGURE 1 | (A) Excitation and emission spectra of two color morphs of *Hydnophora grandis*. Peak maxima indicated by dashed vertical lines with peak wavelengths (nm) being indicated. Excitation spectra are scaled to the maximum of the corresponding emission spectra. **(B)** Photographs of representative colonies of HF (top) and LF (bottom) morphs under daylight (left) and blue light excitation (~470 nm; imaged with a yellow long-pass filter) (right). **(C)** Emission spectra of blue LED (blue line) and orange LED (orange line) used in aquarium experiments. The CFP excitation spectrum of the HF morph is included for comparison (green line). **(D)** Fluorescence emission intensity (measured at the peak wavelength) of both morphs at the end of each experiment under low (10 μmol photons m^{-2} s^{-1}), medium (300 μmol photons $m^{-2}s^{-1}$), and high (1,100 μmol photons $m^{-2}s^{-1}$) intensities of blue light. Bars display mean values of 5 colonies. Error bars show standard deviation. Brackets above two bars indicate *p*-values for statistically significant ($p < 0.05$) differences between the fluorescence emission intensity of each morph at the end of each treatment, determined by one-way ANOVAs.

To measure photodamage of the coral symbionts, three colonies of each morph were placed either under 2,000 μmol photons $m^{-2}s^{-1}$ of blue light (~470 nm) provided by Aquaray Reef Blue LEDs or under the same photofluxes of orange light (~595 nm) produced by P4 Amber Star LEDs (Seoul Semiconductor, Korea, Smith et al., 2013). Light intensity was measured and adjusted as described above. The colonies were kept under blue light for 2 months and under orange light for 6 days. The maximum quantum yield (Fv/Fm) of the algal symbionts was measured using a Waltz Diving PAM as an indicator of photodamage (Warner et al., 1999). Measurements were taken after 14 h of darkness and colonies were exposed to the minimal light levels during measurements to minimize the effects of chlororespiration (Warner et al., 2010). Dark adapted Fv/Fm was used as an indicator of the efficiency of Photosystem II (Krause and Weis, 1991), and the degree of photodamage suffered by the zooxanthellae (Genty et al., 1989; Warner et al., 1999). A precision hole saw was used to remove circular tissue samples of identical size from the center of the treated area of the flat replicate colonies or from control regions in the periphery of the same corals. The tissue samples were homogenized in sterile seawater and zooxanthellae were isolated by differential centrifugation (1,000 g/10 min). After a wash step in sterile seawater, the algal cells were recovered by centrifugation, resuspended and their numbers were determined using a hemocytometer. Zooxanthellae numbers were then normalized to the surface of the cut-out samples.

Statistical Analysis

Coral growth and fluorescence intensity data were plotted and analyzed using GraphPad Prism 7. Paired *t*-tests were used to analyse weight data at the end of each experiment.

The significance of the differences in fluorescence emission intensity between the two morphs under all light treatments were calculated with a fully orthogonal two-way ANOVA with fixed effects, followed by a Tukey's multiple comparison test. The significance of the differences in the fluorescence emission intensity of each morph at the end of each experiment were calculated with one-way ANOVAs, followed by Tukey's multiple comparison tests.

Fv/Fm data were plotted in GraphPad Prism 7. Data was log transformed prior to generation of linear models using R.

Zooxanthellae numbers from coral tissue samples were plotted and analyzed using GraphPad Prism 7. Unpaired *t*-tests were used to calculate the significance of the differences in zooxanthellae numbers from tissue samples of treated and untreated areas of tissue in both morphs after exposure to high intensities of blue and orange light.

RESULTS

Characterization of the Color Morphs

The sequences of the ITS2 region isolated from both color morphs under study matched those of *Symbiodinium* C40a and C40b (GenBank accession numbers AY589747 and AY589748), indicating that the symbiont complement of both color morphs is dominated by the same *Symbiodinium* sp.

Both morphs contained CFPs, with a broad excitation spectrum ranging from ∼350–500 nm with maxima at ∼420, 443, and 473 nm (**Figures 1A,B**). Emission spectra peaked at ∼492 nm (LF morph) and ∼495 nm (HF morph), respectively. In colonies growing side by side under a photon flux of ∼250 μmol photons $m^{-2}s^{-1}$ of white light illumination prior to the start of the experiment, the cyan fluorescence of the high fluorescent (HF) morph was approximately ∼3.1-fold more intense compared to the low fluorescent (LF) morph (**Figure 1A**). The fluorescence maxima of each morph remained essentially unaltered throughout the light treatment experiment, while the intensity of the fluorescence emission changed under the different treatments (**Figure 1D**). The HF morph remained more fluorescent than the LF morph in all conditions, but the ratio (HF/LF) of the peak fluorescence emission intensity between the morphs ranged from ∼8.0 (low light), ∼6.9 (medium light), to ∼3.4 (high light). Highest tissue fluorescence was shown at medium light (HF morph) and high light conditions (LF morph). Fluorescence in low light treated corals reached only ∼30% (LF morph) to ∼60% (HF morph) of these maximal values. A two-way ANOVA showed that the HF morph was significantly more fluorescent than the LF morph under all light condition ($p < 0.001$), but that there was a significant interaction between the light intensity and color morph ($p = 0.0255$). A one-way ANOVA showed significant differences in fluorescence of the LF morph between low and high, as well as medium and high light intensities ($p = 0.0003$ and $p = 0.0191$ respectively). Compared to the low light treatment, the fluorescence of the HF morph also increased significantly under medium light intensities ($p = 0.0183$) (**Figure 1D**).

Photodamage under Intense Blue and Orange Light

The efficiency of algal photosynthesis measured as Fv/Fm in both morphs decreased rapidly over the first 4 days of exposure to intense blue light (2,000 μmol photons $m^{-2}s^{-1}$, **Figure 2A**). During this initial phase, the Fv/Fm values from the LF morph were significantly lower compared to those from the HF morph [linear model: $F_{(2, 21)} = 5.944$, $p = 0.0042$]. The response of the symbionts from the two morphs remained significantly different in the following period during which the values increased again [linear model: $F_{(2, 201)} = 148.1$; $p < 0.001$]. After ∼3 weeks, Fv/Fm values of the HF morph reached the initial value of >0.5. In contrast, the photosynthetic efficiency of the LF morph did not show full recovery and the Fv/Fm values remained below 0.5. No bleaching was visible in the HF morphs whereas visible bleaching started among replicates of the LF morphs after 4 days of exposure to blue light. By the end of the experiments, all LF specimens were bleached in the treated central area of the colonies. The HF morph, in contrast, showed only a mild paling in the light exposed areas.

Under the same photon flux of orange light (2,000 μmol photons $m^{-2}s^{-1}$), symbionts of both morphs showed a rapid decrease in Fv/Fm values down to ∼0.2 (**Figure 2B**). There was no significant difference in the response of both morphs to the treatment [linear model: $F_{(2, 33)} = 3.18$, $p = 0.48$]. Bleaching was visible in both morphs after 2 days and became severe after 6 days when the experiment was terminated.

Analysis of zooxanthellae number of the treated parts of the experimental colonies and control areas showed that the visual bleaching (**Figure 2C**) was caused by a loss of algal cells. The treated regions of the LF colonies suffered significant losses of zooxanthellae under both blue and orange light exposure [unpaired *t*-test: $F_{(1, 53)} = 7.3$, $p < 0.001$; $F_{(1, 35)} = 3.0$, $p < 0.001$ respectively]. In contrast, the illuminated region of the HF morph lost significant amounts of zoothanthellae only under orange light [unpaired *t*-test: $F_{(1, 35)} = 6.5$, $p < 0.001$] (**Figure 2D**).

Coral Growth under Different Light Intensities

Under low intensity blue light (**Figure 3A**), colonies of the LF morph showed a 25% gain in weight that was significantly higher [paired *t*-test: $F_{(1, 4)} = 3.8$, $p < 0.001$] compared to the HF morph. The latter showed essentially no weight gain over the duration of the experiment. Under high intensities of blue light (**Figure 3C**), the colonies of the HF morph gained significantly more weight than the LF morph [paired *t*-test: $F_{(1, 4)} = 1.2$, $p = 0.045$]. At the end of the experiment, the weight of the HF morph had increased by ∼33%, compared to the ∼18% increase of the LF morph colonies. Under medium intensity blue light (**Figure 3B**), both morphs showed comparable growth (HF morph: ∼115%; LF morph 127%, non-significant difference). The growth rates of both morphs were substantially higher under medium light conditions compared to both high and low light treatments (**Figure 3D**).

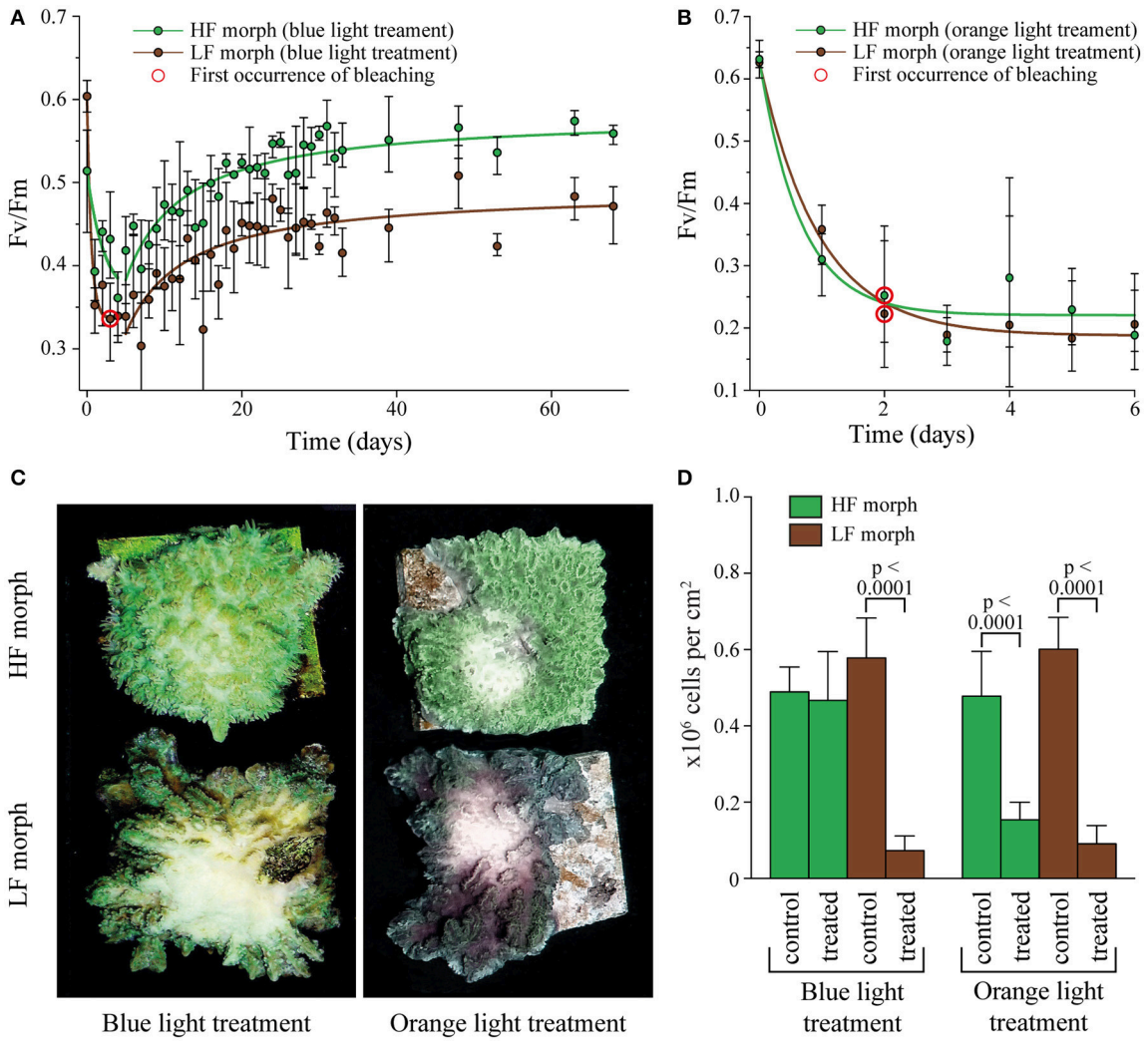

FIGURE 2 | (A) Change in Fv/Fm in two color morphs of *Hydnophora grandis* under high intensity blue light (2,000 μmol photons $m^{-2}s^{-1}$). Error bars indicate the range of mean values of 3 replicate colonies. Red circles highlight the first occurrence of visible bleaching. Lines represent exponential decay and saturation fits, respectively. **(B)** Change in Fv/Fm in the HF and LF color morphs of *Hydnophora grandis* under high intensity orange light (2,000 μmol photons $m^{-2}s^{-1}$). Error bars indicate the range of mean values of 3 replicate colonies. The first occurrence of visible bleaching is marked by red circles. Lines represent exponential decay fits. **(C)** Photographs of representative colonies of the HF morph (top) and LF morph (bottom) taken at the end of the high intensity blue light (left) and orange light (right) treatments. **(D)** Concentration of zooxanthellae in tissue samples of both morphs after exposure to 2,000 μmol photons $m^{-2}s^{-1}$ of blue and orange light (treated) and control tissue samples exposed to ambient light intensities (control). Error bars show standard deviation. Brackets above two bars indicate *p*-values for statistically significant ($p < 0.05$) differences between the zooxanthellae concentrations in treated and untreated tissue samples of each morph under blue and orange light, determined using unpaired *t*-tests.

DISCUSSION

The diversity of coral colors contributes to the visually arresting appearance of coral reefs. Frequently, representatives of different color morphs can be found side-by-side, raising the question of whether these striking differences in color have any ecological significance. Therefore, we tested our hypothesis that the benefits of photoprotection offered by some coral pigments in niches with high levels of light stress might be outweighed by the trade-offs associated with the productions of large pigment quantities in the absence of light stress. Such a scenario could offer an explanation for the evolution of color morphs as a result of balancing selection (Gittins et al., 2015). We chose the coral *H. grandis* as a model since the two distinct morphs differ significantly in the amount of cyan fluorescence proteins from the family of GFP-like proteins that they accumulate in their tissue (D'Angelo et al., 2008). The minimal difference in the spectral properties of the tissue fluorescence such as the 3 nm-shift of the emission peak between the LF morph expressing the protein hgrFP492 (D'Angelo et al., 2008) and the HF morph could be a response to the cellular environment in combination with the deviating pigment concentrations or due to small

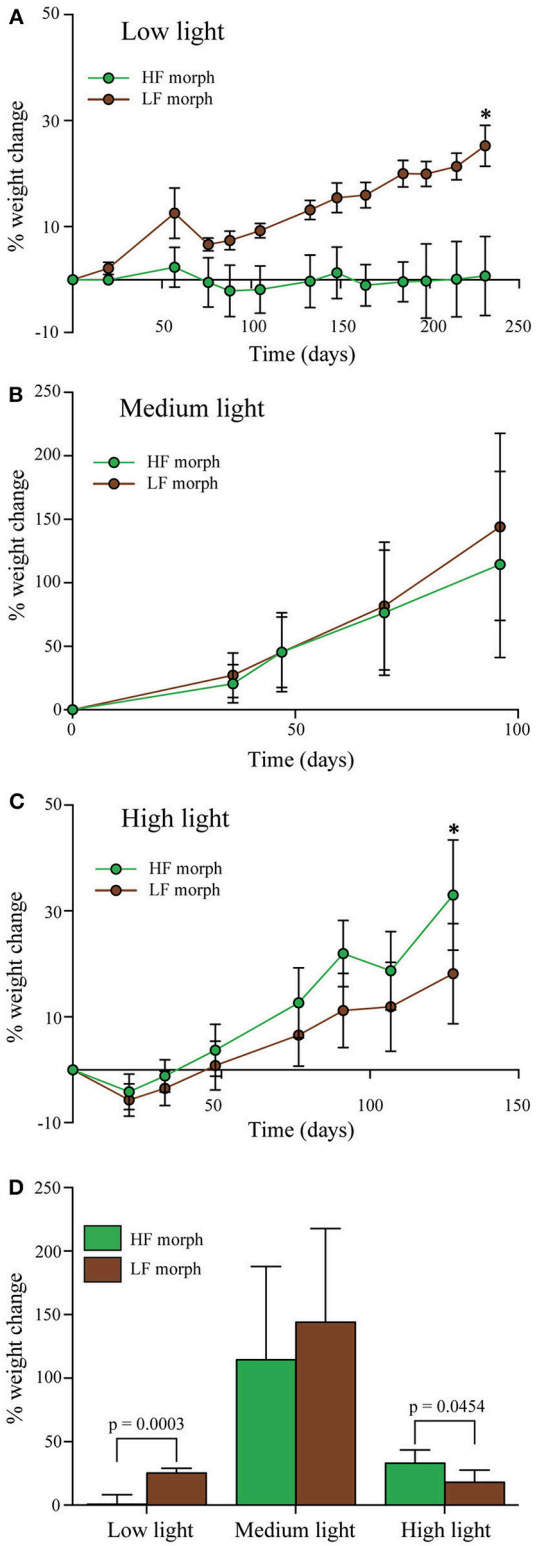

FIGURE 3 | (A–C) Percentage change of wet weight of LF morph (brown circles) and HF morph (green circles) of *Hydnophora grandis* over time under three different intensities of blue light. **(A)** Low light (10 μmol photons $m^{-2}s^{-1}$), **(B)** Medium light (300 μmol photons $m^{-2}s^{-1}$), and **(C)** High light (700–1100 μmol photons $m^{-2}s^{-1}$). Bars display mean values of 5 colonies. Error bars show standard deviation. Asterisks (*) above data points indicate statistically significant ($P < 0.05$) differences between the weighs of the colonies of each morph at the end each experiment, determined using paired *t*-tests. Initial weight for each colony was set to zero. **(D)** Total weight change of each morph under each light intensity at the end of each experiment given as percent of the initial values. Error bars show standard deviation. Brackets above two bars indicate *p*-values for statistically significant ($p < 0.05$) differences between the weighs of the colonies of each morph at the end each experiment, determined using paired *t*-tests.

differences in the amino acid sequence of the proteins (Alieva et al., 2008). Importantly, in both morphs the host pigment absorbs incident photosynthetically active radiation in the blue-green spectral region, covering large sections of the *in situ* absorption spectrum of photosynthetic pigments of the algal symbionts (Smith et al., 2013). We showed that both morphs used in our study were associated with the same *Symbiodinium* subclade, thereby reducing, yet not excluding, the probability that differential responses were due to physiological differences associated with the taxonomic background of the symbionts (Robison and Warner, 2006).

We first tested whether the high CFP concentrations in the tissue of the HF morph could indeed protect the symbionts by screening excess light as it was previously demonstrated for the purple-blue chromoproteins and some green and red fluorescent proteins in shallow water corals (Salih et al., 2000; Smith et al., 2013; Gittins et al., 2015). Measuring changes in the photosynthetic efficiency after dark recovery (Warner et al., 2010) and loss of algal cells in response to exposure of high fluxes of blue light, we show that the HF morph was more tolerant to the light stress. In agreement with a wavelength-dependent screening function of the CFPs, both morphs displayed comparably intense signs of light stress when they were illuminated with orange light outside of the spectral window covered by the protective host pigment. Orange-red light has been shown to negatively affect the photophysiology of *Symbiodinium* in coral tissues (Smith et al., 2013; Wijgerde et al., 2014). The comparable susceptibility of the two morphs to photodamage in this spectral range supports the conclusion that higher resilience of the HF morph under blue light stress is due to the screening by the CFP rather than by other photoprotective mechanisms that might be more dominant in this morph. Our photodamage data are in line with results of an earlier study in which daytime photoinhibition of the algal symbionts of the green fluorescent morph of *Acropora palifera* was reduced as compared to less fluorescent morphs (Salih et al., 2000).

To test whether trade-offs are associated with the high-level expression of the photoprotective CFP, we monitored the growth of the HF and LF morphs under different intensities of blue light. Photon fluxes corresponded to light levels that can be measured around noon in depths of ∼1 m (high light), ∼15 m (medium light), and ∼50–60 m (low light) (Stambler et al., 2008; Eyal et al., 2015; Ziegler et al., 2015). It should be noted that our experimental corals experienced these light levels for 10 h per day, not just around noon, so the dose

of photons received by them per day was higher compared to corals from aforementioned depths in field settings. Corals showed highest growth rates at medium light intensity with no significant differences between the HF and LF morphs. This may indicate that at favorable light levels and in the absence of other forms of stress, the expression of photoprotective pigments may essentially be neutral in the overall performance of the organism. Such a scenario could be supported by the comparably low energetic costs associated with the production of individual pigment molecules (Leutenegger et al., 2007). However, a previous study has reported a higher tolerance of fluorescence corals to heat-stress-induced bleaching (Salih et al., 2000). It should therefore be considered that there might be effects on fitness parameters such as reproduction rate (Loya et al., 2004) or stress tolerance (Salih et al., 2000) that are not assessed by the present experimental set-up.

In the experimental treatments (high vs. low light) that simulated light conditions similar to those at the upper and lower depth distribution limits of several symbiotic reef corals (Eyal et al., 2015; Ziegler et al., 2015), the growth of the HF and LF morphs was strongly reduced in comparison with the medium light treatment. This indicates that both over- and undersupply of light can negatively affect the performance of the corals. Yet, the causes for the reduced growth rates under the two light levels are likely to be very different. A supply of excess light may require an increased investment in several forms of photoprotection, for example in the synthesis of mycosporine-like amino acids (Shick, 2004; Starcevic et al., 2010), antioxidant defense (Lesser and Shick, 1990), or alternative electron transport pathways such as the Mehler reaction (Roberty et al., 2014). Energy may also be invested in repair processes of the photosynthetic apparatus of the symbionts due to photoinhibition and subsequent damage to the D1 protein (Aro et al., 1993; Warner et al., 1999; Gorbunov et al., 2001; Hill and Takahashi, 2014), although it has been suggested that photoinhibiton may protect against oxidative damage caused by excess light (Adams et al., 2008). Furthermore, high light intensities have been shown to cause nutrient limitation of the zooxanthellae, leading to decreased productivity (Dubinsky and Jokiel, 1994). The associated redistribution of energy resources within the coral holobiont and reduction in productivity of the symbioses may result in lower growth rates observed in specimens from the high light treatment. At low photon fluxes, *Symbiodinium* photosynthesis provides only ∼40% of the carbon needed by the coral host (Falkowski et al., 1984), and therefore colony growth may become carbon-limited (Dubinsky and Jokiel, 1994), a potential explanation for the reduced growth of our low light corals.

The growth rates of the two *Hydnophora* color morphs differed significantly under both extreme light conditions. In the high light treatment, the HF morph grew faster compared to the LF morph, suggesting that the high-level expression of a photoprotective CFP could indeed offer a measurable benefit for coral fitness in environments with exposure to excess light. In contrast, under low light levels, the highly pigmented HF specimens ceased to grow, while the LF colonies showed slow yet steady growth. Under these conditions, the expression of photoprotective pigments by the HF morph may represent a disadvantage since it requires an energy investment in the form of the accumulation of large amounts of proteins that offer no functional benefits. On the contrary, the screening of photons by the coral CFPs may actually be detrimental for the productivity of the symbionts since it further deprives photosynthesis from much-needed photons under light-limited conditions. The downregulation of FP expression under low light levels (D'Angelo et al., 2008), visible also in the present experiments, offers a mechanism to reduce these unfavorable side-effects. However, similar to the highly pigmented morphs of *Acropora* sp. (Gittins et al., 2015), this is possible only to a limited extend since the constitutive expression of photoprotective pigments of the HF morph still reaches ∼60% of the maximal expression under high light.

Our study shows that, depending on the light environment, high-level expression of photoprotective GFP-like proteins can have either beneficial or detrimental effects on the fitness of symbiotic corals. Therefore, some form of niche partitioning across the steep light gradient characteristic for coral reefs could be expected. Indeed, corals expressing photoprotective chromoproteins (CPs) (Smith et al., 2013) are most abundant in 1 m depth (Salih et al., 2006). Their share of the total population decreased continuously to depths of 40 m. Also, fluorescent corals were most abundant in 1 m depth and their proportion decreased with depth. At the same time, non-pigmented corals became more abundant (Salih et al., 2006). Furthermore, a recent study showed that CFP-expressing corals were less numerous at lower end of their depth distribution range as compared to GFP-containing or non-fluorescent corals (Roth et al., 2015). Also, the color morphs of *Anemonia viridis* expressing high amounts of cyan and red fluorescent proteins as well as chromoproteins have their distribution maximum in the shallowest waters whereas the non-pigmented morph tends to be more abundant at greater depth (Wiedenmann et al., 1999). Furthermore, a fluorescent clone of this species was more successful than a non-pigmented clone in a long-term competition for space in a shallow water habitat (Wiedenmann et al., 2007). Future work should aim to provide insights in the mechanisms underlying the trade-offs associated with the high-level expression of GFP-like proteins.

We conclude that the extreme light conditions at the upper and lower end of the depth distribution range of symbiotic reef corals exposes them to opposing selective pressures that promote the evolution and persistence of intraspecific color polymorphism. However, as the present study shows, both color morphs performed comparably well under medium light in the absence of other forms of stress. This neutral behavior of the pigmentation under ambient conditions may explain why color morphs can co-exist even in shallow sites (Wiedenmann et al., 1999; Paley and Bay, 2012; Gittins et al., 2015) as the selective advantage of high level pigmentation may become only effective during sporadic episodes of increased stress (Salih et al., 2000; Paley and Bay, 2012). Thereby, color polymorphisms may diversify the niches that can be occupied by a coral species, a capacity that is further enhanced by the light intensity-driven regulation of genes encoding photoprotective GFP-like proteins (D'Angelo et al., 2008).

Notably, the neutral behavior of the pigmentation under ambient conditions together with the fact that multiple gene copies are involved in the color polymorphism could have been a major driver of the evolution of the staggering diversity of GFP-like proteins: mutated gene-copies may have been balanced by functional copies until a gain of function eventually stabilized the novel variants in the gene pool. Examples are chromoproteins in *A. millepora* that are almost exclusively expressed in larvae and have likely evolved from a red fluorescent ancestor protein that also gave rise to a red fluorescent variant with a photoprotective function in adults (Gittins et al., 2015). Interestingly, these larval CPs evolved independently from photoprotective CPs produced in adult corals (Gittins et al., 2015). Other examples include the green-to-red photoconvertible FPs (Ando et al., 2002; Wiedenmann et al., 2004; Oswald et al., 2007; Eyal et al., 2015) that have gained their red fluorescent chromophores by parallel evolution of a green ancestor protein (Field and Matz, 2010). Along with green fluorescent variants (Lyndby et al., 2016), the latter proteins are prevalent in coral species that live preferably in less light exposed habitats where they optimize the internal light environment for symbiont photosynthesis in deeper tissue levels (Bollati et al., 2017; Smith et al., 2017). Thereby, they offer an explanation for the observation that fluorescent corals become again more abundant at greater depth after initially decreasing from the shallowest sites downwards (Salih et al., 2006; Roth et al., 2015; Smith et al., 2017). Due to the different function of the pigments, strongly fluorescent morphs gain an advantage at greater depths (Smith et al., 2017), whereas the trade-offs associated with the high-level production of the pigments give a selective advantage to less colored variants in shallower water.

Our study highlights the critical need to assess different types of GFP-like proteins separately when analyzing their biological function and their ecological significance in structuring reef communities.

AUTHOR CONTRIBUTIONS

CD and JW: provided the research question and designed experiments; CQ: conducted experiments and produced data; CD, JW, and CQ: analyzed and discussed the data; CQ, CD, and JW: wrote the paper.

FUNDING

The study was funded by NERC (NE/I01683X/1 & NE/K00641X/1 to JW), European Research Council under the European Union's Seventh Framework Programme (FP/2007-2013)/ERC Grant Agreement n. 311179 to JW and an IFLS studentship Award to CD.

ACKNOWLEDGMENTS

We thank Tropical Marine Centre (London) and Tropic Marin (Wartenberg) for sponsoring the *Coral Reef Laboratory* at the University of Southampton.

REFERENCES

Adams, W. W. III., Zarter, C. R., Mueh, K. E., Amiard, V., and Demmig-Adams, B. (2008). "Energy dissipation and photoinhibition: a continuum of photoprotection," in *Photoprotection, Photoinhibition, Gene Regulation, and Environment*, eds B. Demmig-Adams, W. W. Adams III, and A. Mattoo (Dordrecht: Springer), 49–64.

Alieva, N. O., Konzen, K. A., Field, S. F., Meleshkevitch, E. A., Hunt, M. E., Beltran-Ramirez, V., et al. (2008). Diversity and evolution of coral fluorescent proteins. *PLoS ONE* 3:e2680. doi: 10.1371/journal.pone.0002680

Ambarsari, I., Brown, B. E., Barlow, R. G., Britton, G., and Cummings, D. (1997). Fluctuations in algal chlorophyll and carotenoid pigments during solar bleaching in the coral Goniastrea aspera at Phuket, Thailand. *Mar. Ecol. Prog. Ser.* 159, 303–307. doi: 10.3354/meps159303

Ando, R., Hama, H., Yamamoto-Hino, M., Mizuno, H., and Miyawaki, A. (2002). An optical marker based on the UV-induced green-to-red photoconversion of a fluorescent protein. *Proc. Natl. Acad. Sci. U.S.A.* 99, 12651–12656. doi: 10.1073/pnas.202320599

Aro, E. M., Virgin, I., and Andersson, B. (1993). Photoinhibition of photosystem-2 - inactivation, protein damage and turnover. *Biochim. Biophys. Acta* 1143, 113–134. doi: 10.1016/0005-2728(93)90134-2

Baker, A. C., Glynn, P. W., and Riegl, B. (2008). Climate change and coral reef bleaching: an ecological assessment of long-term impacts, recovery trends and future outlook. *Estuar. Coast. Shelf Sci.* 80, 435–471. doi: 10.1016/j.ecss.2008.09.003

Banaszak, A. T., LaJeunesse, T. C., and Trench, R. K. (2000). The synthesis of mycosporine-like amino acids (MAAs) by cultured, symbiotic dinoflagellates. *J. Exp. Mar. Biol. Ecol.* 249, 219–233. doi: 10.1016/S0022-0981(00)00192-1

Bhagooli, R., and Hidaka, M. (2003). Comparison of stress susceptibility of in hospite and isolated zooxanthellae among five coral species. *J. Exp. Mar. Biol. Ecol.* 291, 181–197. doi: 10.1016/S0022-0981(03)00121-7

Bollati, E., Plimmer, D., D'Angelo, C., and Wiedenmann, J. (2017). FRET-mediated long-range wavelength transformation by photoconvertible fluorescent proteins as an efficient mechanism to generate orange-red light in symbiotic deep water corals. *Int. J. Mol. Sci.* 18:1174. doi: 10.3390/ijms18071174

D'Angelo, C., Denzel, A., Vogt, A., Matz, M. V., Oswald, F., Salih, A., et al. (2008). Blue light regulation of host pigment in reef-building corals. *Mar. Ecol. Prog. Ser.* 364, 97–106. doi: 10.3354/meps07588

D'Angelo, C., Hume, B. C., Burt, J., Smith, E. G., Achterberg, E. P., and Wiedenmann, J. (2015). Local adaptation constrains the distribution potential of heat-tolerant Symbiodinium from the Persian/Arabian Gulf. *Isme J.* 9, 2551–2560. doi: 10.1038/ismej.2015.80

D'Angelo, C., and Wiedenmann, J. (2012). An experimental mesocosm for long-term studies of reef corals. *J. Mar. Biol. Assoc. U.K.* 92, 769–775. doi: 10.1017/S0025315411001883

D'Angelo, C., and Wiedenmann, J. (2014). Impacts of nutrient enrichment on coral reefs: new perspectives and implications for coastal management and reef survival. *Curr. Opin. Environ. Sustain.* 7, 82–93. doi: 10.1016/j.cosust.2013.11.029

Dove, S. G., Hoegh-Guldberg, O., and Ranganathan, S. (2001). Major colour patterns of reef-building corals are due to a family of GFP-like proteins. *Coral Reefs* 19, 197–204. doi: 10.1007/PL00006956

Dove, S. G., Takabayashi, M., and Hoegh-Guldberg, O. (1995). Isolation and partial characterization of the pink and blue pigments of pocilloporid and acroporid corals. *Biol. Bull.* 189, 288–297. doi: 10.2307/1542146

Dubinsky, Z., and Jokiel, P. L. (1994). Ratio of energy and nutrient fluxes regulates symbiosis between zooxanthellae and corals. *Pac. Sci.* 48, 313–324.

Eyal, G., Wiedenmann, J., Grinblat, M., D'Angelo, C., Kramarsky-Winter, E., Treibitz, T., et al. (2015). Spectral diversity and regulation of coral fluorescence in a mesophotic reef habitat in the Red Sea. *PLoS ONE* 10:e0128697. doi: 10.1371/journal.pone.0128697

Falkowski, P. G., Dubinsky, Z., Muscatine, L., and Porter, J. W. (1984). Light and the bioenergetics of a symbiotic coral. *Bioscience* 34, 705–709. doi: 10.2307/1309663

Field, S. F., Bulina, M. Y., Kelmanson, I. V., Bielawski, J. P., and Matz, M. V. (2006). Adaptive evolution of multicolored fluorescent proteins in reef-building corals. *J. Mol. Evol.* 62, U332–U315. doi: 10.1007/s00239-005-0129-9

Field, S. F., and Matz, M. V. (2010). Retracing evolution of red fluorescence in GFP-like proteins from Faviina corals. *Mol. Biol. Evol.* 27, 225–233. doi: 10.1093/molbev/msp230

Genty, B., Briantais, J. M., and Baker, N. R. (1989). The relationship between the quantum yield of photosynthetic electron-transport and quenching of chlorophyll fluorescence. *Biochim. Biophys. Acta* 990, 87–92. doi: 10.1016/S0304-4165(89)80016-9

Gittins, J. R., D'Angelo, C., Oswald, F., Edwards, R. J., and Wiedenmann, J. (2015). Fluorescent protein-mediated colour polymorphism in reef corals: multicopy genes extend the adaptation/acclimatization potential to variable light environments. *Mol. Ecol.* 24, 453–465. doi: 10.1111/mec.13041

Glynn, P. W., Maté, J. L., Baker, A. C., and Calderón, M. O. (2001). Coral bleaching and mortality in Panama and Ecuador during the 1997–1998 El Niño–Southern Oscillation event: spatial/temporal patterns and comparisons with the 1982–1983 event. *Bull. Mar. Sci.* 69, 79–109.

Gorbunov, M. Y., Kolber, Z. S., Lesser, M. P., and Falkowski, P. G. (2001). Photosynthesis and photoprotection in symbiotic corals. *Limnol. Oceanogr.* 46, 75–85. doi: 10.4319/lo.2001.46.1.0075

Henderson, J. N., and Remington, S. J. (2005). Crystal structures and mutational analysis of amFP486, a cyan fluorescent protein from *Anemonia majano*. *Proc. Natl. Acad. Sci. U.S.A.* 102, 12712–12717. doi: 10.1073/pnas.0502250102

Hill, R., and Takahashi, S. (2014). Photosystem II recovery in the presence and absence of chloroplast protein repair in the symbionts of corals exposed to bleaching conditions. *Coral Reefs* 33, 1101–1111. doi: 10.1007/s00338-014-1188-4

Hoegh-Guldberg, O. (1999). Climate change, coral bleaching and the future of the world's coral reefs. *Mar. Freshw. Res.* 50, 839–866. doi: 10.1071/MF99078

Hughes, T. P., Kerry, J. T., Álvarez-Noriega, M., Álvarez-Romero, J. G., Anderson, K. D., Baird, A. H., et al. (2017). Global warming and recurrent mass bleaching of corals. *Nature* 543, 373–377. doi: 10.1038/nature21707

Hume, B., D'Angelo, C., Burt, J., Baker, A. C., Riegl, B., and Wiedenmann, J. (2013). Corals from the Persian/Arabian Gulf as models for thermotolerant reef-builders: prevalence of clade C3 Symbiodinium, host fluorescence and *ex situ* temperature tolerance. *Mar. Pollut. Bull.* 72, 313–322. doi: 10.1016/j.marpolbul.2012.11.032

Jones, R. J., Hoegh-Guldberg, O., Larkum, A. W. D., and Schreiber, U. (1998). Temperature-induced bleaching of corals begins with impairment of the CO_2 fixation mechanism in zooxanthellae. *Plant Cell Environ.* 21, 1219–1230. doi: 10.1046/j.1365-3040.1998.00345.x

Kelmanson, I. V., and Matz, M. V. (2003). Molecular basis and evolutionary origins of color diversity in great star coral *Montastraea cavernosa* (Scleractinia: Faviida). *Mol. Biol. Evol.* 20, 1125–1133. doi: 10.1093/molbev/msg130

Klueter, A., Loh, W., Hoegh-Guldberg, O., and Dove, S. (2006). Physiological and genetic properties of two fluorescent colour morphs of the coral *Montipora digitata*. *Symbiosis* 42, 123–134.

Krause, G. H., and Weis, E. (1991). Chlorophyll fluorescence and photosynthesis - the basics. *Annu. Rev. Plant Physiol. Plant Molec. Biol.* 42, 313–349. doi: 10.1146/annurev.pp.42.060191.001525

Lesser, M. P. (1997). Oxidative stress causes coral bleaching during exposure to elevated temperatures. *Coral Reefs* 16, 187–192. doi: 10.1007/s003380050073

Lesser, M. P. (2006). Oxidative stress in marine environments: biochemistry and physiological ecology. *Annu. Rev. Physiol.* 68, 253–278. doi: 10.1146/annurev.physiol.68.040104.110001

Lesser, M. P., and Shick, J. M. (1990). Photoadaption and defenses against oxygen toxicity in zooxanthellae from natural populations of symbiotic cnidarians. *J. Exp. Mar. Biol. Ecol.* 134, 129–141. doi: 10.1016/0022-0981(90)90105-L

Leutenegger, A., D'Angelo, C., Matz, M. V., Denzel, A., Oswald, F., Salih, A., et al. (2007). It's cheap to be colorful. Anthozoans show a slow turnover of GFP-like proteins. *FEBS J.* 274, 2496–2505. doi: 10.1111/j.1742-4658.2007.05785.x

Levy, O., Achituv, Y., Yacobi, Y. Z., Stambler, N., and Dubinsky, Z. (2006). The impact of spectral composition and light periodicity on the activity of two antioxidant enzymes (SOD and CAT) in the coral Favia favus. *J. Exp. Mar. Biol. Ecol.* 328, 35–46. doi: 10.1016/j.jembe.2005.06.018

Loya, Y., Lubinevsky, H., Rosenfeld, M., and Kramarsky-Winter, E. (2004). Nutrient enrichment caused by in situ fish farms at Eilat, Red Sea is detrimental to coral reproduction. *Mar. Pollut. Bull.* 49, 344–353. doi: 10.1016/j.marpolbul.2004.06.011

Lyndby, N. H., Kühl, M., and Wangpraseurt, D. (2016). Heat generation and light scattering of green fluorescent protein-like pigments in coral tissue. *Sci. Rep.* 6:26599. doi: 10.1038/srep26599

Matz, M. V., Fradkov, A. F., Labas, Y. A., Savitsky, A. P., Zaraisky, A. G., Markelov, M. L., et al. (1999). Fluorescent proteins from nonbioluminescent Anthozoa species. *Nat. Biotechnol.* 17, 1227. doi: 10.1038/70787

Mazel, C. H., Lesser, M. P., Gorbunov, M. Y., Barry, T. M., Farrell, J. H., Wyman, K. D., et al. (2003). Green-fluorescent proteins in Caribbean corals. *Limnol. Oceanogr.* 48, 402–411. doi: 10.4319/lo.2003.48.1_part_2.0402

Nienhaus, G. U., and Wiedenmann, J. (2009). Structure, dynamics and optical properties of fluorescent proteins: perspectives for marker development. *Chemphyschem* 10, 1369–1379. doi: 10.1002/cphc.200800839

Oswald, F., Schmitt, F., Leutenegger, A., Ivanchenko, S., D'Angelo, C., Salih, A., et al. (2007). Contributions of host and symbiont pigments to the coloration of reef corals. *FEBS J.* 274, 1102–1109. doi: 10.1111/j.1742-4658.2007.05661.x

Paley, A. S., and Bay, L. K. (2012). "Bleaching condition varies among *Acropora millepora* color morphs," in *Proceedings of the 12th International Coral Reef Symposium* (Cairns, QLD), 1–5.

Pospíšil, P. (2016). Production of reactive oxygen species by photo system ii as a response to light and temperature stress. *Front. Plant Sci.* 7:1950. doi: 10.3389/fpls.2016.01950

Rehman, A. U., Szabó, M., Deák, Z., Sass, L., Larkum, A., Ralph, P., et al. (2016). Symbiodinium sp cells produce light-induced intra- and extracellular singlet oxygen, which mediates photodamage of the photosynthetic apparatus and has the potential to interact with the animal host in coral symbiosis. *New Phytol.* 212, 472–484. doi: 10.1111/nph.14056

Reynolds, J. M., Bruns, B. U., Fitt, W. K., and Schmidt, G. W. (2008). Enhanced photoprotection pathways in symbiotic dinoflagellates of shallow-water corals and other cnidarians. *Proc. Natl. Acad. Sci. U.S.A.* 105, 13674–13678. doi: 10.1073/pnas.0805187105

Roberty, S., Bailleul, B., Berne, N., Franck, F., and Cardol, P. (2014). PSI Mehler reaction is the main alternative photosynthetic electron pathway in *Symbiodinium* sp., symbiotic dinoflagellates of cnidarians. *New Phytol.* 204, 81–91. doi: 10.1111/nph.12903

Robison, J. D., and Warner, M. E. (2006). Differential impacts of photoacclimation and thermal stress on the photobiology of four different phylotypes of Symbiodinium (Pyrrhophyta). *J. Phycol.* 42, 568–579. doi: 10.1111/j.1529-8817.2006.00232.x

Rosset, S., D'Angelo, C., and Wiedenmann, J. (2015). Ultrastructural biomarkers in symbiotic algae reflect the availability of dissolved inorganic nutrients and particulate food to the reef coral holobiont. *Front. Mar. Sci.* 2:103. doi: 10.3389/fmars.2015.00103

Rosset, S., Wiedenmann, J., Reed, A. J., and D'Angelo, C. (2017). Phosphate deficiency promotes coral bleaching and is reflected by the ultrastructure of symbiotic dinoflagellates. *Mar. Pollut. Bull.* 118, 180–187. doi: 10.1016/j.marpolbul.2017.02.044

Roth, M. S., Padilla-Gamino, J. L., Pochon, X., Bidigare, R. R., Gates, R. D., Smith, C. M., et al. (2015). Fluorescent proteins in dominant mesophotic reef-building corals. *Mar. Ecol. Prog. Ser.* 521, 63–79. doi: 10.3354/meps11108

Salih, A., Cox, G., Szymczak, R., Coles, S. L., Baird, A. H., Dunstan, A., et al. (2006). "The role of host-based color and fluorescent pigments in photoprotection and in reducing bleaching stress in corals", in *Proceedings of 10th International Coral Reef Symposium* (Okinawa), 746–756.

Salih, A., Larkum, A., Cox, G., Kühl, M., and Hoegh-Guldberg, O. (2000). Fluorescent pigments in corals are photoprotective. *Nature* 408, 850–853. doi: 10.1038/35048564

Shick, J. M. (2004). The continuity and intensity of ultraviolet irradiation affect the kinetics of biosynthesis, accumulation, and conversion of mycosporine-like amino acids (MAAS) in the coral *Stylophora pistillata*. *Limnol. Oceanogr.* 49, 442–458. doi: 10.4319/lo.2004.49.2.0442

Smith, E. G., D'Angelo, C., Salih, A., and Wiedenmann, J. (2013). Screening by coral green fluorescent protein (GFP)-like chromoproteins supports

a role in photoprotection of zooxanthellae. *Coral Reefs* 32, 463–474. doi: 10.1007/s00338-012-0994-9

Smith, E. G., D'Angelo, C., Sharon, Y., Tchernov, D., and Wiedenmann, J. (2017). Acclimatization of symbiotic corals to mesophotic light environments through wavelength transformation by fluorescent protein pigments. *Proc. Biol. Sci.* 284:20170320. doi: 10.1098/rspb.2017.0320

Stambler, N., Levy, O., and Vaki, L. (2008). Photosynthesis and respiration of hermatypic zooxanthellate Red Sea corals from 5-75-m depth. *Isr. J. Plant Sci.* 56, 45–53. doi: 10.1560/IJPS.56.1-2.45

Starcevic, A., Dunlap, W. C., Cullum, J., Shick, J. M., Hranueli, D., and Long, P. F. (2010). Gene expression in the scleractinian acropora microphthalma exposed to high solar irradiance reveals elements of photoprotection and coral bleaching. *PLoS ONE* 5:e13975. doi: 10.1371/journal.pone.0013975

Takahashi, S., Whitney, S. M., and Badger, M. R. (2009). Different thermal sensitivity of the repair of photodamaged photosynthetic machinery in cultured Symbiodinium species. *Proc. Natl. Acad. Sci. U.S.A.* 106, 3237–3242. doi: 10.1073/pnas.0808363106

Vogt, A., D'Angelo, C., Oswald, F., Denzel, A., Mazel, C. H., Matz, M. V., et al. (2008). A green fluorescent protein with photoswitchable emission from the Deep Sea. *PLoS ONE* 3:e3766. doi: 10.1371/journal.pone.0003766

Warner, M. E., Fitt, W. K., and Schmidt, G. W. (1999). Damage to photosystem II in symbiotic dinoflagellates: a determinant of coral bleaching. *Proc. Natl. Acad. Sci. U.S.A.* 96, 8007–8012. doi: 10.1073/pnas.96.14.8007

Warner, M. E., Lesser, M. P., and Ralph, P. J. (2010). "Chlorophyll fluorescence in reef building corals," in *Chlorphyll a Fluorescence in Aquatic Sciences: Methods and Applications,* eds D. J. Suggett, O. Prasil, and M. A. Borowitzka (Dordrecht: Springer), 209–222. doi: 10.1007/978-90-481-9268-7_10

Wiedenmann, J., Ivanchenko, S., Oswald, F., Schmitt, F., Röcker, C., Salih, A., et al. (2004). EosFP, a fluorescent marker protein with UV-inducible green-to-red fluorescence conversion. *Proc. Natl. Acad. Sci. U.S.A.* 101, 15905–15910. doi: 10.1073/pnas.0403668101

Wiedenmann, J., Leutenegger, A., Gundel, S., Schmitt, F., D'Angelo, C., and Funke, W. (2007). Long-term monitoring of space competition among fluorescent and nonfluorescent sea anemones in the Mediterranean Sea. *J. Mar. Biol. Assoc. U.K.* 87, 851–852. doi: 10.1017/S0025315407057050

Wiedenmann, J., Röcker, C., and Funke, W. (1999). "The morphs of Anemonia aff. sulcata (Cnidaria, Anthozoa) in particular consideration of the ectodermal pigments," in *Verhandlungen der Gesellschaft für Ökologie,* ed J. Pfadenhauer (Heidelberg: Spektrum Akademischer Verlag), 497–503.

Wiedenmann, J., Schenk, A., Röcker, C., Girod, A., Spindler, K. D., and Nienhaus, G. U. (2002). A far-red fluorescent protein with fast maturation and reduced oligomerization tendency from *Entacmaea quadricolor* (Anthozoa, Actinaria). *Proc. Natl. Acad. Sci. U.S.A.* 99, 11646–11651. doi: 10.1073/pnas.182157199

Wijgerde, T., van Melis, A., Silva, C. I., Leal, M. C., Vogels, L., Mutter, C., et al. (2014). Red light represses the photophysiology of the *Scleractinian coral Stylophora pistillata*. *PLoS ONE* 9:e92781. doi: 10.1371/journal.pone.0092781

Ziegler, M., Roder, C. M., Büchel, C., and Voolstra, C. R. (2015). Mesophotic coral depth acclimatization is a function of host-specific symbiont physiology. *Front. Mar. Sci.* 2:4. doi: 10.3389/fmars.2015.00004

Conflict of Interest Statement: The authors declare that the research was conducted in the absence of any commercial or financial relationships that could be construed as a potential conflict of interest.

frontiers in Marine Science

ORIGINAL RESEARCH
published: 14 February 2018
doi: 10.3389/fmars.2018.00045

Utility of Photochemical Traits as Diagnostics of Thermal Tolerance amongst Great Barrier Reef Corals

Matthew R. Nitschke[1,2], Stephanie G. Gardner[1], Samantha Goyen[1], Lisa Fujise[1], Emma F. Camp[1], Peter J. Ralph[1] and David J. Suggett[1]*

[1] Climate Change Cluster (C3), University of Technology Sydney, Sydney, NSW, Australia, [2] Centre for Environmental and Marine Studies, University of Aveiro, Aveiro, Portugal

Light availability is considered a key factor regulating the thermal sensitivity of reef building corals, where excessive excitation of photosystem II (PSII) further exacerbates pressure on photochemical pathways already compromised by heat stress. Coral symbionts acclimate to changes in light availability (photoacclimation) by continually fine-tuning the photochemical operating efficiency of PSII. However, how this process adjusts throughout the warmest months in naturally heat-tolerant or sensitive species is unknown, and whether this influences the capacity to tolerate transient heat stress is untested. We therefore examined the PSII photophysiology of 10 coral species (with known thermal tolerances) from shallow reef environments at Heron Island (Great Barrier Reef, Australia), in spring (October-November, 2015) vs. summer (February-March, 2016). Corals were maintained in flow-through aquaria and rapid light curve (RLC) protocols using pulse amplitude modulated (PAM) fluorometry captured changes in the PSII photoacclimation strategy, characterized as the minimum saturating irradiance (E_k), and the extent of photochemical ([1 – *C*], operating efficiency) vs. non-photochemical ([1 – *Q*]) energy dissipation. Values of E_k across species were >2-fold higher in all coral species in spring, consistent with a climate of higher overall light exposure (i.e., higher PAR from lower cloud cover, rainfall and wind speed) compared with summer. Summer decreases in E_k were combined with a shift toward preferential photochemical quenching in all species. All coral species were subsequently subjected to thermal stress assays. An equivalent temperature-ramping profile of 1°C increase per day and then maintenance at 32°C was applied in each season. Despite the significant seasonal photoacclimation, the species hierarchy of thermal tolerance [maximum quantum yields of PSII (F_v/F_m), monitored at dawn and dusk] did not shift between seasons, except for *Pocillopora damicornis* (faster declines in summer) and *Stylophora pistillata* (total mortality in spring). Furthermore, the strategy for dealing with light energy (i.e., preferential photochemical vs. non-photochemical quenching) was unchanged for thermally tolerant species across seasons, whereas thermally sensitive species switched between preferential [1 – *Q*] and [1 – *C*] from spring to summer. We discuss how such traits can potentially be used as a diagnostic of thermal tolerance under non-stressed conditions.

Keywords: coral bleaching, *Symbiodinium*, photoacclimation, photochemical quenching, non-photochemical quenching, thermal tolerance, PSII

OPEN ACCESS

Edited by:
Zvy Dubinsky,
Bar-Ilan University, Israel

Reviewed by:
Itay Cohen,
Hebrew University of Jerusalem, Israel
Stephane Roberty,
University of Liège, Belgium

****Correspondence:***
Matthew R. Nitschke
matthew.nitschke@uts.edu.au

Specialty section:
This article was submitted to Coral Reef Research, a section of the journal Frontiers in Marine Science

Received: *20 April 2017*
Accepted: *31 January 2018*
Published: *14 February 2018*

Citation:
Nitschke MR, Gardner SG, Goyen S, Fujise L, Camp EF, Ralph PJ and Suggett DJ (2018) Utility of Photochemical Traits as Diagnostics of Thermal Tolerance amongst Great Barrier Reef Corals. Front. Mar. Sci. 5:45. doi: 10.3389/fmars.2018.00045

INTRODUCTION

Photosynthetic dinoflagellates of the genus *Symbiodinium* are endosymbionts of scleractinian corals that support reef-building, but are highly susceptible to photochemical destabilization when exposed to anomalous environmental conditions (Smith et al., 2005; Roth, 2014; Warner and Suggett, 2016). Under extreme cases, the light harvesting pigments of *Symbiodinium* are impaired and individual cells are expelled from the host or degraded, which manifests as conspicuous de-colouration referred to as "coral bleaching" (Weis, 2008; Suggett and Smith, 2011). Whilst the term "bleaching" is used interchangeably across scales (i.e., from individual polyps and colonies to reefs) and its process is exacerbated under a number of conditions (from light stress to inorganic nutrient imbalance; Baker et al., 2008; Wiedenmann et al., 2013), widespread "mass bleaching" events are considered a symptom of prolonged anomalous elevated seawater temperatures (Ainsworth et al., 2016) acting synergistically with additional stressors, notably solar radiation (Jones et al., 1998; Mumby et al., 2001; Anthony et al., 2007; Wooldridge et al., 2017). Such conditions led to the single greatest mass bleaching event on the Great Barrier Reef in 2016 (Hughes et al., 2017) and if prolonged, can drive a transition from coral bleaching to coral mortality (Suggett and Smith, 2011).

Whilst anomalous temperatures appear to target numerous physiological pathways of both the coral host and their *Symbiodinium* populations (Baird et al., 2009; Maor-Landaw and Levy, 2016), functional impairment of *Symbiodinium*'s photosystem II (PSII) reaction centers (RCII) often responds as a primary determinant of bleaching-stress susceptibility (Warner et al., 1999; Takahashi et al., 2008). PSII utilizes absorbed light energy to drive electron generation for energy (ATP) and reductant (NADPH) formation, supporting carbon fixation (Oakley et al., 2014). Excitation pressure on PSII is governed by the rate of electron delivery (photon absorption) vs. removal (i.e., electron flow). Thus, (photo)acclimation via constituents of the light harvesting complex (Robison and Warner, 2006; Hennige et al., 2009) and linear electron transport chain (Robison and Warner, 2006; Suggett et al., 2015) ensure that the redox state of the electron carrier molecules (i.e., plastoquinone) are continually fine-tuned to remain optimal. In shallow reef habitats *Symbiodinium* cells exist within highly dynamic light fields (Anthony et al., 2004; Roth, 2014) where ambient photon delivery (incident irradiance) to the light harvesting apparatus and subsequent electron turnover often exceeds the capacity to which cells have acclimatized. Therefore, in order to avoid photoinhibition, cells must employ high rates of protein repair (Takahashi et al., 2004; Ragni et al., 2010; Hill et al., 2011; Jeans et al., 2013), or photoprotection mechanisms that transiently redirect excitation energy from linear electron flow via "non-photochemical" quenching pathways. Non-photochemical quenching in *Symbiodinium* is largely sustained through energy-dependent quenching via "alternate" electron acceptors within the photochemical electron transport chain (Roberty et al., 2014), as well as alteration of pigment protein transfer efficiencies within the PSII light harvesting antenna complex (McCabe Reynolds et al., 2008; Slavov et al., 2016), to dissipate >80% of excitation energy (Gorbunov et al., 2001; Brodersen et al., 2014; Roth, 2014). However, during heat stress, electron transfer through PSII is thought to become increasingly constrained (Tchernov et al., 2004; Smith et al., 2005; Goyen et al., 2017) placing increased reliance on non-photochemical pathways to relieve PSII excitation pressure (Warner et al., 1996; Hill et al., 2004; Roberty et al., 2015). Consequently, light availability can determine the severity with which heat stress manifests (Lesser and Farrell, 2004; Robison and Warner, 2006) resulting in persistent and irreversible PSII photoinhibition of *Symbiodinium*.

Symbiodinium photoacclimation to changes in light availability (photosynthetically active radiation, PAR) has been particularly well-studied *in hospite* of corals distributed along natural spatial light gradients (Iglesias-Prieto et al., 2004), and shallow to mesophotic (Frade et al., 2008; Lesser et al., 2010; Cooper et al., 2011) and clear to turbid (Hennige et al., 2008; Suggett et al., 2012) waters, complimented with reciprocal transplants of coral species across these habitats (Cohen and Dubinsky, 2015). Here, upon moving *Symbiodinium* to darker or deeper habitats, light-harvesting efficiency is altered through adjustment of light-harvesting capacity (Frade et al., 2008). This process likely reflects interactions between the macrostructure of the host (i.e., lateral transfer or local enhancement of light through tissue layers and skeleton; Enríquez et al., 2005, 2017; Terán et al., 2010; Wangpraseurt et al., 2012) and acclimation plasticity of the symbiont, which in the latter case is in part governed by cell size constraints (Suggett et al., 2015). These studies across natural light gradients have proved popular in understanding photoacclimation processes, whereas examining plasticity of photoacclimation at any one depth in response to natural environmental change (i.e., seasons) is comparatively understudied (Titlyanov et al., 2001; Hill and Ralph, 2005; Ulstrup et al., 2008; Winters et al., 2009; Sawall et al., 2014). Some evidence does suggest that processes operating within a species across a depth gradient also potentially operate over time; for example, the maximum photochemical efficiency (F_v/F_m) for *Symbiodinium in hospite* of corals within shallow reefs are often driven to annual low yields in summer (Warner et al., 2002; Ulstrup et al., 2008). Most likely these lows in summer reflect long-term downregulation in response to warmer waters and high PAR in summer (Warner et al., 2002) that is also

Abbreviations: PSII, Photosystem II; F_q'/F_m', Effective photochemical efficiency of PSII; RCII, Photosystem II reaction centers; NPQ, Non-photochemical quenching; [1 – *Q*], Light dependant non-photochemical quenching; [1 – *C*], Light dependant photochemical quenching; SST, Sea surface temperature; PAR, Photosynthetically active radiation; *E*, PAR; RLC, Rapid light curves; *F*, Dark-adapted chlorophyll steady state fluorescence; F_o, Dark-adapted chlorophyll fluorescence minimum; F_m, Dark-adapted chlorophyll fluorescence maximum; F', Light-adapted chlorophyll steady-state fluorescence under actinic light; F_o', Light-adapted chlorophyll fluorescence minimum under actinic light; F_m', Light-adapted chlorophyll fluorescence maximum under actinic light; F_v/F_m, Maximum quantum yield of photosystem II; $F_q'/F_{m'\,(\max)}$, maximum PSII photochemical efficiency; E_k, Minimum saturating irradiance of PSII; E/E_k, E_k normalized to PAR; *S*, Parameter related to the length of the period during which F_v/F_m remains stable; *k*, Rate constant that quantifies the rate of F_v/F_m decrease; $F_v/F_{m(\min)}$, Minimum dark-acclimated maximum quantum yield of photosystem II reached during exposure to heat stress.

accompanied by an increase in photoprotection through non-photochemical quenching (Ulstrup et al., 2008; Sawall et al., 2014; Louis et al., 2016). However, Hill and Ralph (2005) suggest that the same non-photochemical mechanisms for photoprotection to high-light exposure during the diel solar peak in key species of shallow water Great Barrier Reef corals are active across seasons and independent of temperature.

On balance, photoacclimation of *Symbiodinium in hospite* remains generally well-studied across space (i.e., depth) rather than through time. This is surprising given that stability of photochemistry is ultimately dependant on how effectively cumulative excitation pressure that builds over time can be processed. As such, photochemical strategies employed as seasons move toward annual temperature (and/or light) extremes may be particularly pivotal in dictating how coral taxa are differentially impacted by thermal events whilst operating toward the limit of their thermal tolerance (Ulstrup et al., 2008). We targeted 10 species of coral that encompass a diverse range of growth forms, reproductive modes, symbiont transmission strategies, *Symbiodinium* associations, and thermal tolerances at Heron Reef in the southern Great Barrier Reef (GBR, Australia). We initially contrast the extent of photoacclimation (and associated strategies with which absorbed excitation energy is processed) that operates in response to changing light and temperature between spring and summer seasons, and whether this is conserved across species. We subsequently consider the sensitivity of these same species to transient heat stress during summer and spring, and whether any differences potentially reflect alternate strategies of photoacclimation. In doing so, we show for the first time that these coral species vary widely in their strategy of light utilization during high-light doses in spring, but also share an inherent strategy during a low-light event in summer. Furthermore, we demonstrate coral-*Symbiodinium* symbioses that exhibit relative thermally tolerant photochemical function also maintain their strategy of light utilization across seasons.

MATERIALS AND METHODS

Site Location and Retrieval of Seasonal Climate Data

Heron Reef (23°26′32.66″S, 151°54′55.53″E) is part of the Mackay Capricorn management area of the Great Barrier Reef Marine Park in the Southern Great Barrier Reef (Australia). Remotely-sensed weather information was extracted from the GIOVANNI online system for satellite derived climate data, which is maintained by NASA (http://disc.sci.gsfc.nasa.gov/giovanni). Monthly area-averaged data between 2003 and 2016 collected by the Moderate Resolution Imaging Spectroradiometer (MODIS-aqua) were used in this study, including PAR at the ocean surface (Einstein m^{-2} d^{-1}), and daytime sea surface temperature (SST, °C). Satellite data were retrieved for Heron Reef using the bounding box function to define the area of interest. GPS co-ordinates of the bounding box (151.949, −23.463, 151.977, −23.443) were selected to match the location of relay poles RP1 and RP6 (spaning an area of *ca.* 8 km^2) of the Heron Reef Integrated Marine Observing System (IMOS; Bainbridge et al., 2010). Supporting *in situ* information was retrieved from the Heron Reef IMOS network from all eight relay poles (RP1-8) that record high-resolution physical data, including above-water PAR (daily maxima and daily averages from RP8, μmol photons m^{-2} s^{-1}) and sea surface water temperature at 1–2 m depth (RP1-8, daily maxima and daily averages, °C). This data is freely available under a Creative Commons 3.0 license (https://creativecommons.org/licenses/by/3.0/au/deed.en) *via* the Australian Institute of Marine Science (www.aims.gov.au), and was accessed on 18/10/2016 using the database provided rule-based quality control for eliminating outliers or errors.

Further environmental data that relate directly to the optical clarity of the water at Heron Reef (Michael et al., 2012) were accessed from the Bureau of Meteorology (BOM) Heron Island weather station (http://bom.gov.au) which is maintained by the Australian Government. Data for wind speed (km h^{-1}), including; maximum daily gusts; wind speed at 09:00 h and 15:00 h; during the experimental periods in spring and summer (described below) were retrieved from BOM. All available data for total rainfall data (mm) at Heron Island were also retrieved from BOM between 1959 and 2007. The diffuse attenuation coefficient (K_d) of downwelling irradiance at 490 nm, used to approximate seasonal changes in turbidity (Suggett et al., 2012), was collected from the same area of interest from MODIS (as above) during the experimental periods in spring and summer.

Experimental Seasonal Context

The Heron Reef system experiences significant seasonal variability in physical conditions (Kline et al., 2015), and therefore seasonal MODIS (remotely sensed) and IMOS (*in situ*) data were specifically considered for periods coinciding with our experiments (**Figure 1**). The first experiment was conducted between 28th October and 5th November (2015), which we refer to as "spring." The second experiment was conducted between 6th and 16th March (2016); whilst this second period is regarded as post-peak of the summer season, we refer to it as "summer" for the purposes of this study. When strictly considering monthly averaged temperature pooled through 2003 and 2015 (**Figure 1**), the MODIS data indicate that November and March are typically near equal in sea surface temperature (SST) at 26.4 (±0.2 SE) and 25.9 (±0.2) °C, respectively, while the interceding months contain the annual maximum temperatures. However, the *in situ* IMOS data for SST pooled through 2008 and 2015 with higher temporal resolution indicate that the MODIS data likely over-estimate the actual SST here by *ca.* 1.2°C in November, and under-estimate by *ca.* 0.6°C in March (**Figure 1**). Strictly considering monthly averaged PAR (**Figure 1**), the monthly average irradiance of 665.3 (±20.3) μmol photons m^{-2} s^{-1} coincide with the spring experiment in November, but following this month steadily decreases, reaching 457.7 (±13.9) μmol photons m^{-2} s^{-1} in March. This trend is consistent across both MODIS and IMOS data sets. Thus, our two experimental periods contrast "spring" and "summer" as seasonal priming through (i) increases in temperature, and (ii) decreases in light availability.

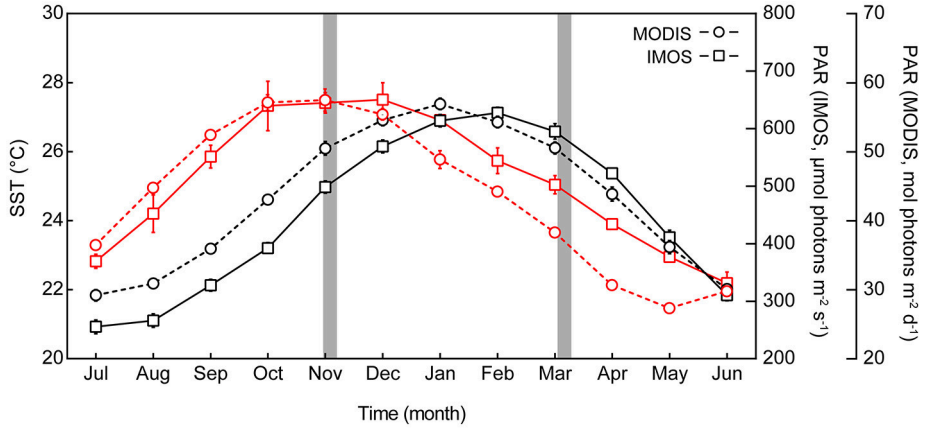

FIGURE 1 | Seasonal profile of sea surface temperature (SST) and photosynthetically active radiation (PAR) at Heron Reef. Monthly average SST (black lines, left axis) and monthly average PAR (red lines, right axes), for Heron Reef lagoon. Remote data sourced from the Moderate Resolution Imaging Spectroradiometer satellite (MODIS 2003–2016, circles) and the *in situ* Integrated Marine Observing System (IMOS 2009–2016, squares) represent monthly averages (±SE) pooled across years including all available data. Experimental periods of this study are indicated by the gray areas.

Key photophysiological parameters of interest in this study (described in further detail in sections below) are known to acclimate in as few as 5–10 days (Anthony and Hoegh-Guldberg, 2003; Roth, 2014). Thus, we utilized the high-temporal resolution (daily) IMOS system for the 14 days pre-experiment (for both spring and summer) to capture the environment under which the photochemical pathways have primed, i.e., the environmental "acclimation history." The environmental conditions immediately following this during the experiment are referred to as "ambient." The summer period of this study in 2016 was conducted directly after Heron Reef was downgraded from "Bleach-Watch" status (low thermal stress for all of February) in the Coral Reef Watch models produced by the National Ocean and Atmospheric Administration (NOAA, http://coralreefwatch.noaa.gov/satellite/index.php).

Species Collection and Maintenance

Ten coral species were used in this study (**Table 1**); *Acropora aspera; Acropora digitifera; Acropora formosa; Acropora millepora*; *Pocillopora damicornis*; *Montipora digitata; Isopora palifera; Stylophora pistillata; Porites cylindrica*; and *Porites lutea* ($N = 4$ per species, <2 m depth). All are considered common on the Great Barrier Reef (Madin et al., 2016) and are typically abundant on the shallow reef-flat and/or reef-crest of Heron Reef. These corals are typically dominated by *Symbiodinium* that broadly fall within clade C (LaJeunesse et al., 2003), and span a range of thermal tolerances that have previously been characterized in studies at Heron Reef (**Table 1**). Notably, corals containing *Symbiodinium* C15 (e.g., *M. digitata, P. cylindrica,* and *P. lutea*) are expected to be significantly more tolerant to transient heat stress than other species (Fitt et al., 2009; Fisher et al., 2012). Only coral colonies that visually appeared healthy (free of lesions or abnormal pigmentation) were selected for collection. No immediate visual signs of bleaching (i.e., significant paling of coral colonies) was observed on the reef during the spring or summer collections. Collected corals were transferred to Heron Island Research Station (The University of Queensland, Australia) and each colony was split into halves (~6 × 2 cm). All species (except *P. lutea* fragments which were mounted in a glass petri dish) were secured onto glass microscope slides using Selleys Epoxy (Selleys Pty Ltd., Australia). Coral collections were performed under the conditions of the Great Barrier Reef Marine Park Authority permits, numbered G15/37922.1 and G15/37538.1

Coral fragments were allowed to recover and acclimate for 5 days prior to experimentation in an unfiltered flow-through aquaria system under 50% of ambient light (using a neutral density shade-cloth) and a continuous flow of ambient lagoon seawater. This was deemed necessary (especially in spring) as the corals would otherwise experience artificially extreme light-doses on a daily basis due to the limited depth (and size) of the holding tanks. After acclimation, corals were distributed to 8 replicate aquaria (20 L, $N = 1$ fragment of each species per tank) also under 50% shaded natural light in a custom built open flow through system utilizing ambient lagoon seawater (minimum flow through of 0.5 L min^{-1}). The water temperature within the system was recorded every 10 min with temperature loggers (HOBO pendant data loggers, Onset Computer Corp., Bourne, MA, USA) and/or temperature buttons (Thermochron, OnSolution, NSW, Australia). This same acclimation protocol and experimental system was used in both spring and summer.

Seasonal Changes in *Symbiodinium* Photochemical Pathways

PSII photochemistry of coral-hosted *Symbiodinium* cells was measured via chlorophyll *a* fluorescence kinetics using a Pulse Amplitude Modulated (PAM) fluorometer (Diving PAM, Walz GmbH, Effeltrich, Germany, settings: MI: 12, Gain: 12, SI: 12, SW: 0.8 s, LC-INT: 3) with a glass optical fiber. Light response curves (applying actinic light to coral tissues incrementally in

TABLE 1 | Coral species used in this study from the shallow reef-flat environments of Heron Reef.

Coral species	Growth form	Reproductive mode + symbiont transmission	Known *Symbiodinium* associations (ITS2)	Thermal tolerance > 31°C
Acropora aspera	Branching (open)	Spawn + horizontal	C3 Hillyer et al., 2017	Sensitive Fisher et al., 2012 Sensitive Middlebrook et al., 2008
Acropora digitifera	Corymbose/digitate	Spawn + horizontal	C3 LaJeunesse et al., 2003	ND
Acropora formosa	Branching (open)	Spawn + horizontal	C3 LaJeunesse et al., 2003	Sensitive Fisher et al., 2012
Acropora millepora	Corymbose	Spawn + horizontal	C3 LaJeunesse et al., 2003	Sensitive Hill et al., 2012 Intermediate Fisher et al., 2012
Pocillopora damicornis	Branching (closed)	Brood + vertical	C1 LaJeunesse et al., 2003 C1c LaJeunesse et al., 2003 C33 Stat et al., 2008 C42 Stat et al., 2008	Intermediate Hill et al., 2012
Montipora digitata	Branching (open)	Spawn + vertical	C15 LaJeunesse et al., 2003 C17 Fisher et al., 2012 C73 Stat et al., 2008	Tolerant Krueger et al., 2015 Tolerant Fisher et al., 2012
Isopora palifera	Branching (open)	Brood + horizontal	C3 LaJeunesse et al., 2003 D1 Stat et al., 2008	ND
Stylophora pistillata	Branching (closed)	Brood + vertical	C1 LaJeunesse et al., 2003 C8a Sampayo et al., 2007 C35 Sampayo et al., 2007 C35a Sampayo et al., 2007 C42 Sampayo et al., 2007 C78 Sampayo et al., 2007 C79 Sampayo et al., 2007	Sensitive Hawkins et al., 2015 Sensitive Fitt et al., 2009
Porites cylindrica	Branching (closed)	Spawn + vertical	C15 LaJeunesse et al., 2003 C17 Fisher et al., 2012	Tolerant Fisher et al., 2012 Tolerant Fitt et al., 2009
Porites lutea	Massive	Spawn + vertical	C15 Fisher et al., 2012	Intermediate Fisher et al., 2012

List of 10 coral species used in this study that are common on the Great Barrier Reef (https://coraltraits.org, Madin et al., 2016). Growth forms, reproductive mode (spawning or brooding), and strategy of Symbiodinium transmission (horizontal or vertical) were also retrieved from Madin et al. (2016). Well-characterized Symbiodinium associations (ITS2 marker) from previously published studies at Heron Island are listed. The thermal tolerances of the PSII function of coral species previously tested at Heron island above 31°C are also listed as described in the respective citations. ND indicates no data.

steps of increasing irradiance) are classified according to the time duration of each light step. Rapid light curves [RLC, *sensu* Ralph and Gademann (2005); Serôdio et al. (2005)] apply light steps of short duration (e.g., 10, 20, 30 s, Perkins et al., 2010) and are widely used in coral photobiology, largely to maximize sample replication while underwater (e.g., Warner et al., 2010). Whilst RLCs provide limited time for photoprotective mechanisms to be maximally induced, steady-state light curves (SSLC) are longer in duration (e.g., 3.5 min of each light step) and are designed to allow the induction of heat-dissipation mechanisms to reach completion. However, assuming a strong diel profile of PSII photochemical efficiency in corals on shallow reef environments (Hill and Ralph, 2005), replicates (or species) may enter different states of acclimation if not sampled rapidly and thus SSLCs are not practical for comparisons of multiple field samples. Furthermore, as coral tissues migrate in response to high-light (Levy et al., 2003; Wangpraseurt et al., 2017b), the assumption that the optical properties related to the structure of the sample remain constant (Serôdio et al., 2006) may be violated during the long-duration of the SSLC and the retrieved fluorescence signals may become error-prone (as seen for corals in Lichtenberg et al., 2016). Suggett et al. (2015) demonstrated that RLCs (20 s light steps) and SSLCs (3.5 min light steps) generally resolve similar light utilization patterns across diverse taxa of *Symbiodinium* in culture, however it is unknown if *Symbiodinium* cells organized into the tissue layers of corals will show similar patterns (although both RLCs and SSLCs are equally limited in this regard). With these factors considered (and discussed in sections below), the use of RLCs are preferred in the present study to conduct all measurements within a narrow time-frame, and we interpret the findings within the limitations of the method. Importantly, we do not interpret the findings as absolute rates of electron transport in photosynthesis (Enríquez and Borowitzka, 2010; Warner et al., 2010) and we do not utilize the RLC as a substitute for a SSLC (Perkins et al., 2010). RLCs with 8 actinic light steps were conducted on low-light acclimated corals during the first 1.5 h of the morning light period ($N = 3$ technical replicates per fragment for $N = 4$ biological replicates) to minimize the effect of night-time reduction of the plastoquinone pool (Hill and Ralph, 2005). Actinic light levels (calibrated against a factory calibrated LI-192 quantum sensor, Li-Cor, Lincoln, NB, USA) of the RLC were 0, 115, 168, 228, 335, 450, 666, 954, 1,356 μmol photons m^{-2} s^{-1}, and 0, 98, 162, 240, 325, 480, 610, 971, 1,350 μmol photons m^{-2} s^{-1} in spring and summer, respectively, and were delivered in 20 s intervals. All RLC measurements were conducted over 4-days, with one replicate per species per day. Distributing the RLCs over a 4-day experimental period was necessary to complete the technical replicates for each fragment within

the naturally low-light acclimated state immediately following sunrise.

All RLCs were initiated with a dark measurement to provide the minimum and maximum dark acclimated fluorescence yields, F_o and F_m, respectively, and all subsequent steps measure the minimum, and maximum fluorescence yields under actinic light, F' and F_m', respectively. These parameters are then used to calculate the maximum ($F_v/F_m = [F_m - F_o]/F_m$) and effective ($F_q'/F_m' = [F_m' - F']/F_m'$) photochemical efficiency. Whilst the latter term is often denoted as Φ_{PSII}, we use F_q'/F_m' to be consistent with Hennige et al. (2008) and Suggett et al. (2012). A light-response curve for F_q'/F_m' was thus generated for each RLC and then fit to a model that characterizes the light-dependent quantum efficiency of PSII using least squares non-linear regression (Equation 1), described in Hennige et al. (2008).

$$F_q'/F_m' = [(F_q'/F_m'_{(\max)}E_k)(1 - \exp(-E/E_k))]/E \quad (1)$$

Briefly, this model provides an estimate of the minimum saturating irradiance (E_k μmol photons m^{-2} s^{-1}) which describes the transition between the light-limited and the light-saturated states of PSII (Hennige et al., 2008). Equation (1) also derives $F_q'/F_m'_{(\max)}$ (dimensionless) which is an alternate estimate of the maximum PSII photochemical efficiency, which can differ from the dark-acclimated maximum quantum yield of photosystem II (F_v/F_m) depending on light history, see Suggett et al. (2012).

To calculate the poise of the photosystem and the activity of pathways of excitation energy transfer other than fluorescence, the extent of light dependant photochemical ([1 – C], Equation 2) and non-photochemical quenching ([1 – Q], Equation 3) parameters were both derived from each RLC light step across seasons and species as follows.

$$[1 - C] = (F_m' - F)/(F_m' - F_o') \quad (2)$$

$$[1 - Q] = (F_v'/F_m')/(F_v/F_m) \quad (3)$$

where [1 – C] is the same as qP referred to in previous studies (Hennige et al., 2008; Oxborough et al., 2012), which assumes zero connectivity (C) between adjacent reaction centers and represents the proportion of excitation energy used to drive photochemistry as the fraction of open reaction centers. [1 – Q] describes the dynamic non-photochemical quenching (Q) that is equivalent to the excitation pressure over PSII (Iglesias-Prieto et al., 2004; Suggett et al., 2015). Use of [1 – Q] is preferred for our study over other calculations of non-photochemical quenching, [e.g., NPQ = $(F_m - F_m')/F_m'$], since the product of [1 – C] and [1 – Q] account for the total energetic dissipation (effective photochemical efficiency) normalized to taxonomic differences in maximum photochemical efficiency, i.e., $(F_q'/F_m')/(F_v/F_m)$ (see Suggett et al., 2015). These parameters decrease over the course of the RLC as they become active or are "utilized."

While all corals were collected from the same light environment (<2 m depth), and care was taken to avoid species at Heron Reef that are characterized as having comparatively thick tissue layers (e.g., *Platygyra* spp. or *Pavona* spp.), it is possible that differences in host pigmentation (Salih et al., 2000), alteration of light fields due to host macrostructure (Enríquez et al., 2005, 2017; Terán et al., 2010; Wangpraseurt et al., 2014), or even the aspect of the colony that fragments were removed from Brown et al. (2000), could potentially introduce variation in the acclimation states of the fragments. Thus, parameters generated from the RLC described below were normalized to E_k to eliminate this source of variability (as per Hennige et al., 2008; Suggett et al., 2012). Examining parameters as E/E_k rather than E allows the differences in photoacclimation to be viewed independent of how photosynthetically usable radiation varies between species, and provides an indication of how mechanisms associated with regulating light-limited (below E_k) or light-saturated (above E_k) PSII are preferentially modified to optimize toward E_k (Hennige et al., 2008).

Both [1 – C] and [1 – Q] were analyzed against the normalized values of E/E_k and assessed with non-linear regression using a standard one phase decay model in Graphpad Prism (version 6). Replicates tests (Graphpad Prism version 6) that test for an inadequate model fit were performed on every curve and confirmed that the one-phase decay model adequately described all quenching curves for all species across both seasons ($p > 0.05$), except for *A. millepora* [1 – C] in spring which did not fit the one phase decay model and was instead fit to a linear model ($R^2 = 0.76$). For every curve (each representing the mean of 4 replicates) the values of [1 – C] and [1 – Q] where $E/E_k = 1$ (i.e., at the minimum saturating irradiance) were interpolated.

Thermal Stress Assay and Monitoring of PSII Photochemical Efficiency

Following the completion of the RLC described above in the non-stressed condition, half of the experimental tanks ($N = 4$) were subjected to changes in temperature to induce transient thermal stress, and the remaining experimental tanks ($N = 4$) were unchanged and served as ambient controls with continuous flow of ambient lagoon seawater. Our approach aimed to maximize synchronicity and equivalency of the ramping profiles in spring and summer (Figure S1) and reach equivalent end-points in temperature. In spring, temperature was increased from 26°C in 1°C increments daily to reach the target treatment temperature of 32°C, and then was held for a further 3 days. 32°C was selected as an environmentally relevant upper limit as the single warmest day recorded by the IMOS network (measured across all RP) reached a maximum of 32.55°C (21st February 2009). In the summer experiment, the ambient lagoon was naturally fluctuating between 26 and 28°C on a diel basis and thus to synchronize the profile with spring, treatment tanks were allowed to fluctuate for the first day under which spring ramped from 26 to 27°C, and then the profiles were synchronized from 28 to 32°C and increased in 1°C increments daily (Figure S1). Temperature was increased by pre-heating continuous flow-through lagoon seawater in a separate sump (200 L) with two custom built, thermostat controlled (±0.1°C) submersible heaters (300 W). Treatment water was pumped from this sump to aquaria at a flow rate matching the flow-through of ambient aquaria.

During the temperature ramp and maintenance at 32°C, dark-acclimated maximum quantum yield of photosystem II (F_v/F_m) was measured twice every day for every coral fragment to monitor for changes in photochemical efficiency (as per Oliver and Palumbi, 2011; Suggett et al., 2012); once in the first hour following sunrise (*ca.* 07:00 h local time) and once again in the evening during the first hour following sunset (*ca.* 19:00 h local time; $N = 3$ technical replicates per fragment). An inverted exponential function (Equation 4, as per Vieira et al., 2009) was used to describe the decrease in F_v/F_m through time as follows.

$$F_v/F_m = F_v/F_{m(0)} - e^{-S+kx} \quad (4)$$

where F_v/F_m is expressed as % ($\%F_v/F_m$, relative to untreated fragments), $F_v/F_{m\ (0)} = \%F_v/F_m$ prior to thermal stress (i.e., $x = 0$), x = time (d), S is a parameter related to the length of the period during which $\%F_v/F_m$ remains stable, and k (d^{-1}) is the rate constant that quantifies the rate of $\%F_v/F_m$ decrease. The minimum (typically reached at the final measurement) dark-acclimated maximum quantum yield of photosystem II reached during exposure to heat stress, will be referred to as $\%F_v/F_{m(\min)}$.

Statistical Analyses

Environmental variables were compared between seasons using unpaired two tailed *t*-tests, assuming unequal variances which were accounted for with Welch's correction. This same statistical test was used to analyse the pooled photoacclimation response (E_k and $F_q'/F_m'_{\ (\max)}$) of all coral species when comparing between spring and summer. To identify specific differences across seasons and species two-way ANOVA was used to investigate the interactions between season (two levels) and species (10 levels) on derived values of E_k and $F_q'/F_m'_{\ (\max)}$, with Sidak's multiple comparisons post hoc tests to locate significant differences. All statistical tests were performed in Graphpad Prism (version 6) against an α of 0.05. To identify functional groupings of corals based on all derived components of the light response curves and thermal tolerance of PSII function, cluster analysis and multidimensional scaling (MDS) were performed with E_k; $F_q'/F_m'_{\ (\max)}$; [1 – *C*]: [1 – *Q*] at $E/E_k = 1$; and $\%F_v/F_{m(\min)}$, with PRIMER-E v6.1 (PRIMER-E Ltd, Ivybridge, Devon, UK). All values were standardized using a square root transformation using PRIMER-E and correlations were drawn based on Pearsons distance. An analysis of similarity (ANOSIM) was used to determine whether the corals separated by MDS ordination significantly differed between seasons.

RESULTS

Spring and Summer Environmental Conditions in the Heron Lagoon

Ambient SST during the experiments in spring (2015) and summer (2016, IMOS *in situ*) closely matched the typical SST for October-November and February-March (2009–2016; **Table 2**). SST increased significantly from spring through summer as expected; daily averages were 24.2°C (±0.7) and 26.9°C (±0.3) during the spring and summer experiments, respectively. Maximum ambient temperatures reached across these periods were 27.3 and 30.2°C, respectively (**Table 2**, Figure S2). Ambient PAR for spring and summer were also consistent with previous years (**Table 2**, Figure S2), whereby ambient daily average PAR during spring was 541.5 (±148.2) μmol photons m^{-2} s^{-1} and was significantly lower during the summer at 442.8 (±142.9) μmol photons m^{-2} s^{-1} (unpaired two tailed *t*-test with Welch's correction, $t_{(43)} = 3.10$ and $t_{(38)} = 2.4$, respectively, $p < 0.05$). Maximum daily PAR values during these periods were 2091.3 and 2004 μmol photons m^{-2} s^{-1}, respectively. This pattern appears to be driven by consistent levels of PAR (i.e., days to weeks) in spring, whereas summer months were frequently punctuated by multiple events of comparatively low PAR (i.e., storm events, Figure S2). Indeed, the acclimation history directly preceding the summer experiment included a significant weather event that lowered the average daily and average maximum PAR to 124 and 560.3 μmol photons m^{-2} s^{-1}, respectively (Figure S2). This pattern of decreasing PAR from spring through summer appears seasonally typical and supported by long-term trends gathered from MODIS (2003–2016; **Figure 1**).

Further physical changes that play a significant role in modulating in-water PAR include the diffuse attenuation coefficient (K_d) of downwelling irradiance, which is used to approximate changes in seawater turbidity (Suggett et al., 2012), elevated wind speeds [which are known to increase K_d at Heron Reef (Michael et al., 2012)], and monthly rainfall. Heron Reef is subjected to significantly faster wind speeds and nearly three-fold greater rainfall in summer (Figure S2). However, this more extreme weather of summer is not reflected in seasonal differences in the remotely-sensed $K_d(490)$ retrieved from the MODIS instrument (Figure S3).

Light Dependant Response of *Symbiodinium* Photochemistry

Eqn. 1 produced a robust description of the light dependant response of F_q'/F_m' across species and seasons (R^2 *ca.* 0.9), except for *A. aspera* and *M. digitata* in spring ($R^2 = 0.76$ and 0.65, respectively) although values for E_k and $F_q'/F_m'_{\ (\max)}$ were still within the range retrieved for all species. Significant seasonal changes in E_k (**Figure 2**) were evident for all species. In spring, the pooled average of E_k across all 10 species was 534.1 (± 67.3) μmol photons m^{-2} s^{-1}, and in summer decreased >2-fold to 227.5 (± 28.5) μmol photons m^{-2} s^{-1} [unpaired two tailed *t*-test with Welch's correction, $t_{(9)} = 17.77$, $p < 0.01$]. These values of minimum saturating irradiance are thus consistent with the differences in acclimation history between spring and summer experiments (**Table 2**, Figure S2). A two-way ANOVA of species × season revealed significant effects of each factor [$F_{(9,59)} = 2.835$, $p < 0.01$, and $F_{(1,59)} = 345.2$, $p < 0.0001$, respectively] and Sidak's multiple comparisons tests confirmed that all comparisons of species from spring to summer had significantly lower E_k (all multiple comparison tests $p < 0.05$). The largest change in E_k between seasons was for *A. aspera* decreasing from 652.9 (±75.4) μmol photons m^{-2} s^{-1} in spring to 244 (±10.4) μmol photons m^{-2} s^{-1} in summer. In contrast, the smallest changes in E_k were observed

TABLE 2 | The physical environment of Heron Reef in spring and summer.

	Spring			Summer		
	Oct-Nov	**Acclimation history**	**Ambient**	**Feb-Mar**	**Acclimation history**	**Ambient**
Temperature (°C)						
Daily average	24.0 (±1.2)	23.5 (±0.7)	24.2 (±0.9)	26.8 (±0.8)	27.3 (±0.4)	26.8 (±0.3)
Daily maximum	25.2 (±1.3)	24.9 (±1.2)	25.5 (±1.1)	27.8 (±1.0)	28.4 (±0.7)	27.7 (±0.5)
PAR (μmol photons m^{-2} s^{-1})						
Daily average	625.6 (±121.5)	616.3 (±30.3)	541.5 (±148.2)	517.9 (±177.9)	476.8 (±151.9)	442.9 (±148.9)
Daily maximum	2090.5 (±180.4)	2019.1 (±97.4)	1930.8 (±224.6)	1982.5 (±516.4)	1777.8 (±391.8)	1700.3 (±424.9)

In situ physical data retrieved from the Heron Reef IMOS network (from all eight relay poles). Data include above-water photosynthetically available radiation (PAR, μmol photons m^{-2} s^{-1}, daily maxima and daily averages) and sea surface water temperature at 1–2 m depth (°C, daily maxima and daily averages). All available data (daily measurements between 2009 and 2016) were used to characterize the typical conditions for spring (October-November) and summer (February-March). The acclimation history reflects the 14 d period directly preceding the spring (2015) and summer (2016) experiments. The ambient environmental conditions during the experiment are also listed. Values represent means for the period ± 1 SD. These data were accessed via the Australian Institute of Marine Science (www.aims.gov.au).

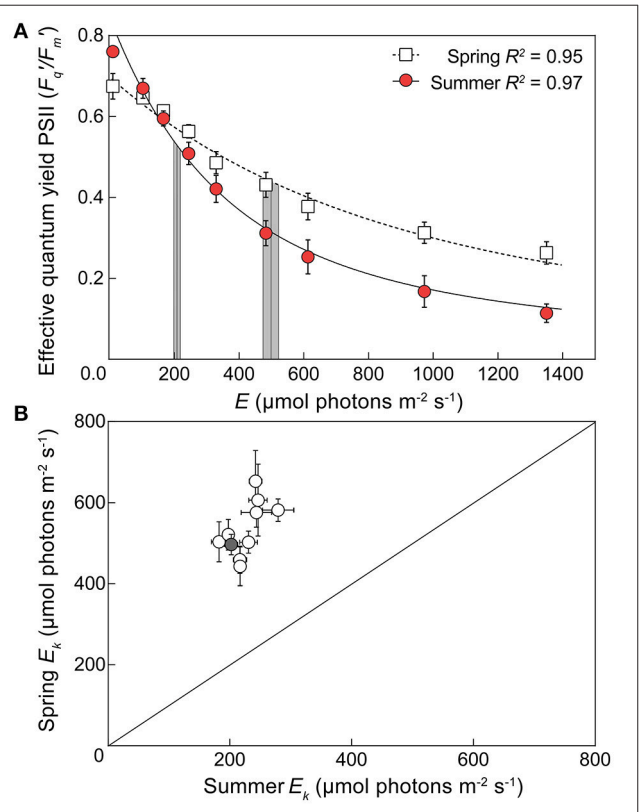

FIGURE 2 | Seasonal changes in minimum saturating irradiance for 10 coral species. **(A)** An example light response curve for the effective quantum yield of PSII (F_q'/F_m') in the coral *Acropora digitifera* in spring (open squares) and summer (red circles). Error bars indicate ±SE. The derived minimum saturating irradiance (E_k) of each curve is indicated by the vertical lines ±SE (gray areas). **(B)** The derived E_k for all 10 species of coral plotted according to season (1:1 ratio indicated by diagonal line) with spring E_k on the vertical axis and summer E_k on the horizontal axis. The gray symbol indicates the example derived values of *Acropora digitifera* shown in **(A)**.

for *P. cylindrica*, decreasing from 442.8 (±47.8) μmol photons m^{-2} s^{-1} to 218.5 (±8.9) μmol photons m^{-2} s^{-1} between seasons.

Values for the derived maximum PSII photochemical efficiency F_q'/F_m' $_{(max)}$ (dimensionless) also differed significantly between seasons and when averaged across all species increased from 0.68 (±0.01) in spring to 0.77 (±0.02) in summer [Figure S4, unpaired two tailed *t*-test with Welch's correction, $t_{(12)} = 4.94$, $p < 0.001$]. This is supported by the measured values of F_v/F_m which also increase across seasons (Figure S5). A two-way ANOVA of species × season revealed a significant interaction between factors [$F_{(9, 59)} = 2.147$, $p < 0.05$]; however, Sidak's multiple comparisons tests confirmed that this was not driven by a consistent response across all species (Figure S4). For example, whilst *M. digitata, P. lutea, P. cylindrica,* and *S. pistillata,* exhibited significant changes in E_k, no corresponding significant shift in F_q'/F_m' $_{(max)}$ was observed (Figure S4). However, all other species demonstrated a shift in F_q'/F_m' $_{(max)}$ with an increase in summer (Sidak's multiple comparisons tests $p < 0.05$), and the largest change in F_q'/F_m' $_{(max)}$ of 0.14 (dimensionless) between seasons was observed in *A. digitifera*. Overall, these general complimentary responses for E_k and F_q'/F_m' $_{(max)}$ are consistent with acclimation to the decrease of light availability (Hennige et al., 2008; Suggett et al., 2012) that appears typical between spring and summer, including our 2015/16 sampling season (above, **Table 2**).

Seasonal Changes in Light Dependant Dynamic Quenching

Values derived for [1 – *C*] at $E/E_k = 1$ pooled across all species differed significantly between seasons [unpaired two tailed *t*-test with Welch's correction, $t_{(10)} = 4.675$, $p < 0.001$], decreasing from 0.79 (±0.02) in spring to 0.72 (±0.01 SE) in summer. Similarly, the derived [1 – *Q*] at $E/E_k = 1$ pooled across all species also differed significantly between seasons [unpaired two tailed *t*-test with Welch's correction, $t_{(13)} = 7.56$, $p < 0.001$], increasing from 0.79 (±0.02) in spring to 0.94 (±0.01) in summer. As such, at the light intensity at which electron transfer rates "saturate" ($E/E_k = 1$), corals generally shifted toward increased reliance of photochemical over non-photochemical quenching from spring into summer as light availability decreased. In fact, three distinct quenching patterns previously described for

Symbiodinium isolates (Suggett et al., 2015) were observed in spring. "Normal quenching," where [1 – *C*] and [1 – *Q*] are utilized equally, *P. damicornis* and *A. digitifera*; preferential photochemical quenching, where the ratio of [1 – *C*] to [1 – *Q*] < 1 for *P. lutea, P. cylindrica, S. pistillata,* and *M. digitata*; and preferential non-photochemical quenching, where the ratio of [1 – *C*] to [1 – *Q*] > 1 for *A. aspera, A. formosa, A. millepora,* and *I. palifera*. However, all coral species switched to preferential utilizing [1 – *C*] in summer (**Figure 3**). The largest seasonal shift in the ratio of [1 – *C*] to [1 – *Q*] at $E/E_k = 1$ was for *A. formosa* (1.23 in spring, decreased to 0.73 in summer), whereas the smallest shift was for *S. pistillata* (0.88 in spring, decreased to 0.79 in summer).

PSII Photochemical Efficiency during Transient Heat Stress Assays

Corals subjected to transient heat stress typically exhibited comparable $\%F_v/F_{m(\min)}$ across spring and summer, except for *P. damicornis* and *S. pistillata* (**Figures 4E,H**). *S. pistillata* suffered total dysfunction in spring, i.e., chlorophyll fluorescence was below the levels of detection (not able to measure F_o), representing the strongest reaction of all species to transient heat stress. In contrast, *S. pistillata* was less sensitive in summer with $\%F_v/F_{m(\min)}$ reaching 41.12 (±13.91) relative to ambient fragments; as such, *S. pistillata* was the only species to show significantly enhanced thermal tolerance from spring to summer. *P. damicornis* exhibited an opposite response whereby $\%F_v/F_{m(\min)}$ reached 75.31 (±8.85) relative to ambient fragments in spring, but had a heightened sensitivity in summer [$\%F_v/F_{m(\min)}$ was reduced to 19.91 (±8.89) relative to ambient fragments].

PSII photochemical efficiency of *M. digitata* and *P. lutea* was tolerant to transient heat stress across both seasons (**Figures 4F,I**). However, in summer, *P. lutea* fragments raised to 32°C demonstrated increased diel variability (i.e., morning vs. evening $\%F_v/F_m$) relative to ambient fragments. All other coral species exhibited compromised PSII photochemical efficiency via heat stress for both seasons. Parameters retrieved by the inverted exponential function fit to changes in $\%F_v/F_m$ (Equation 4, Table S1) indicate that PSII photochemical efficiency for multiple species declined earlier in summer than in spring (i.e., $S_{\text{summer}} < S_{\text{spring}}$), however, the rate of decline (once it began) was comparatively more rapid in spring than in summer (i.e., $k_{\text{summer}} < k_{\text{spring}}$). For example, for *A. aspera, S* (dimensionless) was 5.18 (±3.26) in spring, but declined to 1.64 (±0.53) in summer, whereas k (d^{-1}) declined from 0.94 (±0.40) d^{-1} to 0.58 (±0.06) d^{-1} from spring to summer (Table S1, **Figure 4A**). Despite these minor seasonal differences in kinetics of PSII photochemical efficiency, $\%F_v/F_{m(\min)}$ for *A. aspera* after 3 d at 32°C was not significantly different across seasons [83.33 (±8.43) in spring vs. 75.76 (±4.19) in summer]. This same pattern of an earlier, more gradual decline in PSII photochemical efficiency during the summer experiment was also seen in *A. digitifera*, *A. millepora,* and *P. cylindrica* (Table S1). *A. formosa* and *I. palifera* were more sensitive to transient heat stress than the other Acroporid species, and $\%F_v/F_{m(\min)}$ reached 44.63 (±25.81) and 50.75 (±23.43) % for the two species respectively in spring compared to 56.83 (±19.87) and 60.88 (±20.53) % in summer. Additionally, *A. formosa* and *I. palifera* demonstrated

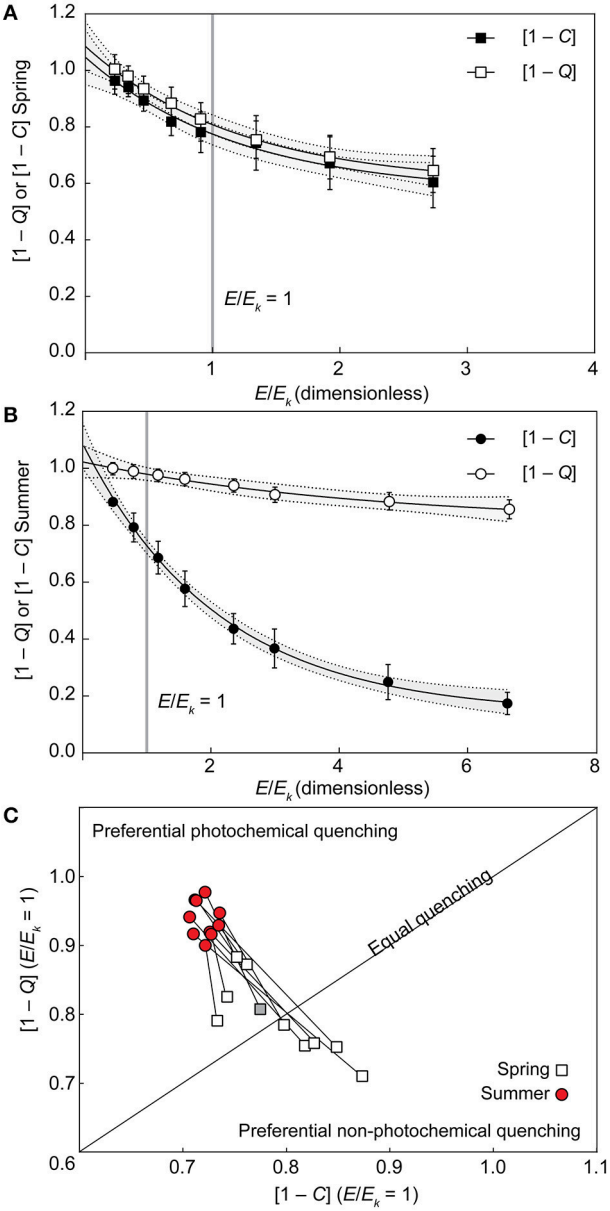

FIGURE 3 | Seasonal changes in photochemical and non-photochemical quenching. **(A,B)** Example of photochemical ([1 – *C*], black symbols) and non-photochemical ([1 – *Q*], open symbols) quenching light-response curves fit to non-linear, one-phase exponential decay models in spring **(A)** and summer **(B)** in the coral *Acropora digitifera*. Error bars indicate ±SE and the gray areas inside dashed lines indicate the ±95% prediction bands of the model fit. **(C)** Interpolated values of [1–*Q*] (vertical axis) and [1–*C*] (horizontal axis) at $E/Ek = 1$ [indicated by the vertical gray lines in **(A,B)**] are plotted for all 10 species according to season (1:1 ratio indicated by the diagonal line) with spring (open squares) and summer (red circles) species pairs joined by lines that indicate the direction of the photoacclimation shift. The example from *Acropora digitifera* in spring is indicated by the gray square.

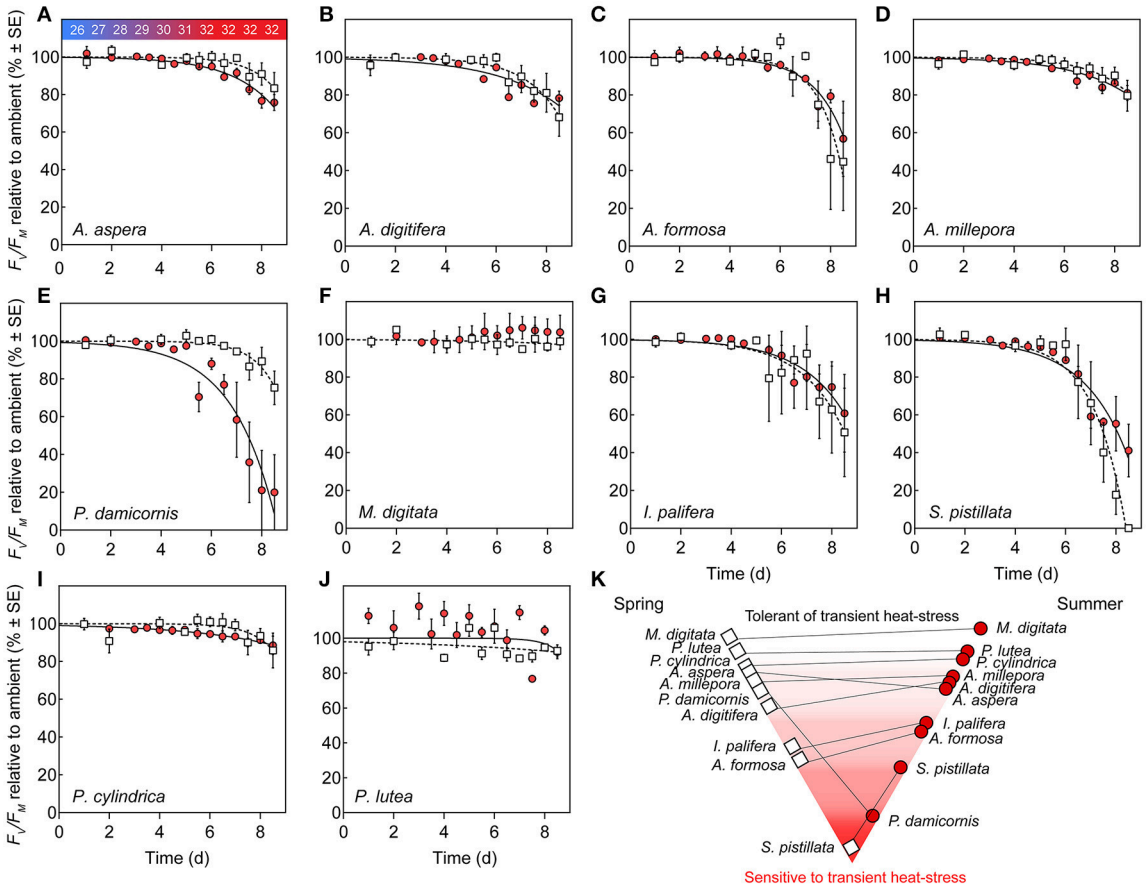

FIGURE 4 | Photosystem II (PSII) function under transient heat stress. **(A–J)** Species-specific declines in maximum PSII quantum yield (%F_v/F_m) of corals under a thermal stress experiment expressed relative to ambient controls (%) at each corresponding time point in spring (open squares) and summer (red circles). Lines represent the non-linear regression, inverted exponential fit in spring (hashed lines) and summer (solid lines). Values represent means ($N = 4$) ±SE. **(K)** Pyramid graph of the hierarchy of thermal tolerance from most tolerant (top) to the most sensitive species (bottom). Horizontal lines between spring (left, open squares) and summer (right, red circles) indicate the direction of change in minimum dark-acclimated quantum yield of photosystem II reached during exposure to heat stress as %$F_v/F_{m(\min)}$ across seasons.

high inter-fragment variability. For example, the %F_v/F_m of *I. palifera* exposed to transient heat stress in spring ranged from 0.62 to 0.15 (dimensionless) across all four replicates.

Functional Diversity in Photobiology across Species and Seasons

All of the derived photophysiological parameters, including E_k, $F_q'/F_m'_{(\max)}$, [1 – C] and [1 – Q] at $E/E_k = 1$, as well as %$F_v/F_{m(\min)}$, for both spring and summer, were analyzed using MDS to examine functional differences across species. ANOSIM further confirmed the significant separation of photobiology across seasons (**Figure 5**, global $R = 0.88$, $p < 0.001$), whereby separation of seasonal clusters was driven primarily by the RLC-derived parameters (horizontal vectors of E_k, $F_q'/F_m'_{(\max)}$, [1 – C] and [1 – Q], **Figure 5**). Within each season, the ordinations of individual species did not cluster exclusively according to growth form, host taxonomy, or known symbiont associations (**Table 1**). For example, in spring, three distinct genera (*Acropora, Porites,* and *Montipora*) cluster together at 97% similarity. Species within each season were thus largely ordinated according to the response of PSII photochemical efficiency to heat stress (vertical vector of %$F_v/F_{m(\min)}$) with the most thermally tolerant species (*M. digitata* and *P. lutea*) clustered together at 97% similarity in both seasons. *S. pistillata* was the most dissimilar to all other species (<80% similarity) and this is primarily driven by the complete dysfunction in response to temperature [i.e., %$F_v/F_{m(\min)} = 0$], rather than differences in the non-stressed photobiology (above). For species that survived the transient heat stress (i.e., excluding *S. pistillata*), the only RLC parameter demonstrating a significant linear relationship with PSII photochemical efficiency under stress was the extent of light-dependant dynamic quenching (**Figures 5B,D**). Specifically, a negative linear relationship between %$F_v/F_{m(\min)}$ and [1 – C] at $E/E_k = 1$ ($R^2 = 0.48$, $p < 0.05$), and a positive linear relationship between %$F_v/F_{m(\min)}$ and [1 – Q] at $E/E_k = 1$ ($R^2 = 0.50$, $p < 0.05$), indicating that species inherently primed to preferentially employ greater photochemical over non-photochemical quenching during non-stressed conditions also

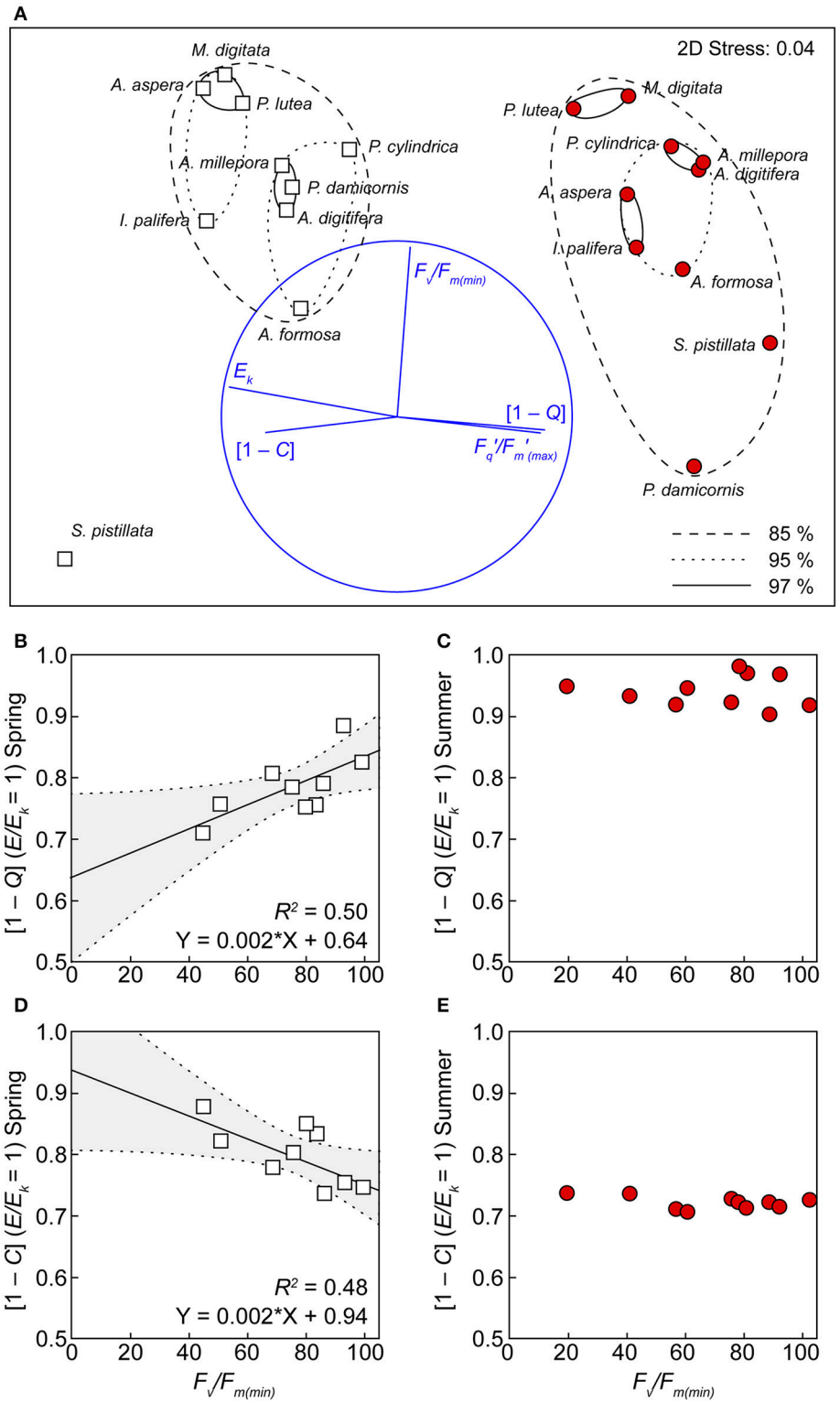

FIGURE 5 | Functional groupings according to photochemistry and thermal tolerance. **(A)** Multi-dimensional scaling (MDS) analysis, using the derived values of E_k, $F_q'/F_m'_{(max)}$ (dimensionless), [1 – *C*] and [1 – *Q*] at $E/E_k = 1$, and $\%F_v/F_{m(min)}$ in both spring (white squares) and summer (red circles). Clusters represent 85 (hashed ovals), 95 (dotted ovals), and 97 (solid ovals) % similarity (based on a Bray–Curtis dissimilarity matrix) between species. Significant linear correlations between [1 – *Q*] **(B),** [1 – *C*] **(D)** and $\%F_v/F_{m(min)}$ are indicated by lines with 95% confidence band (gray areas) of the fit. This correlation is absent for the same parameters in summer **(C,E)**.

have PSII that are more thermally tolerant. However, this linear relationship was absent in summer (**Figure 5**).

DISCUSSION

Our study from the shallow-reef flat environment of Heron lagoon captured photochemical seasonal low-light acclimation from spring to summer across all coral species. Species-independent reductions in the minimum PSII saturating irradiance (E_k μmol photons m^{-2} s^{-1}) were consistent with seasonal reductions in PAR (i.e., E/E_k approaching 1), and reflected a general shift to preferential utilization of [1 – *C*] (i.e., increased reliance on linear electron transport), which is expected as *Symbiodinium* acclimate toward low-light (Ragni et al., 2010; Suggett et al., 2015). Whilst such acclimation did not reorganize species hierarchy of thermal tolerance across seasons (except *S. pistillata* and *P. damicornis*), the strategy for dealing with light energy was unchanged for thermally tolerant species across seasons. We discuss how these findings expand our understanding of *Symbiodinium* photobiology and how such studies can potentially be used to identify diagnostics of thermal susceptibility under non-stressed conditions.

Symbiodinium spp. use various acclimation processes to increase their photosynthetic capacity and inhabit light-reduced habitats (e.g., mesophotic reefs or cryptic habitats), commonly reflected by reducing E_k; for example, acclimation from open, high-light habitats to light-reduced reef walls and caves (*Montipora monasteriata* at Wistari Reef, neighboring Heron Reef, Anthony and Hoegh-Guldberg, 2003), and with increasing depth (*Madracis* spp., Curacao, Frade et al., 2008); and across both clear and turbid sites (*Porites lutea*, Indonesia, Hennige et al., 2008). In the latter case, these trends shift in parallel with increases in $F_q'/F_m'_{(max)}$ (Hennige et al., 2008). Such acclimation can in fact be described by a linear function with changing optical depth (Hennige et al., 2008) until corals inhabit extreme light regimes (see Suggett et al., 2012). Our data from spring to summer are thus entirely consistent with this classical view of a reduction in E_k and increase in $F_q'/F_m'_{(max)}$ indicating that the same photoacclimation processes that are well-described to operate across space, also operate through time.

In contrast to our observations, Ulstrup et al. (2008) previously demonstrated that E_k is greater in summer (January) than in winter (July), especially for the shade-adapted sides of branches, for *P. damicornis* and *Acropora valida* at Heron Reef. However, this is not entirely at odds with our findings, as without data for the interceding months in spring, it is not possible to ascertain if corals examined by Ulstrup et al. (2008) cycled through a period of spring high-light acclimation. Immediately prior to and during the first days of our summer experiment, where average daily PAR levels (above water, IMOS network) dropped below 300 μmol photons m^{-2} s^{-1} due to a significant weather event. The kinetics of photoacclimation in corals in response to stochastic low-light events have not been explored extensively for the corals used in our study; however, the coral *Turbinaria mesenterina* can exhibit changes in E_k to changes in light levels in as few as 5–10 d (Anthony and Hoegh-Guldberg, 2003). Roth et al. (2010) also demonstrated that maximum quantum PSII yields increase in response to low-light conditions within a period of 5–10 d for the coral *Acropora yongei*. Such relatively rapid timeframes suggest that our E_k and $F_q'/F_m'_{(max)}$ acclimation could therefore perhaps reflect a chance capturing of a stochastic low-light acclimation event, exacerbating any typical seasonal response that might have occurred. Such experiments would thus benefit from frequent sampling intervals (ideally daily measurements), to tease apart seasonal vs. stochastic weather acclimation. These challenges aside, we still observed an acclimation response consistent with changes in light availability across seasons and thus a basis to examine different acclimation states in the context of thermal sensitivity.

Our observed changes in E_k [and $F_q'/F_m'_{(max)}$] reflect the seasonal light environment; however, the apparent synergy between light and temperature in bleaching stress (Jones et al., 1998; Mumby et al., 2001; Anthony et al., 2007) indicate the potential role of factors other than light (i.e., temperature) in driving changes in the saturation of PSII reaction centers. E_k is governed by changes in both light harvesting and utilization (Frade et al., 2008; Hennige et al., 2008; Suggett et al., 2012); however, the maximum rate of linear electron transport is further constrained by downstream processes, including CO_2 limitation and the kinetics of enzymatic function, both of which are likely altered under changes in temperature (Jones et al., 1998), in particular, under extreme and relatively rapid temperature excursions for *Symbiodinium* (Lilley et al., 2010). For example, Claquin et al. (2008) demonstrated for six species of diatoms grown under a range of temperatures (between 5 and 35°C), that E/E_k is driven to > 1 for temperatures both above and below the optimum for growth, i.e., inherent acclimation processes under non-optimal conditions cannot balance light-harvesting and downstream photosynthetic reactions. Given that the optimal temperature range for enzymes involved in photosynthesis and growth in corals of the present study are unknown, the deconvolution of temperature and light as factors in E_k regulation is presently not possible. Ultimately this will be important as a loss of linear electron transport chain, but maintenance of absorption, inevitably places more pressure on the photosystem and the ability of *Symbiodinium* cells to buffer transient stressors.

Light utilization strategies were markedly different between seasons, and in spring three distinct patterns were observed: a "normal quenching profile" (equal utilization of [1 – *C*] and [1 – *Q*]), preferential dynamic non-photochemical quenching, and preferential photochemical quenching (*sensu* Suggett et al., 2015). Such variability of inherent photosynthetic "strategy" is entirely consistent with the idea of *Symbiodinium* "ecotypes" (Iglesias-Prieto and Trench, 1997) or species optimized to different regimes, but able to co-exist within a single habitat through acclimation plasticity, i.e., the shallow reef flat of Heron Reef. Interestingly, light utilization strategies of *Symbiodinium* under spring conditions partially corresponded to phylogenetic groups (both host and symbiont, **Table 1**) that may reflect the light field of specific corals (Wangpraseurt et al., 2012). For example, coral species with symbionts utilizing preferential non-photochemical quenching were closely related (all in

the family Acroporidae) and are known to harbor host-generalist *Symbiodinium* types (i.e., *Symbiodinium* ITS2 type C3, **Table 1**) that are typically acquired horizontally from a pool of free-living *Symbiodinium* (Nitschke et al., 2016). This supports the concept that host-specific differences in physical architectures (both skeletal and tissue structure) produce unique optical environments (Terán et al., 2010; Enríquez et al., 2017; Wangpraseurt et al., 2017a) that may force the photobiology of *Symbiodinium* to converge on host-specific strategies of light-utilization. Furthermore, a high capacity (or rapid induction) of non-photochemical quenching allows photosynthetic microorganisms (i.e., diatoms) to thrive in environments that have a high rate of change in light regimes (Lavaud et al., 2007), which for *Symbiodinium* that enter hosts horizontally, spans both free-living niches (e.g., sediment Nitschke et al., 2015) as well as symbiosis.

While it is tempting to interpret this photobiological trait and patterns of contrasting life history modes (i.e., symbiotic vs. free-living) and coral species-specific light fields (Enríquez et al., 2017) as reflecting trade-offs to a range of light regimes (Suggett et al., 2015), such a hypothesis requires extensive testing to fully establish whether such a pattern holds across a greater range of *Symbiodinium* genotypes and hosts. However, this notion is further supported by the observation that coral species with preferential photochemical quenching in this study harbor symbionts that are acquired vertically (i.e., maternal transmission), and include a number of ITS2 types which (at present) are not culturable (Krueger and Gates, 2012); e.g., *P. lutea*, *P. cylindrical,* and *M. digitata* all host *Symbiodinium* C15 (ITS2) at Heron Reef (**Table 1**), suggesting that *Symbiodinium* restricted to a specific light environment (i.e., host tissues) may have become optimized in regards to a single strategy of light-utilization. It must be noted, however, that the host-tissues themselves may interact with the fluorescence signals of the *Symbiodinium* cells and that the complex multi-cellular arrangement, varied pigment content, and mobile nature of the tissue add a level of uncertainty to inter-species comparisons. For example, Lichtenberg et al. (2016) retrieved fluorescence signatures inside coral tissues with a fiber-optic micro-probe and demonstrated that deeper tissue layers achieve different states of acclimation. However, this micro-scale technique was sensitive to tissue contraction and thus any correction factors that account for tissue depth require continuous knowledge of the physical (i.e., contracted or relaxed) state of the tissue. Ultimately, multiple attenuation coefficients that correspond to the coral tissue directly underneath the instrument fiber-optic are required; one each for the measuring light, the actinic light, and the fluorescence signals (e.g., Serôdio, 2004). Until a method is developed for the simultaneous measuring of these during the application of a light response curve, PSII fluorescence measurements deconvoluted for tissue depth and/or holobiont pigments will remain elusive in coral optics.

Low-light acclimation was observed in summer via upregulation of preferential utilization of [1 – *C*] at $E/E_k = 1$, over non-photochemical quenching. Enhanced photochemical quenching, i.e., the closure of PSII reaction centers under exposure to high-light, is a response that is observed in *Symbiodinium* grown under or adapted to low-light conditions (Robison and Warner, 2006; Ragni et al., 2010) and/or exposure to elevated temperatures (Warner et al., 1996), potentially reflecting a reduction in the capacity of photosynthesis (Ragni et al., 2010). Given the range of quenching strategies adopted across all species in spring, it is perhaps surprising that a ubiquitous response was observed for the utilization of light under low-light conditions. However, this observation is consistent with the paradigm demonstrated in Hennige et al. (2008) (also Suggett et al., 2012) where *Symbiodinium*, independent of host species and depth, inherently optimize to maintain comparable utilization of [1 – *C*]. Such a pattern is achieved through modulating the excitation energy that is dissipated via non-photochemical quenching pathways across the range of light environments (i.e., deep vs. shallow corals). In our study, optimisation of [1 – *C*] at the minimum saturating irradiance to similar levels across all species was consistent with this mechanism, i.e., the downregulation of [1 – *Q*] utilization, rather than major shifts in [1 – *C*]. That our study does not adhere to this paradigm in spring may indicate that such patterns of [1 – *C*] optimisation become complex or non-linear under extremes (Suggett et al., 2012), such as the Heron reef flat habitat we examined here, and thus high-light environments may demand specific photoprotective requirements that exceed any capacity to buffer constant rates of photochemistry. An alternative explanation for the apparent downregulation of [1 – *Q*] utilization in summer may be related to limited time for induction of heat-dissipation mechanisms under RLC protocols. Whilst 20 s actinic light steps characterized species-specific differences in [1 – *Q*] utilization in spring, there is the potential that patterns are masked in summer by a seasonal change in the induction rate of [1 – *Q*] and that species-specific differences may only be evident beyond the transition from light-limited to light-saturated states of PSII (i.e., at $E/E_k > 1$). As such, the time-dependent dynamics for non-photochemical quenching induction clearly warrant more targeted investigation in the future, particularly in the context of resolving photochemical dynamics of RLCs of differing light step durations.

The thermal tolerances or sensitivities are known for many species at Heron Reef and have been quantified at different times of year (**Table 1**), i.e., November (Hill et al., 2012), and February through March (Fitt et al., 2009; Fisher et al., 2012; Hillyer et al., 2017), utilizing similar experimental thresholds of *ca.* 32°C. Whilst experimental studies of thermal-tolerance are typically limited to few species, our approach allows us to broadly characterize the relative hierarchy of tolerance under transient heat stress (strictly in relation to PSII photochemical efficiency), *sensu* Fisher et al. (2012), from high to low-sensitivity as follows; *S. pistillata* (being the only species to suffer total mortality) < *I. palifera* = *A. formosa* = *P. damicornis* < *A. aspera* = *A. digitifera* < *A. millepora* = *P. cylindrica* < *P. lutea* = *M. digitata*.

A broad range of thermal ramping profiles utilized across other previous studies unfortunately limits inter-experiment comparability (Middlebrook et al., 2010). Furthermore, while we utilized identical heating rates and upper thermal limits across

seasons, seasonal differences in the ambient temperatures (and also differences in light utilization strategies) could account for the minor alterations in the kinetics of PSII degradation (i.e., earlier, more gradual decline) between seasons. For example, under relatively acute thermal stress (0.5°C increases per hour to 31°C), the kinetics of PSII function in *A. millepora* has previously been characterized as more sensitive compared to *P. damicornis* in spring (Hill et al., 2012), which is in contrast to our findings for these two species for this time of year. However, our data suggest that such inter-species comparisons of thermal tolerance must be interpreted cautiously and within a limited temporal context as *P. damicornis* changes significantly in thermal sensitivity following the height of summer. Overall our data are broadly consistent with corals exposed to similar thermal profiles. For example, the $\%F_v/F_m$ of *A. aspera* (in March) exposed to an equivalent heat stress (1°C d^{-1} to 32°C) decreased to 70% relative to ambient controls (Hillyer et al., 2017). *M. digitata* (and to a lesser extent *P. cylindrica*) generally maintained PSII photochemical efficiency with little decline in $\%F_v/F_m$ in both seasons, consistent with the findings of Fisher et al. (2012) under a heat stress between 31 and 34°C. *P. lutea* has previously been characterized as having a more "intermediate" thermal tolerance, i.e., equivalent to *A. millepora* (Fisher et al., 2012). Whilst control *P. lutea* demonstrated strong daily fluctuations in $\%F_v/F_m$ yields (potentially suggesting a significant night-time reduction of the plastoquinone pool; Hill and Ralph, 2005), $\%F_v/F_m$ in heat treated fragments did not change significantly and thus *P. lutea* is regarded as relatively thermally tolerant within this study. Our data thus contribute to the established hierarchy of thermal tolerance/sensitivity of corals and, whilst it should be noted that abiotic factors that vary on reefs but were not tested here (e.g., water movement) could alter susceptibility, our observations are consistent with expectations for Heron Reef with *P. damicornis* and *S. pistillata* the most likely to be susceptible to transient thermal stress.

Approximately 50% of the variance of PSII heat stress susceptibility was explained by a linear relationship with non-stressed [1 – *C*] (and [1 – *Q*]) utilization (at $E/E_k = 1$) in spring. Thus, corals that preferentially down-regulated photochemistry (i.e., the closure of PSII reaction centers) at and above the saturation point of PSII were also more resistant to subsequent heat stress. While this relationship is intriguing, utilization of photochemical quenching at any single point in time cannot serve as a diagnostic of thermal tolerance, especially as all species subsequently acclimated to utilize preferential photochemical quenching in summer (and the linear function was no longer apparent). Additionally, thermally induced changes in photochemical downregulation have been observed in both heat-sensitive and heat-tolerant *Symbiodinium* strains in culture (Robison and Warner, 2006) and *in hospite* (Warner et al., 1996). Thus, there is high potential for the environmental conditions in summer (decreasing-light, increasing temperature) to synergistically drive strong species-independent down-regulation of photochemistry and mask any potential light utilization diagnostic of heat-stress tolerance. That said, it is worth noting that our seasonal approach reveals that the strategy for dealing with light energy was unchanged for thermally tolerant species, i.e., thermally tolerant corals successfully balanced their innate ratio of [1 – *Q*] to [1 – *C*], despite significant seasonal changes in E_k, and thermally sensitive species exhibited seasonal swapping of light utilization strategies (especially in the heat sensitive *A. formosa*).

Ability of *Symbiodinium* to maintain light-utilization strategies across a range of environmental conditions has been discussed already (Hennige et al., 2008; Suggett et al., 2012); however, our data indicate that variability in light-utilization through time (at the scale of weeks to months) may be empirically related to differences in heat stress susceptibility. Such a framework is ripe for further experimentation, as temporal (long-term) stability or variability of photosystem function should be evident at the level of functional gene transcription (Scheibe et al., 2005), and thermally tolerant species may be "front-loaded" (*sensu* Barshis et al., 2013) with proteins that enable maintenance of physiological homeostasis that track or anticipate environmental change. Such a hypothesis requires extensive testing across a diverse range of coral-*Symbiodinium* symbioses, especially as exceptions are likely where anomalous temperatures target physiological pathways inherent to the coral host (Baird et al., 2009) or associated microbes (Diaz et al., 2016), that consequently cause *Symbiodinium* degradation. Indeed, the coral *S. pistillata* in our study is an exception to the linear relationship between [1 – *C*] utilization and thermal tolerance in spring, and despite utilizing preferential [1 – *C*] at similar levels to *M. digitata* and *P. lutea*, photochemical efficiency collapsed entirely for this species in response to transient heat stress. In other regions such as the Red Sea, *S. pistillata* exhibits robust host-specific responses to temperature stress and are considered thermally tolerant (Maor-Landaw et al., 2014; Maor-Landaw and Levy, 2016). However, the overall sensitive nature of the *S. pistillata*-*Symbiodinium* symbioses at Heron Reef is well-documented (**Table 1**) and the host seems to be inherently less prepared to cope with transient heat stress than other species in this study (comparatively low mucus production, antioxidant enzyme function, and heat-shock protein content; Fitt et al., 2009).

Our novel study examining the photobiology of diverse coral *Symbiodinium* symbioses within a single environment allowed us to demonstrate the extent of symbiont photoacclimation that operates in response to changing light and temperature between seasons. Further characterisation of fundamental adaptive traits that underlie species-specific differences in commonly measured photobiological descriptors (such as the ratio of [1 – *Q*] to [1 – *C*]) will undoubtedly prove crucial in defining the niche-range of *Symbiodinium* (Suggett et al., 2015). As *Symbiodinium* play a core role in the resilience of corals under environmental stress (especially during elevated temperatures), determining the utility and plasticity of such traits will enhance efforts to predict "winner and loser" coral-*Symbiodinium* symbioses under future climates (Loya et al., 2001; Fabricius et al., 2011). As widespread mass-bleaching events are predicted to become even more frequent under global climate change (Ainsworth et al., 2016), higher-throughput technologies in the area of coral-optics are required if photosynthesis-related traits are to be

effectively utilized in the anticipative management of coral reef ecosystems.

AUTHOR CONTRIBUTIONS

MN and DS: Planned the study; MN, SGG, SG, and LF: Ran the experiments and performed fluorescence measurements. All authors interpreted the data, and MN and DS led the writing of the manuscript. All authors contributed to the final edited version of the manuscript.

FUNDING

This study was supported by ARC Discovery Grant DP160100271 to DS.

ACKNOWLEDGMENTS

Coral collections were performed under the conditions of the Great Barrier Reef Marine Park Authority permits, numbered G15/37922.1 and G15/37538.1 held by MN and DS, respectively. We thank João Serôdio for valuable insight relating to the interpretation of the data. We also thank the staff of Heron Island Research Station for their assistance in the field.

SUPPLEMENTARY MATERIAL

The Supplementary Material for this article can be found online at: https://www.frontiersin.org/articles/10.3389/fmars.2018.00045/full#supplementary-material

REFERENCES

Ainsworth, T. D., Heron, S. F., Ortiz, J. C., Mumby, P. J., Grech, A., Ogawa, D., et al. (2016). Climate change disables coral bleaching protection on the Great Barrier Reef. *Science* 352, 338–342. doi: 10.1126/science.aac7125

Anthony, K., Connolly, S. R., and Hoegh-Guldberg, O. (2007). Bleaching, energetics, and coral mortality risk: effects of temperature, light, and sediment regime. *Limnol. Oceanogr.* 52, 716–726. doi: 10.4319/lo.2007.52.2.0716

Anthony, K., and Hoegh-Guldberg, O. (2003). Variation in coral photosynthesis, respiration and growth characteristics in contrasting light microhabitats: an analogue to plants in forest gaps and understoreys? *Funct. Ecol.* 17, 246–259. doi: 10.1046/j.1365-2435.2003.00731.x

Anthony, K., Ridd, P. V., Orpin, A. R., Larcombe, P., and Lough, J. (2004). Temporal variation of light availability in coastal benthic habitats: effects of clouds, turbidity, and tides. *Limnol. Oceanogr.* 49, 2201–2211. doi: 10.4319/lo.2004.49.6.2201

Bainbridge, S., Steinberg, C., and Furnas, M. (2010). "GBROOS—an ocean observing system for the Great Barrier Reef," in *International Coral Reef Symposium* (Ft. Lauderdale, FL), 529–533.

Baird, A. H., Bhagooli, R., Ralph, P. J., and Takahashi, S. (2009). Coral bleaching: the role of the host. *Trends Ecol. Evol.* 24, 16–20. doi: 10.1016/j.tree.2008.09.005

Baker, A. C., Glynn, P. W., and Riegl, B. (2008). Climate change and coral reef bleaching: an ecological assessment of long-term impacts, recovery trends and future outlook. *Estuar. Coast. Shelf Sci.* 80, 435–471. doi: 10.1016/j.ecss.2008.09.003

Barshis, D. J., Ladner, J. T., Oliver, T. A., Seneca, F. O., Traylor-Knowles, N., and Palumbi, S. R. (2013). Genomic basis for coral resilience to climate change. *Proc. Natl. Acad. Sci. U.S.A.* 110, 1387–1392. doi: 10.1073/pnas.1210224110

Brodersen, K. E., Lichtenberg, M., Ralph, P. J., Kühl, M., and Wangpraseurt, D. (2014). Radiative energy budget reveals high photosynthetic efficiency in symbiont-bearing corals. *J. R. Soc. Interface* 11:20130997. doi: 10.1098/rsif.2013.0997

Brown, B. E., Dunne, R. P., Goodson, M., and Douglas, A. (2000). Marine ecology: bleaching patterns in reef corals. *Nature* 404, 142–143. doi: 10.1038/35004657

Claquin, P., Probert, I., Lefebvre, S., and Veron, B. (2008). Effects of temperature on photosynthetic parameters and TEP production in eight species of marine microalgae. *Aquat. Microb. Ecol.* 51, 1–11. doi: 10.3354/ame01187

Cohen, I., and Dubinsky, Z. (2015). Long term photoacclimation responses of the coral *Stylophora pistillata* to reciprocal deep to shallow transplantation: photosynthesis and calcification. *Front. Mar. Sci.* 2:45. doi: 10.3389/fmars.2015.00045

Cooper, T. F., Ulstrup, K. E., Dandan, S. S., Heyward, A. J., Kühl, M., Muirhead, A., et al. (2011). Niche specialization of reef-building corals in the mesophotic zone: metabolic trade-offs between divergent *Symbiodinium* types. *Proc. R. Soc. Lond. B Biol. Sci.* 278, 1840–1850. doi: 10.1098/rspb.2010.2321

Diaz, J., Hansel, C., Apprill, A., Brighi, C., Zhang, T., Weber, L., et al. (2016). Species-specific control of external superoxide levels by the coral holobiont during a natural bleaching event. *Nat. Commun.* 7:13801. doi: 10.1038/ncomms13801

Enríquez, S., and Borowitzka, M. A. (2010). "The use of the fluorescence signal in studies of seagrasses and macroalgae," in *Chlorophyll a Fluorescence in Aquatic Sciences: Methods and Applications*, eds D. J. Suggett, O. Prášil, and M. A. Borowitzka (Cham: Springer), 187–208.

Enríquez, S., Méndez, E. R., Hoegh-Guldberg, O., and Iglesias-Prieto, R. (2017). Key functional role of the optical properties of coral skeletons in coral ecology and evolution. *Proc. R. Soc. Lon. B Biol. Sci.* 284:20161667. doi: 10.1098/rspb.2016.1667

Enríquez, S., Méndez, E. R., and Prieto, R. I. (2005). Multiple scattering on coral skeletons enhances light absorption by symbiotic algae. *Limnol. Oceanogr.* 50, 1025–1032. doi: 10.4319/lo.2005.50.4.1025

Fabricius, K. E., Langdon, C., Uthicke, S., Humphrey, C., Noonan, S., De'ath, G., et al. (2011). Losers and winners in coral reefs acclimatized to elevated carbon dioxide concentrations. *Nat. Clim. Chang.* 1, 165–169. doi: 10.1038/nclimate1122

Fisher, P. L., Malme, M. K., and Dove, S. (2012). The effect of temperature stress on coral-*Symbiodinium* associations containing distinct symbiont types. *Coral Reefs* 31, 473–485. doi: 10.1007/s00338-011-0853-0

Fitt, W., Gates, R., Hoegh-Guldberg, O., Bythell, J., Jatkar, A., Grottoli, A., et al. (2009). Response of two species of Indo-Pacific corals, *Porites cylindrica* and *Stylophora pistillata*, to short-term thermal stress: the host does matter in determining the tolerance of corals to bleaching. *J. Exp. Mar. Biol. Ecol.* 373, 102–110. doi: 10.1016/j.jembe.2009.03.011

Frade, P., Bongaerts, P., Winkelhagen, A., Tonk, L., and Bak, R. (2008). *In situ* photobiology of corals over large depth ranges: a multivariate analysis on the roles of environment, host, and algal symbiont. *Limnol. Oceanogr.* 53, 2711–2723. doi: 10.4319/lo.2008.53.6.2711

Gorbunov, M. Y., Kolber, Z. S., Lesser, M. P., and Falkowski, P. G. (2001). Photosynthesis and photoprotection in symbiotic corals. *Limnol. Oceanogr.* 46, 75–85. doi: 10.4319/lo.2001.46.1.0075

Goyen, S., Pernice, M., Szabó, M., Warner, M. E., Ralph, P. J., and Suggett, D. J. (2017). A molecular physiology basis for functional diversity of hydrogen peroxide production amongst *Symbiodinium* spp.(Dinophyceae). *Mar. Biol.* 164:46. doi: 10.1007/s00227-017-3073-5

Hawkins, T. D., Krueger, T., Wilkinson, S. P., Fisher, P. L., and Davy, S. K. (2015). Antioxidant responses to heat and light stress differ with habitat in a common reef coral. *Coral Reefs* 34, 1229–1241. doi: 10.1007/s00338-015-1345-4

Hennige, S. J., Smith, D. J., Perkins, R., Consalvey, M., Paterson, D. M., and Suggett, D. J. (2008). Photoacclimation, growth and distribution of massive coral species in clear and turbid waters. *Mar. Ecol. Prog. Ser.* 369, 77–88. doi: 10.3354/meps07612

Hennige, S. J., Suggett, D. J., Warner, M. E., McDougall, K. E., and Smith, D. J. (2009). Photobiology of *Symbiodinium* revisited: bio-physical and bio-optical signatures. *Coral Reefs* 28, 179–195. doi: 10.1007/s00338-008-0444-x

Hill, R., Brown, C. M., DeZeeuw, K., Campbell, D. A., and Ralph, P. J. (2011). Increased rate of D1 repair in coral symbionts during bleaching is insufficient to counter accelerated photo-inactivation. *Limnol. Oceanogr.* 56, 139–146. doi: 10.4319/lo.2011.56.1.0139

Hill, R., Larkum, A., Prášil, O., Kramer, D., Szabó, M., Kumar, V., et al. (2012). Light-induced dissociation of antenna complexes in the symbionts of scleractinian corals correlates with sensitivity to coral bleaching. *Coral Reefs* 31, 963–975. doi: 10.1007/s00338-012-0914-z

Hill, R., Larkum, A. W., Frankart, C., Kühl, M., and Ralph, P. J. (2004). Loss of functional Photosystem II reaction centres in zooxanthellae of corals exposed to bleaching conditions: using fluorescence rise kinetics. *Photosyn. Res.* 82, 59–72. doi: 10.1023/B:PRES.0000040444.41179.09

Hill, R., and Ralph, P. J. (2005). Diel and seasonal changes in fluorescence rise kinetics of three scleractinian corals. *Funct. Plant Biol.* 32, 549–559. doi: 10.1071/FP05017

Hillyer, K. E., Dias, D. A., Lutz, A., Wilkinson, S. P., Roessner, U., and Davy, S. K. (2017). Metabolite profiling of symbiont and host during thermal stress and bleaching in the coral *Acropora aspera*. *Coral Reefs* 219(Pt 4), 1–14. doi: 10.1007/s00338-016-1508-y

Hughes, T. P., Kerry, J. T., Álvarez-Noriega, M., Álvarez-Romero, J. G., Anderson, K. D., Baird, A. H., et al. (2017). Global warming and recurrent mass bleaching of corals. *Nature* 543, 373–377. doi: 10.1038/nature21707

Iglesias-Prieto, R., Beltrán, V., LaJeunesse, T., Reyes-Bonilla, H., and Thomé, P. (2004). Different algal symbionts explain the vertical distribution of dominant reef corals in the eastern Pacific. *Proc. R. Soc. Lond. Ser. B Biol. Sci.* 271, 1757–1763. doi: 10.1098/rspb.2004.2757

Iglesias-Prieto, R., and Trench, R. (1997). Acclimation and adaptation to irradiance in symbiotic dinoflagellates. II. Response of chlorophyll–protein complexes to different photon-flux densities. *Mar. Biol.* 130, 23–33. doi: 10.1007/s002270050221

Jeans, J., Campbell, D. A., and Hoogenboom, M. O. (2013). Increased reliance upon photosystem II repair following acclimation to high-light by coral-dinoflagellate symbioses. *Photosyn. Res.* 118, 219–229. doi: 10.1007/s11120-013-9918-y

Jones, R., Hoegh-Guldberg, O., Larkum, A., and Schreiber, U. (1998). Temperature-induced bleaching of corals begins with impairment of the CO_2 fixation mechanism in zooxanthellae. *Plant Cell Environ.* 21, 1219–1230. doi: 10.1046/j.1365-3040.1998.00345.x

Kline, D. I., Teneva, L., Hauri, C., Schneider, K., Miard, T., Chai, A., et al. (2015). Six month *in situ* high-resolution carbonate chemistry and temperature study on a coral reef flat reveals asynchronous pH and temperature anomalies. *PLoS ONE* 10:e0127648. doi: 10.1371/journal.pone.0127648

Krueger, T., and Gates, R. D. (2012). Cultivating endosymbionts —host environmental mimics support the survival of *Symbiodinium* C15 ex hospite. *J. Exp. Mar. Biol. Ecol.* 413, 169–176. doi: 10.1016/j.jembe.2011.12.002

Krueger, T., Hawkins, T. D., Becker, S., Pontasch, S., Dove, S., Hoegh-Guldberg, O., et al. (2015). Differential coral bleaching—Contrasting the activity and response of enzymatic antioxidants in symbiotic partners under thermal stress. *Comp. Biochem. Physiol. Part A Mol. Integr. Physiol.* 190, 15–25. doi: 10.1016/j.cbpa.2015.08.012

LaJeunesse, T. C., Loh, W. K. W., van Woesik, R., Hoegh-Guldberg, O., Schmidt, G. W., and Fitt, W. K. (2003). Low symbiont diversity in southern Great Barrier Reef corals, relative to those of the Caribbean. *Limnol. Oceanogr.* 48, 2046–2054. doi: 10.4319/lo.2003.48.5.2046

Lavaud, J., Strzepek, R. F., and Kroth, P. G. (2007). Photoprotection capacity differs among diatoms: possible consequences on the spatial distribution of diatoms related to fluctuations in the underwater light climate. *Limnol. Oceanogr.* 52, 1188–1194. doi: 10.4319/lo.2007.52.3.1188

Lesser, M. P., and Farrell, J. H. (2004). Exposure to solar radiation increases damage to both host tissues and algal symbionts of corals during thermal stress. *Coral Reefs* 23, 367–377. doi: 10.1007/s00338-004-0392-z

Lesser, M. P., Slattery, M., Stat, M., Ojimi, M., Gates, R. D., and Grottoli, A. (2010). Photoacclimatization by the coral *Montastraea cavernosa* in the mesophotic zone: light, food, and genetics. *Ecology* 91, 990–1003. doi: 10.1890/09-0313.1

Levy, O., Dubinsky, Z., and Achituv, Y. (2003). Photobehavior of stony corals: responses to light spectra and intensity. *J. Exp. Biol.* 206, 4041–4049. doi: 10.1242/jeb.00622

Lichtenberg, M., Larkum, A. W., and Kühl, M. (2016). Photosynthetic acclimation of *Symbiodinium* in hospite depends on vertical position in the tissue of the scleractinian coral Montastrea curta. *Front. Microbiol.* 7:230. doi: 10.3389/fmicb.2016.00230

Lilley, R., Ralph, P. J., and Larkum, A. W. (2010). The determination of activity of the enzyme Rubisco in cell extracts of the dinoflagellate alga *Symbiodinium* sp. by manganese chemiluminescence and its response to short-term thermal stress of the alga. *Plant Cell Environ.* 33, 995–1004. doi: 10.1111/j.1365-3040.2010.02121.x

Louis, Y. D., Kaullysing, D., Gopeechund, A., Mattan-Moorgawa, S., Bahorun, T., Dyall, S. D., et al. (2016). In hospite *Symbiodinium* photophysiology and antioxidant responses in *Acropora muricata* on a coast-reef scale: implications for variable bleaching patterns. *Symbiosis* 68, 61–72. doi: 10.1007/s13199-016-0380-4

Loya, Y., Sakai, K., Yamazato, K., Nakano, Y., Sambali, H., and van Woesik, R. (2001). Coral bleaching: the winners and the losers. *Ecol. Lett.* 4, 122–131. doi: 10.1046/j.1461-0248.2001.00203.x

Madin, J. S., Anderson, K. D., Andreasen, M. H., Bridge, T. C., Cairns, S. D., Connolly, S. R., et al. (2016). The Coral Trait Database, a curated database of trait information for coral species from the global oceans. *Sci. Data* 3:160017. doi: 10.1038/sdata.2016.17

Maor-Landaw, K., Karako-Lampert, S., Ben-Asher, H. W., Goffredo, S., Falini, G., Dubinsky, Z., et al. (2014). Gene expression profiles during short-term heat stress in the red sea coral *Stylophora pistillata*. *Glob. Chang. Biol.* 20, 3026–3035. doi: 10.1111/gcb.12592

Maor-Landaw, K., and Levy, O. (2016). Gene expression profiles during short-term heat stress; branching vs. massive Scleractinian corals of the Red Sea. *PeerJ* 4:e1814. doi: 10.7717/peerj.1814

McCabe Reynolds, J., Bruns, B. U., Fitt, W. K., and Schmidt, G. W. (2008). Enhanced photoprotection pathways in symbiotic dinoflagellates of shallow-water corals and other cnidarians. *Proc. Natl. Acad. Sci. U.S.A.* 105, 13674–13678. doi: 10.1073/pnas.0805187105

Michael, K. J., Veal, C. J., and Nunez, M. (2012). Attenuation coefficients of ultraviolet and photosynthetically active wavelengths in the waters of Heron Reef, Great Barrier Reef, Australia. *Mar. Freshw. Res.* 63, 142–149. doi: 10.1071/MF11106

Middlebrook, R., Anthony, K. R., Hoegh-Guldberg, O., and Dove, S. (2010). Heating rate and symbiont productivity are key factors determining thermal stress in the reef-building coral *Acropora formosa*. *J. Exp. Biol.* 213, 1026–1034. doi: 10.1242/jeb.031633

Middlebrook, R., Hoegh-Guldberg, O., and Leggat, W. (2008). The effect of thermal history on the susceptibility of reef-building corals to thermal stress. *J. Exp. Biol.* 211, 1050–1056. doi: 10.1242/jeb.013284

Mumby, P. J., Chisholm, J. R., Edwards, A. J., Andrefouet, S., and Jaubert, J. (2001). Cloudy weather may have saved Society Island reef corals during the 1998 ENSO event. *Mar. Ecol. Prog. Ser.* 222, 209–216. doi: 10.3354/meps222209

Nitschke, M. R., Davy, S. K., Cribb, T. H., and Ward, S. (2015). The effect of elevated temperature and substrate on free-living *Symbiodinium* cultures. *Coral Reefs* 34, 1–11. doi: 10.1007/s00338-014-1220-8

Nitschke, M. R., Davy, S. K., and Ward, S. (2016). Horizontal transmission of *Symbiodinium* cells between adult and juvenile corals is aided by benthic sediment. *Coral Reefs* 35, 335–344. doi: 10.1007/s00338-015-1349-0

Oakley, C. A., Schmidt, G. W., and Hopkinson, B. M. (2014). Thermal responses of *Symbiodinium* photosynthetic carbon assimilation. *Coral Reefs* 33, 501–512. doi: 10.1007/s00338-014-1130-9

Oliver, T., and Palumbi, S. (2011). Do fluctuating temperature environments elevate coral thermal tolerance? *Coral Reefs* 30, 429–440. doi: 10.1007/s00338-011-0721-y

Oxborough, K., Moore, C. M., Suggett, D. J., Lawson, T., Chan, H. G., and Geider, R. J. (2012). Direct estimation of functional PSII reaction center concentration and PSII electron flux on a volume basis: a new approach to the analysis of Fast Repetition Rate fluorometry (FRRf) data. *Limnol. Oceanogr. Methods* 10, 142–154. doi: 10.4319/lom.2012.10.142

Perkins, R. G., Kromkamp, J. C., Serôdio, J., Lavaud, J., Jesus, B., Mouget, J.-L., et al. (2010). "The application of variable chlorophyll fluorescence to microphytobenthic biofilms," in *Chlorophyll a Fluorescence in Aquatic Sciences: Methods and Applications*, eds D. J. Suggett, O. Prášil, and M. A. Borowitzka (Cham: Springer), 237–275.

Ragni, M., Airs, R. L., Hennige, S. J., Suggett, D. J., Warner, M. E., and Geider, R. J. (2010). PSII photoinhibition and photorepair in *Symbiodinium* (Pyrrhophyta) differs between thermally tolerant and sensitive phylotypes. *Mar. Ecol. Prog. Ser.* 406, 57–70. doi: 10.3354/meps08571

Ralph, P. J., and Gademann, R. (2005). Rapid light curves: a powerful tool to assess photosynthetic activity. *Aquat. Bot.* 82, 222–237. doi: 10.1016/j.aquabot.2005.02.006

Roberty, S., Bailleul, B., Berne, N., Franck, F., and Cardol, P. (2014). PSI Mehler reaction is the main alternative photosynthetic electron pathway in *Symbiodinium* sp., symbiotic dinoflagellates of cnidarians. *New Phytol.* 204, 81–91. doi: 10.1111/nph.12903

Roberty, S., Fransolet, D., Cardol, P., Plumier, J.-C., and Franck, F. (2015). Imbalance between oxygen photoreduction and antioxidant capacities in *Symbiodinium* cells exposed to combined heat and high light stress. *Coral Reefs* 34, 1063–1073. doi: 10.1007/s00338-015-1328-5

Robison, J. D., and Warner, M. E. (2006). Differential impacts of photoacclimation and thermal stress on the photobiology of four different phylotypes of *Symbiodinium* (Pyrrhophyta). *J. Phycol.* 42, 568–579. doi: 10.1111/j.1529-8817.2006.00232.x

Roth, M. S. (2014). The engine of the reef: photobiology of the coral–algal symbiosis. *Front. Microbiol.* 5:422. doi: 10.3389/fmicb.2014.00422

Roth, M. S., Latz, M. I., Goericke, R., and Deheyn, D. D. (2010). Green fluorescent protein regulation in the coral *Acropora yongei* during photoacclimation. *J. Exp. Biol.* 213, 3644–3655. doi: 10.1242/jeb.040881

Salih, A., Larkum, A., Cox, G., Kühl, M., and Hoegh-Guldberg, O. (2000). Fluorescent pigments in corals are photoprotective. *Nature* 408, 850–853. doi: 10.1038/35048564

Sampayo, E. M., Franceschinis, L., Hoegh-Guldberg, O., and Dove, S. (2007). Niche partitioning of closely related symbiotic dinoflagellates. *Mol. Ecol.* 16, 3721–3733. doi: 10.1111/j.1365-294X.2007.03403.x

Sawall, Y., Al-Sofyani, A., Banguera-Hinestroza, E., and Voolstra, C. R. (2014). Spatio-temporal analyses of *Symbiodinium* physiology of the coral *Pocillopora verrucosa* along large-scale nutrient and temperature gradients in the Red Sea. *PLoS ONE* 9:e103179. doi: 10.1371/journal.pone.0103179

Scheibe, R., Backhausen, J. E., Emmerlich, V., and Holtgrefe, S. (2005). Strategies to maintain redox homeostasis during photosynthesis under changing conditions. *J. Exp. Bot.* 56, 1481–1489. doi: 10.1093/jxb/eri181

Serôdio, J. (2004). Analysis of variable chlorophyll fluorescence in microphytobenthos assemblages: implications of the use of depth-integrated measurements. *Aquat. Microb. Ecol.* 36, 137–152. doi: 10.3354/ame036137

Serôdio, J., Vieira, S., Cruz, S., and Barroso, F. (2005). Short-term variability in the photosynthetic activity of microphytobenthos as detected by measuring rapid light curves using variable fluorescence. *Mar. Biol.* 146, 903–914. doi: 10.1007/s00227-004-1504-6

Serôdio, J., Vieira, S., Cruz, S., and Coelho, H. (2006). Rapid light-response curves of chlorophyll fluorescence in microalgae: relationship to steady-state light curves and non-photochemical quenching in benthic diatom-dominated assemblages. *Photosyn. Res.* 90, 29–43. doi: 10.1007/s11120-006-9105-5

Slavov, C., Schrameyer, V., Reus, M., Ralph, P. J., Hill, R., Büchel, C., et al. (2016). "Super-quenching" state protects *Symbiodinium* from thermal stress—implications for coral bleaching. *Biochim. Biophys. Acta* 1857, 840–847. doi: 10.1016/j.bbabio.2016.02.002

Smith, D. J., Suggett, D. J., and Baker, N. R. (2005). Is photoinhibition of zooxanthellae photosynthesis the primary cause of thermal bleaching in corals? *Glob. Chang. Biol.* 11, 1–11. doi: 10.1111/j.1529-8817.2003.00895.x

Stat, M., Loh, W. K. W., Hoegh-Guldberg, O., and Carter, D. A. (2008). Symbiont acquisition strategy drives host-symbiont associations in the southern Great Barrier Reef. *Coral Reefs* 27, 763–772. doi: 10.1007/s00338-008-0412-5

Suggett, D. J., Goyen, S., Evenhuis, C., Szabó, M., Pettay, D. T., Warner, M. E., et al. (2015). Functional diversity of photobiological traits within the genus *Symbiodinium* appears to be governed by the interaction of cell size with cladal designation. *New Phytol.* 208, 370–381. doi: 10.1111/nph.13483

Suggett, D. J., Kikuchi, R. K., Oliveira, M. D., Spanó, S., Carvalho, R., and Smith, D. J. (2012). Photobiology of corals from Brazil's near-shore marginal reefs of Abrolhos. *Mar. Biol.* 159, 1461–1473. doi: 10.1007/s00227-012-1925-6

Suggett, D. J., and Smith, D. J. (2011). Interpreting the sign of coral bleaching as friend vs. foe. *Glob. Change Biol.* 17, 45–55. doi: 10.1111/j.1365-2486.2009.02155.x

Takahashi, S., Nakamura, T., Sakamizu, M., van Woesik, R., and Yamasaki, H. (2004). Repair machinery of symbiotic photosynthesis as the primary target of heat stress for reef-building corals. *Plant Cell Physiol.* 45, 251–255. doi: 10.1093/pcp/pch028

Takahashi, S., Whitney, S., Itoh, S., Maruyama, T., and Badger, M. (2008). Heat stress causes inhibition of the de novo synthesis of antenna proteins and photobleaching in cultured *Symbiodinium*. *Proc. Natl. Acad. Sci. U.S.A.* 105, 4203–4208. doi: 10.1073/pnas.0708554105

Tchernov, D., Gorbunov, M. Y., de Vargas, C., Yadav, S. N., Milligan, A. J., Häggblom, M., et al. (2004). Membrane lipids of symbiotic algae are diagnostic of sensitivity to thermal bleaching in corals. *Proc. Natl. Acad. Sci. U.S.A.* 101, 13531–13535. doi: 10.1073/pnas.0402907101

Terán, E., Méndez, E. R., Enríquez, S., and Iglesias-Prieto, R. (2010). Multiple light scattering and absorption in reef-building corals. *Appl. Opt.* 49, 5032–5042. doi: 10.1364/AO.49.005032

Titlyanov, E., Titlyanova, T., Yamazato, K., and Van Woesik, R. (2001). Photo-acclimation dynamics of the coral *Stylophora pistillata* to low and extremely low light. *J. Exp. Mar. Biol. Ecol.* 263, 211–225. doi: 10.1016/S0022-0981(01)00309-4

Ulstrup, K. E., Hill, R., Van Oppen, M., Larkum, A., and Ralph, P. (2008). Seasonal variation in the photo-physiology of homogeneous and heterogeneous *Symbiodinium* consortia in two scleractinian corals. *Mar. Ecol. Prog. Ser.* 361, 139–150. doi: 10.3354/meps07360

Vieira, S., Calado, R., Coelho, H., and Serôdio, J. (2009). Effects of light exposure on the retention of kleptoplastic photosynthetic activity in the sacoglossan mollusc *Elysia viridis*. *Mar. Biol.* 156:1007. doi: 10.1007/s00227-009-1144-y

Wangpraseurt, D., Holm, J. B., Larkum, A. W., Pernice, M., Ralph, P. J., Suggett, D. J., et al. (2017a). *In vivo* microscale measurements of light and photosynthesis during coral bleaching: evidence for the optical feedback loop? *Front. Microbiol.* 8:59. doi: 10.3389/fmicb.2017.00059

Wangpraseurt, D., Larkum, A., Ralph, P., and Kühl, M. (2012). Light gradients and optical microniches in coral tissues. *Front. Microbiol.* 3:316. doi: 10.3389/fmicb.2012.00316

Wangpraseurt, D., Larkum, A. W., Franklin, J., Szabó, M., Ralph, P. J., and Kühl, M. (2014). Lateral light transfer ensures efficient resource distribution in symbiont-bearing corals. *J. Exp. Biol.* 217, 489–498. doi: 10.1242/jeb.091116

Wangpraseurt, D., Wentzel, C., Jacques, S. L., Wagner, M., and Kühl, M. (2017b). *In vivo* imaging of coral tissue and skeleton with optical coherence tomography. *J. R. Soc. Interface* 14:20161003. doi: 10.1098/rsif.2016.1003

Warner, M., Chilcoat, G., McFarland, F., and Fitt, W. (2002). Seasonal fluctuations in the photosynthetic capacity of photosystem II in symbiotic dinoflagellates in the Caribbean reef-building coral *Montastraea*. *Mar. Biol.* 141, 31–38. doi: 10.1007/s00227-002-0807-8

Warner, M. E., Fitt, W. K., and Schmidt, G. W. (1999). Damage to photosystem II in symbiotic dinoflagellates: a determinant of coral bleaching. *Proc. Natl. Acad. Sci. U.S.A.* 96, 8007–8012. doi: 10.1073/pnas.96.14.8007

Warner, M. E., Lesser, M. P., and Ralph, P. J. (2010). "Chlorophyll fluorescence in reef building corals," in *Chlorophyll a Fluorescence in Aquatic Sciences: Methods and Applications*, eds D. J. Suggett, O. Prášil, and M. A. Borowitzka (Cham: Springer), 209–222.

Warner, M. E., and Suggett, D. J. (2016). "The Photobiology of *Symbiodinium* spp.: linking physiological diversity to the implications of stress,"in *The Cnidaria, Past, Present and Future: The World of Medusa and Her Sisters*, eds S. Goffredo and Z. Dubinsky (Cham: Springer), 489–509.

Warner, M., Fitt, W., and Schmidt, G. (1996). The effects of elevated temperature on the photosynthetic efficiency of zooxanthellae in hospite from four different species of reef coral: a novel approach. *Plant Cell Environ.* 19, 291–299. doi: 10.1111/j.1365-3040.1996.tb00251.x

Weis, V. M. (2008). Cellular mechanisms of cnidarian bleaching: stress causes the collapse of symbiosis. *J. Exp. Biol.* 211, 3059–3066. doi: 10.1242/jeb.009597

Wiedenmann, J., D'Angelo, C., Smith, E. G., Hunt, A. N., Legiret, F.-E., Postle, A. D., et al. (2013). Nutrient enrichment can increase the susceptibility

of reef corals to bleaching. *Nat. Clim. Chang.* 3, 160–164. doi: 10.1038/nclimate1661

Winters, G., Beer, S., Zvi, B. B., Brickner, I., and Loya, Y. (2009). Spatial and temporal photoacclimation of *Stylophora pistillata*: zooxanthella size, pigmentation, location and clade. *Mar. Ecol. Prog. Ser.* 384, 107–119. doi: 10.3354/meps08036

Wooldridge, S. A., Heron, S. F., Brodie, J. E., Done, T. J., Masiri, I., and Hinrichs, S. (2017). Excess seawater nutrients, enlarged algal symbiont densities and bleaching sensitive reef locations: 2. A regional-scale predictive model for the Great Barrier Reef, Australia. *Mar. Pollut. Bull.* 114, 343–354. doi: 10.1016/j.marpolbul.2016.09.045

Conflict of Interest Statement: The authors declare that the research was conducted in the absence of any commercial or financial relationships that could be construed as a potential conflict of interest.

frontiers in Marine Science

ORIGINAL RESEARCH
published: 27 November 2018
doi: 10.3389/fmars.2018.00450

Relating Coral Skeletal Structures at Different Length Scales to Growth, Light Availability to *Symbiodinium*, and Thermal Bleaching

Timothy D. Swain[1,2], *Simon Lax*[3†], *Natalie Lake*[1], *Hannah Grooms*[1], *Vadim Backman*[4] and *Luisa A. Marcelino*[1,2*]

[1] Department of Civil and Environmental Engineering, Northwestern University, Evanston, IL, United States, [2] Integrative Research Center, Field Museum of Natural History, Chicago, IL, United States, [3] Department of Ecology and Evolution, University of Chicago, Chicago, IL, United States, [4] Department of Biomedical Engineering, Northwestern University, Evanston, IL, United States

OPEN ACCESS

Edited by:
Daniel Wangpraseurt,
University of Cambridge,
United Kingdom

Reviewed by:
Steven L. Jacques,
Tufts University, United States
Robert Ong,
University of Sydney, Australia

***Correspondence:**
Luisa A. Marcelino
l-marcelino@northwestern.edu

†Present Address:
Simon Lax,
Physics of Living Systems,
Department of Physics,
Massachusetts Institute of
Technology, Cambridge, MA,
United States

Specialty section:
This article was submitted to
Coral Reef Research,
a section of the journal
Frontiers in Marine Science

Received: 09 May 2017
Accepted: 08 November 2018
Published: 27 November 2018

Citation:
Swain TD, Lax S, Lake N, Grooms H, Backman V and Marcelino LA (2018) Relating Coral Skeletal Structures at Different Length Scales to Growth, Light Availability to Symbiodinium, and Thermal Bleaching. Front. Mar. Sci. 5:450. doi: 10.3389/fmars.2018.00450

Light scattering of coral skeletons and tissues increases light availability to photosynthetic endosymbionts to form one of the most efficient biological collectors of solar radiation. Rapid increases in light availability during thermally-induced symbiont loss (bleaching) impair photosynthetic performance of the remaining *Symbiodinium* and precipitate a more severe bleaching response (optical feedback-loop hypothesis). Here we focus on light scattering of the skeleton, which is determined by light interaction with skeletal components assembled in a hierarchical fractal-like structure from tens of nanometers (e.g., calcium carbonate nanograins) to micro- and milli-meters (septa, corallites, and coenosteum) to centimeters and higher (colony form). We examined the association between skeletal structures, their role in light scattering, and species-specific bleaching responses for 88 coral species using phylogenetically-corrected analysis. We also explored the effect of growth on light scattering by modeling the fractal-like accretive growth of the skeleton (assuming a diffusion limited process of biomineralization) as a function of skeletal density, size of nanograins, fractal range of biomineralized clusters, and overall mass-fractal dimension, and validated the model with experimental data. Our results show that differences in light scattering from the top ~200 μm (*micro-*μ_s') of the skeleton, and not from the whole skeleton (bulk-μ_s'), are related to bleaching susceptibility. We also demonstrate how differences in *micro-*μ_s' of corallites and coenosteum could explain, in part, the heterogeneous light environment between polyp and coenosarc. The average effective light transport distance of coenosteum measured in 14 coral species indicates that coenosteum could transport light to the corallites, which could then function as "light-trapping devices" where photons are scattered multiple times by septa and corallite walls until absorbed by *Symbiodinium*. Furthermore, our fractal skeletal growth model suggests that corals that grow faster typically have lower mass-fractal dimension, denser skeletons, lower skeletal micro-μ_s', and higher bleaching susceptibility. Finally, our results demonstrate that several skeletal structures of varying

length scales known to modulate the light microenvironment of *Symbiodinium* in coral tissue are not associated with bleaching susceptibility. This work provides evidence of the relationship between skeletal growth, light scattering, and bleaching, and further supports the optical feedback-loop hypothesis of coral bleaching.

Keywords: coral bleaching, light scattering, light transport, optical feedback-loop hypothesis, skeletal growth model

INTRODUCTION

Hermatypic corals are optical machines, adapted for collection of solar energy through complex endosymbioses with photosynthetic dinoflagellates representing the genus *Symbiodinium*. While the basic components of these machines are simple to envision, a thin layer of largely transparent tissue that suspends solar collectors over a light-scattering surface, the diversity of interacting forms and functions are complex. Structural components, and the interactions between components, combine to maximize photosynthesis while simultaneously minimizing photo-damage to their symbionts and themselves. Optimization of these functions has derived a diversity of forms that make corals some of the most efficient biological collectors of solar radiation (Enríquez et al., 2005, 2017; Brodersen et al., 2014), and allows them to occupy habitats characterized by diverse light conditions ranging over two orders of magnitude from the intense solar irradiances of reef crests to near darkness of mesophotic reefs (Anthony and Hoegh-Guldberg, 2003; Pochon et al., 2015). However, light collection optimization in corals comes with a cost when thermal anomalies induce disruption of coral-*Symbiodinium* symbioses (bleaching), which has become an urgent focus of research as global temperatures continue to increase under climate change (Hoegh-Guldberg et al., 2007; Baker et al., 2008; Frieler et al., 2013; Hughes et al., 2017). Thermal stress impairs function of the photosynthetic apparatus of *Symbiodinium* (Iglesias-Prieto et al., 1992; Warner et al., 1999), reducing the light intensity threshold for bleaching (Mumby et al., 2001; Bhagooli and Hidaka, 2004; Lesser and Farrell, 2004). *Symbiodinium* photosynthesis is the primary source of fixed carbon for reef-building corals (Muscatine, 1990), and loss of *Symbiodinium* during bleaching may lead to mortality of the holobiont (Jokiel, 2004; Jones, 2008). This increased sensitivity to light may be determined, in part, by the same mechanisms responsible for modulating the internal light environment that allow corals to inhabit such diverse light regimes.

Increase in light availability to *Symbiodinium* is modulated by the coral host through multiple scattering in the coral skeleton and tissue (Kühl et al., 1995; Enríquez et al., 2005, 2017; Stambler and Dubinsky, 2005; Terán et al., 2010; Marcelino et al., 2013; Wangpraseurt et al., 2016) and through dynamic light redistribution due to tissue contraction and expansion (Wangpraseurt et al., 2012, 2014a; Lichtenberg et al., 2016), as well as light scattering or absorption by host fluorescent pigments (Salih et al., 2000; Lyndby et al., 2016). Fluorescent pigments in coral tissues have been shown to affect light absorption, scattering, and heating (Lyndby et al., 2016), while also reducing the harmful effects of short-wavelength radiation and providing photoprotection through light absorption (Schlichter et al., 1986; Salih et al., 2000; Lesser and Farrell, 2004; Smith et al., 2013).

Here we focus on modulation of light microenvironment by the skeleton, which is dependent on the ability of light to reach the skeleton (i.e., >95% of downwelling or tissue-scattered irradiance is absorbed by *Symbiodinium*; e.g., Magnusson et al., 2007) and the diffuse reflectance of the skeleton (i.e., scattering properties of skeletal material determined by the interaction of light with skeletal structures; Kühl et al., 1995; Enríquez et al., 2005, 2017; Stambler and Dubinsky, 2005; Terán et al., 2010; Kahng et al., 2012; Marcelino et al., 2013; Wangpraseurt et al., 2017). Skeletal reflectance has been shown to increase light availability to *Symbiodinium* in tissue up to six times (depending on the concentration of symbiont cells) relative to cultures (Kühl et al., 1995; Enríquez et al., 2005). This observation lead to the optical feedback-loop (or positive feedback-loop) hypothesis of coral bleaching: as symbionts and/or their pigments are lost in the initial stages of a bleaching event, the reduction of light absorbers further exposes the skeleton, which disproportionately increases excess light availability to the remaining *Symbiodinium*, causing greater symbiont loss and acceleration of the bleaching response (Enríquez et al., 2005; Marcelino et al., 2013; Swain et al., 2016b). Skeletal reflectance is influenced by overall morphology, light absorption, and light scattering. Light scattering is characterized by the reduced scattering coefficient, bulk-μ_s' or μ_s', which is the inverse distance a photon travels before it is randomized in direction (i.e., transport mean free path length, $l_s' = 1/\mu_s'$; Anthony et al., 2005; Enríquez et al., 2005; Stambler and Dubinsky, 2005; Rodríguez-Roman et al., 2006; Marcelino et al., 2013). Light is scattered by interacting with skeletal structures ranging from ∼30–100 nm (e.g., $CaCO_3$ nanograins; Stolarski, 2003; Cuif and Dauphin, 2005a) to ∼1–10 mm (e.g., corallites and septa; Enríquez et al., 2005; Stambler and Dubinsky, 2005) to ∼1–10 cm or more (Enríquez et al., 2005; Stambler and Dubinsky, 2005; Wangpraseurt et al., 2017; e.g., corallite walls and coenosteum).

Skeletal light scattering in the top ∼200 μm superficial layer of the skeleton has been described as microscopic-μ_s' or $\mu_{s,m}'$ (Rogers et al., 2009; Marcelino et al., 2013) and is primarily affected by skeletal microstructures, but not larger features or voids known to affect bulk-μ_s' (Marcelino et al., 2013). Skeletal $\mu_{s,m}'$ is highly variable among coral species and inversely correlated to their bleaching responses (Marcelino et al., 2013). This relationship has been hypothesized to be due to the inverse relationship between $\mu_{s,m}'$ and the *rate of excess light increase* in coral tissue as symbionts are lost, as demonstrated

by physical models of simulated bleaching (Marcelino et al., 2013). The inverse dependence of bleaching response on $\mu_{s,m}{}'$ was also observed experimentally among ten coral species (while differences in *Symbiodinium* thermotolerance and host tissue thickness were insufficient to explain differential bleaching; Swain et al., 2016b). Microscopic-$\mu_s{}'$ was also shown to be capable of modulating a 2- to 5-fold increase in light absorption per unit pigment in *Symbiodinium* when modeling skeleton-dependent light absorption (Swain et al., 2016b). These observations lead to the prediction that $\mu_{s,m}{}'$ is responsible for the rate of optical feedback, where corals with low-$\mu_{s,m}{}'$ may scatter less light to *Symbiodinium*, however once thermally-induced bleaching reduces absorber concentrations in the tissue, low-$\mu_{s,m}{}'$ corals have higher rates of light increase to its symbionts resulting in compounded stress and accelerated bleaching (Marcelino et al., 2013; Swain et al., 2016b). Skeletal optical feedback was also demonstrated with direct micro-sensor measurements of light within live coral tissue, which detected up to a 5-fold enhancement of light directly above the skeleton of bleached corals (relative to healthy corals) at a rate of increase that approximated a power-law function relative to decreasing *Symbiodinium* densities (Wangpraseurt et al., 2017).

Coral skeletons, similar to other biominerals (e.g., mollusk nacre, bone, or glass sponge spicules; Kamat et al., 2000; Aizenberg et al., 2005; Benzerara et al., 2011), contain 30–100 nm calcium carbonate crystals (orthorhombic structure aragonite) assembled in a hierarchical fractal-like structure. These structures spanfrom nanometer–scale interactions between calcium carbonate grains and organic matrix, to micrometer–scale associations of crystal fibers forming "thickening deposits" between "centers of calcification" (COC), to millimeter–scale assemblies of septa in corallites, to overall colony formation (Stolarski, 2003; Cuif and Dauphin, 2005a,b; Stolarski and Mazur, 2005; Nothdurft and Webb, 2007; Przeniosło et al., 2008; Benzerara et al., 2011). Recent observations suggest that skeletal organic matrix (SOM) found in the COCs works as an organic substrate where nanoparticles of amorphous calcium carbonate (40–50 nm in diameter) are deposited and combine to form aragonite crystals that lead to the formation of the skeletal fibers (Von Euw et al., 2017). This process of crystal formation, designated as crystallization by particle attachment (CPA), has been observed to occur in biomineralized materials, such as sea urchin spicules or zebrafish fin bone, and could be due, in part, to diffusion-limited kinetics (De Yoreo et al., 2015). In corals, accretion of aragonite nanograins in the skeleton is a diffusion-limited process, dependent on the secretion of ions (calcium, carbonate, and protons) and organic matrix molecules (involved in crystal nucleation) by specialized cells in the basal ectoderm of the coral tissue (calicoblastic cells), and occurs through a combination of linear extension and thickening (Stolarski, 2003; Cuif and Dauphin, 2005b; Nothdurft and Webb, 2007; Frankowiak et al., 2016). Growth of fractal-like structures can be described by mass-fractal dimension, or D_f , which characterizes the overall size distribution of skeletal structural elements at different length scales (Basillais, 1997; Martin-Garin et al., 2007; Przeniosło et al., 2008; Young et al., 2017). In the case of branching corals, D_f has been hypothesized to reflect their optimal growth strategies along gradients of light and nutrient-flow that result in high morphological plasticity (Kaandorp et al., 2005; Chindapol et al., 2013). Skeletal D_f was shown to be highly correlated with skeletal $\mu_{s,m}{}'$ in 94 coral taxa (Marcelino et al., 2013).

Furthermore, several skeletal structures have been implicated in light collection due to light-induced morphological plasticity. Corallite morphology and spacing among corallites can be plastic in response to differing light environments. Calices can become deeper and septa shorter (Todd et al., 2004; Ow and Todd, 2010), corallite diameter smaller (Nir et al., 2011), and three-dimensional topography of calice surfaces (calical relief) greater (Klaus et al., 2007) under higher radiation. Distances among corallites may increase and corallite surface area decrease under higher radiation (Nir et al., 2011) or change under different spectral conditions (Rocha et al., 2014). There are also differences in light enhancement observed during bleaching in polyp (above corallites) and coenosarc (above coenosteum) tissues, with greater enhancement above the more structurally complex corallites (Wangpraseurt et al., 2017).

At longer length scales, colony morphology is known to change dramatically within some coral species across light (with colony form becoming less compact; Muko et al., 2000; Kaniewska et al., 2008; Todd, 2008) and nutrient-flow gradients (e.g., Smith and Birkeland, 2007; Jimenez et al., 2011; Chindapol et al., 2013), and to be highly diverse between species (e.g., plating, massive, branching, etc.). Internal light fields within tissues have been shown to vary across different colony morphologies and between coenosarc and polyps (Wangpraseurt et al., 2014b). Additionally, differential bleaching among various morphologies has been extensively reported, with massive and encrusting forms thought to be generally more resistant to bleaching then branching and digitate forms (e.g., Marshall and Baird, 2000; Loya et al., 2001; van Woesik et al., 2011; but see McCowan et al., 2012; Swain et al., 2018).

Here we evaluated the role of skeletal structures in light scattering, examined the effect of skeletal growth on light scattering, and tested the effect of coral skeletal structures and traits on bleaching response with the goal of identifying individual or groups of skeletal structures that could be predictive of bleaching susceptibility. Specifically, we evaluated (1) if high variability in light microenvironments within a colony, especially between coenosarc (over coenosteum) and the polyp (over corallite) tissues which yield different photosynthetic efficiencies (Ralph et al., 2002; Ulstrup et al., 2006, 2007; Wangpraseurt et al., 2017), could be partially explained by differences in skeletal $\mu_{s,m}{}'$ between the coenosteum and corallites; (2) the relationship between skeletal features and bleaching response of 88 coral species by performing phylogenetically-corrected regression analysis with overall skeletal architecture (mass-fractal dimension, D_f), colonial unit dimensions (corallite diameter) and organization (corallite complexity and coenosteum surface area), and colony structure (cumulative fractality); and (3) the effect of skeletal growth on light scattering and bleaching susceptibility by modeling the relationship between skeletal density (n), D_f, and growth rate.

METHODS

Coral skeletal characters were collected from museum specimens, literature, or trait databases (values and their sources reported in **Table S1** and **Text S1**), and their relationship to bleaching response was assessed through phylogenetically corrected regression and principal components analyses. Out of 95 coral taxa previously characterized for bleaching response (Swain et al., 2016a), microscopic-μ_s', and mass-fractal dimension D_f by Marcelino et al. (2013), we retained the 88 that were identified to species such that further species-specific data could be applied to these analyses. Bleaching response values for species not reported, or with fewer than three observations, in Swain et al. (2016a) were taken as the mean of responses across the genus (**Table S1**).

Character Collection

Characters related to skeletal light scattering and micro-architecture of the skeleton are described below; the remaining characters are described here. **Skeletal density (*n*)**, the maximum mass of skeletal material per cubic cm ($g{\cdot}cm^{-3}$), is affected by skeletal extension and thickening of nanograins (Bucher et al., 1998) and species-specific values were either obtained from the literature or directly measured from museum specimens of Marcelino et al. (2013) using standard methods (mass divided by volume determined by displacement of water; Hughes, 1987). Species-specific **skeletal growth rate** values, characterized by the maximum linear increase in skeleton deposits measured over a year ($mm{\cdot}yr^{-1}$), were obtained from the literature and related to n and D_f by a coral growth model (see equations 9–13). Species-specific corallite arrangement (**corallite size** measured as corallite max diameter, corallite complexity, and percent of surface area composed of coenosteum) were also obtained. **Corallite complexity**, was parameterized by counting the number of septa within each cycle, and weighing septal counts within cycles by their extension from the corallite wall toward the columella (sum of the number of septa per cycle · extension weight) within 10 corallites for each species from the museum specimens of Marcelino et al. (2013). Primary septal cycles (i.e., those that extend to the columella) were weighted by a factor of three, intermediate cycles were weighted by a factor of two, and cycles that extend minimally from the corallite wall were unweighted. The percent of surface area composed of coenosteum (**% $SA_{coenosteum}$**) was parameterized through direct measurements of museum specimens of Marcelino et al. (2013) captured in size-standardized digital photos and subtracting the area occupied by corallites from the total area of skeletal surface in photographs using ImageJ (version 1.47; NIH). Colony growth morphology was estimated by calculating **cumulative fractality** for each of 10 growth forms characterizing the 88 coral species, which is the product of *apparent surface fractality* of the colony and mass-fractal dimension D_f. *Apparent surface fractality* was measured by visually scoring the structural complexity (i.e., rugosity, or the 3D surface area occupying a given volume) of individual specimens representing each growth form such that encrusting forms were scored the lowest given their low surface area per volume ratio and branching forms (especially closed branches) were scored the highest (modified from Young et al., 2017).

Differential Light Scattering of Coral Skeletal Components

Bulk skeletal scattering (bulk-μ_s', characterized by the reduced light scattering coefficient μ_s' measured in mm^{-1}), is the inverse distance a photon travels before it is randomized in direction, and results from light interaction with voids and skeletal structures at different length scales throughout the entire skeleton (Enríquez et al., 2005; Stambler and Dubinsky, 2005; Terán et al., 2010). **Micro-skeletal light scattering** (micro-μ_s' or $\mu_{s,m}'$) is the reduced light scattering coefficient within the top ∼200 μm of the skeleton and is not influenced by voids (Marcelino et al., 2013; Swain et al., 2016b). Micro-μ_s' was measured using low-coherence enhanced backscattering spectroscopy (LEBS) on tissue-free coral skeletons. The LEBS instrument and principles were described in detail by Marcelino et al. (2013) and references therein, but briefly, LEBS can measure microscopic light-scattering through broadband partial spatial coherence of illumination (*Lsc*) which selectively isolates the scattering spectrum from photons that propagate paths such that the distance between light entry and light exit points is comparable to *Lsc*.

Measurements of $\mu_{s,m}'$ of corallites and coenosteum were taken for a subset of 14 species (previously characterized for skeletal $\mu_{s,m}'$ at the colony level by Marcelino et al., 2013), with corallite diameters and distances between corallites (i.e., coenosteum) larger than the instrument spot size (∼1 mm in diameter). Their ratio was calculated as,

$$\mu_{S,m\_Ratio}{}' = \frac{\mu_{S,m,\ corallite}{}'}{\mu_{S,m,\ coenosteum}{}'} \quad (1)$$

Values for $\mu_{s,m\_corallite}{}'$ and $\mu_{s,m\_coenosteum}{}'$ are reported as the means of ten replicate measurements. To evaluate the potential for coenosteum to transport light into adjacent corallites, we calculated the effective light transport distance of coenosteum ($ETD_{coenosteum}$), which measures how much light can be transported by coenosteum given its intrinsic $\mu_{s,m}'$ (and therefore transport mean free path length, $l'_{S,m} = 1/\mu_{s,m}'$) and inter-corallite distance ($D_{inter-corallite}$) such that:

$$ETD_{coenosteum} = \frac{D_{inter-corallite}}{l_{s,m}{}'} \quad (2)$$

where $l'_{S,}$and $D_{inter-corallite}$ are measured in millimeters. A high $ETD_{coenosteum}$ value indicates low potential for coenosteum to transport light into adjacent corallites. $D_{inter-corallite}$ is the mean distance between ten haphazardly chosen adjacent corallites captured in size-standardized digital photos of the museum specimens of Marcelino et al. (2013), extracted using ImageJ (version 1.47; NIH).

Modeling of Irradiance at the Corallite Surface

The effect of light transport in the coenosteum on corallite irradiance was modeled based on the diffusion approximation to

the light transport equation (Zonios et al., 1999). Corallites were approximated as semi-infinite axially-symmetrical cylindrical regions of turbid media, surrounded by semi-infinite regions of coenosteum, with the scattering properties measured by LEBS. In this approximation, irradiances relative to the incident intensity that would be observed at the surface layer of the corallite (R_1) and the coenosteum (R_2) regions due to a uniform illumination of the coral surface are, respectively,

$$R_1(r) = \int_0^{r_c} \int_0^{2\pi} R\left(\sqrt{r^2 + r'^2 - 2rr'cos\phi};\, \mu'_{s1}, \mu_{a1}\right) r'\, d\phi\, dr' \tag{3}$$

where r is the radial distance from the center of the corallite, r_c is the radius of the corallite, μ'_{s1} and μ_{a1} are the reduced scattering and the absorption coefficients of the corallite, respectively, and $R(x; \mu'_s, \mu_a)$ is the irradiance observed at a distance x from a point source at a surface of a semi-infinite slab of turbid media with the reduced scattering and absorption coefficients μ'_s and μ_a, respectively. The point-source reflectance is derived from the diffusion approximation as follows from Zonios et al. (1999):

$$R_{(\lambda,r)} = \frac{z_0}{4\pi} \frac{\mu_s'}{\mu_s' + \mu_a} \left[\left(\mu + \frac{1}{r_1}\right) \frac{\exp(-\mu r_1)}{r_1^2} + \left(1 + \frac{4}{3}A\right) \left(\mu + \frac{1}{r_2}\right) \frac{\exp(-\mu r_2)}{r_2^2} \right] \tag{4}$$

with

$$\mu = \left[3\mu_a(\mu_a + \mu_s')\right]^{1/2};\ z_0 = \frac{1}{\mu_s' + \mu_a};\ r_1 = \left(z_0^2 + r^2\right)^{1/2};$$
$$r_2 = \left[z_0^2 \left(1 + \frac{4}{3}A\right)^2 + r^2 \right]^{1/2}$$

Some light illuminating the corallite at any given point gets diffusely scattered within the corallite and returns to its surface after which it leaves the coral. A portion of the light, however, may reach the coenosteum region and reach the surface of the coenosteum after being multiply scattered in that region. This irradiance is modeled as the result of the diffusion of light reaching the outer radius of the corallite:

$$R_{1\to 2}(r) = R_1(r_c) \frac{\int_0^{2\pi} R\left(\sqrt{r^2 + r'^2 - 2rr'cos\phi};\, \mu'_{s2}, \mu_{a2}\right) d\phi}{\int_0^{2\pi} R\left(2r_c\sqrt{1 - cos\phi};\, \mu'_{s2}, \mu_{a2}\right) d\phi} \tag{5}$$

where μ'_{s2} and μ_{a2} are the reduced scattering and the absorption coefficients of the coenosteum.

Similarly, the surface irradiance relative to the illumination intensity in the coenosteum region due to the illumination of the coenosteum is

$$R_2(r) = \int_{r_c}^{r_c + L/2} \int_0^{2\pi} R\left(\sqrt{r^2 + r'^2 - 2rr'cos\phi};\, \mu'_{s2}, \mu_{a2}\right) r'\, d\phi\, dr' \tag{6}$$

where L is the average intercorallite distance, and the irradiance of light that is transported from the coenosteum and reaches the corallite surface is

$$R_{2\to 1}(r) = R_2(r_c) \frac{\int_0^{2\pi} R\left(\sqrt{r^2 + r'^2 - 2rr'cos\phi};\, \mu'_{s1}, \mu_{a1}\right) d\phi}{\int_0^{2\pi} R\left(2r_c\sqrt{1 - cos\phi};\, \mu'_{s1}, \mu_{a1}\right) d\phi} \tag{7}$$

Taken together, the irradiance in each of the two regions, corallite and coenosteum, has two components: the "endogenous" light due to the illumination of the specific region and the light transported from the other region:

$$R(r) = \begin{cases} R_1(r) + R_{2\to 1}(r), & r < r_c \\ R_2(r) + R_{1\to 2}(r), & r \geq r_c \end{cases} \tag{8}$$

Micro-Architecture Organization of the Skeleton

Skeletal Mass-Fractal Dimension (D_f)

Micro-skeletal structures of different sizes vary in micro-density and these variations in density, which give rise to light scattering, result in different refractive indices (Kim et al., 2004; Rogers et al., 2009, 2014). Since optical refractive index is linearly dependent on local mass density, the overall organization of structures with size r between ~30–1,000 nm can be characterized by the optical refractive index correlation function C(r) (Kim et al., 2004; Rogers et al., 2009, 2014). LEBS measures fractal-dimension D_f, which quantifies the shape of C(r) (Marcelino et al., 2013). D_f was measured for all 88 species and determined to be consistent with a "mass-fractal" structure (i.e., $D_f < 3$) and varied significantly between low- and high-$\mu_{s,m}{}'$ corals (Marcelino et al., 2013).

Relating Skeletal Density and Fractal-Like Skeletal Organization to Growth Rate

Skeletal growth can be expressed as a function of (1) the size of the elementary unit block (nanograin), which has been observed between 30 and 100 nm in a few species using atomic force microscopy (Cuif and Dauphin, 2005a) and 40–50 nm in *Stylophora pistillata* using scanning helium ion microscopy (Von Euw et al., 2017), and its density (assumed to be 2.73 g/cm^3 or the density of calcium carbonate), (2) the size of larger clusters as biomineralization occurs over different length scales through a mass-fractal equation of crystal growth (Uwaha and Saito, 1990; Peitgen et al., 1992; Miyashita et al., 2005), and (3) the distance between the cellular release of ions (e.g., calcium, carbonate and protons) and organic matrix molecules by calicoblastic cells and their incorporation into the mineralization site (incorporation diffusion length, l) assuming a diffusion-limited process (Furukawa et al., 2001; Allemand et al., 2004).

$$M = M_{\min} \left(\frac{R}{r}\right)^{D_f} \tag{9}$$

$$n = \frac{M}{V} = \frac{M_{\min}}{r^{D_f} R^{3-D_f}} = \left(\frac{r}{R}\right)^{3-D_f} n_0 \tag{10}$$

$$\frac{n}{n_0} = \left(\frac{r}{R}\right)^{3-Df} \quad (11)$$

where, M represents the mass of a biomineralized fractal cluster, M_{min} represents the mass of the elementary unit block (i.e., nanograin), D_f is the mass-fractal dimension of the coral skeleton, r represents radius of the nanograin, R represents the radius of a biomineralized cluster (possibly the "mesocrystals"; domains in "calcification centers" of *Porites sp* skeletons consisting of nanograins organized crystallographically as one large crystal over several micrometers; Benzerara et al., 2011), n represents the average skeletal density, V is the volume of the fractal cluster, and $n_0 = \frac{M_{\min}}{r^3}$ represents the density of the nanograin. Incorporation diffusion length l, (Furukawa et al., 2001) can be expressed as:

$$l = 2Diff/G \quad (12)$$

where, *Diff* is the diffusion coefficient of the ions and other elements involved in the mineralization process and G is the growth rate (interface velocity or the rate of linear increase of the skeletal surface at the deposition interface). Since the radius of a cluster R should be half the diffusion length (Uwaha and Saito, 1990; Furukawa et al., 2001; Miyashita et al., 2005), then:

$$R = \frac{1}{2}l => R = \frac{Diff}{G} => G \propto \frac{1}{R} \propto \left(\frac{n}{n_0}\right)^{\frac{1}{3-D_f}} \quad (13)$$

Since $D_f < 3$ (Furukawa et al., 2001), it follows that denser skeletons (i.e., higher n) tend to grow faster than less dense skeletons and the relationship between G and n is a power-law with an exponent depending on D_f.

In order to test these model predictions, we used previously measured mass-fractal dimension D_f values for the 88 targeted species. The data showed that the majority of coral skeletons had $D_f < 3$ (Marcelino et al., 2013; see **Text S2**). This implies that the density auto-correlation function typically follows an inverse power-law relationship, between the minimal length scale r and the maximal length scale R, thus supporting the notion that coral skeletons are mass fractal-like structures. We tested the experimental relationship between growth rate G (characterized by maximum linear extension rates of species-specific skeletons), skeletal density n, and D_f, of each skeleton and compared it to the relationship obtained by the model (equation 13). Using available datasets and literature we compiled species-specific (1) maximum linear extension rates of skeleton ($mm \cdot yr^{-1}$) as a proxy for growth rates and (2) maximum skeletal density values ($g\ CaCO_3 \cdot cm^{-3}$) (**Table S1**).

Phylogenetic Statistical Analyses

Coral species characters were mapped onto a molecular phylogeny for assessment of homoplasy, phylogenetically-corrected regression, and phylogenetically-corrected principal components analysis. Patterns among species traits may be determined by a combination of ecological and evolutionary processes, and the ecological process can only by accurately assessed once the patterns of shared evolutionary history are accounted for (Rezende et al., 2007; Ivens et al., 2016). The patterns of shared evolutionary history violate an assumption of standard statistical analyses that individual data points are independent, and must be corrected for phylogeny (Revell, 2010). The comprehensive coral phylogeny of Huang (2012) was trimmed to include only the targeted species, the 88 species tree and a 14 species sub-set tree, using the Phylotools R package (Revell, 2012) to preserve proper branch lengths. These trimmed phylogenetic trees were used to define the evolutionary relationships and distances between species for phylogenetic correction of the raw data.

Characters were mapped onto the trimmed Huang (2012) phylogenies using Mesquite 2.75 (Maddison and Maddison, 2011) and visualized with Evolview (Zhang et al., 2012). Homoplasy of categorical data were assessed through the Retention Index (RI) in Mesquite, which is the fraction of apparent synapomorphy (character present in ancestor and shared exclusively by its evolutionary descendants) retained after mapping to the phylogeny, where highly homoplasious characters have low RI values (Farris, 1989). Relationships between continuous variables were assessed with Phylogenetic Independent Contrasts (PIC) analysis within the Phenotypic Diversity Analysis Programs (PDAP) of Mesquite, which corrects an ordinary least squares linear regression for non-independence due to evolutionary relationships among species (Midford and Garland, 2010). We report the results of phylogenetic independent contrasts through the Pearson Product-Moment Correlation Coefficient, or PCC, as well as its p-value. Skeletal features that were not found to be associated with bleaching response through PIC analyses were further assessed to determine if combinations of these features could be correlated with bleaching. Phylogenetically-corrected linear combinations of skeletal features were identified through phylogenetic principal component analysis (phylo-PCA) (Revell, 2009) using the Phytools R package (Revell, 2012). Phylogenetically corrected logistic regressions (Ives and Garland, 2010) of dichotomous variables (branching/massive colony morphology) were performed in Phyloglm v2.4 (Phylogenetic Generalized Linear Model; Ho and Ané, 2014) in R. Because of incomplete taxon sampling for n and G, and the order of magnitude greater parameters for solitary species (which made them extreme outliers in our analyses), the taxa included in the phylo-PCA were reduced to 59 species (**Table S1**). Phylo-PCAs were based on variable correlation rather than covariance due to their vastly different distributions. Principal components are reported in non-corrected space, therefore assessment of correlation with bleaching response was performed with PIC as above.

RESULTS AND DISCUSSION

Skeletal light scattering, which increases the light microenvironment of *Symbiodinium* in coral tissue and accelerates bleaching response (Enríquez et al., 2005; Marcelino et al., 2013; Swain et al., 2016b; Wangpraseurt et al., 2017), is due to light interaction with structures varying in size from tens of nanometers (30–100 nm calcium carbonate nanograins) to micrometers and millimeters (corallite septa and walls) or higher

(coenosteum and colony morphology; Enríquez et al., 2017). Here we evaluated skeletal structures at length scales spanning seven orders of magnitude that are known to affect within-tissue light environment and their relationship with light scattering and bleaching response of 88 coral species. We also modeled the interaction between skeletal growth rate and skeletal density given the fractal-like accretive growth of the skeleton and its potential association with bleaching.

Differences in Skeletal Micro-μ_s', and Not in Bulk-μ_s', Are Related to Bleaching Susceptibility

Bleaching responses of the 88 targeted coral species are highly diverse (bleaching response index, taxon-BRI, ranged from 2.75 to 72.85%, Swain et al., 2016a) and appear to have multiple independent evolutionary origins (i.e., bleaching response is homoplasious across the phylogeny resulting in a low RI = 0.33, **Figure 1**), providing an opportunity to detect correlations with skeletal characters that may otherwise closely reflect evolutionary history. Homoplasious characters provide a better opportunity to reveal the underlying relationships between character states, after correction for phylogenetic non-independence (Revell, 2010) among species.

The pattern of increased taxon-BRI associated with decreased $\mu_{s,m}'$ (Phylogenetic independent contrast tests, PCC = −0.24, $p = 0.024$, $n = 88$; **Figure 1**; **Table S2**), is consistent with earlier work of our lab (Marcelino et al., 2013) and supports the optical feedback-loop hypothesis (Enríquez et al., 2005; Marcelino et al., 2013; Swain et al., 2016b; Wangpraseurt et al., 2017). This pattern is robust to decreased sample size (88, rather than 95 taxa), increased precision of the phylogeny used for correction of non-independence (using the updated and more comprehensive phylogeny of Huang, 2012), and increased precision of the species-specific estimation of bleaching response (using the updated and more comprehensive bleaching response values of Swain et al., 2016a). Association with bleaching response is specific to the light-scattering properties within the top ∼200 μm of the coral skeleton ($\mu_{s,m}'$) and was not detected in the light scattering properties within the overall skeleton (bulk-μ_s', PCC = 0.06, $p = 0.708$, $n = 42$), mirroring our earlier findings using 10 experimentally bleached coral species (Swain et al., 2016b).

While we cannot currently explain these patterns, we hypothesize that they may be due, in part, to significant structural and chemical differences between the top ∼200 μm layer and the rest of the skeleton. Separation between the most recently deposited biomineral and older parts of the skeleton is made by exothecal dissepiments; thin horizontal plates of biomineralized calcium carbonate laid as the colony extends upwards which varies among species. Dissepiment spacing was measured at 60–460 μm in *Porites lobata*, 180–720 μm in *Goniastrea favulus*, 200–1,000 μm in *Pocillopora damicornis*, (overall mean of ∼400 μm; Nothdurft and Webb, 2007), 550–620 μm in *Orbicella annularis* and *Montastrea faveolata*, 800–850 μm in *Montastrea cavernosa*, and 680–720 μm in *Montastrea franski* (overall mean of ∼600 μm; Dávalos-Dehullu et al., 2008). Micro-μ_s' may result from light scattering by the most recently biomineralized calcium carbonate and organic matrix located above the latest dissepiment (e.g., the >60 nm voids in *Goniastrea stelligera* skeleton; Frankowiak et al., 2016), while bulk-μ_s' would result from light scattering by new and old skeleton where older voids could potentially be filled with water or gas due to degradation of organic material. However, how the structural and chemical composition of the top skeletal layer is associated with bleaching susceptibility will require further investigation.

Differences in Skeletal Micro-μ_s' of Corallites and Coenosteum Explain, in Part, Heterogeneous Light Environment Between Polyp and Coenosarc and Are Associated With Bleaching Susceptibility

Differential photosynthetic efficiencies between polyp (above corallite) and coenosarc (above coenosteum) tissues have been attributed to high variability in within-colony light environments (Kühl et al., 1995; Ralph et al., 2002; Ulstrup et al., 2006, 2007). We reasoned that this high variability could be explained, in part, by differences in skeletal light scattering and transport between corallites and coenosteum. To that effect, we first measured light scattering properties and morphometrics of corallites and coenosteum in 14 coral species and then modeled the irradiance that reaches the corallite from coenosteum-transported light in three coral species with differing efficacy of light transport.

We measured $\mu_{s,m}'$ of corallites ($\mu_{s,m\_corallite}'$) and coenosteum ($\mu_{s,m\_coenosteum}'$), calculated their ratio (μ_{S,m_Ratio}', Equation 1) and determined the effective light transport distances of coenosteum ($ETD_{coenosteum}$) for 14 coral species (**Figure 2**). The $ETD_{coenosteum}$ (equation 2), corresponds to the probability that light that enters the coenosteum could be diffusely transported into a corallite and is dependent on the distance traveled by a photon before scatter and randomization (transport mean free path in the top ∼200 μm of the skeleton, $l_S'_m$, where $l'_{S,m} = 1/\mu_{s,m}'$), and on the mean inter-corallite distance ($D_{inter-corallite}$) within a colony. A high $ETD_{coenosteum}$ indicates low probability that light entering coenosteum will be transported to neighboring corallites; similarly to within-tissue transport, the coenosteum could effectively transport light into corallites with inter-corallite distances up to ∼20× $l_S'_{m\_coenosteum}$, (Ishimaru, 1999). In corals with ($\mu_{s,m\_corallite}'/\mu_{s,m\_coenosteum}'$) > 1, and $D_{inter-corallite}$ < 20× $l_S'_m$, the coenosteum could transport light to corallites which could then work as "light-trapping devices" where photons could be scattered multiple times by corallite septa and walls until absorbed by *Symbiodinium*. The 14 corals examined had (mean ± standard deviation) $l_S'_{m\_coenosteum} = 0.24 \pm 0.12$ mm; $D_{inter-corallite} = 2.3 \pm 1.8$ mm; $ETD_{coenosteum} = 13.48 \pm 12.97$ and $\mu_{S,m\_Ratio}' = 1.11 \pm 0.33$, indicating that coenosteum could effectively transport light into corallites and be trapped by multiple scattering. Accordingly, corals with low-scattering coenosteum and high scattering corallites that are spaced within effective transport distances would be more likely to increase light availability to their *Symbiodinium* and precipitate a more rapid bleaching response under increased thermal

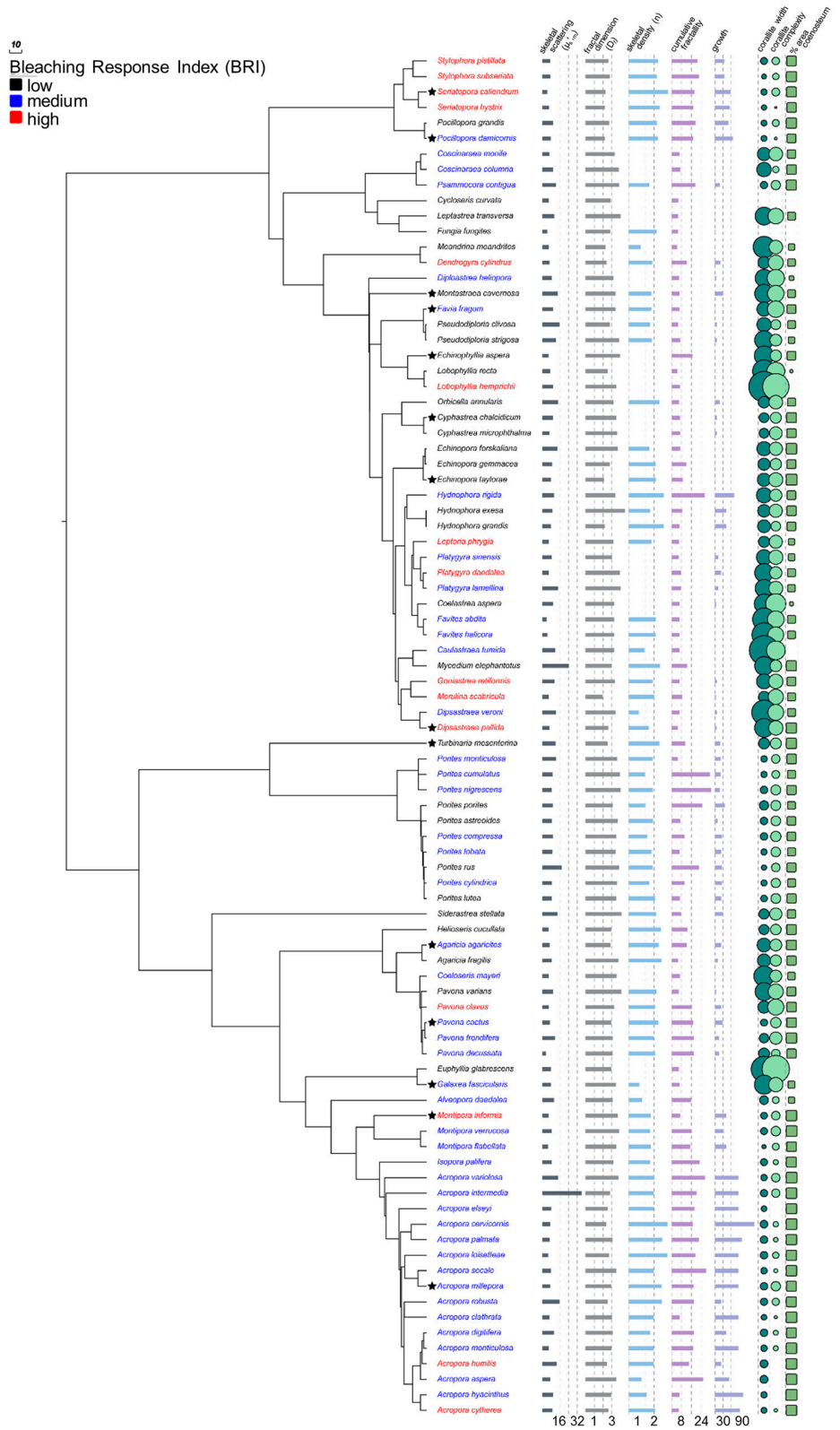

FIGURE 1 | Coral phylogeny of 88 species modified from Huang (2012) with skeletal characters. Coral species color coded by bleaching response and bar graphs, circular plots, and rectangular plots represent variation in skeletal characters. Values for *Cycloseris curvata* and *Fungia fungites* are omitted from circular plots as they are an order of magnitude larger than all other species (see **Table S1**). Stars indicate species for which additional $\mu_{s,m}{}'$ data were collected for corallites and coenosteum. Lower $\mu'_{s,m}$ values are associated with increased bleaching response (PCC $= -0.24$, $p = 0.024$), but other characters are not. See **Figure 5** for phylogenetic principal components analysis of non-light-scattering characters and **Table S2** for complete phylogentic regression analysis of all characters.

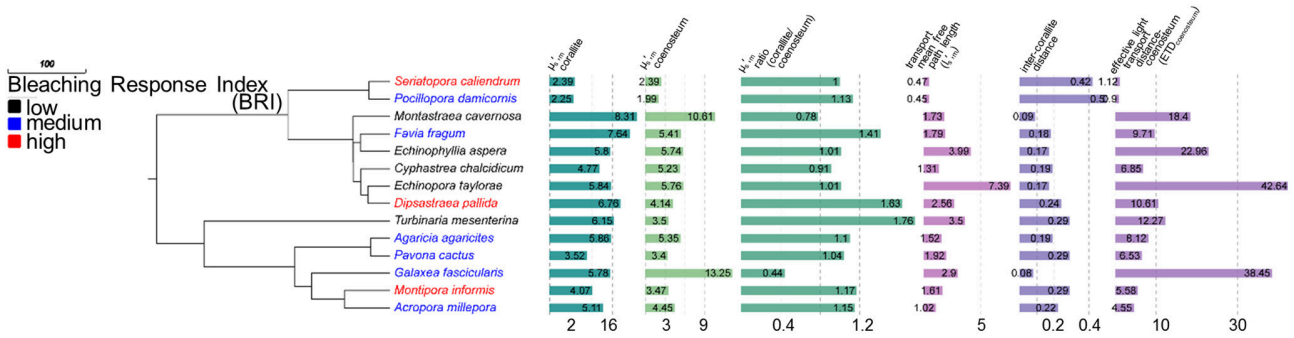

FIGURE 2 | Coral phylogeny of 14 species modified from Huang (2012) with isolated skeletal scattering ($\mu_{s,m}'$) values for corallites and coenosteum. Coral species color coded by bleaching response and bar graphs represent variation in skeletal characters. Higher corallite $\mu_{s,m}'$ values, relative to coenosteum, are associated with increased bleaching response (PCC = 0.69, $p = 0.006$). Lower coenostem effective transport distances ($ETD_{coenosteum}$) are associated with increased bleaching response (PCC = −0.603, $p = 0.022$, $n = 14$).

stress, as predicted by the optical feedback-loop hypothesis (Enríquez et al., 2005; Marcelino et al., 2013; Swain et al., 2016b; Wangpraseurt et al., 2017). Indeed, higher μ_{S,m_Ratio}' (i.e., $\mu_{s,m\_corallite}' > \mu_{s,m\_coenosteum}'$, PCC = 0.69, $p = 0.006$, $n = 14$) and lower $ETD_{coenosteum}$ (i.e., more effective transport, PCC = −0.603, $p = 0.022$, $n = 14$) are significantly associated with increased bleaching response among the coral species examined here. This pattern is consistent with the within-tissue micro-sensor measurements of Wangpraseurt et al. (2017), who demonstrated much larger increases in scalar irradiance enhancement within corallites than at either the coenosarc surface or oral surface of the polyps between bleached and non-bleached corals.

Using the light scattering properties and morphometrics of corallites and coenosteum, we then modeled the irradiance at the corallite surface due to light transport within the coenosteum, assuming that no other light hits the corallite and absorption is negligible (equations 4–8). The distribution of coenosteum-originated irradiance at the corallite surface ($R_{2\to1}(r)$) was modeled for three representative coral species with increasingly higher taxon-BRI and correspondingly progressively smaller $ETD_{coenosteum}$ (*Montastraea cavernosa, Seriatopora caliendrum,* and *Montipora informis,* **Figures 2**, **3A–C**). This can be quantified as the fraction of light that "escapes" the coenosteum and leaks into the corallite: $T_{2\to1} = \frac{\langle R_{2\to1}\rangle}{(\langle R_{2\to1}\rangle + \langle R_2\rangle)}$, where $\langle R_{2\to1}\rangle = \frac{1}{\pi r_c^2}\int_0^{r_c}\int_0^{2\pi} R_{2\to1}(r) r d\phi dr$ is the average irradiance at the corallite surface due to the light transported from the coenosteum and $\langle R_2\rangle = \frac{1}{\pi}\left(\left(r_c + l/2\right)^2 - r_c^2\right)\int_{r_c}^{r_c+l/2}\int_0^{2\pi} R_2(r) r d\phi dr$ is the average irradiance at the coenosteum. In case of *M. cavernosa* (high-$ETD_{coenosteum}$), only a small fraction of the coenosteum illumination reaches corallites (6%, **Table S3**). This fraction is much higher for the two species with more efficient light transport in the coenosteum (lower $ETD_{coenosteum}$); in *S. caliendrum,* and *M. informis*, nearly half of the light irradiating from the coenosteum gets transported into corallites (43 and 35%, respectively, **Table S3**). **Figures 3D,E** shows corresponding profiles of $R_{2\to1}$ as a function of the radial distance from the center of the corallites. In *M. cavernosa,* the species with the least efficient $ETD_{coenosteum}$ (low bleaching susceptibility, high-$ETD_{coenosteum}$), the small fraction of light that diffuses into the corallite stays in its periphery, hardly ever reaching the center ($\langle R_{2\to1}\rangle = 0.04$, **Figure 3D**). Conversely, corallites of the more efficient light transporters, *S. caliendrum* and *M. informis* (higher bleaching susceptibility and lower $ETD_{coenosteum}$) receive more light from the coenosteum, which also propagates further into the center of the corallites ($\langle R_{2\to1}\rangle = 0.07$ and $\langle R_{2\to1}\rangle = 0.2$, respectively, **Figures 3E,F**). Thus, *S. caliendrum* and *M. informis* corallites work as "light-trapping devices," diffusing light all the way through its center. This light-trapping effect of corallites is even more pronounced in *M. informis* which shows the highest bleaching susceptibility in our dataset (taxon-BRI = 73%, **Figure 3F**). Concomitantly, the fraction of the average corallite irradiance due light transport from the coenosteum, $F_{2\to1} = \frac{\langle R_{2\to1}\rangle}{(\langle R_{2\to1}\rangle + \langle R_2\rangle)}$, where $\langle R_1\rangle = \frac{1}{\pi} r_c^2 \int_0^{r_c}\int_0^{2\pi} R_1(r) r d\phi dr$, progressively increases from *M. cavernosa* to *S. caliendrum* and *M. informis*. While coenosteum-transported irradiance plays only a small role in the total irradiation of the corallites of *M. cavernosa* (5%, **Table S3**), the fraction is considerably higher for *S. caliendrum* (46%, **Table S3**), and *M. informis* corallites (64%, **Table S3**).

Both observational and simulated results suggest that higher μ_{S,m_Ratio}' and lower $ETD_{coenosteum}$ correlate with increased bleaching susceptibility in corals. The variable light environment between corallites and coenosarc is likely also a function of other effects, such as the spatially heterogeneous distribution of host pigments in the tissue; green fluorescent protein-like (GFP) pigments in the host are more abundant in polyps then in coenosarc (Salih et al., 2000; Kaniewska et al., 2011; Lyndby et al., 2016; Ong et al., 2018). Additionally, morphological plasticity in corals has been implicated in regulation of within-colony light levels to optimize light capture and photosynthesis (Kaniewska et al., 2008, 2014) and temperature microenvironments within the colony have been found to result from variations in colony morphology, irradiance, and flow patterns within and around the colony (Jimenez et al., 2011; Ong et al., 2017). Future work could look at the combined effect of tissue and skeleton in modulating light environment to the algae, in particular at the level of the polyp/corallite and coenosarc/coenosteum.

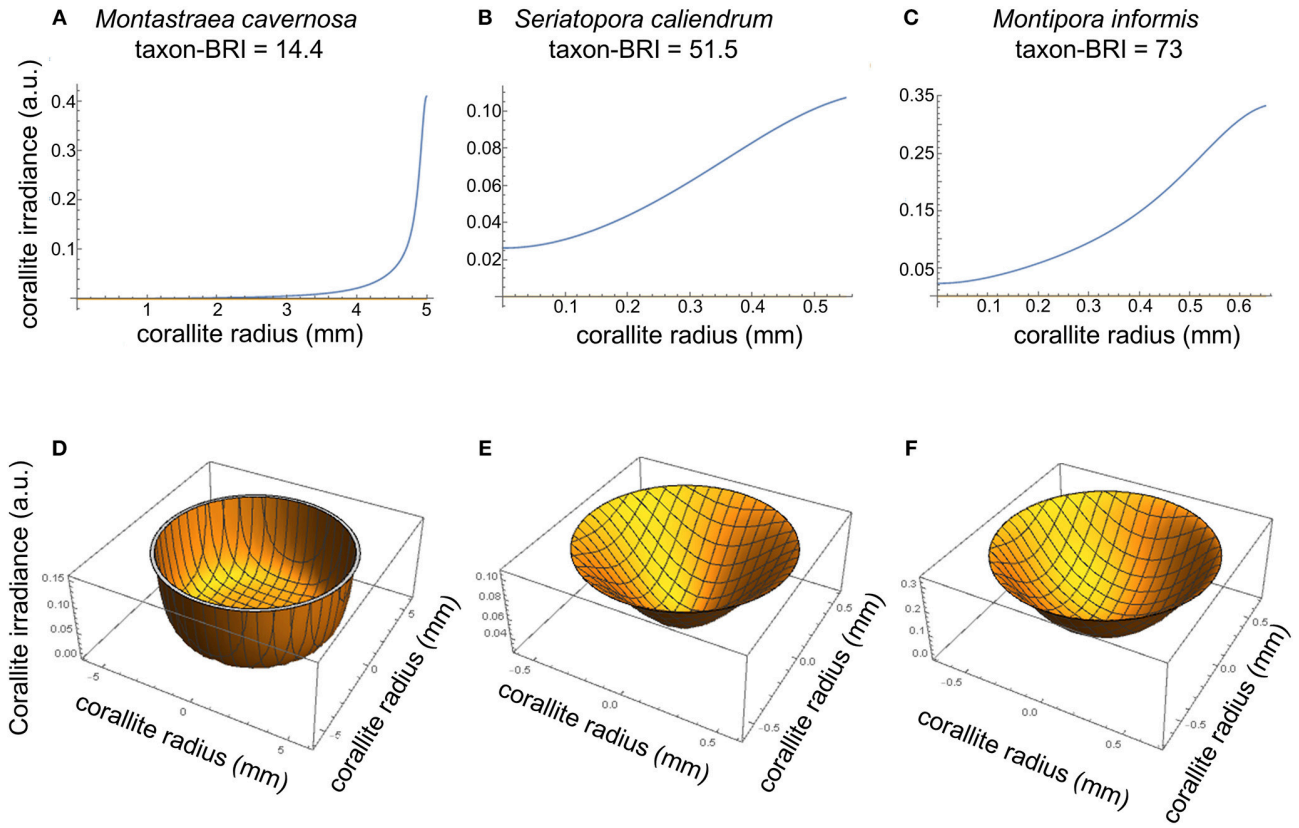

FIGURE 3 | Modeled irradiance at the corallite surface for *M. cavernosa* **(A,D)**, *S. caliendrum* **(B,E)** and *M. informis* **(C,F)** with increasing bleaching susceptibility scores (taxon-BRI of 14.4, 51.5, and 73, respectively) and differential $ETD_{coenosteum}$ and light scattering properties of both corallites and coenosteum (see **Figure 2** and **Table S3**). Plots of 2-D cross-sections through the middle of corallites **(A–C)** and 3-D top view cross-section representations of modeled irradiance in corallites due to light transport in the coenosteum **(D–F)**. The irradiance reaching the corallite was modeled as a function of the size of the corallite (mm), intercorallite distance (mm), and light scattering coefficient (μ_s') of corallite and coenosteum (equations 3–8).

Corals That Grow Faster Typically Have Lower Mass-Fractal Dimension, Denser Skeletons, Lower Skeletal Micro-μ_s' and Likely Show Higher Bleaching Susceptibility

Rate of deposition of calcium carbonate material (calcification rate) is the result of the linear extension of bio-aragonite deposited at the "centers of calcification" over time (linear growth or extension rate; mm yr^{-1}) and increased density from infilling by "thickening deposits" (bulk density or density of the deposited material and the volume of voids in the overall architecture; $gCaCO_3$ cm^{-3}) (reviewed in Stolarski, 2003; Cuif and Dauphin, 2005b; Lough and Cooper, 2011). The fractal coral growth model derived here relates linear extension rate of skeleton (G) and skeletal density (n) through a power-law (which has the property of invariance across a range of length-scales, thus representing fractal growth) with an exponent depending on D_f (Equations 3–7). Since $D_f < 3$ (Marcelino et al., 2013), the model showed that denser skeletons (i.e., higher n) tend to grow faster. This trend was confirmed by observational data with measured G and n for each coral species showing a positive correlation; branching and corymbose corals showed the highest skeletal density (1.94–2.33 $gCaCO_3$ cm^{-3}, $n = 26$) and linear extension rates (48.1–86.2 mm yr^{-1}) while massive, encrusting and columnar corals had the lowest skeletal density and linear extension rates (1.61–1.99 $gCaCO_3$ cm^{-3} and 12.38–20.44 mm yr^{-1}, $n = 29$; **Figure 4A**, $r = 0.35$, $p = 0.02$). These results agree with previously reported differences in growth strategies (i.e., higher investment in linear extension and/or skeletal density) which are due, in part, to the expected mechanical properties of different growth forms. Branching and digitate forms typically have higher extension rates and denser skeletons, while massive and encrusting forms show lower extension rates and lower skeletal density (Hughes, 1987; Jimenez and Cortes, 1993; Marshall, 2000; Morgan and Kench, 2012). However, rapidly growing branch tips of *Acropora* species are much less dense than their colony base due to secondary infilling of older parts of the colony to provide strength (Hughes, 1987; Bucher et al., 1998).

On average, dependence $G(n)$ followed a power-law form $G \propto n^{\alpha}$ with exponent $\alpha \sim 3.8$ (i.e., power law best fit to the experimental data). From Equation 13, $\alpha = \frac{1}{(3-D_f)}$, this exponent corresponds to the average value of $D_f \sim 2.74$,

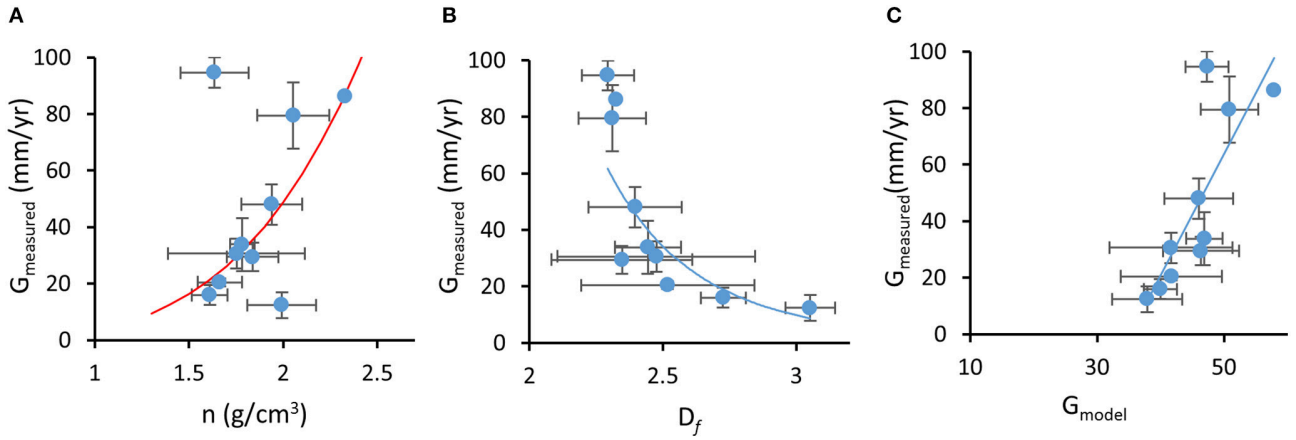

FIGURE 4 | Fractal coral growth model relating **(A)** measured growth (G) to measured skeletal density (*n*), where the red line represents model prediction, **(B)** measured growth to measured mass-fractal dimension (D_f), where the line represents power-law regression ($r^2 = 0.73$), and **(C)** measured growth to model-predicted growth, where the line represents linear regression ($r^2 = 0.67$). Error bars represent standard error.

which approximates the fractal dimension of diffusion-limited aggregation in three-dimensions (Peitgen et al., 1992). The model also predicts that G and D_f are inversely related: corals that exhibit faster linear growth rates are expected to form skeletons with lower fractal dimensions. This trend was also confirmed in our observational data with independently measured species-specific G and D_f averaged for each one of the 10 growth forms, which showed a significant negative correlation (in spite of the large variations in D_f for some growth forms, **Figure 4B**, $r = -0.30$, $p = 0.025$, $n = 59$). Furthermore, the fractal growth model was able to predict growth rates of coral taxa. We compared measured species-specific linear extension rates with linear extension rates predicted by the model (G in Equation 13) based on reported maximal skeletal density for each coral species and measured D_f for each coral skeleton. Although skeletal density is affected by processes that are not directly related to the linear fractal growth (e.g., infilling; Stolarski, 2003; Cuif and Dauphin, 2005b; Nothdurft and Webb, 2007), model-predicted G correlated well with measured growth rates (**Figure 4C**, $r = 0.39$, $p = 0.003$, $n = 59$). Additionally, the model prediction that skeletal density is inversely related to D_f was also validated ($r = 0.35$, $p = 0.009$, $n = 59$).

Predictions of the skeletal growth model, that corals with faster linear extension rates will have denser skeletons and will form skeletons with lower mass-fractal skeletal dimension, are in agreement with experimental data. D_f is one of the parameters that influence light scattering: according to light scattering theory (Rogers et al., 2014), $\mu_{s,m}{}'$ is expected to be proportional to D_f. This positive relationship between D_f and $\mu_{s,m}{}'$ was confirmed by our data (PCC = 0.224, $p = 0.036$, $n = 88$). Furthermore, the model shows inverse dependence between growth rate of the skeleton (i.e., linear extension rate) and the size of the biomineralized cluster R (Equation 13), which light theory describes as positively correlated with $\mu_{s,m}{}'$ (Rogers et al., 2009). Consequently, and although growth rate is influenced by several factors (reviewed in Dávalos-Dehullu et al., 2008; Lough and Cooper, 2011), the model predicts an inverse relationship between growth rate and $\mu_{s,m}{}'$, which is confirmed by our data (PCC = −0.292, $p = 0.017$). Since an inverse dependence between $\mu_{s,m}{}'$ and bleaching response has been shown through experimental and correlational evidence (Marcelino et al., 2013; Swain et al., 2016b), corals that grow faster are expected to have denser skeletons, lower skeletal D_f, lower $\mu_{s,m}{}'$, and are likely to show higher bleaching susceptibility. However, growth rate was not found to be significantly associated with bleaching susceptibility with phylogenetically-corrected regression analysis (**Table S2**) although taxon-BRI and measured G show an increasing linear relationship that plateaus (**Figure S1**).

Skeletal Structures of Varying Length Scales Known to Modulate the Light Microenvironment of Symbiodinium in Coral Tissue Are Not Associated With Bleaching Susceptibility

Several structures demonstrated to either directly modulate the internal light microenvironment, or to change in response to variation in external light fields at different length scales, were evaluated for possible association with bleaching susceptibility. Since $\mu_{s,m}{}'$ is inversely correlated with bleaching susceptibility (Marcelino et al., 2013; Swain et al., 2016b), we reasoned that skeletal structures that partially determine $\mu_{s,m}{}'$ could also conceivably be associated with bleaching susceptibility.

Micro-$\mu_s{}'$, similarly to light-scattering in tissue, is determined by interaction with several skeletal structures: (1) average size of nanograin (30–100 nm, Cuif and Dauphin, 2005a; Von Euw et al., 2017), and (2) extent of the fractal range in the biomineralized cluster R (which relate positively to $\mu_{s,m}{}'$; Rogers et al., 2009 and are currently unknown for individual species), (3) the shape of the optical refractive index correlation function C(r) given by mass-fractal dimension D_f (which inversely correlates with $\mu_{s,m}{}'$; Rogers et al., 2009) and was previously determined for

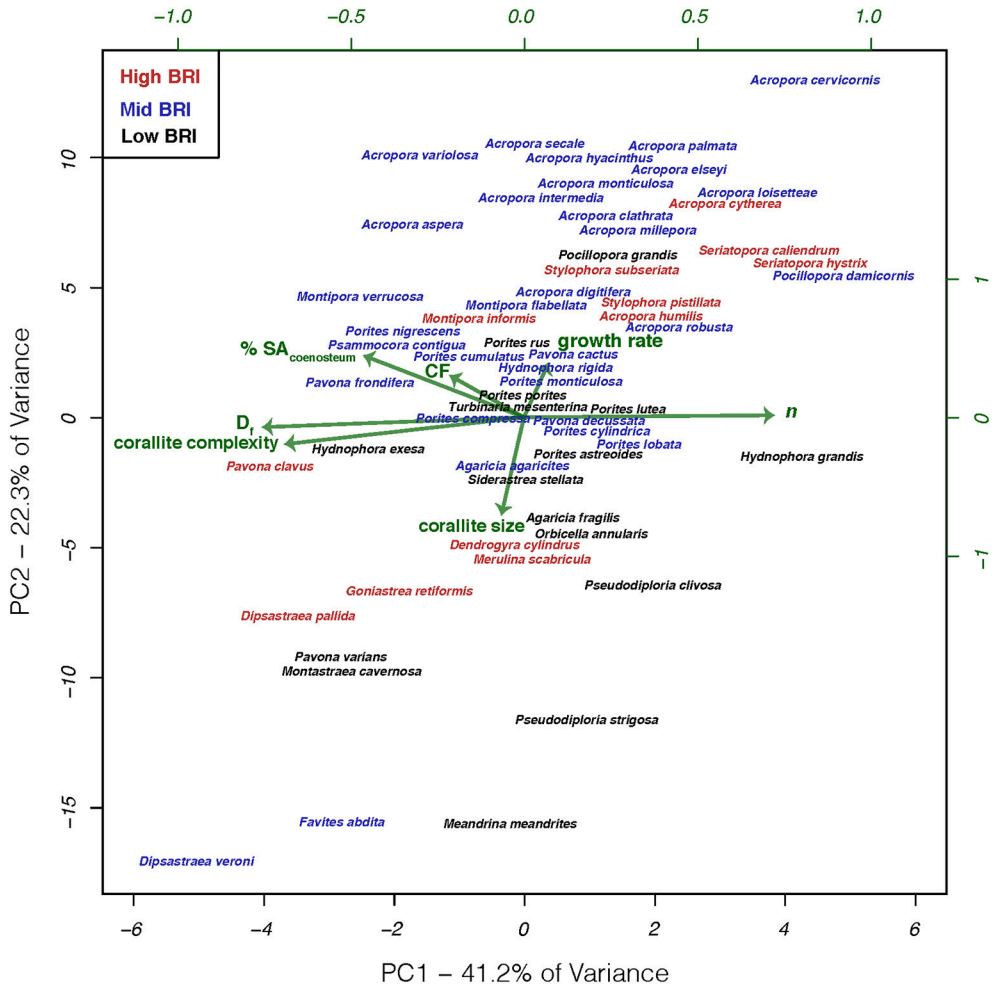

FIGURE 5 | Phylogenetic principal components analysis of characters thought to affect light microenvironments of *in hospite Symbiodinium* for 59 coral species. Phylogenetic correction based on the phylogeny modified from Huang (2012). Coral species color coded by bleaching response and arrows represent the relative contribution to each principal component.

all 88 targeted species (Marcelino et al., 2013), (4) the variance of the of the optical refractive index correlation function, *C(r)* (unknown for each species), and (5) macroscopic structures with voids (which will lower bulk- or micro-μ_s'; Enríquez et al., 2005; Stambler and Dubinsky, 2005; Rogers et al., 2009, 2014; Terán et al., 2010; Marcelino et al., 2013; and have been measured for some species).

Although D_f showed a significant association with $\mu_{s,m}'$ as expected from light theory, when D_f was tested for possible association with bleaching response, phylogenetically-corrected regression analysis revealed a non-significant negative relationship, indicating that although the mass-fractal organization of the skeleton is implicated in light scattering it is not correlated with bleaching susceptibility via the $\mu_{s,m}'$ pathway.

Macroscopic structures at higher length scales were also evaluated for possible association with bleaching susceptibility: colonial module dimensions (corallite size) and organization (corallite complexity, percent colony surface area composed of coenosteum—% $SA_{coenosteum}$). While it is clear that these features are related to each other in specific patterns across the coral phylogeny, since larger diameter corallites are also more complex (PCC = 0.809, $p < 0.001$, $n = 88$) and are surrounded by less coenosteum (PCC = −0.359, $p < 0.001$, $n = 88$; **Figure 1**; **Table S2**), none of these structures was significantly associated with bleaching response (**Figure 1**; **Table S2**). Finally, colony morphology (10 different growth forms listed in **Table S1**) was examined for correlation with bleaching susceptibility, since massive and encrusting colonies are historically reported to bleach and die at lower rates than branching and digitate colonies (Marshall and Baird, 2000; McClanahan, 2004; van Woesik et al., 2011).

We quantified each growth form by calculating *cumulative fractality*, or the product of the *apparent surface fractality* of each growth form, and D_f measured for each species. No significant correlation between taxon-BRI and *cumulative fractality* was detected (PCC = −0.08, $p = 0.47$, $n = 81$). We further performed phylo-log regression analysis on coral species that could be

classified as massive (coded as 0, $n = 44$) or branching (coded as 1, $n = 27$) and could not identify a significant association with bleaching response ($Z = -0.58$, $p = 0.56$). Additionally, we used growth form-specific ratios of surface area to volume described by Madin et al. (2016) (see **Text S2**) to quantify growth forms and also found no significant correlation with bleaching response. Recently it has been shown that the perceived relationship between growth forms and bleaching susceptibility is partially the result of their phylogentic relationships (McCowan et al., 2012; Swain et al., 2018); for example, while in the Faviidae family branching species bleached less than massive, the opposite was observed in the *Acroporidae* and *Poritidae* families (McCowan et al., 2012). Furthermore, due to the largely unknown effect of phenotypic plasticity within species (observed along gradients of light and nutrient flow) and species boundaries on colony morphology (reviewed in Veron, 2013), it has been challenging to accurately quantify and examine possible associations between species-specific growth forms and their bleaching response.

We reasoned that there may not be a clear relationship between bleaching response and individual features, but in combination with other skeletal characters known to modulate the light microenvironment, we may reveal their relationship with bleaching response. To that effect, we applied phylogenetically-corrected principal components analysis (phylo-PCA; **Figure 5**) to the seven characters that were not associated with taxon-BRI, to identify groups of characters that could be linearly combined in multi-dimensional space into principal components that explain the data variance: PC1 explained 41.2% and PC2 explained 22.3% of the data variance (PC3 explained only 15% of the data and was not considered further). Correlations between the two main principal components and the seven skeletal variables show that D_f, n, corallite complexity, and $\%\ SA_{coenosteum}$ were important components of PC1 while growth rate, corallite size and *cumulative fractality* were important components of PC2. Neither PC1 (PCC = 0.07, $p = 0.6$, $n = 59$) nor PC2 (PCC = 0.14, $p = 0.31$, $n = 59$) were significantly related to bleaching response.

These results show that variation in the skeletal structures targeted in this study, which have either been directly associated with modulating the light microenvironment surrounding *Symbiodinium* or shown to respond to variation in external light, are not related to bleaching response of these species. The lack of significant relationships should not be taken as an indication that these features do not actually modulate the internal light microenvironment of *in hospite Symbiodinium*, just that variation in these features and their abilities to modulate light microenvironments were not able to explain the observed variation in bleaching response across species. Variation in bleaching response among coral species has been attributed to diverse factors both intrinsic to the holobiont (e.g., thermotolerance of *Symbiodinium* and the interactions between coral, *Symbiodinium*, and other microbes; Baird et al., 2009; Leggat et al., 2011; Cunning and Baker, 2013; Krediet et al., 2013) and extrinsic from the environment (e.g., site-specific environmental conditions and frequency of thermal anomalies; McClanahan and Maina, 2003; Guest et al., 2012; Pratchett et al., 2013). Furthermore, the diversity of skeletal macro features observed among coral species are the result of simultaneous optimization of light capture and other vital functions including respiration and metabolite exchange between tissues and the environment (mass transfer; van Woesik et al., 2012), particle capture (Sebens et al., 1997), reproduction (Soong and Lang, 1992), and structural stability (Baldock et al., 2014). These forms are constrained by physical limitations imposed by the materials (Jimenez and Cortes, 1993; Boller et al., 2002) and three dimensional geometry of assembling modules (polyps) into a colony (Barbeitos, 2012), the physiological integration of those units (Coates and Oliver, 1973; Coates and Jackson, 1987; Soong and Lang, 1992 and Swain et al., 2018), and the evolutionary history of the species (Barbeitos et al., 2010; Budd et al., 2012). Perhaps the multitude of competing selection pressures directed at skeletal features may reveal correlations with bleaching susceptibility via pathways that are not light-scattering related, such as life-history strategies which have their own sets of specific morphological features (Darling et al., 2012, 2013). Corals with stress-tolerant strategies typically have massive morphologies, large corallites or meandroid polyp organization, grow slowly and have high fecundity, while corals with competitive strategies have large branching and plating morphologies, with smaller corallites, grow quickly, are more sensitive to storm breakages and bleach and die at greater rates during thermal stress events (Darling et al., 2012). Additionally, different morphologies are known to differ in their mass transfer abilities and within-tissue temperatures. Corals with higher surface area to volume ratios have faster gas and metabolite exchange across tissues (van Woesik et al., 2012), although ciliary movement (across the entire colony surface) can actively enhance mass transfer rates by 400% relative to passive molecular diffusion (Shapiro et al., 2014). Massive corals, due to their thick tissues and thicker thermal boundary layers, have higher within-tissue temperatures than branching corals with a thin veneer of tissue overlaying the skeleton and higher surface area to volume ratios (Jimenez et al., 2008, 2011). Furthermore, several non-photosynthetic fluorescent pigments present in host cells, such as GFP-like proteins, UV-absorbing compounds and other pigments, have been implicated in modulating the light microenvironment of *Symbiodinium* (Schlichter et al., 1986; Salih et al., 2000; Smith et al., 2013; Lyndby et al., 2016). In the case of GFP-like proteins, their role in modulating light microenvironment of *Symbiodinium* changes with pigment density. When present at low densities in the tissue, GFP-pigments scatter downwelling light, thus increasing light absorption and heating in the tissue, but at high pigment densities strong scattering reduces absorption and heating (Lyndby et al., 2016). The presence of GFP-pigments in the tissues may partially account for differential coral bleaching susceptibility and should be carefully investigated.

CONCLUSION

Skeletal light scattering, which has been shown to modulate the light microenvironment of *Symbiodinium* in coral tissue, is due to light interaction with structures ranging over several orders of

magnitude. Multiple lines of evidence predict that light scattering from the top ~200 μm (*micro-*μ_s') of skeleton is responsible for the rate of light increase to *Symbiodinium* and accelerated bleaching response to thermal stress (optical feedback-loop hypothesis). Here, phylogenetically-corrected regression analysis identified a relationship between *micro-*μ_s', but not bulk-μ_s' (light-scattering from the whole skeleton), and bleaching susceptibility in 88 coral species. Exploration of within-colony variation in *micro-*μ_s' in the 14-species subset, identified differences between *micro-*μ_s' of corallites and coenosteum, which can partially explain heterogeneity of light environments between polyp and coenosarc tissues. These results indicate that differential skeletal scattering between these structures could facilitate transport of light through the coenosteum to corallites which could then function as "photon-trapping" devices by repeatedly scattering photons off of septa and walls. Those species with inter-corallite spacing and skeletal optical properties that most facilitate this effect are the same species with elevated bleaching responses. However, when the size and complexity of corallites and the extent of coenosteum were measured, no correlation with bleaching could be identified. Furthermore, the well-known connection between colony morphology and bleaching response could not be verified, by either applying cumulative fractality or surface area to volume ratios as parameterizations of growth form, or by compiling growth forms into massive or branching groups in a phylogenetically-corrected regression. These results reveal the importance of performing phylogenetically-corrected correlations with skeletal characters that may otherwise closely reflect species evolutionary history and, as in the case of growth form, are also influenced by genetic and environmental factors. Finally, the effect of the fractal-like accretive growth of the skeleton on *micro-*μ_s' was examined by modeling growth as a function of density, size of nanograins, fractal range of biomineralized clusters, and overall mass-fractal dimension. The model, which was validated with experimental data, indicates that corals that grow faster typically have lower mass-fractal dimension, denser skeletons, lower skeletal micro-μ_s' and higher bleaching susceptibility. While this skeletal growth model was developed to estimate the average growth of skeleton at the colony-level, it should also be applicable to model growth of specific skeletal structures within the colony. Heterogeneity in calcification rates across skeletal structures have been observed in *Pocillopora damicornis* using nanoSIMS isotopic imaging, where skeletal extension in coenosteum is slower than corallite wall and dissepiments (Brahmi et al., 2012a,b). Future improvements to the model could account for this heterogenenous skeletal extension patterns to evaluate whether differences in calcification rates could potentially explain the difference between optical properties of coenosteum and corallites observed in this study.

AUTHOR CONTRIBUTIONS

LM, TS, and VB conceived and designed the research. HG, LM, NL, TS, and VB collected and compiled data. SL and TS performed phylogenetic analysis. LM, SL, TS, and VB analyzed the data and wrote the manuscript. All authors contributed to content revisions and approve of the final text.

FUNDING

This research was supported by the US National Science Foundation (EFRI-1240416 and CBET-1249311), and US National Institutes of Health (EB 003682).

ACKNOWLEDGMENTS

We thank R. Bieler and J. Gerber of the Field Museum for expertise and access to the FMNH museum collections and S. Cairns and T. Coffer of the National Museum of Natural History for expertise and access to the NMNH museum collections. Special thanks to D. Huang for providing us with the tree files for his comprehensive phylogeny of corals and M. Westneat for help analyzing them.

SUPPLEMENTARY MATERIAL

The Supplementary Material for this article can be found online at: https://www.frontiersin.org/articles/10.3389/fmars.2018.00450/full#supplementary-material

Figure S1 | Relationship between bleaching response and mean growth rate per growth form.

Table S1 | Character states and sources for each coral species.

Table S2 | Phylogenetically independent contrasts (PIC) analysis results.

Table S3 | Metrics quantifying the efficacy of the corallite irradiance due to light transport from the coenosteum (see section on "*Differences in Skeletal Micro-*μ_s' *of Corallites and Coenosteum Explain, in Part, Heterogeneous Light Environment Between Polyp and Coenosarc and are Associated With Bleaching Susceptibility*" for details).

Text S1 | Full references of **Table S1**.

Text S2 | Supplemental methods.

REFERENCES

Aizenberg, J., Weaver, J. C., Thanawala, M. S., Sundar, V. C., Morse, D. E., and Fratzl, P. (2005). Skeleton of *Euplectella* sp.: structural hierarchy from the nanoscale to the macroscale. *Science* 309, 275–278. doi: 10.1126/science.1112255

Allemand, D., Ferrier-Pages, C., Furla, P., Houlbreque, F., Puverel, S., Reynaud, S., et al. (2004). Biomineralisation in reef-building corals: from molecular mechanisms to environmental control. *Comptes Rendus Palevol* 3, 453–467. doi: 10.1016/j.crpv.2004.07.011

Anthony, K. R. N., and Hoegh-Guldberg, O. (2003). Variation in coral photosynthesis, respiration and growth characteristics in contrasting light microhabitats: an analogue to plants in forest gaps and understoreys? *Funct. Ecol.* 17, 246–259. doi: 10.1046/j.1365-2435.2003.00731.x

Anthony, K. R. N., Hoogenboom, M. O., and Connolly, S. R. (2005). Adaptive variation in coral geometry and the optimization of internal colony light climates. *Funct. Ecol.* 19, 17–26. doi: 10.1111/j.0269-8463.2005.00925.x

Baird, A. H., Bhagooli, R., Ralph, P. J., and Takahashi, S. (2009). Coral bleaching: the role of the host. *Trends Ecol. Evol.* 24, 16–20. doi: 10.1016/j.tree.2008.09.005

Baker, A. C., Glynn, P. W., and Riegl, B. (2008). Climate change and coral reef bleaching: an ecological assessment of long-term impacts, recovery trends and future outlook. *Estuar. Coast. Shelf Sci.* 80, 435–471. doi: 10.1016/j.ecss.2008.09.003

Baldock, T. E., Karampour, H., Sleep, R., Vyltla, A., Albermani, F., Golshani, A., et al. (2014). Resilience of branching and massive corals to wave loading under sea level rise—a coupled computational fluid dynamics-structural analysis. *Mar. Pollut. Bull.* 86, 91–101. doi: 10.1016/j.marpolbul.2014.07.038

Barbeitos, M. (2012). "Does polyp size constrain the morphological diversity of coral colonies?" in *12th International Coral Reef Symposium*, 30 (Cairns, QLD).

Barbeitos, M. S., Romano, S. L., and Lasker, H. R. (2010). Repeated loss of coloniality and symbiosis in scleractinian corals. *Proc. Natl. Acad. Sci. U.S.A.* 107, 11877–11882. doi: 10.1073/pnas.0914380107

Basillais, E. (1997). Coral surfaces and fractal dimensions: a new method. *Comptes Rendus Acad. Sci. Ser. III Sci. Vie* 320, 653–657.

Benzerara, K., Menguy, N., Obst, M., Stolarski, J., Mazur, M., Tylisczak, T., et al. (2011). Study of the crystallographic architecture of corals at the nanoscale by scanning transmission X-ray microscopy and transmission electron microscopy. *Ultramicroscopy* 111, 1268–1275. doi: 10.1016/j.ultramic.2011.03.023

Bhagooli, R., and Hidaka, M. (2004). Photoinhibition, bleaching susceptibility and mortality in two scleractinian corals, *Platygyra ryukyuensis* and *Stylophora pistillata*, in response to thermal and light stresses. *Comp. Biochem. Physiol. Part A* 137, 547–555. doi: 10.1016/j.cbpb.2003.11.008

Boller, M. L., Swain, T. D., and Lasker, H. R. (2002). Skeletal morphology and material properties of a fragmenting gorgonian coral. *Mar. Ecol. Prog. Ser.* 228, 131–141. doi: 10.3354/meps228131

Brahmi, C., Domart-Coulon, I., Rougee, L., Pyle, D. G., Stolarski, J., Mahoney, J. J., et al. (2012a). Pulsed 86Sr-labeling and NanoSIMS imaging to study coral biomineralization at ultra-structural length scales. *Coral Reefs* 31, 741–752. doi: 10.1007/s00338-012-0890-3

Brahmi, C., Kopp, C., Domart-Coulon, I., Stolarski, J., and Meibom, A. (2012b). Skeletal growth dynamics linked to trace-element composition in the scleractinian coral *Pocillopora damicornis*. *Geochim. Cosmochim. Acta* 99, 146–158. doi: 10.1016/j.gca.2012.09.031

Brodersen, K. E., Lichtenberg, M., Ralph, P. J., Kühl, M., and Wangpraseurt, D. (2014). Radiative energy budget reveals high photosynthetic efficiency in symbiont-bearing corals. *J. R. Soc. Interface* 11:20130997. doi: 10.1098/rsif.2013.0997

Bucher, D. J., Harriott, V. J., and Roberts, L. G. (1998). Skeletal micro-density, porosity and bulk density of acroporid corals. *J. Exp. Mar. Biol. Ecol.* 228, 117–136. doi: 10.1016/S0022-0981(98)00020-3

Budd, A. F., Fukami, H., Smith, N. D., and Knowlton, N. (2012). Taxonomic classification of the reef coral family Mussidae (Cnidaria: Anthozoa: Scleractinia). *Zool. J. Linn. Soc.* 166, 465–529. doi: 10.1111/j.1096-3642.2012.00855.x

Chindapol, N., Kaandorp, J. A., Cronemberger, C., Mass, T., and Genin, A. (2013). Modelling growth and form of the scleractinian coral *Pocillopora verrucosa* and the influence of hydrodynamics. *PLoS Comput. Biol.* 9:e1002849. doi: 10.1371/journal.pcbi.1002849

Coates, A. G., and Jackson, J. B. C. (1987). Clonal growth, algal symbiosis, and reef formation by corals. *Paleobiology* 13, 363–378. doi: 10.1017/S0094837300008988

Coates, A. G., and Oliver, W. A. J. (1973). "Coloniality in zoantharian corals," in *Animal Colonies: Development and Function Through Time*, eds R. S. Boardman, A. H. Cheetham, W. A. J. Oliver (Stroudsburg, PA: Hutchinson and Ross, Inc.), 3–27.

Cuif, J. P., and Dauphin, Y. (2005a). The environment recording unit in coral skeletons–a synthesis of structural and chemical evidences for a biochemically driven, stepping-growth process in fibres. *Biogeosciences* 2, 61–73. doi: 10.5194/bg-2-61-2005

Cuif, J. P., and Dauphin, Y. (2005b). The two-step mode of growth in the Scleractinian coral skeletons from the micrometre to the overall scale. *J. Struct. Biol.* 150, 319–331. doi: 10.1016/j.jsb.2005.03.004

Cunning, R., and Baker, A. C. (2013). Excess algal symbionts increase the susceptibility of reef corals to bleaching. *Nat. Clim. Chang.* 3, 259–262. doi: 10.1038/nclimate1711

Darling, E. S., Alvarez-Filip, L., Oliver, T. A., McClanahan, T. R., and Côté, I. M. (2012). Evaluating life-history strategies of reef corals from species traits. *Ecol. Lett.* 15, 1378–1386. doi: 10.1111/j.1461-0248.2012.01861.x

Darling, E. S., McClanahan, T. R., and Côté, I. M. (2013). Life histories predict coral community disassembly under multiple stressors. *Glob. Chang. Biol.* 19, 1930–1940. doi: 10.1111/gcb.12191

Dávalos-Dehullu, E., Hernández-Arana, H., and Carricart-Ganivet, J. P. (2008). On the causes of density banding in skeletons of corals of the genus *Montastraea*. *J. Exp. Mar. Biol. Ecol.* 365, 142–147. doi: 10.1016/j.jembe.2008.08.008

De Yoreo, J. J., Gilbert, P. U., Sommerdijk, N. A., Penn, R. L., Whitelam, S., Joester, D., et al. (2015). Crystallization by particle attachment in synthetic, biogenic, and geologic environments. *Science* 349:aaa6760. doi: 10.1126/science.aaa6760

Enríquez, S., Méndez, E. R., Hoegh-Guldberg, O., and Iglesias-Prieto, R. (2017). Key functional role of the optical properties of coral skeletons in coral ecology and evolution. *Proc. R. Soc. B Biol. Sci.* 284:20161667. doi: 10.1098/rspb.2016.1667

Enríquez, S., Méndez, E. R., and Iglesias-Prieto, R. (2005). Multiple scattering on coral skeletons enhances light absorption by symbiotic algae. *Limnol. Oceanogr.* 50, 1025–1032. doi: 10.4319/lo.2005.50.4.1025

Farris, J. S. (1989). The retention index and the rescaled consistency index. *Cladistics* 5, 417–419. doi: 10.1111/j.1096-0031.1989.tb00573.x

Frankowiak, K., Kret, S., Mazur, M., Meibom, A., Kitahara, M. V., and Stolarski, J. (2016). Fine-scale skeletal banding can distinguish symbiotic from asymbiotic species among modern and fossil scleractinian corals. *PLoS ONE* 11:e0147066. doi: 10.1371/journal.pone.0147066

Frieler, K., Meinshausen, M., Golly, A., Mengel, M., Lebek, K., Donner, S. D., et al. (2013). Limiting global warming to 2 degrees C is unlikely to save most coral reefs. *Nat. Clim. Chang.* 3, 165–170. doi: 10.1038/nclimate1674

Furukawa, Y., Nakajima, K., and Sato, K. (2001). *Advances in Crystal Growth Research*. New York, NY: Elsevier Science.

Guest, J. R., Baird, A. H., Maynard, J. A., Muttaqin, E., Edwards, A. J., Campbell, S. J., et al. (2012). Contrasting patterns of coral bleaching susceptibility in 2010 suggest an adaptive response to thermal stress. *PLoS ONE* 7:e33353. doi: 10.1371/journal.pone.0033353

Ho, L. s., and Ané, C. (2014). A linear-time algorithm for Gaussian and non-Gaussian trait evolution models. *Syst. Biol.* 63, 397–408. doi: 10.1093/sysbio/syu005

Hoegh-Guldberg, O., Mumby, P. J., Hooten, A. J., Steneck, R. S., Greenfield, P., Gomez, E., et al. (2007). Coral reefs under rapid climate change and ocean acidification. *Science* 318, 1737–1742. doi: 10.1126/science.1152509

Huang, D. (2012). Threatened reef corals of the world. *PLoS ONE* 7:e34459. doi: 10.1371/journal.pone.0034459

Hughes, T. P. (1987). Skeletal density and growth form of corals. *Mar. Ecol. Prog. Ser.* 35, 259–266. doi: 10.3354/meps035259

Hughes, T. P., Kerry, J. T., Álvarez-Noriega, M., Álvarez-Romero, J. G., Anderson, K. D., Baird, A. H., et al. (2017). Global warming and recurrent mass bleaching of corals. *Nature* 543, 373–377. doi: 10.1038/nature21707

Iglesias-Prieto, R., Matta, J. L., Robins, W. A., and Trench, R. K. (1992). Photosynthetic response to elevated temperature in the symbiotic dinoflagellate *Symbiodinium microadriaticum* in culture. *Proc. Natl. Acad. Sci. USA.* 89, 10302–10305. doi: 10.1073/pnas.89.21.10302

Ishimaru, A. (1999). *Wave Propagation and Scattering in Random Media*. New York, NY: Wiley-IEEE Press.

Ivens, A. B., von Beeren, C., Blüthgen, N., and Kronauer, D. J. (2016). Studying the complex communities of ants and their symbionts using ecological network analysis. *Annu. Rev. Entomol.* 61, 353–371. doi: 10.1146/annurev-ento-010715-023719

Ives, A. R., and Garland, T. (2010). Phylogenetic logistic regression for binary dependent variables. *Syst. Biol.* 59, 9–26. doi: 10.1093/sysbio/syp074

Jimenez, C., and Cortes, J. (1993). Density and compressive strength of the coral *Siderastrea siderea* (Scleractinia, Siderastreidae): intraspecific variability. *Rev. Biol. Trop.* 41, 39–43.

Jimenez, I. M., Kühl, M., Larkum, A. W., and Ralph, P. J. (2011). Effects of flow and colony morphology on the thermal boundary layer of corals. *J. R. Soc. Interface* 8, 1785–1795. doi: 10.1098/rsif.2011.0144

Jimenez, I. M., Kühl, M., Larkum, A. W. D., and Ralph, P. J. (2008). Heat budget and thermal microenvironment of shallow-water corals: do massive corals get warmer than branching corals? *Limnol. Oceanogr.* 53, 1548–1561. doi: 10.4319/lo.2008.53.4.1548

Jokiel, P. L. (2004). "Temperature stress and coral bleaching," in *Coral Health and Disease*, eds E. Rosenberg, Y. Loya (Berlin, Heidelberg: Springer-Verlag), 401–425.

Jones, R. J. (2008). Coral bleaching, bleaching-induced mortality, and the adaptive significance of the bleaching response. *Mar. Biol.* 154, 65–80. doi: 10.1007/s00227-007-0900-0

Kaandorp, J. A., Sloot, P. M., Merks, R. M., Bak, R. P., Vermeij, M. J., and Maier, C. (2005). Morphogenesis of the branching reef coral *Madracis mirabilis*. *Proc. R. Soc. B Biol. Sci.* 272, 127–133. doi: 10.1098/rspb.2004.2934

Kahng, S. E., Hochberg, E. J., Apprill, A., Wagner, D., Luck, D. G., Perez, D., et al. (2012). Efficient light harvesting in deep-water zooxanthellate corals. *Mar. Ecol. Prog. Ser.* 455, 65–77. doi: 10.3354/meps09657

Kamat, S., Su, X., Ballarini, R., and Heuer, A. H. (2000). Structural basis for the fracture toughness of the shell of the conch *Strombus gigas*. *Nature* 405, 1036–1040. doi: 10.1038/35016535

Kaniewska, P., Anthony, K. R. N., and Hoegh-Guldberg, O. (2008). Variation in colony geometry modulates internal light levels in branching corals *Acropora humilis* and *Stylophora pistillata*. *Mar. Biol.* 155, 649–660. doi: 10.1007/s00227-008-1061-5

Kaniewska, P., Anthony, K. R. N., Sampayo, E. M., Campbell, P. R., and Hoegh-Guldberg, O. (2014). Implications of geometric plasticity for maximizing photosynthesis in branching corals. *Mar. Biol.* 161, 313–328. doi: 10.1007/s00227-013-2336-z

Kaniewska, P., Magnusson, S. H., Anthony, K. R. N., Reef, R., Kühl, M., and Hoegh-Guldberg, O. (2011). Importance of macro-versus microstructure in modulating light levels inside coral colonies. *J. Phycol.* 47, 846–860. doi: 10.1111/j.1529-8817.2011.01021.x

Kim, Y. L., Liu, Y., Turzhitsky, V. M., Roy, H. K., Wali, R. K., and Backman, V. (2004). Coherent backscattering spectroscopy. *Opt. Lett.* 29, 1906–1908. doi: 10.1364/OL.29.001906

Klaus, J. S., Budd, A. F., Heikoop, J. M., and Fouke, B. W. (2007). Environmental controls on corallite morphology in the reef coral *Montastraea annularis*. *Bull. Mar. Sci.* 80, 233–260. Available online at: https://www.ingentaconnect.com/contentone/umrsmas/bullmar/2007/00000080/00000001/art00015#expand/collapse

Krediet, C. J., Ritchie, K. B., Paul, V. J., and Teplitski, M. (2013). Coral-associated micro-organisms and their roles in promoting coral health and thwarting diseases. *Proc. R. Soc. B Biol. Sci.* 280:20122328. doi: 10.1098/rspb.2012.2328

Kühl, M., Cohen, Y., Dalsgaard, T., Jorgensen, B. B., and Revsbech, NP (1995). Microenvironment and photosynthesis of zooxanthellae in scleractinian corals studied with microsensors for O_2, pH and Light. *Mar. Ecol. Prog. Ser.* 117, 159–172. doi: 10.3354/meps117159

Leggat, W., Seneca, F., Wasmund, K., Ukani, L., Yellowlees, D., and Ainsworth, T. D. (2011). Differential responses of the coral host and their algal symbiont to thermal stress. *PLoS ONE* 6:e26687. doi: 10.1371/journal.pone.0026687

Lesser, M. P., and Farrell, J. H. (2004). Exposure to solar radiation increases damage to both host tissues and algal symbionts of corals during thermal stress. *Coral Reefs* 23, 367–377. doi: 10.1007/s00338-004-0392-z

Lichtenberg, M., Larkum, A. W., and Kühl, M. (2016). Photosynthetic acclimation of *Symbiodinium in hospite* depends on vertical position in the tissue of the scleractinian coral *Montastrea curta*. *Front. Microbiol.* 7:230. doi: 10.3389/fmicb.2016.00230

Lough, J. M., and Cooper, T. F. (2011). New insights from coral growth band studies in an era of rapid environmental change. *Earth Sci. Rev.* 108, 170–184. doi: 10.1016/j.earscirev.2011.07.001

Loya, Y., Sakai, K., Yamazato, K., Nakano, Y., Sambali, H., and van Woesik, R. (2001). Coral bleaching: the winners and the losers. *Ecol. Lett.* 4, 122–131. doi: 10.1046/j.1461-0248.2001.00203.x

Lyndby, N. H., Kühl, M., and Wangpraseurt, D. (2016). Heat generation and light scattering of green fluorescent protein-like pigments in coral tissue. *Sci. Rep.* 6:26599. doi: 10.1038/srep26599

Maddison, W. P., and Maddison, D. R. (2011). *Mesquite: A Modular System for Evolutionary Analysis*. Available online at: http://mesquiteproject.org

Madin, J. S., Hoogenboom, M. O., Connolly, S. R., Darling, E. S., Falster, D. S., Huang, D. W., et al. (2016). A trait-based approach to advance coral reef science. *Trends Ecol. Evol.* 31, 419–428. doi: 10.1016/j.tree.2016.02.012

Magnusson, S. H., Fine, M., and Kühl, M. (2007). Light microclimate of endolithic phototrophs in the scleractinian corals *Montipora monasteriata* and *Porites cylindrica*. *Mar. Ecol. Prog. Ser.* 332, 119–128. doi: 10.3354/meps332119

Marcelino, L. A., Westneat, M. W., Stoyneva, V., Henss, J., Rogers, J. D., Radosevich, A., et al. (2013). Modulation of light-enhancement to symbiotic algae by light-scattering in corals and evolutionary trends in bleaching. *PLoS ONE* 8:e61492. doi: 10.1371/journal.pone.0061492

Marshall, P. A. (2000). Skeletal damage in reef corals: relating resistance to colony morphology. *Mar. Ecol. Prog. Ser.* 200, 177–189. doi: 10.3354/meps200177

Marshall, P. A., and Baird, A. H. (2000). Bleaching of corals on the Great Barrier Reef: differential susceptibilities among taxa. *Coral Reefs* 19, 155–163. doi: 10.1007/s003380000086

Martin-Garin, B., Lathuiliére, B., Verrecchia, E. P., and Geister, J. (2007). Use of fractal dimensions to quantify coral shape. *Coral Reefs* 26, 541–550. doi: 10.1007/s00338-007-0256-4

McClanahan, T. R. (2004). The relationship between bleaching and mortality of common corals. *Mar. Biol.* 144, 1239–1245. doi: 10.1007/s00227-003-1271-9

McClanahan, T. R., and Maina, J. (2003). Response of coral assemblages to the interaction between natural temperature variation and rare warm-water events. *Ecosystems* 6, 551–563. doi: 10.1007/s10021-002-0104-x

McCowan, D. M., Pratchett, M. S., and Baird, A. H. (2012). "Bleaching susceptibility and mortality among corals with differing growth forms," in *12th International Coral Reef Symposium*. Vol. 9A (Cairns, QLD), 1–6.

Midford, P. E., Garland, T Jr, and Maddison, W. P. (2010). *PDAP Package*. Available online at: http://mesquiteproject.org

Miyashita, S., Saito, Y., and Uwaha, M. (2005). Fractal aggregation growth and the surrounding diffusion field. *J. Cryst. Growth* 283, 533–539. doi: 10.1016/j.jcrysgro.2005.05.074

Morgan, K. M., and Kench, P. S. (2012). Skeletal extension and calcification of reef-building corals in the central Indian Ocean. *Mar. Environ. Res.* 81, 78–82. doi: 10.1016/j.marenvres.2012.08.001

Muko, S., Kawasaki, K., Sakai, K., Takasu, F., and Shigesada, N. (2000). Morphological plasticity in the coral *Porites sillimaniani* and its adaptive significance. *Bull. Mar. Sci.* 66, 225–239. Available online at: https://www.ingentaconnect.com/search/article?option1=tka&value1=Morphological+plasticity+in+the+coral+Porites+sillimaniani+and+its+adaptive&pageSize=10&index=1

Mumby, P. J., Chisholm, J. R. M., Edwards, A. J., Andrefouet, S., and Jaubert, J. (2001). Cloudy weather may have saved Society Island reef corals during the 1998 ENSO event. *Mar. Ecol. Prog. Ser.* 222, 209–216. doi: 10.3354/meps222209

Muscatine, L. (1990). "The role of symbiotic algae in carbon and energy flux in reef corals," in *Coral Reefs*, ed Z. Dubinsky (Amsterdam: Elsevier), 75–87.

Nir, O., Gruber, D. F., Einbinder, S., Kark, S., and Tchernov, D. (2011). Changes in scleractinian coral *Seriatopora hystrix* morphology and its endocellular *Symbiodinium* characteristics along a bathymetric gradient from shallow to mesophotic reef. *Coral Reefs* 30, 1089–1100. doi: 10.1007/s00338-011-0801-z

Nothdurft, L. D., and Webb, G. E. (2007). Microstructure of common reef-building coral genera *Acropora*, *Pocillopora*, *Goniastrea* and *Porites*: constraints on spatial resolution in geochemical sampling. *Facies* 53, 1–26. doi: 10.1007/s10347-006-0090-0

Ong, R. H., King, A. J. C., Caley, M. J., and Mullins, B. J. (2018). Prediction of solar irradiance using ray-tracing techniques for coral macro- and micro-habitats. *Mar. Environ. Res.* 141, 75–87. doi: 10.1016/j.marenvres.2018.08.004

Ong, R. H., King, A. J. C., Kaandorp, J. A., Mullins, B. J., and Caley, M. J. (2017). The effect of allometric scaling in coral thermal microenvironments. *PLoS ONE* 12:e0184214. doi: 10.1371/journal.pone.0184214

Ow, Y. X., and Todd, P. A. (2010). Light-induced morphological plasticity in the scleractinian coral *Goniastrea pectinata* and its functional significance. *Coral Reefs* 29, 797–808. doi: 10.1007/s00338-010-0631-4

Peitgen, H.-O., Jürgens, H., and Saupe, D. (1992). *Chaos and Fractals: New Frontiers of Science*. New York, NY: Springer-Verlag. doi: 10.1007/978-1-4757-4740-9

Pochon, X., Forsman, Z. H., Spalding, H. L., Padilla-Gamiño, J. L., Smith, C. M., and Gates, R. D. (2015). Depth specialization in mesophotic corals (*Leptoseris* spp.) and associated algal symbionts in Hawai'i. *R. Soc. Open Sci.* 2, 1–14. doi: 10.1098/rsos.140351

Pratchett, M. S., McCowan, D., Maynard, J. A., and Heron, S. F. (2013). Changes in bleaching susceptibility among corals subject to ocean warming and recurrent bleaching in Moorea, French Polynesia. *PLoS ONE* 8:e70443. doi: 10.1371/journal.pone.0070443

Przeniosło, R., Stolarski, J., Mazur, M., and Brunelli, M. (2008). Hierarchically structured scleractinian coral biocrystals. *J. Struct. Biol.* 161, 74–82. doi: 10.1016/j.jsb.2007.09.020

Ralph, P. J., Gademann, R., Larkum, A. W. D., and Kühl, M. (2002). Spatial heterogeneity in active chlorophyll fluorescence and PSII activity of coral tissues. *Mar. Biol.* 141, 639–646. doi: 10.1007/s00227-002-0866-x

Revell, L. J. (2009). Size-correction and principal components for interspecific comparative studies. *Evolution* 63, 3258–3268. doi: 10.1111/j.1558-5646.2009.00804.x

Revell, L. J. (2010). Phylogenetic signal and linear regression on species data. *Methods Ecol. Evol.* 1, 319–329. doi: 10.1111/j.2041-210X.2010.00044.x

Revell, L. J. (2012). Phytools: an R package for phylogenetic comparative biology (and other things). *Methods Ecol. Evol.* 3, 217–223. doi: 10.1111/j.2041-210X.2011.00169.x

Rezende, E. L., Lavabre, J. E., Guimarães, P. R., Jordano, P., and Bascompte, J. (2007). Non-random coextinctions in phylogenetically structured mutualistic networks. *Nature* 448, U925–U926. doi: 10.1038/nature05956

Rocha, R. J., Silva, A. M., Fernandes, M. H., Cruz, I. C., Rosa, R., and Calado, R. (2014). Contrasting light spectra constrain the macro and microstructures of scleractinian corals. *PLoS ONE* 9:e105863. doi: 10.1371/journal.pone.0105863

Rodríguez-Roman, A., Hernández-Pech, X., Thomé, P. E., Enríquez, S., and Iglesias-Prieto, R. (2006). Photosynthesis and light utilization in the Caribbean coral *Montastraea faveolata* recovering from a bleaching event. *Limnol. Oceanogr.* 51, 2702–2710. doi: 10.4319/lo.2006.51.6.2702

Rogers, J. D., and Capoglu, I. R., Backman, V. (2009). Nonscalar elastic light scattering from continuous random media in the Born approximation. *Opt. Lett.* 34, 1891–1893. doi: 10.1364/OL.34.001891

Rogers, J. D., Radosevich, A. J., Yi, J., and Backman, V. (2014). Modeling light scattering in tissue as continuous random media using a versatile refractive index correlation function. *IEEE J. Select. Top. Quant. Electronics* 20, 173–186. doi: 10.1109/jstqe.2013.2280999

Salih, A., Larkum, A., Cox, G., Kühl, M., and Hoegh-Guldberg, O. (2000). Fluorescent pigments in corals are photoprotective. *Nature* 408, 850–853. doi: 10.1038/35048564

Schlichter, D., Fricke, H. W., and Weber, W. (1986). Light harvesting by wavelength transformation in a symbiotic coral of the Red Sea twilight zone. *Mar. Biol.* 91, 403–407. doi: 10.1007/BF00428634

Sebens, K. P., Witting, J., and Helmuth, B. (1997). Effects of water flow and branch spacing on particle capture by the reef coral *Madracis mirabilis* (Duchassaing and Michelotti). *J. Exp. Mar. Biol. Ecol.* 211, 1–28. doi: 10.1016/S0022-0981(96)02636-6

Shapiro, O. H., Fernandez, V. I., Garren, M., Guasto, J. S., Debaillon-Vesque, F. P., Kramarsky-Winter, E., et al. (2014). Vortical ciliary flows actively enhance mass transport in reef corals. *Proc. Natl. Acad. Sci. USA.* 111, 13391–13396. doi: 10.1073/pnas.1323094111

Smith, E. G., D'Angelo, C., Salih, A., and Wiedenmann, J. (2013). Screening by coral green fluorescent protein (GFP)-like chromoproteins supports a role in photoprotection of zooxanthellae. *Coral Reefs* 32, 463–474. doi: 10.1007/s00338-012-0994-9

Smith, L. W., and Birkeland, C. (2007). Effects of intemittent flow and irradiance level on back reef *Porites* corals at elevated seawater temperatures. *J. Exp. Mar. Biol. Ecol.* 341, 282–294. doi: 10.1016/j.jembe.2006.10.053

Soong, K., and Lang, J. C. (1992). Reproductive integration in reef corals. *Biol. Bull.* 183, 418–431. doi: 10.2307/1542018

Stambler, N., and Dubinsky, Z. (2005). Corals as light collectors: an integrating sphere approach. *Coral Reefs* 24, 1–9. doi: 10.1007/s00338-004-0452-4

Stolarski, J. (2003). Three-dimensional micro- and nanostructural characteristics of the scleractinian coral skeleton: a biocalcification proxy. *Acta Palaeontol. Pol.* 48, 497–530.

Stolarski, J., and Mazur, M. (2005). Nanostructure of biogenic versus abiogenic calcium carbonate crystals. *Acta Palaeontol. Pol.* 50, 847–865. Available online at: https://www.app.pan.pl/article/item/app50-847.html

Swain, T. D., Bold, E. C., Osborn, P. C., Baird, A. H., Westneat, M. W., Backman, V., et al. (2018). Physiological integration of coral colonies is correlated with bleaching resistance. *Mar. Ecol. Prog. Ser.* 586, 1–10. doi: 10.3354/meps12445

Swain, T. D., DuBois, E., Gomes, A., Stoyneva, V. P., Radosevich, A. J., Henss, J., et al. (2016b). Skeletal light-scattering accelerates bleaching response in reef-building corals. *BMC Ecol.* 16:10. doi: 10.1186/s12898-016-0061-4

Swain, T. D., Vega-Perkins, J. B., Oestreich, W. K., Triebold, C., DuBois, E., Henss, J., et al. (2016a). Coral bleaching response index: a new tool to standardize and compare susceptibility to thermal bleaching. *Glob. Chang. Biol.* 22, 2475–2488. doi: 10.1111/gcb.13276

Terán, E., Méndez, E. R., Enríquez, S., and Iglesias-Prieto, R. (2010). Multiple light scattering and absorption in reef-building corals. *Appl. Opt.* 49, 5032–5042. doi: 10.1364/AO.49.005032

Todd, P. A. (2008). Morphological plasticity in scleractinian corals. *Biol. Rev.* 83, 315–337. doi: 10.1111/j.1469-185X.2008.00045.x

Todd, P. A., Ladle, R. J., Lewin-Koh, N. J. I., and Chou, L. M. (2004). Genotype x environment interactions in transplanted clones of the massive corals *Favia speciosa* and *Diploastrea helippora*. *Mar. Ecol. Prog. Ser.* 271, 167–182. doi: 10.3354/meps271167

Ulstrup, K. E., Ralph, P. J., Larkum, A. W. D., and Kühl, M. (2006). Intra-colonial variability in light acclimation of zooxanthellae in coral tissues of *Pocillopora damicornis*. *Mar. Biol.* 149, 1325–1335. doi: 10.1007/s00227-006-0286-4

Ulstrup, K. E., van Oppen, M. J. H., Kühl, M., and Ralph, P. J. (2007). Inter-polyp genetic and physiological characterisation of *Symbiodinium* in an *Acropora valida* colony. *Mar. Biol.* 153, 225–234. doi: 10.1007/s00227-007-0806-x

Uwaha, M., and Saito, Y. (1990). Fractal aggregation and dendritic crystal-growth. *J. Cryst. Growth* 99, 175–178. doi: 10.1016/0022-0248(90)90507-H

van Woesik, R., Irikawa, A., Anzai, R., and Nakamura, T. (2012). Effects of coral colony morphologies on mass transfer and susceptibility to thermal stress. *Coral Reefs* 31, 633–639. doi: 10.1007/s00338-012-0911-2

van Woesik, R., Sakai, K., Ganase, A., and Loya, Y. (2011). Revisiting the winners and the losers a decade after coral bleaching. *Mar. Ecol. Prog. Ser.* 434, 67–76. doi: 10.3354/meps09203

Veron, J. (2013). Overview of the taxonomy of zooxanthellate Scleractinia. *Zool. J. Linn. Soc.* 169, 485–508. doi: 10.1111/zoj.12076

Von Euw, S., Zhang, Q., Manichev, V., Murali, N., Gross, J., Feldman, L. C., et al. (2017). Biological control of aragonite formation in stony corals. *Science* 356, 933–938. doi: 10.1126/science.aam6371

Wangpraseurt, D., Holm, J. B., Larkum, A. W., Pernice, M., Ralph, P. J., Suggett, D. J., et al. (2017). *In vivo* microscale measurements of light and photosynthesis during coral bleaching: evidence for the optical feedback loop? *Front. Microbiol.* 8:59. doi: 10.3389/fmicb.2017.00059

Wangpraseurt, D., Jacques, S. L., Petrie, T., and Kühl, M. (2016). Monte Carlo modeling of photon propagation reveals highly scattering coral tissue. *Front. Plant Sci.* 7:1404. doi: 10.3389/fpls.2016.01404

Wangpraseurt, D., Larkum, A. W. D., Franklin, J., Szabó, M., Ralph, P. J., and Kühl, M. (2014a). Lateral light transfer ensures efficient resource distribution in symbiont-bearing corals. *J. Exp. Biol.* 217, 489–498. doi: 10.1242/jeb.091116

Wangpraseurt, D., Larkum, A. W. D., Ralph, P. J., and Kühl, M. (2012). Light gradients and optical microniches in coral tissues. *Front. Microbiol.* 3:316. doi: 10.3389/fmicb.2012.00316

Wangpraseurt, D., Polerecky, L., Larkum, A. W. D., Ralph, P. J., Nielsen, D. A., Pernice, M., et al. (2014b). The *in situ* light microenvironment

of corals. *Limnol. Oceanogr.* 59, 917–926. doi: 10.4319/lo.2014.59.3.0917

Warner, M. E., Fitt, W. K., and Schmidt, G. W. (1999). Damage to photosystem II in symbiotic dinoflagellates: a determinant of coral bleaching. *Proc. Natl. Acad. Sci. U.S.A.* 96, 8007–8012. doi: 10.1073/pnas.96.14.8007

Young, G. C., Dey, S., Rogers, A. D., and Exton, D. (2017). Cost and time-effective method for multi-scale measures of rugosity, fractal dimension, and vector dispersion from coral reef 3D models. *PLoS ONE* 12:e0175341. doi: 10.1371/journal.pone.0175341

Zhang, H., Gao, S., Lercher, M. J., Hu, S., and Chen, W. H. (2012). EvolView, an online tool for visualizing, annotating and managing phylogenetic trees. *Nucleic Acids Res.* 40, W569–W572. doi: 10.1093/nar/gks576

Zonios, G., Perelman, L. T., Backman, V., Manoharan, R., Fitzmaurice, M., Van Dam, J., et al. (1999). Diffuse reflectance spectroscopy of human adenomatous colon polyps *in vivo*. *Appl. Opt.* 38, 6628–6637. doi: 10.1364/AO.38.006628

Conflict of Interest Statement: The authors declare that the research was conducted in the absence of any commercial or financial relationships that could be construed as a potential conflict of interest.

frontiers in Marine Science

ORIGINAL RESEARCH
published: 06 August 2019
doi: 10.3389/fmars.2019.00472

Optical Properties of Living Corals Determined With Diffuse Reflectance Spectroscopy

Steven L. Jacques[1], Daniel Wangpraseurt[2,3,4]* and Michael Kühl[3,5]*

[1] Department of Biomedical Engineering, Tufts University, Medford, MA, United States, [2] Department of Chemistry, Cambridge University, Cambridge, United Kingdom, [3] Marine Biology Section, University of Copenhagen, Copenhagen, Denmark, [4] Scripps Institution of Oceanography, University of California, San Diego, San Diego, CA, United States, [5] Climate Change Cluster, University of Technology Sydney, Ultimo, NSW, Australia

The internal light field and thus light exposure of the photosymbiotic microalgae (*Symbiodinium* sp.) in corals is strongly modulated by the optical properties of coral tissue and skeleton. While there are numerous studies documenting the light microenvironment in corals, there are only few measurements of the inherent optical properties of corals in the literature, and this has hampered a more quantitative understanding of coral optics. Here we present a study of the optical properties of 26 live coral samples, representative of 11 coral species and spanning a variety of morphotypes. We employed well-established fiber-optic reflectance spectroscopy techniques from biomedical optics using two methods: (1) A source and a detection fiber separated by a variable distance measured the lateral spread of light in corals, dominated by the skeleton; (2) A fiber-optic field radiance probe measured the diffuse reflectance from the coral surface, dominated by the living coral tissue. Analysis based on diffusion theory and Monte Carlo simulation yielded estimates of the bulk scattering and absorption coefficients of the coral tissue and skeleton, in the 750–1030 nm wavelength range. Extrapolating into the spectral region of photosynthetically active radiation (PAR, 400–700 nm) allowed estimation of the optical depth of absorption by the main *Symbiodinium* photopigment chlorophyll *a*. Coral tissue scattering was on average ~1.9x stronger than the scattering of the skeleton, consistent with the model that corals trap photons by high scattering to enhance absorption by algal pigments, while the lower scattering of the skeleton allows spread of light to otherwise shaded coral tissue areas.

Keywords: coral optics, photobiology, light scattering, coral-algal symbiosis, light harvesting, Monte Carlo (MC)

OPEN ACCESS

Edited by:
Oren Levy,
Bar-Ilan University, Israel

Reviewed by:
Nadav Shashar,
Ben-Gurion University of the Negev, Israel
David F. Gruber,
Baruch College (CUNY), United States

****Correspondence:***
Steven L. Jacques
stevjacq@gmail.com
Daniel Wangpraseurt
dw527@cam.ac.uk

Specialty section:
This article was submitted to Coral Reef Research, a section of the journal Frontiers in Marine Science

Received: *10 September 2018*
Accepted: *12 July 2019*
Published: *06 August 2019*

Citation:
Jacques SL, Wangpraseurt D and Kühl M (2019) Optical Properties of Living Corals Determined With Diffuse Reflectance Spectroscopy. Front. Mar. Sci. 6:472. doi: 10.3389/fmars.2019.00472

INTRODUCTION

Calcifying, symbiont-bearing corals are the key architects and builders of (sub)tropical coral reefs, one of the most diverse marine habitats on Earth. Coral fitness and thus reef-building is largely dependent on the interactions of the cnidarian animal host and its endosymbiotic microalgae belonging to the dinoflagellate genus *Symbiodinium*. An additional feature of corals is their close interaction with associated microbes that form a diverse microbiome (Bourne et al., 2009). While microbes and nighttime feeding on particles and zooplankton provide essential nutrients and some organic carbon, the coral mainly relies on the supply of labile carbon from *Symbiodinium* photosynthesis (Muscatine et al., 1981). By regulating the nutrient supply to the microalgae and ensuring sufficient light and inorganic carbon supply, the coral host keeps its photosymbionts in

a state of unbalanced growth stimulating net O_2 production and the excretion of photosynthates in the form of simple carbohydrates from *Symbiodinium* to the host (Falkowski et al., 1984). It is estimated that *Symbiodinium* photosynthesis can cover up to >90% of the energy demand of the coral host (Muscatine et al., 1981). Optimization of *Symbiodinium* light exposure for photosynthesis and photoprotection against high UV and solar radiation is thus a key trait in corals, and several strategies for such optimization have been identified in corals (summarized in Wangpraseurt et al., 2016). Coral optics have also been linked to coral bleaching susceptibility (Enriquez et al., 2005; Rodriguez-Roman et al., 2006; Swain et al., 2016; Wangpraseurt et al., 2017a).

The use of fiber-optic microprobes (Kühl et al., 1995; Wangpraseurt et al., 2012) and various types of reflectance measurements (Salih et al., 2000; Enriquez et al., 2005; Marcelino et al., 2013; Wangpraseurt et al., 2014) have revealed the presence of light gradients and intense scattering of light in both coral tissue and skeleton, which are modulated by coral tissue plasticity and thickness (Wangpraseurt et al., 2014), and the presence and distribution of fluorescent and scattering host pigments in the coral tissue (Salih et al., 2000; Lyndby et al., 2016; Smith et al., 2017). Studies of clean coral skeletons indicate that differences in defined skeleton scattering properties can also play an important role for the light field in corals (Marcelino et al., 2013), which was further supported by Enríquez et al. (2017) studying different museum coral skeleton specimens for relative light enhancement, a less defined measure of scattering.

Modeling and simulation of coral light fields based on estimates of inherent optical parameters remain underexplored with so far only two publications in the literature (Teran et al., 2010; Wangpraseurt et al., 2016). This is mainly reflecting the limited knowledge about the inherent optical properties (IOP) of corals, i.e., the absorption and scattering coefficients and the angular characteristics of scattering in tissue and skeleton. Recently, we have started to apply experimental methods from biomedical optics such as diffuse reflectance spectroscopy and optical coherence tomography in combination with diffusion theory and Monte Carlo modeling to alleviate this knowledge gap (Wangpraseurt et al., 2016, 2017b). In the present study, we present a survey of the absorption and scattering characteristics of 11 different coral species spanning a range of morphotypes. The aim was to obtain robust average values for IOP of tissue and skeleton of intact corals rather than present detailed high-resolution studies linking such measurements to the fine-structure of individual coral species, which is possible with, e.g., optical coherence tomography (Levitz et al., 2004; Wangpraseurt et al., 2019).

MATERIALS AND METHODS

Field Site and Coral Sampling

Corals were collected by snorkeling from the shallow reef flat on Heron Island, Great Barrier Reef, Australia (152°06′ E, 20°29′ S). Corals were fragmented by hammer and chisel and mounted with clay on small tiles for handling and species identification according to Veron (2000). We used a total of 26 fragments representing 11 different species (**Supplementary Table S1**). Prior to measurements, coral fragments were kept in a shaded outdoor tank at Heron Island Research Station, which was constantly flushed with seawater from the lagoon. At the end of the 5-day measuring period, some fragments were used for determination of *Symbiodinium* cell counts, while the remaining fragments were returned to their original habitat.

Experimental Measurements

Optical fiber-based spectroscopy was used to measure the spreading and reflectance of light from the corals by two different experimental approaches (**Figure 1**). First, the spreading of light in the skeleton was characterized. Such a point-spread function of light was measured by injecting light into randomly chosen coral tissue areas with one optical fiber collecting light at a distance, r [mm] from the source fiber, which was positioned into the coral tissue (**Figure 1A**). We note that this volumetric approach mainly probes skeleton scattering. These experiments used 400 μm wide, flat cut optical glass fibers (Ocean Optics, United States), where the source fiber was connected to a white tungsten-halogen light source (HL2000, Ocean Optics, United States), and the collecting fiber was connected to a sensitive fiber-optic spectrometer (QE65000, Ocean Optics, United States). Spectral measurements of light at defined distances from the source fiber, M(r) [counts], were acquired over a wavelength range of 300–1100 nm, where spectral data from 500 to 1030 nm were of sufficient quality for further analysis. Fiber placement was controlled by a manually operated micromanipulator (MM33, Märtzhäuser, Germany), such that the inter-fiber distance, r, was varied in 1 mm steps from 1 to 10 mm distance from the incident light spot on the coral.

Secondly, we measured the diffuse reflected light from coral tissue, $M_{d,coral}$, relative to the reflected light from a gray slate reflectance standard, $M_{d,std}$ positioned at identical distance as the coral surface. These measurements were done with a fiber-optic reflection probe (MODEL QR450-7-XSR, Ocean Optics, United States) consisting of six illumination fibers surrounding a central collection fiber (all fibers had a diameter of 400 μm). The collection fiber was connected to

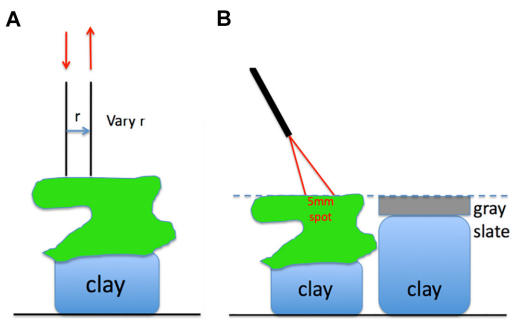

FIGURE 1 | (A) Two optical fibers measure the lateral spread of light within the coral. **(B)** An optical fiber probe delivers to and collects from a 5-mm-dia. spot on the coral, at a 30° angle off the normal to the coral surface.

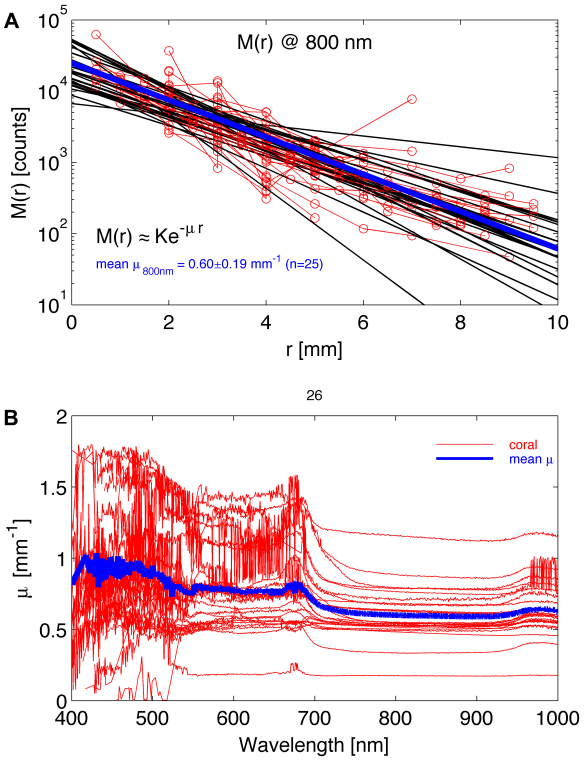

FIGURE 2 | Experimental determination of lateral light attenuation in corals. **(A)** M(r) data at 800 nm for 26 coral samples fitted with the exponential function $M(r) = K{\cdot}e^{-\mu\cdot r}$ (black lines). Blue line is the average fit. **(B)** The lateral attenuation spectrum of μ versus wavelength for the 26 coral specimens. Blue line is average spectrum.

a fiber-optic spectrometer (QE65000, Ocean Optics), while the illumination fibers were connected to a fiber-optic halogen light source (QE65000, Ocean Optics). The fiber-probe was oriented at an angle of 30° relative to normal with the probe tip positioned at a distance of ∼1.5 cm from the coral or reflectance standard surface. This orientation produced a ∼5 mm wide spot of illumination on the coral or gray slate standard. The probe collection matched the same 5 mm spot as the light delivery. The 30° illumination mitigated any specular reflectance from the coral or reflectance standard. The coral samples and the reflectance standard were mounted on lumps of clay enabling careful adjustment of their respective heights to ensure identical distance to the fiber probe. After measuring reflected light from the coral, the reflectance standard was shifted into position for measurements allowing correction for any small differences in coral distance from the fiber probe. The reflectance spectrum of a coral was calculated as:

$$R_d = \frac{M_{d.coral}}{M_{d.std}} R_{d.std} \quad (1)$$

where Rd,std is the known reflectance of the reflectance standard (=99%),and $M_{d,coral}$ and $M_{d,std}$ [counts] denote the reflected light spectrum of the coral and reflectance standard, respectively.

TABLE 1 | List of abbreviations and their descriptions.

Abbreviation	Description	Unit
PAR	Photosynthetically available radiation	μmol photons m^{-2} s^{-1}
M(r)	Uncalibrated radial reflectance measurement	Arbitrary
R(r)	Calibrated radial reflectance measurement	Dimensionless
$M_{d,coral}$	Uncalibrated reflected light from coral	Arbitrary
$M_{d,std}$	Reflected light from reflectance standard	Arbitrary
R_d	Diffuse reflectance	Dimensionless
R_{dstd}	Diffuse reflectance from reflectance standard	Dimensionless
μ	Attenuation coefficient	mm^{-1}
K	Scaling constant	Dimensionless
μ	Scattering coefficient	mm^{-1}
g	Anisotropy of scattering	Dimensionless
μ_s'	Reduced scattering coefficient = $\mu_s \cdot(1\text{-}g)$	mm^{-1}
a_s	Skeletal Scattering coefficient at 500 nm	mm^{-1}
a_c	Tissue scattering coefficient at 500 nm	mm^{-1}
b_s	Skeletal scattering power (scales scattering over wavelength)	Dimensionless
m_a	Absorption coefficient	mm^{-1}
W_s	Water content of skeleton	Dimensionless
W_c	Water content of coral tissue	
n	Refractive index	Dimensionless
λ	Wavelength	Nm
KR_d	Uncalibrated diffuse reflectance	Dimensionless
pKR_d	Predicted reflectance spectrum based on scattering and water absorption only	Dimensionless
f_{coll}	Light collection efficiency factor	Dimensionless
K_d	Scaling constant	Dimensionless
OD	Optical depth	Dimensionless
T	Transmittance	Dimensionless
A	Absorbance	Dimensionless

Model Development

Optical Properties of Skeleton

The measurements of M(r) described the lateral spreading of light within the coral, and hence were dominated by the skeleton optical properties. Such measurements yielded spectra of laterally transported light as a function of radial distance from the source, M(r) [counts], which could be fitted with an exponential function as:

$$M(r) \approx K \cdot e^{-\mu\cdot r} \quad (2)$$

The approximation $K{\cdot}e^{-\mu\cdot r}$, where K is a scaling constant and μ is the attenuation coefficient of light [mm^{-1}], ignores the initial 1/r dependence of M(r) at short r, which is expected from diffusion theory (Farrell et al., 1992), since experiments showed that all coral species followed this approximation with

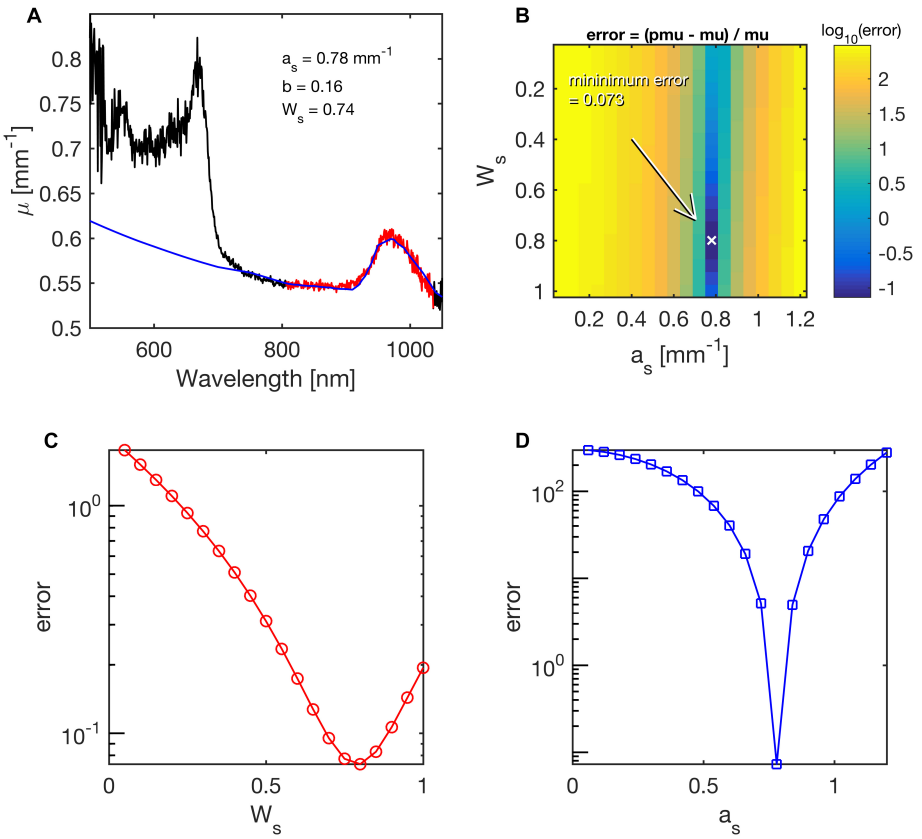

FIGURE 3 | Example of fitting coral skeletal scattering (a_s) and water content (W_s) during least-squares fitting of the lateral attenuation coefficient $\mu(\lambda)$ for 750 nm < l < 1030 nm in *Acropora millepora*. The mapping of errors for a_s and W_s, yielded best values of 0.78 mm^{-1} and 0.74 mm^{-1}, respectively. **(A)** The fit (blue line) to the spectral range in red. **(B)** Map of the error for various choices of a_s and W_s. The parameter b was held at its fitted value of 0.16. Arrow points to minimum error. **(C)** Error in W_s, while a_s was held at its best value. **(D)** Error in a_s, while W_s was held at its best value.

no obvious 1/r behavior. Hence, the point-spread function could be well-described by the lateral attenuation coefficient μ [mm^{-1}], and analysis of M(r) spectra thus yielded values of $\mu(\lambda)$ according to Eq. 2. **Figure 2A** shows an example of M(r) for 800 nm light, indicating a value of μ = 0.60 ± 0.19 mm^{-1} (n = 26 corals; mean ± SD). **Figure 2B** shows spectra of $\mu(\lambda)$ for the 26 coral samples, illustrating significant variability among the investigated corals around the overall mean attenuation spectrum (blue line in **Figure 2B**).

Subsequently, $\mu(\lambda)$ was fitted by a least-squares method (multidimensional unconstrained non-linear minimization, Nelder-Mead, fminsearch.m in MATLAB) to determine the reduced scattering coefficient of the coral skeleton, $\mu_s'_{sk}$ [mm^{-1}] and the average skeletal water content, W_s. The analysis used the 750–1030 nm wavelength range, where algal pigments did not affect the spectrum. The wavelength behavior of $\mu_s'_{sk}$ was described by:

$$\mu'_{ssk} = a_s\left(\frac{\lambda}{500nm}\right)^{-b_s} \quad (3)$$

where a_s = μ_s'(500 nm), and b_s is the skeletal scattering power (**Table 1**).

Assuming absence of strong spectral signatures by the coral skeleton material (Marcelino et al., 2013), the wavelength dependence of the skeletal absorption coefficient can be approximated by:

$$\mu_{a,sk}(\lambda) = W_s\,\mu_{a,water} \quad (4)$$

Where W_s is the skeletal water content (dimensionless), and $\mu_{a,water}(\lambda)$ is the absorption spectrum of water (Hale and Querry, 1973). The analysis used least-squares fitting, where the behavior of the point spread function, R(r), was calculated for each wavelength using a custom written algorithm that calculates the diffuse reflectance based on diffusion theory (Farrell et al., 1992; Tuchin, 2007). This approach has been intensively used in biomedical tissue optics and provides consistent results with other approaches (e.g., Monte Carlo simulation) when light scattering dominates over light absorption for a given tissue; as a rule of thumb, if $\mu_s(1\text{-}g)/\mu_a$ is >10 (Jacques and Pogue, 2008). Briefly, the model uses a set of μ_a and μ_s' values to predict R(r). The model is varied over a range of μ_a and μ_s' values until a set of values closely match the experimentally measured values. The model assumes a refractive index mismatch between the coral surface and water. We assumed a refractive

index of 1.4 for coral tissue and 1.33 for water (Wangpraseurt et al., 2016), thus the refractive index mismatch was calculated as $n_r = n_{coral}/n_{water} = 1.4/1.33$.

The R(r) was first interpreted using Eq. 2, $R(r) = K{\cdot}e^{-\mu \cdot r}$, to yield a simple attenuation coefficient (μ). Iteration then adjusted the values of a_s, b_s and W_s until the predicted μ and measured μ agreed. **Figure 3** illustrates the ability of least-squares fitting to find the a_s and W_s of a coral by showing the relative error in a predicted μ versus the experimentally measured μ as:

$$\text{error} = (\mu_{predicted} - \mu_{experimental})/\mu_{experimental} \quad (5)$$

Optical Properties of Coral Tissue

The diffuse reflected light collected from the 5 mm wide illumination spot was used to estimate the optical properties of the living coral tissue on top of the coral skeleton. The normalized spectra were divided by the reflected light spectrum from a 99% diffuse reflectance standard (Spectralon) in air, $M_{d.sp}(\lambda)$, to calculate $KR_d(\lambda)$ as:

$$KR_d = \frac{M_{d.c}}{M_{d.gs}\, M_{d.sp}} \quad (6)$$

where K is an unknown scaling factor. This procedure canceled the wavelength dependence of the light source and the spectrometer response. **Figure 4A** shows the raw spectra $M_{d.c}(\lambda)$, $M_{d.gs}(\lambda)$, and $M_{d.sp}(\lambda)$. **Figure 4B** shows spectra of $KR_d(\lambda)$.

Each diffuse reflectance spectrum on the coral, $KR_{d.coral}$, was matched by a predicted reflectance spectrum pKR_d using least-squares fitting based on the expression:

$$pKR_d = f_{coll}\, K_d\, R_{d.theory}\,(\mu_{a.c}, \mu_{sc}^{'}, n_r) \quad (7)$$

where

$$\mu_{sc}^{'} = a_c\left(\frac{\lambda}{500nm}\right)^{-b_c} \quad (8)$$

$$\mu_{a.c} = W_c\, \mu_{a.water} \quad (9)$$

and n_r is the refractive index mismatch between coral tissue and water (ncoral/nwater = 1.4/1.33). The fitting parameters were (i) the reduced scattering coefficient at 500 nm, ac, and (ii) a scaling constant Kd.

The coral water content, W_c, was assumed to be 0.60, which allowed the scattering to be specified so as to match the water absorption peak seen at 960 nm. Such use of water as an internal standard in reflectance spectroscopy depends on the assumed value of the water content, and hence is subject to some, albeit modest, error (Jacques and Pogue, 2008), but the method allows specification of an approximate value for the scattering coefficient. The coral scattering power, b_c (**Table 1**) was assumed to be 0.50, and variation in this assumption had little effect on the fitting.

The factor f_{coll} in Eq. 7 is a light collection efficiency factor specifying the fraction of the total diffuse reflectance collected by the optical fiber probe. The optical fiber probe only collected light from a 5 mm wide spot, and hence failed to collect all the diffuse light escaping the coral. We determined a f_{coll} value of 0.448, by running a two-layer Monte Carlo simulation (Wangpraseurt et al., 2016) that placed a 2-mm-thick living coral layer on top of a semi-infinite skeleton (see more details in the **Supplementary Information**).

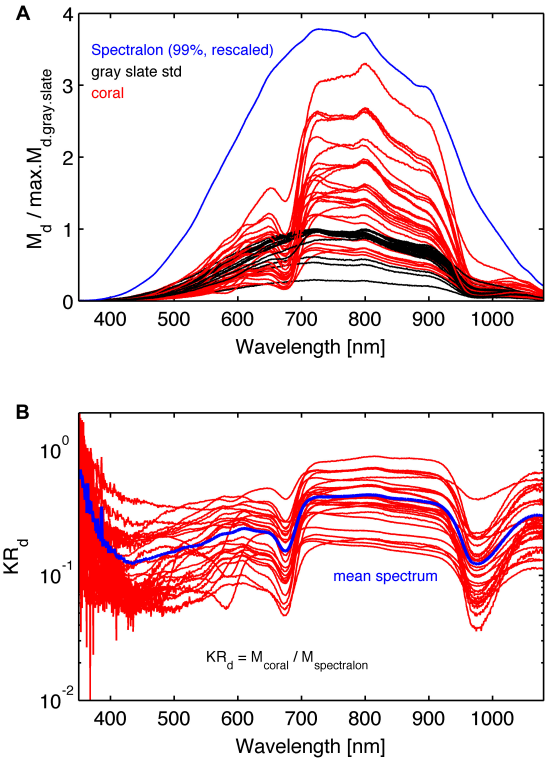

FIGURE 4 | (A) The raw spectra: red lines are the coral reflected light spectra $M_{d.coral}(\lambda)$, black lines are reflected light spectra, $M_{d.gs}(\lambda)$, from the gray reflectance standard spectra, and the blue line is reflected light spectrum, $M_{d.sp}(\lambda)$, from the 99% Spectralon reflection standard scaled arbitrarily. The coral and gray reference spectra were normalized by the maximum reflection in the gray reference spectrum for each coral. **(B)** Normalized reflectance spectra, $KR_d(\lambda)$ (see Eq. 3). The blue line is the mean spectrum of the 26 coral samples.

Figure 5 shows an example fit for one of the investigated corals (*Acropora millepora*), where **Figure 5A** shows the map of errors indicating the locus of minima (white line), while **Figure 5B** plots the error along this locus, and a blue diamond indicates the minimum along this locus. **Figure 5C** plots the measured spectrum KR_d (red line) and the predicted pKR_d (blue line) based on the 750–1030 nm range, i.e., outside the range of coral pigment absorption.

Algal Pigments

The coral spectra shown in **Figures 2**, **4B** clearly have absorption by algal pigments at wavelengths <700 nm, including a clear peak absorption in the red part of the spectrum due to Chl *a*, and a range of other pigments at shorter wavelengths. The optical density (OD) is the negative natural logarithm of transmittance (T) and is thus related to absorbance (A) of a material via $OD = A\, ln10$ (Welch and van Gemert, 2011). We can thus calculate OD as a proxy for spectral pigment absorption as:

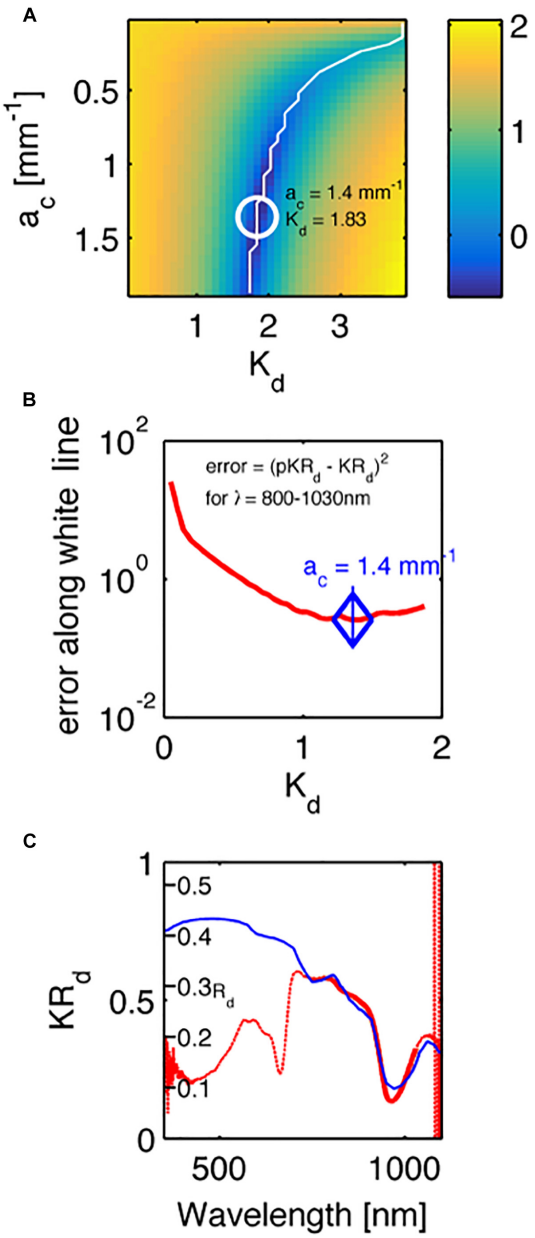

FIGURE 5 | An example fit of the KR_d spectrum of a *Acropora millepora*. **(A)** A map of the errors in measured KR_d vs. predicted pKR_d (Eq. 4), as choices of a_c and K_d were varied. White line indicates a range of minima. White circle indicates the best minimum using least-squares fitting. Color bar is $\log_{10}$ scale. **(B)** The profile of the error along the white line in **(A)**. **(C)** The experimental spectrum (red line) and the fit to the data from 800 to 1030 nm. The y-axis is the measured KR_d. A second set of tic marks labeled R_d indicate the true reflectance collected from the 5-mm-dia. spot by the optical fiber probe, as predicted by $R_d = pKR_d/K_d$.

$$OD = -\ln\left(\frac{KR_d}{pKR_d}\right) \quad (10)$$

where KR_d is the measured reflectance spectrum at the apparent peak of Chl *a* absorption and pKR_d is the spectrum devoid of algal pigments as predicted from the scattering plus water absorption (see above). **Figure 6** summarizes the values of the OD of Chl *a*, with a mean value of 1.8 ± 0.5 SE.

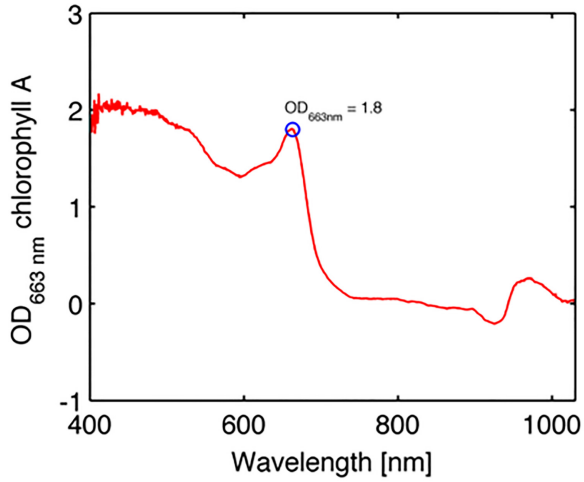

FIGURE 6 | Example of optical density (OD) spectrum of chlorophyll *a* in the coral *Favites abdita* (Eq. 7).

TABLE 2 | Average of coral tissue and skeleton optical parameters.

	μ_s' (500 nm)	Scatter power	Water content
	a [mm^{-1}]	b	W
Coral skeleton	0.83 ± 0.16	0.17 ± 0.05	0.64 ± 28
Coral tissue	1.55 ± 1.06	(0.5 assumed)	(0.6 assumed)

RESULTS AND DISCUSSION

The present study develops a rapid, non-invasive approach to characterize the optical properties of living intact corals. In contrast to previous studies that focused on analyzing the scattering of dead coral skeletons (Marcelino et al., 2013; Enríquez et al., 2017), we provide a first characterization of optical properties for a range of intact shallow water corals. The main findings of the present study show that coral tissue scattering was ∼87% stronger than skeletal scattering for a wide range of investigated corals (**Table 2**). These results confirm earlier observations of high tissue scattering and low skeletal scattering (Wangpraseurt et al., 2016). It is important to point out what low skeletal scattering implies for coral light transport as different interpretations of the significance of scattering in corals have been promoted (Marcelino et al., 2013; Wangpraseurt et al., 2016; Enríquez et al., 2017).

Marcelino et al. (2013) characterized the reduced scattering coefficient of coral skeletons and showed that corals with low μ_s' are characterized by a higher spread of light within the

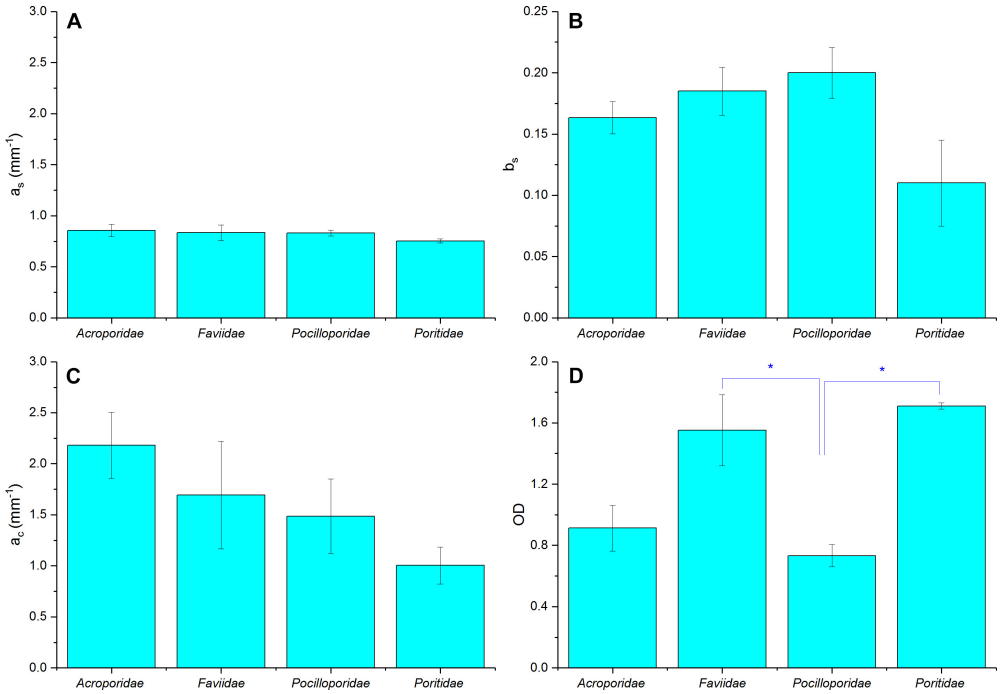

FIGURE 7 | Summary of optical properties of tissue and skeleton for four different coral families. **(A)** Skeletal scattering coefficient @ 500 nm (a_s, mm^{-1}), **(B)** Skeletal scattering power (b_s), **(C)** Tissue scattering coefficient @ 500 nm (a_c, mm^{-1}), **(D)** Optical depth (OD). Data are means ± SE for *Acroporidae* (n = 9), *Faviidae* (n = 8), *Pocilloporidae* (n = 5), and *Poritidae* (n = 3). Significant differences ($p < 0.05$) are marked with asterisk.

skeleton. In contrast, Enríquez et al. (2017) visualized the spreading of a laser beam on coral skeletons and argued that high scattering in coral skeletons, in this case not quantified in terms of μ_s or μ_s', leads to a high spreading of light. The relationship between light spreading and skeletal scattering is however non-linear and requires detailed quantification of μ_s' values. We illustrate this with a simple Monte Carlo model-based simulation of light propagation and fluence rate (= scalar irradiance) in a coral model (see **Supplementary Information**). Assuming a simple light absorbing medium (i.e., $\mu_s' = 0$), an incident collimated light beam will attenuate exponentially according to Lambert Beer's law. All light will be absorbed along the central line of illumination and no lateral spread of light is visible (**Supplementary Figures S1A,B**). Using a low skeletal scattering value ($\mu_s' = 1$ mm^{-1}), the fluence rate spreads within the skeleton and can be measured as a high radial reflectance away from the point of illumination (**Supplementary Figure S1C**). In this scenario, ($\mu_s' = 1$ $\mu_a = 0.1$ mm^{-1}) increasing μ_s' has increased the spread of light. However, increasing μ_s' 10 fold to $\mu_s' = 10$ mm^{-1} (e.g., Marcelino et al., 2013), reduces the spread of light (**Supplementary Figure S1D**). Now higher skeletal scattering leads to lower spreading of light, and most of the light is backscattered from a smaller area within the skeleton. Visual observations of intense light spreading of a laser beam from a skeleton do not imply that the scattering coefficient of the skeleton is high (Enríquez et al., 2017).

It has been argued that skeletal light scattering plays a key role in enhancing photosynthetic efficiency of corals (Enriquez et al., 2005), which can be disadvantageous during periods of excess irradiance, where the scattered light causes additional stress leading to photoinhibition and loss of symbionts further increasing light stress in the tissue (Teran et al., 2010; Marcelino et al., 2013; Wangpraseurt et al., 2017a). However, it has also been reported that coral tissue scattering can have a central role in affecting coral light propagation and the contribution of skeletal scattering to coral light absorption (Wangpraseurt et al., 2012, 2014; Wangpraseurt et al., 2016). To illustrate the combined role of tissue and skeletal scattering in coral light transport, we developed a set of Monte Carlo simulations based on the optical properties determined in the present study (see **Supplementary Information**). We first used average optical properties, i.e., high tissue scattering and lower skeletal scattering (**Table 2**). Secondly, the coral tissue scattering was reduced 10-fold to test whether the coral tissue scattering had an effect on light absorption by Chl *a*. We calculated the integral of fluence rate in the coral tissue layer, which is proportional to the amount of light absorbed by Chl *a*. The results show that the scattering properties of the living coral tissue clearly affects how light is concentrated in that layer, leading to an approximate 17% increase in light absorption for the high tissue scattering scenario (**Supplementary Figure S2A**). With high coral tissue scattering, the photons are trapped in the coral layer and thus enhance the absorption, while low coral tissue scattering leads to photons passing through the coral layer entering the skeleton, where it is backscattered to the coral tissue

layer. The oblique angle of backscatter of diffuse light doubles the opportunity of algae to absorb light compared to the nearly collimated incident sunlight that enters the coral (Enriquez et al., 2005), this effect is due to enhancement of scalar irradiance in coral tissue (Kühl et al., 1995) where for an isotropic distribution of backscattered light, the average path-length for upwelling photons is twice that of photons in a collimated beam traversing a thin plane of tissue or sediment (Kühl and Jørgensen, 1994).

Symbiodinium density controls the absorption of Chl *a*, and *Symbiodnium* cell density is highly variable between corals and over time due to, e.g., seasonal fluctuations and/or environmental stress (Hoegh-Guldberg and Jones, 1999). Therefore, we also varied the absorption coefficient over a range of values, (μ_a = 0.001 to 0.050 mm^{-1}) corresponding to a range of realistic Chl *a* concentrations (Teran et al., 2010). Using a high absorption coefficient (μ_a = 0.050 mm^{-1}), our Monte Carlo simulations, show that high coral tissue scattering leads to a 6.8% decrease in light absorbed by Chl *a*, relative to the low coral tissue scattering scenario (**Supplementary Figure S2**). Thus, depending on *Symbiodinium* cell density, increasing tissue scattering can increase or decrease light absorption. This is an important finding as it suggests that the role of light scattering in corals has to be evaluated with respect to algal cell density and Chl *a* content (**Supplementary Figures S2A,B**). Additionally, it is important to consider that a realistic prediction of light absorption by *Symbiodinium* cells would also require to take into account the structural complexity of both coral tissue (e.g., tissue thickness, surface structure, *Symbiodinium* distribution, and coral host pigments) (Wangpraseurt et al., 2017b) and skeletons (Enríquez et al., 2017), which is beyond the scope of the present study.

We found no species-specific differences in optical parameters and data was thus grouped by coral families (**Figures 7A–D**, see **Supplementary Table S1**, ANOVA $p > 0.05$). Mean tissue scattering [mm^{-1}] ranged between 1.0 (Poritidae) and 2.2 (Acroporidae) and was not significantly different between the investigated coral families (**Figure 7C**, ANOVA, $p > 0.05$). Grouping of optical parameters in coral families showed that the average skeletal scattering ranged between 0.7 and 0.8 [mm^{-1}] and was not significantly different between the four coral families (**Figure 7A**, ANOVA, $p > 0.05$). Our results show that due to the small scattering power of the skeleton ($b = 0.17$), skeletal scattering varies little with wavelength between 400 nm (μ_s' = 0.86) and 800 nm (μ_s' = 0.76, **Figure 7B**). The estimated skeletal scattering is similar to previous estimates from a Faviid coral (about 0.3–0.4 mm^{-1}; Wangpraseurt et al., 2016). In contrast, Marcelino et al. (2013) and Swain et al. (2016) have reported species-specific differences in skeletal light scattering and their estimates are about one order of magnitude higher than reported here. However, Marcelino et al. (2013) used low coherence enhanced backscattering spectroscopy to determine the reduced scattering coefficient for a range of coral skeletons for short photon pathlengths (<100 μm). This approach allows for estimating the reduced scattering coefficient in the locally monitored aragonite structure, while the present approach estimates bulk scattering properties of the skeleton, across the coral surface including the structural complexity of the skeleton and its voids (**Supplementary Figure S3**). Thus, the lower values could be explained by the different measuring techniques.

Although the focus of the present study was on characterizing light scattering, diffuse reflectance spectroscopy also allows for characterizing pigment absorption properties. The optical density (OD) was thus calculated as an indication of pigment absorbance (**Figure 7D**). We found a mean OD value of 1.8, which characterizes the product of pigment concentration and the average pathlength of photons within the pigmented algal layer. Mean OD differed significantly between coral families, with lowest OD measured in Pocilloporidae (mean = 0.73 ± 0.07 SE) and highest in Poritidae (mean = 1.71 ± 0.02 SE; ANOVA, $p < 0.05$). In contrast, volumetric cell density estimates suggested highest cell densities for Pocilloporidae (**Supplementary Table S2**). The low OD in Pocilloporidae is due to the thin tissue in these corals, as the OD estimates measure OD per projected surface area and thus integrates over the entire tissue volume.

We note that our study only investigated the IOPs of coral species sampled from a shallow reef flat habitat. It is possible that corals exhibit changes in IOP in response to environmental light gradients spanning over high light shallow waters to mesophotic deeper waters. Such investigation can now be realized with the presented methodology but was beyond the scope of the present study, which aimed at obtaining first estimates of average IOP for different coral species.

CONCLUSION

Both the coral skeleton and the coral tissue have a central role in modulating light transport and harvesting in corals. The coral skeleton can play a major role in backscattering light toward the overlying living tissue, thereby increasing the harvest of sunlight by Chl *a*, but the skeleton is translucent and can also play a key role in redistributing light to shaded regions in coral colonies. The efficiency of harvesting sunlight by Chl *a* is affected by high scattering in coral tissue when algal/Chl *a* levels are low, and diminished when algal/Chl *a* density is high, which may compensate for fluctuations of low and high algal densities in corals.

AUTHOR CONTRIBUTIONS

SJ, DW, and MK designed the study, analyzed and interpreted the data, and wrote the manuscript. SJ and DW performed the experimental measurements, developed the optical simulations, and provided the analytical tools.

FUNDING

This study was funded by a Carlsberg Foundation distinguished post-doctoral fellowship to DW, and from the European Union's Horizon 2020 Research and Innovation Programme under the Marie Skolodowska-Curie grant agreement no. 702911, a Carlsberg Foundation infrastructure grant (CF14-0573 to MK), and a Sapere Aude advanced grant

from the Independent Research Fund Denmark (DFF-1323-00065B to MK).

This research was conducted under a research permit from the Great Barrier Reef Marine Parks authority (G18-41571.1).

ACKNOWLEDGMENTS

We thank the staff at Heron Island Research Station as well as Sofie Lindegaard Jakobsen, Erik Trampe, Camilla Wentzel, and Anthony Larkum for excellent assistance during the field work.

SUPPLEMENTARY MATERIAL

The Supplementary Material for this article can be found online at: https://www.frontiersin.org/articles/10.3389/fmars.2019.00472/full#supplementary-material

REFERENCES

Bourne, D. G., Garren, M., Work, T. M., Rosenberg, E., Smith, G. W., and Harvell, C. D. (2009). Microbial disease and the coral holobiont. *Trends Microbiol.* 17, 554–562. doi: 10.1016/j.tim.2009.09.004

Enríquez, S., Méndez, E. R., Hoegh-Guldberg, O., and Iglesias-Prieto, R. (2017). Key functional role of the optical properties of coral skeletons in coral ecology and evolution. *Proc. R. Soc. Lond. B* 284, 20161667. doi: 10.1098/rspb.2016.1667

Enriquez, S., Mendez, E. R., and Iglesias-Prieto, R. (2005). Multiple scattering on coral skeletons enhances light absorption by symbiotic algae. *Limnol. Oceanogr.* 50, 1025–1032. doi: 10.1364/AO.49.005032

Falkowski, P. G., Dubinsky, Z., Muscatine, L., and Porter, J. W. (1984). Light and the bioenergetics of a symbiotic coral. *Bioscience* 34, 705–709. doi: 10.2307/1309663

Farrell, T. J., Patterson, M. S., and Wilson, B. (1992). A diffusion theory model of spatially resolved, steady–state diffuse reflectance for the noninvasive determination of tissue optical properties in vivo. *Med. Phys.* 19, 879–888. doi: 10.1118/1.596777

Hale, G. M., and Querry, M. R. (1973). Optical constants of water in the 200-nm to 200-μm wavelength region. *Appl. Opt.* 12, 555–563. doi: 10.1364/AO.12.000555

Hoegh-Guldberg, O., and Jones, R. J. (1999). Photoinhibition and photoprotection in symbiotic dinoflagellates from reef-building corals. *Mar. Ecol. Prog. Ser.* 183, 73–86. doi: 10.3354/meps183073

Jacques, S. L., and Pogue, B. W. (2008). Tutorial on diffuse light transport. *J. Biomed. Opt.* 13:041302. doi: 10.1117/1.2967535

Kühl, M., Cohen, Y., Dalsgaard, T., Jørgensen, B. B., and Revsbech, N. P. (1995). Microenvironment and photosynthesis of zooxanthellae in scleractinian corals studied with microsensors for O_2, pH and light. *Mar. Ecol. Prog. Ser.* 117, 159–172. doi: 10.3354/meps117159

Kühl, M., and Jørgensen, B. B. (1994). The light-field of microbenthic communities – radiance distribution and microscale optics of sandy coastal sediments. *Limnol. Oceanogr.* 39, 1368–1398. doi: 10.4319/lo.1994.39.6.1368

Levitz, D., Thrane, L., Frosz, M., Andersen, P., Andersen, C., Andersson-Engels, S., et al. (2004). Determination of optical scattering properties of highly-scattering media in optical coherence tomography images. *Opt. Express* 12, 249–259. doi: 10.1364/opex.12.000249

Lyndby, N. H., Kühl, M., and Wangpraseurt, D. (2016). Heat generation and light scattering of green fluorescent protein-like pigments in coral tissue. *Sci. Rep.* 6:26599. doi: 10.1038/srep26599

Marcelino, L. A., Westneat, M. W., Stoyneva, V., Henss, J., Rogers, J. D., Radosevich, A., et al. (2013). Modulation of light-enhancement to symbiotic algae by light-scattering in corals and evolutionary trends in bleaching. *PLoS One* 8:e61492. doi: 10.1371/journal.pone.0061492

Muscatine, L., McCloskey, L. R., and Marian, R. E. (1981). Estimating the daily contribution of carbon from zooxanthellae to coral animal respiration. *Limnol. Oceanogr.* 26, 601–611. doi: 10.4319/lo.1981.26.4.0601

Rodriguez-Roman, A., Hernandez-Pech, X., Thome, P. E., Enriquez, S., and Iglesias-Prieto, R. (2006). Photosynthesis and light utilization in the Caribbean coral *Montastraea faveolata* recovering from a bleaching event. *Limnol. Oceanogr.* 51, 2702–2710. doi: 10.4319/lo.2006.51.6.2702

Salih, A., Larkum, A., Cox, G., Kühl, M., and Hoegh-Guldberg, O. (2000). Fluorescent pigments in corals are photoprotective. *Nature* 408, 850–853. doi: 10.1038/35048564

Smith, E. G., D'angelo, C., Sharon, Y., Tchernov, D., and Wiedenmann, J. (2017). Acclimatization of symbiotic corals to mesophotic light environments through wavelength transformation by fluorescent protein pigments. *Proc. R. Soc. Lond. B* 284:20170320. doi: 10.1098/rspb.2017.0320

Swain, T. D., DuBois, E., Gomes, A., Stoyneva, V. P., Radosevich, A. J., Henss, J., et al. (2016). Skeletal light-scattering accelerates bleaching response in reef-building corals. *BMC Ecol.* 16:10. doi: 10.1186/s12898-016-0061-4

Teran, E., Mendez, E. R., Enriquez, S., and Iglesias-Prieto, R. (2010). Multiple light scattering and absorption in reef-building corals. *Appl. Opt.* 49, 5032–5042. doi: 10.1364/AO.49.005032

Tuchin, V. (2007). *Tissue Optics*. Bellingham, WA: SPIE Press.

Veron, J. E. N. (2000). *Corals of the World*, Vol. 1–3. Townsville: Australian Institute of Marine Science, 295.

Wangpraseurt, D., Holm, J. B., Larkum, A. W. D., Pernice, M., Ralph, P. J., Suggett, D. J., et al. (2017a). *In vivo* microscale measurements of light and photosynthesis during coral bleaching: evidence for the optical feedback loop? *Front. Microbiol.* 8:59. doi: 10.3389/fmicb.2017.00059

Wangpraseurt, D., Wentzel, C., Jacques, S. L., Wagner, M., and Kühl, M. (2017b). In vivo imaging of coral tissue and skeleton with optical coherence tomography. *J. R. Soc. Interface* 14:20161003. doi: 10.1098/rsif.2016.1003

Wangpraseurt, D., Jacques, S., Petri, T., and Kühl, M. (2016). Monte Carlo modeling of photon propagation reveals highly scattering coral tissue. *Front. Plant Sci.* 7:1404. doi: 10.3389/fpls.2016.01404

Wangpraseurt, D., Jacques, S. L., Lyndby, N., Holm, J. B., Ferrier-Pages, C., and Kühl, M. (2019). Microscale light management and inherent optical properties of intact corals studied with optical coherence tomography. *J. R. Soc. Interface* 16:20180567. doi: 10.1098/rsif.2018.0567

Wangpraseurt, D., Larkum, A. W. D., Franklin, J., Szabo, M., Ralph, P. J., and Kühl, M. (2014). Lateral light transfer ensures efficient resource distribution in symbiont-bearing corals. *J. Exp. Biol.* 217, 489–498. doi: 10.1242/jeb.091116

Wangpraseurt, D., Larkum, A. W. D., Ralph, P. J., and Kühl, M. (2012). Light gradients and optical microniches in coral tissues. *Front. Microbiol.* 3:316. doi: 10.3389/fmicb.2012.00316

Welch, A. J., and van Gemert, M. J. (2011). *Optical-Thermal Response of Laser-Irradiated Tissue*. New York, NY: Plenum Press.

Conflict of Interest Statement: The authors declare that the research was conducted in the absence of any commercial or financial relationships that could be construed as a potential conflict of interest.

Advantages of publishing in Frontiers

OPEN ACCESS
Articles are free to read for greatest visibility and readership

FAST PUBLICATION
Around 90 days from submission to decision

HIGH QUALITY PEER-REVIEW
Rigorous, collaborative, and constructive peer-review

TRANSPARENT PEER-REVIEW
Editors and reviewers acknowledged by name on published articles

Frontiers
Avenue du Tribunal-Fédéral 34
1005 Lausanne | Switzerland

Visit us: www.frontiersin.org
Contact us: info@frontiersin.org | +41 21 510 17 00

REPRODUCIBILITY OF RESEARCH
Support open data and methods to enhance research reproducibility

DIGITAL PUBLISHING
Articles designed for optimal readership across devices

FOLLOW US
@frontiersin

IMPACT METRICS
Advanced article metrics track visibility across digital media

EXTENSIVE PROMOTION
Marketing and promotion of impactful research

LOOP RESEARCH NETWORK
Our network increases your article's readership